I. Sol-Gel Deposition of Oxide-Ion Conducting Thin Films
II. Liquid Precursors to Hafnium and Tantalum Carbides

by

Jennifer Woodbridge Pell

B.S., Brandeis University

(1993)

M.S., Brandeis University

(1993)

SUBMITTED TO THE DEPARTMENT OF CHEMISTRY
IN PARTIAL FULFILLMENT OF THE REQUIREMENTS
FOR THE DEGREE OF DOCTOR OF PHILOSOPHY

at the

MASSACHUSETTS INSTITUTE OF TECHNOLOGY

May 1999

[June 1999]

Signature of Author _____

Department of Chemistry
13 May, 1999

Certified by _____

Dietmar Seyferth
Thesis Supervisor

Accepted by _____

Dietmar Seyferth
Chairman, Departmental Committee on Graduate Students

Science

V.1

This doctoral thesis has been examined by a Committee of the Department of Chemistry as follows:

Professor Alan Davison _____

<div align="right">Chairman of Thesis Committee</div>

Professor Dietmar Seyferth _____

<div align="right">Thesis Supervisor I</div>

Professor Hans-Conrad zur Loye_____

<div align="right">Thesis Supervisor II</div>

I. Sol-Gel Deposition of Oxide-Ion Conducting Thin Films
II. Liquid Precursors to Hafnium and Tantalum Carbides

By

Jennifer Woodbridge Pell

SUBMITTED TO THE DEPARTMENT OF CHEMISTRY ON

May 13, 1999 IN PARTIAL FULFILLMENT OF THE REQUIREMENTS FOR

THE DEGREE OF DOCTOR OF PHILOSOPHY IN CHEMISTRY

ABSTRACT

I. The deposition of thin films of the BiMeVOx oxygen ion conducting ceramics was studied. The sol-gel precursor solution included a soluble form of bismuth acetate, a vanadium alkoxide, and the acetate or alkoxide of the dopant metal (Me). Copper-doped films were spin-coated onto nonporous quartz substrates and pyrolyzed. These were initally defect-free, but became agglomerated on heating at higher temperatures. The use of a number of different additive compounds was tried, but did not greatly improve the behavior of the films on quartz substrates. These films, when deposited onto platinum-coated substrates, remained defect-free to all temperatures. Niobium-doped films remained defect-free on quartz substrates at all heating temperatures. The reasons for these behaviors are examined. Copper-doped films were deposited defect-free onto porous alumina substrates. The structure of a single-molecule bismuth-vanadium precursor in the sol-gel solution is suggested.

II. Liquid precursors to refractory transition metal carbides were produced via both organometallic and metal alkoxide starting materials. These precusors were pyrolyzed under inert atmosphere and found to convert to the metal carbide, plus excess carbon, between 1100 °C and 1500 °C.

The use of Grignard reagents to functionalize (chloromethyl)silyl-terminated carbosilane dendrimers was investigated briefly. The syntheses were plagued by long reaction times and low purities, contrary to the behavior expected for the (chloromethyl)silyl group. Reasons for this behavior are discussed.

Thesis Supervisor, Part I: Dr. Hans-Conrad zur Loye
Thesis Supervisor, Part II: Dr. Dietmar Seyferth
Title: Robert T. Haslam and Bradley Dewey Professor of Chemistry

Acknowledgments

TABLE OF CONTENTS:

Part II: Liquid Precursors to Hafnium and Tantalum Carbides

Chapter One

Oxygen Ion Conducting Membranes: Brief Survey and Introduction

1.1 Mass Transport in Solids: Fast Ionic Conduction

In most solid state materials, ionic conduction does not occur to any appreciable extent. Defects in the crystal lattice or large interstitial spaces, however, can provide empty sites (vacancies) via which ions can migrate in a "hopping" mechanism, wherein ions move sequentially into adjacent energy-equivalent empty sites. (Figure 1.1) Cooperative motion of the ions also occurs. At room temperature, most ionic solids do not have enough vacancies to permit appreciable conduction of ions. However, when defect concentrations become high, as they do near the material's melting point, the ionic conductivity of the material increases. For example, NaCl, which is an insulator at room temperature, can reach a conductivity of 10^{-3} S cm^{-1} at 800 °C, just below the melting point of the material. Doping aliovalent "impurities" into the parent structure of a material creates vacancies on the opposite ionic lattice to maintain charge electroneutrality. In addition, some materials, such as AgCl, accommodate ions in the interstitial space to compensate for vacancies on the lattice (Frenkel defects), so that movement of ions from lattice sites to interstitial sites and *vice-versa* provides a second potential mechanism for mass transport. (Figure 1.2) In both of the examples given, it is the cation that is the mobile species, although examples where anion Frenkel defects provide the mode for mass transport are known (e.g. AgF).

Certain metal oxides, as well, experience a gradual increase in defect concentration on the oxide sublattice as the sample

temperature rises, resulting in the potential for oxide ion conductivity. Oxides that crystallize in the fluorite structure, such as HfO_2, CeO_2, ThO_2, and stabilized zirconia have sufficient unoccupied volume in the unit cell that anions can move into interstices. These materials can also accommodate a large concentration of lower-valent dopant cations such as Ca^{2+} and Y^{3+} in their structures, resulting in a high oxygen vacancy concentration and thus a high oxide ion conductivity. Zirconias can be doped with heterometals to maintain them in the cubic fluorite structure, yielding, for instance, the industry standard oxide ion conductor yttria-stabilized zirconia (YSZ). They have conductivities on the order of 5×10^{-2} S cm^{-1} at 1000 $^{\circ}$C, and are classified as "solid electrolytes."

Solid electrolytes, also known as fast ionic conductors or superionic conductors, are a class of materials with a significantly higher low-temperature (below the material's melting point) conductivity than would be expected from a simple statistical assumption regarding the number of vacancies. In these materials, either a cationic or an anionic component of the structure is not confined to specific lattice sites, resulting in a high concentration of mobile species and a low activation energy for ion migration. As noted above, this situation may come about due to a large interstitial volume native to the structure type, which accommodates ion movement; or because of a large impurity concentration which produces extrinsic vacancies on the lattice of the conducted species. However, dopant ions and vacancies tend to interact, and the extra energy required to overcome this attraction increases the activation energy for conduction. Therefore simply doping a structure reaches

a point beyond which further increases in dopant concentration actually decrease the conductivity realized.[1]

A high degree of intrinsic vacancy disordering on the ionic sublattice, whether in the room temperature phase or in a metastable high temperature phase, can also provide for fast ionic conductivity because the random distribution of ions over an excess number of sites having equal potential permits all of the ions on that sublattice to be mobile, at least in principle. For instance, disorder on both the cation and oxygen sublattices of the pyrochlore ($A_2B_2O_7$) materials, where A and B may switch positions and O move into interstitial sites, provides the high oxygen ion conductivities seen in these materials; furthermore, the pyrochlore materials have a vacant oxygen site, when compared with the closely-related fluorite structure AO_2 (A_4O_8, compare with $A_2B_2O_7$).[2]

A major goal of research in oxygen ion conducting materials is the development of new compounds having high oxygen ion conductivity at relatively low temperatures (400-800 °C), for use in a number of different applications. The design of new conductors attempts to combine the extrinsic vacancies made through doping with the intrinsic vacancies already in the parent structure. The provision of a low activation energy barrier for hopping between adjacent sites by using structures with a large free volume and highly polarizable ions, is a second consideration. "Intergrowth" hybrids of known structures are possible. For example, while the perovskite structure (ABO_3) is stoichiometric, it accepts a large variation in A' and B' dopants, so that the net compound $A_xA'_{1-x}B_yB'_{1-y}O_{3-\delta}$ can become oxygen-deficient and therefore conductive. The Brownmillerite oxides ($A_2B'B''O_5$) have essentially

the perovskite structure with ordered oxygen vacancies in alternate layers along the [101] direction. A number of examples of good oxygen ion conductivity above the temperature of an order-disorder transition in the Brownmillerite family exist.[3,4] The Brownmillerites may be intergrown with perovskites to produce hybrid oxygen ion conducting materials.[4,5] Another hybrid-type family, the Aurivillius[6] phases ($Bi_2A_{n-1}M_nO_{3n+3}$) sandwich perovskitic $\{A_{n-1}M_nO_{3n+1}\}^{2-}$ regions between sheets of $\{Bi_2O_2\}^{2+}$. Oxygen vacancies in the perovskite region lead to the high conductivity reported for Bi_2WO_6 and $Bi_2VO_{5.5}$ (n=1).[7-10] (Figure 1.3) The intergrowth of Brownmillerite and Aurivillius structures produced a new class of oxygen ion conductors.[11]

Figure 1.1: Hopping mechanism for ionic conductivity.

net O_2 conduction via O^{2-} of lattice

◯ = lattice vacancy

⬤ = atom in lattice
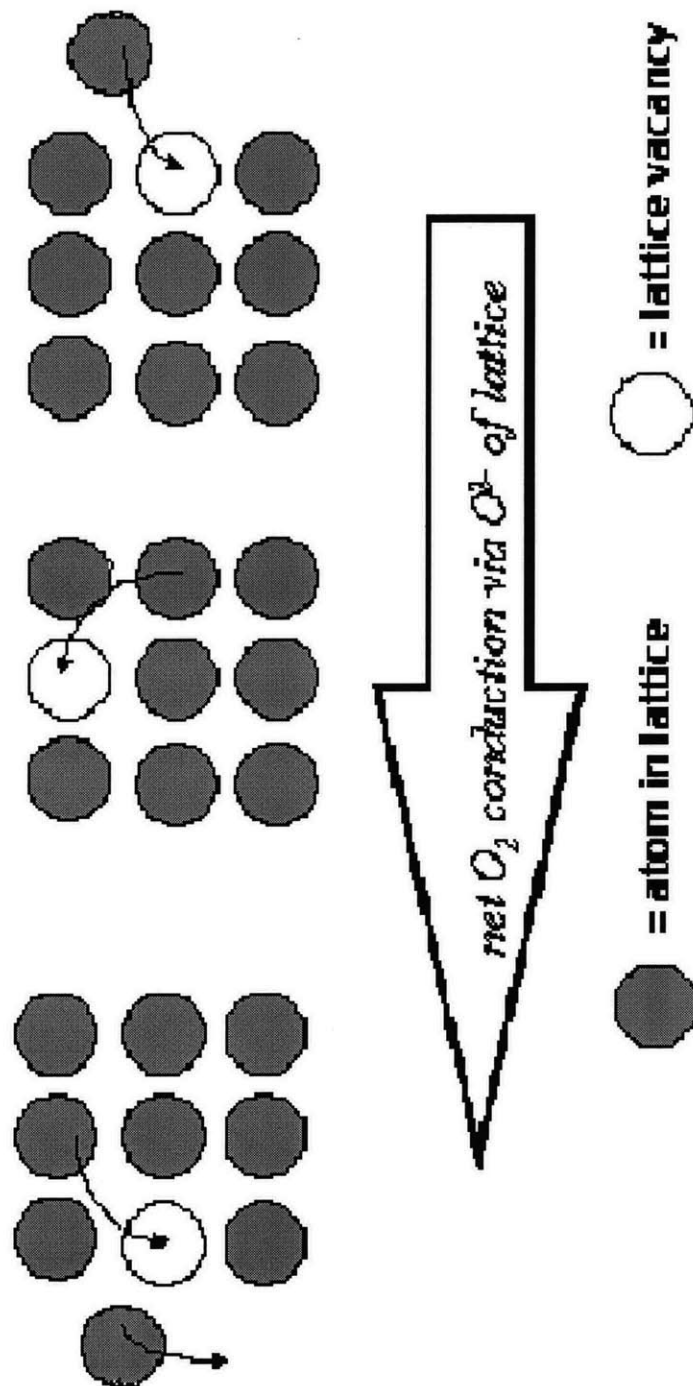
Figure 1.2: Ionic conductivity via Frankel defects (interstitial atoms).
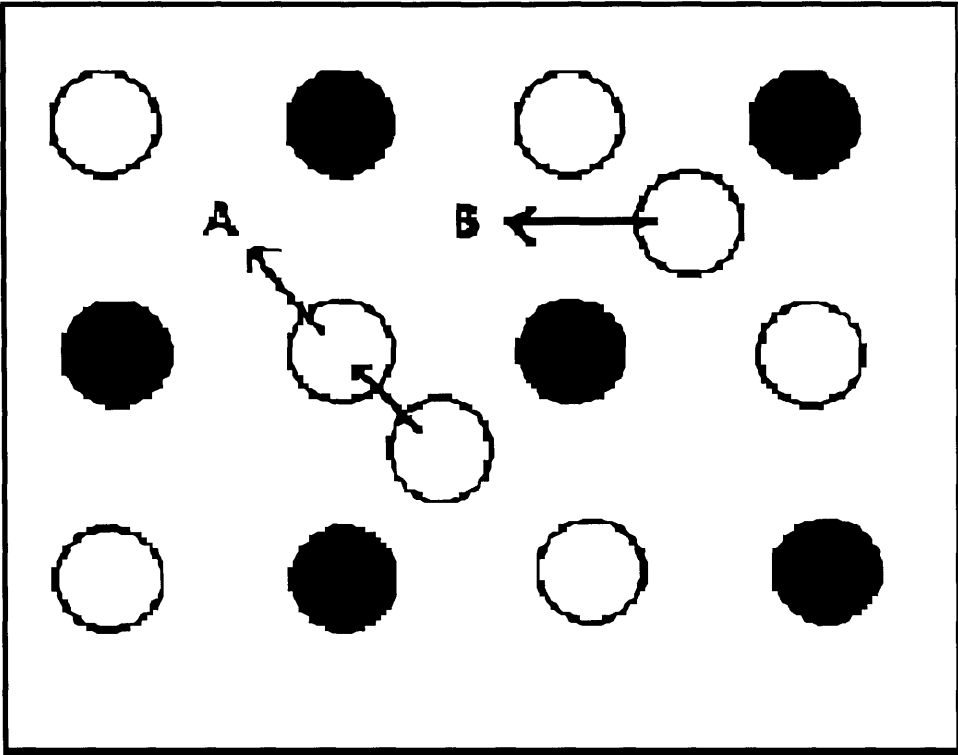
A -- interstitial to lattice site
B -- interstitial to interstitial

= atom # 1   = atom # 2

1.2 The BiMeVOx Family of Oxygen Ion Conductors

It is the Aurivillius phases that have given us materials with some of the highest oxygen-ion conductivities measured to date. These materials were first reported by Bush[12] and Debreuille-Gresse.[7,13] The solid-state synthesis is accomplished by heating two equivalents of bismuth oxide, Bi_2O_3, with one of vanadium pentoxide, V_2O_5, to 600 °C, followed by re-grinding of the pelletized sample and calcination at 850 °C in air.[14] Two phase changes occur in the parent structure on heating prior to congruent melting at 890 °C. (Equation 1.1)

$$(1.1) \quad \alpha \xrightarrow{450\ ^{\circ}C} \beta \xrightarrow{570\ ^{\circ}C} \gamma$$

The α phase, stable at room temperature, has a face-centered orthorhombic mean cell, $a=5.533(1)$, $b=5.611(1)$, $c=15.288(4)$ Å, by powder XRD. Single-crystal X-ray data were consistent with the powder data. In the β phase, the mean cell is tetragonal and some weak reflections indicate doubled cell parameters to give $a=b=11.285(8)$, $c=15.400(9)$ Å at 500 °C. The γ phase is tetragonal $I4/mmm$ with parameters $a=b=4.004(1)$ and $c=15.488(8)$ Å at 700 °C. The X-ray data indicate a layered structure of $\{Bi_2O_2\}^{2+}$ sheets and perovskite-like slabs similar to those found in Bi_2MO_6 (M=W, Mo), but the cell parameters and elemental composition indicate that the perovskite slabs are incomplete. While the O atoms in the puckered sheets are easily located, those in the vanadium

octahedra of the perovskitic regions are split among high-multiplicity crystallographic sites. There is a certain degree of debate in the literature about the details of the structure, partially due to the ambiguity introduced by the site disordering, and partially due to the superlattice reflections observed by a number of authors. [15]

Whatever the particulars of the structure, the overall formulation indicates vacancies and therefore high oxygen-ion mobility in the perovskitic planes: $\{Bi_2O_2\}^{2+}\{VO_{3.5}\square_{0.5}\}^{2-}$ (where $\square$ is a vacancy). The measured oxide-ion conductivities were indeed quite high, and the transport number near unity. Abraham's report spurred a flurry of other papers reporting various partial substitutions of other elements for the Bi, V, or both metals in the structure, and the resulting modifications to the ionic conductivity.[16,17]

The puckered $\{Bi_2O_2\}^{2+}$ sheets have basal edge-shared BiO_4 groups in which the Bi is at the apex of a square pyramid and the four oxygen atoms form the base plane. Partial substitution of the Bi with Sb, Pb, and Te has been achieved but with no real improvement in the ionic conductivity.[18-22] The A and B sites of the perovskite block can be substituted by a wide range of cations, provided that the perovskite and bismuth oxide layers continue to match structurally. Substitution of aliovalent cations onto the vanadium sites can stabilize the high-temperature, high-conductivity γ phase to room temperature, as well. The collective term for the metal-substituted members of this family is "BiMeVOx", with the general formula $BiM_xV_{1-x}O_{5.5-\delta}$.

Further work by Abraham[14] led to the initial members of the BiMeVOx family. He doped the parent structure with up to 12 atom% of Cu^{2+} and found that for $0<x<0.07$ in the general formula above, the material is found in the orthorhomic (α) phase, while for $0.07<x<0.12$ the tetragonal γ phase is stabilized to ambient temperature. The formulation $Bi_2Cu_{0.1}V_{0.9}O_{5.35}$ was found to have ionic conductivity (pressed pellet) of 1×10^{-2} S cm^{-1} at 300 °C, some three orders of magnitude greater than that of YSZ at the same temperature. (Figure 1.4) Measurement of the conductivity of a single crystal of the parent (undoped) material and of $Bi_2Cu_{0.1}V_{0.9}O_{5.35}$ demonstrated a marked anisotropy, with the conductivity parallel to the $\{Bi_2O_2\}^{2+}$ planes (crystallographic ab plane) some 100 times higher than that perpendicular to the $\{Bi_2O_2\}^{2+}$ planes (crystallographic c plane).[23,24] This is consistent with the perovskitic layer's being primarily responsible for the ionic conduction. The addition of the dopant prevents the ordering of the metal positions and oxygen vacancies, and permits the stabilization of the high-symmetry γ phase; the disorder on these sites also provides the high conductivity observed in these samples. Substitution of Li^+, Zn^{2+}, and Ti^{4+}, at 10 atom%, all led to the stabilization of the γ structure to room temperature, while use of Al^{3+} and Ge^{4+} did not lead to the γ structure.[9] Surprisingly, the Ti-substituted materials showed the highest conductivities in this set of compounds – higher, even, than for the 10% Cu-doped compounds reported by Abraham. This illustrates that oxygen-ion vacancy concentration alone does not determine the ionic conductivity. The conductivity order among those ion substituents

that stabilized the γ structure is $Ti^{4+}>Cu^{2+} \approx Zn^{2+}>Li^+$, paralleling the order of the ability of the cation to polarize anions. The authors suggest that the polarization of the oxygen ions somehow "eases" the hopping of oxide ions from filled sites to vacant sites. Among 4+ cation substituents Pb, Zr, Sn, and Ti, the conductivity increased with decreasing ionic radius,[25] as expected from the model developed by Cherry et al. for migration of oxygen ions in perovskite-type oxides.[26] The conductivities of the BiMeVOx materials and the quantity of dopant required for their stabilization in the γ phase are listed in Tables 1.1 and 1.2.[27]

The coordination geometry around the dopant cation is, similarly, important. Substitution of Sb(V) and Nb(V) into the parent structure to generate $Bi_2M_{0.3}V_{0.7}O_{5.5}$ (M=Sb, Nb) stabilizes the tetragonal phase and gives materials with conductivities comparable to or slightly better than BiCuVOx and BiTiVOx.[28] However, the conductivity of the Sb-substituted material is higher than for the Nb-substituted material, and this appears to be correlated with the regular octahedral geometry around the Sb, *versus* the off-center positioning of Nb in its coordination octahedron, as well as with the polarizability of Sb relative to that of Nb. The distorted and oxygen-deficient surroundings of the Nb may act as a trapping area during anionic diffusion, thereby lowering the conductivity. In Cr(III)-doped samples, the tendency for Cr(III) to adopt a full regular octahedral coordination and form clusters seems to be associated with the rise the number of tetrahedrally coordinated V(V) in the lattice.[29] This clustering, as well as the increase in the number of unfavorable tetrahedral V(V) sites, may

cause the poor oxide ion conductivity of Cr(III)-doped samples. Conversely, in the high-conductivity Cu-doped BiCuVOx, EPR and UV-VIS spectroscopic data suggest that the Cu^{2+} sites are distorted-octahedral, with the oxygen atoms compressed along the apical direction.[30]

Most of this discussion must be taken with somewhat of a grain of salt, however, since cations of suitable charge and size may substitute onto either the Bi or V sites. West et al. demonstrates that three or four mechanisms of accommodating the aliovalent cations may take place: V $\leftrightarrow$ Bi, V $\leftrightarrow$ M, Bi $\leftrightarrow$ M, and possibly interstitial M. [31,32] Double substitutions, either of two different metals for V or of heterometals on the V and Bi sites, have been reported. These failed to give an improvement in conductivity over the BiCuVOx standard, and the authors report that the resulting solid solutions are metastable.[22] The questionable nature of the assumption that all the dopants introduced are going into given sites may account for the variation among reports of the minimum dopant levels required to stabilize the γ phase.[23,31,33]

The high oxide ion conductivity reported for the BiMeVOx family is believed to be due to the disorder of the oxygen vacancies that are associated with the vanadium atoms in the perovskitic layer. Mairesse has summarized results for the substitutions of various metal cations onto the vanadium site.[17] The highest conductivities are found for BiCuVOx, BiTiVOx, and BiNbVOx; doping with other metals results in compounds with lower oxide ion conductivities, though in all doped materials the conductivities are still higher than in the undoped parent phase. (Figure 1.5)

All told, the BiMeVOx family of materials, with their exceptionally high oxygen ion conductivity at low temperatures, have been extensively studied and show potential for a number of applications. However, because the electronic transport number has been shown to be at least a few percent (t_i=0.987 at 557 °C),[34] these materials cannot be used in devices where electrical "shorting" of the circuit is detrimental: e.g. in oxygen sensors and fuel cells. For other applications, the presence of some electronic conductivity is beneficial. $Bi_2VO_{5.5}$ and BiMeVOx (Me=Cu, Fe, Sr) have also been tested as catalysts for the oxidative coupling of methane (*vide infra*). [35]

Figure 1.3: Bi$_2$VO$_{5.5}$ structure.

$=VO_5^{5-}$ $=$oxygen

$=$bismuth
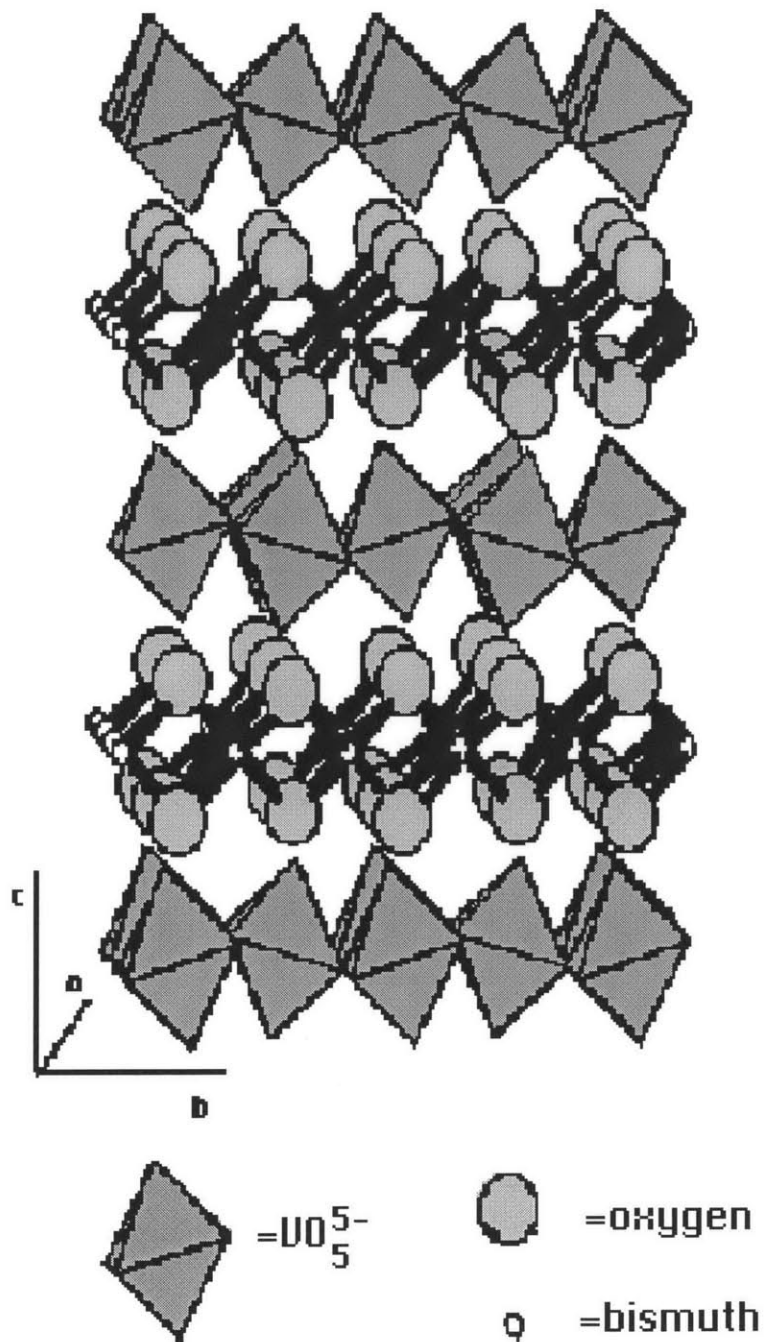
Figure 1.4: Comparison of YSZ, $Bi_2VO_{5.5}$, $Bi_2Cu_{0.1}V_{0.9}O_{5.5-\delta}$ ionic conductivities over a range of temperatures.[14]
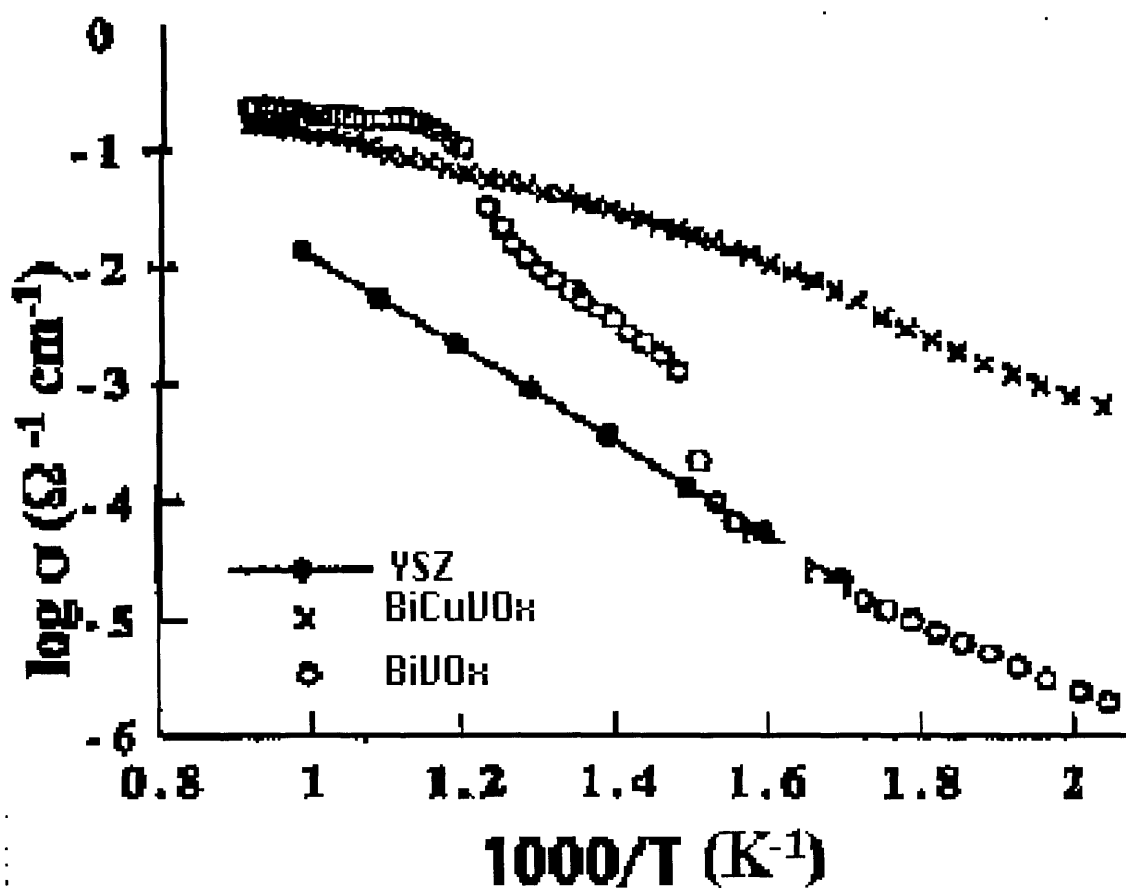
Figure 1.5: Comparison of $Bi_2VO_{5.5}$, $Bi_2Cu_{0.1}V_{0.9}O_{5.5-\delta}$, $Bi_2Ti_{0.1}V_{0.9}O_{5.5-\delta}$, $Bi_2Nb_{0.3}V_{0.7}O_{5.5-\delta}$ ionic conductivities over a range of temperatures.[33]
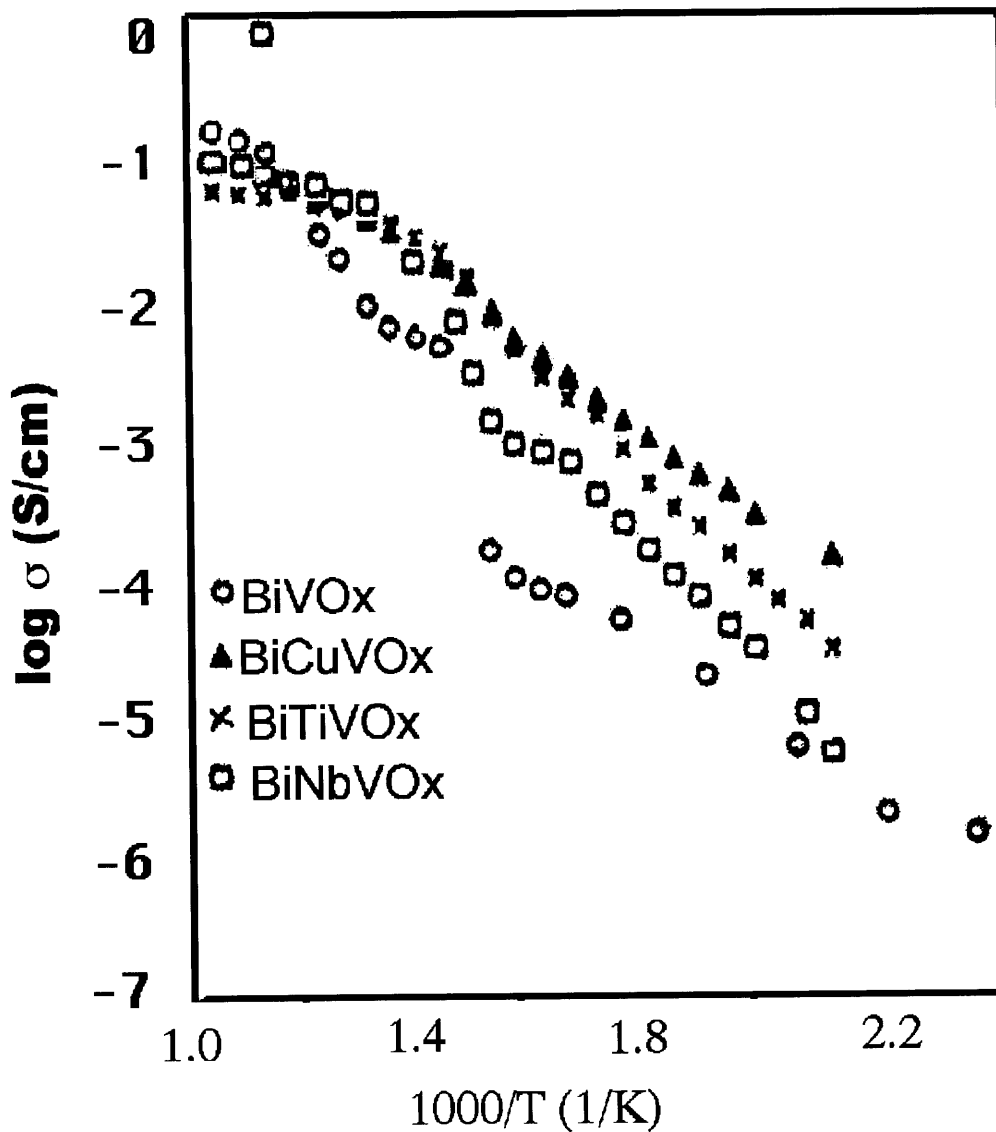
Table 1.1: Conductivities of the Aurivillius phase oxygen ion conductors.[27]

Compound	T (°C)	σ (S/cm)	Comments
Bi_2WO_6	900	1×10^{-2}	
Bi_2WO_6	900	1×10^{-1}	single crystal, parallel to **ab** plane
$Bi_2VO_{5.5}$	300	5×10^{-5}	α-phase
	300	1×10^{-5}	single crystal, parallel to **ab** plane
	300	1×10^{-5}	single crystal, perpendicular to **ab** plane
	500	1×10^{-2}	β-phase
	500	1×10^{-2}	single crystal, parallel to **ab** plane
	500	1×10^{-4}	single crystal, perpendicular to **ab** plane
	600	1×10^{-1}	γ-phase
	600	3×10^{-1}	single crystal, parallel to **ab** plane
$Bi_2V_{0.8}Al_{0.2}O_{5.4}$	500	1.8×10^{-2}	polycrystalline
$Bi_2V_{0.9}Cu_{0.1}O_{5.35}$	500	5×10^{-2}	polycrystalline
$Bi_2V_{0.9}Co_{0.1}O_{5.35}$	500	7×10^{-2}	polycrystalline
$Bi_2V_{0.9}Fe_{0.1}O_{5.40}$	650	6.7×10^{-2}	polycrystalline

Table 1.1 (continued).

Compound	T (°C)	σ (S/cm)	Comments
$Bi_2V_{0.8}La_{0.2}O_{5.4}$	500	6.6×10^{-3}	polycrystalline
$Bi_2V_{0.7}Nb_{0.3}O_{5.5}$	500	5×10^{-2}	polycrystalline
$Bi_2V_{0.93}Ni_{0.07}O_{5.395}$	500	1×10^{-1}	polycrystalline
$Bi_2V_{0.7}Sb_{0.3}O_{5.5}$	500	1×10^{-1}	polycrystalline
$Bi_2V_{0.9}Sr_{0.1}O_{5.35}$	650	1.2×10^{-2}	polycrystalline
$Bi_2V_{0.9}Ti_{0.1}O_{5.35}$	500	5×10^{-2}	polycrystalline
$Bi_2V_{0.9}Zn_{0.1}O_{5.35}$	500	5×10^{-2}	polycrystalline

Table 1.2: Cation dopant concentrations required to stabilize the high-temperature (γ) phase of $Bi_2VO_{5.5}$.[27]

Dopant Cation	% of Vanadium Substitution
Li^+	10
Zn^{2+}	10
Pb^{2+}	9-10
Cu^{2+}	7-12
Ni^{2+}	10
Co^{2+}	7.5-25
Sb^{5+}	15-50
Nb^{5+}	10-50
Ta^{5+}	10-25
Ti^{4+}	10-20
Zr^{4+}	10-15
Mg^{2+}	7.5-15

1.3 Measurement of Oxygen Ion Conductivity[36,37]

1.3.1 Impedance Spectroscopy

Ionic conductivity, σ, is generally treated the same way as is electronic conductivity, and is expressed by the Equation 1.2:

(1.2) $\sigma = neZ\mu$

where n is the number of charge carriers per unit volume, e is the charge on the electron, Z is the charge on the carriers, and μ is a measure of the carrier mobility.

Because the hopping mechanism described in Section 1.1 is an activated process the carrier mobility is expressed by an Arrhenius-type equation. (Equation 1.3)

(1.3) $\mu = \mu_0 e^{(-Ea/kT)}$

where μ_0 depends on the attempt frequency (the number of times per second that a given ion tries to move), the distance moved by the ion, and the magnitude of the imposed external field (if this is small, about 300 V cm^{-1}, μ_0 will include a 1/T dependence as well).

All told, the expression for the conductivity has the form given by Equation 1.4.

(1.4) $\sigma = (\sigma_0/T)e^{(-Ea/T)}$

Thus a plot of $\ln(\sigma T)$ against $1/T$ will give a line of slope $-E_a$. Over a range of temperatures this plot may have regions of different activation energies corresponding to different sources (extrinsic or intrinsic) of the conductivity observed.

While the electrical conductivity of materials can be measured directly by imposing a dc current and measuring the voltage drop across the material according Ohm's law, the measurement of ionic conductivity is not so straightforward. Imposition of a dc voltage across an ion-conducting solid will result in an initial current which will be the sum of the ion current and any electronic current. Because many electrode materials are blocking to the ions being conducted, the solid will become polarized over time and the voltage will drop to zero. Thus the ionic conductor behaves as a capacitor when blocking electrodes are used. One solution to the problem of making the conductivity measurement is, of course, to use an electrode that permits conduction of both electrons and the mobile ions; however, such electrodes are not available for all materials.

A second commonly used alternative is to impose an ac voltage oscillating at a range of different frequencies, and measure the impedance (or the admittance; the equations cited below are for the impedance). A Wheatstone bridge type of apparatus is used, where for impedance measurements the resistive and capacitative circuit elements are in series. Gold or platinum blocking electrodes are typical, and the interface between the electrode and the sample therefore adds a double-layer capacitance in series with the simple bulk resistance and with the resistance due to grain boundary effects (the latter is seen in polycrystalline samples only).

Each of these sample resistances has a capacitance in parallel with it, and the electronic resistance of the sample is parallel the ionic resistances and capacitances. (Figure 1.6) Because the apparatus measures only the composite R and C values the sample is a sort of "black box," so that the interpretation of ac impedance or admittance measurements to yield R and C values for each of the circuit components is somewhat of an art.

According to Ohm's law, $I=ER^{-1}$ and is frequency-independent for direct current passing through a resistor. For a capacitor, a frequency-dependent ac current can pass through (Equation 1.5).

(1.5) $I=j(\omega)CE$

$j=(-1)^{1/2}$, ω=angular frequency $2f\pi$

Ohm's law can also be written in terms of impedance, Z, as $Z=E(t)/I(t)$, where $E(t) = E_m \sin \omega t$ and $I(t) = I_m \sin (\omega t+\phi)$. Since the total voltage drop across a circuit containing resistive and capacitive elements is a simple sum of the voltage drops across each element, $E=E_R + E_C$; the total impedance for such a circuit is given by Equation 1.6:

(1.6) $Z = R + 1/j\omega C = R - j/\omega C$.

The impedance of a parallel RC circuit is given by Equation 1.7. After some algebra, this separates into real and imaginary parts as in Equations 1.8a-b. Elimination of the frequency ω gives the equation of a circle with its center at (R/2, 0) and radius R/2. (Equation 1.9) Thus, when the imaginary part Z″ of the complex impedance is

plotted against the real part Z′, each parallel RC circuit gives rise to a semicircle in the Z* plane and each series RC element gives a vertical line in this plane. (Figure 1.7) The R value of each circuit element is the intersection of either the line or the semi-circle with the Z′ axis. The maximum of the semicircle occurs such that $\omega RC=1$. When the frequencies are not sufficiently far apart, the semi-circles often overlap, so that some curve-fitting is necessary to deduce the locations of the useful points in the Z* plane. (Figure 1.7) The overall sample resistance will be the sum of the bulk and grain boundary resistance. As shown in Figure 1.7, the zero intercept of the net arc is this sum. Furthermore, since the electrodes are normally blocking for the ion conducted, their frequency response curve is a line inclined at a slope of $\pi/4$ to the horizontal (Z′) axis, and thus may be distinguished easily from the material's resistances. Closer analysis of the data can differentiate the contributions to the total conductivity of the current carrier concentration and the rates of ion hopping from site to site.[38] As the number of circuit elements increases, the expressions for Z′ and Z″ become increasingly complicated, so that the circuit in Figure 1.7 would have the complex impedance expression given by Equation 1.10.

(1.7) $Z = [1/R + j*(2\pi\omega C)]^{-1}$

(1.8a) $Z' = 1/R * [(1/R)^2 + (2\pi\omega C)^2]^{-1}$

(1.8b) $Z'' = 2\pi\omega C * [(1/R)^2 + (2\pi\omega C)^2]^{-1}$

(1.9) $(Z'')^2 + (Z' - R/2)^2 = R^2/4$

(1.10) $Z^* = R_e + [1/j\omega C_{dl} + (1/R_b + j\omega C_b)^{-1} + (1/R_{gb} + j\omega C_{gb})^{-1}]$

The impedance of a sample is typically measured over a range of frequencies ω from 1 mHz to 1 MHz.[37]

1.3.2 Non-ac Methods

Other methods of measuring ionic conductivity include far infrared[39] and Raman[40] spectroscopy, where the vibrations of mobile ions can provide a direct measurement of hop-attempt frequencies; examination of the motional narrowing of NMR absorption lines;[41,42] and examination of the diffusion rate of labeled ions such as $[O^{17}]^{2-}$ and radioactive $[Na*]^+$. Non-blocking electrodes can be used to obtain a value of the transport number. Use of the Hall Effect, where a potential difference is created across a current-carrying sample in a transverse magnetic field, can give a measure of the charge on, and number per unit volume of, the conducted species. Finally, electrochemical oxygen pumping (see Section 1.4.2 below) has been used to study the oxygen transport characteristics of a number of materials. [43]

Figure 1.6: Equivalent circuit diagram for a polycrystalline oxygen ion conductor. R_e = electronic resistance; C_{dl} = double-layer capacitance at the blocking electrode; C_b, R_b = bulk capacitance and resistance; C_{gb}, R_{gb} = grain boundary capacitance and resistance.
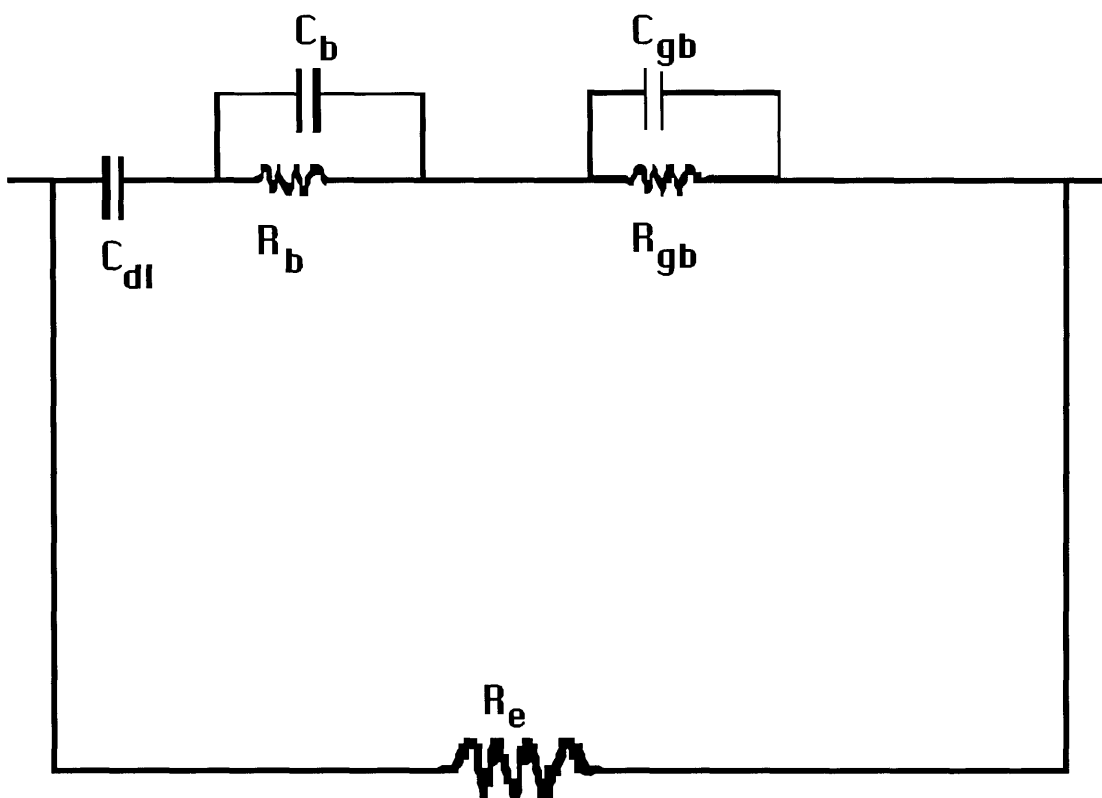
Figure 1.7: Typical plot resulting from complex impedance measurements on the circuit shown in Fig. 1.6.
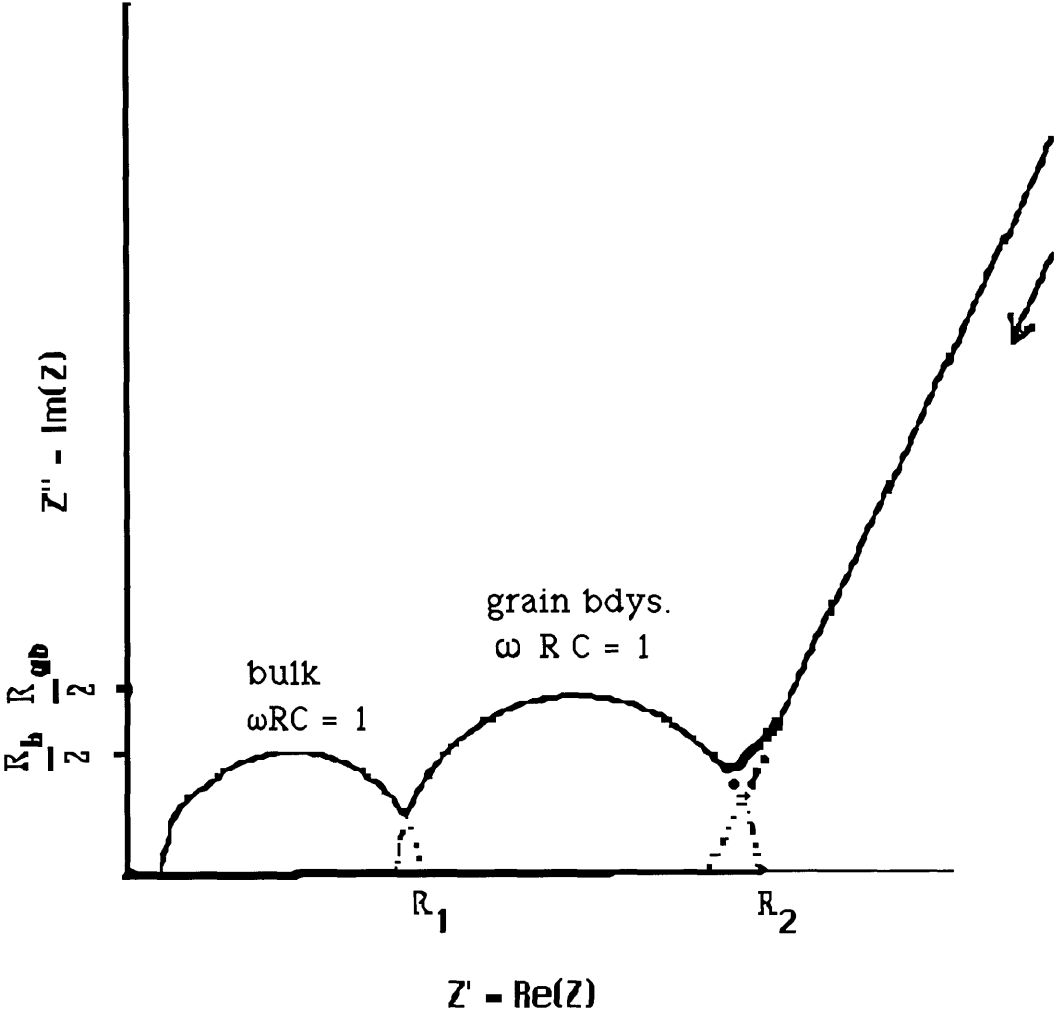
1.4 Applications of Oxygen Ion Conductors

1.4.1 Solid Oxide Fuel Cells (SOFCs)

In a fuel cell two electrodes are separated by an electrolyte, which in a solid oxide fuel cell (SOFC) is the oxide ion conducting ceramic. Fuels such as hydrogen (fed directly or produced *in situ* by hydrocarbon reforming) or carbon monoxide are fed to the anode where they are oxidized, releasing electrons to an external circuit. On the cathode side, oxygen fed into the SOFC unit is reduced by the electrons arriving through the external circuit. (Figure 1.8) The electron flow through the external circuit produces dc electricity at an open-circuit voltage which can be derived from the Gibbs energy expression for the chemical reaction taking place combined with Faraday's law. The actual closed-circuit voltage falls off with increasing current density and power as more and more chemical potential is converted to heat rather than to electrical energy.[44] However, because a fuel cell converts chemical potential directly into electrical work without going though the intermediate of heat, as in steam turbine-based electrical generators, its conversion efficiency is not Carnot-limited. To build up to the desired voltage, single fuel cell units are arranged as a stack and connected in series or in parallel or in a combination of the two, depending on the application. Compared with traditional steam-turbine generators, fuel cells are also higher in efficiency at partial load,[44] may be constructed modularly on virtually any site, and are less polluting. Ceramic fuel cells – SOFCs – have been constructed for

multikillowatt applications and operated for thousands of hours; they offer a number of benefits over other types of fuel cells.[45]

One of the difficulties with SOFCs, however, is that maintaining the high operating temperature (1000 °C) required for sufficient ionic conductivity in the electrolyte (usually stabilized zirconia[45]), uses up some of the energy benefit realized by the greater theoretical efficiency. Furthermore, the operating conditions put stringent requirements on the other materials (anode, cathode, interconnects) to be used in the cell. The other materials to be used must be stable and compatible with each other at high temperatures. While temperatures over 600 °C are desirable to permit *in situ* hydrocarbon fuel reforming, it is also preferable to be able to operate the fuel cell at temperatures less than 800 °C to reduce the material-based problems associated with other cell components. Some research[11, 15,16,46] has sought to develop new materials that exhibit high oxide ion conductivities below 800 °C, while having other desirable properties such as low cost and stability over a wide range of temperatures and oxygen partial pressures, many present-day technologies seek simply to reduce the thickness of the YSZ solid electrolyte. By reducing the path length for oxide ion conduction, such electrolyte films or membranes can increase the effective oxygen flux at a given temperature.

Figure 1.8: Solid oxide fuel cell.

Anode side reactions: $H_2 + O^{2-} \rightarrow H_2O + 2\ e^-$ or $CO + H_2O \rightarrow H_2 + CO_2$. Cathode side reaction: $O_2 + 4\ e^- \rightarrow 2\ O^{2-}$.
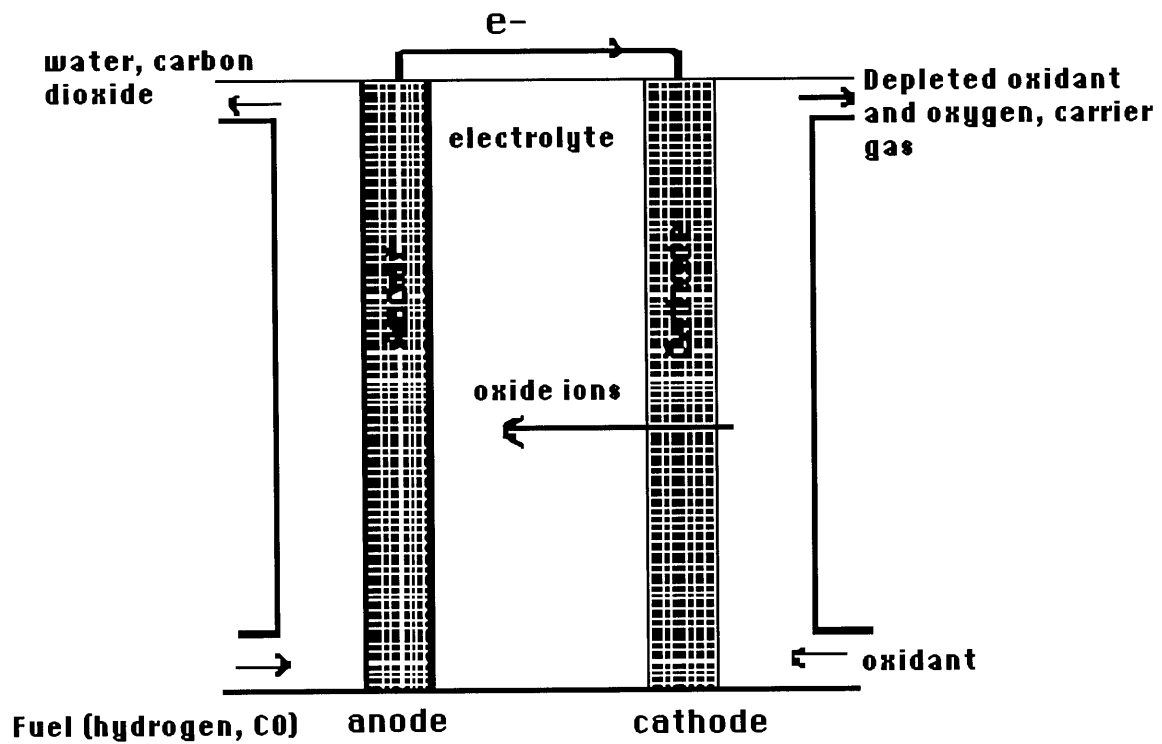
1.4.2 Oxygen Sensors

Increasing demands for efficient combustion processes which maximize energy output while minimizing polluting partial-combustion products such as raw hydrocarbons, CO, and NO_x, have made the development of accurate methods for monitoring the oxygen-content of process streams essential. On-line monitoring requires good sensor technology. Oxide-ion conducting materials are the basis for such sensors.

Nernst, in 1900, first observed the electrolytic evolution of oxygen from a sample of zirconia stabilized with 15 mol% yttria.[47] He theorized that the electrical conduction was due to ionic motion and developed the equation that bears his name to quantify it: $E=kT/4q \ln (PO_2'/PO_2'')$, where PO_2'' and PO_2' are the oxygen partial pressures on either side of the sample. This development of electrical potential can be measured and used to determine the oxygen partial pressure in an unknown gas mixture, if that in a reference gas is known.

In automobile emissions control equipment, for example, the exhaust from the engine is passed over a platinum-containing catalyst downstream of the engine. For efficient operation of the catalytic converter, the fuel-to-air ratio must be kept near 0.07 over the entire range of driving conditions.[2] A feedback circuit enabling constant adjustment of the fuel injection system employs an oxygen sensor in which a yttria-stabilized zirconia (YSZ) oxide-ion conductor is exposed on one side to the exhaust gas stream and on the other to a reference gas of known oxygen content (air). (Figure 1.9) The

difference in oxygen partial pressures on either side of the YSZ barrier produces an electrical potential difference across the YSZ according to the Nernst equation. However, because many oxide ion conductors are partially "shorted out" by some electronic conduction, the actual voltage falls below the Nernst potential (Equation 1.11).

(1.11) $E_{meas} = t_{ionic} \, kT/4q \, \ln (PO_2'/PO_2'')$

where t_{ionic}, is the fraction of the total conductivity which is due to ion movement.

The electrical conductivity comes about through partial reduction of the metal oxide. Because electrons are significantly more mobile than ions, a few excess electrons will lead to a large electronic contribution to the total conductivity; thus a small degree of reduction can short out the sensor.

Oxide ion conducting ceramics proposed for use in oxygen sensor applications must therefore have an initial transference number near unity and be stable to reduction over the whole range of oxygen partial pressures – and temperatures – which it will encounter in the process stream to be monitored. In addition, the present operating temperature of YSZ-based sensors is over 800 °C, while a desirable operating temperature is lower, in the 200-400 °C range. Thus methods of lowering the operating temperature of these units, either by finding new oxide ion conductive materials that satisfy the requirements, or by using thin films or membranes of known conductive materials, are being sought. [46]

Figure 1.9: Oxygen sensor probe in an automotive exhaust gas stream.

Exhaust Gases

$P2$ = exhaust gas oxygen content

Pt electrodes

air ($P1 = 0.21$ atm)

YSZ ceramic
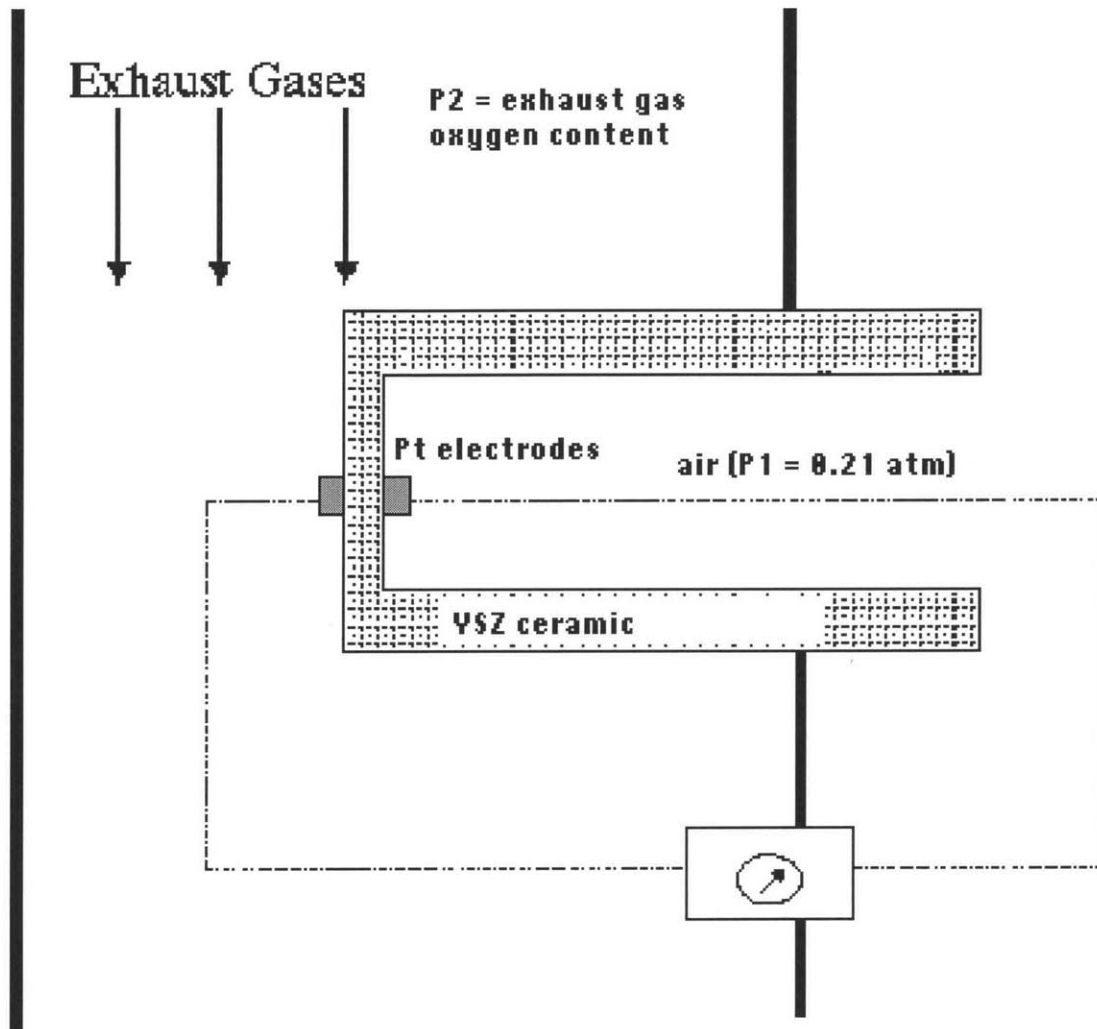
1.4.3 Air Separators

The situation of oxygen pumping is essentially the reverse of the oxygen sensing: an applied voltage E produces an oxygen partial pressure difference on either side of a solid electrolyte, in accordance with the Nernst equation. (Equation 1.11) A device designed to take advantage of this may be used to separate oxygen out of air or specialty gases to obtain, for example, oxygen-free nitrogen or argon. In other cases, the pure oxygen is the desired product of the separation process, frequently to be used in chemical oxidation processes or industrial combustion or oxidation processes, or in health-related industries.

Cryogenic distillation is the preferred process, currently, for large-scale (50-2000 tons/day) production of high-purity (>95%) oxygen. Contaminants in the compressed air feed, such as water, carbon dioxide, and hydrocarbons, must be removed prior to the distillation to prevent blockage of heat exchangers and hazardous waste buildup in the distillation column sump.[48] Removal of these contaminants is expensive both in terms of the extra capital equipment requirement and the energy requirements. Crude argon (1% in air) is one product of the cryogenic air separation process. At this stage it contains some 2-7% oxygen, which must be removed prior to the argon's use in inert atmosphere applications; but because of the proximity of the boiling point of argon (87.28 K) and oxygen (90.19 K), further purification of the argon by distillation is extremely uneconomical. Currently, oxygen contamination in crude argon streams is reduced to the ppm level by reduction to

water using excess hydrogen over a platinum catalyst, followed by drying and distillation to remove water, hydrogen, and nitrogen contaminants.[49] In addition to the expense of using hydrogen in this way, the drying and distillation steps introduce large capital and operating costs into the purification process. A number of cyclic adsorption/desorption processes for removing oxygen from argon are also reported in the patent literature.[50]

An air separator constructed from a pore- and defect-free oxide-ion conductor, on the other hand, is completely permselective for oxygen, and offers significant advantages over air separation methods based on conventional technology.[51,52] The feed stock may be crude argon,[53] air, or the hot exhaust from a combustion process.[52,54] Application of an electrical potential difference across the ionic conducting ceramic will "pump" oxide ions against an unfavorable concentration gradient at a reasonable rate to induce separation.[52] Air separator designers prefer to have concomitant electrical and ionic conduction ($t_{ionic} < 1$), as this situation makes it unnecessary to have an external circuit prevent charge buildup on the membrane. Potential losses associated with the ohmic resistance of the electrolyte and electrodes, in addition to nonohmic rate processes such as charge transfer, adsorption, and slow gas phase and surface diffusion of oxygen and oxide ions, cause the actual applied potential to exceed the theoretical (Nernst) potential required to achieve a given PO_2.[55] Furthermore, air separators must be operated at temperatures at or above 800 °C where the ceramic material, typically YSZ, has sufficient ionic conduction to be useful.[56] Both of these problems have clear associated costs,

driving research into improving oxygen pump/air separator efficiencies. One approach to the problem is the development of low-temperature (200-400 °C) oxide ion conducting materials.[11,15,16,46] For instance, Dumelie et al. used a highly conductive solid solution, called β (σ at 600 °C = 1 S cm^{-1}), in the Bi$_2$O$_3$-PbO system as a pressed pellet "membrane" some 4 mm thick to take advantage of the high conductivity of this material compared with YSZ.[56] They found that the air separator performance declined after a few operating hours as grain coarsening and the development of orientation in the pellet caused cracks.

A second approach to improving the performance of solid electrolyte air separators is to fabricate the oxide ion conductive material as a thin film or membrane. The resulting decrease in the conduction path will result in a corresponding increase in the total oxygen flux realizable at a given temperature, as well as decreasing the required overpotential.

1.4.4 Catalytic Inorganic Membrane Reactors

The ability to include in-line air separation in a chemical process is particularly attractive for designers of catalytic inorganic membrane reactors (CIMRs) for partial oxidation reactions. Partial oxidation reactions are among the most widespread in use in industry, and lead to a number of important organic intermediates. (Table 1.3) The current technology for performing these reactions on an industrial scale uses the standard fixed-bed reactor design in which a mixture of reagent and inert gases flow over a heterogeneous catalyst; air or oxygen is injected at the outset of

45

the reactor flow and possibly at intermediate points. Reactant profiles tend to decrease monotonically with distance from oxygen (air) inlets and the selectivity for the desired partial oxidation product is low near the inlet due to complete oxidation in this high-PO_2 area. The organic materials must be diluted to below explosive concentrations with inert gases to ensure safety. Such diluent gases or air (as opposed to pure oxygen) create an additional need for downstream separation processes.

The potential benefits of using a membrane reactor geometry, where components of the feed stock are kept separated by a barrier permselective to oxygen are clear. In plants where pure oxygen is the desired reagent, a membrane reactor setup eliminates the need for off-line cryogenic air separation. The ability to add oxygen continually and gradually to the reagent stream can increase conversion rates and will increase the selectivity for the desired partial oxidation products. Modulation of oxygen injection by varying the partial pressure or electrical overpotential gives a finer reaction control than is realizable with a finite-point injection design. Finally, the ability to "leak" in oxygen permits the use of pure (undiluted) feedstocks and reduces the downstream separator load. While polymer-based membrane reactors were used in biotechnology applications during the 1970s and 1980s, catalytic *inorganic* membrane reactors were not used until the mid-1980s, when methods of fabrication became sufficiently well-advanced.[57] Commercialization of such reactor geometries was first accomplished in 1991.[58] Initial work focused on the oxidative coupling of methane (OCM) to ethene or higher (C_{2+}) products, on partial oxidation to methanol or formaldehyde, or on methane

conversion to synthesis gas ("syngas," CO + H_2), which is then converted via Fischer-Tropsch technology to higher-value products— because the high temperatures required for methane activation (> 600 °C) are also required by YSZ for achieving a reasonable oxygen flux.

Large worldwide reserves of methane make it an inexpensive gas to obtain and increase the potential economic benefit of a system of converting it to higher value products. The selectivity of conversion of methane to ethane, then to ethylene, is determined by the rate at which oxygen is made available to the reagent stream. Selectivity – avoidance of losses of carbon into low-value CO_x – is more important economically than is achieving a high raw yield.[59] The best catalytic reactors offer 20% conversion at 80% selectivity for C_2H_4 and C_2H_6.[60] The use of steam reforming to convert methane to syngas, followed by conversion to C_{2+} products via Fischer-Tropsch processes, is energy and capital intensive; syngas production by steam reforming accounts for upwards of 60% of the integrated cost of a plant.[60] Some 40% of the capital investment goes into the air separation and syngas generation equipment.[61]

A process using a dense solid electrolyte hollow-tube reactor packed with an Rh-based catalyst achieved up to 99% conversion with 90-95% CO and H_2 selectivity. The tube reactor (Figure 1.10) was cast from a perovskite in the La-Sr-Fe-Co-O system (a mixed conductor) and was 0.25-1.20 mm thick; it was operated at 800 °C for up to 500 h.[60] Work at British Petroleum using both the La-Sr-Fe-Co-Cr-O perovskites and an In_2O_3/PrO_2-doped zirconia gave

similar results for a range of reaction geometries. There, the focus was on making thinner solid electrolyte membranes for achieving the same flux at lower temperatures, and on improving fabrication processes for the membranes, rather than on examining new materials which may give higher fluxes at still-high temperatures.[61]

Other processes using CIMRs have been reported. DiCosimo reports and patents a process for oxidative dehydrodimerization of propylene over a Bi_2O_3-La_2O_3 oxide-ion conductive catalytic membrane some 0.5 mm thick in a counterflow reactor operated at 600 °C.[62,63] However, he found that he needed to add oxygen (1% by volume) to the propylene feedstock to stabilize the membrane against Bi^{3+} reduction to the metal, and had a conversion rate to C_3 dimers of less than 5% of the propylene, with selectivity near 50% for C_3 dimers. A later patent discloses a 5-300 μm-thick dense membrane of titania-doped YSZ atop a porous YSZ support (0.2-1 mm thick) used at 700-900 °C for OCM at conversions of 10-50% of methane (MnO_2•Na or MgO•Li catalyst) with C_{2+} selectivity of over 50%.[64] The patent also claims partial oxidation of ethylene to ethylene oxide and propylene to propylene oxide or acrylonitrile over assorted catalysts, also with high conversion rates (> 20%) and selectivities (>50%) at lower temperatures. The permselectivity of YSZ to oxygen has also been used to shift the equilibrium of the decomposition of CO_2 to CO + O_2.[65]

As the discussion above indicates, there is an interest in partial oxidation reactions which must be run in the 200-600 °C range, below the temperatures where a reasonable oxygen flux can be expected from traditional YSZ electrolytes. All of the reactions in

Table 1.3, except for those involving methane, are best run at 270-500 °C; higher temperatures result in excessive oxidation to CO_x. While some work has accomplished these partial oxidations in CIMRs by making thinner YSZ membranes and by adding Bi_2O_3 dopants to provide for electronic conduction so that oxygen pumping increases the activity of partial oxidation catalysts,[57,66] conversion numbers are still low.[57] The oxygen flux achievable through a 1-mm thickness 8% Y_2O_3-doped zirconia is 10^{-11} mol cm^{-2} s^{-1} at 800 °C and La-Sr-Mn-O perovskite systems can achieve 10^{-10} mol cm^{-2} s^{-1} at the same temperature. This creates quite a limitation on the conversion reaction.[57]

The largest hurdles faced in the construction of commercially useful CIMRs include[67] (1) improvement of the oxygen fluxes available at the temperatures desired for the partial oxidation reactions, (2) prevention of cracking during thermal cycling, (3) design issues including how to seal the membrane into existing plant components or how to fabricate a standalone membrane reactor unit, (4) matching the oxygen supply rates to the reaction rates to optimize yield and selectivity, and (5) issues of heat transfer. While several of these points are chemical engineering problems, the initial advances must be made in the area of materials chemistry. New mixed oxygen-ion/electronic conductors with good material strength and high flux at lower temperatures need to be developed; methods of fabricating a defect-free membrane either as a supported film or as a standalone design are vital.

Table 1.3: Industrial Partial Oxidation Processes[68]

Organic Reactant	Products	Current Catalysts
napthalene	maleic anhydride	V_2O_5
o-xylene	maleic anhydride	V_2O_5 + MoO_3
methanol	formaldehyde	$Fe_2(MoO_4)_3$ + MoO_3 or Ag
ethylene	ethylene oxide	Ag
proplyene aldehyde	acrolein	bismuth molybdates
propylene	acrolein	bismuth molybdates
methane	syngas (CO + H_2)	Rh-based catalyst
methane	ethylene + C_{2+}	Rh-based catalyst
1-butene	butadiene	bismuth scheelites
propylene (+ NH_3)	acrylonitrile	bismuth molybdates

1.4.5 Expected Benefits of Use of BiMeVOx Compounds

The devices described above all suffer from the need to be operated at high temperatures (> 600 °C) to achieve economic oxygen fluxes. While part of the solution to the problem involves reducing the length of the conduction path by fabrication of thinner membranes of the solid electrolyte atop porous supports to provide the proper structural integrity, there is a natural limit to how thin membranes can become before pinholes and other defects become technically unavoidable.[57] Thus, the thinner-membrane approach is best combined with the use of novel materials with higher oxide ion conductivities. The BiMeVOx materials, with some of the highest oxygen-ion conductivities, are not appropriate for all the devices discussed above due to their concomitant electronic conductivity, which increases as the bismuth in the lattice is reduced to the metal over long-term use at very low PO_2. Still, the BiMeVOx compounds can be useful for oxygen pumps and air separators, and for CIMRs. Fabricated as membranes, they can be extremely powerful. For comparison, a 1 cm^2 area of a 1 mm-thick membrane of YSZ operated at 500 °C has an expected oxygen flux of 2.3×10^{-12} mol cm^{-2} s^{-1} while under the same conditions a BiCuVOx membrane gives 2.3×10^{-7} mol cm^{-2} s^{-1} oxygen flux. For 1 μm films, the flux jumps to 2.3×10^{-9} mol cm^{-2} s^{-1} and 2.3×10^{-4} mol cm^{-2} s^{-1} for YSZ and BiCuVOx, respectively.[69]

In addition to the benefits realizable due to the BiMeVOx phases' high low-temperature oxide ion conductivity, these

materials are expected to be catalytically active in partial oxidation reactions, so that in a CIMR including a BiMeVOx membrane, the membrane may contribute to the catalysis. In general, metal oxides, especially mixed oxygen ion/electronic conductors, are superior to metals as catalysts for partial oxidation reactions.[57,67] The active sites on the catalyst are variously thought to be oxygen vacancies with local migration of electrons to or away from these sites[70] or lattice oxygen near the surface. Adsorbed oxygen is responsible for nonselective reactions on the surface of the catalyst.[71] The most active catalysts are able to cycle between two valence states and thereby store and release oxygen. Ready incorporation of oxygen into the lattice minimizes the adsorbed (non-selective) oxygen species.

Bismuth-containing species, particularly those based on the scheelite structure, are known to be active partial oxidation catalysts. The scheelite structure (named for the mineral $CaWO_4$) is tetragonal AMX_4 with tetrahedral $(MX_4)^{n-}$ units and A^{n+} cations. It is not a layered or chainlike structure. Anion vacancies exist in the scheelite structure and oxygen ion mobility is significant in many of the bismuth-containing scheelites.[72] The scheelite polymorph of bismuth orthovanadate, $BiVO_4$ has been found to have low but measurable mixed conduction which is accounted to anion vacancies.[73-75] It is catalytically active for OCM, though the bismuth molybdates are more commonly used due to their higher activity.[67,72] Tests of the Aurivillius phases $Bi_2O_2(A_{n-1}B_nO_{3n+1})$, A= Ca, Sr, Ba, Pb; B=Nb, Ta; n=2-4 showed that these materials are selective and stable in the OCM reaction.[76] Direct tests on the

BiMeVOx family show a correlation between methane conversion and oxygen conductivity, and for M=Fe, Cu, Sr doping at 10 mol%, the C_2 selectivity increases.[35] In all these cases the catalyst was used in a packed-bed reactor geometry.

In partial oxidation systems other than OCM, the bismuth-containing scheelite catalysts are effective, and their activity and selectivity increases with increasing vacancy concentration,[72] which leads to increased oxygen ion mobility. On the other hand, catalysts with vacancies but no bismuth in the lattice have high isomerization activity and low oxidation activity for olefin oxidation or coupling; so while bismuth is not directly involved in the first step of olefin oxidation, it is relevant for selective oxidation of the allyl intermediate.[72] Furthermore, catalysts containing bismuth are re-oxidized more readily than those that have no bismuth. The evidence suggests, then, that the BiMeVOx family promises at least some catalytic activity in partial oxidation applications, so that a membrane fabricated from BiMeVOx for use in a CIMR would have a dual function of permselectivity and catalytic activity.

1.5 Conclusions and Project Goals

While the electronic conductivity of the BiMeVOx family of oxygen-ion conductors prevents them from being useful in fuel cell and oxygen sensor applications, this same property is desirable in air separation and CIMR technology. In both cases there is a industrial strong interest in lowering the temperatures presently required for economical oxygen fluxes (600-900 °C). The high oxygen conductivity at low temperatures (200-600 °C) characteristic of some members of the BiMeVOx family can be used in combination with fabrication of these materials as membranes or thin films to

obtain very high oxygen fluxes. Furthermore, the experience with bismuth-based oxide catalysts suggests that BiMeVOx membranes may be catalytically active in appropriate devices. It is vital that these films be defect-free so that the permselectivity is uncompromised, and that they be able to maintain their integrity in reducing conditions during thermal cycling.

The practical goal of the research described in Part I of this thesis was to produce defect-free thin films (<1-10 μm thick on a porous support) of BiMeVOx solid oxide conductors, test and verify their oxide ion conductivity, and use them – in collaboration with the Ying group in the Chemical Engineering Department at MIT – in a CIMR. The research eventually succeeded in the deposition of $Bi_2Cu_{0.1}V_{0.9}O_{5.5-\delta}$ and $Bi_2Nb_{0.3}V_{0.7}O_{5.5-\delta}$ films onto porous alumina substrates. Further progress was checked by the termination of the project.

The succeeding chapters describe the deposition of BiMeVOx films onto a number of substrates using pulsed laser deposition (Chapter Two) and two sol-gel based methods of preparing a film-castable precursor (Chapters Three and Four). Characterization of the precursor solution is reported in Chapter Five. Film-casting onto non-porous and porous substrates, finally, is described (Chapter Six). Because much of the work described relies on techniques and ideas often outside the purvey of traditional chemistry, each chapter includes, where appropriate, a brief introductory review of the relevant material. This part of the thesis will conclude with a discussion of future directions and usefulness of this work (Chapter Seven).

Figure 1.10: Tube type CIMR for oxidative dehydrodimerization of propylene.
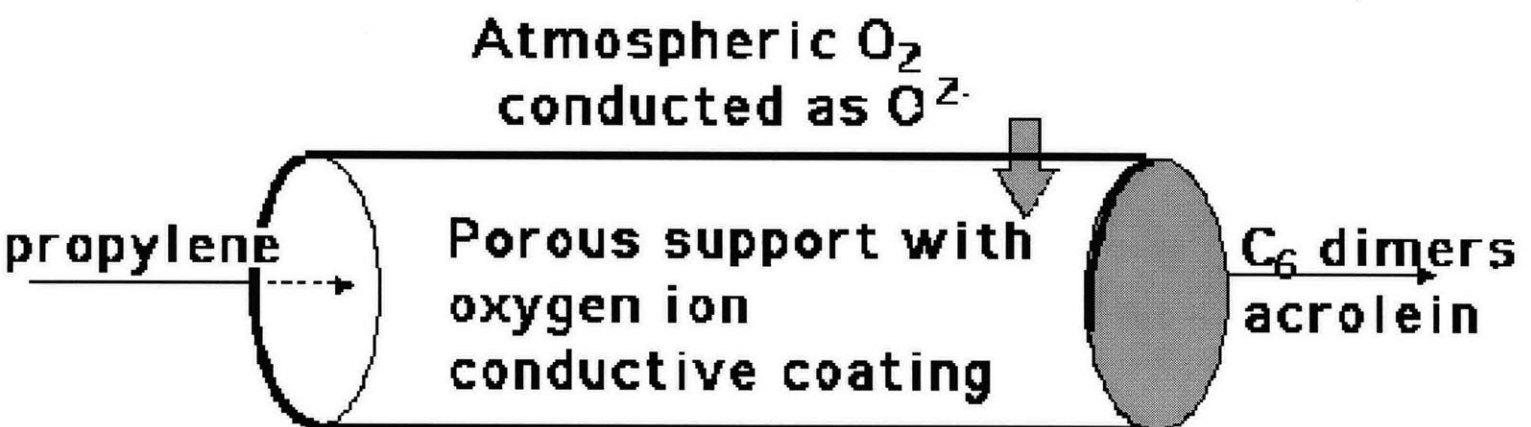
1.6 References

1) Kilner, J. A.; Brook, R. J. *Solid State Ionics* **1982**, *6*, 237.

2) Tuller, H. L.; Moon, P. K. *Mater. Sci. and Eng. B1* **1988**, 171.

3) Schwartz, M.; Link, B. F.; Sammells, A. F. *J. Electrochem. Soc.* **1993**, *140*, L62.

4) Goodenough, J. B.; Ruiz-Diaz, J. E.; Zhen, Y. S. *Solid State Ionics* **1990**, *44,* 44.

5) Thomas, J. K.; Krause, W. E.; zur Loye, H.-C. *Solid State Ionics*; Nazri, G.-A., Tarascon, J.-M. and Armand, M., Ed.; Mater. Res. Soc.: Boston, MA, 1992; Vol. 293, pp 307.

6) Aurivillius, B. *Ark. Kemi.* **1949**, *1*, 463.

7) Abraham, F.; Debreuille-Gresse, M. F.; Mairesse, G.; Nowogrocki, G. *Solid State Ionics* **1988**, *28-30*, 529.

8) Lee, C. K.; Sinclair, D. C.; West, A. R. *Solid State Ionics* **1993**, *62*, 193.

9) Sharma, V.; Shukla, A. K.; Gopalakrishnan, J. *Solid State Ionics* **1992**, *58*, 359.

10) Yanovskii, V. K.; Voronkova, V. I.; Aleksandrovskii, A. L.; Dyakov, V. A. *Sov. Phys. Dokl. Engl. Trans.* **1975**, *20*, 306.

11) Kendall, K. R.; Thomas, J. K.; zur Loye, H.-C. *Chem. Mater.* **1995**, *7*, 50.

12) Bush, A. A.; Venetsev, Y. N. *Zh. Neorg. Khim.* **1986**, *31*, 1346.

13) Debreuille-Gresse, M.-F., Ph.D. Thesis, Universite de Lille, 1986.

14) Abraham, F.; Boivin, J. C.; Mairesse, G.; Nowogrocki, G. *Solid State Ionics* **1990**, *40-41*, 934.

15) Kendall, K. R.; Navas, C.; Thomas, J. K.; zur Loye, H.-C. *Solid State Ionics* **1995**, *82*, 215.

16)Kendall, K. R.; Navas, C.; Thomas, J. K.; zur Loye, H.-C. *Chem. Mater.* **1996**, *8*, 642.

17)Mairesse, G. in *Fast Ion Transport in Solids*; Scrosati, B. *et al*, Ed.; Kluwer Academic Publishers: Netherlands, 1993, pp 271-290.

18)Millan, P.; Castro, A.; Torrance, J. B. *Mater. Res. Bull.* **1993**, *28*, 117.

19)Ramirez, A.; Millan, P.; Castro, A.; Torrance, J. B. *Eur. J. Solid State Inorg. Chem.* **1994**, *31*, 173.

20)Castro, A.; Millan, P.; Martinez-Lope, M. J.; Torrance, J. B. *Solid State Ionics* **1993**, *63-65*, 897.

21)Castro, A.; Millan, P.; Enjalbert, R.; Snoeck, E.; Galy, J. *Mater. Res. Bull.* **1994**, *29*, 871.

22)Vannier, R. N.; Mairesse, G.; Abraham, F.; Nowogrocki, G. *Solid State Ionics* **1994**, *70-71*, 248.

23)Pernot, E.; Anne, M.; Bacmann, M.; Strobel, P.; Fouletier, J.; Vannier, R. N.; Mairesse, G.; Abraham, F.; Nowogrocki, G. *Solid State Ionics* **1994**, *70-71*, 259.

24)Vannier, R. N.; Mairesse, G.; Abraham, F.; Nowogrocki, G.; Pernot, E.; Anne, M.; Bacmann, M.; Strobel, P.; Fouletier, J. *Solid State Ionics* **1995**, *78*, 183.

25)Yan, J.; Greenblatt, M. *Solid State Ionics* **1995**, *81*, 225-233.

26)Cherry, M.; Islam, M. S.; Catlow, C. R. A. *J. Solid State Chem.* **1995**, *f118*, 125.

27)Kendall, K. R.; Ph.D. Thesis, Massachusetts Institute of Technology: Cambridge, MA, 1996.

28)Joubert, O.; Jouanneaux, A.; Ganne, M.; Vannier, R. N.; Mairesse, G. *Solid State Ionics* **1994**, *73*, 309.

29) Joubert, O.; Ganne, M.; Vannier, R. N.; Mairesse, G. *Solid State Ionics* **1996**, *83*, 199.

30) Aboukais, A.; Delmaire, F.; Rigole, M.; Hubaut, R.; Mairesse, G. *Chem. Mater.* **1993**, *5*, 1819.

31) Lee, C. K.; Lim, G. S.; West, A. R. *J. Mater. Chem.* **1994**, *4*, 1441.

32) Lee, C. K.; Tan, M. P.; West, A. R. *J. Mater. Chem.* **1994**, *4*, 525.

33) Goodenough, J. B.; Manthiram, A.; Parantham, M.; Zhen, Y. S. *Mater. Sci. Eng. B,* **1992**, *12*, 357.

34) Iharada, T.; Hammouche, A.; Fouletier, J.; Kleitz, M.; Boivin, J. C.; Mairesse, G. *Solid State Ionics* **1991**, *48*, 257.

35) Cherrak, A.; Hubaut, R.; Barbaux, Y.; Mairesse, G. *Catal. Lett.* **1992**, *15*, 377.

36) this section is based on the discussion in West, A. R. *Solid State Chemistry and Its Applications*; John Wiley and Sons: New York, 1984, pp 482-489.

37) Macdonald, J. R. *Impedance Spectroscopy: Emphasizing Solid Materials and Systems*; John Wiley & Sons: New York, 1987.

38) Almond, D. P.; Hunter, C. C.; West, A. R. *J. Mater. Sci.* **1984**, *19*, 3236.

39) Allen, S. J.; Remeika, J. P. *Phys. Rev. Letters* **1974**, *33*, 1478.

40) Harley, R. T.; Hayes, W.; Rushworth, A. J.; Ryan, J. F. *J. Phys. C* **1975**, *8*, L530.

41) McGeehin, P.; Hooper, A. *J. Mater. Sci.* **1977**, *12*, 1.

42) Abragam, A. *The Principles of Nuclear Magnetism*; Clarendon Press: Oxford, 1961.

43) Doshi, R.; Shen, Y.; Alcock, C. B. *Solid State Ionics* **1994**, *68*, 133.

44) Cross, J. *Fuel Cell Technology*, 1998; Vol. 76, pp 11-13, 21.

45) Minh, N. Q. *J. Am. Ceram. Soc.* **1993**, *76*, 563.

46) Hagenmuller, P. ; Laskar, A. L. and Chandra, S., Eds. *Superionic Solids and Solid Electrolytes*; Academic Press: New York, 1989, pp 679-704.

47) Nernst, W. *Z. Elektrochem.* **1900**, *3*, 41.

48) Carolan, M.F., Dyer, P.N., LaBar Sr., J.M., Thorogood, R.M., Air Products and Chemicals Co: U.S. Patent No. 5,240,473, 1992.

49) Latimer, R. E. *Chem. Eng. Process* **1967**, *February*, 35.

50) Erickson, D.C., U.S. Patent No. 4,132,766, 1979.

51) Thorogood, R. M.; Srinivasan, R.; Yee, T. F.; Drake, M. P., Air Products and Chemicals: US Patent No. 5,240,480, 1993.

52) Chen, M. S.; Hegarty, W. P.; Steyert, W. A., Air Products and Chemicals, Inc.: US Patent No. 5,118,395, 1992.

53) Chen, M.S., Cook, P.J., Air Products and Chemicals Co.:U.S. Patent No. 5,035,726, 1991.

54) Chen, M.S., Hegarty, W.P., Steyert, W.A., Air Products and Chemicals Co.: U.S. Patent No. 5,174,866, 1992.

55) Rincon-Rubio, L. M.; Nguyen, B. C.; Mason, D. M. *J. Electrochem. Soc.* **1985**, *132*, 2919.

56) Dumelie, M.; Nowogrocki, G.; Boivin, J. C. *Solid State Ionics* **1988**, *28-30*, 524.

57) Saracco, G.; Specchia, V. *Catal. Rev. - Sci. Eng.* **1994**, *36*, 305.

58) Hsieh, H. P. *Catal. Rev. - Sci. Eng.* **1991**, *33*, 1.

59) Lunsford, J. H. *Angew. Chem. Int. Ed. Engl.* **1995**, *34*, 970.

60) Balachandran, U.; al., e. *Amer. Ceram. Soc. Bull.* **1995**, *74*, 71.

61) Mazenek, T., talk given to zur Loye group.

62) DiCosimo, R.; Burrington, J. D.; Grasselli, R. K., The Standard Oil Company: U.S. Patent No. 4,571,443, 1986.

63) DiCosimo, R.; Burrington, J. D.; Grasselli, R. K. *J. Catal.* **1986**, *102*, 234.

64) Hazbun, E.A., U.S. Patent No. 4,791,079, 1988.

65) Itoh, N.; Sanchez, M. A.; Xu, W.-C.; Haraya, K.; Hongo, M. *J. Membrane Sci.* **1993**, *77*, 245.

66) Stoukides, M.; Vayenas, C. G. *J. Catal.* **1981**, *70*, 137.

67) Harold, M. P.; Lee, C.; Burggraaf, A. J.; Keizer, K.; Zaspalis, V. T.; de Lange, R. S. A. *MRS Bulletin* **1994**, *April*, 34.

68) Gates, B.C.; Katzer, J.R., Schuit, G.C.A. *Chemistry of Catalytic Processes*, New York: McGraw-Hill, pp 325-388.

69) Numbers were calculated using literature values for σ for YSZ and BiCuVOx at 500 °C, and setting $t_{ionic} = 1$, $P_1 = 0.001$ atm, and $P_2 = 0.21$ atm (atmosphere side) in the Nernst equation. Thus, $E = t_{ionic} RT/4F \ln(P_2/P_1)$, $R = LA\sigma^{-1}$ ($A = 1$ cm^2; $L = 1$ mm, 1μm), $i = E/R$, and $G_{ox} = i/4F$, giving the final equation $G = EA\sigma/4LF$.

70) Nguyen, B. C.; Lin, T. A.; Mason, D. M. *J. Electrochem. Soc.* **1986**, *133*, 1807.

71) Zhang, Z.; Verykios, X.; Baerns, M. in *Catalysis : An Integrated Approach to Homogeneous, Heterogeneous and Industrial Catalysis;* Mouljin, J.A., *et al.*, Eds.; Marcel Dekker, 1994, pp 507-556.

72) Sleight, A. W. in *Heterogeneous Catalysis: Principles and Applications;* Bond, G.C., Ed., New York: Clarendon Press, pp 181.

73) Wood, P.; Sinclair, D. C.; Glasser, F. P. *Solid State Ionics* **1993**, *66*, 151.

74) Lu, T.; Steele, B. C. H. *Solid State Ionics* **1986**, *21*, 339.

75) Vinke, I. C.; Diepgrond, J.; Boukamp, B. A.; de Vries, K. J.; Burggraaf, A. J. *Solid State Ionics* **1992**, *57*, 83.

76) Barrault, J.; Grosset, C.; Dion, M.; Ganne, M.; Tournoux, M. *Catal. Lett.* **1992**, *16*, 203.

Chapter Two

Pulsed Laser Deposition of Bi(Me)VOx onto Non-Porous Substrates

The experimental work described in this chapter was adapted, in part, from Pell, J.W., Auyeung, R.C.Y., Chrisey, D.B., zur Loye, H.-C., *Thin Solid Films* **300** (1997), 154-158.

2.1 Introduction: Pulsed Laser Deposition

We initially attempted to deposit films of the BiMeVOx materials using pulsed laser deposition. The actual depositions were done at the Naval Research Laboratory in Bethesda, MD, by Ray Auyeung and Dr. Doug Chrisey, using targets provided by us; characterization work was done by us at MIT. The idea had been that if we could produce thin films of the BiMeVOx materials by this route, we could get a "head start" on designing the equipment needed to check that the ionic conductivity of the material was not significantly lessened by the large surface-to-bulk ratio of the thin film, as well as on building an appropriate reactor for testing the membranes in CIMR applications.

2.1.1 Method: How it works

In a pulsed laser deposition (PLD) process, an ultraviolet (UV) laser spot rastered over the surface of a target made of the material – metal or ceramic – to be deposited, causes a rapid heating and excitation of the target material. A plume of atoms, molecules, ions, clusters, micron-sized particles, and molten globs of the target material spews off the target and deposits onto a substrate, held some distance away and usually heated. (Figure 2.1) The precise mechanism of this ablation is a function of the laser properties (pulse rate, rastering rate, wavelength, energy/fluence) and the target properties (optical, thermodynamical, topological). The laser light hitting the target is

absorbed in three main ways: (1) volume absorption by electrons and phonons in the crystal lattice, (2) free carrier absorption at the surface (mainly in metal targets), and (3) thermal absorption by the plume. The absorbed light produces a molten layer (Knudsen layer) at the target surface. Thermal evaporation of the material is a minor contributor to the plume content: instead, the rapid vaporization process gives a strong recoil pressure on the liquid layer and expels material directly.[1] The behavior of the plume of spewed material is therefore difficult to model, and development of the technique has relied on a trial-and-error phenomenological approach.

The general idea of PLD has been known for some time. Since most materials absorb strongly in the 200-400 nm region, early research used a standard Nd:YAG laser (primary energy 1064 nm), frequency-doubled to 532 nm and mixed with the original 1064-nm beam to obtain 355 nm radiation, or frequency-doubled a second time to achieve a 266 nm beam. However, the resulting beam had only 15-20% of the power of the fundamental, so real use of PLD had to await advances in eximer laser technology, where the fundamental emission is directly in the UV region (KrF lasers, for example, emit at 248 nm). As a result of this gradual development, PLD appeared in a number of sub-fields of physics and materials science under a number of different names, including "pulsed laser evaporation (PLE)," "laser molecular beam epitaxy (LMBE)," "laser-induced flash evaporation (LIFE)," "laser-assisted deposition and annealing (LADA)," and "laser sputtering." At the Spring 1989 Materials Research Society (MRS) symposium meeting the membership voted for the standardization of the term "pulsed laser

deposition (PLD)" to describe the process, but the other terms continue to appear occasionally in the literature.[2]

The advantages of film deposition by PLD include (1) the flexibility of the system design – different targets can be brought into position during a deposition, so that multilayer or gradient films can be produced. (2) The congruent evaporation permits the stoichiometry of the deposited film to mirror more closely that of the target – a problem with certain other film deposition methods. (3) A single eximer laser can be "time shared" among multiple deposition chambers, so that costs can be kept low – about ten times less than a molecular beam epitaxy (MBE) system.[1] (4) There are a relatively small number of control parameters. (5) High vacuum is not necessary, so a reactive background gas – such as O_2, O_3, NO_2, and N_2O, all used to maintain oxidative conditions in high-temperature superconductor (HTS) depositions – may be used. The dynamic range of deposition pressures is the largest of all the physical (vapor) deposition techniques.[3] (6) Virtually any material can be laser-evaporated.

Other deposition techniques include thermal evaporation (TE); accelerated molecular beam epitaxy (AMBE), ion cluster beam deposition (ICBD), and ionized vapor deposition (IVD), where the vapor flux is ionized by electron impact and a bias placed on the substrate; molecular beam epitaxy (MBE) and atomic layer epitaxy (ALE), where continuous molecular beams are deposited – layer-by-layer, in ALE; chemical vapor deposition (CVD) and metal-organic chemical vapor deposition (MOCVD), where chemical vapors react on or above the substrate to form the desired phase; plasma-enhanced or laser-assisted CVD, which include reaction energy

supplied to the chemical vapor cloud by production of a plasma or heating by laser light, near the substrate; ion beam deposition (IBD) and its combination with TE as ion-beam assisted deposition (IBAD), where a low-energy ion beam is produced by decelerating a high-energy ion beam or by accelerating a gas species in a broad-beam source; and sputter deposition (S), where extracting ions (usually Ar) from a plasma strike the target and cause the expulsion of target material onto the substrate. Table 2.1 compares the assorted deposition techniques for their deposition parameters. Table 2.2 compares the materials depositable by these techniques.

In addition, the details of the deposition event – where a wave of the material, at high energy (and therefore high surface mobility) appears suddenly at the substrate surface, followed by a delay which may be on the same time-scale as adatom rearrangement and film nucleation processes – are unique among film deposition techniques, and provides a number of opportunities for research into the physics of film depositions.

Table 2.1: Comparison of Film Deposition Parameters.[4] See text for explanation of abbreviations.

Method	Plume energy(eV)	Vacuum	Deposition Rate (A/s)	Use of >10 mtorr gas?
AMBE	0.1-100	UHV	3	no
ALE	0.1	UHV	1	no
CVD forms	0.1 (~500 PECVD)	HV (UHV for MOCVD)	10-20	yes
IBAD	0.1-1000	HV	10	no
IBD	20-200	UHV	0.1	no
ICBD	0.1-10	HV	10	no
IVD	0.1-1000	HV	20	no
MBE	0.1	UHV	3	no
PLD	1-1000	HV	10	yes
S	1-1000	HV	10	no
TE	0.1	HV	20	no

Table 2.2: Comparison of Common Materials Deposited by Various Techniques[4] See text for explanation of abbreviations.

Method	Semi-conductors	Carbides	Nitrides	1-2 Element Oxides	3-4 Element Oxides
AMBE	X				
ALE	X				
CVD		X	X	X	
IBAD			X	X	
IBD	X				
ICBD					
IVD				X	
LACVD	X				
MOCVD	X				
MBE	X	X			
PECVD	X				
PLD	X	X	X	X	X
S		X	X	X	X
TE				X	

Figure 2.1: Pulsed laser deposition (PLD) setup for deposition of $Bi_2VO_{5.5}$ and $Bi_2Cu_{0.1}V_{0.9}O_{5.35}$ described in this chapter.
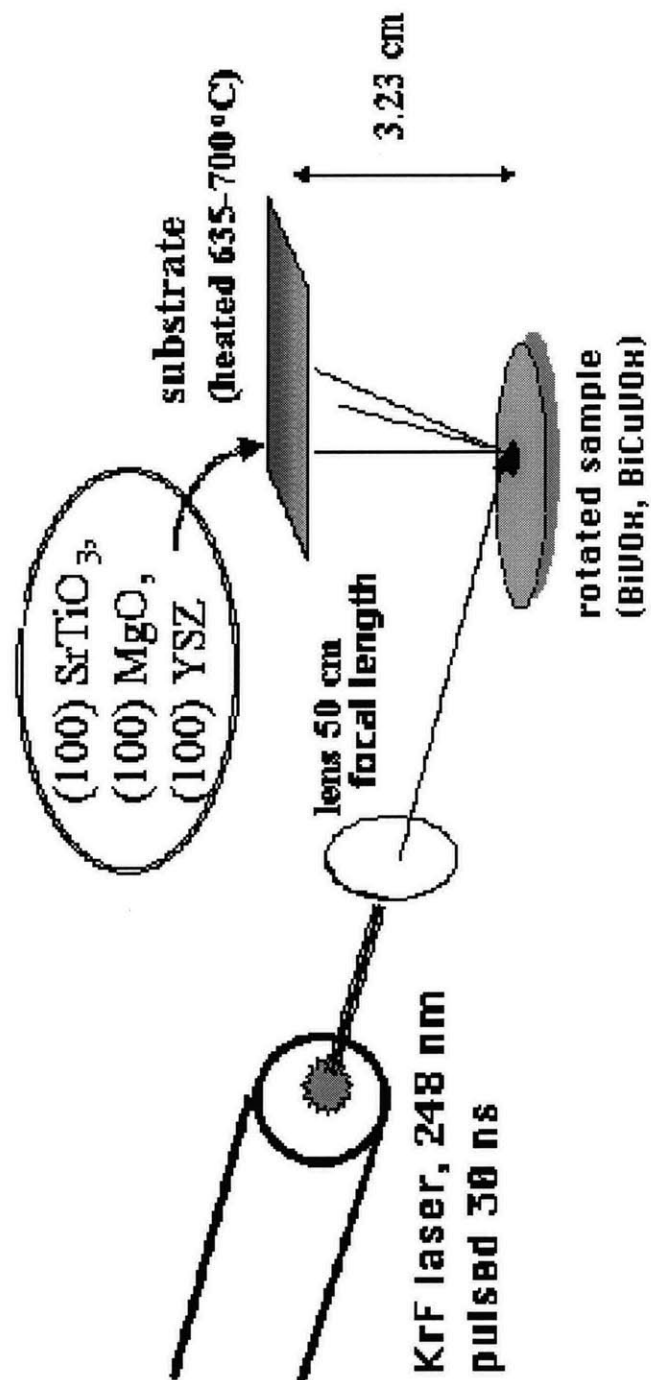
2.1.2 Pitfalls and Problems

Two major problems in the PLD method impede its more wide-scale commercial use. First, the deposited film often contains particulates – like boulders on a smooth sandy beach – of a size unacceptable in films intended for high-performance electronic and optical applications such as high-temperature superconductors, dielectrics, and ferroelectrics. Second, scale-up of the process so that large areas can be covered with film in a high-throughput setting remains an ongoing challenge.

The particulates found on the deposited film are believed to be from large clusters or molten globules of material ejected from the target and depositing as a unit onto the substrate. They can range in size from the nanometers to microns. There are a number of possible mechanisms,[5] including (1) break-off of protruding features on the target surface, either when it is fresh or after damage due to the laser irradiation, (2) rapid expansion of trapped gas bubbles beneath the target surface causing ejection of surface material, (3) splashing of the molten layer of the target due to a subsurface superheated region or recoil due to the rapid surface evaporation, and (4) condensation from a supersaturated vapor. Several techniques for reducing the size and number of particulates or eliminating them entirely have been tried. A shutter mechanism ("velocity filter") switching in and out of the plume path permits passage of the small, high-velocity plume particles while stopping the large, slow chunks.[5] This, however, reduces the total throughput and therefore the overall deposition rate. "Off-axis"

depositions, in which the substrate is 180° to the initial plume direction (0°, or line-of-sight, is the usual geometry) has been used to benefit.[6] A second laser aimed at the plume breaks apart the large particles in it. Finally, reduction of the laser power density and wavelength may eliminate the splashing that gives particulate deposition, though with too-low power density and wavelength, incongruent deposition occurs. Thus, while the problem of the particulates in a PLD thin film has not been eliminated, progress has been made toward solving it.

Scale-up of PLD to enable deposition of films onto large (>100 mm diameter substrates) has been approached mainly through adjustments to the deposition chamber geometry. Offsetting the rotating target from the substrate center, and counter-rotating the substrate in the resulting off-center plume, combined with a rastering laser, has been used to deposit films over 125-mm diameter substrates.[7] Other approaches have used (1) an off-axis stationary beam focused on a rotating target, with deposition onto a counter-rotating substrate; (2) increasing the target-substrate distance; (3) and a stationary beam focused on a rotating target, with the substrate rotating and translating across the plume. While these approaches are reasonably satisfactory, the major challenges remain. Currently, the target must be resurfaced – usually with sandpaper – between depositions to smooth out the grooves caused by the laser's impinging on the target surface. The resulting waste of material and time is uneconomical in a commercial setting. Other problems are technical in nature: the challenges of uniformly heating a large substrate, of monitoring the deposition rate, of reducing the particulate deposition, and of finding a way to deposit

films onto non-planar substrates. Until solutions to these difficulties are found, the commercialization of PLD is unlikely. See Table 2.3 for a comparison of PLD with other deposition techniques.

Despite these major problems with PLD, a number of companies had entered the arena as of 1994,[3] and were producing films of high-temperature superconductors. Ferroelectric films for use in nonvolatile memories and other novel devices, dielectric films for microwave and field effect devices, and semiconductor films have been deposited successfully by PLD and shown high quality and performance. Bioceramics and tribological coatings, as well as polymer thin films, are potential areas for application of PLD. To our knowledge, however, the work reported in this chapter is the first PLD of a thin film of a material intended for use as an oxide-ion conductive membrane.

Table 2.3: Comparison of Deposition Techniques – Commercial Factors[4]

HDR=high deposition rate, LST=low substrate temperature, LA = large area, LC = low cost, EMC = easy material change, MC = material conservation

Method	HDR	LST	LA	LC	EMC	MC	Problems
AMBE		X					Uniformity
ALE							Slow
CVD	X		X	X			High T substrates
IBAD		X			X		Impurities, uniformity
IBD		X			X	X	Slow growth, small area
ICBD		X	X				Impurities reproducibility
IVD	X	X	X	X	X		Impurities
LACVD		X					Selected areas only
MOCVD	X		X	X			High T substrates
MBE			X				High T substrates
PECVD	X	X		X			Uniformity
PLD	?	X	?	X	X	X	Particulates, small area
S		X	X		X	X	Impurities
TE	X		X	X	X		Impurities

2.2 Results and discussion

As noted in Chapter One, $Bi_2VO_{5.5}$, a member of the Aurivillius family of compounds, undergoes two consecutive phase transitions on heating (Equation 2.1). The higher temperature forms exhibit higher oxygen ion conductivity.

$$(2.1) \quad \alpha \xrightarrow{\text{450 °C}} \beta \xrightarrow{\text{570 °C}} \gamma$$

These phase transitions are reversible but can be suppressed by a 10-30% doping of the parent $Bi_2VO_{5.5}$ structure ("BiVOx") with a wide range of elements.[8] In particular, a 10 mol% doping with copper results in the stabilization of the high-temperature (γ) polymorph as the compound $Bi_2Cu_{0.1}V_{0.9}O_{5.35}$ ("BiCuVOx").

$Bi_2VO_{5.5}$ and $Bi_2Cu_{0.1}V_{0.9}O_{5.35}$ were deposited by PLD onto a number of substrates, including MgO, YSZ, and $SrTiO_3$ (STO). The BiMeVOx target materials were made originally by solid state synthesis and verified phase-pure by XRD. (Figure 2.2 a, b)

BiVOx films deposited on MgO and YSZ underwent severe delamination during post-deposition cooling. This is due to a combination of the thermal expansion mismatch and lattice mismatch between BiVOx and these substrates, and because of the severe strains developed in the films during the γ–α phase transitions. See Table 2.4 for a summary of relevant lattice parameters.

As can be seen in Table 2.4, based on their lattice parameters neither MgO nor YSZ can accommodate both the γ (high-temperature) and the α (room temperature) phases. On the other

hand, the $SrTiO_3$ (STO) lattice matches that of the γ phase along its **a** direction and that of the α phase along its face diagonal. Samples deposited on STO were thus of better quality. See Table 2.5 for a summary deposited film thicknesses. The substrate temperature listed for each film was the one that yielded the X-ray diffraction patterns with the best phase purity and the narrowest rocking curve.

All films on STO were strongly **c**-axis oriented, as shown by the absence of all but the 00l peaks in the X-ray diffraction patterns. (Figure 2.3) No other oxide phases were observed in the XRD patterns of any of the deposited films, and Rutherford back-scattering showed the stoichiometry to be correct within detection limits. Both of the BiVOx films showed large-scale cracking and delamination, but were smooth, without granularity in the uncracked areas. (Figure 2.4 a, b) The films were cooled slowly to minimize the effects of thermal strains; however, thermal contraction and phase-change strains were exacerbated by the 45° crystallite re-orientation required for the ingrowing α-BiVOx phase to match the substrate STO lattice. The results of the second heating and cooling illustrates the extent of grain disorder and internal strain in the α-$Bi_2VO_{5.5}$ films. (Figure 2.5) This cracking occurs in spite of the low temperature (below the α–β transition) of the heating step, and the strain relief that may be expected from the cracks already present in the film. The light areas in the electron micrographs are probably due to hillock formation during the second annealing step; similar results have been observed in

BiMeVOx films made by sol-gel deposition methods. (See Chapter Six.)

The stabilized γ-$Bi_2Cu_{0.1}V_{0.9}O_{5.35}$ (BiCuVOx) films deposited onto STO were adherent and smooth, free of microcracking and granularity, unlike the undoped parent phase. (Figure 2.6) Since it can be expected that the thermal expansion coefficient of BiCuVOx is similar to that of BiVOx, the absence of cracking and delamination in the BiCuVOx films indicates that the phase transition and the corresponding lattice-match problem were the main causes of the cracking observed in the BiVOx films, rather than the development of thermal strains. As with the BiVOx films, the BiCuVOx film is **c**-axis oriented (Figure 2.7) with non-00l peaks completely absent. However, while the quality of the as-deposited BiCuVOx films is high, the severe cracking that occurred during the second heating to 400 °C (well below the mp of 890 °C) and subsequent medium-rate cooling (10 °C min^{-1}) suggests that the membrane, when deposited via PLD, is still too strained to accommodate thermal expansion mismatch. Moreover, the results of the second annealing step (Figure 2.8) indicate little or no randomness to the orientation of the **a-b** plane with respect to the STO lattice (Figure 2.9) as would be expected, given the near-perfect match of the two lattices (Table 2.4).

Pulsed laser deposition of films of the parent (α) phase $Bi_2VO_{5.5}$ onto $LaNiO_3$ and $SrTiO_3$ substrates has been previously reported.[9] In the latter paper, while the rapid (10 °C min^{-1}) cooling from the deposition temperature (675 °C) was not reported to cause cracking or delamination of the films, the films exhibit a more or less random grain orientation in the plane of the substrate,

although the XRD reported there shows strong **c**-axis orientation, as seen in our results, and a high degree of granularity, as evidenced by inspection of the published SEM micrographs. Grain-boundary grooving in these samples may relieve strain in the film, preventing the cracking that we see in our films.[10] If so, it may be that higher-temperature treatment of those films would have lead to agglomeration and dewetting (See Chapter 6). On the other hand, the films deposited in the experiments described above are oriented, smooth, and defect-free as deposited, without obvious graininess. The extremely slow cooling rate may have permitted quasi-single crystal film nucleation in the case of our films. The film quality in the BiCuVOx case seems to be due mostly to a combination of the close lattice match to the substrate and the suppression of phase transitions. In the undoped BiVOx film the change in cell parameter size and in the direction of the primary cell axes required to match the substrate lattice induces severe strains in the film, causing the observed cracking pattern and delamination.

Table 2.4: Lattice parameters of substrates and PLD films.

Compound	Lattice Parameters (Å)	Face Diagonal (Å)
α-$Bi_2VO_{5.5}$	a=5.54, b=5.62, (c=15.32)	7.89
γ-$Bi_2VO_{5.5}$	a=b=4.004 (c=15.488)	5.66
$Bi_2Cu_{0.1}V_{0.9}O_{5.35}$	a=b=3.92	5.54
MgO	a=b=c=4.16	5.88
YSZ (15% Y_2O_3/85% ZrO_2)	a=b=c=5.14	7.27
$LaNiO_3$	a=b=c=3.83	5.41
$SrTiO_3$	a=b=c=3.94	5.57

Table 2.5: Results for BiMeVOx Films PLD onto STO

Film	Substrate Temp. (°C)	Laser Pulses	Thickness (μm)*
BiVOx-A	700	3000	1.05 (0.84[+])
BiVOx-B	635	2000	0.22
BiCuVOx	635	2000	0.20

*by profilometry [+]by Rutherford back-scattering (RBS)

Figure 2.2a: $Bi_2VO_{5.5}$ sample prepared by solid state methods and used as a target in the PLD depositions.

BiVO$_4$
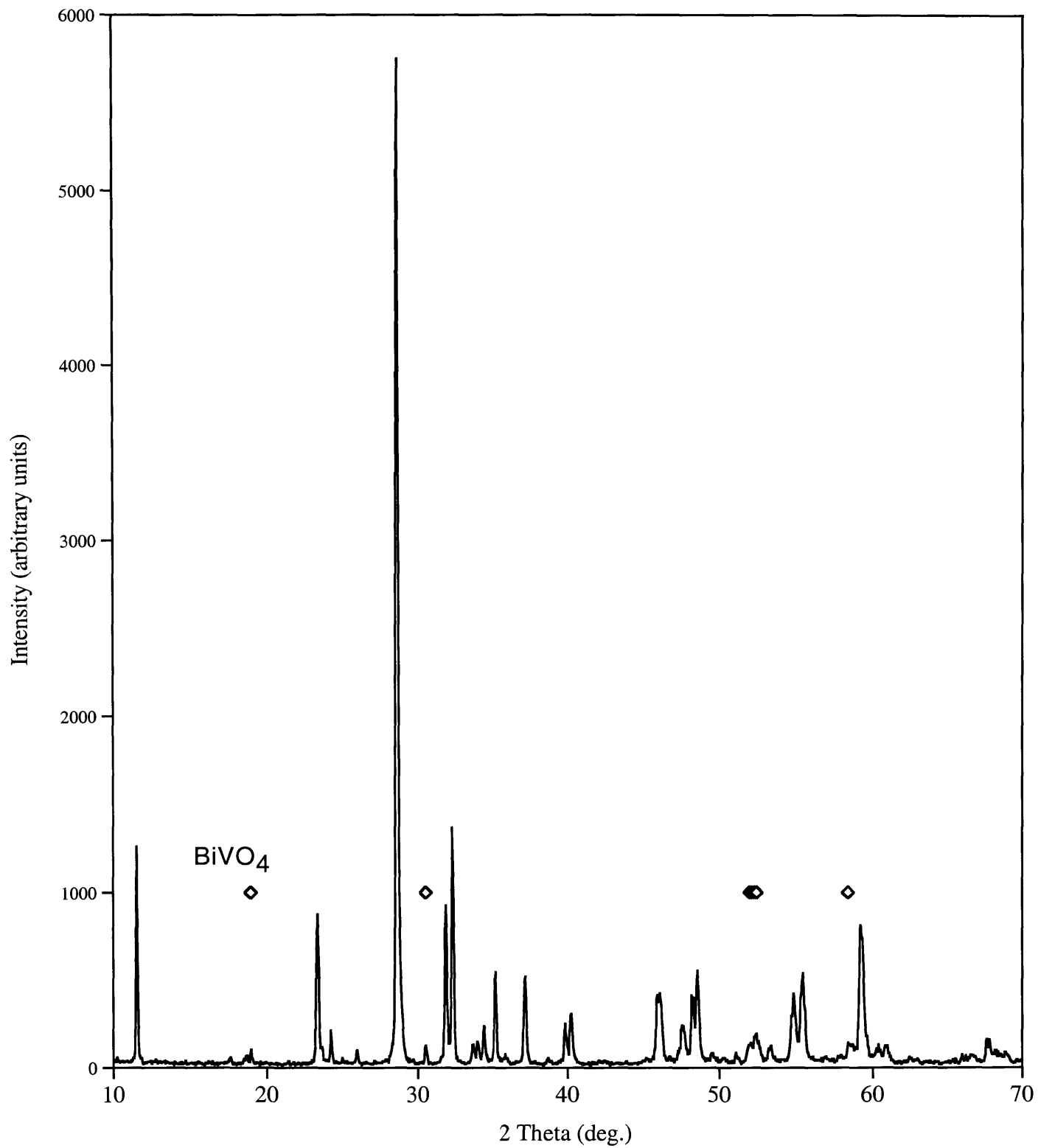
Figure 2.2b: $Bi_2Cu_{0.1}V_{0.9}O_{5.5-\delta}$ sample prepared by solid state methods and used as a target in the PLD depositions.
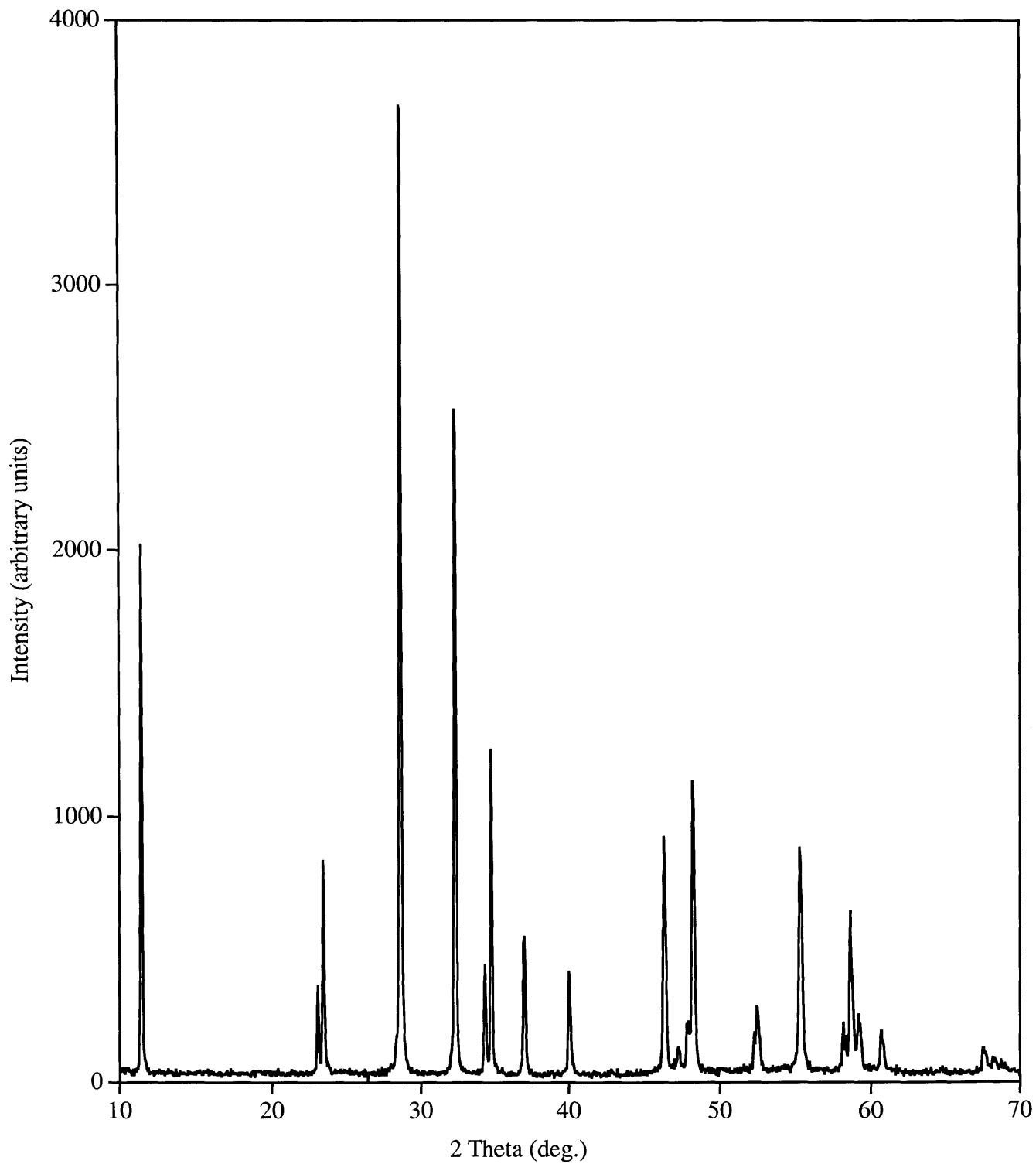
Figure 2.3: Grazing incidence XRD (GIXRD, grazing angle 1°) of $Bi_2VO_{5.5}$ films deposited by PLD onto STO. Deposition temperature 700 °C.
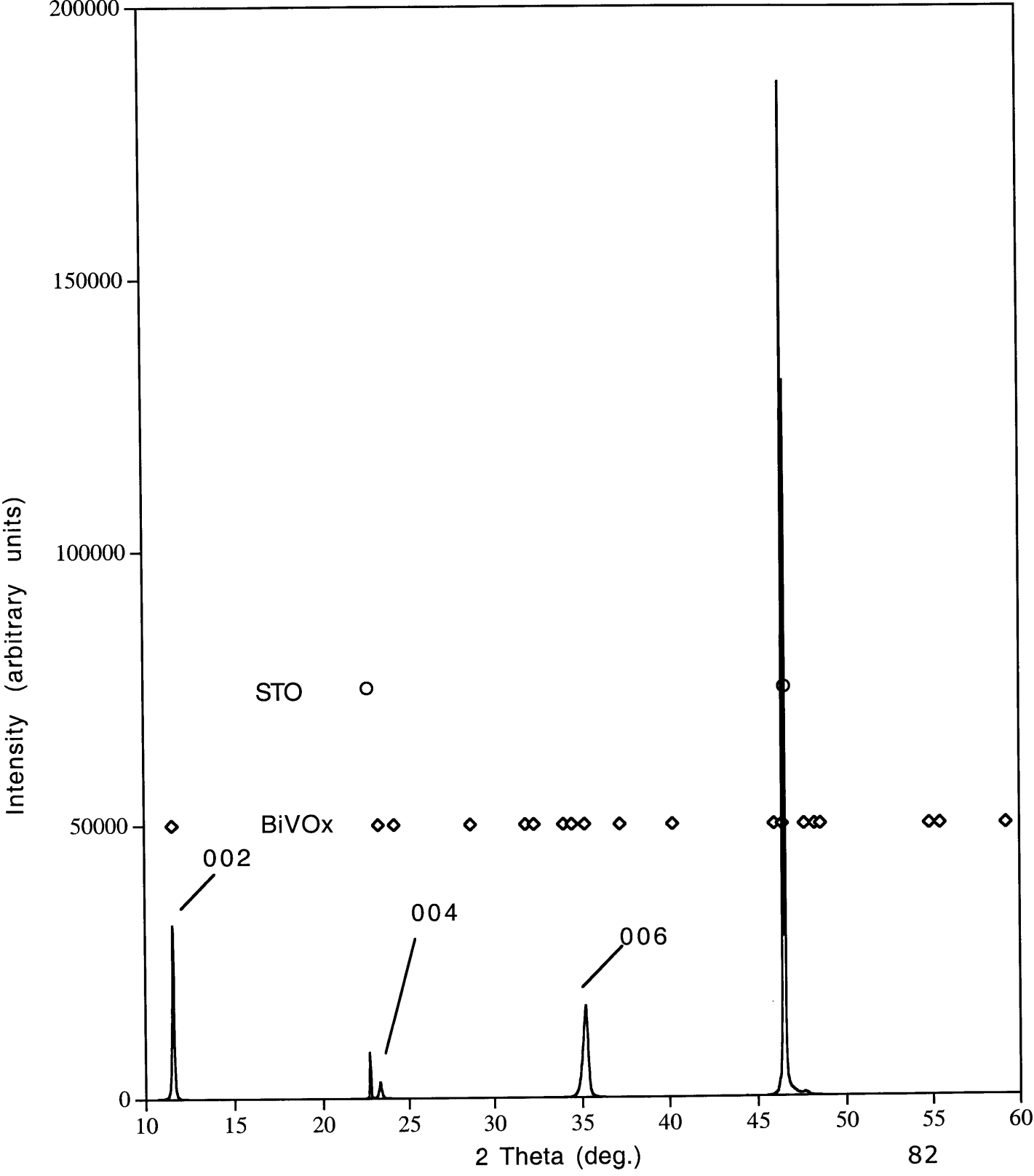
Figure 2.4: (a) $Bi_2VO_{5.5}$ film on STO, deposited at 635 °C, X 2500. (b) $Bi_2VO_{5.5}$ film on STO, deposited at 700 °C, X 515.

(a)
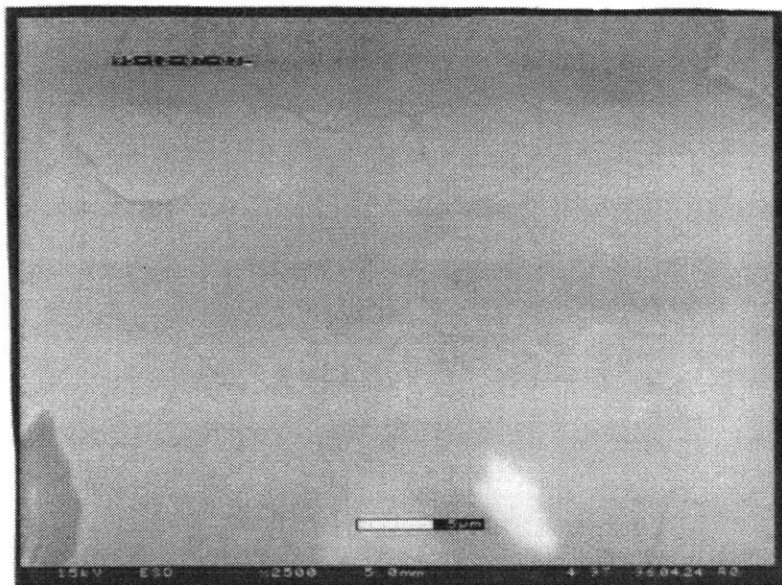
(b)
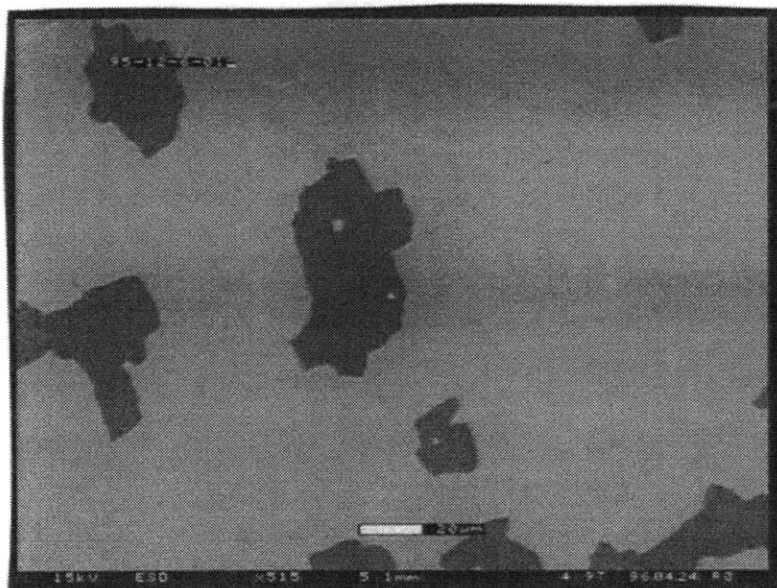
Figure 2.5: $Bi_2VO_{5.5}$ film on STO after 2nd heating cycle, X 740.
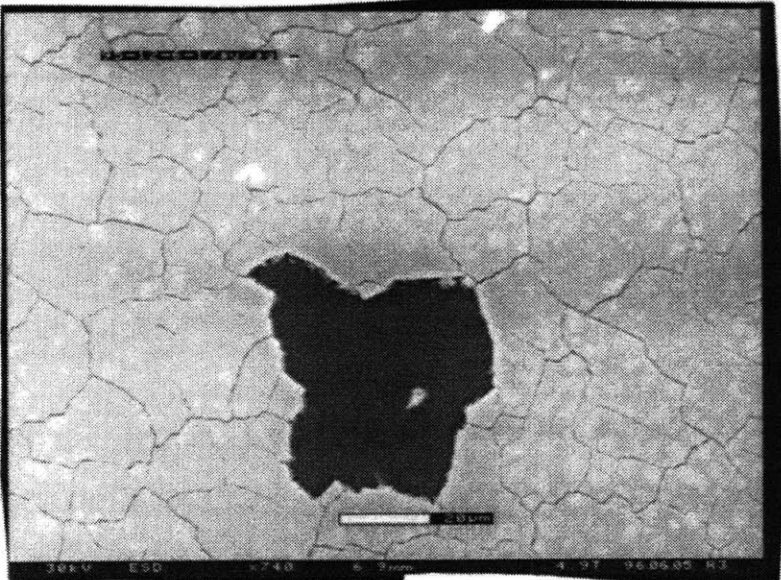
Figure 2.6: $Bi_2Cu_{0.1}V_{0.9}O_{5.5-\delta}$ film on STO after initial PLD at 635 °C, X 1350.

Figure 2.7: GIXRD of BiCuVOx films deposited on STO by PLD.
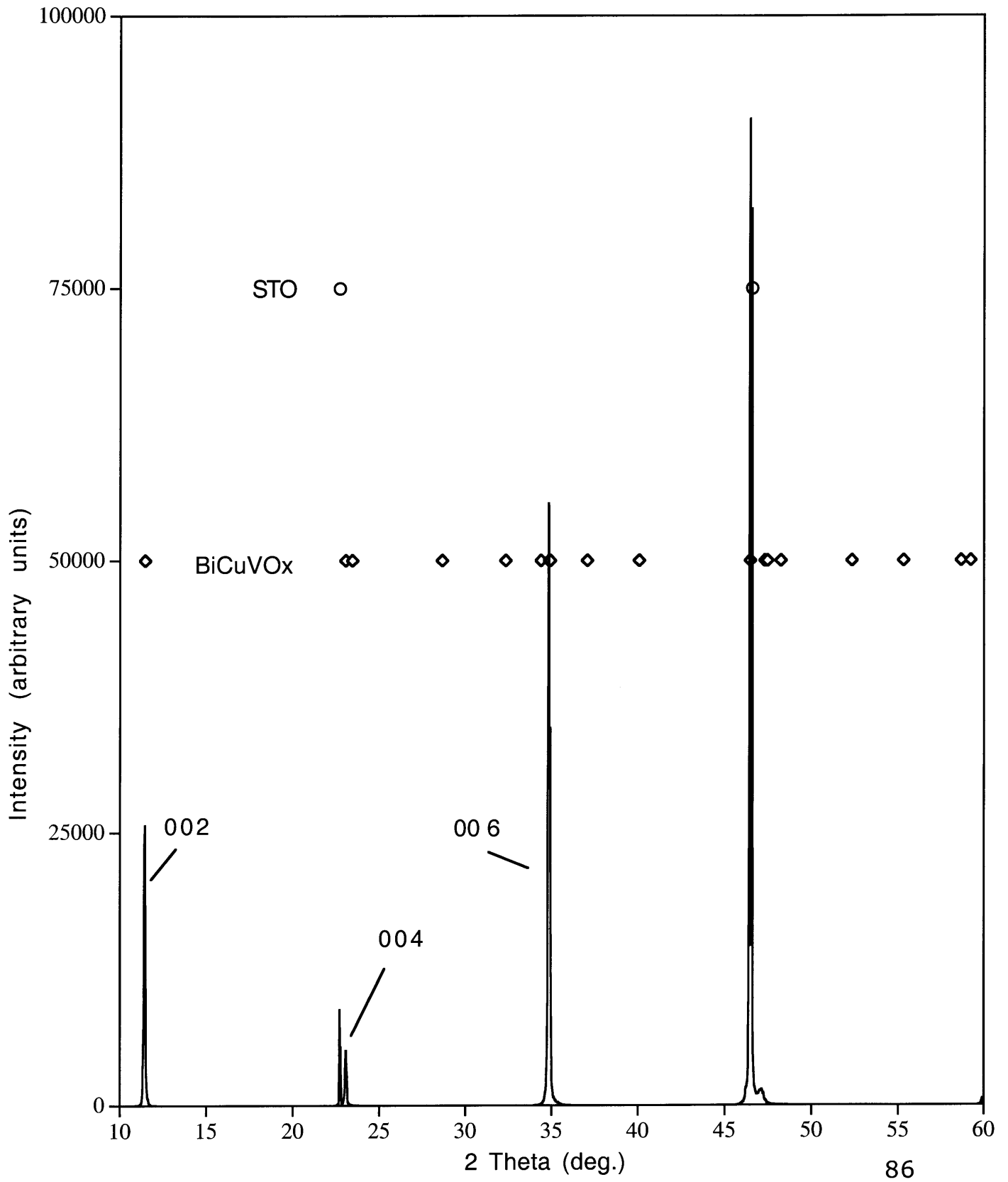
Figure 2.8: BiCuVOx film on STO after 2nd heating cycle, X 785.
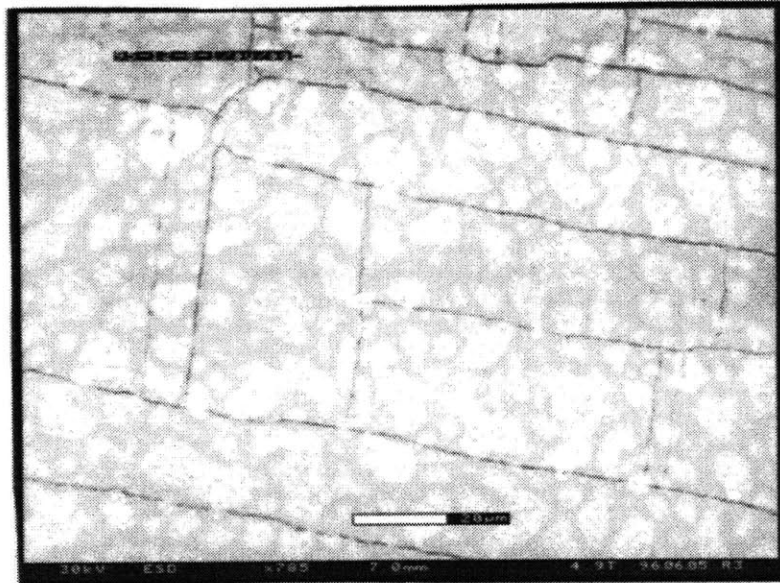
Figure 2.9: Alignment of the deposited BiCuVOx film with the a or b substrate directions ensures that cracking (dark lines) occurs in a rectilinear manner. (a) This is also the case for γ-$Bi_2VO_{5.5}$. (b) However, grain reorientation to align the α-$Bi_2VO_{5.5}$ with the STO face diagonal during the γ-α transition results in a circular cracking pattern (c).

α-BiVOx	γ-BiVOx	BiCuVOx

c   b   a
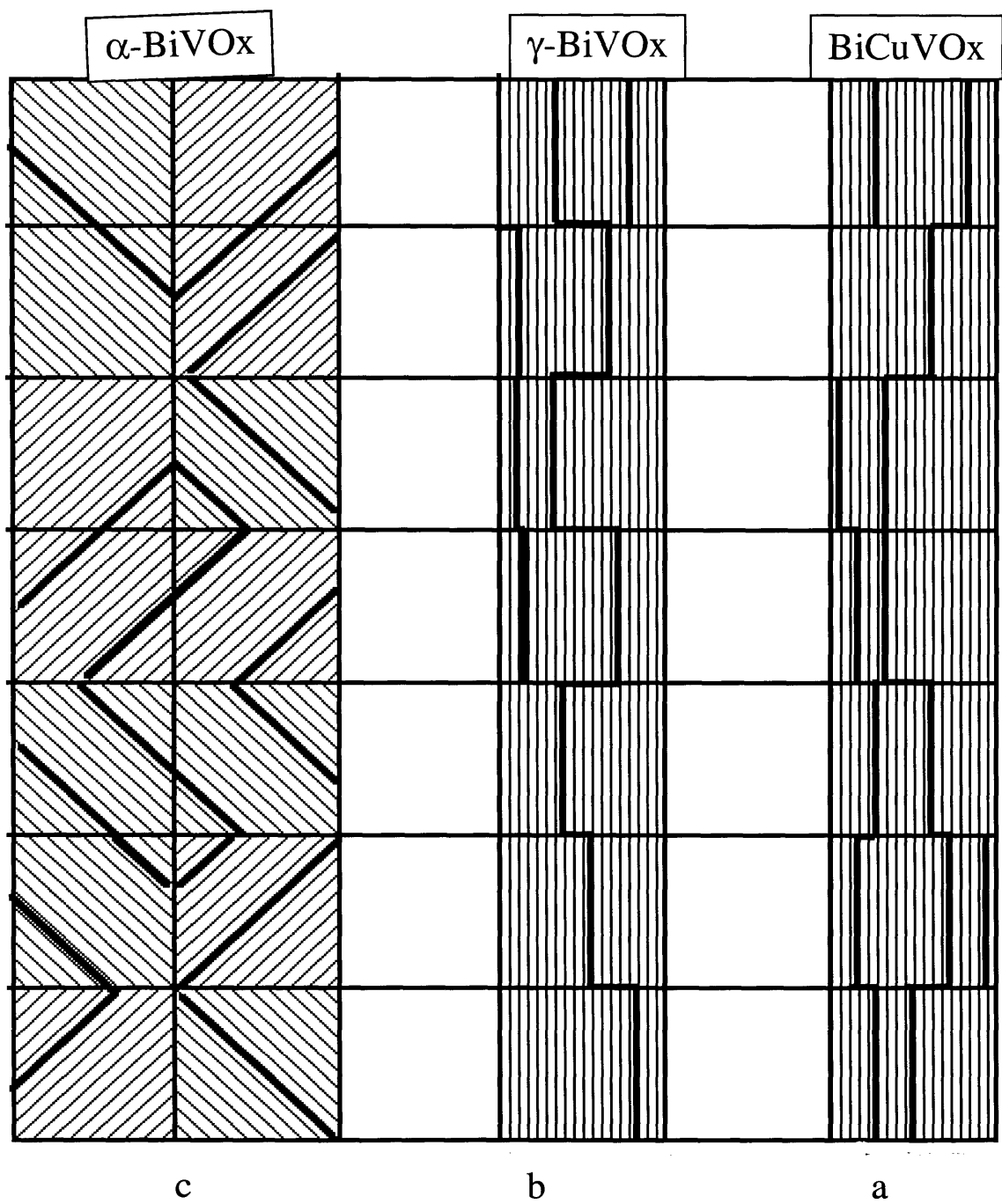
2.3 Conclusions

Smooth and defect-free BiCuVOx films were successfully deposited onto STO substrates by PLD, while BiVOx films were smooth, but cracked due to the rotation of the film lattice with respect to the STO lattice during the cooling-step γ–α phase transition undergone by these films.

Both BiVOx and BiCuVOx films were subjected to a second low-temperature (400 °C) heating cycle with moderately fast heating and cooling to determine whether the instantaneous-deposition nature of the PLD process had created films which were highly strained and merely metastable. This temperature was chosen to be well below the film's melting point (890 °C for $Bi_2VO_{5.5}$[11], 895 °C for $Bi_2Cu_{0.1}V_{0.9}O_{5.35}$, see DTA/TGA results in Chapter Six) to limit the atomic mobility expected in the film and prevent island formation, and to be below the temperature for the α–β phase transition (450 °C) so that strains in the films generated by their initial depositions and cooling would be highlighted without interference from additional phase transitions. It was expected also that this temperature would be sufficiently low that thermal expansion would not contribute greatly to any cracking seen. Both films exhibited severe strain-cracking. The cracking pattern reflected the underlying orientation of the film with respect to the substrate lattice. While BiCuVOx, oriented along the lattice-matched **a-b** direction of the STO lattice, cracked in a rectilinear pattern, the BiVOx films cracked in a rounded pattern reflective of

their re-orientation during cooling from the γ phase matching of the **a-b** direction to the α phase matching of the cell diagonal. (See Figure 2.6.)

The results highlight the importance of judicious substrate choice in thin film depositions. Substrates must not only be lattice matched, but also compatible in terms of their thermal expansion coefficients. Finally, phase transitions in the film must be suppressed. While many thin films are inspected for quality directly post-deposition, the result of the second heating cycle reported here points up the need for testing films under a variety of heating and cooling regimes, if they are to be used in a practical application.

2.4 Experimental

Details on the reagents and instruments used in this Chapter may be found in the Appendix to Part I of this thesis.

Experiment #1 Synthesis of Target Pellets (JWP/II/99A, B)

Stoichiometric quantities of Bi_2O_3 (9.3190 g, 20 mmol) and V_2O_5 (1.8188 g, 10 mmol) were ground together in an agate mortar under acetone and a pellet pressed of the resulting mixed solid. The pellet was heated in air on platinum foil for 20 h at 850 °C with an intermediate grinding to prepare $Bi_2VO_{5.5}$ (BiVOx), phase purity verified by powder X-ray diffraction (PXRD). Similarly, bulk $Bi_2Cu_{0.1}V_{0.9}O_{5.35}$ (BiCuVOx) was prepared from stoichiometric quantities of Bi_2O_3 (9.3190 g, 20 mmol), V_2O_5 (1.637g, 9 mmol) and CuO (0.1591 g, 2 mmol) heated in air on a platinum foil for 20 h at 850 °C. Pressed and sintered pellets, approximately 2 cm in diameter, of each compound, were used as targets for the deposition.

Experiment #2 PLD of BiMeVOx Films (performed at Naval Research Laboratory)

The BiVOx and BiCuVOx films were prepared by pulsed laser deposition on (100) $SrTiO_3$, (100) MgO, and (100) 15 %Y_2O_3-doped ZrO_2 (yttria-stabilized zirconia, YSZ) using a KrF laser (248 nm).

Laser pulses of approximately 30 ns duration were focused through a 50 cm focal length lens onto the BiVOx or BiCuVOx target. With an incident power of 0.8 W at 5 Hz, the focal spot size of 0.07-0.08 cm^2 yielded a fluence of 1.8-2 J cm^{-2} at the target. Before each deposition, the targets were pre-burned for 2000 shots in oxygen to remove surface contaminants and to reach a steady state ablation composition. Targets were rotated in the rastered beam to minimize surface cratering. The target-to-substrate distance was 3.23 cm. Substrates were not specially prepared before deposition. Substrate temperatures from 635 °C to 700 °C were tried. The depositions were carried out in 0.3 Torr O_2 with slow cooling (< 1 °C min^{-1}) in approximately 100 Torr O_2. A faster cooling rate resulted in delamination of the films.

Experiment #3 Characterization of PLD Films (JWP/III/139)

The surface morphology of the films was examined without further sample preparation using environmental scanning electron microscopy (ESEM, Electro-Scan) at 15 kV beam energy and 4.9 Torr water vapor pressure to prevent surface charging and achieve the desired resolution. Film thicknesses were determined by profilometry (Dektak, 2.5 μm stylus). Some material was removed from a small area of each film sample using concentrated HCl to create a step for the profilometer. The thickness and stoichiometry was verified in one of the BiVOx samples by Rutherford backscattering spectroscopy (RBS). Films were checked for orientation and phase purity at the Naval Research Laboratory by rocking-curve XRD using Cu Kα radiation (1.5418 Å). Full X-ray

diffraction patterns were collected with rocking and re-aligning on the $\Gamma(002)$ peak of BiVOx.

Experiment #4 Post Deposition Thermal Treatment (JWP-III-142)

Samples were subjected to a second annealing in air at 400 °C for 2h and cooled at 10 °C min^{-1}. These films were re-examined for changes in surface morphology using ESEM. For the latter examination, approximately 50 Å of gold was evaporated onto the film surfaces to relieve charging effects.

2.5 References

1) Cheung, J. in *Pulsed Laser Deposition of Thin Films*, Chrisey, D. B. and Hubler, G. K., Ed.; John Wiley & Sons: New York, 1994.

2) Chrisey, D. B. in *Pulsed Laser Deposition of Thin Films,* Chrisey, D. B. and Hubler, G. K., Ed.; John Wiley & Sons: New York, 1994.

3) Venkatesan, T. in *Pulsed Laser Deposition of Thin Films*; Chrisey, D. B. and Hubler, G. K., Ed.; John Wiley & Sons: New York, 1994.

4) Hubler, G. K. in *Pulsed Laser Deposition of Thin Films*; Chrisey, D. B. and Hubler, G. K., Ed.; John Wiley & Sons: New York, 1994.

5) Chen, L.-C. in *Pulsed Laser Deposition of Thin Films*; Chrisey, D. B. and Hubler, G. K., Ed.; John Wiley and Sons: New York, 1994.

6) Kennedy, R. J. *Thin Solid Films* **1992**, *214*, 223.

7) Greer, J. A. in *Pulsed Laser Deposition of Thin Films*; Chrisey, D. B. and Hubler, G. K., Ed.; John Wiley & Sons: New York, 1994.

8) Mairesse, G. in *Fast Ion Transport in Solids*; Scrosati, B. and al., e., Ed.; Kluwer Academic Publishers: Netherlands, 1993.

9) Prasad, K. V. R.; Varma, K. B. R.; Raju, A. R.; Satyalakshmi, K. M.; Mallya, R. M.; Hegde, M. S. *Appl. Phys. Lett.* **1993**, *63*, 1898.

10) Srolovitz, D. J.; Goldiner, M. G., *JOM,* **1995**, *March*, 31.

11) Abraham, F.; Debreuille-Gresse, M. F.; Mairesse, G.; Nowogrocki, G. *Solid State Ionics* **1988**, *28-30*, 529.

Chapter Three:

Sol-Gel Approaches to Bulk BiMeVOx

3.1 Introduction to the Sol-Gel Method

In addition to the films of the BiMeVOx materials produced by pulsed laser deposition described in Chapter Two, a number of BiMeVOx films were produced by the sol-gel method. This work is described in the remainder of Part I of this thesis. Chapter Three provides background information on the sol-gel method and reports our early and informative, albeit unsuccessful, attempts at developing a formulation which would produce BiMeVOx membranes on casting and pyrolysis. Chapters Four and Five report and discuss the formulation that was eventually found to be most useful, and the work done to characterize that precursor. Chapter Six reports deposition of the BiMeVOx films onto a number of substrates.

While the majority of the background material needed for discussion of the work reported in these chapters is provided below, some significant pieces of information are left to be introduced as needed in subsequent chapters.

3.1.1 Definitions, History, Background

Brinker and Scherer, in their text on the subject, define the "sol-gel" process as "the preparation of ceramic materials by the preparation of a sol, gelation of the sol, and removal of the solvent."[1] Most definitions by the many reviewers of the sol-gel process are similar; however, throughout the literature the term has been more widely applied to include systems that form neither true sols nor true gels. Therefore the term "sol-gel" has come to

refer to virtually any ceramic preparative technique that involves dissolved or colloidal ceramic precursors. Sol-gel-type chemistry has also appeared in the literature under the terms "soft-solution processing" and "chimie douche," where the "soft" refers to the differences between this technique and those involving grinding and firing to high temperatures of dry ceramic powders.

Most reviewers cite Ebelman's 1846 synthesis of silicon alkoxides as the earliest step in sol-gel processing's development.[2,3] By the early 1900s Walter A. Patrick of the Silica Gel Corporation was issued dozens of patents revealing sol-gel processes for making silica-gel supported catalysts, mixed oxides, adsorbents, and porous glasses, thereby demonstrating the potential industrial uses of this chemistry.[4-6] Later advances by Moulton (American Optical Company, 1943),[7-9] in which mixtures of silicon, titanium, and tin alkoxychlorides were partially hydrolyzed and used as antireflective coatings on glass; by Kimberlin (1953),[10,11] who used aluminum alkoxides to produce high-purity fine powders of aluminum metal; and by Yoldas (1975),[12,13] who found that alumina sols could be used to produce transparent gel monoliths, set the stage for rapid development and copious publishing on the potential and actual uses of the sol-gel process. The sol-gel process has made it into the realm of quasi-political discussion, as well: one recent paper points out the "environmentally friendly" aspects of sol-gel and other "soft chemistry" methods, insofar as lower firing temperatures are necessary for making solid ceramic items via sol-gel-type processes,

and water (or recyclable organic solvents) can be used as the liquid carrier for the precursors.[14]

Because the term "sol gel" has come to refer both to a process where the ceramic precursor is a true sol (a colloidal suspension of solid particles in a liquid) and where the precursor is a macromolecular network, (from condensation polymerization of metal alkoxides), some care must be taken in identifying what sort of chemical and physical processes are occurring in a preparation identified as "sol-gel." Inorganic precursor salts, including chlorides, nitrates, sulfides, and, ultimately, hydroxides, are usually used to create true sols. Metal or silicon alkoxides are the precursors to macromolecular suspensions; metal carboxylates and other organic acid salts may be used to introduce the primary or additional metals into solution in either case. Flocculation (in the sol) or hydrolysis/condensation (in the alkoxide case) results in a *gel*, a continuous semisolid or viscoelastic skeleton enclosing or enclosed by a continuous liquid phase. Aging or drying of the gel results in further condensation, which leads to shrinkage of the gel as the liquid is expelled. If the expulsion occurs more rapidly than the evaporation, the process is called *syneresis*; under normal drying conditions, however, a porous and high-surface area *xerogel* results, while under supercritical conditions, little shrinkage occurs and the resulting low-density material is called an *aerogel*. Aside from the environmental conditions of the drying, the final dry product properties are controlled by a number of parameters active during the condensation or flocculation and as the solvent evaporates out of the gel pores. Ionic strength or pH variation and the steric properties of the precursor lead to different degrees of

condensation and branching in the condensed material. Drying control chemical additives can reduce the development of the capillary pressures that lead to cracking during solvent evaporation. Firing of the dry product "greenbody" results in pyrolysis of residual (unhydrolyzed) organic groups, usually with concomitant gas production, followed by crystallization and sintering. The intimate mixing of the constituents ensures that the crystallization and sintering will occur at temperatures several hundreds of degrees lower than those required for more traditional mixed-oxide powder processes, at least in principle. These issues will be discussed in more detail below.

3.1.2 True Sols

A sol is a colloidal suspension of solid particles in a liquid. In sol-gel preparations, the sol is generally polydisperse. The high surface free energy of the particles makes them tend to collapse together to form aggregate larger particles with reduced surface energy; van der Waals and Coulomb forces further attract the particles to each other. Thus, a colloid is kinetically stable only; thermodynamically, it is unstable if colloid particles alone are considered.

However, for oxide and hydroxide sols, where the particles have low to mid-range surface potentials, the behavior can be well-described by the Derjaguin, Landau, Verwey, and Overbeek (DLVO) Theory.[15] In this model, an electric double layer is formed when the surface of the colloid particle acquires a charge in a polar solvent and becomes surrounded by a diffuse layer of counter-ions

and some opposite-charge co-ions. This ionic atmosphere protects the colloid particle from the approach of other likewise-screened particles. The particle surface acquires the charge by: (1) ionization, where a functional group on the surface dissociates and forms an ion, depending on the pH of the solution; (2) preferential adsorption of ions from solution; and (3) dissolution of the colloid particle surface into its cationic and anionic parts at different rates. The ionic strength of the solution determines the degree of screening of the colloidal particle's native charge; at high ionic strength the surface potential falls rapidly within a short distance and van der Waals forces drive the ensuing flocculation. Likewise, flocculation will occur in any situation where close approach of the particles – due to thermal (Brownian) or mechanical agitation – permits the short-range van der Waals forces to dominate the system.

The addition of a surfactant will stabilize a colloid against coagulation of its particles. For example, soap (long-chain fatty acids) will collect ionic carboxylate-ends toward the colloid particle, and the hydrophobic chains will thus protect the particle from coming within coagulation distance of other particles.

If the electric double layer or surfactant preventing coagulation is removed, so that sol particles can approach within the active distance of van der Waals forces and coagulate, they may form a densely packed sediment, a re-suspendable loose sediment, or a network of aggregated particles where the "sediment" volume is equal to that of the solvent. In the last case, the aggregate particles may cross-link and immobilize the solvent, providing a viscoelastic gelatinous mass. The degree of cross-linking

determines the physical properties of the gel. The induction of gelation can be accomplished by a gradual change of ionic strength or by removal of solvent by evaporation. Gently heating a sol in an aqueous solvent (enthalpy-stabilized sol), or gently cooling one which is in a non-aqueous solvent (entropy-stabilized sol) can also induce gelation.

Multicomponent gels, where several metals need to be simultaneously present in the sol, suffer from co-solubility and preferential precipitation problems. The additional ionic strength provided by the addition of metal A, in some form, to a sol of metal B may disrupt the sol of metal B and cause it to flocculate; or metal A simply will "refuse" to form a sol in the presence of metal B. Careful control of the pH, temperature, and ionic strength, and sometimes the addition of surfactant materials, is usually necessary if a multicomponent gel is required. High dilution, of course, aids in getting all metal components into the sol but does not permit gel formation. These difficulties are exacerbated by an increased number of metals required to be simultaneously in the final gel.

3.1.3 Macromolecular "Sols"

Polymeric or macromolecular gels, which are not formed from true sols, are usually formed from metal alkoxide-based precursor solutions. Most studies have dealt with the reactivity of silicon alkoxides, because their hydrolysis is slow in "neutral" solutions (insofar as the concept of pH can be applied to non-aqueous regimes) and the relative rates of hydrolysis and condensation can be controlled by the use of acid, base, or nucleophilic catalysts.

Metal alkoxides, on the other hand, are extremely reactive to water and other hydroxyl compounds, so that while reports of applications involving metal-based sol-gel preparations are manifold, studies of the kinetics and mechanism of the reactions they undergo are few. The chemistry and behavior of multicomponent alkoxide systems, and of systems with metal alkoxides and metal salts together, is more complex still.

In general, the reactions of alkoxides can be broken into two categories: hydrolysis and condensation (Equations 3.1-3.2). Via these reactions, a network of M-O-M- bonds form.

(3.1) Hydrolysis: $M(OR)_n + x\ H_2O \Leftrightarrow M(OR)_{n-x}(OH)_x + x\ ROH$

(3.2a) Condensation by dehydration:

$$2\ (RO)_3M(OH) \rightarrow (RO)_3M\text{-}O\text{-}M(OR)_3 + H_2O$$
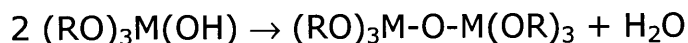
(3.2b) Condensation by dealcoholation:

$$2\ (RO)_3M(OH) \rightarrow (RO)_3M\text{-}O\text{-}M(OR)_2(OH) + ROH$$
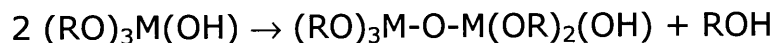
The mechanisms and rates of these reactions depend on pH, temperature, and the concentration of water in the nonaqueous solvent. Furthermore, depending on these factors and the identities of M and R, the morphology of the resulting oligimers may be either linear or branched. For tetraethoxysilane (TEOS), the hydrolysis rate increases with increasing $[H^+]$ or $[OH^-]$ in acidic and basic conditions, respectively. In acid, the rate of the hydrolysis reactions exceed that of the condensation reactions, and a linear gel morphology results. Under basic conditions the rapidity of the condensation reactions leads to a branched and cross-linked gel morphology.[16]

The oligimer chains may cross-link to form a gel either as evaporative losses of solvent cause them to approach, or as the condensation reactions continue to propagate. The gel network is formed as continued polymerization splits off alcohol groups and forms an extended M-O-M- structure. The degree of crosslinking determines the physical properties of the gel, including its ability to wet a substrate.[17,18]

One of the difficulties with using alkoxides to make multicomponent gels is that different metal alkoxides hydrolyze at different rates. If one component hydrolyzes too rapidly relative to the other(s), it may precipitate as a hydroxide within the gel, or the gel micromorphology will be similar to that of a block co-polymer, with regions of mostly one metal type, and other regions of mostly the other. The resulting inhomogeneity in the gel undoes one of the major benefits of the sol-gel method, the atomic-level mixing of the assorted metal species that provides for a reduced crystallization temperature. This difficulty can be addressed by the judicious choice of pH and solvent polarity and viscosity. Adjusting the identities of the alcohol groups can modify the hydrolysis rate as well. Other processes based on decreasing the reactivity of the metal alkoxide precursors by chemical modification (alcohol exchange, addition of carboxylic acid ligands or β-diketones), or by controlling the local concentration of water (by alcohol dehydration, esterification, and emulsion reaction) have been used with success.[19]

Because metal alkoxides are usually expensive and difficult to obtain in large quantities, it is often the case that only some of the metals of a multicomponent gel are added as alkoxides. The

103

remainder are provided as metal salts chosen to be soluble in the alcoholic solvent. Citrates, acetates, formates, tartrates, and nitrates are typically used. Chlorides and sulfates, due to their stability, are often hard to remove, leading to impurities in the final ceramic. Nitrates, being highly oxidizing, can lead to fires or explosions if care is not taken during the gel drying, and tend to crystallize out during solvent evaporation. Metal acetates and other salts of weak organic acids are usually soluble in a range of alcoholic solvents; however, their thermal degradation occurs at a higher temperature than for nitrates, so that their removal from the gel is more difficult. Heating a mixture of metal acetate and alkoxide can create some non-hydrolytic M-O-M' formation, with liberation of the alkyl acetate (Equation 3.3).

(3.3) $M(OR)_x + M'(OAc)_y \rightarrow (RO)_{x-1}M-O-M'(OAc)_{y-1} + ROAc$
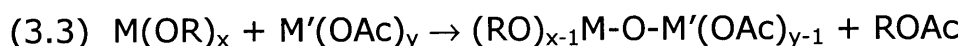
Likewise, a metal halide may be used in conjunction with a metal alkoxide to produce a mixed alkoxide, with liberation of the alkyl chloride (Equation 3.4).[20]

(3.4) $M(OR)_x + M'X_y \rightarrow (RO)_{x-1}M-O-M'X_{y-1} + RX$
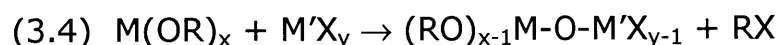
Nonhydrolytic routes to gels, particularly where silicon and a transition metal are required in the same gel, are an active area of research.[19] Such routes provide a work-around for the problem of the faster hydrolysis of transition metal alkoxides, compared with the hydrolysis rate of the analogous silicon alkoxides.

3.1.4 Gel-to-Ceramic Transition

Once the gel is formed, heat treatment converts it to an inorganic oxide ceramic. During this step, the organic solvent further evaporates from the gel and organic ligands are pyrolyzed; some structural rearrangement and densification occurs; the structure crystallizes (and at higher temperature, sinters). The structure of the gel and the degree of real atomic-level mixing that has occurred in the gel will greatly affect the temperatures at which each of these stages will occur.

Differences in the gel morphology can lead to different behavior on solvent removal and densification. Linear polymeric chains undergo considerable collapse and structural rearrangement and pack into a high-density, low-porosity dried gel. Highly crosslinked gels, on the other hand, tend to maintain their structure on solvent removal, leaving pores where solvent had been and leading to a low-density dried gel. In both cases, as normal drying occurs, the gel shrinks by a large amount, and it often cracks due to the high capillary forces developed by the solvent in the gel pores. Slow drying permits the gel to dissipate the stresses built up in this way, so that the resulting xerogel will be uncracked. Gels with a particle-type or cluster-type morphology tend to have larger pores than those with a highly-crosslinked polymer morphology, so that the capillary stresses associated with the solvent drying out of the pores are smaller.

The use of drying control chemical additives (DCCAs) in alkoxide sol-gel preparations minimizes the vapor pressure of the solvent in the pores, reduces the pore size distribution, and

decreases the drying stresses. Common DCCAs include formamide, glycerol, oxalic acid, glycols, and ethanolamines.[21,22]

Drying the gel under supercritical conditions for the solvent in question – e.g. at a position in its phase diagram where the liquid/vapor phase boundary has disappeared – leads to uncracked and mostly unshrunken aerogels. These materials have low density and very high porosity.

No matter how the drying process is done, there still will remain unhydrolyzed organic-containing ligands that need to be driven out of the gel by pyrolysis. This must be done while there is still some porosity to the gel, so that gases produced from pyrolysis of the organics can escape without cracking the gel. As the processing temperature is increased, viscous sintering, driven by the reduction in surface free energy, occurs. Finally, the metal and oxygen atoms rearrange into the crystal structure predicted by the elements' phase diagram according to composition of the gel and the treatment temperature, or kinetic products may result. This occurs at a much lower temperature than it would in a traditional solid-state synthesis, in which metal oxide powders are mixed and heated, because the intimate mixing of the metals has already occurred in the gel formation, while in solid state syntheses atoms of each metal must cross grain boundaries in order to come into proximity with each other.

While much of the above discussion of the care required in the drying step applies to gel monoliths, the principles of gel densification and drying are similar for sol-gel production of films. Films deposited as a single thick coating are prone to crack due to capillary pressure in the pores. On the other hand, films created by

the repeated deposition of thin layers must be dried and in many cases pyrolyzed as each layer is deposited, so that gases created by the decomposition of organics in layer *n* do not escape in such a way as to destroy layer *n+1*. An additional problem in the drying stage of film deposition is that anisotropic shrinkage can cause "mud cracking" or "islanding," as the film shrinks back from cracks. Delamination, or peeling, of the film from the substrate can also occur. (Figure 3.1)

3.1.5 Applications and Outlook

As indicated above, the sol-gel method brings with it a number of benefits over more traditional methods of ceramic synthesis due to the atomic-level mixing of the metals which can occur in the sol and gel. This permits crystallization and sintering to happen at a lower temperature than for mixed-oxide powder methods, producing savings in time, capital equipment, and energy. Furthermore, lower temperatures help to avoid contamination of the sample from the pyrolysis container or furnace materials, so that sol-gel processes can provide higher-purity materials than powder syntheses. Phases and microstructures not available in high-temperature processing are accessible via the sol-gel method. Because some sintering occurs during a high-temperature powder synthesis, finely-divided powders are difficult to obtain, while sol-gel precursors – often combined with spray pyrolyses – may lead to high-surface-area, fine, and reasonably monodisperse powders. Finally, the sol-gel method permits solids to be fabricated in a

number of forms, including not only powders, but monoliths, fibers, and films.

In particular, films of ceramics for electronic and magnetic applications have been extensively produced by the sol-gel process.[23] High-temperature superconductors, most notably $YBa_2Cu_3O_{7-\delta}$,[24,25] electrochromic ceramics such as V_2O_5 and WO_3,[23] ionic conductors (YSZ),[26-28], dielectrics such as $SrTiO_3$,[29] and ferroelectric perovskites, particularly those in the lanthanum-modified lead zirconate titanate (PLZT) system,[30,31] have been widely studied for sol-gel depositions. Another ferroelectric, lithium niobate, $LiNbO_3$ (LNO), melts incongruently at an equimolar ratio of Li and Nb, resulting in inhomogenous single crystals. As a result, it is extremely difficult to prepare LNO by conventional (solid state) methods. However, there are a number of reports for the preparation of LNO by sol-gel processing.[32,33] Finally, the layered ferroelectric $Bi_4Ti_3O_{12}$ has been prepared in bulk[34,35] and in thin film form[36,37] by the sol-gel method.

Commercialization of the sol-gel process requires the ability to fabricate on a large scale or with high throughput, and profitability must be demonstrated. Recently, sol-gel derived electrical and magnetic ceramics, including alumina substrates (Mitsubishi), layered ceramic capacitors (NEC), and silica display panel spacers and printed circuit boards (GelTech) went into production.[23] Trends in the microelectronics industry are expected to lead to further commercial application of sol-gel derived materials. Antireflective and other optical coatings have been applied by dip-coating sol-gel precursor solutions onto glass panes and mirrors for years,[21] and it

can be expected that this trend will continue. The technology, therefore, is present or within reach for scale-up and commercial application of the sol-gel deposition of oxide-ion conducting films described in this work.

3.1.6 Other precursor routes

Certain other precursor routes to oxide ceramics show potential for the production of film-castable multicomponent solutions. Hydroxycarboxylic acids (citric, lactic, or tartaric), which form polybasic acid chelates with metal ions, metal salts (nitrates, carbonates, and hydroxides), and polyhydroxyl alcohols (ethylene glycol) may be co-dissolved; the condensation reaction between the metal chelate and the alcohol may then form an ester. On heating, polyesterification occurs, resulting in a homogenous solution of the metal ions in an organic matrix. This stable solution is film-castable and dries to a glass, which can then be calcined to a dense material.[38] The process is variously known as the "Pechini process" or the "amorphous citrate process." Powders of $Pb_3MnNb_2O_9$ are reported to have been synthesized by this route,[39] as have strontium and lanthanum manganese oxides;[40] however, there have been few, if any, reports of the use of this process in film casting. A similar process, entailing the use of glycine and metal nitrates, has been reported, but due to the sometimes violent exothermic decomposition that occurs on heating, it is unlikely to be of use in the synthesis of anything but powders.[41] Polyacrylamide gels[42] and polyethylenimine[43] have also been used as an organic matrix for maintaining multiple metal ions in simultaneous solution.

Finally, yttria, zirconia, and YSZ thin films have been prepared from solution of metal carboxylate precursor salts in a carboxylic acid/amine solvent system. The precursor salts were prepared by reacting the metal nitrates with ammonium trimethylacetate and dissolved in propionic acid/amylamine/xylene. The resulting solution was spin-cast onto Si(111) substrates to produce dense, if somewhat granular films.[44]

3.1.7 Outline of the Research Done

Our initial approaches to producing a film-castable sol containing 2 Bi: 1 V centered on the use of vanadic acid condensation to polyvanadic acid to produce a gel network. The bismuth was to be introduced as a salt dissolved in the trapped solvent. As discussed below, most attempts along this line of research led to preferential precipitation of 1:1 Bi:V materials. Other formulations led to thick granular films with large-scale cracking. Reports of this work make up the remainder of Chapter Three. Chapter Four discusses work in which the gel-producing materials were vanadium alkoxides.

3.1.8 Vanadic Acid Background

Vanadium pentoxide gels have been the subject of extensive research due to their electrical properties. Their electrical conductivity is high, and they exhibit semiconducting behavior. They have been examined for use in antistatic coatings and switches.[45]

Vanadium pentoxide gels may be prepared by pouring molten V_2O_5 into cold water[46] or by the polycondensation of decavanadic acid, which in turn is obtained by running sodium metavanadate, $NaVO_3$, over an acidic ion-exchange resin.[47] In reality, the specific vanadate species present in a solution, and their degrees of condensation, depend on the pH and total concentration of vanadium. While in very basic solution the primary species is $[VO_4]^{-3}$, protonation of the orthovanadate ion followed by condensation leads to pyrovanadate ion $[V_2O_7]^{4-}$, and repetition of the protonation and condensation reactions lead up through $[V_4O_{12}]^{4-}$ as the acidity rises. In acidic solution, protonation and condensation of the species $[V_3O_9]^{3-}$ leads to the decavanadate anion[48] $[H_2V_{10}O_{28}]^{5-}$ until the pH drops far below the isoelectric point of pH 2.2, when the polymer is broken up and VO_2^+ and/or VO^{3+} are formed.[49] Decavanadic acid ($H_4V_{10}O_{27}$), in turn, undergoes polycondensation to create fiberlike sol particles which may then make up a gel. While the gels can be produced by adding acids, e.g. HNO_3, to vanadate salts (NH_4VO_3, $NaVO_3$), this leaves unwanted ions in the gel.[23] Depending on the concentration of the vanadium species and the pH, the gelation will occur within 2-50 hours.

Tetravalent vanadium serves as a polymerization inititator. It may be formed (at about 1%)[45] during the ion exchange process from sodium metavandate to vanadic acid, or from the oxidation of organics in the solution by V^{5+}. The polymerization is autocatalytic.[47]

The vanadium oxide gel structure is made up of flat ribbons some 1000 Å long and 100 Å wide and having a structure similar to

that of the **ac** plane of orthorhombic V_2O_5, *i.e.* edge-shared VO_5 pyramids.[45,50] This basic ribbon structure is considered to be the root of the gel's layered nature. When deposited as thin films, vanadium pentoxide sols produce a highly-oriented layered structure where the layer planes are parallel to the substrate.[51]

The layered structure of the V_2O_5 gel has been pillared with a number of cations of varying sizes and charges: the alkali and alkaline earth metal cations, NH_4^+, several transition metal cations, and Al^{3+}, as well as with the Al_{13} cation and the Mo_6 and Nb_6 chloride clusters.[52] Therefore, we thought that vanadic acid sols would be a good starting point for creating precursors to the BiMeVOx oxides.

Figure 3.1: ESEMs of films showing mudcracking (a, X 710; b, X 310) and delamination (c, X 1150).

(a)
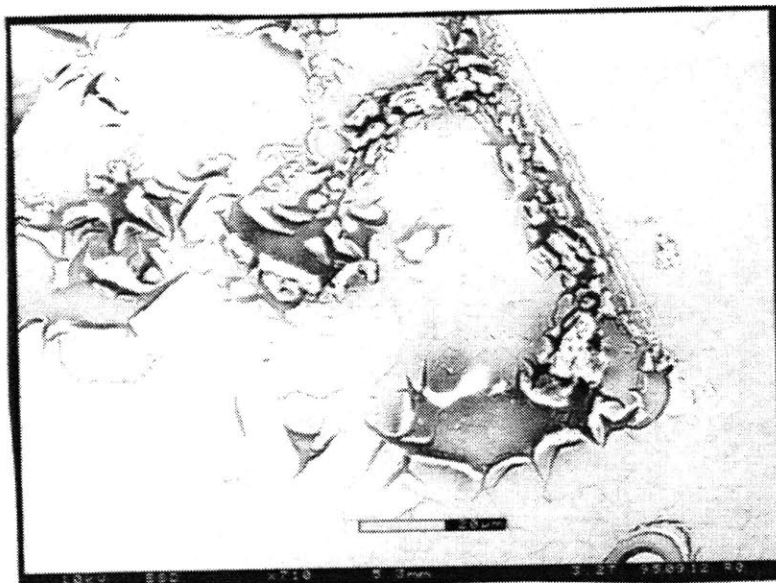
(b)

(c)

3.2 Results and Discussion

Initially, 0.1M solutions of $NaVO_3$ were ion-exchanged and mixed with $Bi(NO_3)_3 \cdot 5H_2O$ dissolved in glacial acetic acid at room temperature or with Bi_2O_3 partly dissolved in hot glacial acetic acid. In both cases an immediate precipitate formed—this was calcined and found to be $BiVO_4$. (Expts. 1-2, Figure 3.2) Higher concentrations of $NaVO_3$ in the initial solution were tried in the hope of providing a higher probability for gelation (0.1M solutions gelled after 24 hours in the absence of the bismuth salts). Therefore 0.5 M vanadate solution, which gelled after 12 hours in the absence of the bismuth salts, was used with each of $Bi(NO_3)_3 \cdot 5H_2O$ and Bi_2O_3, and an alcohol (2MOE) provided as a sacrificial reductant, so that V(IV) would be generated to catalyze the gel-forming polymerization. In both cases here as well, a precipitate formed immediately, and after calcining these precipitates were identified as a mix of Bi_2O_3 and $BiVO_4$, plus an unidentified minor phase. (Expts. 3-4, Figure 3.3) The minor phase may be a sodium-containing oxide of Bi and/or V, which would occur if the ion-exchange on the column was incomplete. A still-higher concentration (0.6 M) of $NaVO_3$ was also tried; Bi^{3+} was put into solution by dissolving Bi_2O_3 in HNO_3. This provided more free H^+ for exchange with the sodium metavanadate, so that even if the column failed to exchange the sodium for protons, the strong acid was likely to work. In addition, it was hoped that the decreased pH would serve to prevent preferential precipitation of any bismuth-containing species prior to gelation.

However, the initial try here (Experiment 5) still resulted in a precipitate which on calcining was identified as a mixture of $BiVO_4$ and $Bi_2VO_{5.5}$ (Figure 3.4); the mother liquor gave $BiVO_4$ only. Aging of the ion-exchanged vanadate solution prior to the addition of the bismuth-containing solution permitted polymerization of the vanadic acid to begin, as evidenced the appearance of red fibrils in the beaker (Experment 6); addition of the bismuth solution gave a clear solution which was stable at least overnight. Slow evaporation of the solvent gave a precipitate which even prior to calcination could be identified as a mix of $BiVO_4$ and $Bi_2VO_{5.5}$. Repetition of the experiment gave a solution which was stable for at least two days (Experiment 7). The solid left behind from evaporation of the solution was calcined for 10 hours at a number of temperatures. For temperatures up to 550 °C the solid was identified by XRD as a mixture of $BiVO_4$ and Bi_2O_3; by 650 °C peaks associated with $Bi_2VO_{5.5}$ started to appear, and by 750 °C the calcined product was a mixture of $BiVO_4$ and $Bi_2VO_{5.5}$ only. No Bi_2O_3 was found in any of these samples, but it may have been hidden under the background as an amorphous phase.

Ion-exchanged $NaVO_3$ solutions did not prove to be useful precursor solutions at any of the concentrations tried. The presence of acetic or nitric acids inhibited the gelation of vanadate solutions somewhat, but in the presence of the bismuth salts, these solutions would not gel at all. Instead, precipitates formed which were often identifiable by powder XRD as $BiVO_4$, even prior to calcination. Whether this is due to destabilization of the poly(vanadic acid) sol because of the bismuth salts' ionic strength contribution (or in the case of the suspensions, the presence of

nucleation sites for flocculation), or because of a disruption of the condensation reactions leading to poly(vanadic acid) in the first place, is unclear.

Due to the doubt regarding whether complete ion exchange was occurring between the sodium metavanadate and the resin, we began to test ammonium metavanadate for its ability to ion-exchange with a strong acid and thereby to produce the vanadic acid required for polymerization and gelation. Excess ammonium-containing salt was expected to burn out during the calcination step in air, unlike sodium-containing salts in the $NaVO_3$ preparations. Several concentrations of NH_4VO_3 were tested for gelation using glacial acetic acid and a combination of nitric and acetic acids to provide excess H^+. (Expts. 8-10) While acetic acid alone gave gel-like chunks in the solvent with 0.5 M NH_4VO_3, it gave a fibrous semigel which became a chunky gel overnight with 0.25 M NH_4VO_3. The use of HNO_3 alone or with acetic acid gave similar results. Thus both acids, at least in principle, could be expected to work with the ammonium metavanadate to give the V_2O_5 gel as required.

Initial experiments combining 0.25 M NH_4VO_3 with bismuth solutions (Experiments 11-13) gave precipitates which in all cases were identified as $BiVO_4$. Evaporation of the solvent from a suspension of supernatant and precipitate gave a homogenous solid which after calcination at 725 °C gave $Bi_2VO_{5.5}$ or a mixture of $BiVO_4$ and $Bi_2VO_{5.5}$. (Figures 3.6, 3.7) At about the time this work was being done a report appeared in which $Bi(NO_3)_3 \cdot 5H_2O$ and NH_4VO_3 were co-dissolved in concentrated HNO_3—quantities are not reported—and the solution subsequently diluted and anion-extracted to precipitate a solid which, after heating to 350 °C, had

the composition $Bi_4V_{2.1}O_{11.2}$ and was isomorphous with the γ phase

of $Bi_2VO_{5.5}$.[53] However, in our similar experiment (Experiment 11)

we observed a precipitate immediately on dilution.

Because it was suspected that the "precipitate" observed was

the flocculant from an unstable sol, several experiments used gum

arabic, a polysaccharide colloidal stabilizer, to keep all of the ions in

a common liquid phase. (Expts. 13-14) The precursor "solution"

was opalescent when the bismuth and vanadium components were

mixed at 40 °C. This suspension was evaporated and the calcined

solid identified as V_2O_5 + Bi_2O_3. (Expt. 13) For room temperature

mixing a clear solution was obtained (Expt. 14) but a solid settled

out over several days. This solid, when calcined, was identified as

$BiVO_4$. The suspension, with plasticizers ethylene glycol and glycine

added, gave $Bi_2VO_{5.5}$ after 22 h at 750 °C. This compares with the

behavior of a simple mixture of Bi_2O_3 and V_2O_5, which – unground

and not pressed into a pellet – remained as the starting materials

after a similar heat treatment. The precipitates in these

experiments could be redissolved with the addition of more nitric

acid; evaporation of these solutions gave Bi_2O_3 and V_2O_5, or in some

cases $BiVO_4$ (experiments not detailed here).

A number of reports cite the use of ethylene glycol alone or in

combination with glycine (Pechini process[38]) to obtain a gellable

sol.[23,28,54] Co-dissolution of NH_4VO_3 and $Bi(NO_3)_3 \cdot 5H_2O$ in

ethylene glycol and water gave a precipitate (Experiment 15).

Addition of glycine did not redissolve the solid, which after

calcination was identified as a mix of $BiVO_4$ and $Bi_2VO_{5.5}$. Likewise,

adding glycine to a similar mix initially (Experiment 16) gave a

reasonably stable paintlike suspension that after calcination was identified as $BiVO_4$ plus Bi_2O_3.

Thus the approach using NH_4VO_3 was only able to produce a stable solution (sol) in the presence of colloidal stabilizer gum arabic and excess nitric acid, and even then, a flocculant/precipitate appeared after 24-48 hours at room temperature. Plasticizers ethylene glycol and glycine did not improve matters. In all cases, the precipitate, even after high-temperature calcination, gave the 1:1 $BiVO_4$ phase with some $Bi_2VO_{5.5}$ in many cases, for the highest calcination temperatures.

Several factors appear to be at work in causing the failure of these experiments to produce a stable film-castable solution that would result in the formation of $Bi_2VO_{5.5}$. In many cases, the concentration of vanadic acid may have been too low to provide for sufficient polymerization. That $BiVO_4$ precipitated out, in a form sufficiently crystalline, in many experiments, to diffract X-rays even without heat treatment, points to a certain thermodynamic stability that the assorted methods tried just could not overcome. Experiments with the solid-state reaction of $BiVO_4$ with Bi_2O_3 demonstrate that the former will indeed incorporate more bismuth to form the desired $Bi_2VO_{5.5}$ phase (Experiment 16). In light of the solid state experiments, however, it is surprising that even in experiments where the solution was boiled down along with the precipitate, so that no metals should have been lost, in most cases the major phase produced was $BiVO_4$. This suggests that the degree of homogeneity and intimate contact between the bismuth and vanadium species in these preparations is *less* than that obtainable by hand-grinding in a mortar! However, in cases where

the solids were not ground together, but were simply stirred, neither $BiVO_4$ nor $Bi_2VO_{5.5}$ formed after 20-25 h at > 700 °C, so those experiments reported here which gave $Bi_2VO_{5.5}$ had at least some advantage over a simple mixing of the solid reagents. Preferential precipitation of the $BiVO_4$ certainly played a role in the dehomogenization; also, the crystallization of bismuth nitrate out of the gels during the drying stage may have contributed to the loss of homogeneity.[1,55]

Figure 3.2: Precipitate from Experiment #1, calcined. Lines marked show positions of BiVO₄ (JCPDS 14-688) peaks.
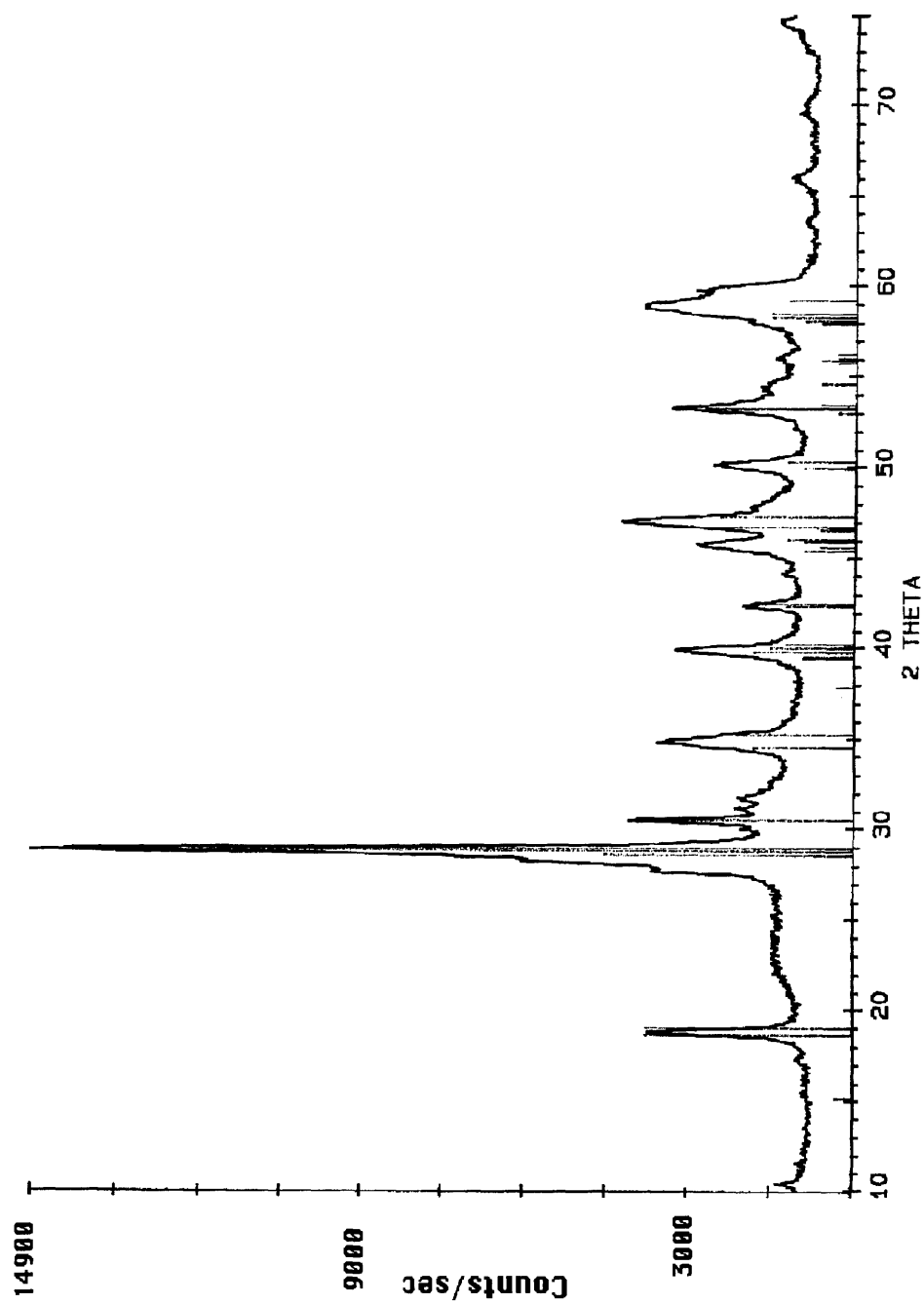
Figure 3.3: Precipitate from Experiment #3, calcined. o = BiVO₄ peak positions (JCPDS 14-688), x = Bi₂O₃ peak positions (JCPDS 14-699), unmarked peaks are an unidentified phase.
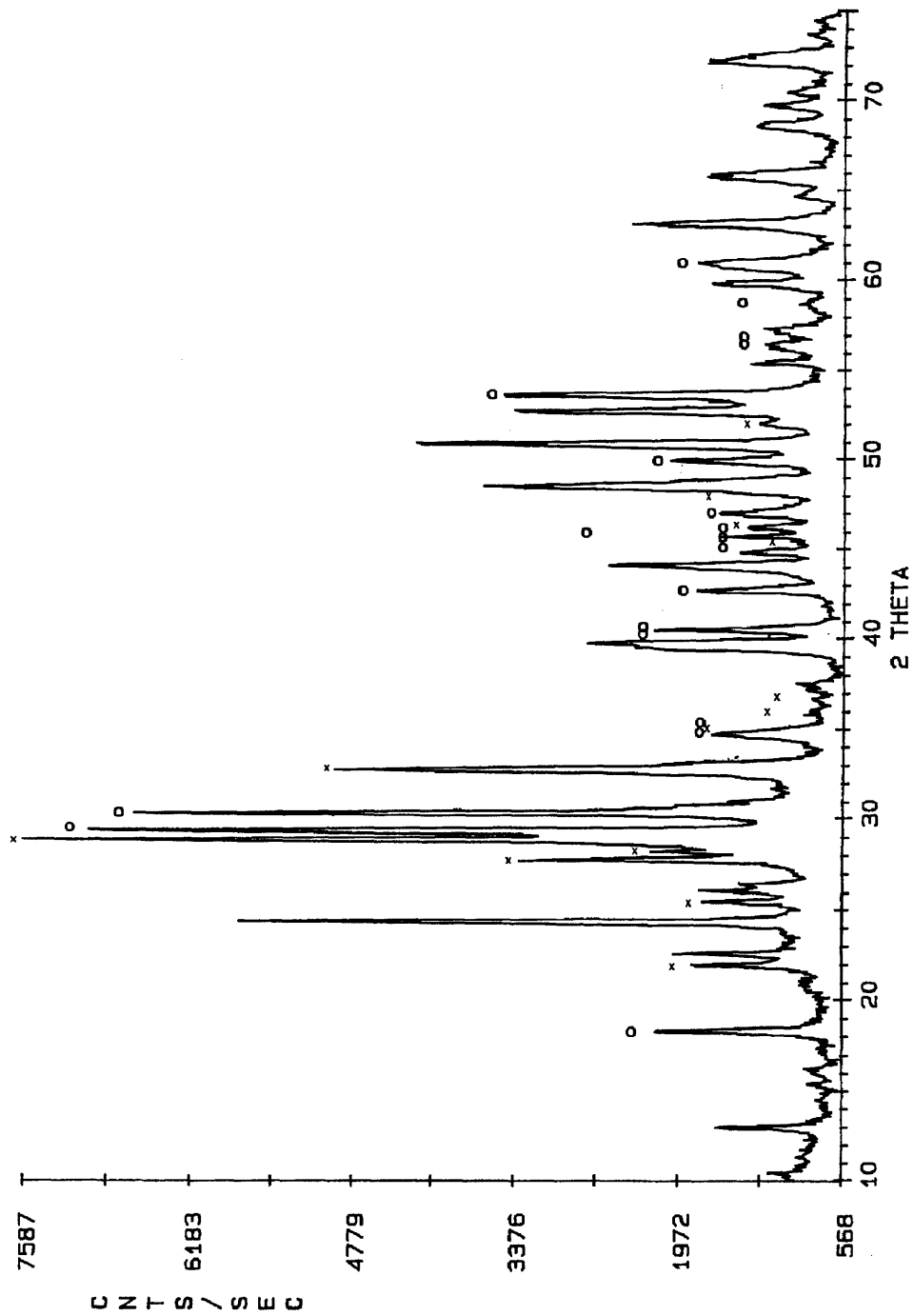
Figure 3.4: Precipitate from Expt. #5, calcined. Lines marked indicate $BiVO_4$ (JCPDS 14-688) peak positions; o = α-$Bi_2VO_{5.5}$ peak positions (based on Abraham et al.[56]).
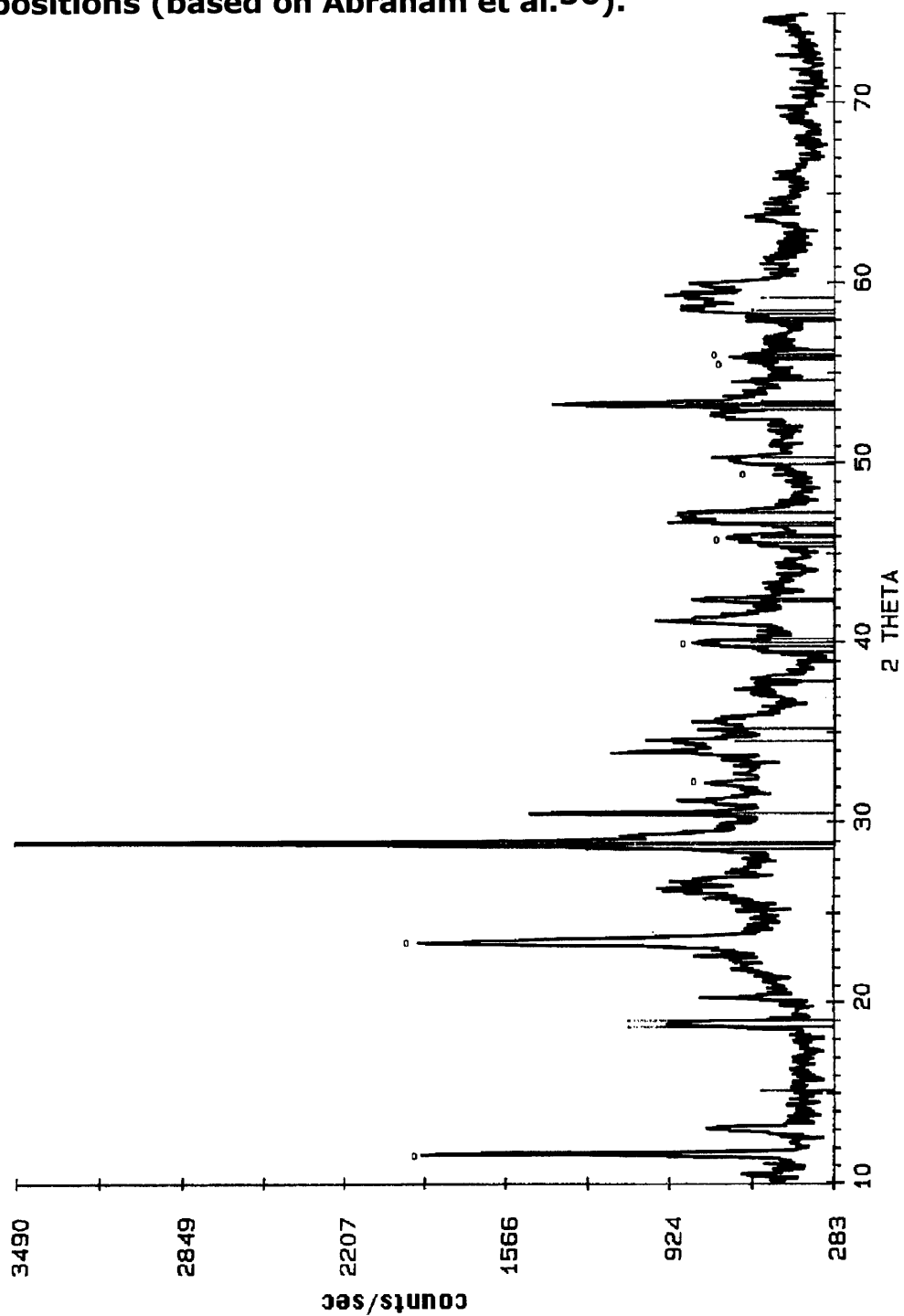
Figure 3.5a: Experiment #7, solvent evaporated from preparation, solid calcined at 350 °C. Lines indicate position of BiVO₄ (JCPDS 14-688) peaks.
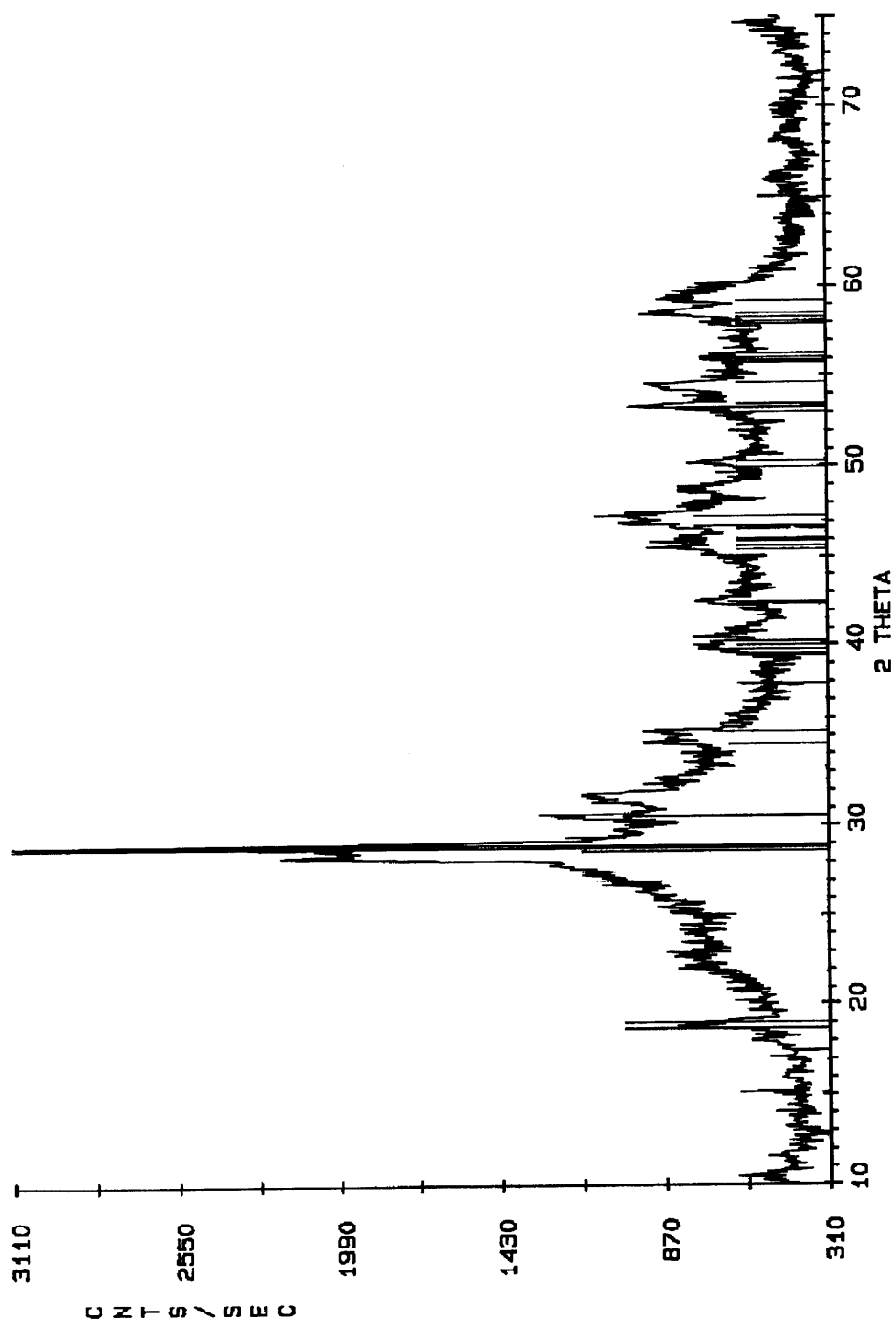
Figure 3.5b: Experiment #7, solvent evaporated from preparation, solid calcined at 550 °C. Lines indicate position of BiVO$_4$ (JCPDS 14-688) peaks.
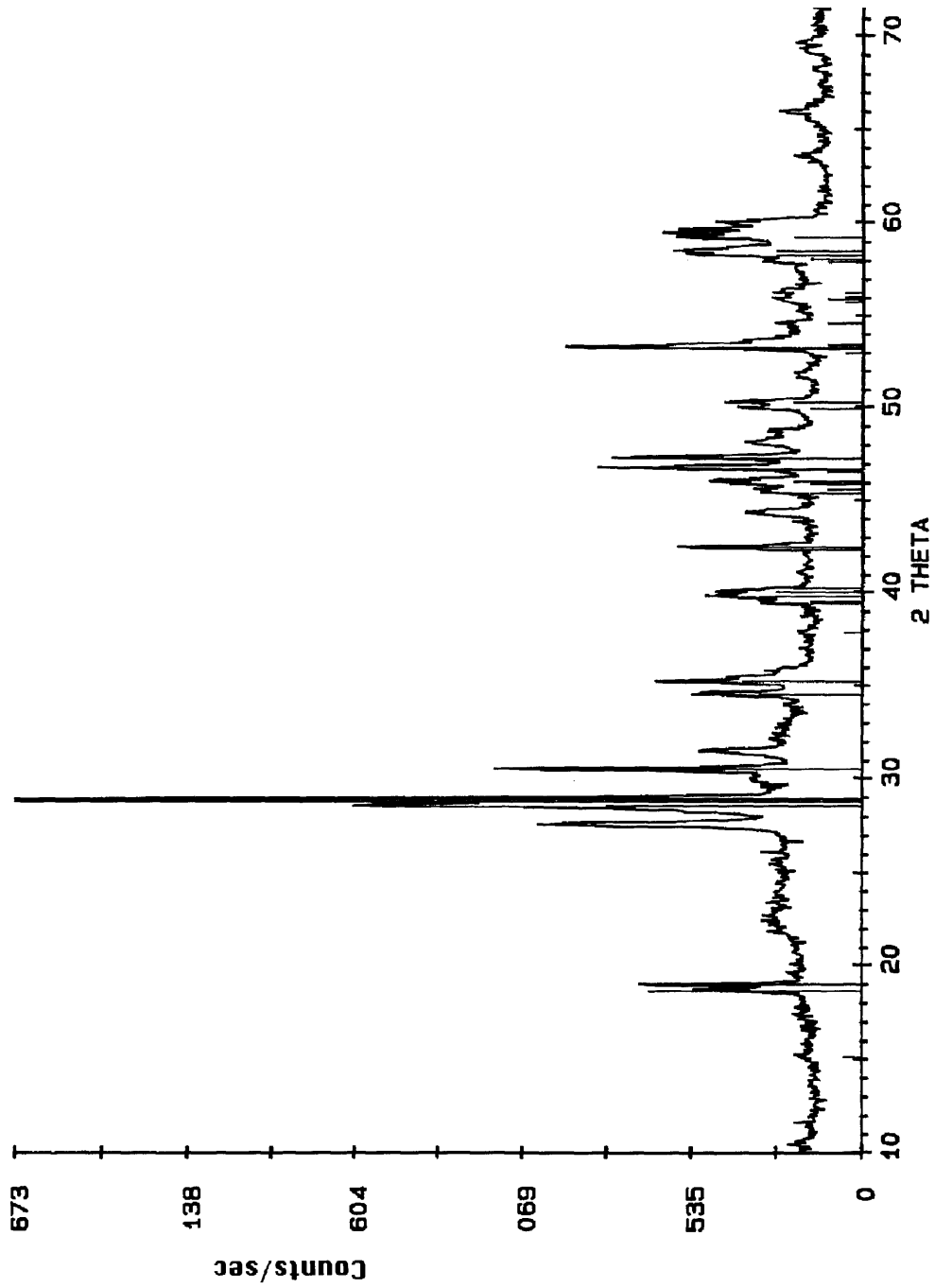
Figure 3.5c: Experiment #7, solvent evaporated from preparation, solid calcined at 750 °C. Lines indicate position of BiVO$_4$ (JCPDS 14-688) peaks, * = α-Bi$_2$VO$_{5.5}$ peak positions.
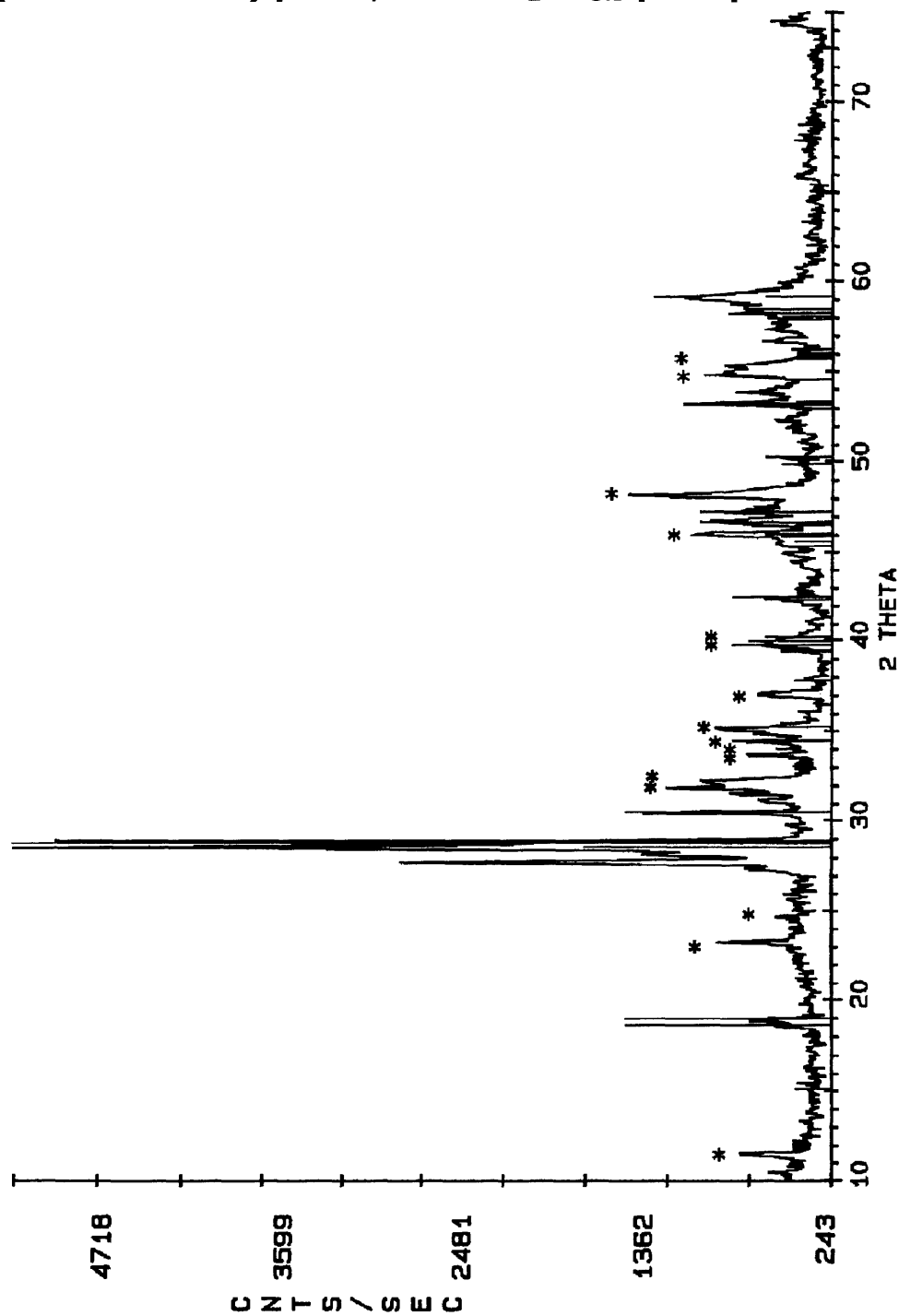
Figure 3.6: Experiment #11, solvent evaporated from preparation and solid heated at 400 °C for 6 h, then 725 °C for 36 h. Lines marked show positions expected for $BiVO_4$ (JCPDS 14-688), * = peak positions for α-$Bi_2VO_{5.5}$.
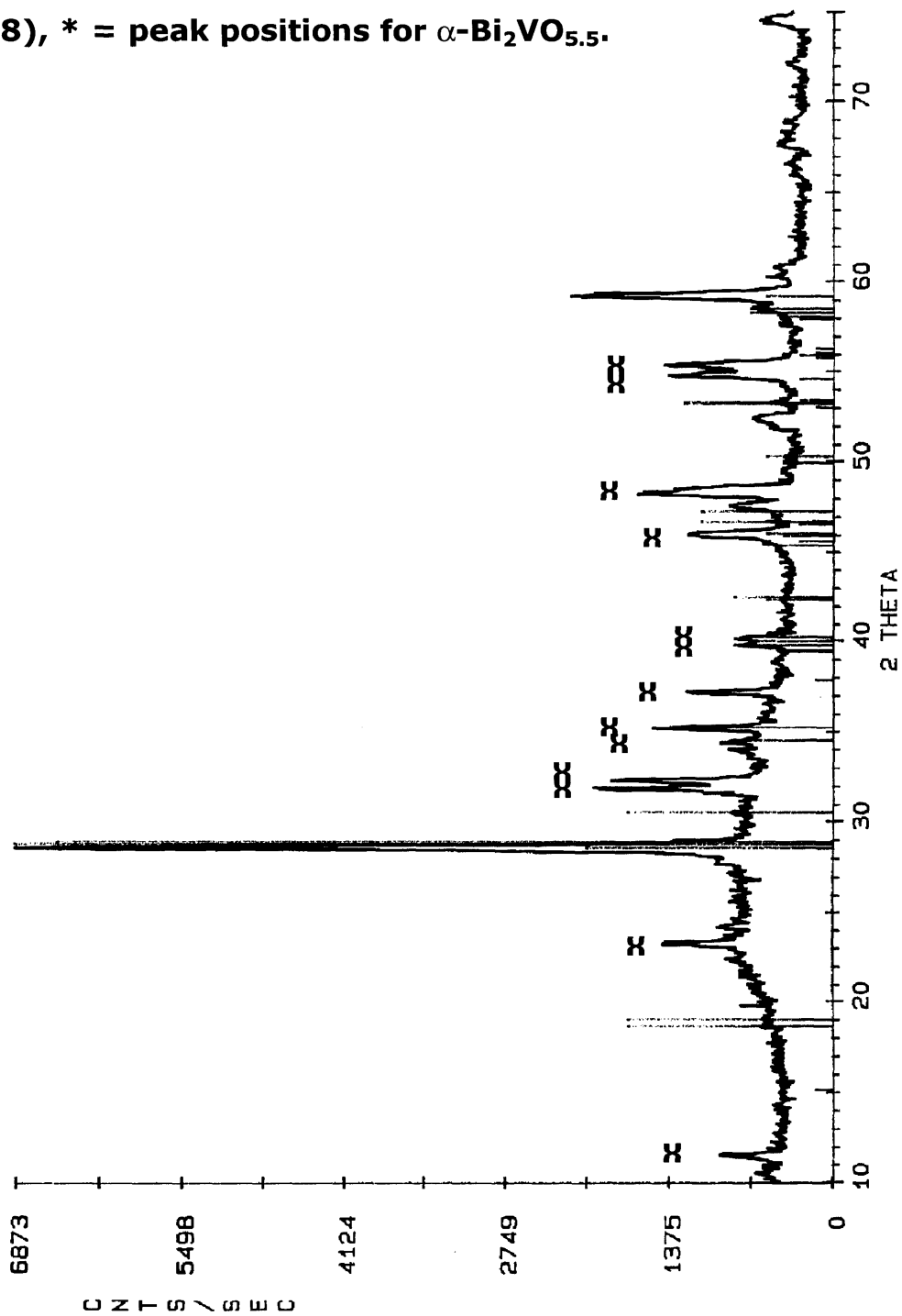
Figure 3.7a: Experiment #12, solvent evaporated from suspension and solid heated 400 °C for 6 h. Lines marked indicate positions of BiVO$_4$ (JCPDS 14-688) peaks, o = Bi$_2$O$_3$ peaks (JCPDS 14-699).
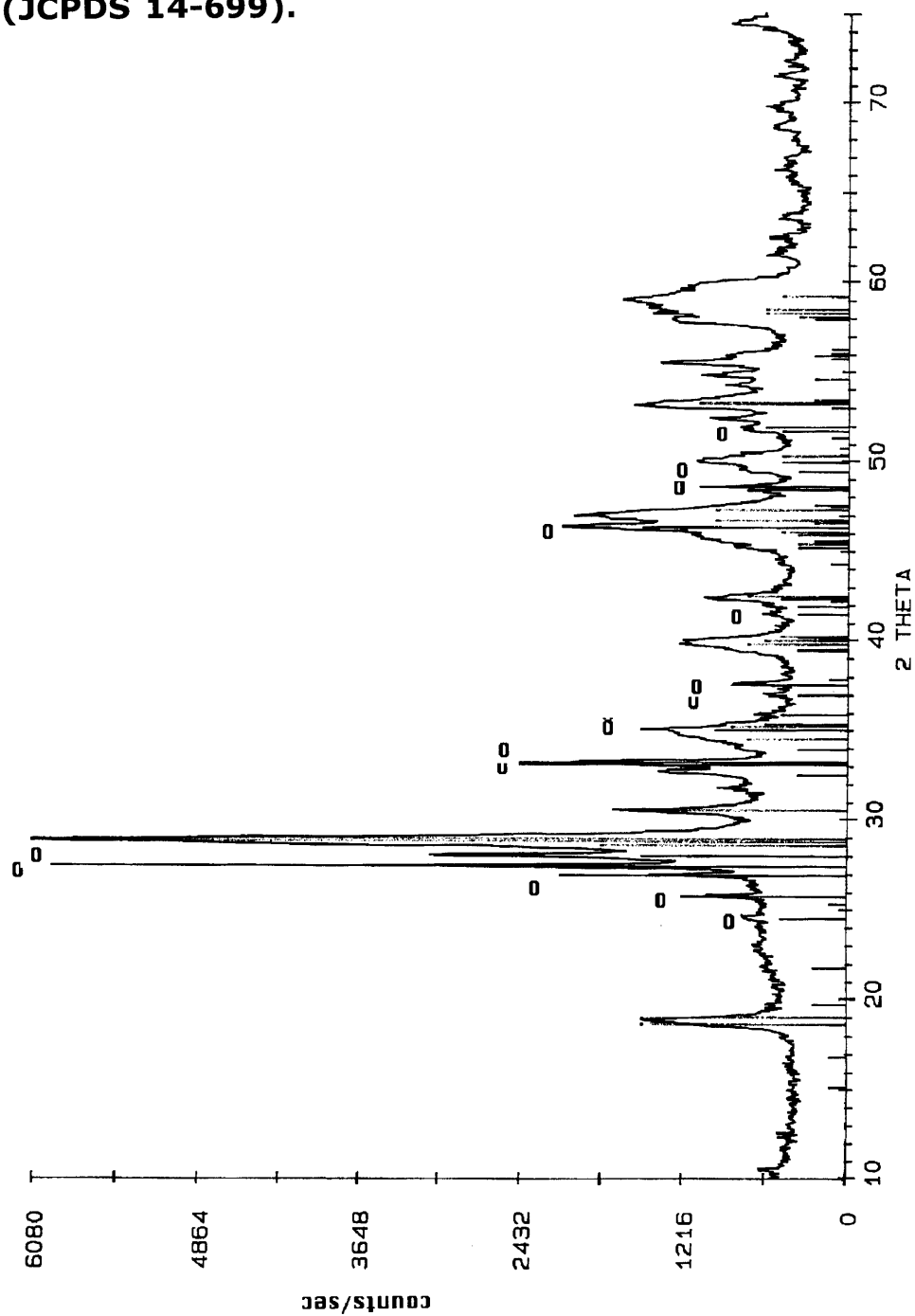
Figure 3.7b: Solid shown in Figure 3.7a, heated at 725 °C for 36 h. All peaks are in the proper positions for α-Bi$_2$VO$_{5.5}$.
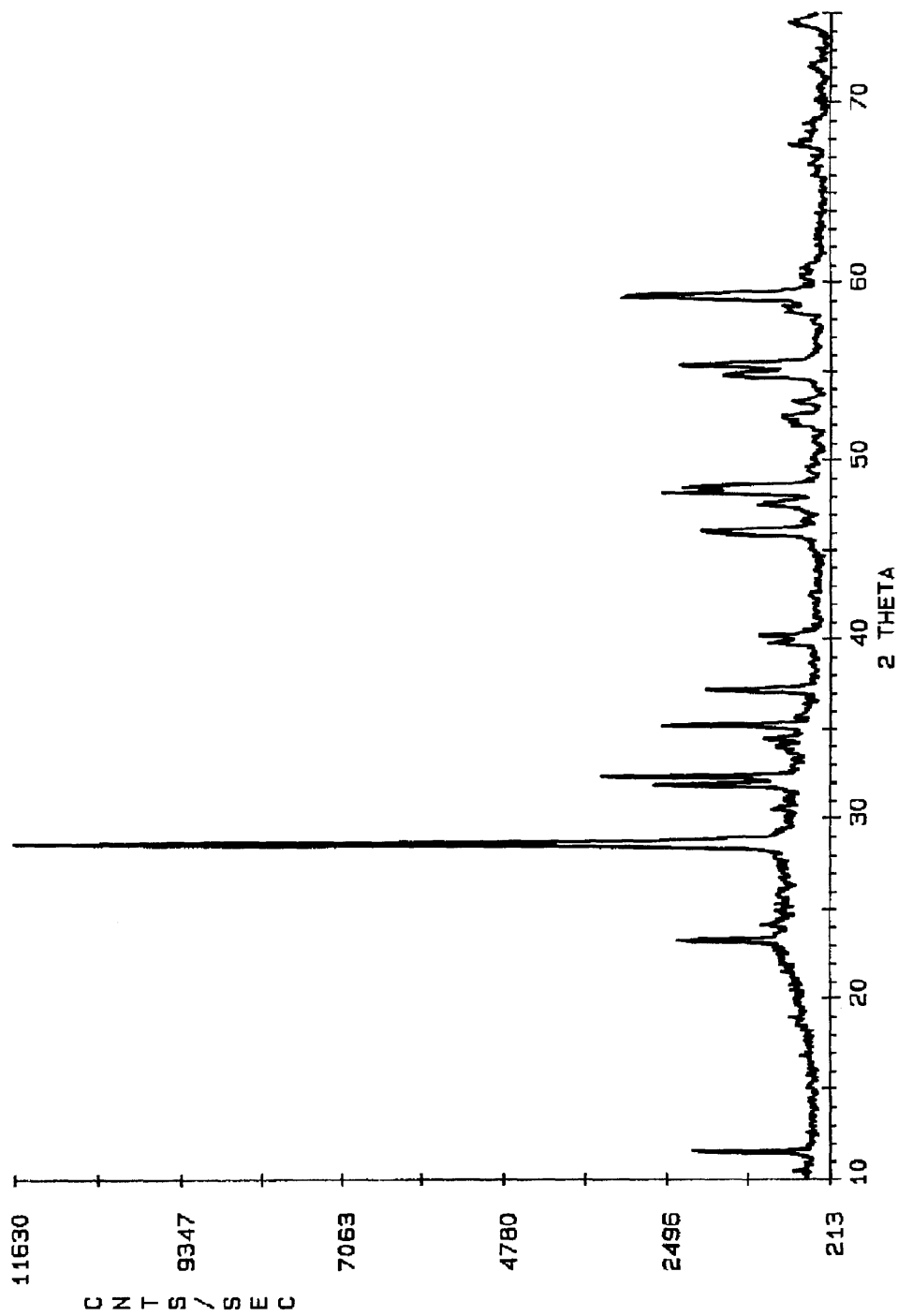
3.3 Conclusions

Vanadic acid gels were intended for use as a gel matrix in which bismuth ions would be trapped in solvent pockets. Gels were successfully made by ion-exchange of sodium metavanadate solutions or by providing excess acid to ammonium metavanadate solutions. However, the conditions under which the bismuth salts were soluble were anathemic to the vanadic acid. In most cases, a precipitate which was directly identifiable by powder XRD as $BiVO_4$, or which formed $BiVO_4$ after calcination at low temperatures, appeared on mixing or brief standing of the Bi/V precursor solutions. Those solutions which were stable contained large amounts of acid, and were found to be non-gelling and not film-castable. Due to the problems found with this particular approach to forming a film-castable solution, vanadium alkoxides were next tried, again to produce a gel matrix which would hopefully trap the bismuth ions homogeneously. That work is the subject of Chapter Four.

3.4 Description of Salient Experiments

All experiments were performed in open air. The ion-exchange resin was packed in a 1-inch diameter glass tube fitted with a burette valve and having glass wool at the bottom to prevent loss of the resin. The tube was loaded with approximately 100 g of the resin to create a column some 14 inches high. Between uses, the resin was regenerated by washing with 1M H_2SO_4. All pyrolyses

were done in Al_2O_3 crucibles in air. Materials and instrumentation used in this Chapter are listed and described in the Appendix to Part I of this thesis.

It should be noted that the term "solution" below is being used loosely to refer to both true solutions and colloidal suspensions where the liquid phase was clear to the eye (e.g. particles small enough not to scatter visible light). Where the distinction is important, "sol" will be used. The abbreviation "2MOE" indicates 2-methoxyethanol.

3.4.1 Experiments using NaVO₃

Experiment 1 (JWP/I/110N) 0.1 M NaVO₃ + Bi(NO₃)₃·5H₂O in acetic acid

A 0.1M aqueous solution of $NaVO_3$ (1.2191g, 10 mmol in 100 ml water) was made. A solution of 10 mmol of $Bi(NO_3)_3 \cdot 5H_2O$ (4.8516g) in approximately 50 ml of glacial acetic acid was made. The $NaVO_3$ solution was poured down the ion-exchange column and, after the first 10 ml of eluant were discarded, 50 ml were measured to deliver 5 mmol of vanadium. This yellow-orange solution was mixed immediately with the bismuth nitrate solution, and became slightly milky. Heating the solution for 5 minutes with stirring resulted in a dark orange solution and precipitate. The mixture was allowed to stand, covered, at room temperature for 24 h. The mixture was filtered to remove precipitated solids and 15 ml ethanol (95%) added. After another 24 h the liquid was decanted

off and the solid calcined at 200 °C for 1 h, then for 11 h at 450 °C. The resulting pale yellow solid was characterized by XRD as $BiVO_4$, JCPDS 14-688. (Figure 3.2)

Experiment 2 (JWP/I/110A) 0.1 M $NaVO_3$ + Bi_2O_3/acetic acid

A 0.1 M solution of $NaVO_3$ was prepared as above. Bi_2O_3 was dissolved in hot glacial acetic acid and the white crystals that formed on cooling collected (JP/I/106). This solid, thought to be $Bi(OAc)_3$, (3.8616g, 10 mmol) was stirred in 150 ml hot glacial acetic acid; most of it dissolved. The $NaVO_3$ solution was poured down the ion exchange column and after the first 10 ml was discarded, 50 ml (5 mmol vanadium) added to the hot bismuth acetate solution. A fluffy precipitate formed immediately. The mixture was filtered after 24 h and 15 ml ethanol (95%) added; after another 24 h the liquid was decanted off and the solids calcined as above. The XRD pattern was that of $BiVO_4$, 14-688.

Experiment 3 (JWP/I/113N) 0.5 M $NaVO_3$ + $Bi(NO_3)_3·5H_2O$/ acetic acid/ 2MOE

A 0.5 M solution of $NaVO_3$ was prepared by dissolving the solid (6.095g, 50 mmol) in 100 ml deionized water. A solution of $Bi(NO_3)_3·5H_2O$ was prepared by dissolving (4.8527g, 10 mmol) in 20 ml warm glacial acetic acid. 2-methoxyethanol (5 ml, 66 mmol) was added. The $NaVO_3$ solution was poured down the ion exchange column and the first 10 ml discarded, then 10 ml (5 mmol) mixed with the $Bi(NO_3)_3$ solution. A milky yellow-white gel-precipitate

instantly formed. This was permitted to age at room temperature 24 h, then added directly to a crucible as a wet gel. After calcining as above, the XRD pattern showed a mixture of $BiVO_4$ (14-688), Bi_2O_3 (14-699), and peaks belonging to an unknown phase(s). (Figure 3.3)

Experiment 4 (JWP/I/113A) 0.5 M NaVO$_3$ + Bi$_2$O$_3$/acetic acid/ 2MOE

A 0.5 M solution of $NaVO_3$ was prepared as above. The white bismuth solid prepared in Expt. 2 (1.9305 g, 5 mmol) was stirred in 85 ml hot glacial acetic acid and 5 ml 2MOE (66 mmol). Most of the solid dissolved. To this was added 5 ml (2.5 mmol vanadium) of the ion exchange eluant as described above. A milky yellow-white slurry formed instantly. This was permitted to age 24 h at room temperature, then the liquid removed and the yellow solid washed with water, then ethanol and acetone. After drying in air the material was calcined as above. The XRD pattern showed $BiVO_4$ (14-688), Bi_2O_3 (14-699), and peaks belonging to an unknown phase(s).

Experiment 5 (JWP/I/131) 0.6 M NaVO$_3$ + Bi$_2$O$_3$/HNO$_3$

A 1.2 M Bi^{3+} solution of 13.9788g Bi_2O_3 (30 mmol) was made by dissolving the solid in a hot mixture of 15 ml conc. HNO_3 and 10 ml deionized H_2O. A 0.6 M solution of $NaVO_3$ was made by the solid dissolving (7.3158 g, 60 mmol) in 100 ml deionized water. This was poured down an ion-exchange column and when the eluant became

dark yellow-orange, 50 ml were taken off and poured slowly into the bismuth solution. A fine orange precipitate formed. The mixture was permitted to stand three days at room temperature, covered. The liquid was decanted off and evaporated (JWP/I/131B); the residue was identified by XRD as $BiVO_4$. The remaining solid was dried (JWP/I/131A) and identified by XRD as $BiVO_4$ (14-688) plus some peaks in the expected positions for $Bi_2VO_{5.5}$. (Figure 3.4)

Experiment 6 (JWP/I/134) 0.5 M NaVO₃ + Bi₂O₃/HNO₃, aged

A solution of Bi_2O_3 was made by dissolving (6.9894 g, 15 mmol) in a hot mixture of 20 ml conc. HNO_3 and 15 ml H_2O. A 0.6 M sodium vanadate solution was made as in Expt. 5. After enough of the vanadate solution eluted from the ion exchange column to deliver 15 mmol of vanadium (25 ml), it was permitted to sit for 15 minutes at room temperature so that the polymerization could begin. Red fibrous structures were observed in the beaker. This was then added slowly to the Bi^{3+} solution with stirring to break up the polymer. A clear orange solution resulted; this was heated for 10 minutes with heating and stirring. The solvent was slowly evaporated to deposit brown-and-white solids. The brown part was, after calcining at 400 °C for 4 hours, found to be mostly $BiVO_4$, while the white part was mostly Bi_2O_3.

Experiment 7 (JWP/I/139-2) 0.5 M NaVO₃ + Bi₂O₃/HNO₃, aged

Solutions of Bi^{3+} and $NaVO_3$ were prepared and mixed as in Expt. 6 above. The resulting clear yellow-orange solution was left

at room temperature, covered, 2 days with no change noted. This material was distributed among 6 crucibles and the solvent evaporated. Each crucible was heated in O_2 for 10 h at 350, 450, 550, 650, 700, and 750 °C, respectively. The calcined solids were identified by XRD (Table 3.1).

Table 3.1: Results of Experiment 7 (JWP/I/139-2)

Calcining Temp (°C)	XRD results	Figure
350	$BiVO_4 + Bi_2O_3$	3.5a
450	$BiVO_4 + Bi_2O_3$	
550	$BiVO_4 + Bi_2O_3$	3.5b
650	$BiVO_4 + ? Bi_2VO_{5.5}$	
700	$BiVO_4 + ? Bi_2VO_{5.5}$	
750	$BiVO_4 + Bi_2VO_{5.5}$	3.5c

3.4.2 Experiments using NH₄VO₃

Experiment 8 (JWP/I/123A) 0.5M NH₄VO₃/acetic acid, gel test

A 0.5 M solution of NH_4VO_3 was made by adding 1.4622g (12.5 mmol) of solid to 25 ml deionized water and heating to dissolve, giving a light yellow solution. To this was added 25 ml glacial acetic acid. The solution turned red-orange immediately, and a yellow precipitate appeared but redissolved quickly. On cooling, and standing overnight, the preparation yielded a chunky, fibrous precipitate in a supernatant liquid.

Experiment 9 (JWP/I/123B) 0.5M NH$_4$VO$_3$/acetic acid / HNO$_3$, gel test

A 0.5 M solution of NH$_4$VO$_3$ was made as in Expt. 8. To 25 ml of this solution were added 7.8 ml of 16 M HNO$_3$ and 17.2 ml glacial acetic acid. The solution immediately becomes orange-red, and becomes darker red over time. Red-orange fibers appear on the beaker sides within 5 minutes of mixing. After standing overnight a chunky solid had developed within a supernatant liquid.

Experiment 10 (JWP/I/123C) 0.25M NH$_4$VO$_3$/acetic acid, gel test

A 0.25 M solution of NH$_4$VO$_3$ was made by dissolving 0.7310 g of solid (6.25 mmol) in 25 ml deionized water and 25 ml of glacial acetic acid were added. The solution remained clear but became orange in color. Within an hour of cooling fibers appeared in the beaker. After standing overnight a chunky solid developed within a supernatant liquid.

Experiment 11 (JWP/I/124-IV) 0.25M NH$_4$VO$_3$ + Bi(NO$_3$)$_3$•5H$_2$O / acetic acid

A 0.25 M solution of NH$_4$VO$_3$ was made by dissolving (0.7311g, 6.25 mmol) of the solid in 25 ml hot deionized water. A 0.5 M solution of bismuth nitrate was made by dissolving the solid in 25 ml hot acetic acid. The bismuth-containing solution was poured slowly into the vanadium-containing solution with rapid stirring, and the

heating continued. An orange precipitate appeared instantly. After standing overnight the preparation was split into two parts: one part (JWP/I/124-IV-A) was filtered and the solid added to an alumina crucible, while the other part (JWP/I/124-IV-B) was added directly to a crucible and the solvent evaporated. Both were heated in air for 4 h at 300 °C and for 6 h at 400 °C and the resulting solids X-rayed. JWP/I/124-IV-A was identified as $BiVO_4$ (14-688); and JWP/I/124-IV-B identified as a mixture of $BiVO_4$ and Bi_2O_3 (14-699). JWP/I/124-IV-B, after calcining, was pressed into a pellet without intermediate grinding and heated for 36 h at 725 °C. The resulting solid was identified by XRD as a mixture of $Bi_2VO_{5.5}$ (identified by comparison with standard made by a solid-state route) and $BiVO_4$ (14-688). (Figure 3.6)

Experiment 12 (JWP/I/124-V) 0.25M NH_4VO_3 + Bi_2O_3/ acetic acid

A white suspension/solution of Bi_2O_3 was prepared by heating the solid (2.9122g, 6.25 mmol) in 75 ml hot acetic acid. A 0.25 M solution of NH_4VO_3 was prepared (0.7311 g, 6.25 mmol) in 25 ml hot deionized water. The hot bismuth preparation was poured slowly, with rapid stirring, into the vanadium preparation. An orange precipitate instantly formed. After standing overnight, the preparation was split into two parts and calcined as in Expt. 11. The solid part, JWP/I/124-V-A, was identified after calcining as $BiVO_4$ (14-688); and the combined precipitate-plus-solution part, JWP/I/124-V-B, was identified after calcining as a mix of $BiVO_4$ (14-688) and Bi_2O_3 (14-699). (Figure 3.7a) JWP/I/124-V-B, after

calcining, was pressed into a pellet and heated at 725 °C for 36 h. The resulting solid was identified by XRD as $Bi_2VO_{5.5}$ (Figure 3.7b).

Experiment 13 (JWP/I/142-1) 0.25M NH_4VO_3 + Bi_2O_3/HNO_3 + gum arabic, mix at 40 °C

A solution of Bi^{3+} was made by dissolving Bi_2O_3 (JM 99%, 6.9894 g, 15 mmol) in 25 ml conc. HNO_3 with warming; the solution was cooled to room temperature. A solution of NH_4VO_3 was made by dissolving solid (1.7547 g, 15 mmol) in 300 ml deionized water with heating and stirring; the solution was cooled to room temperature. To this solution was added 10 ml of a 2 g/100 ml gum arabic solution, followed by the bismuth solution, with stirring, at 40 °C. The resulting material was slightly milky orange-yellow. The suspension was transferred to a crucible and the solvent evaporated off to leave a red-orange coating (V_2O_5) on the crucible sides and a yellow-white powder (Bi_2O_3) on the crucible bottom.

Experiment 14 (JWP/I/142-3) 0.25M NH_4VO_3 + Bi_2O_3/HNO_3 + gum arabic, mix at room temperature

A Bi^{3+} solution was prepared as in Expt. 13. A solution of NH_4VO_3 was prepared by dissolving the solid (1.7547g, 15 mmol) in 350 ml hot deionized water along with 3 g of gum arabic. Both solutions were permitted to cool to room temperature; the bismuth solution was added slowly to the vanadate solution with stirring. The initially cloudy solution became a clear yellow-orange after a few minutes. The clear mixture was placed in a capped bottle to

settle. Over several days a solid settled out and was filtered off and heated at 350 °C for 2h, then 725 °C for 12 h in air. The resulting calcined solid was identified by XRD as $BiVO_4$. To the other half of the suspension ethylene glycol and glycine were added. The resulting slightly milky solution was heated to dryness – with a violent reaction and evolution of brown gas – and the solid heated for 22h at 750 °C. The calcined solid was identified by XRD as $Bi_2VO_{5.5}$.

Experiment 15 (JWP/I/149-2) $Bi(NO_3)_3 \cdot 5H_2O$ + NH_4VO_3 + ethylene glycol/glycine

To 20 ml hot deionized water was added $Bi(NO_3)_3 \cdot 5H_2O$ (12.1268g, 25 mmol) 1.14 g (15 mmol) glycine, and 80 ml (1.42 mol) ethylene glycol, resulting in a white-yellow milky suspension. NH_4VO_3 was added (1.4622 g, 12.5 mmol) to 20 ml deionized water and heated to dissolve. The vanadate solution was added to the bismuth suspension to give a red-orange paintlike mixture. This was heated to 60 °C for 3 h with stirring, in open air, then brought to 85 °C for another 2 h, then brought to 130 °C and let cool. The volume was thereby reduced to less than 100 ml. This was removed from the heat and left uncovered overnight with slow stirring. The suspension was relatively stable, like a paint. After evaporation of the solvent, the solid was calcined at 350 °C/2h, then 725 °C/12 in air. The resulting material was identified as $BiVO_4$ + Bi_2O_3.

Experiment 16 (JWP/I/83L21) BiVO$_4$ + Bi$_2$O$_3$, solid state

BiVO$_4$ (JWP/I/68, as above), and one-half the moles of Bi$_2$O$_3$ (to deliver total 2 Bi : 1 V) were ground together in an agate mortar, pressed into a pellet, and heated in an alumina crucible for 21 h at 725 °C. XRD of the pellet showed clean Bi$_2$VO$_{5.5}$. The same amounts of BiVO$_4$ and Bi$_2$O$_3$ were simply stirred together for 5 minutes with a stirring rod, and the loose powder heated according to the same heating scheme. XRD of the powder showed starting materials with some indication of peaks in the expected locations for Bi$_2$VO$_{5.5}$.

Table 3.2: Summary of Experiments Reported

Expt. #	Formulation	Result
1	0.1 M $NaVO_3$ + $Bi(NO_3)_3 \cdot 5H_2O$, HOAc	precipitate: $BiVO_4$
2	0.1 M $NaVO_3$ + Bi_2O_3, HOAc	precipitate: $BiVO_4$
3	0.5 M $NaVO_3$ + $Bi(NO_3)_3 \cdot 5H_2O$, HOAc/2MOE	suspension evaporated for $BiVO_4$ + Bi_2O_3
4	0.5 M $NaVO_3$ + Bi_2O_3, HOAc/2MOE	precipitate: $BiVO_4$ + Bi_2O_3
5	0.6 M $NaVO_3$ + Bi_2O_3, HNO_3	precipitate calcines to: $BiVO_4$ + $Bi_2VO_{5.5}$; supernatant: $BiVO_4$
6	0.6 M $NaVO_3$ + Bi_2O_3, HNO_3, pre-gelled	suspension evaporated for $BiVO_4$ + Bi_2O_3
7	0.6 M $NaVO_3$ + Bi_2O_3, HNO_3, pre-gelled and aged	suspension evaporated, range of heating gives $BiVO_4$ + Bi_2O_3 (low T) to $BiVO_4$ + $Bi_2VO_{5.5}$ (high T)
11	0.25 M NH_4VO_3 + $Bi(NO_3)_3 \cdot 5H_2O$, HOAc	precipitate: $BiVO_4$ suspension evaporated for $BiVO_4$ + Bi_2O_3, calcined to $BiVO_4$ + $Bi_2VO_{5.5}$

Table 3.2 continued.

12	0.25 M NH_4VO_3 + Bi_2O_3, HOAc	precipitate: $BiVO_4$ suspension evaporated for $BiVO_4$ + Bi_2O_3, calcined to $Bi_2VO_{5.5}$
13	0.25 M NH_4VO_3 + Bi_2O_3, HNO_3, gum arabic, 40 °C mixing	suspension evaporated, pyrolyzed for Bi_2O_3 + V_2O_5
14	0.25 M NH_4VO_3 + Bi_2O_3, HNO_3, gum arabic, room temperature mixing	precipitate: $BiVO_4$ suspension (eth. gly. and glycine added) evaporated, calcined to $Bi_2VO_{5.5}$
15	0.25 M NH_4VO_3 + $Bi(NO_3)_3 \cdot 5H_2O$, glycine, ethylene glycol	paintlike precursor pyrolyzed to Bi_2O_3 + $BiVO_4$
16	Bi_2O_3 + $BiVO_4$, grind and pellet, 725 °C/21h	$Bi_2VO_{5.5}$
16	Bi_2O_3 + $BiVO_4$, mixed, 725 °C/21h	starting materials

3.5 References

1) Brinker, C. J.; Scherer, G. W. *Sol-Gel Science: The Physics and Chemistry of Sol-Gel Processing*; Academic Press: New York, 1990.

2) Ebelmen, J. J. *Compt. Rend.* **1844**, *19*, 398.

3) Ebelmen, J. J. *Ann. Chim. Phys.* **1846**, *16*, 129.

4) Patrick, W. A., Silica Gel Corporation: U.S. Patent No. 1,696,645, 1928.

5) Patrick, W. A., Silica Gel Corporation: U.S. Patent No. 1,297,724, 1919.

6) Patrick, W. A., Silica Gel Corporation: U.S. Patent No. 1,520,305, 1924.

7) Moulton, H. R., American Optical Company: U.S. Patent No. 2,601,123, 1952.

8) Moulton, H. R., American Optical Company: U.S. Patent No. 2,432,484, 1947.

9) Moulton, H. R., American Optical Company: U.S. Patent No. 2,531,945, 1950.

10) Kimberlin Jr., C. N., U.S. Patent No. 2,636,865, 1953.

11) Kimberlin Jr., C. N., U.S. Patent No. 2,754,176, 1956.

12) Yoldas, B. E., U.S. Patent No. 3,941,719, 1976.

13) Yoldas, B. E. *Ceramic Bull.* **1975**, *54*, 286.

14) Yoshimura, M. *J. Mater. Res.* **1998**, *13*, 796.

15) Shaw, D. J. *An Introduction to Colloid and Surface Chemistry*; Butterworths: London, 1970.

16) Hench, L. L.; West, J. K. *Chem. Rev.* **1990**, *90*, 33.

17)Lee, G. R.; Crayston, J. A. *Adv. Mater.* **1993**, *5*, 434.

18)Kordas, G.; Moore, G. A.; Jorgenson, J. D.; Rotella, F.; Hitterman, R. L.; Volin, K. J.; Faber, J. *J. Mater. Chem.* **1991**, *1*, 175.

19)Corriu, R. J. P.; Leclercq, D. *Angew. Chem. Int. Ed. Engl.* **1996**, *35*, 1420.

20)Corriu, R.; Leclercq, D.; Lefevre, P.; Mutin, P. H.; Vioux, A. *Chem. Mater.* **1992**, *4*, 961.

21)Jones, R. W. *Fundamental Principals of Sol Gel Technology*, 1989.

22)Calzada, M. L.; Sirera, R.; Carmona, F.; Jimenez, B. *J. Am. Ceram. Soc.* **1995**, *78*, 1802.

23)Lakeman, C. D. E.; Payne, D. A. *Mater. Chem. and Phys.* **1994**, *38*, 305.

24)Wedemeyer, H.; Zhang, J.-Y. in *Eurogel '91*; Vilminot, S., Nass, R. and Schmidt, H., Ed.; Eslevier Science Publishers: Netherlands, 1992.

25)Kenzer, D. S.; Teepe, M. R.; Moore, G. A.; Kordas, G.; *Mater. Res. Soc. Symp. Proc.*, **1990**, *180*, 947.

26)Shane, M.; Mecartney, M. L. *J. Mater. Sci.* **1990**, *25*, 1537.

27)Kueper, T. W.; Visco, S. J.; DeJonghe, L. C. *Solid State Ionics* **1992**, *52*, 251.

28)Chen, C. C.; Nasrallah, M. M.; Anderson, H. U. *Solid State Ionics* **1994**, *70/71*, 101.

29)Selvaraj, U.; Prasadarao, A. V.; Komarneni, S.; Roy, R. *Mater. Lett.* **1995**, *23*, 123.

30)Selvaraj, U.; Prasadarao, A. V.; Komarneni, S. *Mater. Lett.* **1994**, *20*, 71.

31)Kim, C. J.; Yoon, D. S.; Lee, J. S.; Choi, C. G.; No, K. *Jpn. J. Appl. Phys.* **1994**, *33*, 2675.

32) Eichorst, D. J.; Payne, D. A.; Wilson, S. R.; Howard, K. E. *Inorg. Chem.* **1990**, *29*, 1458.

33) Yanovskaya, M. I.; Turevskaya, E. P.; Leonov, A. P.; Ivanov, S. A.; Kolganova, N. V.; Stefanovich, S. Y.; Turova, N. Y.; Venevtsev, Y. N. *J. Mater. Sci.* **1988**, *23*, 395.

34) Yamaguchi, O.; Maruyama, N.; Hirota, K. *Br. Ceram. Trans. J.* **1991**, *90*, 111.

35) Toyoda, M.; Payne, D. A. *Mater. Lett.* **1993**, *18*, 84.

36) Toyoda, M.; Hamaji, Y.; Tomono, K.; Payne, D. A. *Jpn. J. Appl. Phys.* **1993**, *32*, 4158.

37) Dayalan, E.; Peng, C. H.; Desu, S. B. *Ceram. Trans.* **1992**, *25*, 189.

38) Pechini, M., U.S. Patent No. 3,330,697, 1967.

39) Anderson, H. U.; Pennell, M. J.; Guha, J. P., in *Ceramic Powder Science (Advances in Ceramic Science Vol. 21)*; New York: American Ceramic Society, 1987; pp 91-98.

40) Baythoun, M. S. G.; Sale, F. R. *J. Mater. Sci.* **1982**, *17*, 2757.

41) Chick, L. A.; Pederson, L. R.; Maupin, G. D.; Bates, J. L.; Thomas, L. E.; Exarhos, G. J. *Mater. Lett.* **1990**, *10*, 6.

42) Douy, A.; Odier, P. *Mat. Res. Bull.* **1989**, *24*, 1119.

43) Miao, H.; Sapina, F.; Ibanez, R.; Beltran, A.; Beltran, D.; de la Fuente, G. F. *Solid State Ionics* **1993**, *66*, 231.

44) Chu, P.-Y.; Buchanan, R. C. *J. Mater. Res.* **1991**, *6*, 1736.

45) Legendre, J.-J.; Livage, J. *J. Colloid and Interface Sci.* **1983**, *94*, 75.

46) Gharbi, N.; R'Kha, C.; Ballutaud, D.; Michaud, M.; Livage, J.; Audiere, J. P.; Schiffmacher, G. *J. Non-Crystalline Solids* **1981**, *46*, 247.

47) Lemerle, J.; Nejem, L.; Lefebvre, J. *J. Inorg. Nucl. Chem.* **1980**, *42*, 17.

48) Greenwood, N. N.; Earnshaw, A. *Chemistry of the Elements*; 1st ed.; Pergamon Press: New York, 1984.

49) Hazel, J. F.; McNabb, W. M.; Santini Jr., R. *J. Phys. Chem.* **1953**, *57*, 681.

50) Legendre, J.-J.; Aldebert, P.; Baffier, N.; Livage, J. *J. Colloid and Interface Sci.* **1983**, *94*, 84.

51) Bullot, J.; Cordier, P.; Gallais, O.; Gauthier, M. *J. Non-Crystalline Solids* **1984**, *68*, 123.

52) Khairy, M.; Tinet, D.; van Damme, H. *J. Chem. Soc. Chem. Commun.* **1990**, 856.

53) Bhattacharya, A. K.; Mallick, K. K.; Thomas, P. A. *Solid State Communications* **1994**, *91*, 357.

54) Wedemeyer, H.; Zhang, J. Y. in *Eurogel '91,* Vilminot, S., Nass, R. and Schmidt, H., Ed.; Elsevier Science Publishers: Netherlands, 1992.

55) Gugliemi, M.; Carturan, G. *J. Non-Crystalline Solids* **1988**, *100*, 16.

56) Abraham, F.; Boivin, J. C.; Mairesse, G.; Nowogrocki, G. *Solid State Ionics* **1990**, *40-41*, 934.

Chapter Four

Synthesis of Bulk BiMeVOx (Me = Cu, Nb, Fe, Ti, Mn)

The experimental work described in this chapter was adapted, in part, from Pell, J.W., Ying, J.Y., and zur Loye, H.-C., *Mater. Lett.* 25, 1995, 157-160.

4.1 Introduction and general approach

In Chapter Three, initial attempts at producing bulk undoped $Bi_2VO_{5.5}$ from a precursor solution that contained bismuth as the acetate or nitrate, and vanadium as poly(vanadic acid) were described. However, these precursors failed to yield phase-pure $Bi_2VO_{5.5}$ at temperatures significantly lower than the solid-state synthesis required, and were plagued by preferential precipitation of bismuth nitrate or $BiVO_4$, leading to multiple phases in the pyrolyzed product and mud-cracked films. True gelation never occurred in these precursor solutions.

Another way of forming vanadium-oxide gels is by hydrolysis of vanadyl alkoxides.

4.1.1 Transition metal alkoxides[1-7]

The majority of this section is culled from literature reviews, many of which are by R. C. Mehrotra and co-workers, as referenced above.

4.1.1.1 Synthetic Methods

There are a variety of synthetic routes available for making almost any alkoxide of any metal. The best method for synthesizing a given metal alkoxide depends on the electronegativity and ionic radius of the metallic element and the steric and electronic nature of the alcohol group.

Alkoxides of strongly electropositive metals may be made by direct reaction of the alcohol with the metallic element (Equation 4.1).

(4.1) $M + n\ ROH \rightarrow M(OR)_n + n/2\ H_2$
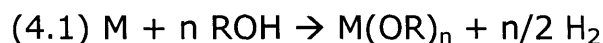
M=alkali or alkaline earth metal

For less strongly electropositive elements, a catalyst may assist this process (Equation 4.2).

(4.2) $M + cat + n\ ROH \rightarrow M(OR)_n + n/2\ H_2 + cat$
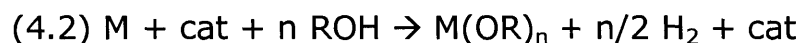
M= Mg, Be, Al, lanthanides, Tl; cat= I_2, HgX_2, O_2

As the acidity of the alcohol decreases, the facility with which these reactions proceed also decreases.

Alkoxides of less electropositive elements may sometimes be made by reaction of the alcohol with the oxide or hydroxide (Equation 4.3a,b).

(4.3a) $M(OH)_n + n\ ROH \Leftrightarrow M(OR)_n + n\ H_2O$

(4.3b) $MO_{n/2} + n\ ROH \Leftrightarrow M(OR)_n + n/2\ H_2O$
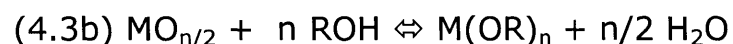
M = B, Si, Ge, Sn, Pb, As, Se, V, Hg

The reaction goes significantly to the right only if the displaced water is removed from the reaction system. The ramification, or degree of branching, (and therefore the acidity) and the boiling point of the alcohol influence the position of the equilibrium.

Alkoxides of somewhat electronegative metals may be made by reaction of the metal halide with alcohol (Equation 4.4).

(4.4) $MX_n + n\ ROH \rightarrow M(OR)_n + HX$

X = Cl

For electropositive metals, the mixture of metal halide and alcohol tends to yield the solvate rather than the alkoxide, while many transition metal halides will undergo only partial substitution of alcohol groups for halides. However, these reactions can in most cases be driven to completion if ammonia is added to scavenge HCl.

Alkoxides of transition metals may be made by exchange between the metal halide and an alkali alkoxide (Equation 4.5).

(4.5) $MX_n + n\ M'OR \rightarrow M(OR)_n + n\ M'X$

M= transition metal; M' = Li, Na, K; X = Cl

(4.6) $M(OR)_n + n\ HOR' \rightarrow M(OR')_n + n\ HOR$

M= early transition metal or non-transition metal

Alkoxides may be made by alcohol-exchange reactions (Equation 4.6). In general this reaction will not provide complete substitution of one alcohol group for another unless it is driven to the right by the removal of the lower-boiling alcohol. The facility for alcohol group interchange increases as the ramification of the group decreases, i.e. primary alcohols will easily substitute tertiary alcohols. For later transition metals, the degree of interchange is partially determined by the stability of different coordination forms.

Alkoxides may be made by ester exchange reactions (Equation 4.7) where again, the reaction may be driven toward complete

substitution of the original alcohol groups by removal of the ester from the system.

(4.7) $M(OR)_n + x\ CH_3COOR' \rightarrow M(OR')_n + x\ CH_3COOR$

M= Al, Ga, Fe, Ti, Zr, Hf, Nb, Ta, lanthanides

Alkoxides may be made by alcoholysis of metal dialkylamides (Equation 4.8). This is driven forward by the high reactivity of metal amides with hydroxy compounds, as well as by the volatility of the resulting dialkylamine, which can be driven off from the reaction system.

(4.8) $M(NR_2)_n + n\ R'OH \rightarrow M(OR')_n + HNR_2$

4.1.1.2 Properties and Reactions

Although metal-alcohol bonds could be expected to be highly polar based on consideration of Pauling electronegativities, many metal alkoxides are volatile and soluble in organic solvents. (Methoxides are an exception.) Inductive effects, which increase with increasing ramification of the alcohol group, explain the decreased polarity of the M-OR bond. The formation of oligimers through dative bonds likewise may decrease the polarity of the M-OR bond by increasing the electron density around the metal. Oligimerization and polymerization that occurs to satisfy the coordination demands of the metal may result in an insoluble alkoxide complex, but may be suppressed by the use of sterically demanding alcohols.

Metal alkoxides are extremely sensitive to atmospheric moisture and therefore must be handled under dry conditions. They react with hydroxy compounds (water, other alcohols, esters, glycols, and organic acids) with partial or full substitution of the attacking reagent for the original alcohol group. They also react with ketones and diketones, β-ketoamines, alkanolamines, hydroxylamines, thiols, and coordinating ligands. These reactions are sensitive to steric factors, with reactivity decreasing in the order MeO > EtO > iPrO > tBuO; they may be pushed to completion by removal of the displaced alcohol group.

The hydrolysis of a metal alkoxide in solution is usually followed by polycondensation (dehydration and dealcoholation) reactions (Equations 4.9a-c). These polycondensation reactions can, depending on the concentration of the solution, result in sufficient crosslinking to give a gel. The balance of pH, temperature, and water-to-alkoxide ratio determines how much each of these reactions contributes to the final product distribution.

(4.9a) $M(OR)_n + x\ H_2O \rightarrow M(OH)_x(OR)_{n-1} + x\ ROH$ (hydrolysis)

(4.9b) $-M-OH + H-O-M \rightarrow -M-O-M- + H_2O$ (dehydration)

(4.9c) $-M-OH + R-O-M \rightarrow -M-O-M- + ROH$ (dealcoholation)
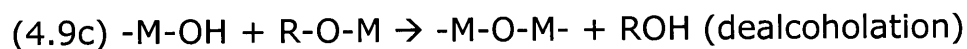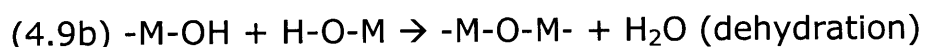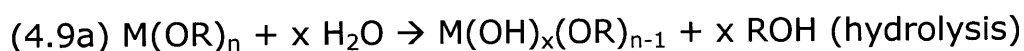
4.1.2 Synthesis of Vanadium Alkoxides

Vanadyl alkoxides have recently been examined as model compounds for research on the interaction of vanadate with the tyrosine and serine amino acids in enzymes involved in

151

phosphorylation reactions. The enzymatic cleavage and formation of phosphoester bonds proceeds via a transition state where the phosphorus has a trigonal bipyramidal geometry similar to that of oxovanadium alkoxides in the solid state;[8] these reactions are often inhibited or catalyzed by vanadate.[9] Vanadium complexes have been identified as insulin mimics and as cofactors for haloperoxidases and nitrogenases.[10,11] As a result of the interest in vanadium alkoxides in bioinorganic research, a relatively large number of papers have been published on the structure and reactivity of vanadium alkoxides and the reaction products with diols, amine-alcohols, and other molecules with biologically-relevant motifs.

"Vanadic acid esters" – vanadium alkoxides – were first prepared by Prandtl and Hess[12] by refluxing together V_2O_5 and alcohol. Later work by Funk et al.[13] involved the alcoholysis of $VOCl_3$ followed by the passage of dry ammonia through the reaction mix to trap evolved HCl as NH_4Cl. These methods resulted in yields of 10-35%. Alcohol interchange reactions are reported to give better yields, some 70%, when the evolved alcohol can be removed as an azeotrope with benzene[14] (Equation 4.10). All of these reactions, however, suffer from the reduction of vanadium(V) to vanadium(IV) by the alcohol, even when the latter reagent is not in excess.

(4.10) $VO(OEt)_3$ + 3 ROH → $VO(OR)_3$ + 3 EtOH
R=Me, iPr, tBu, sAm, tAm, sHex, tHex, cyHex

Gels prepared from vanadyl alkoxides have fibrous structures,[15-18] as do those formed from the poly(vanadic acid); but the fibers are finer and form thinner films.[19] Acid catalysis gives faster hydrolysis but slower gelation, with gel collapse (syneresis) which is not observed for hydrolysis at neutral pH.[20] This is due to the change in fiber with changing hydrolysis-to-condensation rate ratios. This is analogous to the effect of pH on silicon alkoxide hydrolysis, where the presence of H^+ in solution increases the rate of hydrolysis and increase of OH^- increases the rate of condensation, leading to more branched oligimers in basic solution, and more linear ones in acidic medium.[21] Under conditions of intermediate-to-high alkoxide concentrations and water-to-alkoxide ratios, and neutral pH, a monolithic gel is produced. This becomes green over time from the reduction of V^{5+}. There is debate about the source of the reduction of V(V) to V(IV), with some argument for reduction by the alcohol. However, since this reduction is also seen in vanadic acid solutions not containing organic materials, another possible reaction is analogous to the reaction which forms the vanadium bronzes (Equation 4.11).[8,22]

(4.11) $2 V^{5+}O(OR)_3 + (3+n+x/2)H_2O \rightarrow$

$$H_xV_x^{4+}V_{2-x}^{5+}O_5 \cdot nH_2O + 6 ROH + (x/4)O_2$$
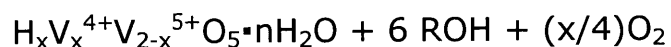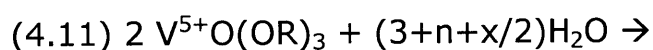
To prepare film-castable precursor solutions for bismuth vanadium oxide, we used vanadium 2-methoxyethoxide and introduced the bismuth as bismuth acetate, prepared by us in an alcohol-soluble form. This preparative procedure permitted the

production of phase-pure $Bi_2VO_{5.5}$ at exceptionally low pyrolysis temperatures, and was extended to making bulk powders of the doped BiMeVOx materials for a number of metal dopants. Furthermore, the solutions did achieve true gelation, without precipitation of any species, and were therefore film castable.

4.1.3 Bismuth part of the precursor

In Chapter Three we described experiments in which the precursor solution used poly(vanadic acid) and either bismuth nitrate or bismuth acetate. The bismuth acetate, used as-received from a commercial source, would not dissolve except in hot acetic acid solutions, consistent with what is reported in the literature;[23,24] and the bismuth nitrate tended to dissolve readily but to crystallize out as the solution was being concentrated. Therefore, a number of other bismuth compounds were tested for use with the vanadium alkoxides. These included commercial bismuth 2-ethylhexanoate and a bismuth nitrate-poly(ethylene glycol) complex,[25] neither of which gave very good results. Bismuth 2-methoxyethoxide proved to be a successful starting material for the Bi-V precursor solution. It was prepared both directly from bismuth chloride and sodium 2-methoxyethoxide[26] and via the bismuth dimethylsilamide as an intermediate.[27]

Mehrotra et al.[26] first synthesized bismuth alkoxides Bi(OR)₃ (R=Me, Et, and Pr) which were insoluble or sparingly soluble in the parent alcohol. The synthesis was by reflux of bismuth chloride with the sodium alkoxide of the alcohol, in a mixture of benzene and the parent alcohol. While a number of workers have reported success

154

in obtaining monomeric or at least soluble bismuth alkoxides using this general method with more sterically demanding alcohol groups, for example $-OCH(CF_3)_2$, $-OC_6F_5$,[28] $-OCMe_3$, $-OC_6H_3Me_2$-2,6,[29] $-OCH_2CH_2OMe$,[30-33]$-OC_6H_3(iPr)_2$-2,6,[27] reactions with more common alcohols have been accompanied by the formation of insoluble materials and have produced yields of only 50% or so. It is possible in some of these cases that trace water in the commercially produced bismuth chloride is forming condensed oxo-alkoxides which precipitate from solution.[27] Freshly synthesized BiI_3 reacted with potassium alkoxide gives potassium bismuth iodides K_2BiI_5 and K_3BiI_6 due to side reactions with the KI, leading to a low (<30%) yield of $Bi(OR)_3$: thus BiI_3 is not a good alternative to $BiCl_3$ as a starting material.[27]

Several workers have obtained bismuth alkoxides by alcoholyzing bismuth amides, rather than using bismuth halides. Matchett et al. used $Bi(NMe_2)_3$ to obtain $[Bi(OR)_3]_n$ for R=iPr, CH_2CH_2OMe, $CH_2CH_2NMe_2$, $CHMeCH_2NMe_2$, and CMe_2Et.[32] They found that the crystal structure of the soluble 2-methoxyethoxide is polymeric, with a $[Bi(\mu\text{-}O)_2O]$ backbone and a μ-O dimeric asymmetric unit. Massiani et al. used both the sodium alkoxide and alcoholysis of $Bi(N(SiMe_3)_2)_3$ to obtain the 2-methoxyethoxide,[30] while Sauer et al. alcoholyzed $Bi(N(SiMe_3)_2)_3$ with t-butoxide and diisopropylphenoxide to obtain the alkoxides in high yields.[27] The bismuth amides, in turn, may be synthesized by the reaction of $BiCl_3$ with the lithium salt of the amine in appropriate solvent: benzene or hexane for silylated amines,[34] and petroleum ether-THF for non-silylated amines.[35] There is also a report of bismuth

2-methoxyethoxide having been prepared by alcoholysis of [Bi(OEt)$_3$]$_\infty$.[33] Unless very sterically demanding ligands are used, even the bismuth alkoxide species prepared in these are insoluble. Although the metal is an 18-electron center for the tris(alkoxide), bismuth is also Lewis acidic with a large ionic radius: therefore it will seek to become hypervalent through oligimerization if steric demands by the alkoxy groups do not prevent this.

Due to reports of the solubility of the bismuth tris(2-methoxyethoxide) "(Bi-2MOE)$_3$",[27,30,32,33] we synthesized it using the alkali metal alkoxide method and the trimethylsilylamide method. We also returned to look at the carboxylates of bismuth as potential starting materials. In addition to the acetate, a number of other carboxylates are reported in the literature, and all decompose cleanly under 400 °C in air.[36]

4.1.4 Synthesis of Bulk Oxygen-Ion Conductors

The bismuth precursor species and vanadium 2-methoxyethoxide were first used to make bulk Bi$_2$VO$_{5.5}$ so that water ratios and pyrolysis temperatures and times could be examined and optimized. Due to the lessons learnt in the PLD experiments (Chapter 2) film-casting experiments were not done until dopant-stabilized γ-BiMeVOx was available from a sol-gel preparation.

As reported by Abraham et al.[37] (see Chapter 1), Bi$_2$VO$_{5.5}$ undergoes transitions to higher-conductivity phases at 450 °C and 570 °C. The highest-temperature phase, designated γ, may be stabilized to room temperature by the doping of 5-40% of assorted

metal ions into the structure.[38] The dopant is thought mainly to occupy the V positions, though some site-mixing is suspected.[39] Doping onto the Bi sites has been claimed by one group.[40] The conductivities of the doped materials are higher than that of the parent (undoped) γ phase (Figure 1.5), even in cases where the charge on the dopant does not lead to an increase in the number of vacancies. In addition to the extrinsic vacancies brought about through doping, and the higher conductivity achievable due to the higher symmetry of the high-temperature phase, the dopants make the passage of oxide ions through the lattice easier due to increased polarizability.

The oxygen ion conductivities are reported to be the highest for $Bi_2Cu_{0.1}V_{0.9}O_{5.35}$, $Bi_2Nb_{0.3}V_{0.7}O_{5.5}$, $Bi_2Ti_{0.1}V_{0.9}O_{5.5-\delta}$, $Bi_2Fe_{0.1}V_{0.9}O_{5.5-\delta}$, and $Bi_2Mn_{0.15}V_{0.85}O_{5.5-\delta}$.[38] (See Table 1.1) We synthesized these materials in bulk form by a modification of the sol-gel method described above: bismuth acetate, synthesized as described, was dissolved in 2MOE and mixed with V-2MOE, synthesized by alcoholysis of V_2O_5; the (commercial product) metal carboxylate or alkoxide was dissolved in this precursor solution, all in ratios such that the final metals content was those of the desired phases.

4.2 Results

4.2.1 Vanadium Alkoxides Synthesis

Our first attempts at making the vanadium alkoxide precursor solutions centered on alcoholysis of $VOCl_3$. The alcoholysis reaction

did not go to completion, leaving a product $VO(OR)_xCl_{3-x}$ (R=Et, iPr, nBu, 2MOE) which was extremely sensitive to hydrolysis and precipitated rather than gelling. Bubbling anhydrous ammonia into the reaction vessel lead to a white-grey gelatinous precipitate or black gum accompanied by loss of the yellow color characteristic of the higher vanadium alkoxides. The use of alkali metal alcoholates[8] to remove the final Cl atom was not explored.

We chose to focus our efforts on using vanadium 2-methoxyethoxide to introduce vanadium into the sol-gel precursor because it is more reactive than the common alcohols and is known for some metals, most notably yttrium, to be able to convert the oxoalkoxide into the complete alkoxide. We thus expected high yields in synthesizing the alkoxide from V_2O_5 or from lower alkoxides. It is also associated with producing soluble alkoxides – not by reduction in the degree of condensation of the metal alkoxide but by formation of a cyclic oligimer that exposes the organic parts of the alkoxide ligand to the solvent, ensuring solubility.[33] Metal 2-methoxyethoxides are for the same reason less susceptible to nucleophilic attack and therefore more stable to hydrolysis.

Synthesis of vanadium 2-methoxyethoxide via alcohol interchange of commercially available $VO(OiPr)_3$ was attempted. However, even with attempted removal of the lower-boiling alcohol by repeated distillation, complete substitution of the isopropyl groups was not realized. Nor was the new alkoxide purifiable by vacuum distillation, as the products decomposed at all pressures available to us. The deep green color of the alkoxide produced by the alcohol exchange indicated some degree of reduction to V(IV),

presumably due to the action of V(V) on the alcohols. The substituted alkoxide in solution was analyzed for total vanadium content by hydrolysis followed by pyrolysis and gravimetric determination of V_2O_5. Vanadium alkoxide so formed was used in some precursor syntheses, as described below.

To ensure uniformity of the alkoxy groups, we typically prepared vanadium alkoxides for the precursor solutions by the alcoholysis of V_2O_5: e.g., by boiling finely-ground V_2O_5 in the alcohol, with continuous removal of water as an azeotrope in benzene.[9] This method resulted in a green solution apparently containing primarily $V(OR)_4$.[41] Vanadium content was determined as described above. Attempts to purify the alkoxide by vacuum distillation failed, again due to the decomposition of the alkoxide under all the pressures available. (Anticipated conditions were approximately 150-160°C/0.5mm based on $V(OnBu)_4$, which is the closest analogue to $V(2MOE)_4$ reported in the literature.[41]) The best yields for this method were approximately 70-80% based on V_2O_5 recovered after hydrolysis and pyrolysis of the alkoxide product. Literature yields of $V(OnBu)_4$ near 70% of vacuum-purified material were reported.[9] Concentration ranges where the hydrolysis of the alkoxide yielded a gel were tested. DTA/TGA of the vanadium oxide gels prepared in this manner showed that decomposition was complete by 370 °C. (Figure 4.1)

Figure 4.1: DTA/TGA of vanadium oxide gel from hydrolysis of V-2MOE. Heating rate: 25 °C/min.

Temperature Difference (°C)

melting

690°C

loss of water

gain of oxygen

loss of water, alcohol

370°C

350°C

290°C

Temperature (°C)

Weight (mg)
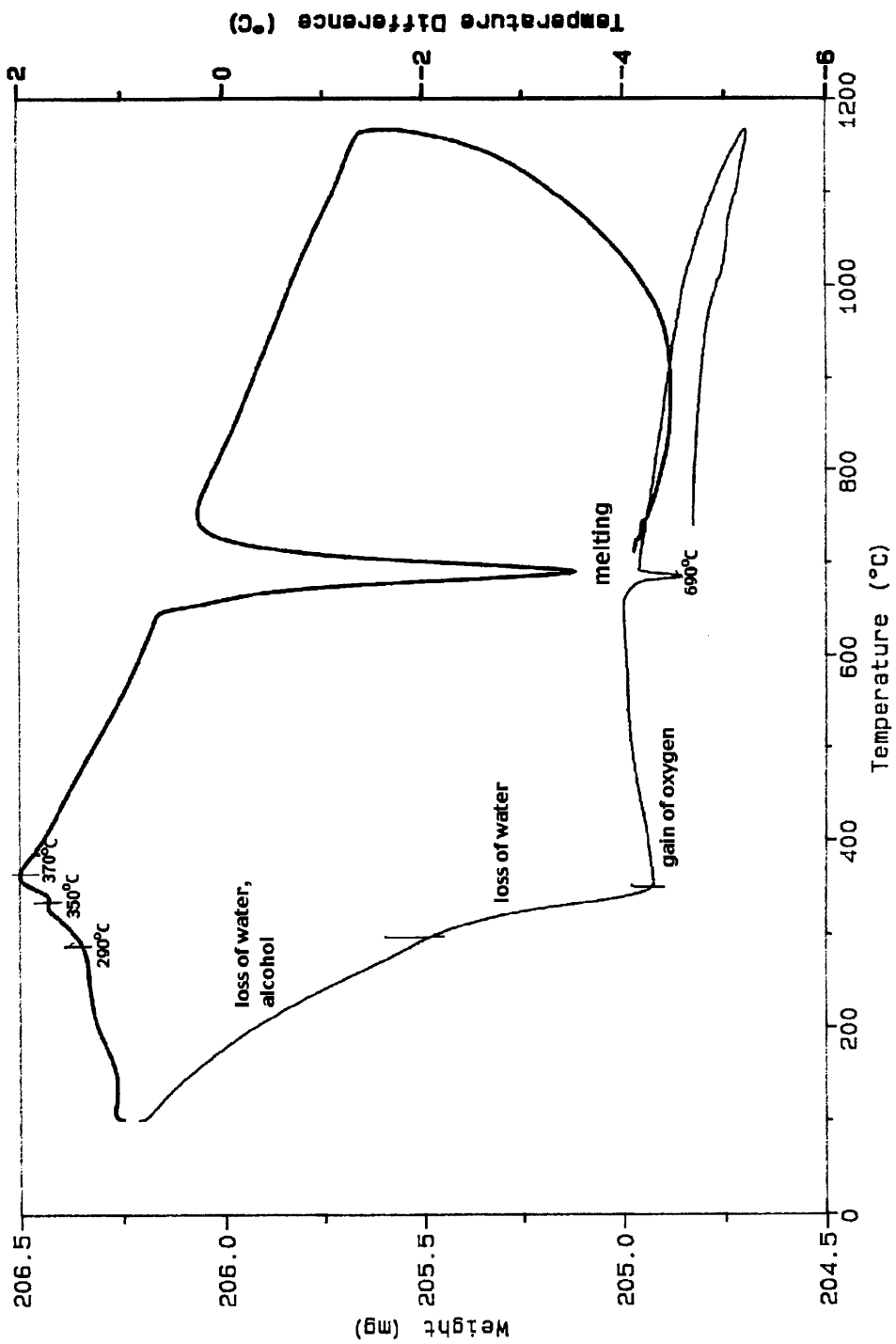
4.2.2 Synthesis and characterization of alcohol-soluble bismuth acetate

Bismuth acetate that is soluble in 2-methoxyethanol – the parent alcohol of choice for the vanadium alkoxide – was prepared by reaction of Bi_2O_3 with glacial acetic acid with continuous removal of the water produced. To our knowledge, this is the only report of the solubility of bismuth acetate in a solvent other than hot acetic acid. The synthesis of insoluble $Bi(OAc)_3$ via a method similar to our procedure, has been reported by Späth[42] and by Gattow and Schwank.[43] The latter reports the powder X-ray diffraction pattern, which does not match that of the JCPDS (#14-726) or our pattern. (Figure 4.2) Our powder XRD pattern does, however, resemble the pattern reported by Troyanov and Pisarevskii[44], if the severe preferential orientation in our sample is ignored. (Table 4.1) In both cases, the synthesis is by refluxing $Bi(NO_3) \cdot 5H_2O$[42] or Bi_2O_3[43] in acetic anhydride. Their procedures give no indication of having protected the synthesized material from air. It is likely that Gattow and Späth produced materials heavily contaminated with BiO(OAc). We found a mixture of $Bi(OAc)_3$ and BiO(OAc) (JCPDS # 14-0800) when we attempted to perform the synthesis in an open dish (Expt. 11) or when the material synthesized under inert atmosphere was left open to air. (Figure 4.3) Gattow and Späth report that their "bismuth acetate" is insoluble in all solvents tried.

Our DTA/TGA data, showing percent weight loss during the conversion to the oxide and decomposition temperatures (Figure 4.4), are consistent with the identification of our soluble precursor

as $Bi(OAc)_3$, as is elemental analysis. This is further supported by the PA-FTIR data (Figure 4.5).[43,45] The sample was decomposed at 700 °C in air to Bi_2O_3 and the weight retention was found to be 60.07%, consistent with $Bi(OAc)_3$ (60% expected) and not with BiO(OAc) (82% expected). The sample that had been synthesized in open-air conditions was similarly oxidized to Bi_2O_3 and found to have a weight retention of 82%. This sample, as well as a sample of bismuth acetate synthesized under inert atmosphere that was left open in air two days, would not dissolve in 2MOE.

Single-crystal X-ray diffraction on the compound synthesized by our procedure (Experiment 12) showed space group $P2_1/a$, with lattice parameters **a**=12.0848 Å, **b**=10.8859 Å, **c**=7.2889 Å, β=106.173, Z=4. (Figure 4.6) This slightly different from that reported by Troyanov and Pisarevskii,[45] who find $P2_1/c$, **a**=12.082 Å, **b**=10.858 Å, **c**=7.348 Å, β=105.83 °, Z=4; however, the bonding in the asymmetric unit and the layered chain disposition of the bismuth acetate trimers described by them were identical to what we found. They report that the compound is insoluble in all solvents tried. The basic unit in bismuth acetate is a bismuth atom surrounded by the three acetate groups bonded through both oxygens, as expected. Bismuth centers are linked via secondary bonding with the oxygens on the acetate groups, so that the asymmetric unit is a bismuth-acetate trimer, which lies in chains in the crystal. The lone pair is stereochemically active: the acetate groups bonded as bidentate ligands are found on one side of the bismuth atom, while the secondary-bonded ones are on the other side. On this basis we may guess that the lone pair is pointed in

the direction of the latter ligands.[25,32,46] The powder X-ray diffraction pattern of the sample before and after exposure to air (Figures 4.2, 4.3) demonstrated decomposition of the original sample to (eventually) one matching the known powder pattern for bismuth oxide acetate (JCPDS #14-800). The before-exposure XRD pattern, however, did not match the one listed in the JCPDS database (#14-726), even accounting for preferential orientation, but did match the pattern simulated using the crystal structure information provided by the single crystal data once preferential orientation was accounted-for, demonstrating the purity of the material examined by powder XRD. The bismuth acetate purchased from commercial sources (See Appendix to Part I), although sold and handled "under inert atmosphere," was likewise heavily contaminated with bismuth oxide acetate according to powder XRD. This is probably the major reason for the commercial materials' failure to dissolve, as observed in the experiments described in Chapter Three.

Reports of sol-gel preparations using commercial bismuth acetate have all mentioned its insolubility. Toyoda et al.[23,24] twice-refluxed commercial bismuth acetate in glacial acetic acid, removing the solvent each time, then dissolved the resulting powder in a 2-methoxyethanol solution of titanium 2-methoxyethoxide. In this case it may be argued that the dissolution of the bismuth species was associated with the formation of a heterobimetallic alkoxy-acetate;[47] however, the bismuth acetate prepared by us is soluble directly in 2-methoxyethanol and several other alcohol ethers. The key to the solubility of our bismuth acetate preparation probably involves the

careful exclusion of air and moisture after synthesis, so that the conversion to the insoluble oxyacetate was impeded. The acetate, as prepared here, forms an adduct with pyridine[48] in which the bismuth center retains three acetate ligands and adds two pyridine ligands. The pyridine and pyrazine-carboxylates of bismuth may be made in a similar synthetic process to that given here for bismuth acetate, but the resulting compounds are insoluble.[49] It likewise forms an adduct with thiourea.[50] We suggest that a similar interaction with the alcohol ether 2MOE assists the dissolution. The white crystalline bismuth acetate prepared in this way was dissolved in 2MOE with warming to produce a clear, faintly yellow solution which could be cooled to room temperature without precipitation. On standing 1-2 hours, however, a white fibrous semisolid occupied the entire solvent volume. A clear solution could be re-obtained on warming or vigorous stirring at ambient temperature; however, the solid could not be redissolved if the mother liquor was removed from it. Very dilute preparations remained clear for periods up to several days, even without stirring. The PA-FTIR of the solid is nearly identical to that of the alcoholysis product of $Bi(N(SiMe_3)_2)_3$, with some extra peaks attributed to acetate groups. (Figure 4.7 a, b) Their TGA traces are similar. (Figure 4.8 a,b) Alcoholysis of $Bi(NO_3)_3 \cdot 5H_2O$ by polyethylene glycols has been reported[25] and the exchange $Pb(OAc)_2 + HOiPr \rightarrow Pb_4O(OiPr)_6$ is known.[51] The white fibrous semisolid is thus thought to be an alcoholysis product of the acetate, supposed formula $[Bi(OAc)_x(2MOE)_{3-x}]_\infty$. The $Bi(OAc)_3$ could also be dissolved in diglyme but was insoluble in THF, DMSO, benzene, and isopropanol.

Table 4.1: Powder X-ray diffraction pattern for bismuth acetate prepared by method described in text.

Indexing and d(lit) from Troyanov.[44] Literature values (single crystal) $P2_1/c$, a=12.082 Å, b=10.858 Å, c=7.348 Å, β=105.83°, Z=4. Cell parameters from single crystal XRD: $P2_1/a$, a=12.0848 Å, b=10.8859 Å, c=7.2889 Å, β=106.173°, Z=4.

h	k	l	d(exp) Å	d(lit) Å	I/Io (exp, %)
			12.51		1.29
1	0	0	11.46	11.54	100
1	1	0	7.87	7.847 5.851 (11$\underline{1}$)	3.59
2	0	0	5.78	5.786	42.10
2	1	0	5.10	5.112 4.912 (12$\underline{0}$) 4.866 (111)	4.74
3	0	0	3.86	3.877	25.38
2	2	$\underline{1}$	3.75	3.766 3.739 (211)	0.34
3	1	0	3.64	3.649 3.481 (11$\underline{2}$) 3.472 (20$\underline{2}$) 3.360 (012) 3.208 (13$\underline{1}$) 3.057 (30$\underline{2}$) 3.040 (12$\underline{2}$)	0.50
2	2	$\underline{2}$	2.94	2.920	0.42
4	0	0	2.90	2.904	9.34

Table 4.1, continued.

h	k	l	d(exp) Å	d(lit) Å	I/Io (exp, %)
4	1	0	2.80	2.806 2.623 (40$\underline{2}$)	2.84
4	2	0	2.56	2.562 2.550 (41$\underline{2}$) 2.475 (331)	0.38
5	0	0	2.32	2.324 2.305 (431)	1.21
5	1	0	2.27	2.272 2.24 (50$\underline{2}$)	2.54
1	2	$\underline{3}$	2.22	2.227 2.205 (521) 2.196 (51$\underline{2}$) 2.180 (14$\underline{2}$) 2.130 (322)	0.96
2	5	0	2.03	2.034 2.013 (511) 2.006 (53$\underline{1}$)	0.26
6	1	$\underline{1}$	1.98	1.978	0.41
5	3	0	1.96	1.955	0.29
6	0	0	1.94	1.935	4.86
5	1	$\underline{3}$	1.92	1.910 1.885 (42$\underline{2}$)	0.33
4	0	$\underline{4}$	1.73	1.733	0.31
			1.70		0.36
			1.66		2.18
			1.64		0.52
			1.44		0.73
			1.42		0.40

Figure 4.2: Powder XRD pattern of bismuth acetate. Note the preferred orientation.
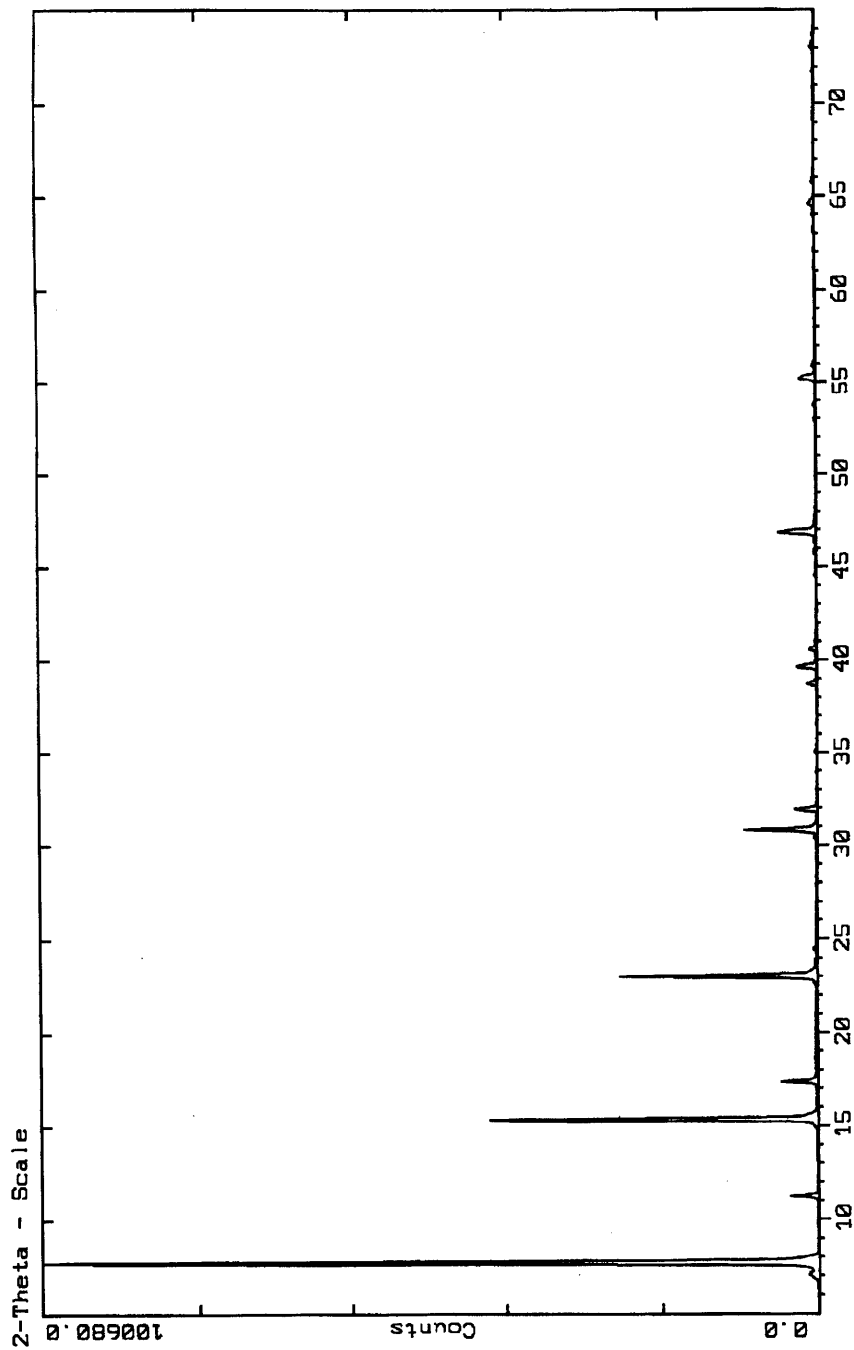
Figure 4.3: Powder XRD pattern of bismuth acetate (a) freshly-made, fast scan in air; (b) left open to air for two days.
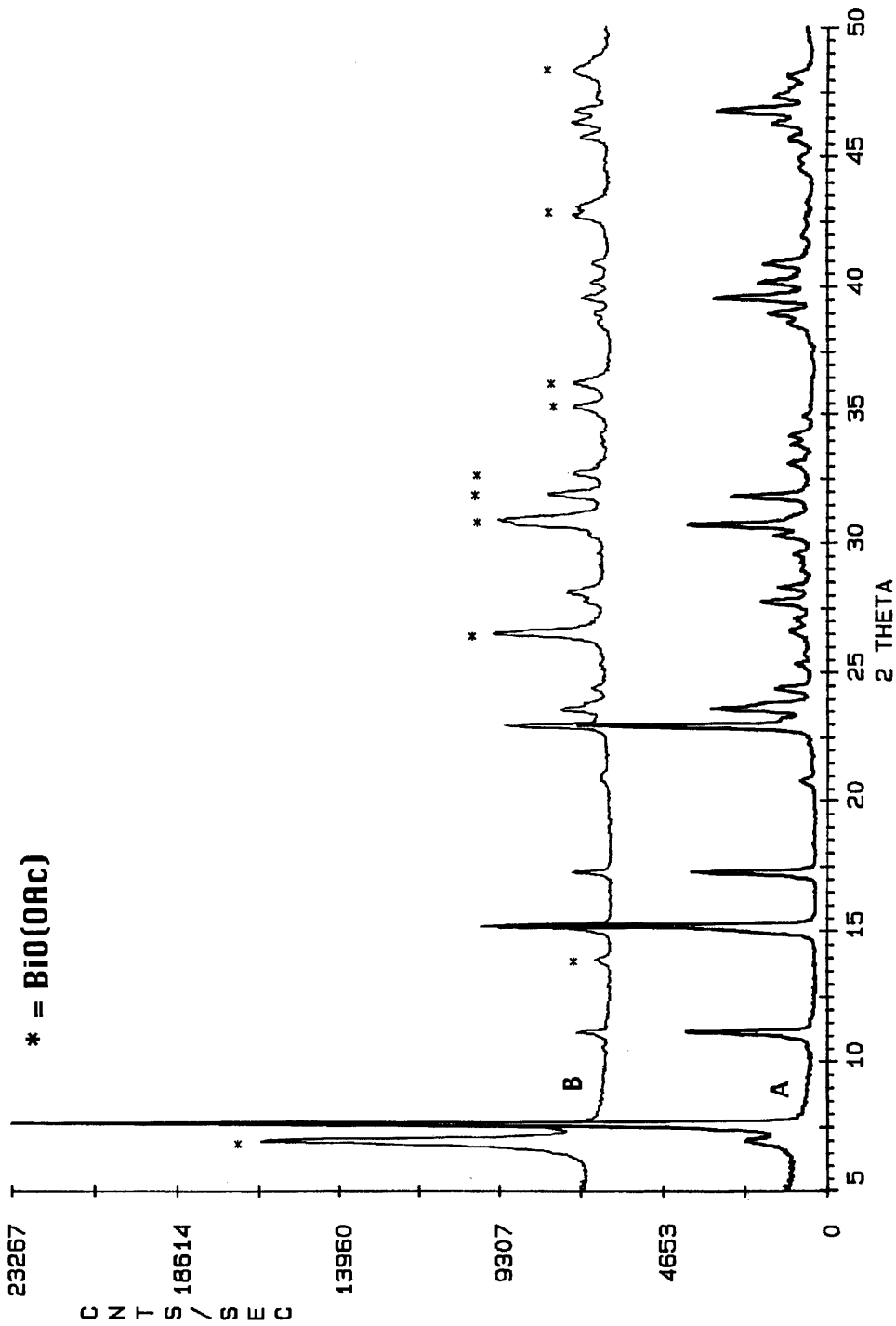
Figure 4.4: DTA/TGA of bismuth acetate. Heating rate: 25 °C/min.
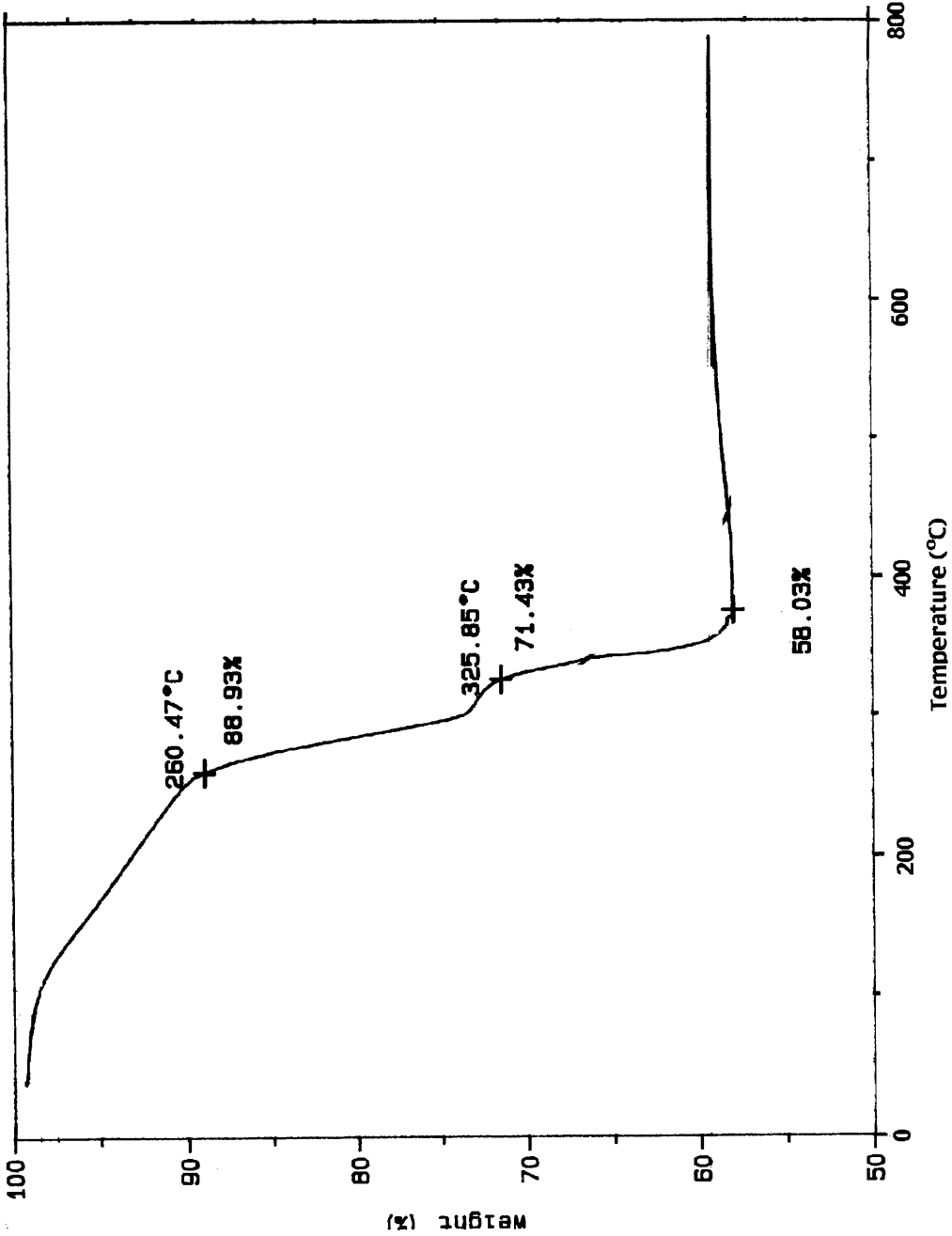
Figure 4.5: Photoaccoustic FTIR of bismuth acetate.
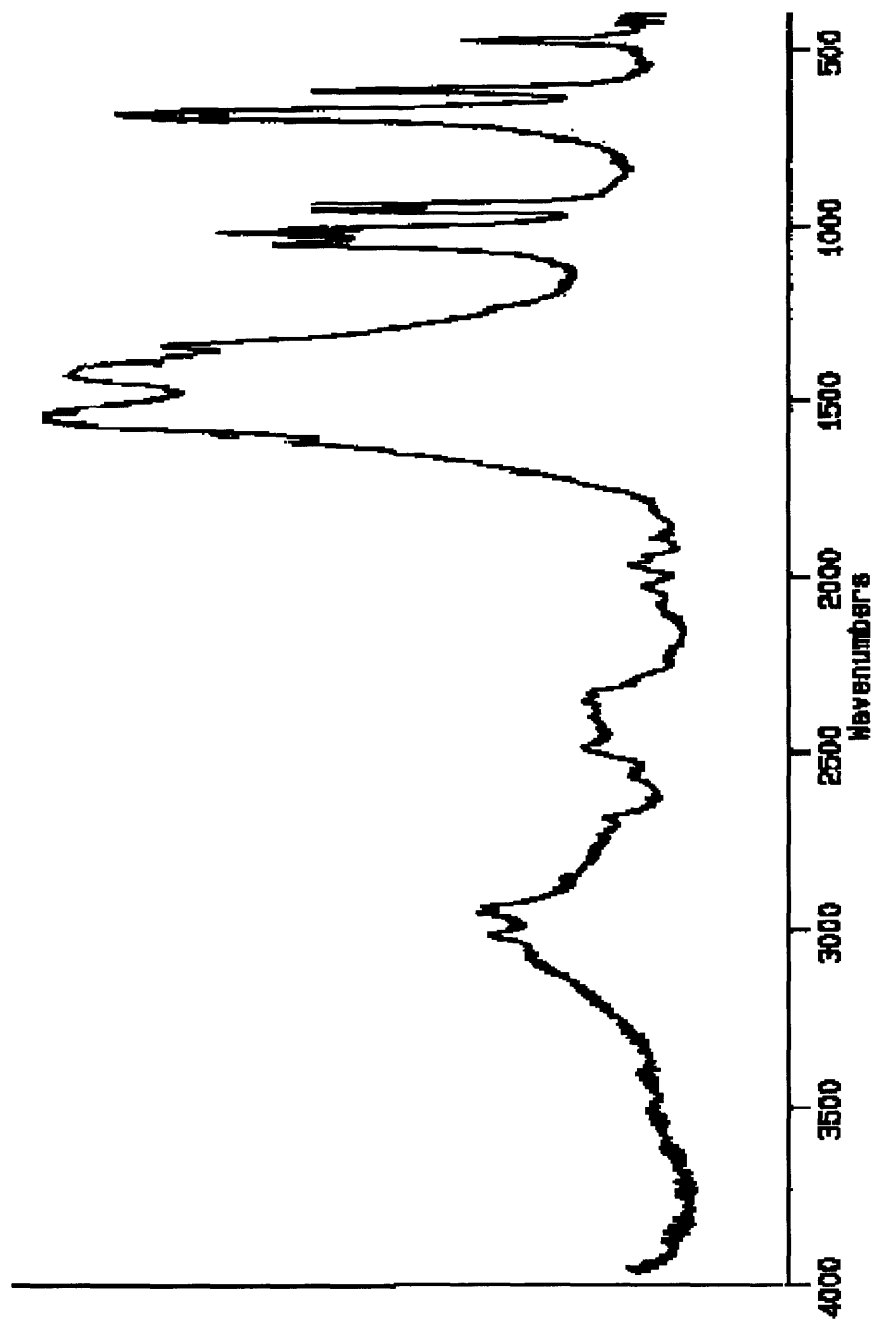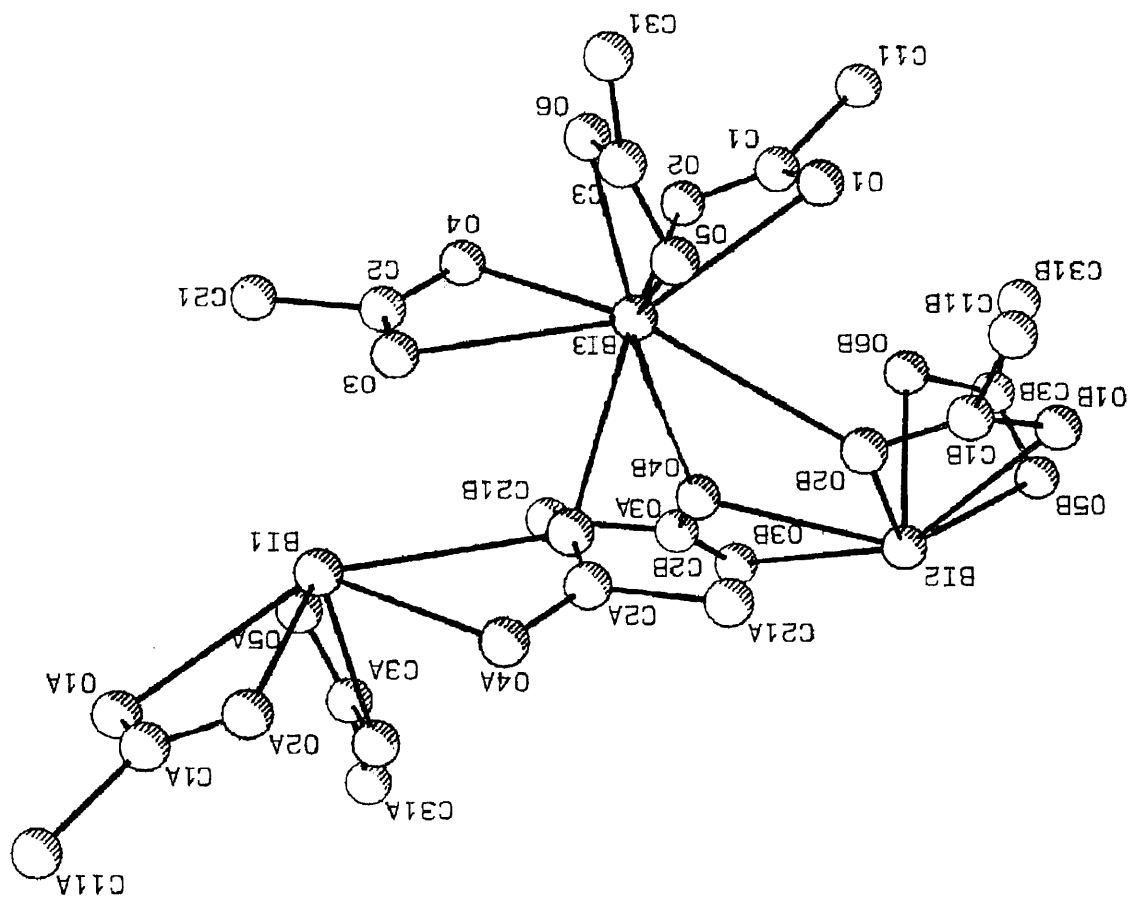
Figure 4.6: ORTEP of bismuth acetate. Selected bond lengths (pm) and angles: Bi(3)-O(1) 254, Bi(3)-O(2) 230, Bi(3)-O(3) 267, Bi(3)-O(4) 240, Bi(3)-O(5) 252, Bi(3)-O(6) 224, Bi(3)-O(2B) 294, Bi(3)-O(4B) 283, Bi(3)-O(3A) 280; O(1)-Bi(3)-O(3) 152.5°, O(1)-Bi(3)-O(4) 117°, O(1)-Bi(3)-O(5) 80°, O(1)-Bi(3)-O(6) 74°, O(4)-Bi(3)-O(6) 80°, O(3)-Bi(3)-O(6) 79°, O(3)-Bi(3)-O(4) 50.5°, O(5)-Bi(3)-O(6) 53°, O(1)-Bi(3)-O(2) 53.4°

Figure 4.7a: Photoaccoustic FTIR of bismuth acetate-2MOE polymer.
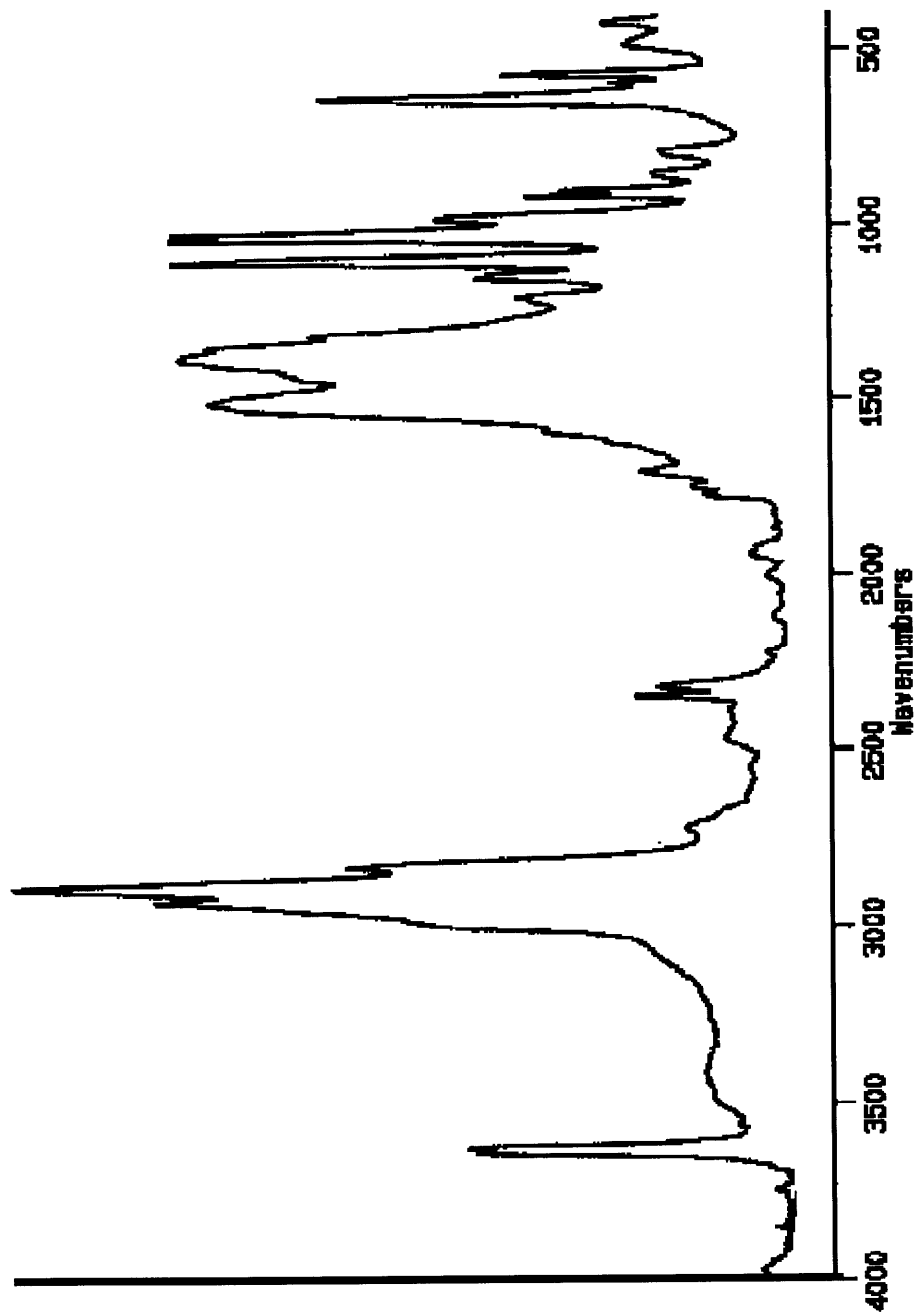
Figure 4.7b: Photoaccoustic FTIR of product of alcoholysis of Bi(N(SiMe₃)₂)₃ by 2MOE.
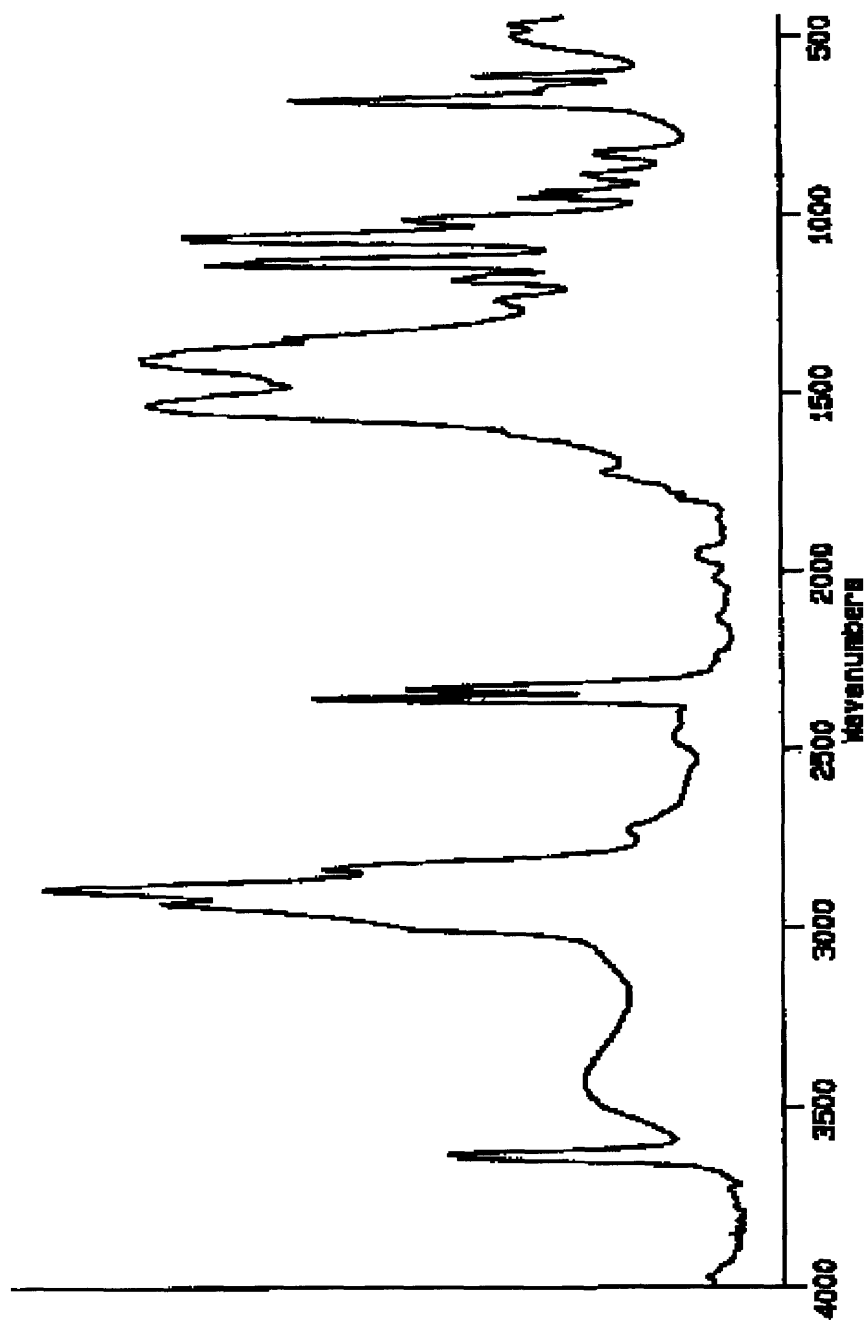
Figure 4.8a: DTA/TGA of bismuth acetate-2MOE polymer.
Heating rate: 25 °C/min.

Temperature Difference (°C)

20   15   10   5   0   -5

92.4%, 251°C

77.6%, 287°C
75.7%, 309°C

58%, 333°C

Temperature (°C)

0   200   400   600   800

Weight (%)

100   90   80   70   60   50
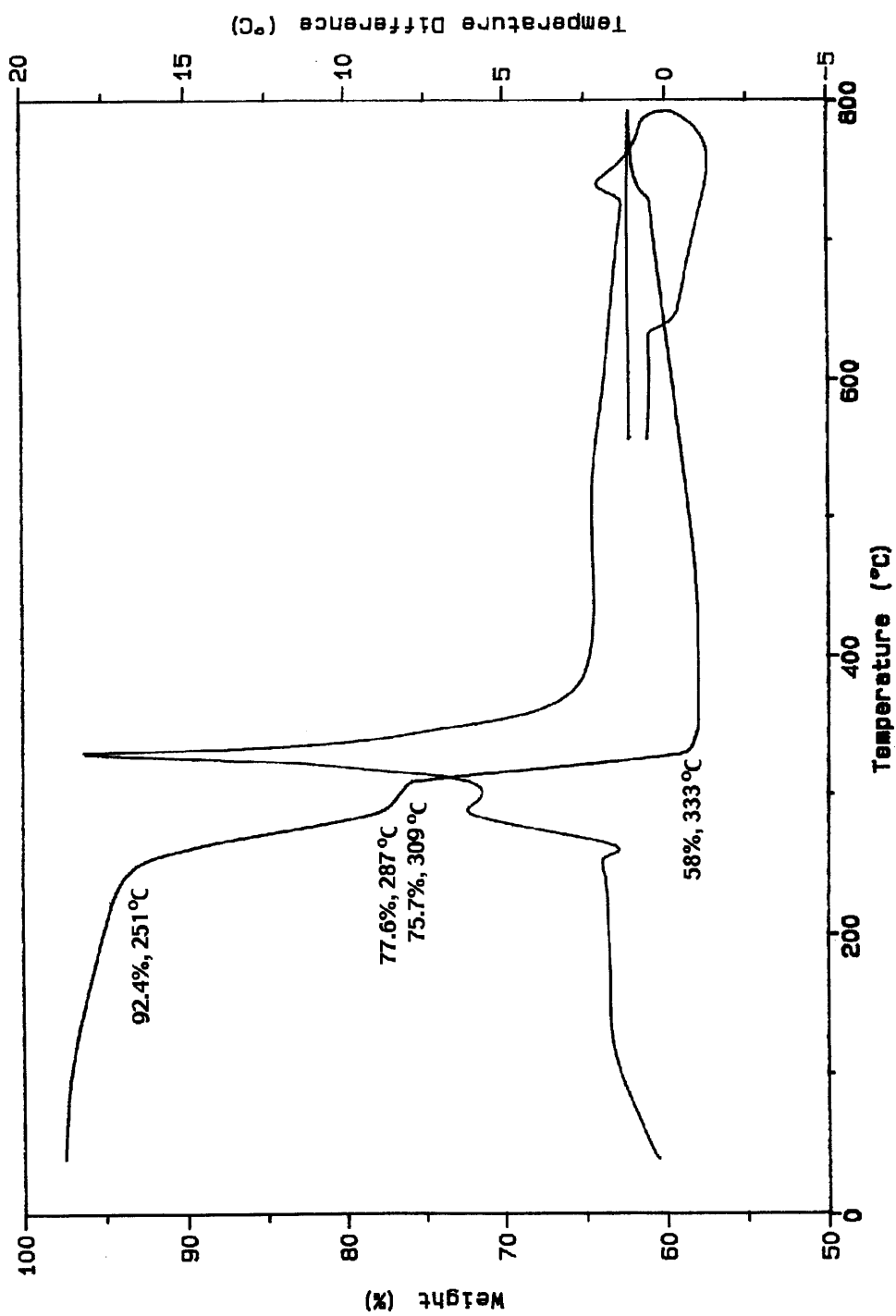
Figure 4.8b: DTA/TGA of product of alcoholysis of Bi(N(SiMe₃)₂)₃ by 2MOE. Heating rate: 25 °C/min.
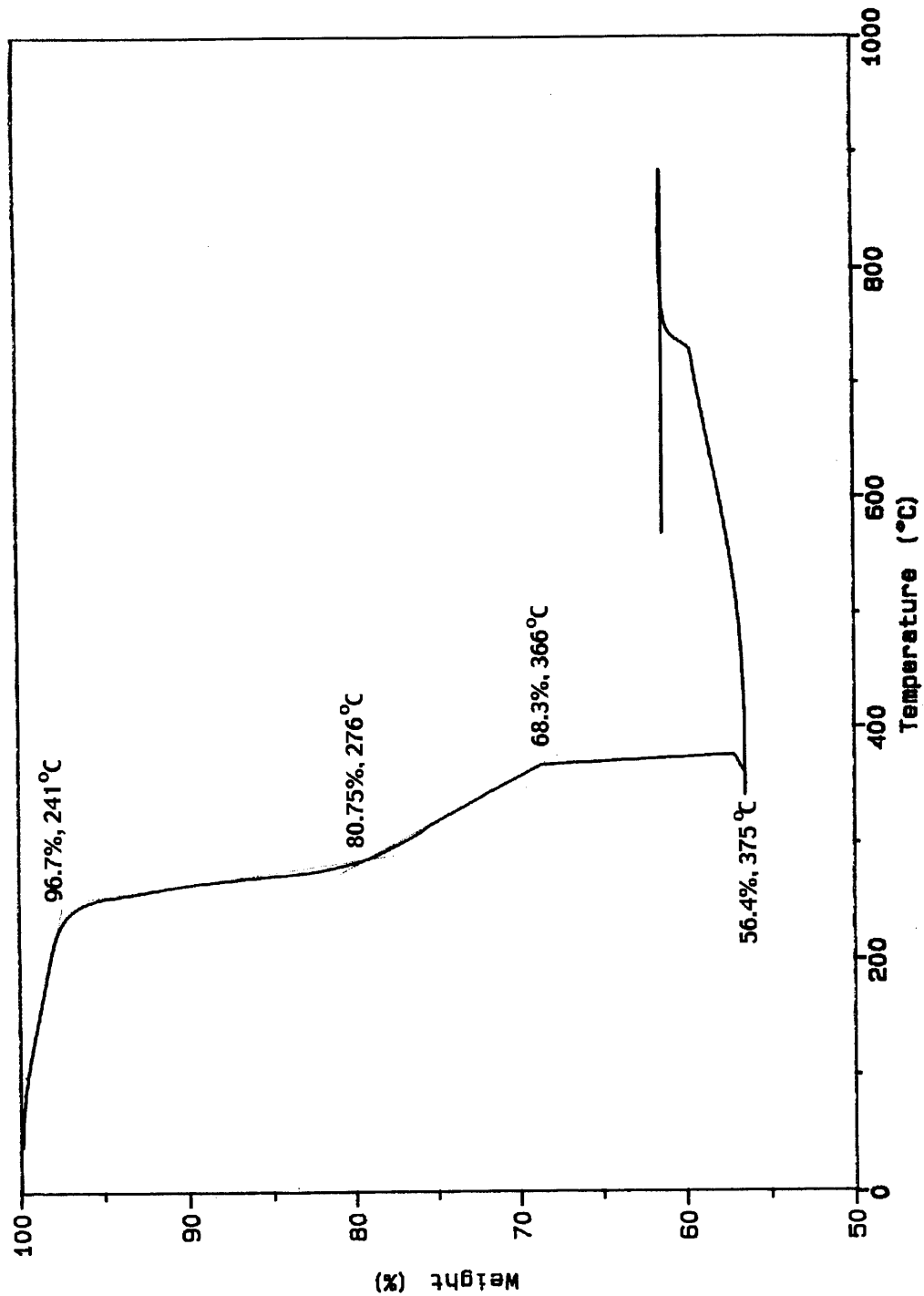
4.2.3 Bulk Bi$_2$VO$_{5.5}$ Synthesis

Vanadium 2-methoxyethoxide (V-2MOE) was prepared by azeotropic distillation of finely ground V$_2$O$_5$ in excess 2MOE and benzene.[12] Alternatively, the 2-methoxyethoxide could be made by twice-refluxing VO(OiPr)$_3$ in 2MOE with distillation each time above 100 °C.[14] In either case, the concentration of the resulting yellow solution was verified by gravimetric determination of V$_2$O$_5$ following hydrolysis of the alkoxide and heating the resulting gel in air to 700 °C. Direct use of VO(OiPr)$_3$ resulted in poor gel quality due to the extremely fast hydrolysis of the isopropoxide group, yielding the α-Bi$_2$VO$_{5.5}$ only after extended heating to temperatures (750 °C) higher than those required for gels made from V-2MOE (450 °C). Soluble bismuth acetate was prepared as described above and dissolved in 2MOE. Vanadium 2-methoxyethoxide (V-2MOE) and bismuth acetate solutions in 2-methoxyethanol were mixed in quantities to give a 1:2 V:Bi mole ratio. The clear yellow solution which resulted was stable under nitrogen for weeks, though hydrolysis was evident within an hour of being opened to the air. Refluxing this precursor solution overnight resulted in precipitation of a brown solid which after heating at 625 °C for 1 h in air became a mixture of BiVO$_4$ (JCPDS 14-688) and Bi$_2$VO$_{5.5}$[37] as identified by powder XRD.

The precursor solution was hydrolyzed with water or water mixed with concentrated ammonium hydroxide or glacial acetic acid. Immediate precipitation was seen in precursor solutions containing

NH_4OH, presumably due to a complex formation between NH_3 and the vanadium alkoxide.[11,52] However, translucent gels were obtained for precursor solutions hydrolyzed with pure water or with water and acetic acid. Different alkoxide/water/acid ratios resulted in varying gel qualities. Pyrolysis of the gel occurred with initial formation of $BiVO_4$, with ingrowth of the desired $Bi_2VO_{5.5}$ phase as pyrolysis temperature increased. (Figure 4.9) The presence of acetic acid did not appear to make a difference in the pyrolysis temperature at which the α-$Bi_2VO_{5.5}$ appeared in the XRD patterns. There was, however, a correlation between gel quality and the temperature at which the desired α-$Bi_2VO_{5.5}$ phase appeared in the powder XRD pattern, with more homogenous-looking gels producing cleaner diffraction patterns at low pyrolysis temperatures. TGA/DTA of this gel showed decomposition was complete by 430 °C. (Figure 4.10) Vanadium tris(isopropoxide) oxide was also directly tested for use in the precursor solution, but its rapid hydrolysis resulted in poor-quality gels or fibrous precipitates which on pyrolysis did not show the α-$Bi_2VO_{5.5}$ phase until 750 °C.

Several early experiments had given a mixture of $Bi_2VO_{5.5}$ and $BiVO_4$ (Expts. 16, 17). Because a number of papers suggested that $BiVO_4$, had some significant O^{2-} conductivity,[53] complex impedance (CI) experiments were undertaken to determine the conductivity behavior of pure $BiVO_4$ and of sol gel prepared $Bi_2VO_{5.5}$ contaminated with $BiVO_4$. Complex impedance plots (Z″ vs Z′) for pure $BiVO_4$ showed at low temperatures (340.1 °C) a high-frequency arc with a spike at lower frequencies. As the temperature rose (594.5 °C), the first arc disappeared and the spike resolved into a

second arc. This second arc is attributed to the electrodes' having become non-blocking, and represents electronic conductivity. (Figure 4.11a, b) The total conductivity shown by the $BiVO_4$ pellet was low. (Figure 4.12) A combination pellet, synthesized by a sol-gel method but with the sample having a PXRD pattern showing a mixture of $BiVO_4$ and $Bi_2VO_{5.5}$, was also investigated using CI. In this case, it should be noted that a lower conductivity reading may have resulted from a failure to densify the pellet completely. The high-temperature sintering was omitted in order to maintain the original post-synthesis sample composition for at least the lower temperature readings; thus pressure alone was used in densifying the pellet. The data show very noisy plots at low temperature, probably due to the low pellet density, which would lead to a high grain boundary-type resistance. At higher temperatures (490.2 °C) a single high-frequency arc terminates on its low-frequency side in a line representing the electronic contribution to the conductivity. (Figure 4.13 a-d) The conductivity on the cooling leg of the experiment is higher due to the increased densification of the pellet. (Figure 4.14)

Synthesis of α-$Bi_2VO_{5.5}$ was also accomplished by mixing appropriate ratios of V-2MOE with $Bi(2MOE)_3$ made by the alcoholysis of $Bi(N(Si(CH_3)_3)_2)_3$.[27] Hydrolysis and heating of the bulk gel result in a material that undergoes direct conversion to α-$Bi_2VO_{5.5}$ at 450 °C. DTA/TGA shows a single-step decomposition by 310 °C. (Figure 4.15) The X-ray powder diffraction patterns (Figure 4.16) show no evidence of $BiVO_4$ peaks, although at intermediate temperatures some unidentified peaks appear. These peaks disappear and the desired phase increases in crystallinity at

subsequent heating to higher temperatures. The precursor solution that included alkoxides of both metals had a lower temperature for formation of the desired α-$Bi_2VO_{5.5}$ phase because (1) the possible formation of a bimetallic alkoxide in solution may have provided stable atomic-level mixing and adjacent placement of Bi and V atoms before hydrolysis, or (2) the fact that both compounds were hydrolyzable permitted the formation of Bi-O-V bonds – i.e. intimate metal mixing – in the condensation reactions leading to the gel. The lesser susceptibility of the $Bi(OAc)_3$ to hydrolysis or alcoholysis may have decreased its incorporation in the gel structure relative to that of the bismuth alkoxides, so that its main method of incorporation may have been by being dissolved in the solvent trapped in the vanadium oxide gel, rather than by Bi-O-V bonding.

The formation of $Bi_2VO_{5.5}$, which is a layered structure, at low temperatures in the sol-gel process, is due to "templating" by the initial layered structure of the V_2O_5 gel. V_2O_5 gel has a layer structure similar to that of the α- and γ-vanadium bronze, $M_xV_2O_5$, where the M^+ layer is interposed by the layers of VO_6 octahedra.[20,54]

The BiMeVOx materials (Me=Cu, Nb, Ti, Fe, Mn) were successfully synthesized using a modification of the method described for $Bi_2VO_{5.5}$: to bismuth acetate and V-2MOE solutions in 2MOE were added metal salts or alkoxides in the ratios required to obtain the desired metal stoichiometry in the final product. Copper and manganese were added as the acetates, while iron was added as the acetate or acetylacetonate, and niobium and titanium added as the isopropoxides. Several other methods of adding niobium, e.g. as the acetate and as the chloride, failed to give stable

solutions. In all cases, all of the components were soluble in 2MOE. Precursor solutions were hydrolyzed with 1-2 equivalents of water and pyrolyzed. In all cases powder XRD shows low-temperature formation of the desired γ-BiMeVOx phase. (Figures 4.9, 4.17-4.21) $Bi(N(SiMe_3)_2)_3$, $Cu(OAc)_2$, and V-2MOE mixed in a 2MOE solution also led to a low-temperature synthesis of BiCuVOx. (Figure 4.22)

Due to the presence of the dopant, the metal-doped phases are disordered, so that less diffusion of metal atoms needs to occur in order to have these atoms attain their final positions in the structure. This is one mechanism for the lower-temperature formation of the doped phases from a preparation otherwise identical to that which forms the undoped parent structure $Bi_2VO_{5.5}$. In addition, the metal dopants may catalyze the burn-out of the organic materials, as is sometimes seen with polymeric ceramic powder binders.[55]

The total conductivity of a solid electrolyte is the sum of the conductivities of a number of processes – i.e. intergrain and intra-grain conductivity, and grain-boundary conductivity. Because of this, processing parameters may influence the conductivity of a given sample of oxygen-ion conducting material. In particular, the grain size achieved during synthesis, and the density or level of sintering achieved during the later processing of the synthesized powder, is relevant. For BiCuVOx samples prepared by standard solid-state methods, then ball-milled to produce various grain sizes and/or mixed with binder before sintering into a pellet for conductivity testing, some variation in the oxygen ion conductivity with the grain size and degree of sintering/densification of the pellet is reported in the literature.[56] As a result, the oxygen ion

conductivity of a sample of $Bi_2Cu_{0.1}V_{0.9}O_{5.35}$ made by the sol-gel method as described above was tested by complex impedance spectroscopy. (Figure 4.23 a-d) A single arc was observed in the complex impedance data, with a spike occurring at lower frequencies which eventually evolved to a line with increasing temperatures. The line indicated the significant electronic contribution to the total conductivity of the samples. The high frequency arc, arising from oxide ion conductivity, represented the sum of grain boundary and bulk resistances; the individual contributions could not be separated out. It was found that the conductivity was essentially the same as that reported in the literature for samples made by a solid state synthesis procedure.[57] (Figure 4.24)

Figure 4.9: Powder XRD patterns at various pyrolysis temperatures for sol-gel produced $Bi_2VO_{5.5}$. The bismuth precursor was bismuth acetate.
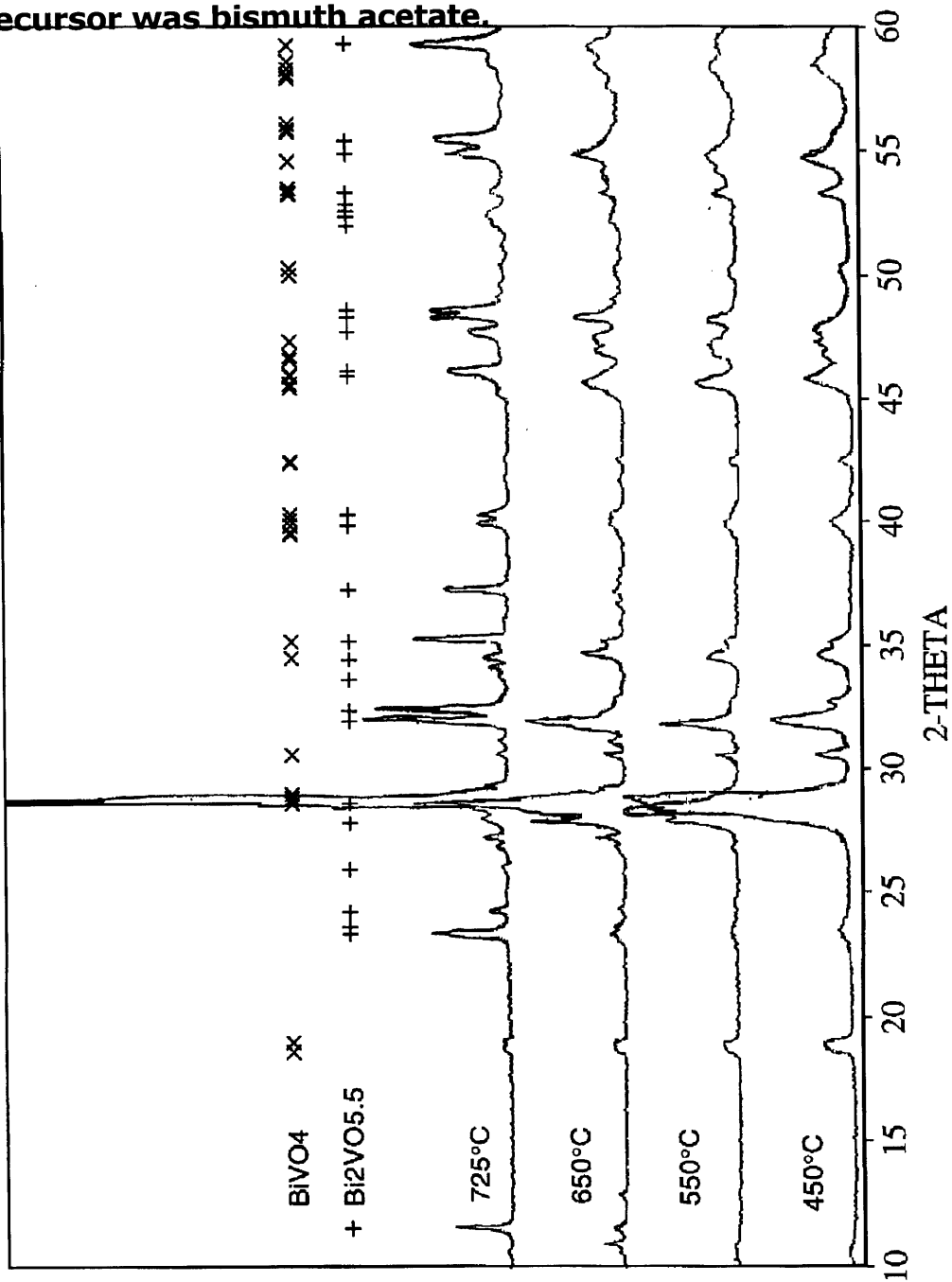
Figure 4.10: TGA of $Bi_2VO_{5.5}$ precursor gel after hydrolysis and removal of solvents. Heating rate: 25 °C/min. (JP-II-39-0)
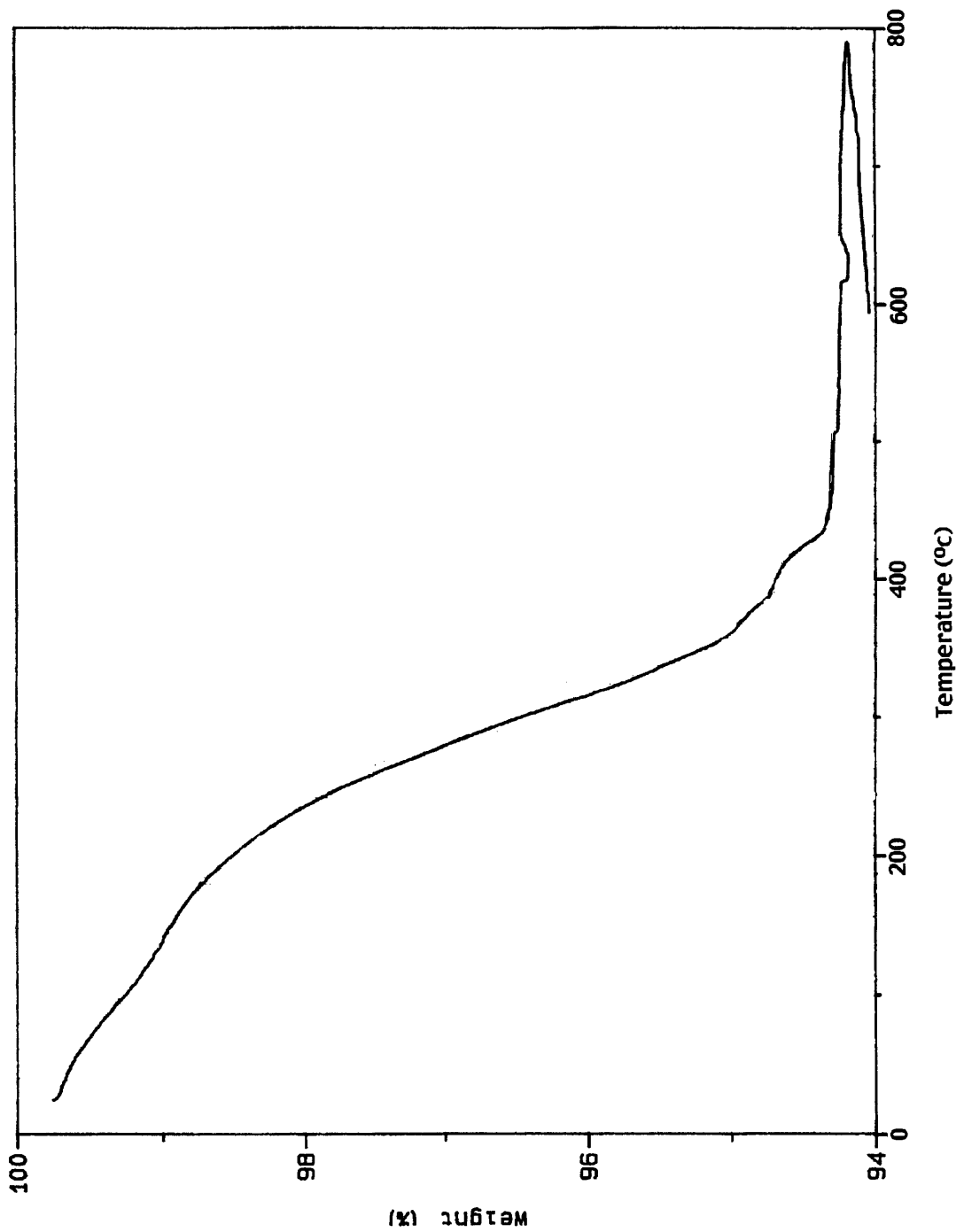
Figure 4.11: Complex impedance plots for BiVO$_4$. (a) 340.1 °C. (b) 594.5 °C.
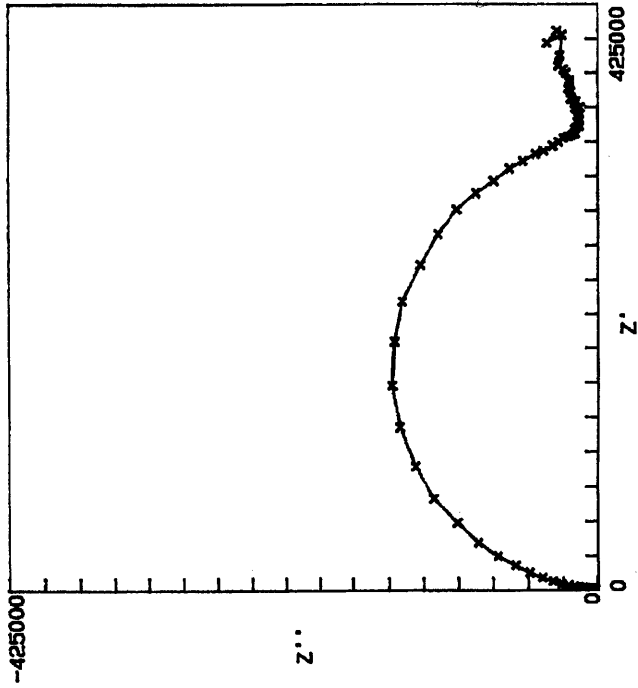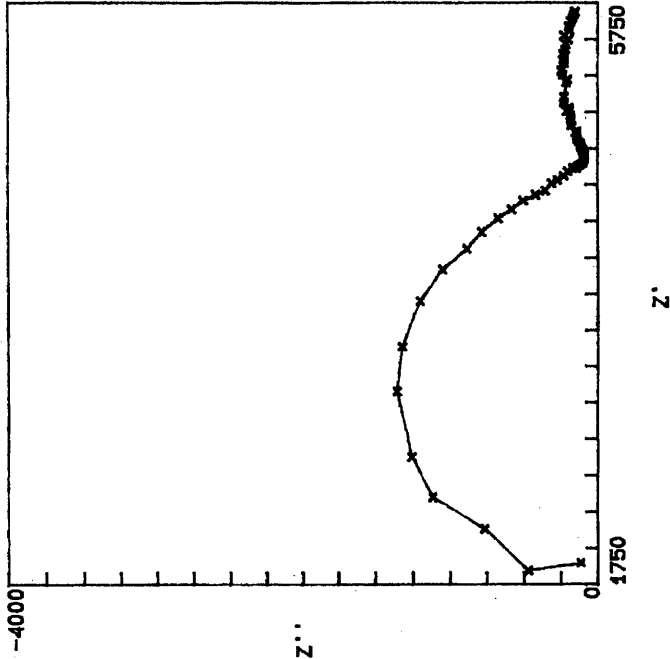
Figure 4.12: Conductivity of BiVO₄ as a function of temperature.
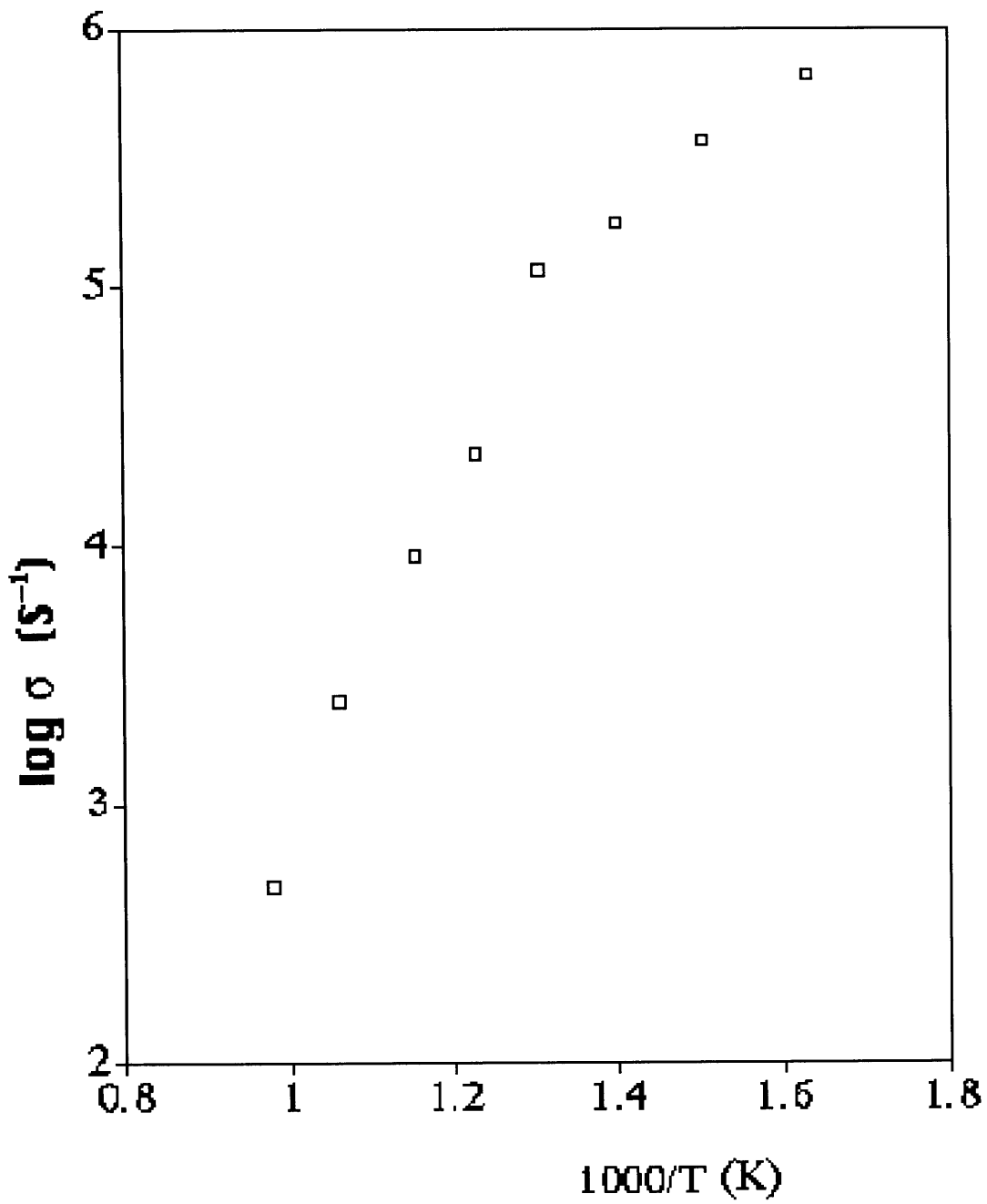
Figure 4.13: Complex impedance plots for $Bi_2VO_{5.5}$ contaminated with $BiVO_4$. (a) 490.2 °C, heating. (b) 542.1 °C, heating.
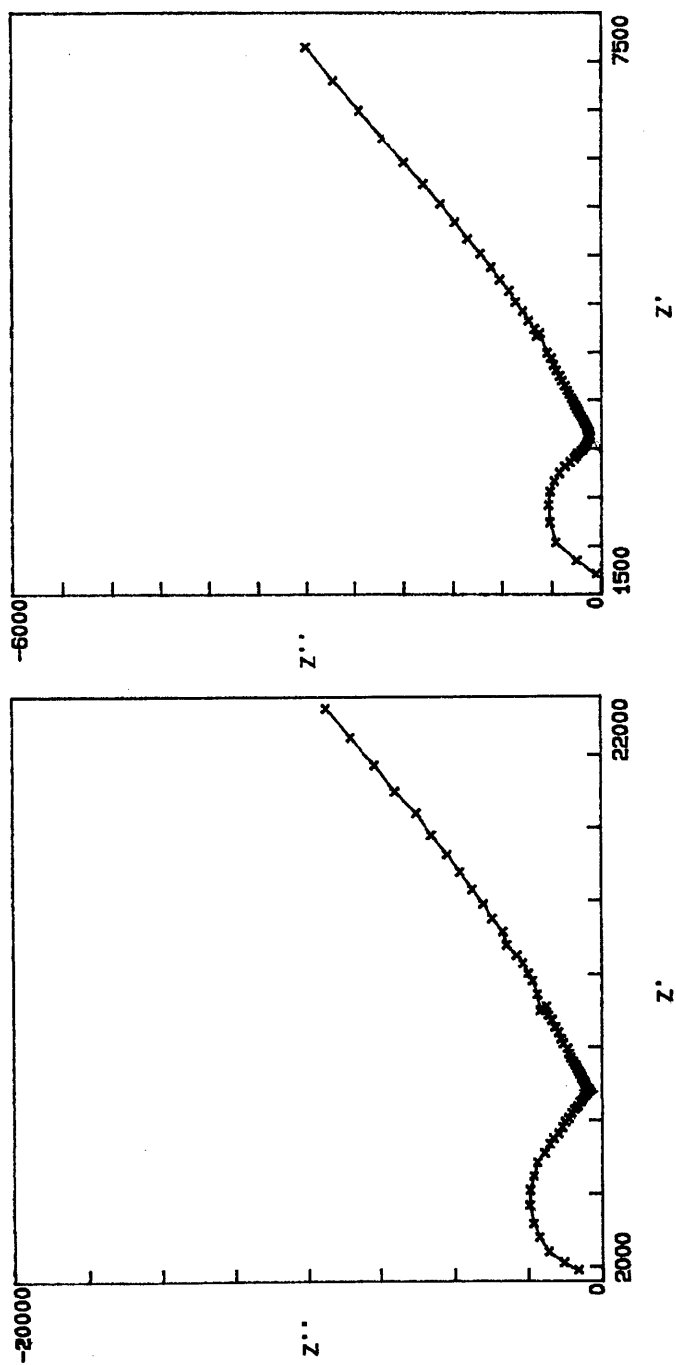
Figure 4.13, continued: (c) 390.0 °C, cooling. (d) 339.8 °C, cooling.
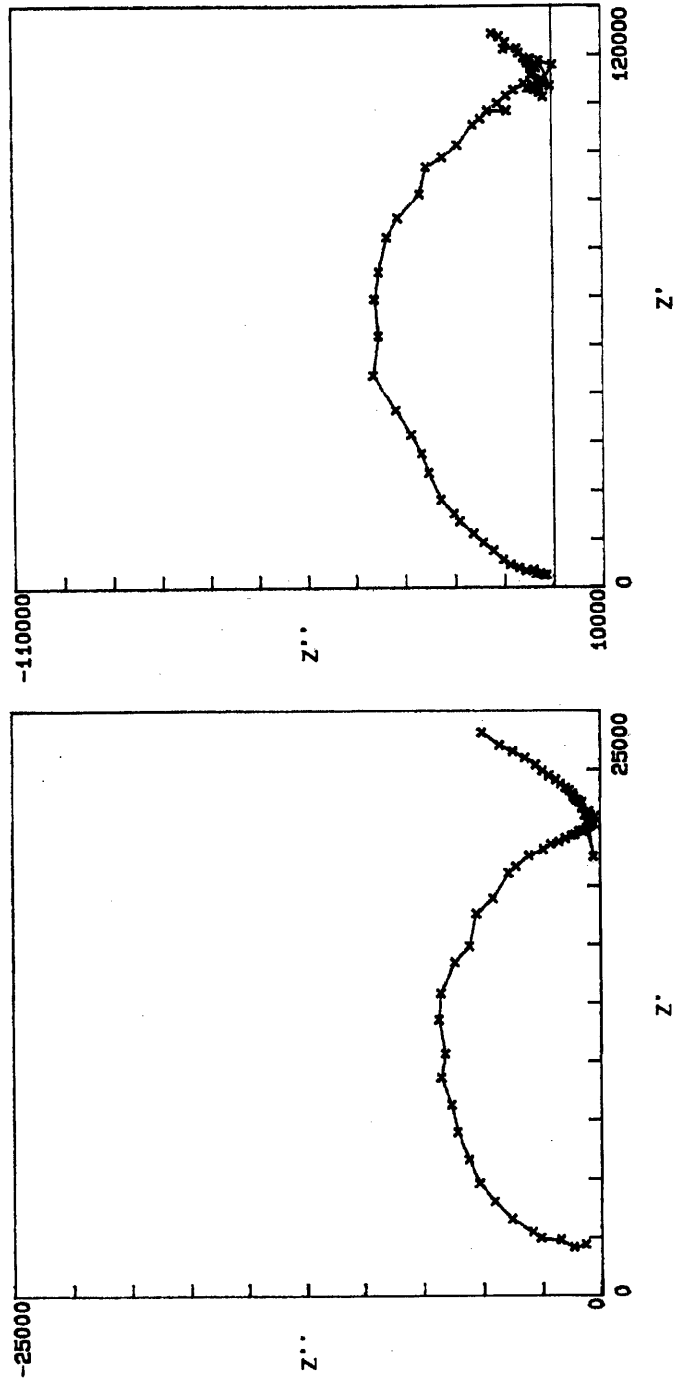
Figure 4.14: Conductivity of $Bi_2VO_{5.5}$ contaminated with $BiVO_4$ as a function of temperature.
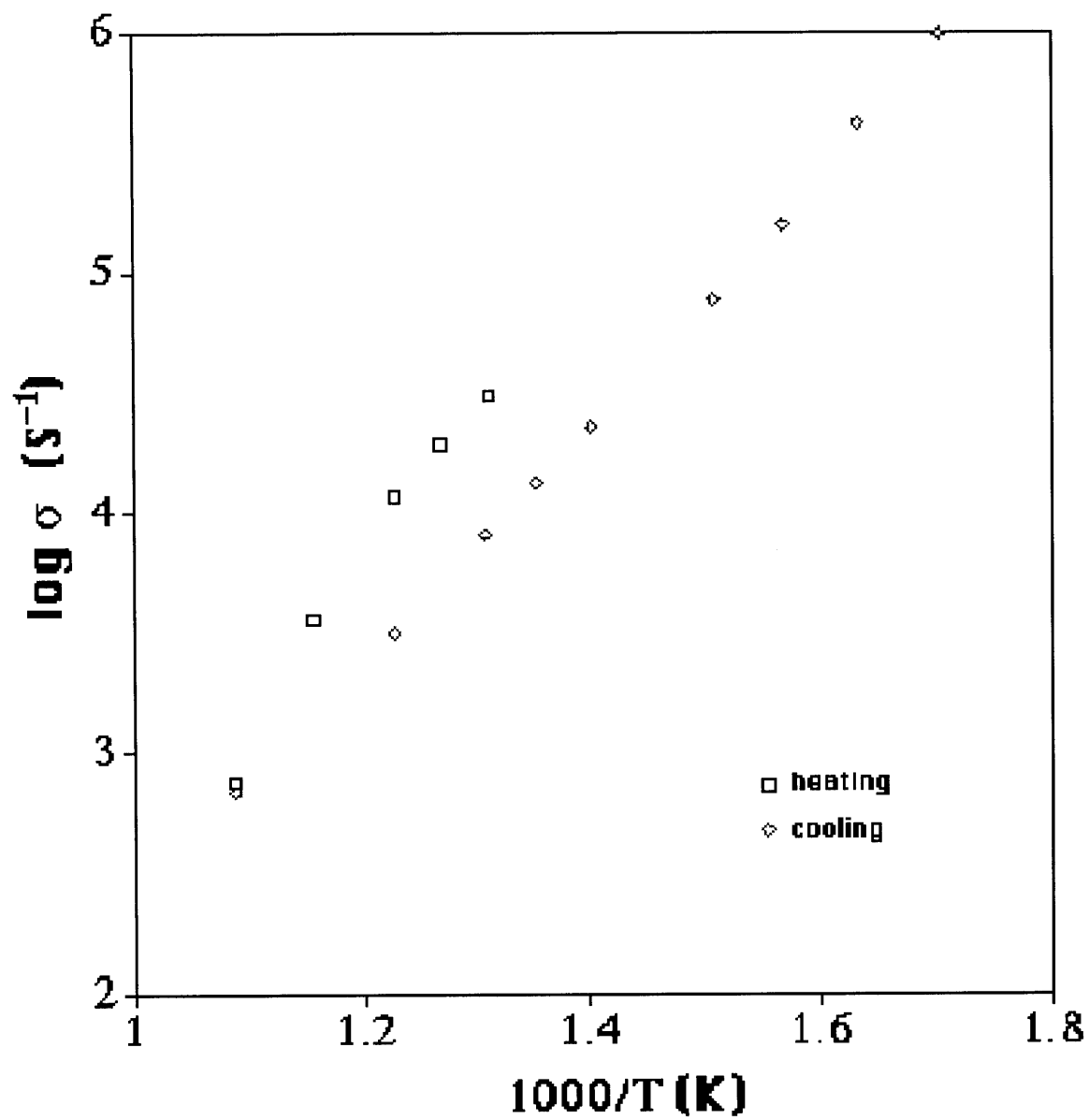
Figure 4.15: DTA of hydrolyzed and gelled precursor to $Bi_2VO_{5.5}$. Bismuth was added as $Bi(N(SiMe_3)_2)_3$. Heating rate: 25 °C/min.

Temperature Difference (°C)

Temperature (°C)

Weight (mg)

99.3%, 213 °C

96.7%, 283 °C

89.9%, 308 °C
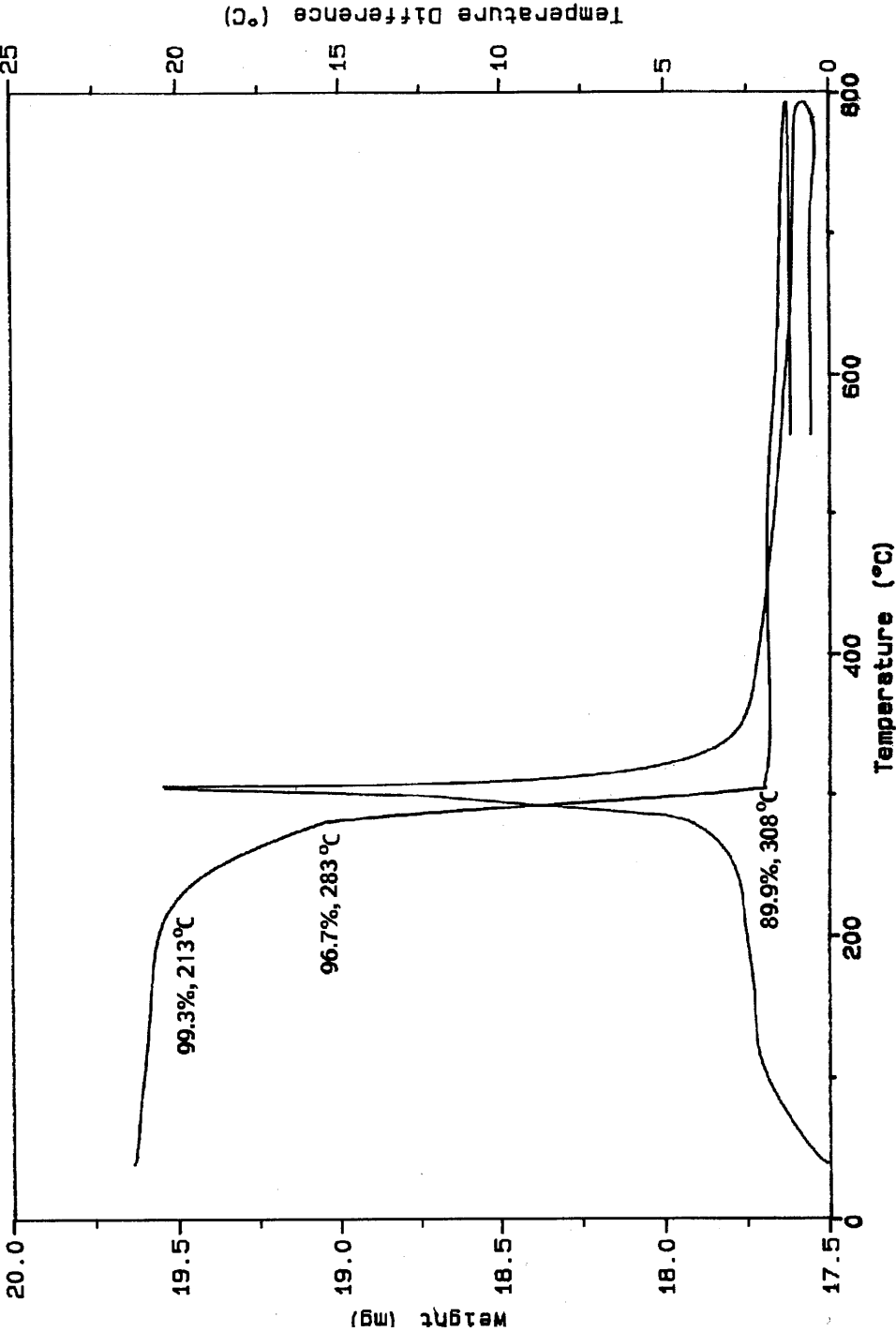
Figure 4.16: Powder XRD patterns at various pyrolysis temperatures for sol-gel produced $Bi_2VO_{5.5}$. The bismuth precursor was $Bi(N(SiMe_3)_2)_3$.
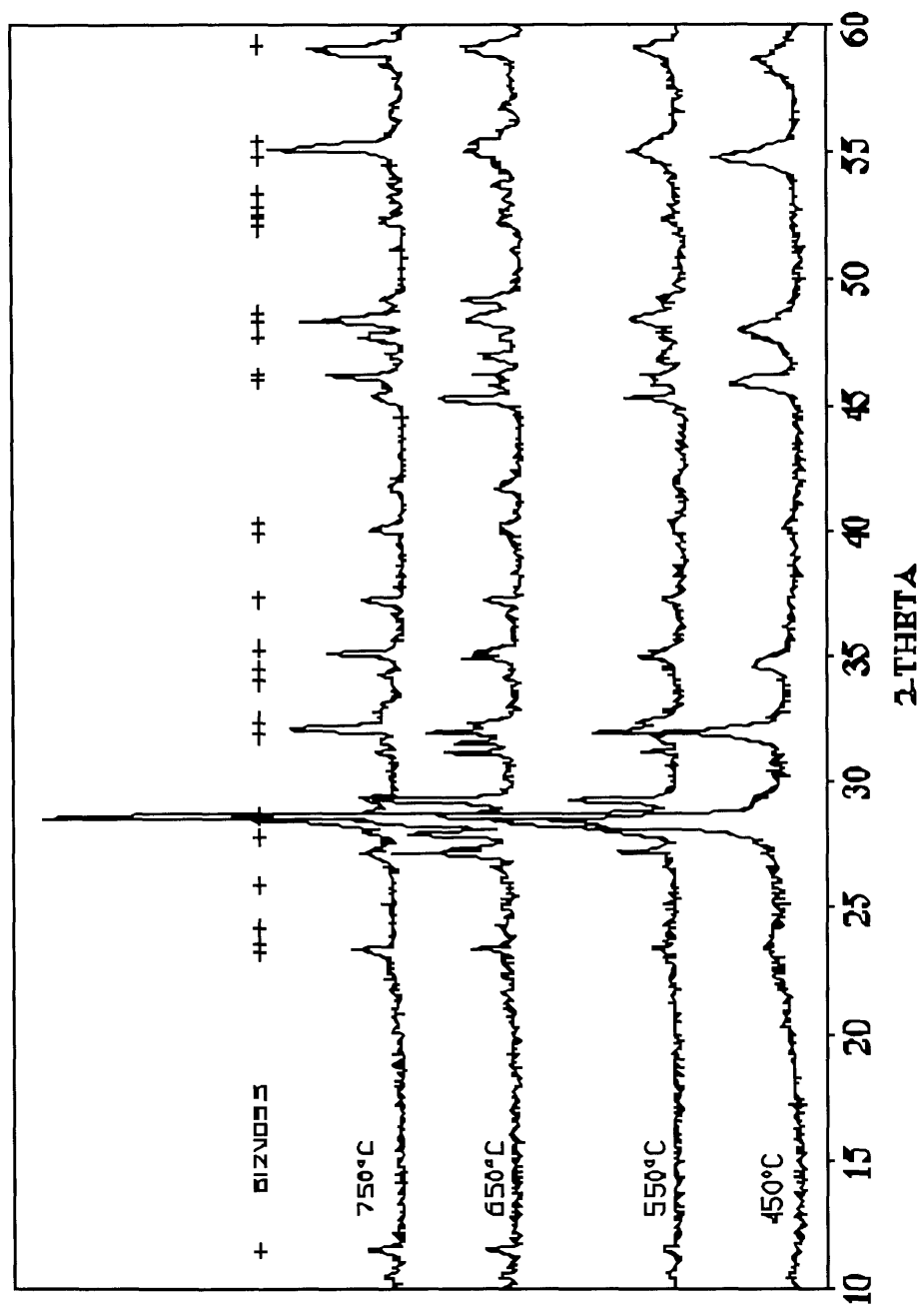
Figure 4.17: Powder XRD patterns at various pyrolysis temperatures for sol-gel produced $Bi_2Cu_{0.1}V_{0.9}O_{5.5}$. The precursor was V-2MOE, $Cu(OAc)_2$, and $Bi(OAc)_3$.
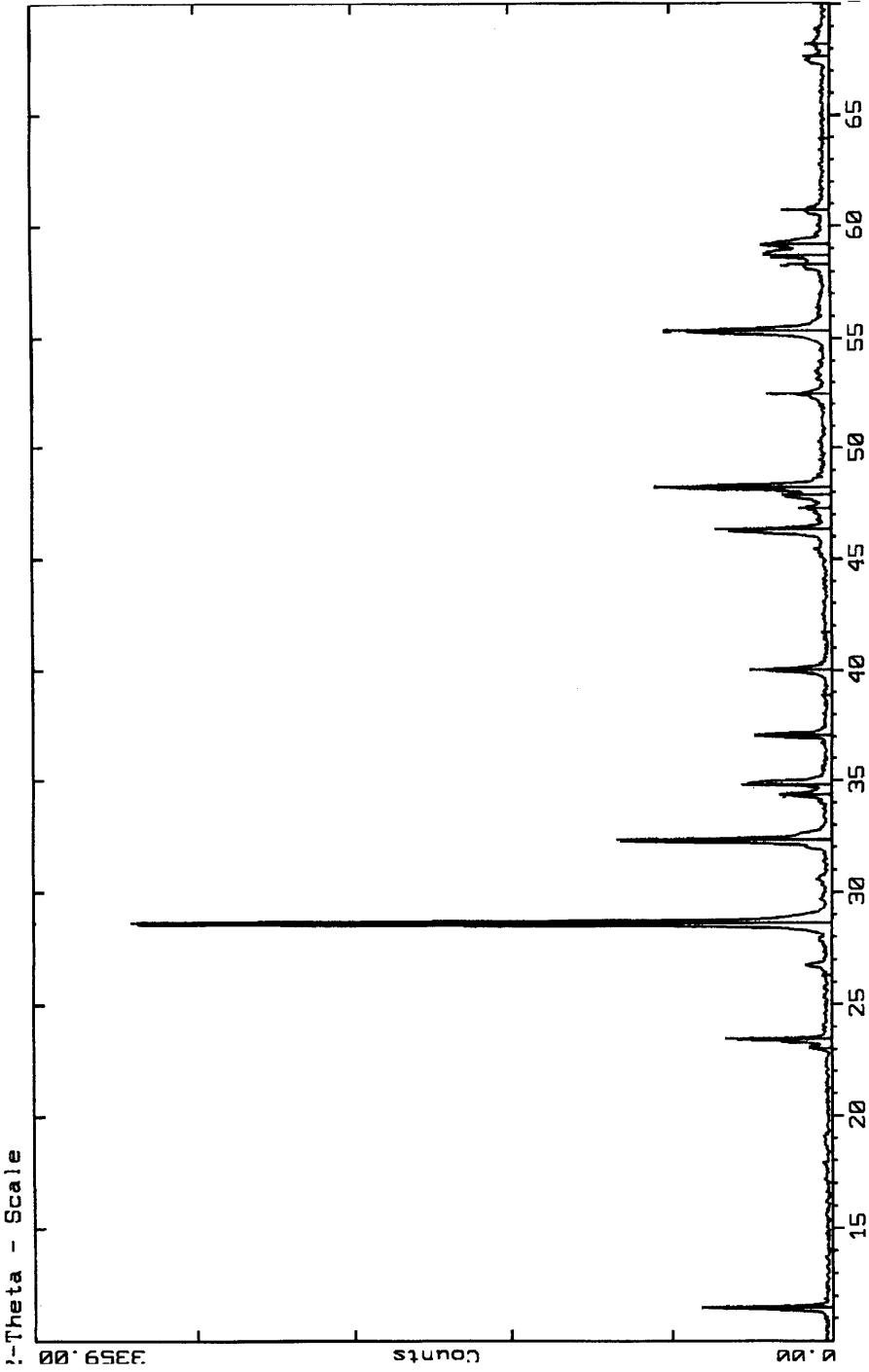
Figure 4.18: Powder XRD patterns at various pyrolysis temperatures for sol-gel produced $Bi_2Nb_{0.3}V_{0.7}O_{5.5}$. The precursor was V-2MOE, $Nb(OiPr)_5$, and $Bi(OAc)_3$.
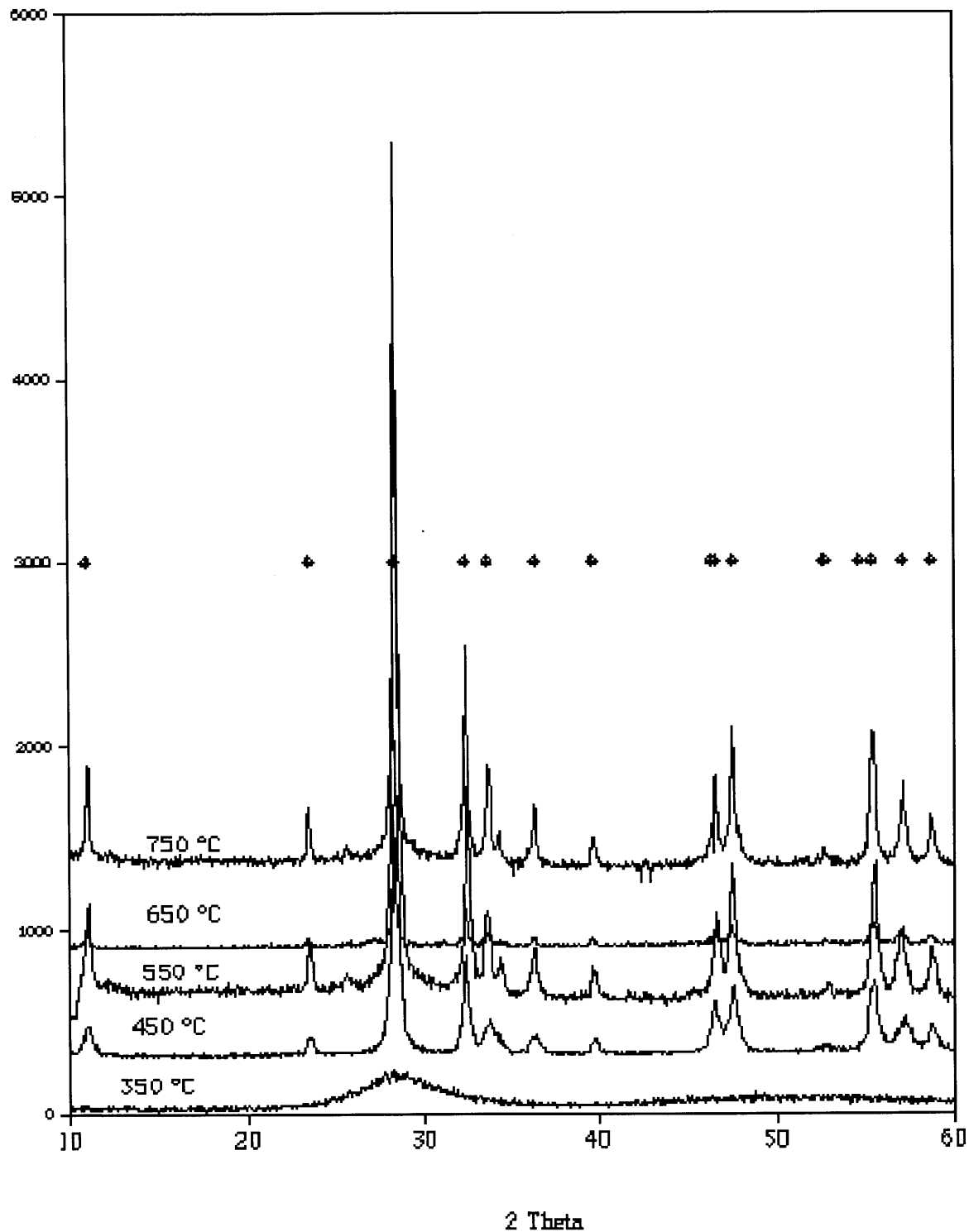
Figure 4.19: Powder XRD patterns at various pyrolysis temperatures for sol-gel produced $Bi_2Mn_{0.15}V_{0.85}O_{5.5-\delta}$. The precursor was V-2MOE, $Mn(OAc)_2$, and $Bi(OAc)_3$.

2 Theta
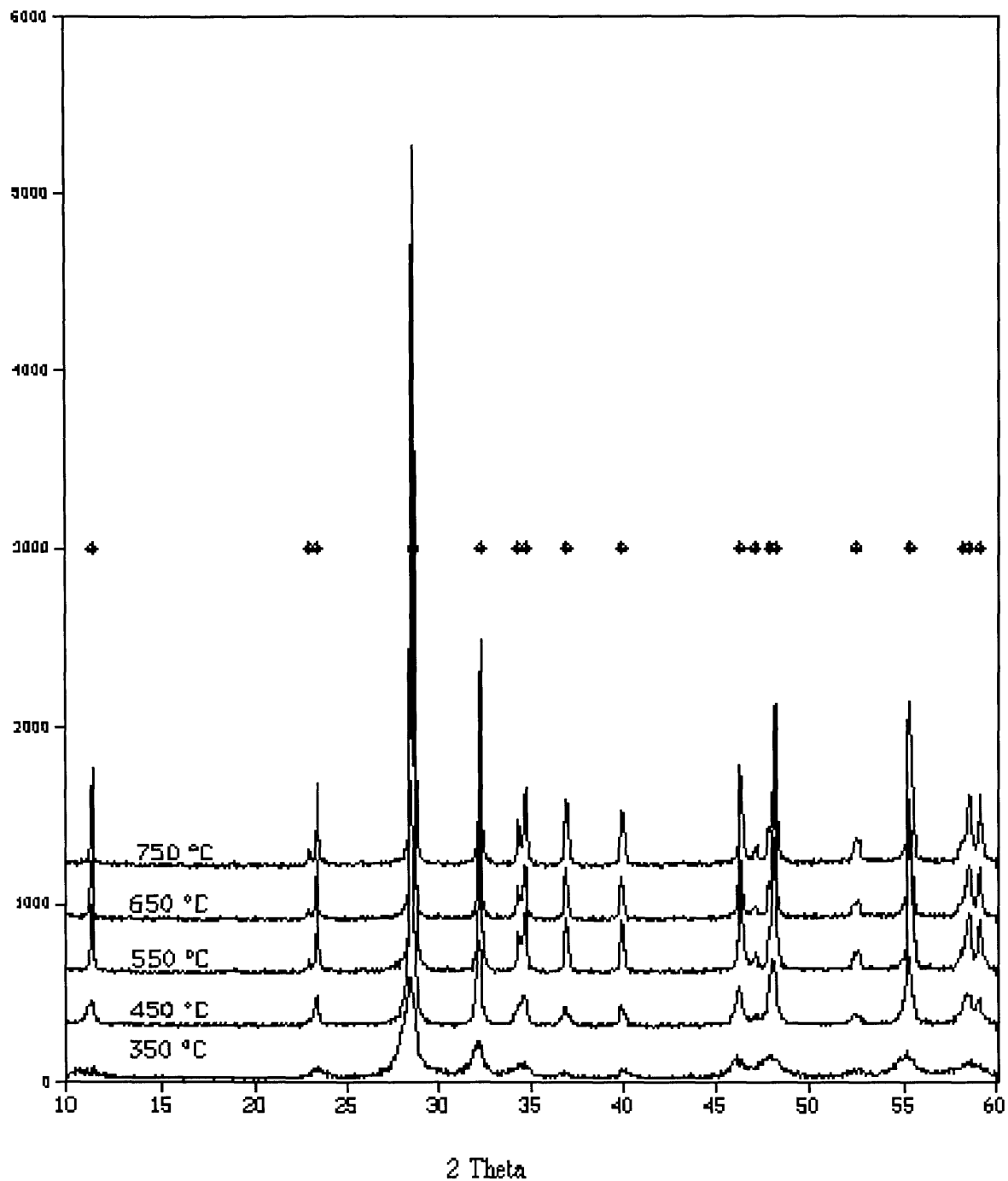
Figure 4.20: Powder XRD patterns at various pyrolysis temperatures for sol-gel produced $Bi_2Fe_{0.1}V_{0.9}O_{5.5-\delta}$. The precursor was V-2MOE, $Fe(OAc)_2$, and $Bi(OAc)_3$.
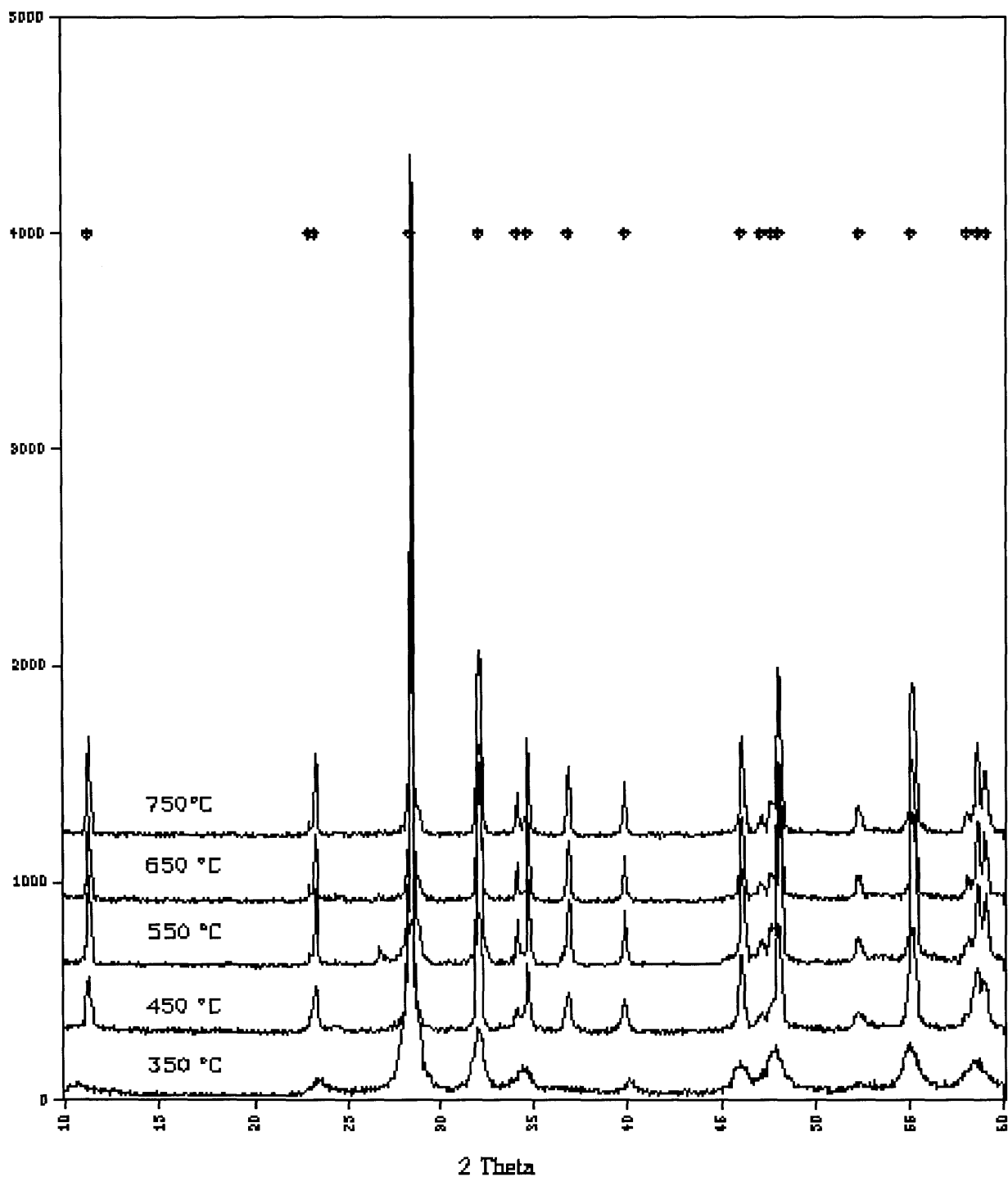
Figure 4.21: Powder XRD pattern at a pyrolysis temperature of 750 °C for sol-gel produced $Bi_2Ti_{0.1}V_{0.9}O_{5.5-\delta}$. The precursor was V-2MOE, $Ti(OiPr)_4$, and $Bi(OAc)_3$.
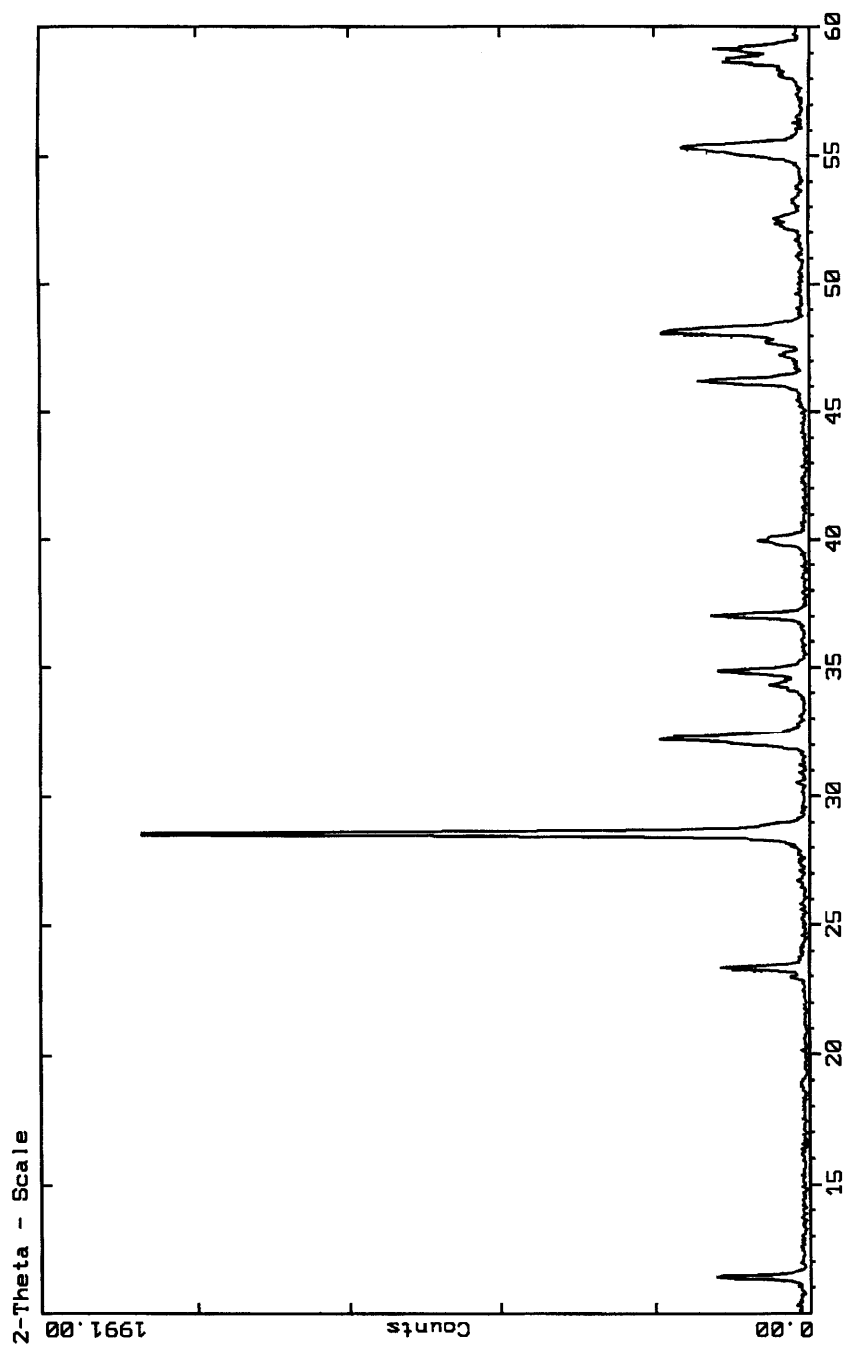
Figure 4.22: Powder XRD patterns at various pyrolysis temperatures for sol-gel produced $Bi_2Cu_{0.1}V_{0.9}O_{5.5}$. The precursor was V-2MOE, $Cu(OAc)_2$, and $Bi(N(SiMe_3)_2)_3$.
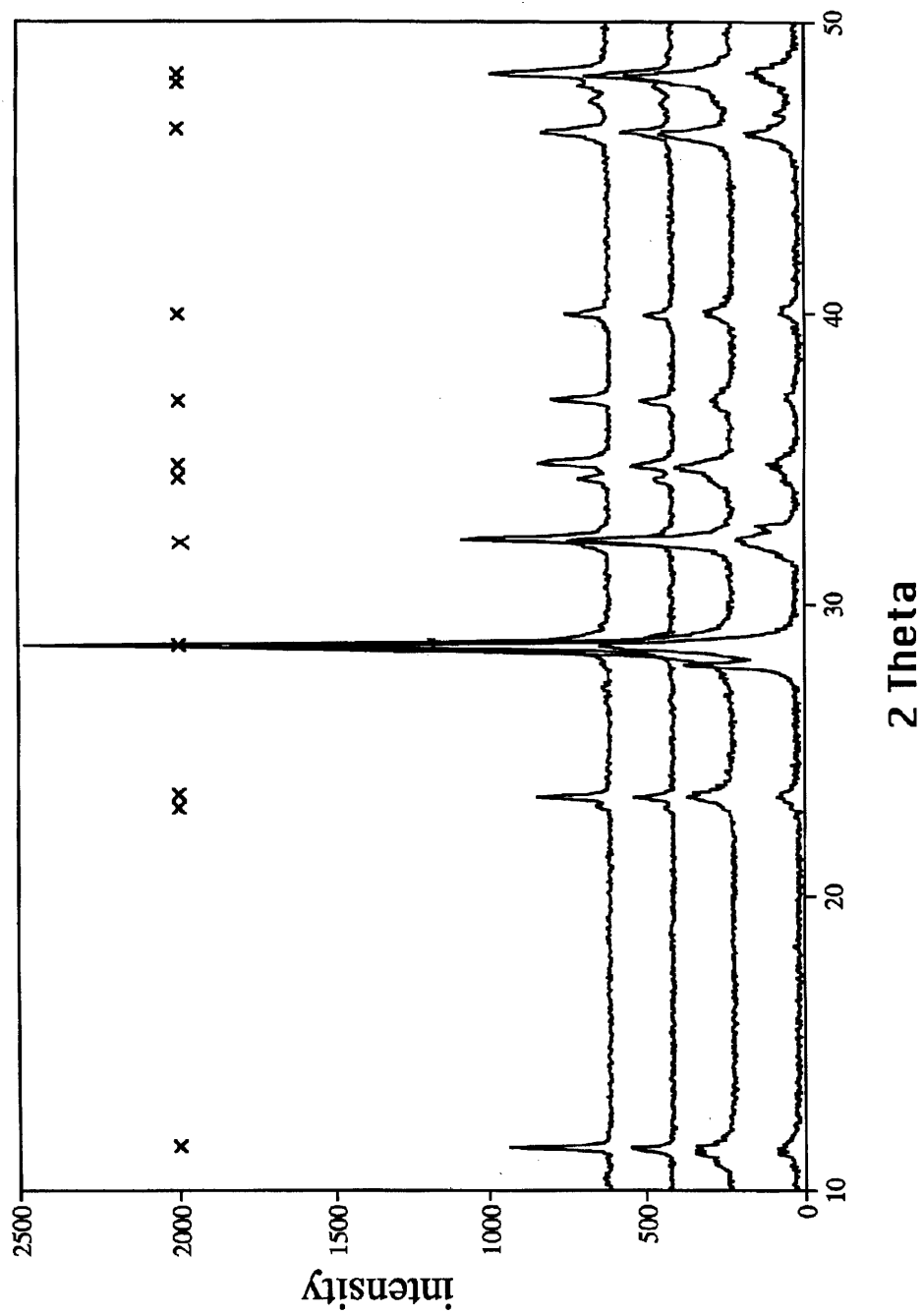
Figure 4.23: Complex impedance plots for sol-gel produced

$Bi_2Cu_{0.1}V_{0.9}O_{5.5}$. (a) 294.8 °C heating. (b) 395.3 °C heating.
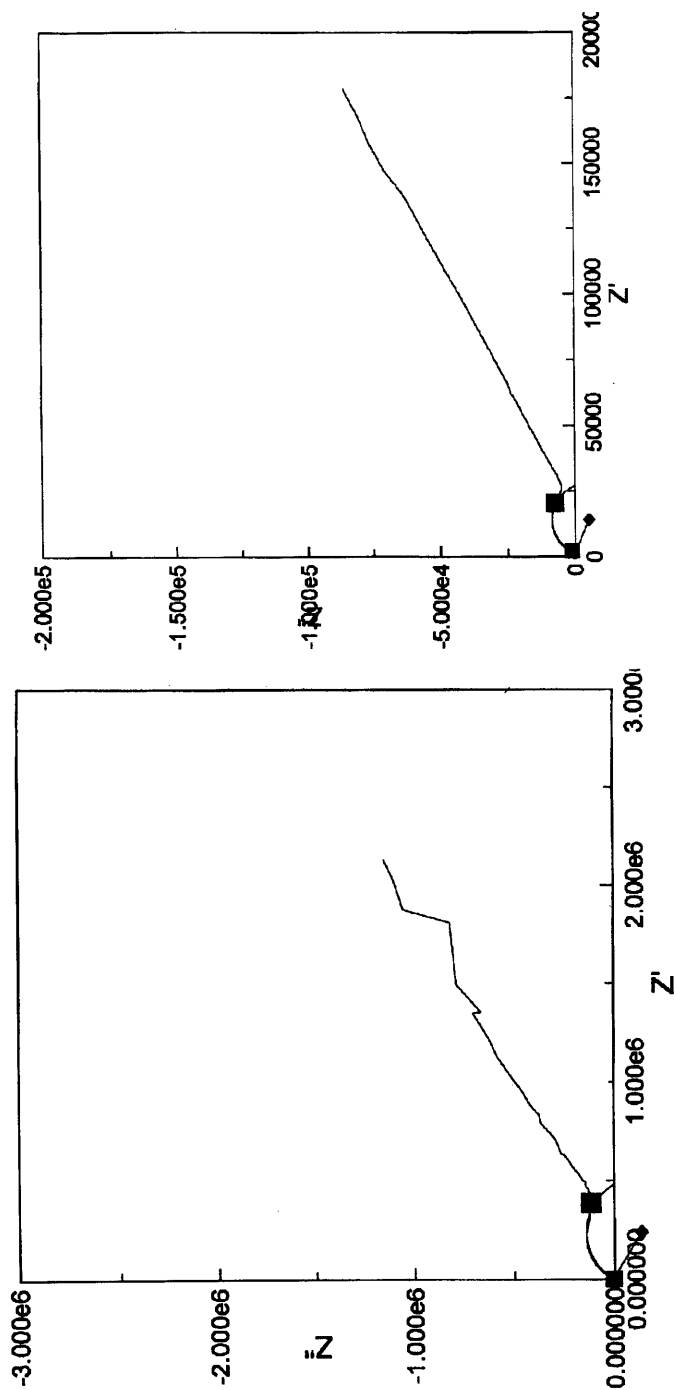
Figure 4.23, continued: (c) 675.1 °C heating. (d) 805.7 °C heating.
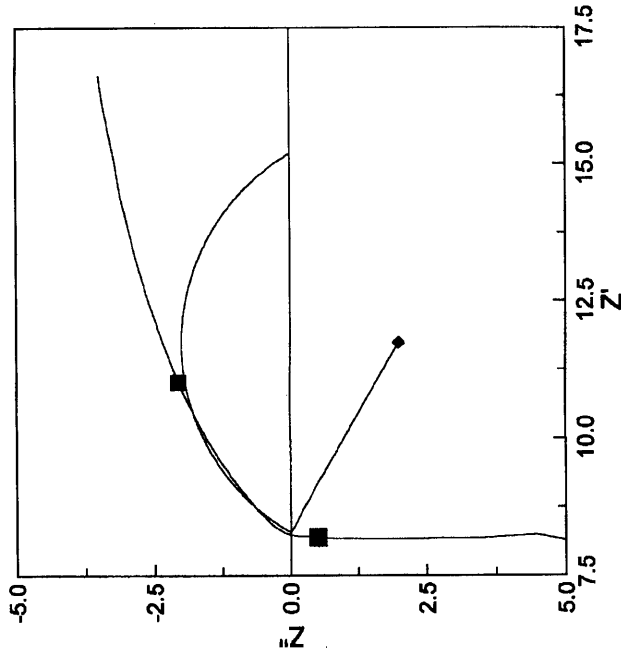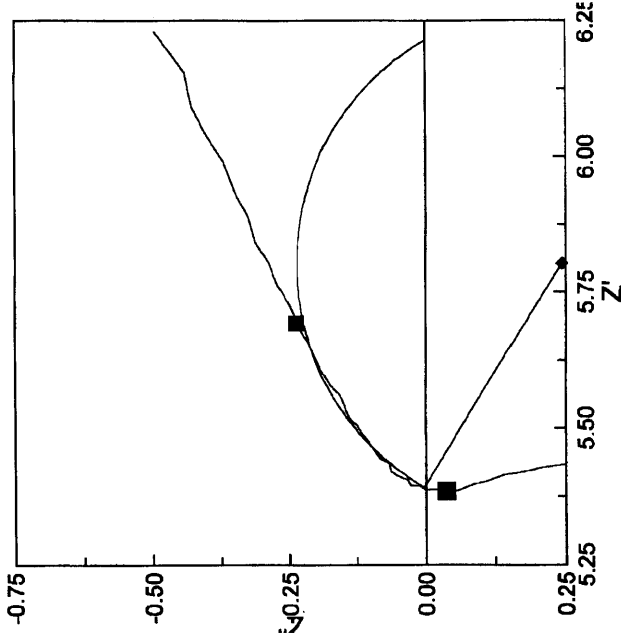
Figure 4.24: Conductivity of sol-gel produced $Bi_2Cu_{0.1}V_{0.9}O_{5.5}$ as a function of temperature.
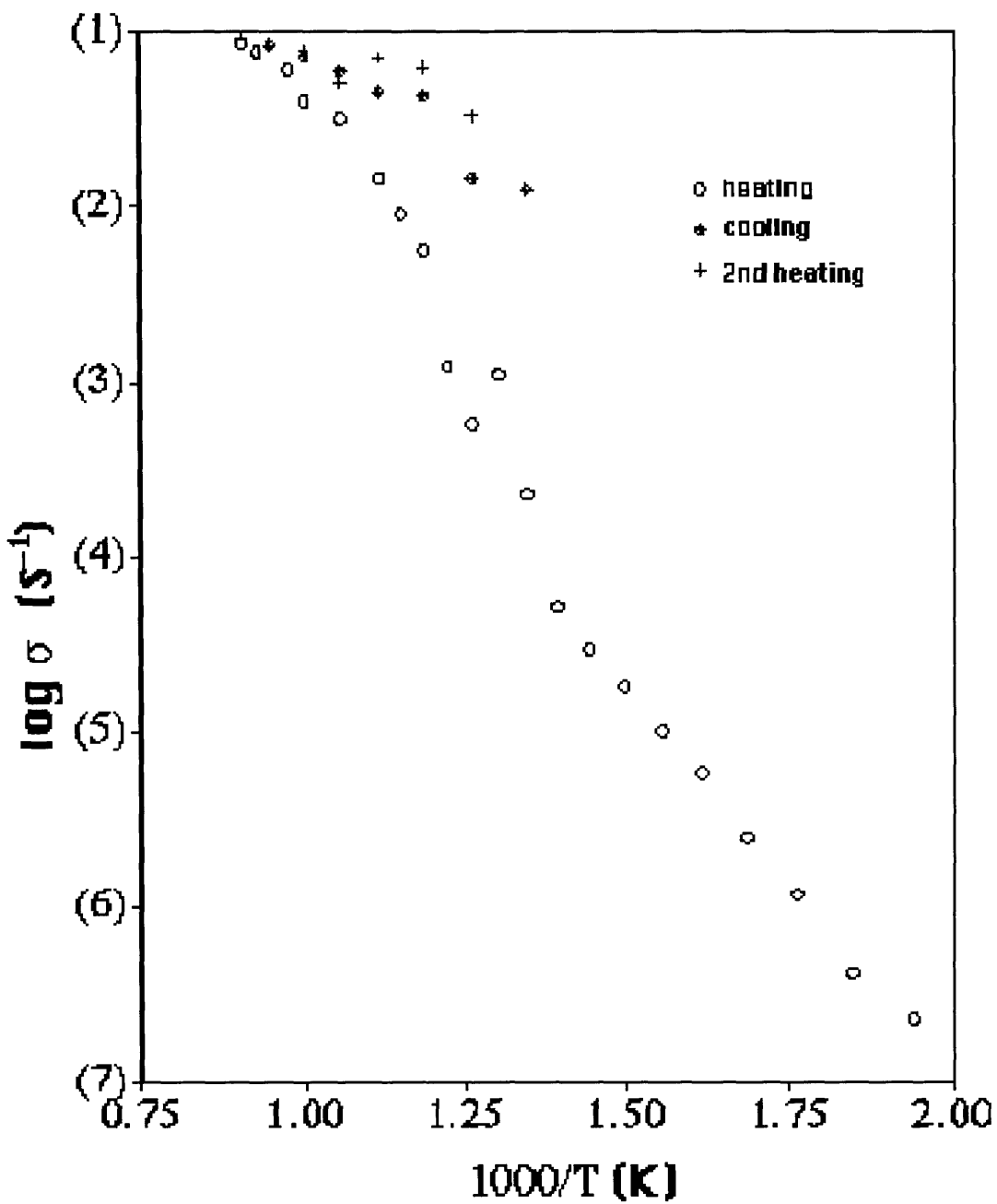
4.3 Conclusions

Vanadium 2-methoxyethoxide was used to generate the gel for sol-gel precursors to BiMeVOx materials with considerably more success than had been found for solutions using poly(vanadic acid), described in Chapter Three. Bismuth acetate prepared from the oxide by repeated reflux in glacial acetic acid under inert atmosphere with removal of water, was found to be soluble in alcohol ethers such as 2-methoxyethanol and was used successfully in precursor solutions. On standing in 2-methoxyethanol solution, the bismuth acetate alcoholyzes to form a fibrous insoluble material thought to be polymerized bismuth 2-methoxyethoxide. The formation of this material is suppressed in the presence of vanadium 2-methoxyethoxide. This suppression could indicate the formation of an associated Bi-O-V complex in solution, which may aid in keeping the bismuth atoms in place in the gel network during gelation, drying, and pyrolysis, assisting the $Bi_2VO_{5.5}$ phase in appearing at a lower temperature than for solid state synthesis. The layered nature of the primary vanadium-based gel component, combined with the linear structure of the alcoholytic Bi-2MOE-OAc polymer that develops on standing, is a second factor in the low-temperature development of the layered $Bi_2VO_{5.5}$ phase. The disordered doped phases form at still lower temperatures.

Bismuth 2-methoxyethoxide made by alcoholysis of the dimethylsilamide was also used successfully in the precursor solution. Here, the desired phase formed directly at 450 °C pyrolysis temperature, with no trace of intermediate $BiVO_4$

formation. Presumably the possibility for the bismuth alkoxide's participation in hydrolysis and condensation reactions permitted this low-temperature formation. However, due to the multistep nature of the procedure, and the low yields, this precursor was deemed uneconomical for scale-up and industrial application and was dropped from further investigation.

Bulk parent α-$Bi_2VO_{5.5}$ and several γ-phase doped BiMeVOx materials, e.g. BiCuVOx, BiNbVOx, BiTiVOx, BiFeVOx, and BiMnVOx, were synthesized from a sol-gel precursor solution made up of soluble bismuth acetate, vanadium alkoxide, and dopant alkoxide or carboxylate. In doped materials, the desired phase formed directly, presumably, as DTA/TGA indicated decomposition at 430 °C and pure γ-phase was found at 450 °C. This is in contrast to the behavior of the undoped parent phase made by the same precursor process, which appears at 450 °C but is not completely formed phase-pure until 725 °C. All of these temperatures are some 300 °C lower than for the standard solid-state synthesis, demonstrating the success of the method in providing for intimate mixing of the metals in the compound. Complex impedance spectroscopy data taken for BiCuVOx made by the sol-gel method described shows oxygen ion conductivity on par with that reported in the literature for samples made by the solid-state powder synthesis route.

The result that the doped BiMeVOx materials could be synthesized by a sol-gel method at low temperature provided the possibility for deposition of films of these materials. The work towards the goal of producing defect-free films of BiMeVOx on porous substrates is described in Chapter Six. However, since a number of observations during the course of the work described in

this Chapter were suggestive of the formation of a single precursor complex between bismuth and vanadium in solution, some experiments were undertaken to elucidate the nature of this putative precursor. That work is described in the next Chapter.

4.4 Experimental Section

See the Appendix to Part I of this thesis for a list of materials and their sources, and for specifics on instrumentation used.

4.4.1 Vanadium Alkoxides

Several attempts to make $VO(OEt)_3$ by refluxing together V_2O_5 and ethanol or butanol with distillation of water/alcohol/benzene azeotrope gave a hydrolyzable product which could not be cleanly isolated by distillation. The distillation was attempted at atmospheric pressure and under vacuum, but the equipment used for vacuum distillation was inadequate. Attempts to make the alkoxide by alcoholysis of $VOCl_3$ with a sweep of inert gas to carry off HCl, gave a yellow undistillable material, and in combination with NH_3 generated by NH_4OH gave a white gelatinous precipitate or a black gum. Combinations of $VOCl_3$ with EtOH, iPrOH, BuOH, and 2MOE gave materials which precipitated on addition of water. These experiments are described in more detail below.

Experiment #1 (JWP-I-19I27) V_2O_5 + nBuOH → $VO(OBu)_3$

Finely ground V_2O_5 (18.185g, 100 mmol) was added to nBuOH (110 ml, 1200 mmol) in 100 ml benzene. A small amount of 3 Å molecular sieve was added to the reaction pot to scavenge evolved water and the mixture refluxed with distillation for 4.5 h. When distillate stopped coming over, the reaction mixture was filtered to yield a green-brown liquid. An attempt to vacuum distill the product decomposed it. Addition of water to a sample of this provided a red

203

gel in under 1 minute. The gel subsequently became green-black on standing for a few minutes. A known amount of solid was hydrolyzed to a fibrous gelatinous solid and carefully heated to dryness, then pyrolyzed 18 hours in air at 600 °C. The orange brown solid, verified by powder XRD as V_2O_5, was weighed and the concentration of the sample found to be 1.350 mmol V/g solution.

Experiment #2 (JWP-I-21) V_2O_5 +excess nBuOH → VO(OBu)$_3$

The same synthesis as Experiment #1 was tried, this time with a 10x excess of BuOH in hopes of getting all of the V_2O_5 to react. A green-grey solid remained in the pot.

Experiment #3 (JWP-I-28) V_2O_5 + 2MOE → VO(2MOE)$_3$, single heating

V_2O_5 was ground finely in a mortar and added (4.0158g, 22 mmol) to 100 ml benzene and 150 ml 2MOE (2 mol). This was heated with distillation for 3 hours and the olive green product filtered. The solid residue was washed with 2x 25 ml 2MOE and the washings combined with the filtrate. The filtrate became red-orange on addition of water. A known amount of the product was hydrolyzed and carefully heated to dryness, then heated for 18 hours in air at 600 °C. The orange-brown solid, verified by XRD as V_2O_5, was weighed and the concentration of the sample found to contain 0.2436 mmol V/g solution, approximately 56% yield from V_2O_5 .

Experiment #4 (JWP-I-53) V_2O_5 + 2MOE → VO(2MOE)$_3$, smaller excess of 2MOE

V_2O_5, finely ground (4.0306 g, 22 mmol), was added to 75 ml benzene and 100 ml (1.32 mol) 2MOE and heated 3 h until distillation of clear and colorless liquid stopped. The reaction mix was filtered to leave a light yellow liquid which was found by the usual method to deliver 0.1018 mmol V/g solution, approximately 59% yield from V_2O_5.

Experiment #5 (JWP-II-93a) VO(OiPr)$_3$ + 2MOE → VO(2MOE)$_3$

VO(OiPr)$_3$, 25 ml (0.1 mol) was added to 75 ml 2MOE (1 mol) and refluxed 1.5 h, followed by distillation at 83-105 °C. An additional 100 ml 2MOE (1.25 mol) were added and distillation continued until the vapor temperature exceeded 100 °C. It was permitted to stand and cool overnight to yield a brown liquid. Standard analysis showed concentration 1.068 mmol V/g solution, approximately 63% yield from the initial vanadium content of the vanadium isopropoxide solution.

Experiment #6 (JWP-II-94a) V_2O_5 + 2MOE → VO(2MOE)$_3$, 2 distillations

Finely ground V_2O_5 (10g, 53.5 mmol) was added to 100 ml benzene and 200 ml (2.63 mol) 2MOE and heated for 1 hour. It was then distilled until the vapor temperature was 105 °C, and 40 ml more (0.52 mol) 2MOE added. Distillation was continued until the

vapor temperature exceeded 105 °C. The green-brown liquid was cooled and filtered twice. The standard analysis found 0.7266 mmol V/g solution, approximately 77% yield based on V_2O_5.

Experiment #7 (JWP-II-201) Standard V-2MOE Preparation

25 g of finely ground V_2O_5 was added to benzene (100 ml) and 2MOE (200 ml) and distilled at 100 °C for 2 hours. Up to 50 ml more 2MOE was added and the mixture again distilled until the temperature exceeded 105 °C. The cooled mixture was left stirring overnight, then filtered under inert atmosphere with 2MOE rinses. Aliquots of known mass were taken, hydrolyzed, and carefully dried, then pyrolyzed in air for 8 h at 750 °C. The remaining solid was weighed as V_2O_5 to calculate moles V delivered per g of solution. Yields were generally 70-80% based on V_2O_5 added.

4.4.2 Bismuth Part of the Precursor

Experiment # 8 (JWP-I-93I5) Bi(NO$_3$)$_3$*5H$_2$O + HO(CH$_2$CH$_2$O)$_4$H → [Bi(NO$_3$)$_2$(O(CH$_2$CH$_2$O)$_4$)]$_2$* 2 MeOH

In inert atmosphere Bi(NO$_3$)$_3$·5H$_2$O (4.865 g, 10 mmol) were added to 7.5 ml acetonitrile and 2.5 ml MeOH and warmed; tetraethylene glycol (2.3g, 11.84 mmol) was added to MeOH (2.5 ml) and dissolved. This was added to the bismuth nitrate solution and warmed 1.5 h. On cooling overnight some crystals appeared; these were redissolved on warming and stirring. After again sitting overnight the flask was left for several hours on ice. The solid was

filter washed with 2x 10 ml of cold MeOH, then vacuum dried. The filtrate was clear and yellow. 3.82 g of the solid was recovered (33%, white solid) and stored in the glove box. The experiment was repeated on (JWP-I-90, 32% yield, white crystals in yellow oil). In that experiment, the product was hydrolyzed to a gellatinous precipitate with TGA/DTA (Figure 4.25). Likewise, the synthesis was repeated on a larger scale (JWP-I-95, again in approximately 30% yield).

Experiment #9 (JWP-II-8) BiCl$_3$ + NaN(SiMe$_3$)$_2$ → Bi(N(SiMe$_3$)$_2$)$_3$ "BiSA"

BiCl$_3$ (3.0208 g, 9.6 mmol) was added to a schlenk flask in the glove box and dissolved to an opalescent solution in 70 ml diethyl ether. NaN(SiMe$_3$)$_2$ (5.5357 g, 30 mmol) was added to a second schlenk flask and suspended in 50 ml diethyl ether. The latter solution was cooled to 0 °C and the BiCl$_3$ solution added slowly to it via cannula. The reaction was stirred at room temperature overnight, then the ether removed *in vacuo* to yield a fine yellow powder. This was dissolved in pentane, leaving a pale yellow solid (^{1}H NMR in C$_6$D$_6$ 0.373 ppm (s)) which was filtered off, pyrolyzed, and identified by XRD as NaCl plus some Bi$_2$O$_3$. Some of the filtrate was hydrolyzed and dried, then pyrolyzed – XRD identified this as Bi$_2$O$_3$. To the remainder of the filtrate excess 2MOE was added, giving a clear and colorless solution. Removal of the solvent *in vacuo* gave a white solid. Hydrolysis and pyrolysis of this material gave Bi$_2$O$_3$ (identified by XRD). DTA/TGA was done on Bi(N(SiMe$_3$)$_2$)$_3$ powder and on the hydrolyzed gel. (Figure 4.26 a,b) The

preparation was repeated on II-18A, II-46 (39% yield), II-57, and II-95 (29% yield).

Experiment #10 (JWP-II-24A) $BiCl_3$ + $NaN(SiMe_3)_2$ → BiSA; BiSA + 2MOE → "Bi(2MOE)$_3$"

$BiCl_3$ (5.0932g, 15 mmol) and $NaN(SiMe_3)_2$ (8.3g, 45 mmol) were each dissolved in 75 ml Et_2O and added, one to the other, at room temperature. The evolved heat boiled the solvent and a yellow green-grey suspension resulted. This was stirred overnight and the ether distilled off to near-dryness, then the remainder removed *in vacuo*. This was extracted with pentane and filtered. To the filtrate was added 10 ml 2MOE to get a clear and colorless solution. The volume was reduced *in vacuo* and the solution's [Bi] determined by hydrolysis and pyrolysis as Bi_2O_3 to be 0.11 mmol/g solution. DTA/TGA (Figure 4.27) and PA-FTIR (Figure 4.7b) were performed on the product, which was assumed to have the formula $Bi(2MOE)_3$.

Experiment #11 (JWP-I-19) Bi_2O_3 + acetic acid in open air → $Bi(OAc)_3$ + BiO(OAc)

Bi_2O_3 (30.692g, 66 mmol) was added to 100 ml glacial acetic acid (1600 mmol) with heating and stirring. The yellow suspension became white and was permitted to cool to room temperature, producing large flat crystals which were covered with a fine white powder. This was filtered and the solid washed with cold ethanol, leaving a fine white powder. The sample was oxidized to Bi_2O_3 and

found to have a weight retention of 82% (82% expected for $BiO(OAc)_3$). Yield 100% based on bismuth oxide acetate.

Experiment #12 (JWP-II-77A) Bi_2O_3 + acetic acid in N_2 sweep → $Bi(OAc)_3$

Bismuth oxide was twice covered with glacial acetic acid in an open Schlenk flask and boiled to near-dryness under rapidly flowing nitrogen. During the first heating the pale yellow oxide suspension became milky white, and during the second a colorless solution was obtained. On cooling, white mica-like crystals formed and were separated by filtration. Drying was completed under vacuum. The material was stable indefinitely at room temperature under inert atmosphere, but decomposed in air to an insoluble off-white talclike powder. Yield: 100% of Bi recovered as $Bi(OAc)_3$. Elemental analysis (Oneida): 18.42 C, 2.10 H (expected for $Bi(OAc)_3$ 18.66 C, 2.35 H). The sample was decomposed at 700 °C in air to Bi_2O_3 and the wt. retention was found to be 60%, consistent with $Bi(OAc)_3$ (60% expected) and not with $BiO(OAc)$ (82% expected). DTA/TGA showed total weight loss 40% actual, expected for conversion to bismuth oxide 39.7%; decomposition steps at 275 °C to oxyacetate, 375 °C to oxide. (Figure 4.4) PA-FTIR: (cm^{-1}) 3013 m, 2935 m, 2486 w, 2334 w, 1970 w, 1622 sh, 1542 s, 1426 s, 1348 sh, 1051 s, 1024 s, 941 s, 687 s, 617 m, 475 m (Figure 4.5). Powder XRD of the material was difficult due to the high degree of orientation of the crystals; the peak positions could not be matched to anything in the JCPDS database, including JCPDS #14-0726 ($Bi(OAc)_3$) nor to the patterns reported in the literature.[43] (Figure 4.2) The material was

ground in air and left open to air overnight, and the powder XRD repeated to give a pattern matching JCPDS #14-0800 (BiO(OAc)). (Figure 4.3)

X-ray diffraction was performed on a single crystal of the bismuth acetate prepared in this experiment. Space group P2$_1$/a **a**=12.0848 Å, **b**=10.8859 Å, **c**=7.2889 Å, β=106.173°, Z=4. Atomic distances and angles to be given in figure caption. (Figure 4.6)

The solubility of -77A in several solvents was tested: it was soluble in 2MOE, ethylene glycol, and diglyme, but not in HOiPr, benzene, or THF. The sample, after being ground and left open to air overnight, would not dissolve even in large amounts of 2MOE with warming.

Experiment #13 (JWP-II-77B) Bi(OAc)$_3$ + 2MOE → [Bi(2MOE)$_x$(OAc)$_{3-x}$]$_\infty$

The procedure of Experiment #6 (II-77A) was repeated, and hot 2MOE was added (20 ml) to dissolve the solid. On cooling, a copious white puffy precipitate formed. This redissolved on heating. 2MOE was added to make up a total volume of 50 ml and the solution left overnight at room temperature. The resulting white solid mass occupied the entire solution volume. Addition of 50 ml more 2MOE would not redissolve the solid, even with heating. The white solid was collected and dried and decomposed at 700 °C for 1 hour in air. The resulting yellow powder, identified as Bi$_2$O$_3$, showed an 80.0% weight retention. Bi(2MOE)$_3$ gives 53.7% weight retention expected.

Experiment #14 (JWP-II-121) Bi(OAc)$_3$ + 2MOE → [Bi(2MOE)$_x$(OAc)$_{3-x}$]$_\infty$

Bi$_2$O$_3$ (6 g, 12.9 mmol) was added to a schlenk flask and covered 3x with glacial acetic acid. The acetic acid was distilled off each time under swift nitrogen flow. Finally, acetic anhydride was added and removed in the same manner, and the resulting white crystalline solid dried *in vacuo* overnight. (II-121A) 50 ml 2MOE was added to this and stirred with warming to 50 °C to get a clear solution which after a few minutes became milky. Another 25 ml 2MOE were added to produce a clear solution and the stirring and heating discontinued. Within 6 hours white woolly fibers appeared to be growing from the flask walls; within 12 hours the entire solvent volume was occupied by a white fibrous material. Some of this was removed and stored in the glovebox. (II-121B) The solvent was removed *in vacuo* from the remainder: during this removal the fibers broke up to give a milky suspension. The resulting white amorphous solid was pumped down on over the weekend, and some of it saved (II-121C). (Figure 4.7a)

The solid was insoluble in deuterated NMR solvents benzene, THF, CHCl$_3$, and dimethoxyethane. It could not be redissolved in 2MOE but would dissolve in the V-2MOE solution in 2MOE. DTA/TGA was done on the solid and showed a two-step decomposition complete by 350 °C. (Figure 4.8a)
PA-FTIR was done on the solid and was found to overlay with that of II-24, the alcoholysis product of Bi(N(SiMe$_3$)$_2$)$_3$. (Figure 4.7b)

Figure 4.25: DTA/TGA of [Bi(NO₃)₂(O(CH₂CH₂O)₄)]₂* 2 MeOH. Heating rate: 25 °C/min.
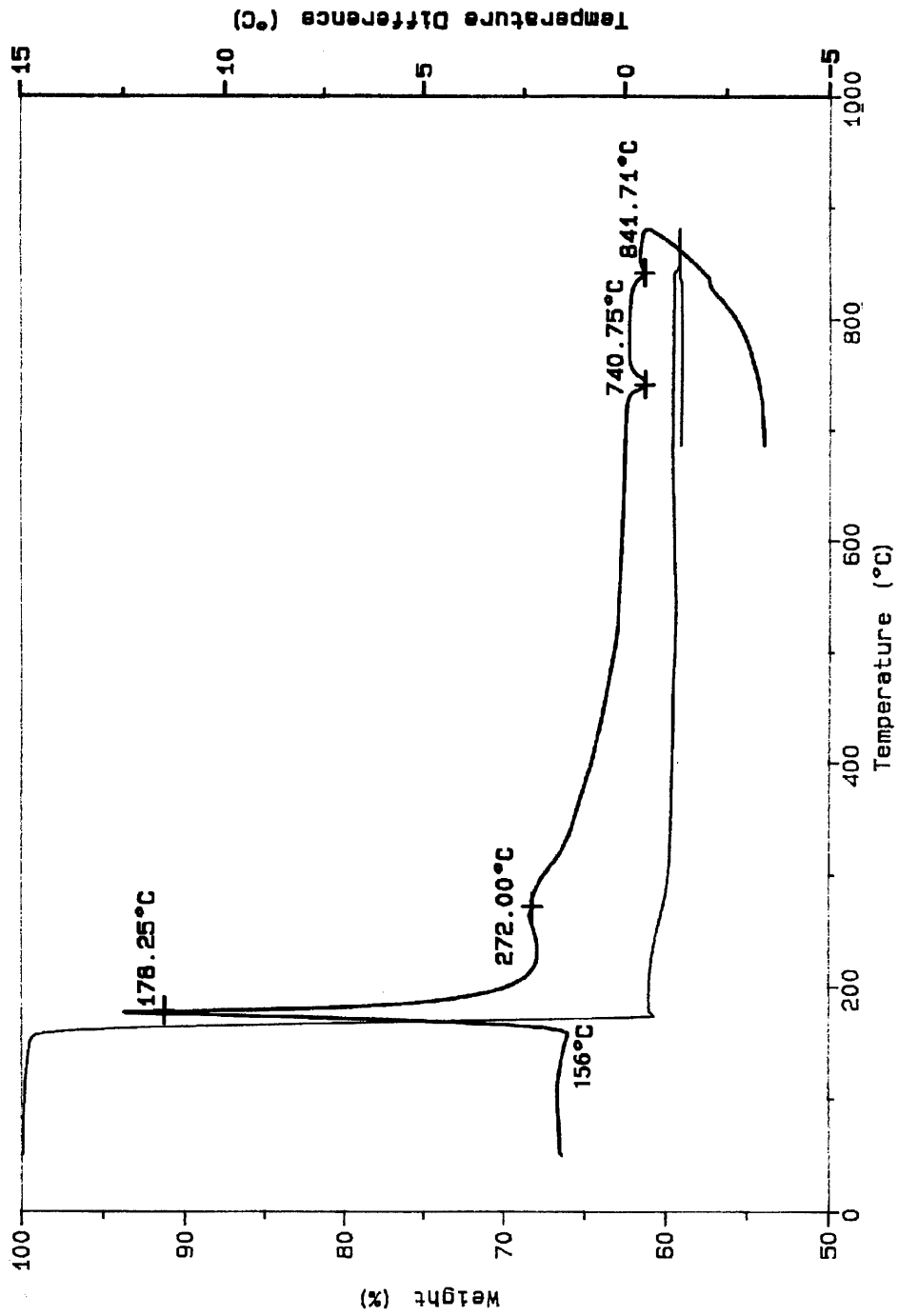
Figure 4.26a: DTA/TGA of Bi(N(SiMe₃)₂)₃. Heating rate: 25 °C/min.
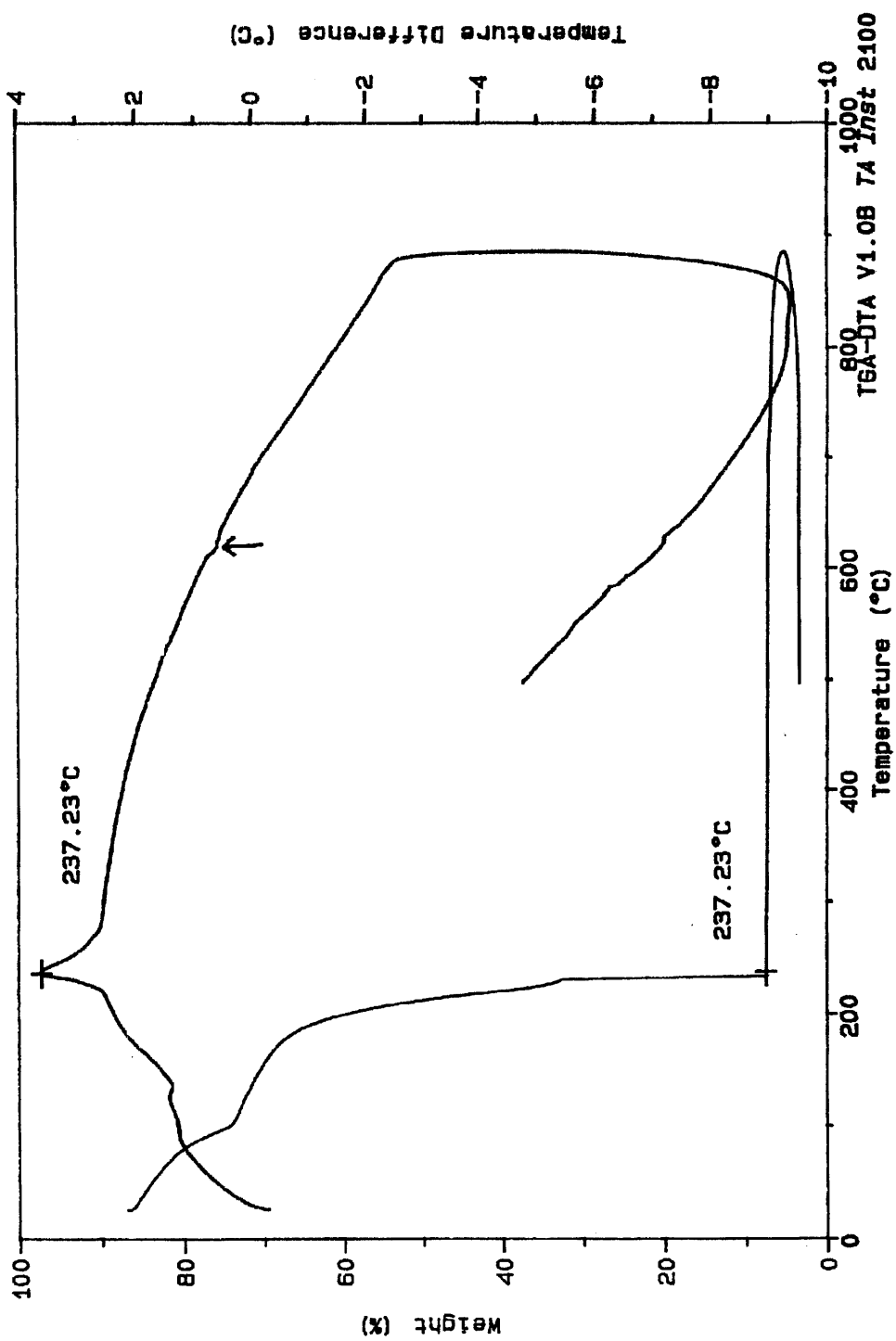
Figure 4.26b: DTA/TGA of the product of the alcoholysis of Bi(N(SiMe₃)₂)₃ with 2MOE, after hydrolysis and removal of solvents. Heating rate: 25 °C/min.

Figure 4.26b: DTA/TGA of the product of the alcoholysis of $Bi(N(SiMe_3)_2)_3$ with 2MOE, after hydrolysis and removal of solvents. Heating rate: 25 °C/min.
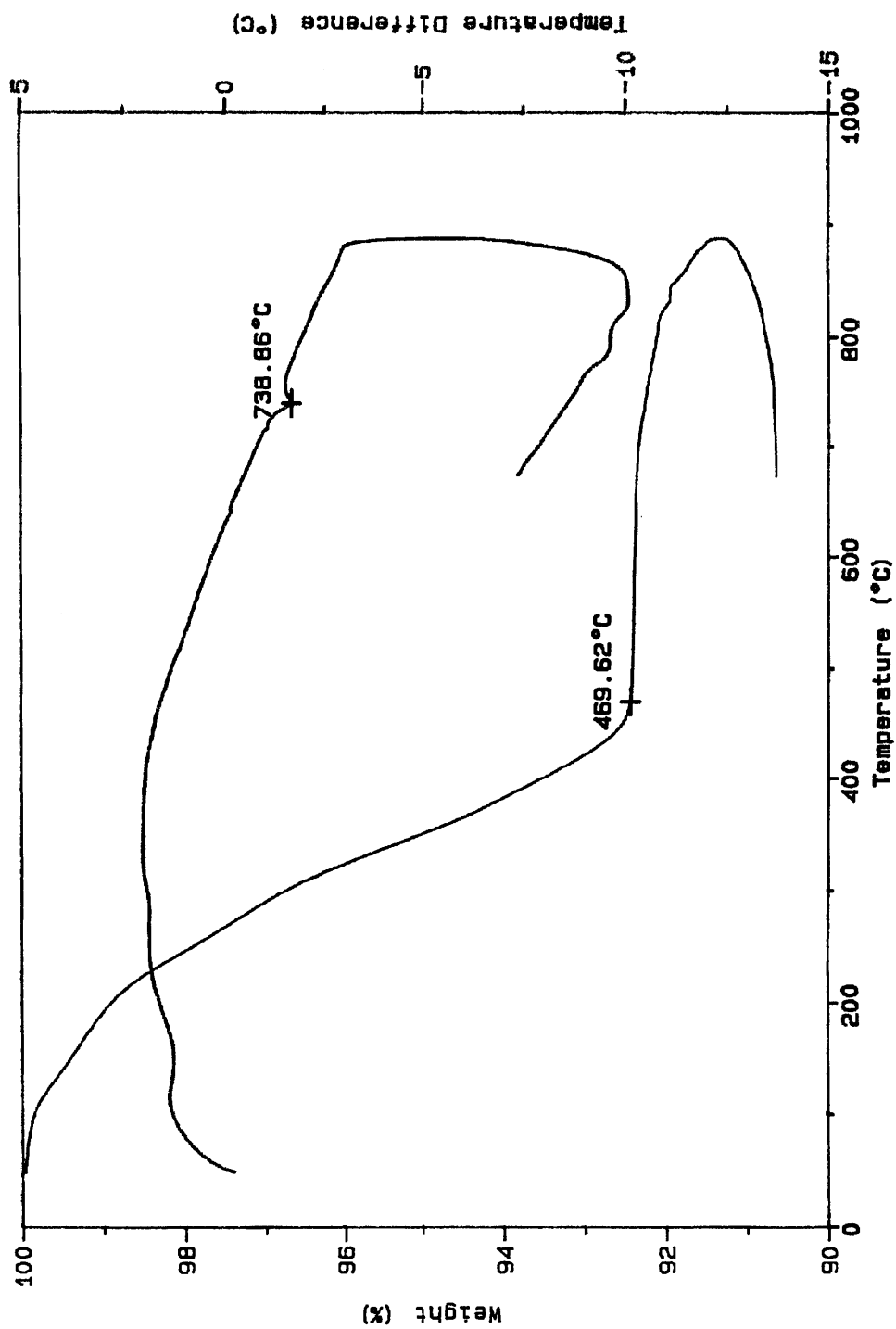
Figure 4.27: DTA/TGA of the product of the alcoholysis of Bi(N(SiMe₃)₂)₃ with 2MOE. Heating rate: 25 °C/min.
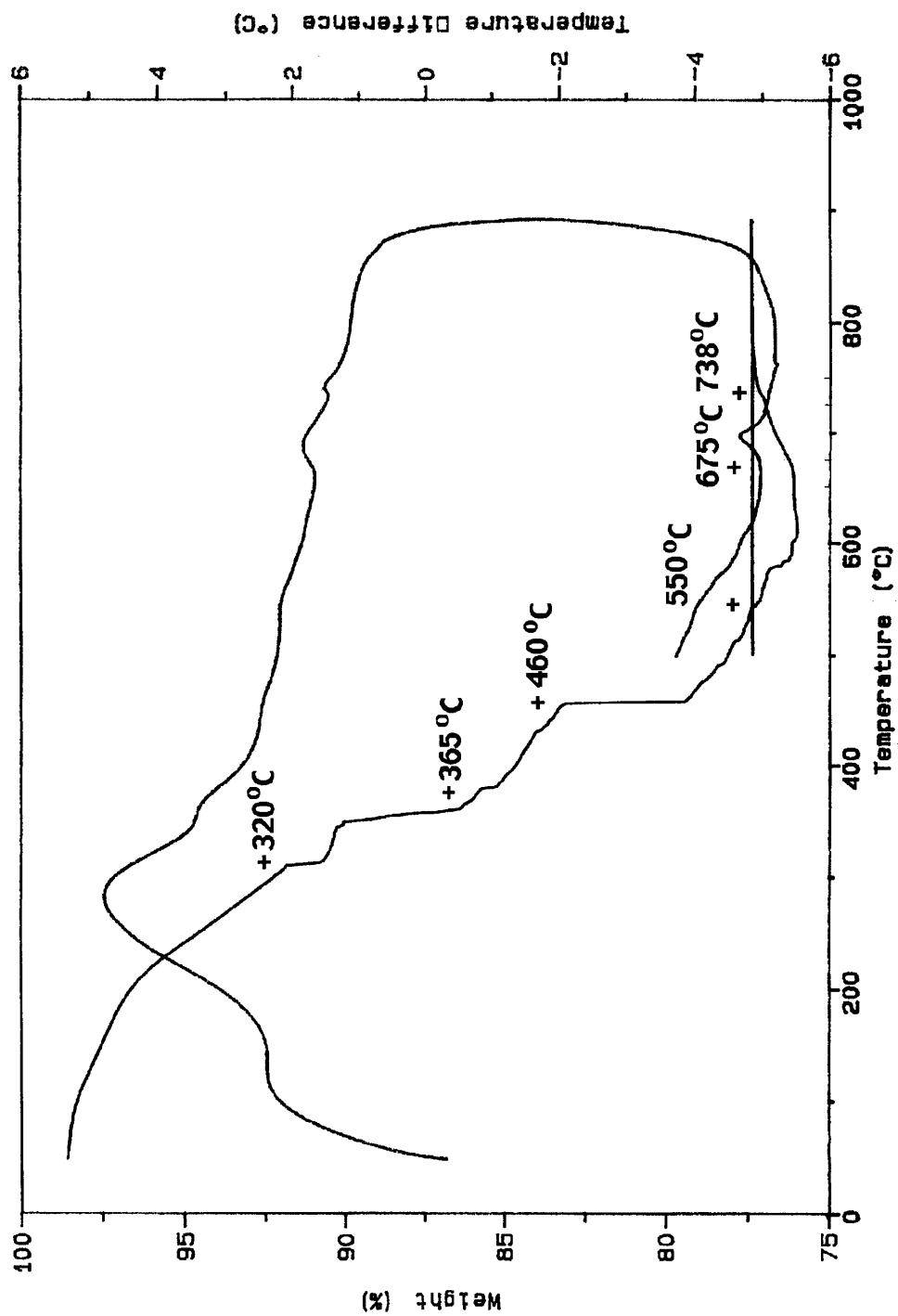
4.4.3 Bulk Bi$_2$VO$_{5.5}$

Experiment #15 (JWP-I-43) Bi(NO$_3$)$_3$·5H$_2$O + V(OBu)$_4$;

Bi(NO$_3$)$_3$·nH$_2$O + V(OBu)$_4$; to make Bi$_2$VO$_{5.5}$

To Bi(NO$_3$)$_3$·5H$_2$O (4.3834 g, 9 mmol) dissolved in 10 ml glacial acetic acid was added V(OBu)$_4$ (3.333 g, 4.5 mmol), resulting in an instant orange precipitate. To the same weight of Bi(NO$_3$)$_3$·5H$_2$O which had been left in a dessicator with P$_2$O$_5$ for several days (34% weight loss), the same amount of V(OBu)$_4$ was added. A deep red liquid, which eventually settled out an orange ppte, was formed. On addition of water to each a yellow ppte settled out. There was no gelation.

Experiment #16 (JWP-I-43) Bi(NO$_3$)$_3$·5H$_2$O + V-2MOE → to make Bi$_2$VO$_{5.5}$

V-2MOE (18.4748 g, 4.5 mmol) was added Bi(NO$_3$)$_3$·5H$_2$O (4.3835g, 9 mmol) dissolved in 10 ml glacial acetic acid. A clear orange-brown solution resulted. This was hydrolyzed to yield a yellow precipitate which, after heating at 350 °C was found by XRD to contain only BiVO$_4$; likewise the solid, pressed as a pellet and heated to 600 °C for 44 h and found to be a mixture of BiVO$_4$ and Bi$_2$VO$_{5.5}$.

Experiment #17 (JWP-I-54(3)) Bi(NO$_3$)$_3$·5H$_2$O + VO(OiPr)$_3$ →

to make Bi$_2$VO$_{5.5}$

#1 (Nitric acid present)

Bi(NO$_3$)$_3$·5H$_2$O (4.3813 g, 9 mmol) was dissolved in 30 ml glacial acetic acid and 10 ml isopropanol and 1 ml concentrated nitric acid (initial pH 2.96). VO(OiPr)$_3$ (1.1210 g, 4.57 mmol) were added. The solution became orange yellow instantly, and was clear. Addition of 1 ml (56 mmol, 4x excess) water give no change. After heating, 1 ml more water was added and a yellow precipitate settled out from a pale green liquid. The dried powder was amorphous to XRD but after heating to 350 °C may have contained poorly crystalline BiVO$_4$ and Bi$_2$VO$_{5.5}$. After heating to 650 °C (12h) the XRD showed BiVO$_4$ and Bi$_2$VO$_{5.5}$ peaks.

#2 (No nitric acid)

Bi(NO$_3$)$_3$·5H$_2$O (4.3804 g,9 mmol) was dissolved in 30 ml glacial acetic acid and 10 ml isopropanol (pH measured 2.65), and VO(OiPr)$_3$ (1.1106 g, 4.53 mmol) added. A light yellow-orange precipitate formed immediately. Addition of 1 ml (56 mmol, 4x excess) water of caused the precipitate to settle. After drying the precipitate was dark orange with white flakes and was mostly BiVO$_4$ by XRD. After decomposition at 350 °C the solid showed BiVO$_4$ only, but after heating as a pellet at 650 °C (12 h) the XRD showed a mix of BiVO$_4$ and Bi$_2$VO$_{5.5}$.

Experiment # 18 (JWP-I-58) Bi(NO$_3$)$_3$·5H$_2$O + VO(OiPr)$_3$;

Bi(NO$_3$)$_3$·nH$_2$O + VO(OiPr)$_3$ → both to make Bi$_2$VO$_{5.5}$

Bi(NO$_3$)$_3$·5H$_2$O (5.0140 g, 10.34 mmol) was stored in a dessicator over P$_2$O$_5$ for 1 week then weighed to find that the new weight was 4.6990, a 33.8% loss attributed to loss of 1.75 H$_2$O. This was added to 30 ml glacial acetic acid and 30 ml HOiPr and warmed to dissolve. VO(OiPr)$_3$ (1.268 g, 5.17 mmol) was added to produce a yellow solution. Water was added to part of the sample (8x excess, 2 ml) and a light yellow precipitate formed. The solvent was evaporated off with heating. XRD showed a mixture of BiVO$_4$ and Bi$_2$VO$_{5.5}$.

The same procedure was followed using Bi(NO$_3$)$_3$·5H$_2$O that had not been left over P$_2$O$_5$. The XRD showed only BiVO$_4$ in the sample.

Experiment #19 (JWP-I-85) Bi(NO$_3$)$_3$·2.5H$_2$O + V-2MOE → to make Bi$_2$VO$_{5.5}$

Bi(NO$_3$)$_3$·5H$_2$O (5.0325 g, 10.4 mmol) was left in a dessicator for 2 weeks over P$_2$O$_5$ (weight loss attributed to loss of 2.5 H$_2$O) was dissolved in 30 ml acetic acid and 20 ml 2MOE. This was added to V-2MOE solution (25.01 g, 2.55 mmol) to give a yellow-orange solution accompanied by a slight exotherm. 2 ml water were added to give instant milkiness. The solvent was evaporated from the

sample, leaving a yellow-white powder which was heated on a hotplate (ca 300 °C) for 1 hr then identified by XRD as $BiVO_4$.

Experiment #20 (JWP-I-97) $[Bi(NO_3)_2(O(CH_2CH_2O)_4)]_2 \cdot 2$ MeOH + V-2MOE → to make $Bi_2VO_{5.5}$

$[Bi(NO_3)_2(O(CH_2CH_2O)_4)]_2 \cdot$ 2 MeOH (See Expt. 8, 2.1178 g, 3.63 mmol) was added to 25 ml each of acetonitrile and methanol with warming and stirring, to produce a white susp. To this was added V-2MOE (17.835 g, 1.82 mmol) to give a dark yellow milky suspension. Part of this was permitted to evaporate, yielding a green powder with orange-yellow flecks. The remainder was hydrolyzed with excess water and the resulting gelatinous precipitate divided: part was and the solid set aside, and part was evaporated. All samples' powder XRD show $BiVO_4$ after heating for 3 h at 525 °C.

Experiment #21 (JWP-I-100) $[Bi(NO_3)_2(O(CH_2CH_2O)_4)]_2 \cdot 2$ MeOH + $VO(OiPr)_3$ → to make $Bi_2VO_{5.5}$

$[Bi(NO_3)_2(O(CH_2CH_2O)_4)]_2 \cdot$ 2 MeOH was made freshly by adding $Bi(NO_3)_3 \cdot 5H_2O$ (4.9607g, 10.02 mmol) in 25 ml methanol and 75 ml acetonitrile to a suspension of tetraethylene glycol (2.5102 g, 12.92 mmol) in methanol in a 250 ml three-neck flask equipped with a condensor. The mixture was refluxed under nitrogen for 2.5 hours, yielding a milky suspension and a white precipitate. This was hot-filtered via a cannula filter and cooled to room temperature

slowly, then left at 0 °C overnight. This was cold-filtered to collect white crystals of [Bi(NO$_3$)$_2$(O(CH$_2$CH$_2$O)$_4$)]$_2$· 2 MeOH (4.34 g, 36%). A second crop was not collected.

The sample of [Bi(NO$_3$)$_2$(O(CH$_2$CH$_2$O)$_4$)]$_2$ made above was added to a 3-neck flask equipped with a condensor (4.0131 g, 3.44 mmol) with 75 ml acetonitrile and 25 ml methanol at reflux. To this was added VO(OiPr)$_3$ solution (0.844g, 3.45 mmol). The mixed solution became a clear yellow-orange. This was stirred for 15 minutes, then cooled and hydrolyzed with one equivalent of water and the liquids evaporated off the sample. The resulting solid was calcined at 600 °C for 12 h, resulting in an inhomogenous material with a powder XRD pattern matching BiVO$_4$ (JCPDS 14-688).

Experiment #22 (JWP-I-103) commercial Bi(OAc)$_3$ + V-2MOE → to make Bi$_2$VO$_{5.5}$

Bi(OAc)$_3$ (2.6743 g, 6.93 mmol commercial product) was added to 50 ml glacial acetic acid and heat to produce a white milky suspension. 25 ml 2MOE were added, followed by 34.02 g V-2MOE (3.47 mmol) in 20 ml 2MOE, yielding a yellow solution. When 1.0 ml water (4 equivalents) was added to the hot solution, a precipitate formed, then redissolved and the solution became yellow-green. The solvent was evaporated to a light green-brown solid. This is pyrolyzed 350 °C/32h and 650 °C/1h in air. Powder XRD showed BiVO$_4$ and trace Bi$_2$VO$_{5.5}$.

Experiment #23 (JWP-II-35 (repeated JWP-II-37)) Bi(OAc)₃ + V-2MOE, refluxed → to make Bi₂VO₅.₅

Bi_2O_3 (1.20g, 2.58 mmol) was added to a 3-neck flask with 25 ml glacial acetic acid and heated to near-dryness, with air blown across the surface of the suspension to increase the rate of evaporation of the acetic acid. This produced a fine white powder, which was air-dried then put under nitrogen. 75 ml 2MOE were added and the mixture warmed to distillation. The white solid nearly dissolved in cold 2MOE but on heating became very milky. Most of the solvent was distilled off; 100 ml more 2MOE was added and the milky white mixture permitted to cool. V-2MOE (19.26 g, 1.3 mmol) was added to yield a milky yellow solution. This was refluxed overnight, leaving a chocolate brown mixture which was distilled to dryness, then heated 1.5 h at 650 °C – XRD showed $BiVO_4$ and $Bi_2VO_{5.5}$; then 625 °C/8 h and 650 °C/20 h – the final XRD showed $Bi_2VO_{5.5}$ and trace amounts of $BiVO_4$.

Experiment #24 (JWP-II-39) Bi(OAc)3 + V-2MOE, assorted hydrolysis conditions

Bi_2O_3 (1.2055 g, 2.59 mmol) was added to 15 ml glacial acetic acid and heated under flowing N_2. Another 15 ml acetic acid was added and evaporated off to near dryness. Finally, air was blown across the solid to dry it. The resulting solid was mostly-dissolved in 25 ml warm 2MOE and V-2MOE solution (19.9225 g, 1.3 mmol) added to give a clear yellow solution. 2MOE was added to a 65 ml

final volume and the mixture stirred 2h at room temperature. II-39-0 was the resulting solution. ^{1}H NMR peaks at (δ, ppm) 1.66(s), 3.08 (s), 3.24 (s, broad) in C_6D_6. This was hydrolyzed to a golden-brown gel.

II-39-1: 10 ml of solution 39-0 (0.4 mmol Bi) was hydrolyzed with 1 ml (70x excess) of (2.5 ml 2MOE + 0.5 ml H_2O + 0.5 ml acetic acid) and became milky instantly. Left open, it became a yellow gel overnight.

II-39-2: 10 ml solution 39-0 was hydrolyzed with 1 ml of (2.5 ml 2MOE + 0.5 ml H_2O + 0.5 ml NH_4OH) to give a white-yellow stringy precipitate. Left open overnight, it became a gelatinous white-yellow precipitate in a clear and colorless solvent.

II-39-3: 10 ml of 39-0 was hydrolyzed with 1 ml of (2.5 ml 2MOE + 1.0 ml H_2O) and became slightly more viscous. Left open overnight, it became a translucent yellow gel.

II-39-4: 5 ml solution 39-0 was hydrolyzed with 1 ml of (1.25 ml 2MOE + 0.25 ml H_2O + 0.25 ml HNO_3) became darker orange but stayed clear. Left open overnight, it remained a yellow liquid.

All of the gels were dried and heated for 8 h at 600 °C in air and XRD to show $BiVO_4$ + $Bi_2VO_{5.5}$ + amorphous phase which is probably Bi_2O_3. A second heating of each of these at 650 °C for 20 h gives in all cases $Bi_2VO_{5.5}$.

DTA/TGA was done on the hydrolyzed and unhydrolyzed 39-0. Solvent was removed from both prior to thermal analysis The unhydrolyzed material showed a two-step decomposition, with a large exotherm at the second step, complete by 350 °C. (Figure 4.28a) A second sample of the unhydrolyzed material was aged for six months; its decomposition is similar but has a more pronounced

first decomposition step. (Figure 4.28b) Formation of an equilibrium complex in the precursor solution may have occurred over the aging period, leading to an initial step in the decomposition involving the breaking of these complex bonds. The hydrolyzed material, conversely, shows a multistep decomposition not complete until 430 °C. (Figure 4.10)

Experiment #25 (JWP-II-12A) Bi(N(SiMe₃)₂)₃ + V-2MOE → to make Bi₂VO₅.₅

Bi(N(SiMe_3)_2)_3 (0.6348g, 0.92 mmol) was added to a round-bottom flask in the glove box and dissolved in 50 ml 2MOE to give a clear and colorless solution. V-2MOE (3.7572 g, 0.45 mmol) in 15 ml 2MOE was added to the bismuth solution. 5 ml of this clear yellow solution was hydrolyzed with 2 ml of water (800x excess) to give a yellow-white translucent material. A gel formed as the volume of the solution was reduced *in vacuo*. This gel was dried and pyrolyzed at 500 °C for 12 hours to produce a powder whose XRD shows only Bi_2VO_{5.5}. Another 5 h at 600 °C improved the crystallinity and confirmed phase-purity. DTA/TGA performed on the 600 °C sample to demonstrate phase changes at proper places. EDX showed some contamination with Na and Si.

Experiment #26 (JWP-II-30-5) "Bi(2MOE)₃" + V-2MOE → to make Bi₂VO₅.₅

To 10 g of the solution of "Bi(2MOE)_3" made in Experiment #10 above (0.1078 mmol Bi) were added 4.378 g V-2MOE (0.05 mmol).

The resulting yellow solution was hydrolyzed with 0.5 ml H_2O in 1.0 ml 2MOE (150x excess) to give a yellow-white gelatinous precipitate. This was left open overnight to leave a yellow gelatinous precipitate that settled out of a clear and colorless liquid. Removal of the solvent by heating left brown lumps which on heating for 8 hours at 500 °C in air gave poorly crystalline $Bi_2VO_{5.5}$; heatings at 600 °C/10h and 650 °C/12h gave $Bi_2VO_{5.5}$ of improved crystallinity

Experiment #27 (JWP-II-58) Bi-2MOE + V-2MOE

A solution of $Bi(N(SiMe_3)_2)_3$ in 2MOE (8.952g, 3.146 mmol Bi) was added to V-2MOE (10.612 g, 1.6 mmol) and the clear yellow solution stirred at room temperature for 3 hours. The volume was reduced by half *in vacuo*. This was stirred another 3 hours and divided in half: to II-58A 1.0 ml (17.5x excess) of water was added, resulting in a white gel formation in a yellow solution, which was left open overnight and gelled throughout; II-58B was left open overnight without addition of water. When hydrolyzed, -B became a gel almost instantly. Both samples were oven dried for 6 hours and heated 8 hours at 450 °C. XRD of each of these showed $Bi_2VO_{5.5}$, with very small or nonexistent $BiVO_4$ peaks; each pyrolyzed sample was then heated at 550, 650, and 750 °C with improvements in crystallinity. Some of the stray peaks could be identified as $Bi_{12}SiO_{20}$ or NaCl. (Figure 4.16)

Experiment # 28 (JWP-I-89) Conductivity of BiVO$_4$

Approximately 4 g of BiVO$_4$ were ground finely in an agate mortar, then pressed into a 1/2" pellet mold at 7500 psi. The pellet was placed on an alumina boat on platinum foil and heated at 10 °C/min. ramp rate to 800 °C for 24 h, then cooled at 5 °C/min. to room temperature. The outside surface of the pellet became purple, but after the very outer layer was removed with fine-grained sandpaper, the underlayer, and presumably the bulk, showed the yellow color expected of BiVO$_4$. The pellet was measured with a vernier calipers and weighed, and density calculated to be 6.457 g/cm^3, some 92.9% of the theoretical density (based on cell dimensions given in JCPDS #14-688) of 6.949 g/cm^3. Opposing faces were painted with platinum ink and the pellet, stood on its edge on a platinum sheet in an alumina boat, heated again with a 20 °C/min ramp to 800 °C for 5 min., followed by cooling to room temperature at 25 °C/min. The conductivity of the pellet was measured by complex impedance spectroscopy, as described in the Appendix to Part I of this thesis. Measurements were made at 50 °C intervals from 350 °C to 750 °C. At several temperatures the data showed spiky or otherwise nonsmooth high-frequency arcs, which may have indicated some separation into bulk and grain boundary resistances, and several cases a second low-frequency arc indicated that the electrode had become non-blocking (e.g. significant electronic conduction). Because the worst-case or lower-limit of the actual conductivity was the information sought, the separation of the bulk and grain boundary contributions was

not calculated. All of the conductivity values given are based on the sum of the grain and bulk resistances, therefore. Figure 4.11 shows the impedance spectra for $BiVO_4$ at several temperatures. Figure 4.12 shows the plot of conductivity with temperature.

Experiment # 29 (JWP-I-109) CI Measurement on a Mixed-Phase Pellet

A three-necked flask equipped with a vigreaux column, side-arm condensor, and receiver, all under nitrogen, was charged with of $VO(OiPr)_3$ (2.453 g, 10 mmol) and 20 ml 2MOE. The mixture was heated until the vapor temperature was 100 °C, then 5 ml more 2MOE were added twice, with distillation to vapor temperature of 100 °C on the first time and to 120 °C on the second time. The distillation was stopped. Meanwhile, "$Bi(OAc)_3$" (7.7222g, 20 mmol) made in an open vessel (Expt. 11) were dissolved with heating and stirring in 180 ml of a 1:1 2MOE/glacial acetic acid mixture. The hot contents of the distillation apparatus were added to the hot bismuth solution, yielding a green-brown mixture with brown precipitate. A mixture of 10 ml each of 2MOE, acetic acid, and water was slowly added, producing a white precipitate. The solution was boiled to remove solvent with stirring, and appeared to homogenize somewhat; it became an orange-green color. After stirring for 2 days, the solvent was completely boiled off, and the yellow/green/brown/white inhomogenous solid transferred to an alumina crucible and heated at 400 °C for 3 hours. It was found by XRD to contain a mixture of $BiVO_4$ and $Bi_2VO_{5.5}$. (Figure 4.29) The sample was pressed into a 1/2" pellet at 10,000 psi and the faces

sanded smooth. The pellet was heated at 250 °C for 12 h, then measured and weighed, and the density found to be 5.06 g/cm^3, 64% of theoretical density (7.80 g/cm^3) if the pellet were all Bi$_2$VO$_{5.5}$ and 78% of theoretical density (6.949 g/cm^3) were the pellet all BiVO$_4$. The faces of the pellet were not prepared with platinum ink due to the high decomposition temperature of the ink binder. This was not anticipated to cause a significant difference in the results.[58] Complex impedance measurements were conducted as described in the Appendix to Part I of this thesis. Measurements were made at temperature intervals of 25 or 50 °C from 200 °C to 700 °C, and back to 275 °C. After removal from the apparatus, the pellet was inhomogenous, with orange and yellow speckles; it was ground for XRD and found to contain (Figure 4.30) unknown peaks (they did not match JCPDS #14-699. 14-688, or 9-387, nor Bi$_2$VO$_{5.5}$).

For the first few temperature data-points the conductivity was insufficiently high to provide a readable arc among the noise points. A clear trend could not be clearly distinguished until approximately 500 °C: here the high-frequency arc was ignored and the conductivity (principally electronic) found from the intercept of the line (see Figure 4.13 for representative impedance plots). Two of the cooling-side plots were analyzed using the high-frequency arc, as the line was indistinguishable. See Figure 4.14 for the plot of conductivity vs. temperature. It should be noted that the main mechanism for the increase in conductivity on the cooling leg of the plot is the increased density of the pellet after being heated to 700 °C.

Table 4.2: Results of BiVO$_4$ Complex Impedance Measurement

Temp. (°C)	Diameter	Z″ Center	Z′ Center	X intercept	ρ (ohm · cm)
340.1	331267.2	19323.15	164114.6	330871.53	662344.6
391.3	180605.7	426.751	92407.5	182711.358	365754.9
441.7	82749.9	-5280.51	46437.47	88148.0235	176456.3
492.1	49041.13	-6181.006	32453.22	57740.8245	115586.632
543.3	9673.28	950.836	6195.08	11124.2965	22268.8191
594.5	2702.237	33.1004	3158.993	4510.51689	9029.23473
672.1	258.8374	97.77968	1087.482	1249.68578	2501.64371
749.1	23.1564	8.5476	222.468	236.859532	474.149717

Table 4.3: Complex Impedance Results for mixed BiVO$_4$/ Bi$_2$VO$_{5.5}$ pellet

Temp. (°C)	Type	y-intercept	slope	diameter	Z″ center	Z′ center	x-intercept	ρ (ohm·cm)
490.2	line	5257.23	0.63825				8236.94455	30812.1
516.4	line	3412.094	0.6585				5181.61579	19382.8
542.1	line	2198.45	0.69996				3140.82233	11748.8
593.6	line	696.124	0.7187				968.587728	3623.18
646.1	line	136.18	0.6725				202.498141	757.482
646.2	line	149.744	0.8059				185.809654	695.056
542.4	line	955.3897	1.1307				844.954188	3160.71
492.1	line	2529.08	1.156				2187.78547	8183.82
466.2	line	4291.03	1.1999				3576.15635	13377.28
441.1	line	7874.011	1.2854				6125.72818	22914.43
390.9	line	26349.2	1.2886				20447.928	76489.29
365.2	line	45113.66	1.0636				42416.0023	158645.0
339.8	arc			112089	20727.33	53320.7	113075.296	422979.2
314.5	arc			259883.9	49452.28	120794	259827.547	971933.3

Figure 4.28a: DTA/TGA of the Bi$_2$VO$_{5.5}$ gel precursor JP II-39-0, solvent removed soon after mixing. Heating rate: 25 °C/min.
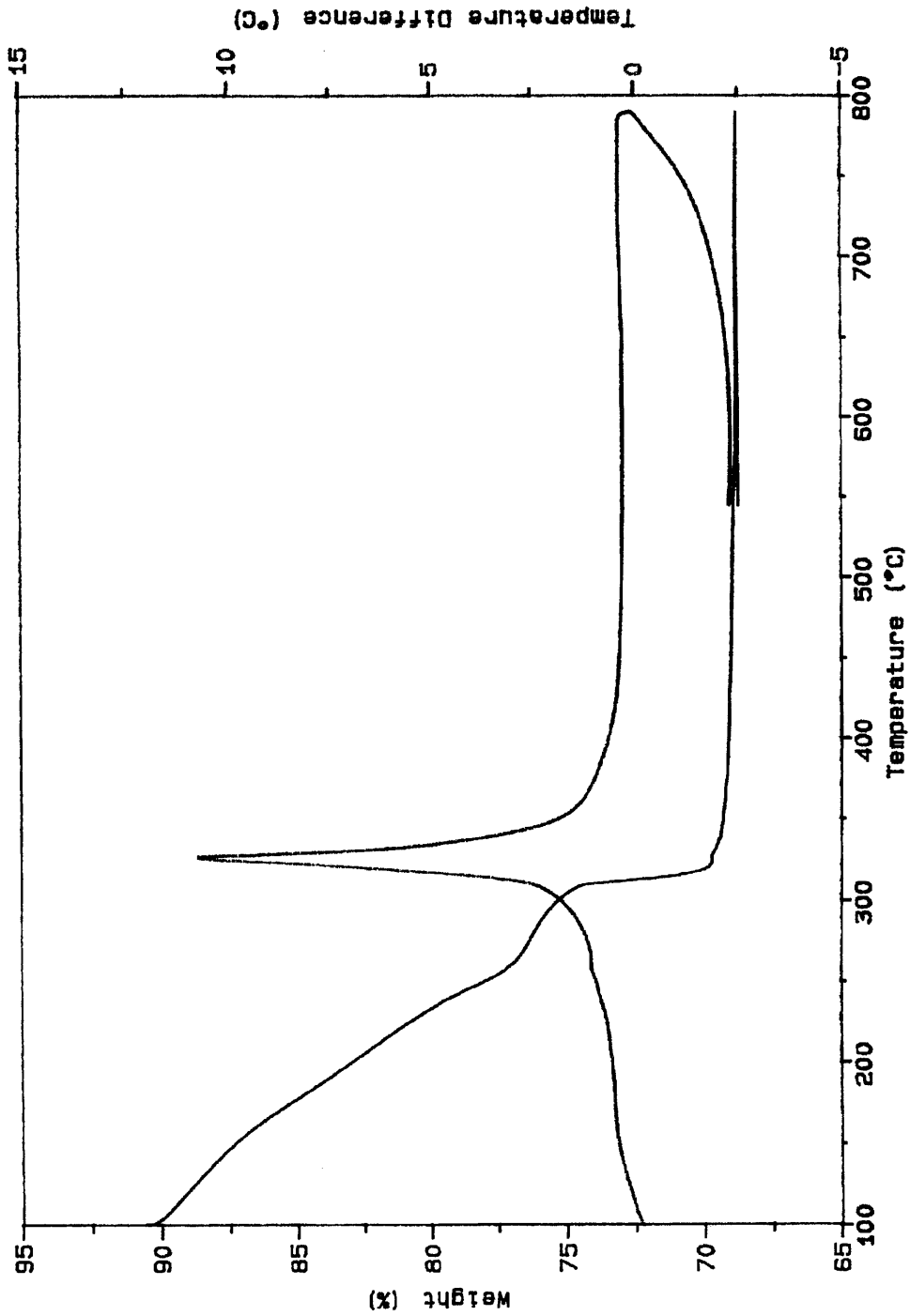
Figure 4.28b: DTA/TGA of the $Bi_2VO_{5.5}$ gel precursor JP-II-39-0, solvent removed after six months' aging of the solution. Heating rate: 25 °C/min.
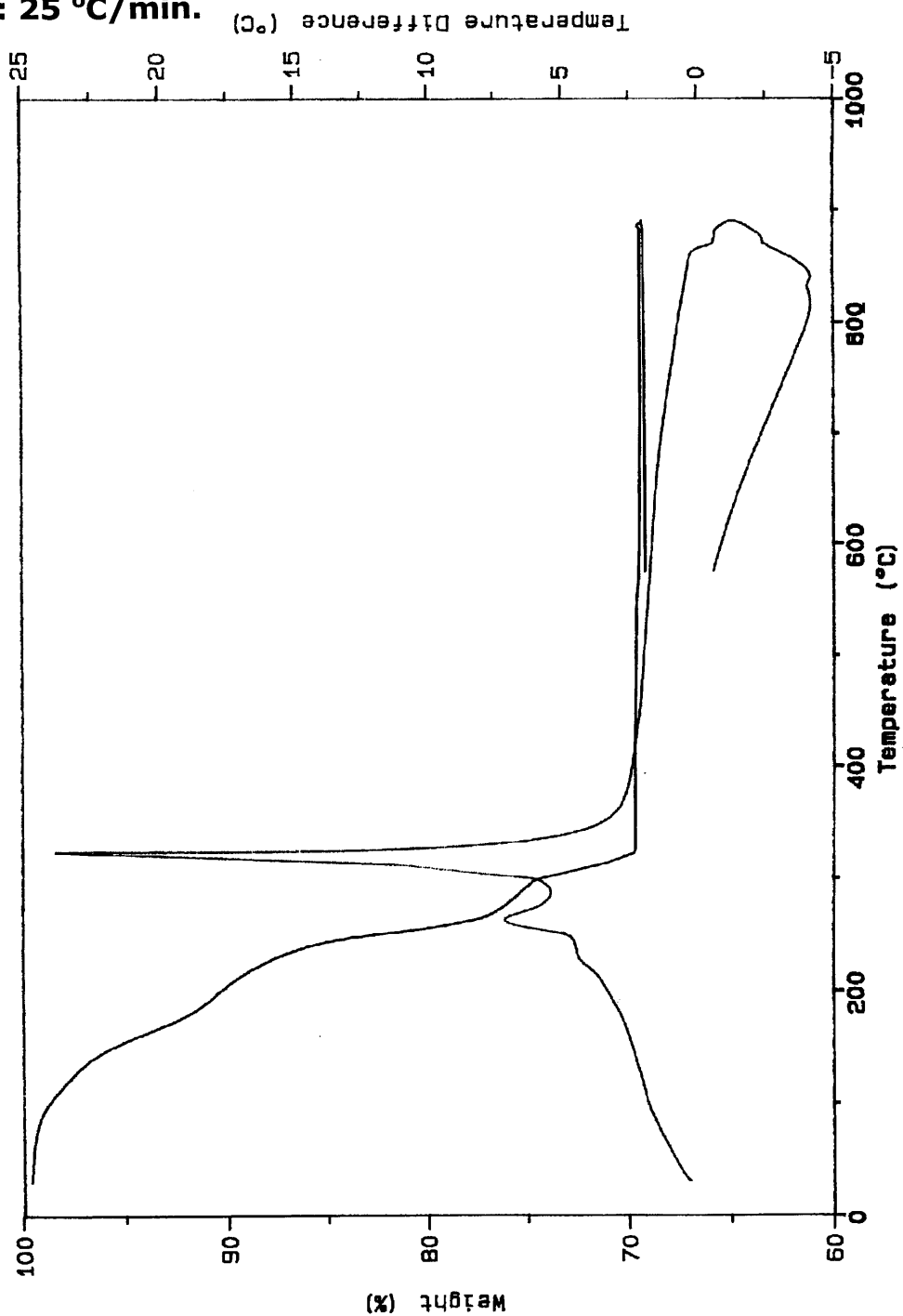
Figure 4.29: Powder XRD of sol-gel Bi$_2$VO$_{5.5}$ contaminated with BiVO$_4$. The sample was pressed into a pellet and its conductivity was checked by CI.
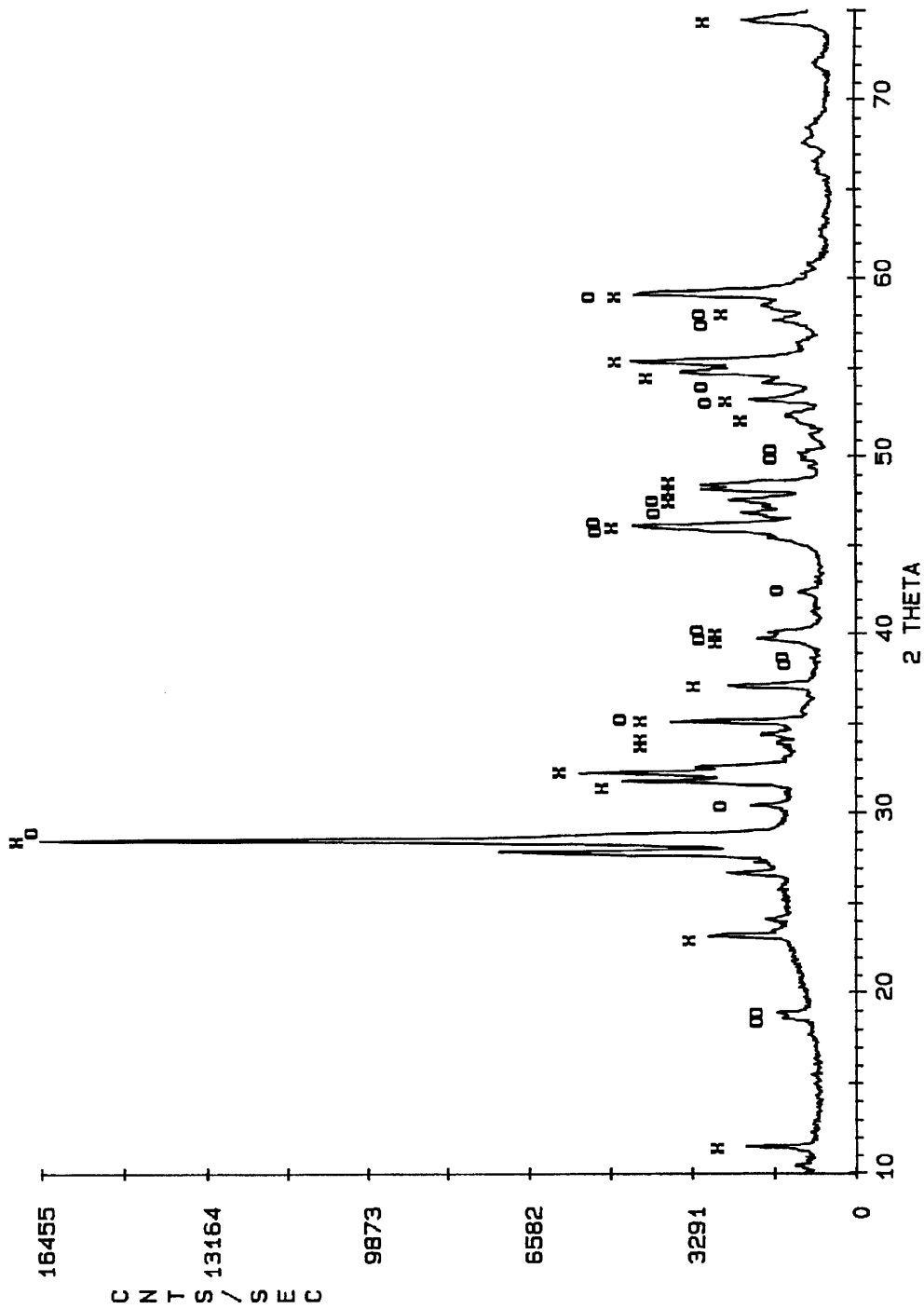
Figure 4.30: Powder XRD of sample from Figure 4.29, after CI data was taken. None of the peaks match the known oxides of Bi and/or V.
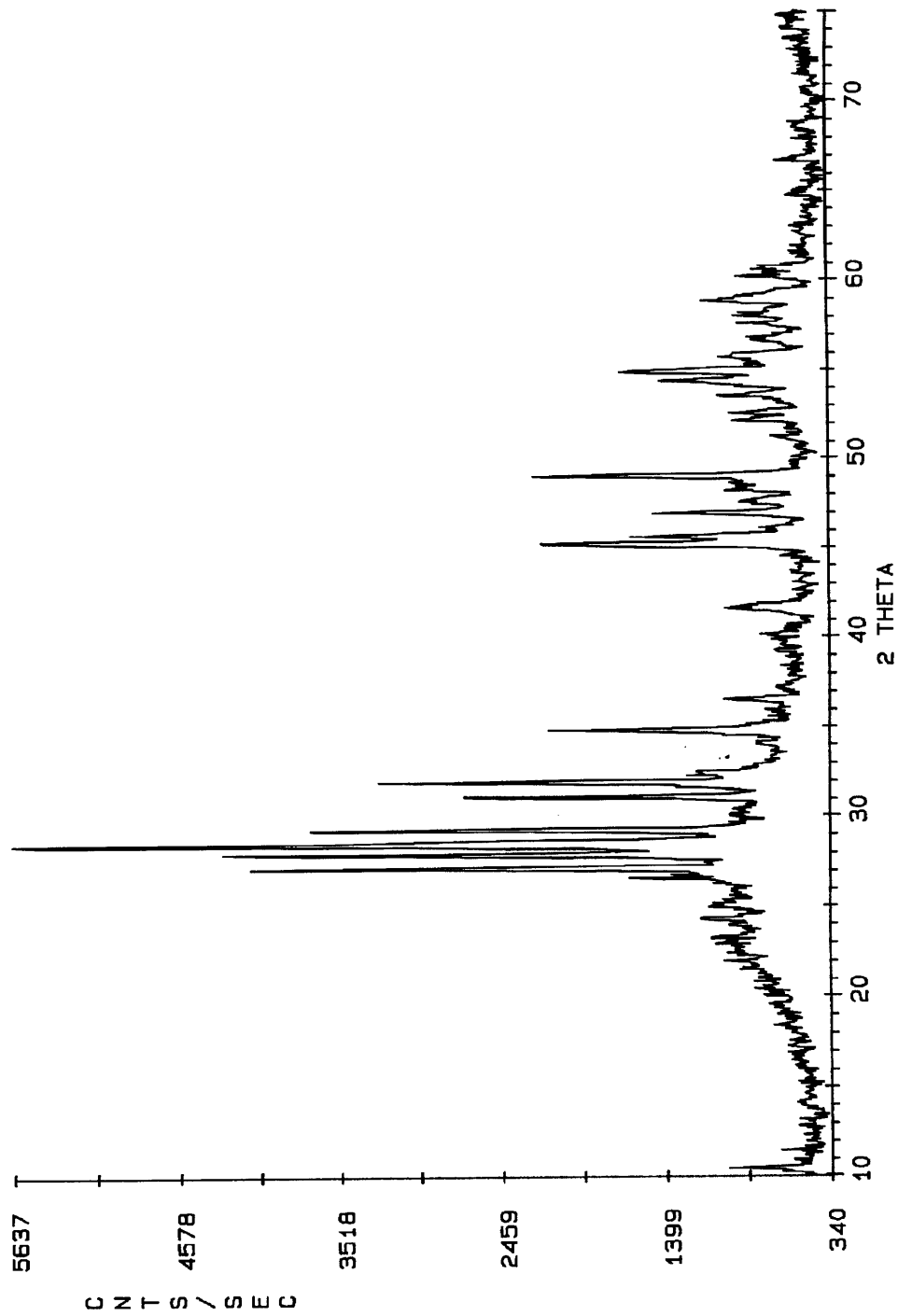
4.4.4 Synthesis of Bulk BiMeVOx

Experiments with a notebook numbering KD-x were performed by UROP Katya M. Delak under my technical guidance.

Experiment #30 (JWP-II-99A1) Solid State Synthesis of Standard $Bi_2VO_{5.5}$

$Bi_2VO_{5.5}$ was made by solid state methods to provide a standard against which sol-gel prepared samples could be checked. Stoichiometric quantities of Bi_2O_3 (9.3190 g, 20 mmol)) and V_2O_5 (1.8188 g, 9.9 mmol) were ground under acetone and pressed into a 1/2" pellet at 7000 psi. The pellet was placed on platinum foil in a small alumina crucible and heated at 850 °C for 20 h (heating 10 °C/min, cooling 4 °C/min), then re-ground and re-pressed, and heated under the same regime for 40 h. The XRD pattern compared favorably with that reported in the literature.[37] (Figure 4.31)

Experiment #31 (JP-II-99B2) Solid state synthesis of standard $Bi_2Cu_{0.1}V_{0.9}O_{5.35}$

$Bi_2Cu_{0.1}V_{0.9}O_{5.35}$ was made by solid state methods to provide a standard against which sol-gel prepared samples could be readily compared. Stoichiometric quantities of Bi_2O_3 (9.3190g, 20 mmol), V_2O_5 (1.637g, 9 mmol), and CuO (0.1591g, 2 mmol) were ground under acetone in an agate mortar ad the mixed powder pressed into a 1/2" pellet at 7000 psi. The pellet was placed on platinum foil

in an alumina crucible and heated for 20 h at 850 °C (10 °C/min heating, 5 °C/min cooling), then removed, reground, re-pressed, and heated for another 40 h at 850 °C (same heating/cooling rates). Powder XRD showed clean γ-phase $Bi_2Cu_{0.1}V_{0.9}O_{5.35}$, indexing gives **a**=3.9179 Å, **c**=15.4478 Å, all angles 90°. (Figure 4.32)

Experiment #32 (JWP-II-97b) Bi(OAc)$_3$ + V-2MOE + Cu(2-ethylhexanoate)$_2$ with acetylacetone → to make Bi$_2$Cu$_{0.1}$V$_{0.9}$O$_{5.35}$

Bi(OAc)$_3$ (1.9306g, 5 mmol) was added in the glove box to a flask and dissolved in 50 ml 2MOE. V-2MOE (3.0972 g, 2.25 mmol) in 25 ml 2MOE was added. Copper 2-ethylhexanoate (0.0875 g, 0.25 mmol) was dissolved in 25 ml 2MOE and added into the Bi/V solution, which became green-yellow. 2,4-pentanedione (10 ml, 100 mmol) in 25 ml 2MOE was added, and the solution turned dark red-brown. This was stirred at room temperature overnight, then hydroyzed with 10 ml water to give a yellow-green viscous solution. Over two days this became a green gel with a green supernatant. The gel was dried together with the supernatant at 120 °C, then heated at 700 °C in air for 10 h to yield an inhomogenous orange and yellow solid. This was identified by XRD as a mixture of $Bi_2VO_{5.5}$, $BiVO_4$, and Bi_2O_3.

A sample of the solution was hydrolyzed and permitted to stand without stirring, then heated to dryness and pyrolyzed as above. XRD showed a combination of $BiVO_4$ and $Bi_2VO_{5.5}$.

Experiment #33 (JWP-II-103) Bi(OAc)₃ + V-2MOE + Cu(2-ethylhexanoate)₂ → to make $Bi_2Cu_{0.1}V_{0.9}O_{5.35}$

Bi(OAc)₃ (7.7222g, 20 mmol) was added to V-2MOE (12.393 g, 8 mmol) and copper 2-ethylhexanoate (0.3501 g, 2 mmol) in 200 ml 2MOE to give a green solution. This was stirred over the weekend then the volume was halved by heating under vacuum. The solution was hydrolyzed with 10 ml H_2O (17x excess) + 5 ml glacial acetic acid in 10 ml 2MOE. A white-green gel formed with a green supernatant liquid. This was stirred and dried together at 120 °C overnight to leave a solid which was green-grey on the bottom and yellow on top; there were blue deposits on the beaker sides. The solid was pyrolyzed at 700 °C/10 h in air and identified by XRD as $Bi_2Cu_{0.1}V_{0.9}O_{5.35}$. However, the solid from the furnace was inhomogenous in color; contaminants at below XRD detection level were assumed.

Experiment #34 (JWP-II-105) Bi(OAc)₃ + V-2MOE + Cu(OAc)₂ → $Bi_2Cu_{0.1}V_{0.9}O_{5.35}$

Bi(OAc)₃ (7.7224 g, 20 mmol) dissolved in 150 ml 2MOE. To a second flask were added Cu(OAc)₂ (0.1816g, 2 mmol) and V-2MOE (12.3889 g, 8 mmol) in 50 ml 2MOE. The bismuth solution was added into the V/Cu solution and stirred over the weekend to leave a green opalescent solution with a small amount of white solid precipitate. The solvent volume was reduced *in vacuo* to about 160 ml and the sample was split into two parts, one of which (B) was hydrolyzed with 5 ml acetic acid/10 ml H_2O/10 ml 2MOE (17x excess) and the other (C) with 10 ml H_2O/10 ml 2MOE (17x excess). Both

236

gelled instantly, B with a loose gel texture and the appearance of white fibers with a teal green supernatant liquid, C with a orange-green firm gel with a more homogenous appearance and a pale yellow supernatant liquid. Both were dried overnight to leave yellow solids with blue copper deposits on the beaker sides. They were heated at 700 °C/10 h. XRD of both show clean γ phase. (Figure 4.17)

Experiment #35 (JWP-II-107) $Bi(N(SiMe_3)_2)_3$ + V-2MOE + $Cu(OAc)_2$ → $Bi_2Cu_{0.1}V_{0.9}O_{5.35}$

$Bi(N(SiMe_3)_2)_3$ (0.9880 g, 1.43 mmol) was dissolved in 10 ml 2MOE. In a second flask $Cu(OAc)_2$ (0.0128g, 0.072 mmol) and V-2MOE (0.8684g, 0.65 mmol) were dissolved in 15 ml 2MOE. This was added to the bismuth solution with 15 ml 2MOE rinse and warmed 5 min with stirring to give a yellow-green solution. This was hydrolyzed with 0.3 ml water (1 equivalent) in 0.7 ml 2MOE. Gelatinous white clusters appeared; the sample was left lightly covered overnight. A blue solid gel in a clear and colorless supernatant resulted; the solvent was driven off with heating and the resulting cohesive gel cake pyrolyzed at 700 °C for 10 h in air. XRD shows clean γ phase.

Experiment #36 (JWP-II-113) $Bi(N(SiMe_3)_2)_3$ + V-2MOE + $Cu(OAc)_2$ → $Bi_2Cu_{0.1}V_{0.9}O_{5.35}$

$Bi(OAc)_3$ (15.4448g, 40 mmol) was dissolved in 225 ml 2MOE with $Cu(OAc)_2$ (0.3639 g, 2 mmol) and V-2MOE (24.7773 g, 18 mmol)

and the solution stirred 2.5 h to yield a clear deep green solution. Some (15 ml) was set aside and the remainder hydrolyzed with 1.0 ml water (0.8 equivalents), giving a dark blue-green opaque solution with some white precipitate. This did not gel on standing overnight. 1 ml more water (total 1.6 equivalents) was added and the solution stirred with warming to get a thick green gel. This was divided into 4 samples and heated for 8 h at 350, 450, 550, and 650 °C in Ni crucibles in air. XRD showed γ phase appearance at 350 °C and clean at 450 °C. (Figure 4.22)

Some of the 650 °C sample was set aside and pressed into a 1/2" pellet at 9000 psi. The pellet dimensions were measured and the density found to be 5.0322 g/cm^3, some 65% of theoretical density (7.784 g/cm^3 theory). The faces were painted with platinum ink and the sample heated at 300 °C for 8 h; however, it was found that the ink did not decompose, so it was sanded off the faces. Complex impedance spectroscopy was done on the sample according to the procedure noted in the Appendix to Part I of this thesis. Impedance measurements were taken at temperature intervals of 25 or 50 °C from 250-825 °C, with a short cooling leg to 475 °C and a second heating leg to 825 °C. The final density was 6.075 g/cm^3, 78% of theoretical.

The first several temperatures were extremely noisy and only barely able to be fitted with a high-frequency arc, but by 325 °C the high-frequency arc arising from the combined bulk and grain-boundary resistances and a line arising from electronic conductivity is clearly evident. (Figure 4.23) By higher temperatures still the high-frequency part of the slightly-curved line is fitted to the left side of the arc; this is justified by the portions of

the data falling below x-axis, which indicate an overlaid semicircle and line. Figure 4.24 shows the conductivity vs. temperature plot.

Experiment #37 (JWP-II-115) $Bi(N(SiMe_3)_2)_3$ + V-2MOE + $Cu(OAc)_2$ → $Bi_2Cu_{0.1}V_{0.9}O_{5.35}$

To a round-bottom flask was added $Bi(N(SiMe_3)_2)_3$ (1.1061 g, 1.6 mmol), $Cu(OAc)_2$ (0.0152g, 0.08 mmol) and V-2MOE (0.9951g, 0.72 mmol). These were dissolved in 25 ml 2MOE. The solution was hydrolyzed with 0.1 ml water (2 equivalents) to a powder blue-green gel which produced a colorless supernatant overnight. The solution was poured off and dried with virtually no residue. The gel was divided into 4 samples which were heated 8 hours at 350, 450, 550, and 650 °C respectively, in Ni crucibles in air. XRD showed γ phase appearance at 350 °C with some amorphous phase contamination; $BiVO_4$ peaks appear in the 450 °C sample, but the 550 °C sample is phase-pure γ-BiCuVOx.

Experiment # 38 (KD-I-7) Solid State synthesis of standard sample of $Bi_2Nb_{0.3}V_{0.7}O_{5.5}$

Stoichiometric quantities of Bi_2O_3 (4.6596g, 10 mmol), V_2O_5 (0.6366g, 3.5 mmol), and Nb_2O_5 (0.3987g, 1.5 mmol) were ground in an agate mortar under acetone, then pressed into a pellet and heated at 850 °C for 40 h (heating 10 °C/min, cooling 5 °C/min). The sample, after XRD, found not to have incorporated the Nb, and it was reground, pressed into a pellet, and heated at 1000 °C for 20 h

(heating 10 °C/min, cooling 5 °C/min). Examination by PXRD showed phase pure $Bi_2Nb_{0.3}V_{0.7}O_{5.5}$. (Figure 4.35)

Experiment #39 (KD-31) Bi(OAc)₃ + NbCl₅/2MOE → Bi₂V₀.₇Nb₀.₃O₅.₅

Bi(OAc)₃ (0.5 g, 1.3 mmol) was dissolved in 40 ml 2MOE and V-2MOE (1.201g, 0.46 mmol) added. In a separate flask, NbCl₅ (0.0725 g, 0.2 mmol) was dissolved with warming in 25 ml 2MOE and added to the Bi/V solution. The solution became cloudy yellow. The solution was hydrolyzed with 0.031 ml water (1.5 equivalents) was added to this solution, resulting in two milky layers, one white, the other yellow. The two layers were separated and heated 450 °C/8 h then 550 °C/ 8h. The XRD pattern did not match the expected γ phase pattern for $Bi_2Nb_{0.3}V_{0.7}O_{5.5}$.

Experiment #40 (KD-50) Bi(OAc)₃/diglyme + V-2MOE + Nb(OiPr)₅ → Bi₂V₀.₇Nb₀.₃O₅.₅

Bi(OAc)₃ (0.5 g, 1.3 mmol) was added to 30 ml diglyme and the mixture warmed to dissolve all solids. Nb(OiPr)₅/HOiPr solution (0.676g, 0.197 mmol) and V-2MOE solution (1.6976 g, 0.46 mmol) were added and warmed with stirring for 1 hour to give a transparent yellow solution. The solution was left open to air (not hydrolyzed) for 12 hours, then heated in a 60 ° oven for 3 h to form an opaque gel, which was heated at 350 and 450 °C for 8 h in air. The 350 °C sample was too poorly crystalline to show much in the

XRD, while the 450 °C sample, while poorly crystalline, showed phase pure $Bi_2Nb_{0.3}V_{0.7}O_{5.5}$. (Figure 4.18)

Experiment #41 (KD-51) Bi(OAc)$_3$/2MOE + V-2MOE + Nb(OiPr)$_5$ → Bi$_2$V$_{0.7}$Nb$_{0.3}$O$_{5.5}$

Bi(OAc)$_3$ (0.5g, 1.3 mmol), V-2MOE (1.6800 g, 0.46 mmol) , and Nb(OiPr)$_5$ solution (0.675 g, 0.196 mmol) were added together with 20 ml 2MOE. With warming and stirring a transparent bright yellow solution resulted. This was stirred 1 hour and hydrolyzed with 29 μl (0.57 equivalents) of water. A solid formed at the point of contact of the water, but redissolved on stirring. A gel formed on standing overnight. This was dried at 120 °C then split into three parts and each part heated at 550, 650, and 750 °C for 8 hours in air. All showed phase-pure $Bi_2V_{0.7}Nb_{0.3}O_{5.5}$ by XRD. (Figure 4.18)

Experiment #42 (JWP-II-175) Bi(OAc)$_3$ + V-2MOE + Mn(OAc)$_2$ → Bi$_2$V$_{0.85}$Mn$_{0.15}$O$_{5.5-\delta}$

Bi(OAc)$_3$ (5g, 130 mmol), 15.622 g V-2MOE solution (15.622g, 55.3 mmol) and Mn(OAc)$_2$·4H$_2$O (0.2380g, 9.75 mmol) were dissolved in 2MOE to give a yellow solution. This was hydrolyzed with excess water to make a fibrous precipitate, which was dried 4 days at 100 °C and pyrolyzed at 625 °C for 8 h in air to give an olive-green solid. XRD shows the appearance of the standard tetragonal γ phase expected for $Bi_2V_{0.85}Mn_{0.15}O_{5.5-\delta}$.

Experiment #43 (JWP-II-199A) Bi(OAc)$_3$ + V-2MOE + Mn(OAc)$_2$ → Bi$_2$V$_{0.85}$Mn$_{0.15}$O$_{5.5-\delta}$

Bi(OAc)$_3$ (2.0007 g, 5.20 mmol) V-2MOE (6.25g, 2.2 mmol), and Mn(OAc)$_2$·4H$_2$O (0.0953g, 0.39 mmol) were mixed in 150 ml 2MOE to dissolve and hydrolyzed with 2 ml H$_2$O (13 equivalents) to give a milky grey-yellow solution. This was warmed at 60 °C to dry for 3 hours, then 100 °C overnight. The resulting gel was split among 5 alumina crucibles and heated for 8 hours at 350, 450, 550, 650, and 750 °C in air. XRDs showed the evolution of the desired γ phase Bi$_2$V$_{0.85}$Mn$_{0.15}$O$_{5.5-\delta}$ with pyrolysis temperature. (Figure 4.19)

Experiment #44 (JWP-II-176B) Bi(OAc)$_3$ + V-2MOE + Fe(OAc)$_2$ → Bi$_2$V$_{0.9}$Fe$_{0.1}$O$_{5.5-\delta}$

Bi(OAc)$_3$ (2.5g, 6.48 mmol), V-2MOE (8.27 g, 2.93 mmol) and Fe(OAc)$_2$ (0.0563g, 0.325 mmol) were mixed in 100 ml 2MOE to give a yellow solution. This was hydrolyzed with 0.5 ml H$_2$O (2.5 equivalents), yielding a milky yellow-grey suspension. This was warmed on a hot plate to remove approximately 1/2 the volume of solvent. After 1 hour a gel was produced; this was dried and pyrolyzed at 625 °C for 8 hours. The XRD showed the appearance of the standard tetragonal γ phase Bi$_2$V$_{0.9}$Fe$_{0.1}$O$_{5.5-\delta}$. (Figure 4.33)

Experiment #45 (JWP-II-176A) Bi(OAc)₃ + V-2MOE + Fe(acac)₂ → Bi₂V₀.₉Fe₀.₁O₅.₅₋δ

Bi(OAc)$_3$ (2.5g, 6.5 mmol) were added to V-2MOE solution (8.27g, 2.93 mmol) and 100 ml 2MOE and stirred to dissolve. Fe(acac)$_2$ (0.1144 g, 0.33 mmol) was added to obtain a red-orange solution. 0.5 ml water (2.5 equivalents) were added, resulting in some milkiness; this was warmed on a hot plate to remove some solvent. After 4 hours a gel was produced; this was dried and pyrolyzed at 625 °C for 8 hours. The XRD pattern showed the appearance of the standard tetragonal γ phase expected for Bi$_2$V$_{0.9}$Fe$_{0.1}$O$_{5.5-\delta}$. (Figure 4.34)

Experiment #46 (JWP-II-199B) Bi(OAc)₃ + V-2MOE + Fe(acac)₂ → Bi₂V₀.₉Fe₀.₁O₅.₅₋δ

Bi(OAc)$_3$ (2.3386g 6.06 mmol), V-2MOE (7.7364 g, 2.73 mmol), and Fe(acac)$_2$ (0.10695 g, 0.30 mmol) were dissolved in 100 ml 2MOE and hydrolyzed with 2 ml H$_2$O (10 equivalents) to yield a milky red solution. This was warmed at 60 °C to dry for 3 hours, then 100 °C overnight. The resulting gel was split among 5 alumina crucibles and heated for 8 hours at 350, 450, 550, 650, and 750 °C in air. XRDs showed the evolution of the desired γ phase Bi$_2$V$_{0.9}$Fe$_{0.1}$O$_{5.5-\delta}$ with pyrolysis temperature. (Figure 4.20)

Experiment #47 (JWP-III-53) Bi(OAc)$_3$ + V-2MOE + Ti(OiPr)$_4$ → Bi$_2$Ti$_{0.1}$V$_{0.9}$O$_{5.5-\delta}$

Bi(OAc)$_3$ (1g, 2.59 mmol), V-2MOE solution (2.35 g, 1.17 mmol), and Ti(OiPr)$_4$ (0.0367 g, 0.129 mmol) were mixed in 60 ml 2MOE to dissolve. This was hydrolyzed with 0.4 ml water (4.3 equivalents) to produce a clear yellow solution which became a tan liquidy gel on standing overnight. The solvent was evaporated from this and the gel pyrolyzed for 8 h at 700 °C. Examination by XRD showed a clean γ phase pattern for Bi$_2$Ti$_{0.1}$V$_{0.9}$O$_{5.5-\delta}$. (Figure 4.21)

Table 4.4: XRD standard, $Bi_2VO_{5.5}$ by solid state, Expt. 30

λ_1=1.54056, λ_2=1.54439, 10-70° step size 0.05°, 2 sec./step; literature a = 5.533, b = 5.611, c = 15.288 Å orthorhombic, indexing based on literature.[37]

h	k	l	2theta	d(exp) Å	I/Io (%)
0	0	2	11.580	7.6352	16.62
3	1	1	23.289	3.8163	14.32
1	1	3	24.200	3.6747	3.70
3	1	3	28.638	3.1145	100
0	2	0	31.852	2.8072	17.05
6	0	0	32.319	2.7677	20.82
2	2	0	33.728	2.6552	2.84
0	2	2	34.000	2.6346	3.63
6	0	2	34.480	2.5990	4.85
0	0	6	35.216	2.5464	14.39
3	1	5	37.223	2.4136	11.09
0	2	4	39.849	2.2603	5.49
6	0	4	40.216	2.2405	5.92
6	2	0	45.955	1.9732	9.19
6	2	2	47.640	1.9073	6.32
0	2	6	48.235	1.8851	12.35
6	0	6	48.573	1.8728	13.17
3	3	3	54.813	1.6734	10.52
9	1	3	55.441	1.6560	13.35
			59.230	1.5587	15.94

Table 4.5: XRD standard, $Bi_2Cu_{0.1}V_{0.9}O_{5.35}$ by solid state, Experiment 31

Scan conditions same as for Table 4.4. Indexing gives a=3.9179 Å, c=15.4478 Å, all angles 90°.

h	k	l	2theta	d(exp) Å	d(calc) Å	I/Io (%)
0	0	2	11.480	7.7020	7.72	54.93
0	0	4	23.025	3.8594	3.862	9.95
1	0	1	23.439	3.7922	3.798	22.61
1	0	3	28.604	3.1181	3.118	100
1	1	0	32.310	2.7684	2.770	68.74
1	1	2	34.349	2.6086	2.608	12.07
0	0	6	34.803	2.5756	2.575	34.00
1	0	5	37.034	2.4254	2.426	14.87
1	1	4	40.018	2.2512	2.251	11.33
2	0	0	46.340	1.9577	1.959	25.06
2	0	2	47.879	1.8983	1.899	6.31
1	1	6	48.213	1.8859	1.886	30.80
2	1	3	55.328	1.6591	1.659	23.95
1	0	9	58.686	1.5719	1.572	17.50
2	0	6	59.222	1.5589	1.559	6.99
2	1	5	60.693	1.5246	1.524	5.33

Table 4.6: Reflections and indexing for BiCuVOx made by sol-gel method, Expt. 34

Scan conditions same as for Table 4.4. Indexing gives a=3.9195 Å, c=15.4045 Å, all angles 90°.

h	k	l	2theta	d(exp) A	d(calc) A	I/Io (%)
0	0	2	11.499	7.6892	7.71	27.57
0	0	4	26.051	3.8551	3.857	3.19
1	0	1	23.408	3.7972	3.800	12.57
1	0	3	28.608	3.1177	3.118	100
1	1	0	32.289	2.7702	2.773	23.41
1	1	2	34.374	2.6068	2.609	5.58
0	0	6	34.894	2.5691	2.571	9.89
1	0	5	37.069	2.4232	2.425	8.01
1	1	4	40.033	2.2504	2.251	6.45
2	0	0	46.267	1.9606	1.961	9.13
2	0	2	47.848	1.8995	1.900	4.75
1	1	6	48.240	1.8850	1.885	17.46
2	1	1	52.470	1.7425	1.742	3.44
2	1	3	55.302	1.6598	1.660	15.18
1	0	9	58.727	1.5709	1.571	8.08
2	0	6	59.179	1.5600	1.559	6.45

Table 4.7: Complex Impedance Data for Sol-Gel Derived $Bi_2Cu_{0.1}V_{0.9}O_{5.35}$

Temp. (°C)	Type	y-intercept	slope	diameter	Z″ real center	Z′ imag. center	x-intercept	ρ (ohm·cm)
242.2	circle			2.227E6	1.05E6	3.61E5	2.109E6	4.360E6
269.3	circle			1.435E6	5.545E6	3.83E6	1.161E6	2.401E6
294.8	circle			4.434E5	2.061E5	8.40E4	4.113E5	8.504E5
320.1	circle			2.118E5	9.762E4	4.27E4	1.945E5	4.021E5
345.4	circle			8.835E4	4.214E4	1.65E4	8.310E4	1.718E5
370.5	circle			5.635E4	2.427E4	1.45E4	4.841E4	1.001E5
395.3	circle			2.751E4	1.4163E4	5042	2.696E4	5.575E4
420	circle			1.582E4	8930.44	2650	1.638E4	3.387E4
444.7	circle			8767.66	5340.4	1709	9.378E3	1.939E4
469.5	circle			1292.5	1536.22	248.1	2.133E3	4.410E3
494.6	line	303.42	-.707				4.291E2	8.872E2
520	circle			737.4	539.64	215.5	9.399E2	1.734E3
545.4	circle			390.28	241.1	117.4	3.970E2	8.208E2
570.7	circle			36.788	70.265	8.103	8.678E1	1.794E2
596.6	circle			27.45	40.304	6.312	5.429E1	1.085E2
622.6	circle			13.60	26.84	2.705	3.307E1	6.837E1
675.1	circle			7.981	11.743	1.993	1.520E1	3.143E1
726.8	circle			5.583	9.473	1.568	1.179E1	2.437E1
753.4	circle			1.556	7.216	0.308	7.931E0	1.640E1

Temp. (°C)	Type	y-intercept	slope	diameter	Z″ real center	Z′ imag. center	x-intercept	ρ (ohm·cm)
805.7	circle			0.958	5.802	0.243	6.215E0	1.285E1
831.8	circle			0.558	5.329	0.117	5.582E0	1.154E1
779.8	circle			0.268	0.035	5.479	5.608E0	1.159E1
727.7	circle			0.926	6.068	0.168	6.500E0	1.344E1
675.6	circle			2.313	7.046	0.486	8.096E0	1.674E1
623	circle			3.941	8.579	0.719	1.041E1	2.153E1
570.9	circle			3.380	9.329	0.430	1.095E1	2.266E1
520	circle			26.493	21.275	5.946	3.311E1	6.846E1
469.2	circle			24.904	26.233	3.824	3.808E1	7.874E1
520.1	circle			5.000	12.144	0.611	1.457E1	3.012E1
571.1	line	8.331	-1.088				7.658E0	1.583E1
623	line	5.7055	-0.858				6.648E0	1.374E1
675.1	circle			3.252	7.717	0.601	9.228E0	1.908E1
726.9	circle			0.431	5.876	0.053	6.085E0	1.258E1
779.6	circle			0.381	5.533	0.065	5.712E0	1.181E1
831.6	circle			0.174	5.102	0.026	5.185E0	1.072E1

Table 4.8: XRD standard $Bi_2Nb_{0.3}V_{0.7}O_{5.5}$ by solid state, Expt. 38.

Scan conditions same as for Table 4.4. Indexing gives a=3.909113 Å, c=15.74489 Å, all angles 90°. Note the preferred orientation problem with the 00ℓ peaks.

h	k	l	2theta	d(exp) A	d(calc) A	I/Io (%)
0	0	2	11.212	7.8852	7.87	14.07
0	0	4			3.943	
1	0	1	23.399	3.7986	3.794	9.85
1	0	3	28.432	3.1366	3.135	100
1	1	0	32.375	2.7630	2.764	29.60
0	0	6	34.150	2.6234	2.624	6.91
1	1	2	34.317	2.6110	2.608	7.91
1	0	5	36.624	2.4516	2.452	6.98
1	1	4	39.830	2.2614	2.262	6.94
2	0	0	46.435	1.9539	1.955	13.48
1	1	6	47.777	1.9021	1.903	18.66
2	1	1	52.638	1.7373	1.738	3.36
2	1	3	55.327	1.6591	1.659	21.05
2	0	6	58.851	1.5679	1.568	7.69

Table 4.9: $Bi_2V_{0.85}Mn_{0.15}O_{5.5-\delta}$, Expt. 43.

Scan conditions same as for Table 4.4. Indexing gives a=3.91805 Å, c=15.49123 Å, all angles 90°.

h	k	l	2theta	d(exp) A	d(calc) A	I/Io (%)
0	0	2	11.383	7.7671	7.75	14.11
0	0	4	22.907	3.8791	3.8728	2.68
1	0	1	23.389	3.8002	3.798	11.67
1	0	3	28.557	3.1232	3.121	100
1	1	0	32.273	2.7715	2.770	31.48
1	1	2	34.313	2.6112	2.6086	6.83
0	0	6	34.718	2.5817	2.582	10.99
1	0	5	36.960	2.4301	2.4302	9.61
1	1	4	39.998	2.2523	2.2533	7.91
2	0	0	46.300	1.9593	1.959	14.33
1	1	6	48.134	1.8888	1.889	22.51
2	1	1	52.509	1.7413	1.7411	4.23
2	1	3	55.332	1.6589	1.659	23.20
1	0	9	58.552	1.5752	1.5759	10.08
2	0	6	59.149	1.5607	1.5606	10.08

Table 4.10: $Bi_2V_{0.9}Fe_{0.1}O_{5.5-\delta}$ by sol gel, Expt. 46

Scan conditions same as for Table 4.4. Indexing gives a=3.9356 Å, c=15.46157 Å, all angles 90°.

h	k	l	2theta	d(exp) A	d(calc) A	I/Io (%)
0	0	2	11.366	7.7784	7.73	14.91
0	0	4	22.900	3.8803	3.8654	2.56
1	0	1	23.252	3.8224	3.814	12.60
1	0	3	28.494	3.1299	3.128	100
1	1	0	32.125	2.7839	2.783	27.48
1	1	2	34.205	2.6192	2.6184	6.73
0	0	6	34.746	2.5797	2.5769	14.50
1	0	5	36.916	2.4329	2.432	10.55
1	1	4	39.888	2.2582	2.258	8.18
2	0	0	46.080	1.9681	1.968	14.78
1	1	6	48.079	1.8909	1.891	24.89
2	1	1	52.241	1.7496	1.7488	4.67
2	1	3	55.110	1.6651	1.666	22.46
1	0	9	58.585	1.5744	1.574	13.99
2	0	6	59.032	1.5635	1.5640	9.79

Table 4.11: $Bi_2Ti_{0.1}V_{0.9}O_{5.5-\delta}$, Expt. 47

Scan conditions same as for Table 4.4. Indexing gives a=3.9312 Å, c=15.4416 Å, all angles 90°.

h	k	l	2theta	d(exp) A	d(calc) A	I/Io (%)
0	0	2	11.412	7.7478	7.72	12.10
0	0	4	22.941	3.8734	3.8604	2.36
1	0	1	23.306	3.8136	3.810	11.45
1	0	3	28.547	3.1242	3.124	100
1	1	0	32.226	2.7755	2.780	19.39
1	1	2	34.319	2.6108	2.6154	5.17
0	0	6	34.828	2.5739	2.574	11.85
1	0	5	37.011	2.4269	2.429	12.76
1	1	4	39.979	2.2533	2.2558	6.63
2	0	0	46.206	1.9631	1.966	14.41
1	1	6	48.150	1.8882	1.888	19.14
2	1	3	55.100	1.6654	1.664	11.15
1	0	9	58.716	1.5711	1.5725	11.05
2	0	6	59.152	1.5606	1.5621	12.31

Figure 4.31: Powder XRD of solid-state synthesized $Bi_2VO_{5.5}$. This is the XRD pattern that has been used to verify the sol-gel synthesis products throughout this research.
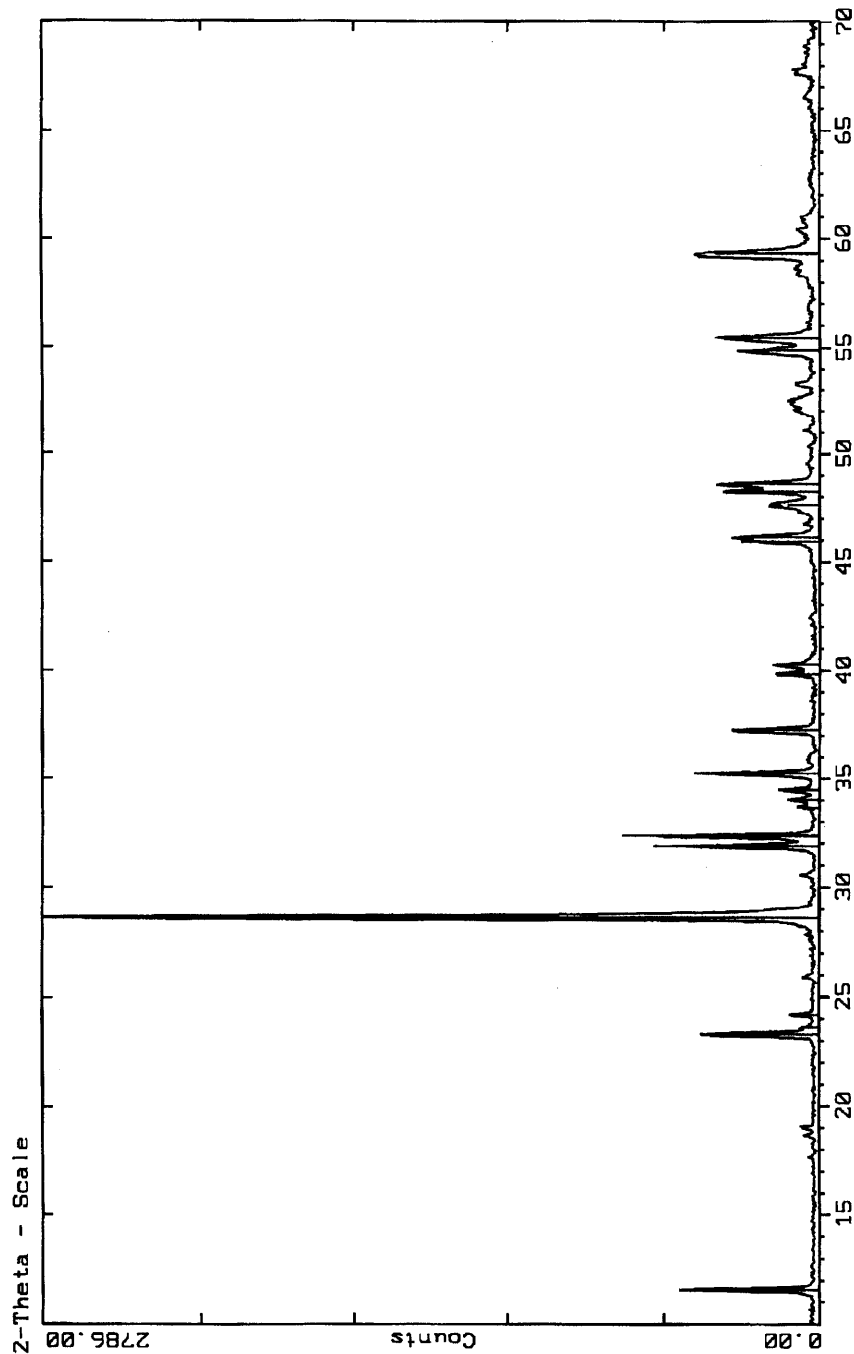
Figure 4.32: Powder XRD of solid-state synthesized $Bi_2Cu_{0.1}V_{0.9}O_{5.5}$. This is the XRD pattern that has been used to verify the sol-gel synthesis products throughout this research.
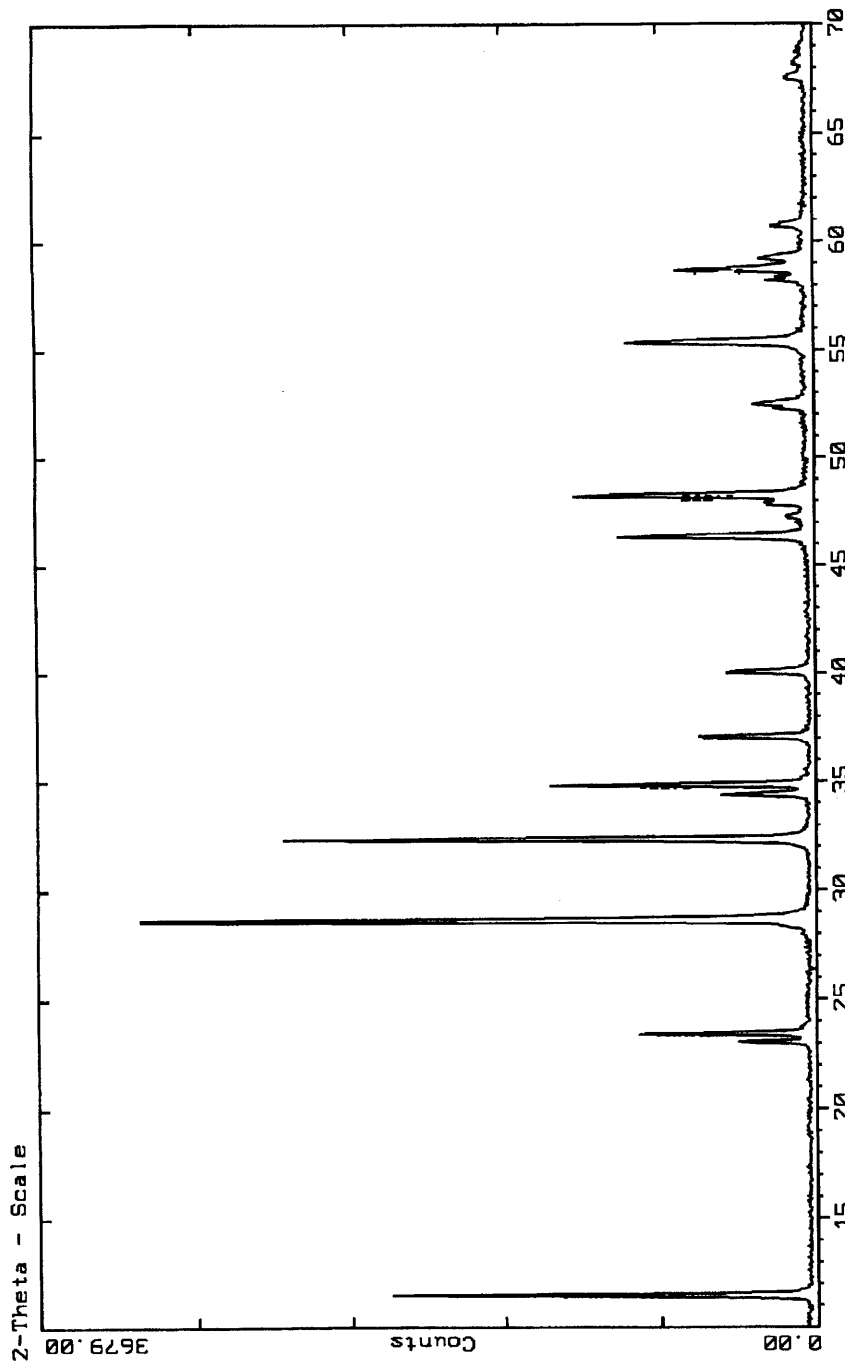
Figure 4.33: Powder XRD of sol-gel produced $Bi_2V_{0.9}Fe_{0.1}O_{5.5-\delta}$. Pyrolysis temperature was: 625 °C. The iron was supplied as $Fe(OAc)_2$.
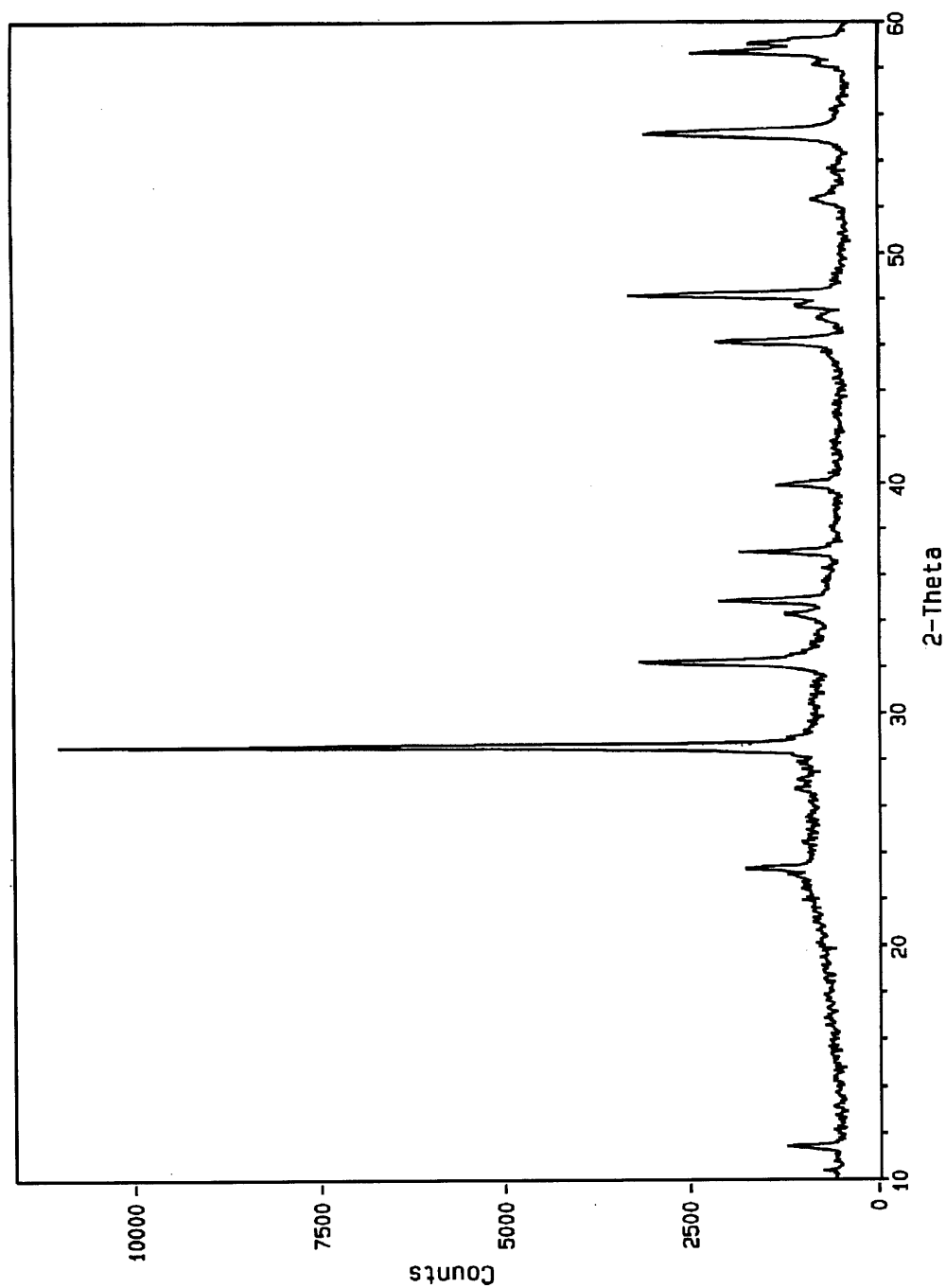
Figure 4.34: Powder XRD of sol-gel produced $Bi_2V_{0.9}Fe_{0.1}O_{5.5-\delta}$. Pyrolysis temperature was: 625 °C. The iron was supplied as $Fe(acac)_2$.
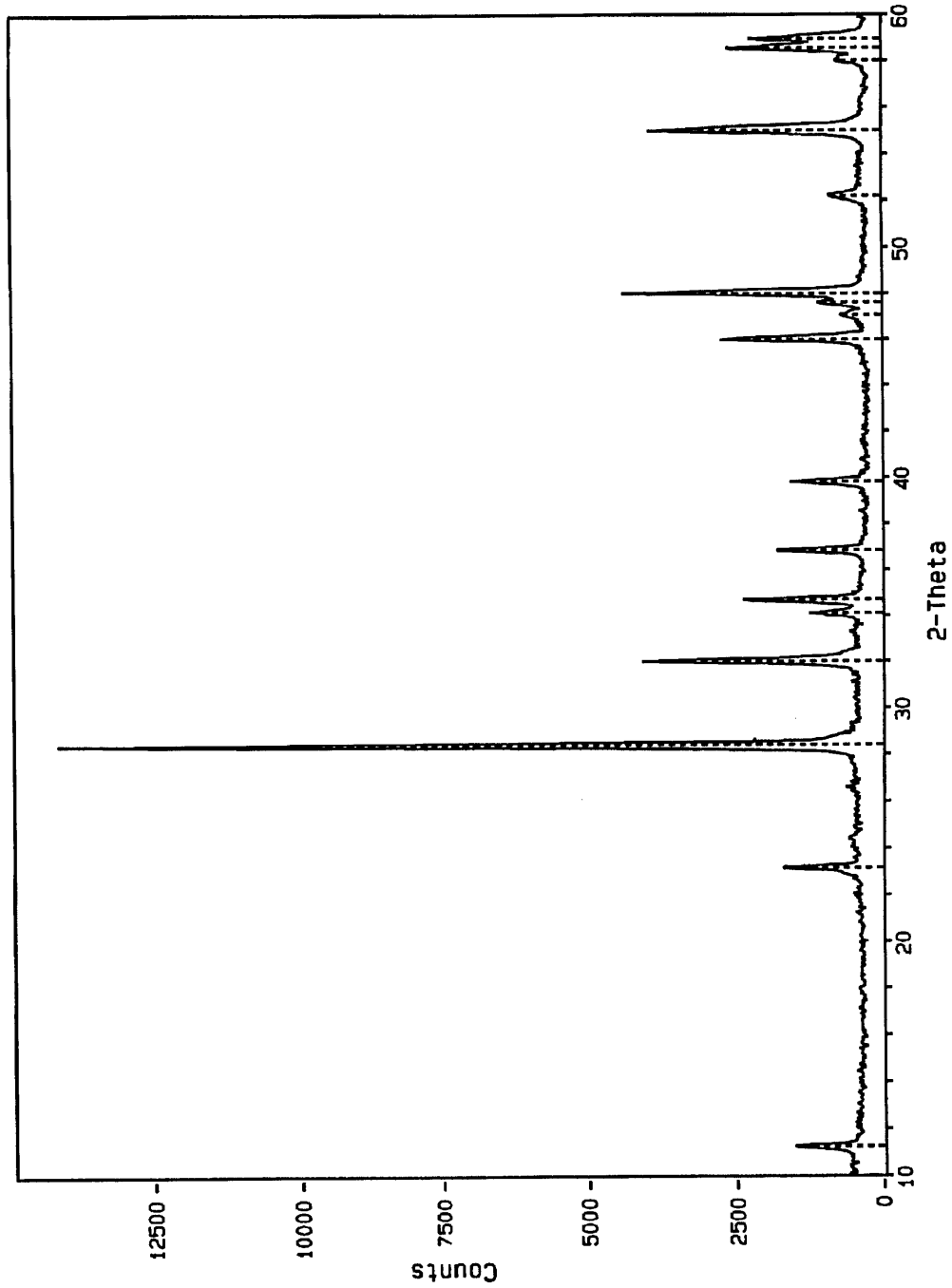
Figure 4.35: Powder XRD of solid-state synthesized

$Bi_2V_{0.7}Nb_{0.3}O_{5.5}$. This is the XRD pattern that has been used to verify the sol-gel synthesis products. Pyrolysis temperature was 1000 °C.
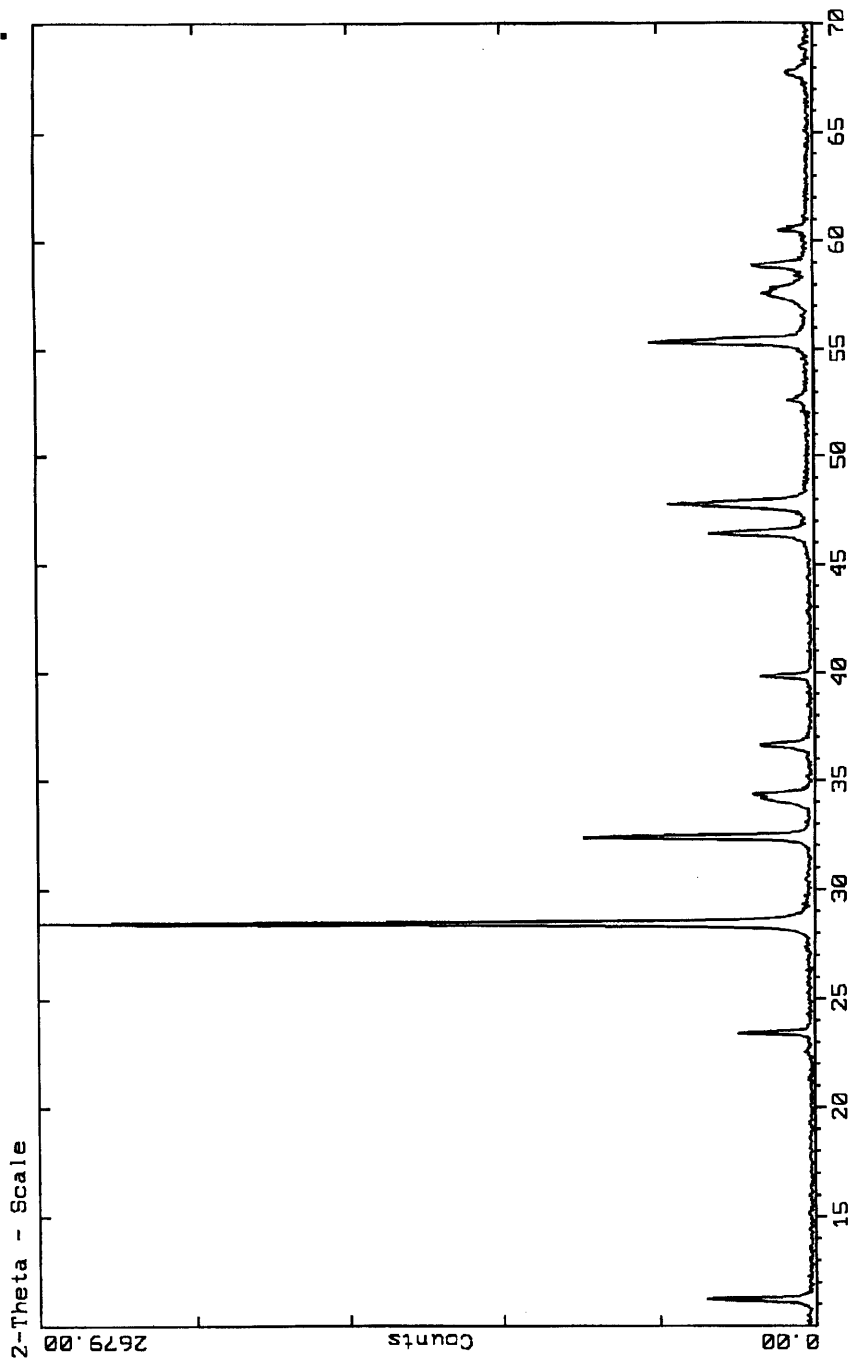
4.5 References

1) Bradley, D. C.; Mehrotra, R. C.; Gaur, D. P. *Metal Alkoxides*; Academic Press: New York, 1978.

2) Mehrotra, R. C. *Inorg. Chim. Acta Rev.* **1967**, *1*, 99.

3) Mehrotra, R. C. *Adv. Inorg. Chem. Radiochem.* **1983**, *26*, 269.

4) Mehrotra, R. C. *J. Non-Crystalline Solids* **1988**, *100*, 1.

5) Mehrotra, R. C. in *Sol-gel Science and Technology : Proceedings of the Winter School on Glasses and Ceramics from Gels, São Carlos (SP), Brazil, 14-19 August 1989* , 1989, p 17.

6) Mehrotra, R. C. in *Sol-gel Science and Technology : Proceedings of the Winter School on Glasses and Ceramics from Gels, São Carlos (SP), Brazil, 14-19 August 1989,* 1989, p 40.

7) Mehrotra, R. C.; Singh, A.; Sogani, S. *Chem. Rev.* **1994**, *94*, 1643.

8) Hillerns, F.; Rehder, D. *Chem. Ber.* **1991**, *124*, 2249.

9) Priebsch, W.; Rehder, D. *Inorg. Chem.* **1990**, *29*, 3013.

10) Crans, D. C.; Chen, H.; Felty, R. A. *J. Am. Chem. Soc.* **1992**, *114*, 4543.

11) Crans, D. C.; Shin, P. K. *J. Am. Chem. Soc.* **1994**, *116*, 1305.

12) Prandtl, W.; Hess, L. *Z. Anorg. Chem.* **1913**, *82*, 103.

13) Funk, H.; Weiss, W.; Zeising, M. *Z. Anorg. Allg. Chem.* **1958**, *296*, 36.

14) Mittal, R. K.; Mehrotra, R. C. *Z. Anorg. Chem.* **1964**, *327*, 311.

15) Legendre, J.-J.; Livage, J. *J. Colloid and Interface Sci.* **1983**, *94*, 75.

16) Legendre, J.-J.; Aldebert, P.; Baffier, N.; Livage, J. *J. Colloid and Interface Sci.* **1983**, *94*, 84.

17) Lemerle, J.; Nejem, L.; Lefebvre, J. *J. Inorg. Nucl. Chem.* **1980**, *42*, 17.

18) Livage, J. *Chem. Mater.* **1991**, *3*, 578.

19) Hirashima, H.; Kamimura, S. in *Better Ceramics Through Chemistry III;* Brinker, C. J., Clark, D. E. and Ulrich, D. R., Eds.; Mater. Res. Soc.: Pittsburgh, 1988, pp 779-784.

20) Hirashima, H.; Tsukimi, K.; Muratake, R. *J. Ceram. Soc. Jpn. Inter. Ed.* **1989**, *97*, 232.

21) Hench, L. L.; West, J. K. *Chem. Rev.* **1990**, *90*, 33.

22) Hirashima, H.; Sato, A.; Yoshida, T. *Yogyo-Kyokai-shi* **1986**, *94*, 875.

23) Toyoda, M.; Payne, D. A. *Mater. Lett.* **1993**, *18*, 84.

24) Toyoda, M.; Hamaji, Y.; Tomono, K.; Payne, D. A. *Jpn. J. Appl. Phys.* **1993**, *32*, 4158.

25) Rogers, R. D.; Bond, A. H.; Aguinaga, S. *J. Am. Chem. Soc.* **1992**, *114*, 2960.

26) Mehrotra, R. C.; Rai, A., K *Ind. J. Chem.* **1966**, *4*, 537.

27) Sauer, N. N.; Garcia, E.; Ryan, R. R. *Mat. Res. Soc. Symp. Proc.,* **1990**; *180*, 921.

28) Jones, C. M.; Burkart, M. D.; Bachman, R. E.; Serra, D. L.; Hwu, S.-J.; Whitmire, K. H. *Inorg. Chem.* **1993**, *32*, 5136.

29) Evans, W. J.; Hain, J. H. J.; Ziller, J. W. *J. Chem. Soc. Chem. Commun.* **1989**, 1628.

30) Massiani, M.-C.; Papiernik, R.; Hubert-Pfalzgraf, L. G. *Polyhedron* **1991**, *10*, 437.

31) Massiani, M. C.; Papiernik, R.; Hubert-Pfalzgraf, L. G.; Daran, J. C. *J. Chem. Soc. Chem. Commun.* **1990**, 301.

32) Matchett, M. A.; Chiang, M. Y.; Buhro, W. E. *Inorg. Chem.* **1990**, *29*, 360.

33) Hubert-Pfalzgraf, L. G.; Poncelet, O.; Papiernik, R.; Boulmaaz, S.; Sirio, C. in *Eurogel '91*, Vilminot, S., Nass, R. and Schmidt, H., Eds.; Elsevier: Netherlands, 1991, pp 293.

34) Clegg, W.; Compton, N. A.; Errington, R. J.; Norman, N. C.; Wishart, N. *Polyhedron* **1989**, *8*, 1579.

35) Ando, F.; Hayashi, T.; Ohashi, K.; Koketsu, J. *J. Inorg. Nucl. Chem.* **1975**, *37*, 2011.

36) Devillers, M.; Tirions, O.; Cadus, L.; Ruiz, P.; Delmon, B. *J. Solid State Chem.* **1996**, *126*, 152.

37) Abraham, F.; Debreuille-Gresse, M. F.; Mairesse, G.; Nowogrocki, G. *Solid State Ionics* **1988**, *28-30*, 529.

38) Mairesse, G. in *Fast Ion Transport in Solids*; Scrosati, B. *et al.*, Eds.; Kluwer Academic Publishers: Netherlands, 1993, pp 271.

39) Kendall, K. R.; Navas, C.; Thomas, J. K.; zur Loye, H.-C. *Chem. Mater.* **1996**, *8*, 642.

40) Vannier, R. N.; Mairesse, G.; Nowogrocki, G.; Abraham, F.; Boivin, J. C. *Solid State Ionics* **1992**, *53-56*, 713.

41) Bradley, D. C.; Mehta, M. L. *Can. J. Chem.* **1962**, *40*, 1183-1188.

42) Spath, E. *Monatsh.* **1912**, *33*, 235.

43) Gattow, G.; Schwank, H. *Z. anorg. Chem.* **1971**, *382*, 49.

44) Troyanov, S. I.; Pisarevskii, A. P. *Koord. Khim.* **1991**, *17*, 909.

45) Pisarevskii, A. P.; Matynenko, L. I.; Dzyubenki, N. G. *Zh. Neorg. Khim.* **1990**, *35*, 1489.

46) Rogers, R. D.; Bond, A. H.; Aguinaga, S.; Reyes, A. *J. Amer. Chem. Soc.* **1992**, *114*, 2967.

47)Sauer, N. N.; Garcia, E.; Salazar, K. V.; Ryan, R. R.; Martin, J. A. *J. Am. Chem. Soc.* **1990**, *112*, 1524.

48)Boyle, T., personal communication via email.

49)Zevaco, T.; Guilhaume, N.; Postel, M. *New. J. Chem.* **1991**, *15*, 927.

50)Bench, W.; Blazso, E.; Dubler, E.; Oswald, H. R. *Acta Crystallogr.* **1987**, *43C*, 1699.

51)Papiernik, R.; Hubert-Pfalzgraf, L. G.; Massiani, M. C. *Polyhedron* **1991**, *10*, 1657.

52)Nugent, W. A.; Harlow, R. L. *J. Am. Chem. Soc.* **1994**, *116*, 6142-6148.

53)Lu, T.; Steele, B. C. H. *Solid State Ionics* **1986**, *21*, 339.

54)West, A. R. *Solid State Chemistry and its Applications*; John Wiley and Sons: New York, 1992.

55)Birchall, J. D.; Mockfort, M. J.; Stanley, D. R., Imperial Chemical Industries, PLC: U.S. Patent No. 4,950,626, 1990.

56)Krok, F.; Bogusz, W.; Kurek, P.; Wasiucionek, M.; Jakubowski, W.; Dygas, J. *Mat. Sci. and Eng. B* **1993**, *B21*, 70.

57)Abraham, F.; Boivin, J. C.; Mairesse, G.; Nowogrocki, G. *Solid State Ionics* **1990**, *40-41*, 934.

58)Kendall, K., personal communication.

Chapter Five

Describing the Bi/V Precursor: Synthesis and Characterization of a Bismuth-Vanadium Heterobimetallic Alkoxide

The experimental work described in this chapter was adapted, in part, from Pell, J.W., Davis, W.C, and zur Loye, H.-C., *Inorg. Chem.* 1996, 5754-5755.

5.1 Introduction: Brief Review of Heterobimetallic Alkoxides

A number of observations made during the work described in Chapter Four suggested that some experiments, tangential to the project goal of producing defect-free films of the BiMeVOx ceramic, be undertaken to investigate whether a single bismuth-vanadium complex was formed in the precursor solution. The observation that the yellow vanadium 2-methoxyethoxide became orange when the bismuth acetate solution was added, suggested that a change occurred in the vanadium coordination sphere due to the $Bi(OAc)_3$. Likewise, the behavior of the fibrous bismuth acetate-alcohol polymer that was formed in the bismuth acetate solution in 2-methoxyethanol, suggested an interaction with the vanadium alkoxide: it would not form in the presence of vanadium alkoxide, even in concentrated solutions of $Bi(OAc)_3$; in solutions where it had formed, addition of the vanadium alkoxide would redissolve it readily. That the bismuth 2-methoxyethoxide made from bismuth tris(dimethylsilamide) formed the $Bi_2VO_{5.5}$ phase directly was also suggestive of a high degree of interaction between the precursor materials.

We expect chemical interactions to occur between the $Bi(OAc)_3$ and V-2MOE in solution. Vanadium alkoxides tend to form μ-alkoxo dimers in order to increase their coordination numbers, as do most transition metal alkoxides.[1-3] While unbridged vanadium alkoxides are colorless, the bridged dimeric or oligomeric derivatives tend to be yellow to red in color; the degree of bridging changes with the

alkoxide's concentration in solution.[4] Likewise, bismuth, even when its compounds have eighteen electrons, also tends to become hypervalent, increasing its coordination number through bridging by its ligands, as seen in bismuth acetate (Chapter Four).[5] The alcohol in use in our sol-gel preparations, 2-methoxyethanol, is capable of acting as a bridging ligand, as seen in $Ba_2Cu_2(OR)_4(acac)_4 \cdot 2HOR$ ($R=CH_2CH_2OCH_3$)[6] and in $Ba_4Ti_{13}(\mu3\text{-}O)_{12}(\mu5\text{-}O)_6(\mu1\text{-}\eta^1\text{-}OCH_2CH_2OCH_3)_{12}(\mu1,\mu3\text{-}\eta^2\text{-}OCH_2CH_2OCH_3)_{12}$.[7]

As we have indicated in the previous Chapters, the use of metal alkoxides in sol-gel processes requires that the hydrolysis and condensation rates of each alkoxide be matched to prevent inhomogeneities in the gel. One method of reaching homogeneity is to use only one alkoxide species and to add other metals as decomposable salts. Another is to modify the ligands of one or more of the alkoxides to be used so that the rate of hydrolysis and condensation of the least stable alkoxide is close to that of the most stable. A more elegant method is to prepare a heterometallic alkoxide which already has locked in its structure the proper metal ratio. The lability of the coordination sphere permits the synthesis of heterometallic alkoxides, often by nothing more complicated than simply mixing them. Incorporation of the metals required in the final oxide product into a single source precursor is the ultimate in attaining atomic-level mixing of the metals.

Despite the widespread interest in multi-metal alkoxide precursors to a number of ceramic classes – mainly those intended for electronic applications (superconductors, ferro- and di- electrics, etc.) where high-temperature processing often creates grain

morphologies that reduce the material's desired performance –
there is little information regarding the exact composition of many
precursor systems, and less about the structure of many purported
heterometallic alkoxide precursor species. Partly this is because the
majority of the research in these areas is goal- or product-oriented,
and the specific details of precursor species' structures usually are
tangential to the question of what precursor "recipe" works the
best. Aside from this, however, it is often difficult to isolate the
putative species because they tend to precipitate or polymerize as
solvent is removed, usually with loss of the solution-stable
structure, rather than crystallize. Combination species may arise
simultaneously in solution from an attempted heterometallic
alkoxide synthesis. Many vanadium alkoxides, in fact, undergo
rearrangement and exchange in solution.[2] The distribution of such
species will be statistical, depending on the thermodynamics and
kinetics of the species' formation and on the concentration of the
solution. In such cases isolation of "the" precursor is problematic.

Despite the difficulties, a number of heterometallic alkoxide
precursors have been reported. A number of bimetallic alkoxides
were synthesized early in this century by the titration of alkali metal
alkoxides with less basic alkoxides of p-block metalloids and
transition metals.[8] They were considered to be alkoxo salts until
the 1958 work of Bartley and Wardlaw, which demonstrated the
covalent nature of $[Na(Zr_2(OR)_9)]$.[9] More recent work has produced
combinations of transition metals in a single alkoxide:

$[(BaTiO)_4(iOPr)_{16}] \cdot 3HOiPr$,[10] $Pb_2Ti_2(\mu4-O)(\mu3-OiPr)_2(\mu-OiPr)_4(OiPr)_4$,[11]

$Ba_2Cu_2(2MOE)_4(acac)_4 \cdot 2H2MOE$;[6] $MNb_2(\mu-OAc)_2(\mu-OR)_4(OR)_6$ (M=Cd,
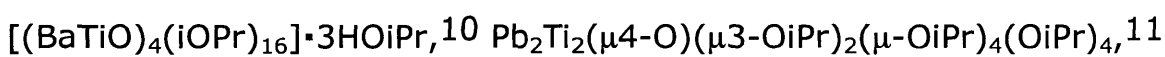
Mg), $PbZr_3(\mu4\text{-}O)(\mu\text{-}OAc)_2(\mu\text{-}OR)_5(OR)_5$, $Gd_2Zr_6(\mu4\text{-}O)_2(\mu\text{-}OAc)_6(\mu\text{-}OR)_{10}(OR)_{10}$, R=iPr;[12] $Pb_4Zr_2(OiPr)_{16}$, $Pb_2Zr_4(OiPr)_{20}$,[13] $Pb_6Nb_4(\mu4\text{-}O)(\mu3\text{-}OEt)_4(\mu2\text{-}OEt)_{12}(OEt)_8$,[14] $Ba_4Ti_{13}(\mu3\text{-}O)_{12}(\mu5\text{-}O)_6(\mu1\text{-}\eta^1\text{-}2MOE)_{12}(\mu1, \mu3\text{-}\eta^2\text{-}2MOE)_{12}$,[7] and a number of others. Most of these are μ-oxo materials; in most cases the appearance of oxo-bridging is due to partial hydrolysis of the parent alkoxides.

There are a number of different methods for making heterometallic alkoxides; which one will work depends on the nature of the metals involved (electronegativity and tendency to increase coordination sphere) and the steric and electronic nature (ramification) of the alkoxo groups. Simply mixing two metal alkoxides, particularly where one of the metals is strongly electropositive, has yielded a heterometallic alkoxide product in a number of examples. A precursor to $LiNbO_3$, for example, is $LiNb(OEt)_6$, made by simply refluxing an ethanolic solution of Li(OEt) with $Nb(OEt)_5$ in 1:1 ratio.[15] Likewise, $Ba(2MOE)_2$ and $Ti(2MOE)_4$ refluxed together in 2-methoxyethanol left a white solid $BaTi(2MOE)_6$;[7] and $Ti(OiPr)_4$ and $[Pb(OiPr)_2]_\infty$ refluxed in toluene gave crystalline $Pb_2Ti_2O(OiPr)_{10}$.[11] Furthermore, the second metal alkoxide may be produced by *in situ* dissolution of the metal; the alkaline earth metals dissolve faster in alcohol in the presence of alkoxides of the transition metals and main group metalloids (Equation 5.1).

(5.1) $M + 2\ ROH + 2\ M'(OR)_x \longrightarrow (HgCl_2/ROH)\ [M(M'(OR)_y)_z]$
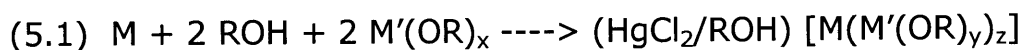
M=Mg, Ca, Sr, Ba; M'=Al, Ga, Zr, Hf, Nb, Ta; R=Et, iPr; x, y, z as needed for electroneutrality.

Such solubilizing of a metal-containing species is often evidence of the formation of a mixed alkoxide. For instance, $Pb_4O(OEt)_6$ dissolves in non-polar solvents when $[Nb(OEt)_5]_2$ is added at room temperature. Cooling the solution gives crystalline $Pb_6O_4(OEt)_4[Nb(OEt)_5]_4$.[12]

Other leaving groups can also be used; for instance, $Ba[N(SiMe_3)_2]_2(THF)_2$ reacted with $Zr_2(OiPr)_8(HOiPr)_2$ gives $[BaZr_2(OiPr)_{10}]_2$.[15] The reaction of a metal alkoxide and a metal carboxylate may be reacted. Where simple ligand exchange does not occur, the metal species may react to form an oxo-bridged heterometallic alkoxide with ester elimination (Equation 5.2).

(5.2) $M(OR)_n + M'(O_2CR')_m \longrightarrow (RO)_{n-1}MOM'(O_2CR')_{m-1} + RO_2CR'.$
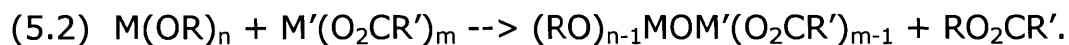
For example, a precursor to YSZ was prepared according to Equation 5.3.[15]

(5.3) $Y(OAc)_3 + Zr(OnBu)_4 \longrightarrow$

$\qquad Y(OAc)_2[OZr(OnBu)_2]OH + C_4H_8 + nBuOAc$

(The origin of the butene was not discussed.)
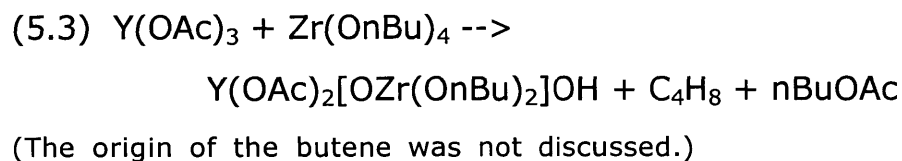
Likewise, production of Nb-containing heterometallic alkoxides has been accomplished (Equation 5.4).[12]

(5.4) $M(OAc)_2 + 2 Nb(OiPr)_5 \longrightarrow MNb_2(OAc)_2(OiPr)_{10}$

(M=Mg, Cd, Pb)
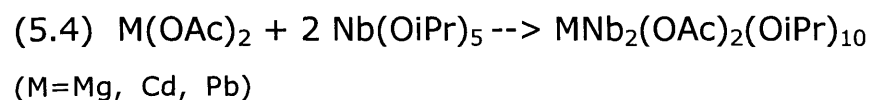
One problem with this approach, however, is that the reaction is thermodynamically controlled, and the factors that determine the distribution of products are not well-understood. Salt-elimination reactions of the type given in Equation 5.5 may occur, but commonly do not result in controlled-stoichiometry products; the reaction is often incomplete. For example, the reaction between $PbCl_2$ and $KNb(OEt)_6$ in refluxing ethanol gives mostly unreacted starting material.[12]

(5.5) $MX_n + nM'M''(OR)_m \longrightarrow M[M''(OR)_m]_n + nM'X$
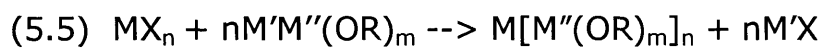
X=Cl, Br, I

Hirota et al. reported that mixing $BiCl_3$ and vanadium(V) tris(ethoxide) oxide in the presence of sodium ethoxide results in the precipitation of a substance they label "a bismuth vanadyl alkoxide." This, after hydrolysis and vacuum drying at 120 °C, produced $BiVO_4$ according to powder XRD. They do not report any characterization work for the precursor alkoxide they claim.[16] Likewise, there are a number of examples where lanthanide-aluminum alkoxides have been made by co-dissolving the chlorides in the presence of potassium alkoxide (Equation 5.6).

(5.6) $LnCl_3 + 3\ AlCl_3 + 12\ KOiPr \longrightarrow [Ln(Al(OiPr)_4)_3] + 12\ KCl$

(Ln= Gd, Ho, Er).[8]

Ter- and tetra-metallic alkoxides have been made using metal alkoxides as chelating ligands $L_M = (M^{(x)}(OR)_{x+y})^{y-}$ according to Equation 5.7.

(5.7) $M'Cl_2 + [KL_M] \rightarrow [ClM'L_M] + KCl$[8] where M=Al, Ga, Nb, Ta, Zr and M'=Fe, Co, Ni, Cu

There has been a flurry of interest in bismuth alkoxides as potential precursors for sol-gel and chemical vapor deposition preparations of bismuth-containing superconductors[17-19] and ferroelectrics, notably $Bi_3Ti_4O_{12}$.[20-22] Heterometallic alkoxides with the correct metal ratios for the final product are especially sought-after. There is, however, a dearth of information about even the homometallic alkoxides of bismuth. Insoluble bismuth alkoxides have been known since 1966[23] and in recent years a number of soluble bismuth alkoxide complexes have been isolated.[17-19,24-28] While several groups have claimed the existence of a bismuth-transition metal precursor in their sol-gel processes[16,22,29,30] and have published IR and mass spectral data, none of these species have been isolated[5] for elemental analysis and/or x-ray crystal structure analysis. During our attempts at synthesizing a 2:1 Bi:V precursor to the oxide-ion conducting ceramic $Bi_2VO_{5.5}$, we were able to isolate and characterize $[BiCl_3(\mu\text{-}O)(\mu\text{-}OC_2H_4OCH_3)_2(OC_2H_4OCH_3)V]_2$, which to our knowledge represents the first structural description of a heterobimetallic bismuth-containing alkoxide complex. After the isolation of this material, we went on to try to prepare analogs, but were unable to obtain isolable products.

5.2 Results and Discussion

5.2.1 Structure and Properties of III-76B

Bismuth (III) chloride was dissolved in a 2:1 molar ratio with VO(OiPr)$_3$ in 2MOE solution. Brief warming, followed by several days' standing, led to the growth of crystals of the dimeric Bi-V complex III-76B. The synthesis was based on a "non-hydrolytic sol-gel method" published in the literature.[31]

There are relatively few compounds available with which to compare [BiCl$_3$(μ-O)(μ-OC$_2$H$_4$OCH$_3$)$_2$(OC$_2$H$_4$OCH$_3$)V]$_2$. The asymmetric unit contains one bismuth and one vanadium atom (Figure 5.1). The vanadium atom is located in a distorted octahedral environment that is unusual among vanadium (V) alkoxides, which prefer a square pyramidal geometry. The shortest V-O distance of 160 pm, belonging to the bridging oxide atom O(4), compares well with the usual vanadyl distance of 158 pm.[4,32,33] A band at 945 cm^{-1} confirms the weakening of the vanadyl bond (usually 950-990 cm^{-1}).[4] (Figure 5.2) Taking O(4) as the "top" vertex of the octahedron, the equatorial plane (defined relative to O(4)) is deflected slightly downward. The trans oxygen, O(2), and V, form an angle of 170° with O(4), the deviation from 180° presumably caused by the short reach of the 2MOE group. Two of the 2MOE groups are bidentate on vanadium, in contrast with the cases found in lead(II) 2-methoxyethoxide[34] and bismuth 2-methoxyethoxide,[24]

where the ligand is monodentate; bidentate 2MOE has been observed in a barium-titanium complex.[7]

The coordination environment around the bismuth atom is a distorted capped octahedron with the chlorine atoms and O(4), O(6), and O(14) as octahedral vertices. The alkoxy oxygen O(1) caps the O(4)-O(6)-O(14) face at 285 pm. This atom connects nearly at the equator (taking the bridging oxygen O(4) as the top vertex), distorting O(6)-Bi-O(14) to 114° and pinching O(6)-Bi-Cl(3) and O(14)-Bi-Cl(1) to 82° and 75°, respectively. The Bi-O(1) bond may be designated as a secondary bond.[35]

The examples of other bismuth alkoxides suggest that a stereochemically active lone pair should be sought.[24,26,27] The distortion around the bismuth center implies that such a lone pair would be directed toward the O(6)-O(14)-O(4) face. Were this the case, it would be expected that the Bi-O(1) bond would be weak; however, this bond is only slightly longer than the complex's other Bi-O bonds. The distortion in the octahedron is small, indicating no real gap in the coordination geometry; and the Bi-Cl(3) and Bi-Cl(2) bonds, which are trans to the expected location of a lone pair, are not significantly shorter than Bi-Cl(1). Thus we conclude that a stereochemically active lone pair is absent.

Combined DTA/TGA of the compound in oxygen (Figure 5.3) shows an endotherm at 144 °C with no attendant weight change, which is assigned to a separation of the complex into the original $BiCl_3$ and $VO(OC_2H_4OCH_3)_3$ parts. If this assignment is correct, the complex is surprisingly stable. Stepped exothermic weight losses up to 328 °C correspond to the removal of the $-OC_2H_4OCH_3$ groups, while the weight loss from 375-450 °C is assigned to the

dissociation of the six chlorine atoms. The final product was identified by powder XRD to be primarily $BiVO_4$ (JCPDS #14-688), with some V_2O_5 (JCPDS # 9-387) and possibly Bi_2O_3 under the amorphous background (Figure 5.4).

The complex is soluble only in donor solvents. ^{51}V NMR of the complex and parent V alkoxide both gave a single peak.[32] (Figure 5.5) In the ^{13}C and ^1H NMR spectra (Figures 5.6, 5.7), peaks corresponding to the bidentate ligands are shifted only slightly from the corresponding peaks of the parent vanadium alkoxide, while additional peaks arise from the bridging 2MOE group. This suggests that the heterometallic complex maintains its structure in DMSO solution. In alcohols (methanol, diglyme) the complex appears to break apart.

To our knowledge, $[BiCl_3(\mu\text{-}O)(\mu\text{-}OC_2H_4OCH_3)_2(OC_2H_4OCH_3)V]_2$ is the first example of a heterobimetallic alkoxide involving bismuth. The presence of chlorine in the structure could allow for further substitution by alkali metal-containing alkoxides, with the potential for increasing the number of metals present. Chemistry similar to that described in this section was used in an attempt to synthesize isolable analogs of JWP-III-76B.

Figure 5.1: ORTEP of JWP-II-76B, bismuth-vanadium alkoxide. Protons have been omitted for clarity. Selected bond distances (pm): Bi-Cl(1) 257.1, Bi-Cl(2) 251.7, Bi-Cl(3) 250.8, Bi-O(6) 259.7, Bi-O(1) 284.9, Bi-O(4) 270.3, Bi-O(14) 279.8, V-O(1) 178.9, V-O(2) 236.0, V-O(3) 180.0, V-O(4) 160.3, V-O(5) 216.8, V-O(6) 190.7, Bi-V (short side) 368.8. Selected bond angles (deg.): Cl(3)-Bi-Cl(2) 93.81, Cl(3)-Bi-Cl(1) 87.44, Cl(2)-Bi-Cl(1) 94.35, Cl(3)-Bi-O(6) 82.28, Cl(2)-Bi-O(6) 88.46, Cl(1)-Bi-O(6) 169.51, Cl(3)-Bi-O(4) 89.31, Cl(2)-Bi-O(4) 176.74, Cl(1)-Bi-O(4) 86.73, O(6)-Bi-O(4) 91.02, O(14)-Bi-O(4) 89.37, O(14)-Bi-O(6) 114.19, O(14)-Bi-Cl(1) 75.8, O(14)-Bi-Cl(2) 91.94, O(14)-Bi-Cl(3) 162.69.
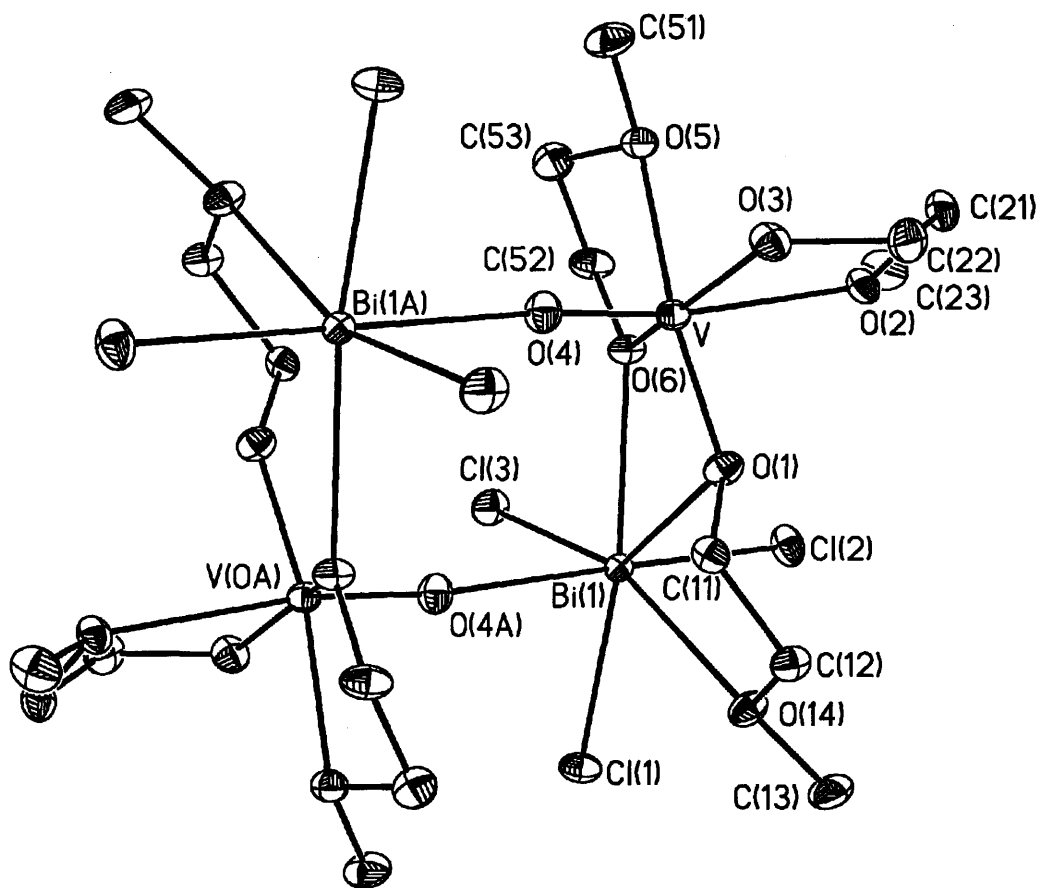
Figure 5.2: FTIR of JWP-II-76B. See text for details.
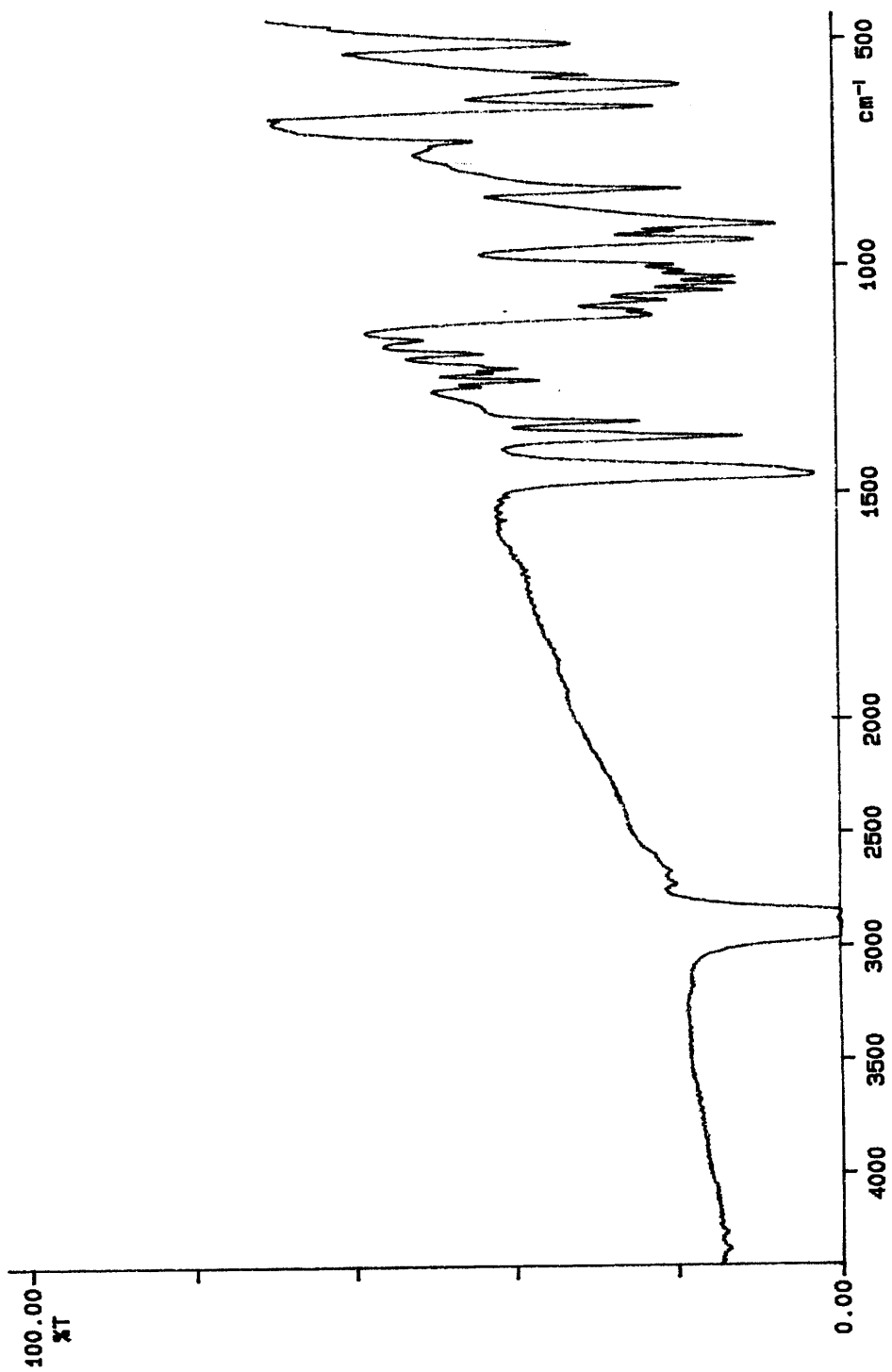
Figure 5.3: DTA/TGA of JWP-II-76B. See text for details.
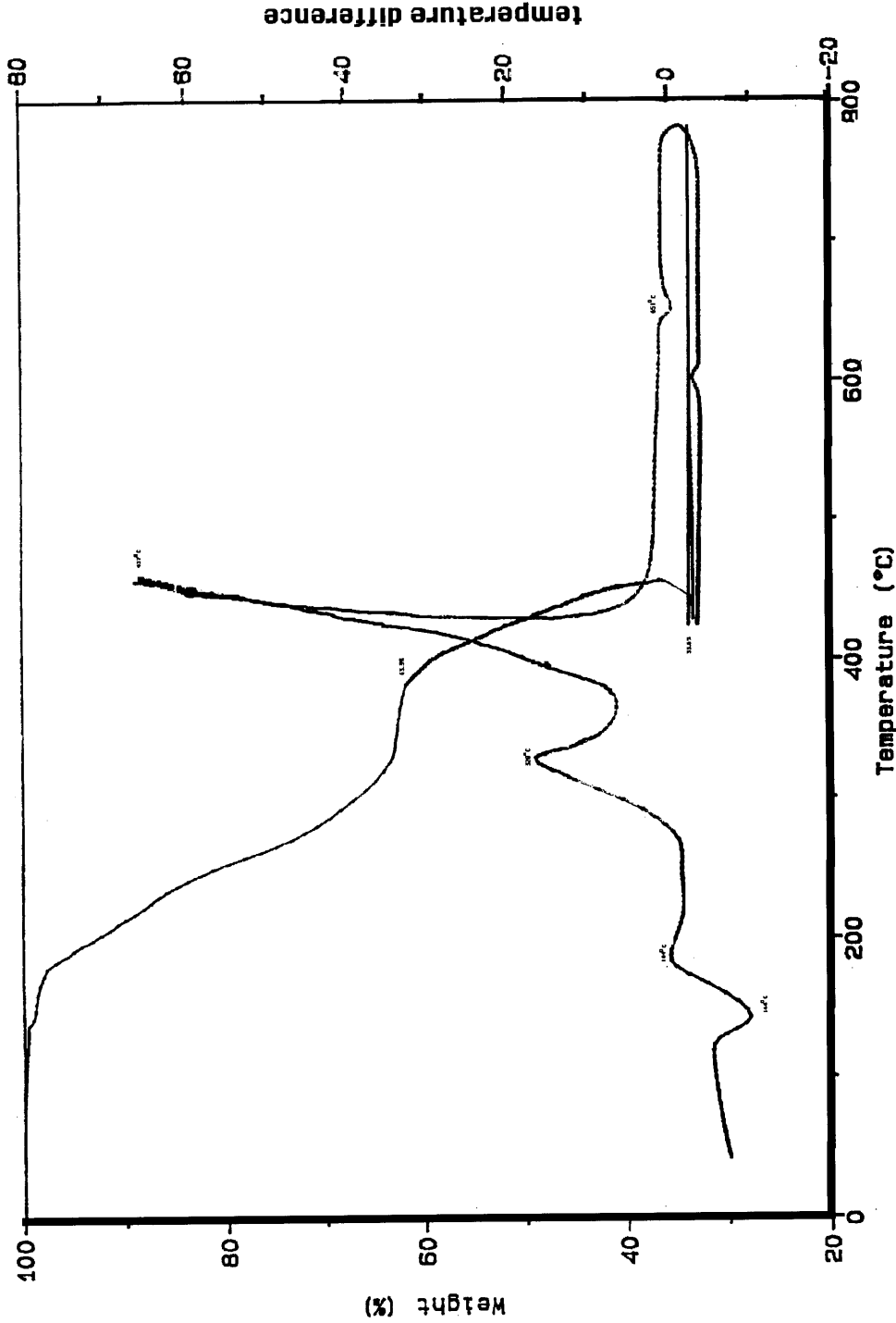
Figure 5.4: Powder XRD of pyrolysis product of JWP-II-76B.
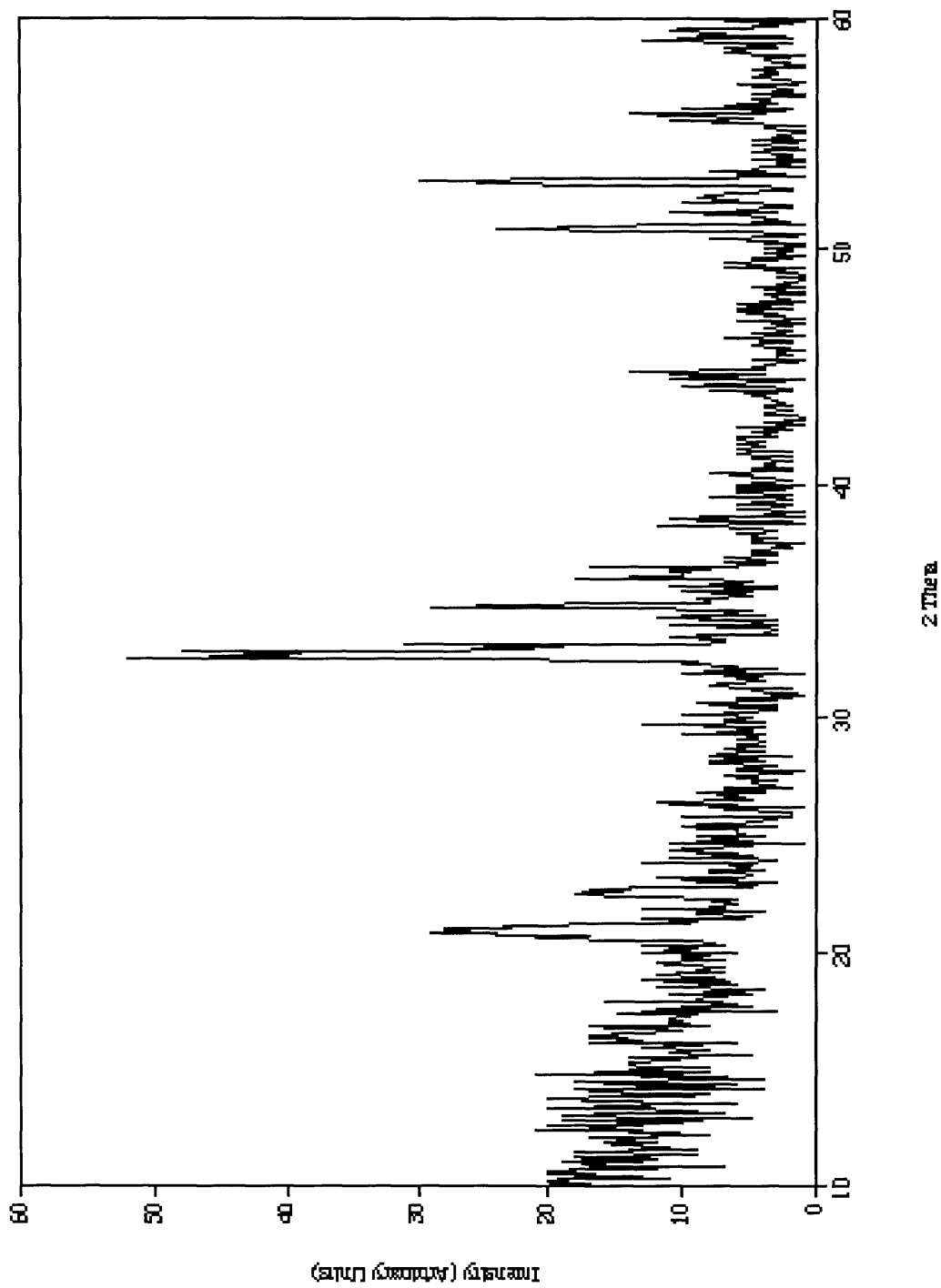
Figure 5.5: ^{51}V NMR of JWP-II-76B (d$_6$-DMSO)
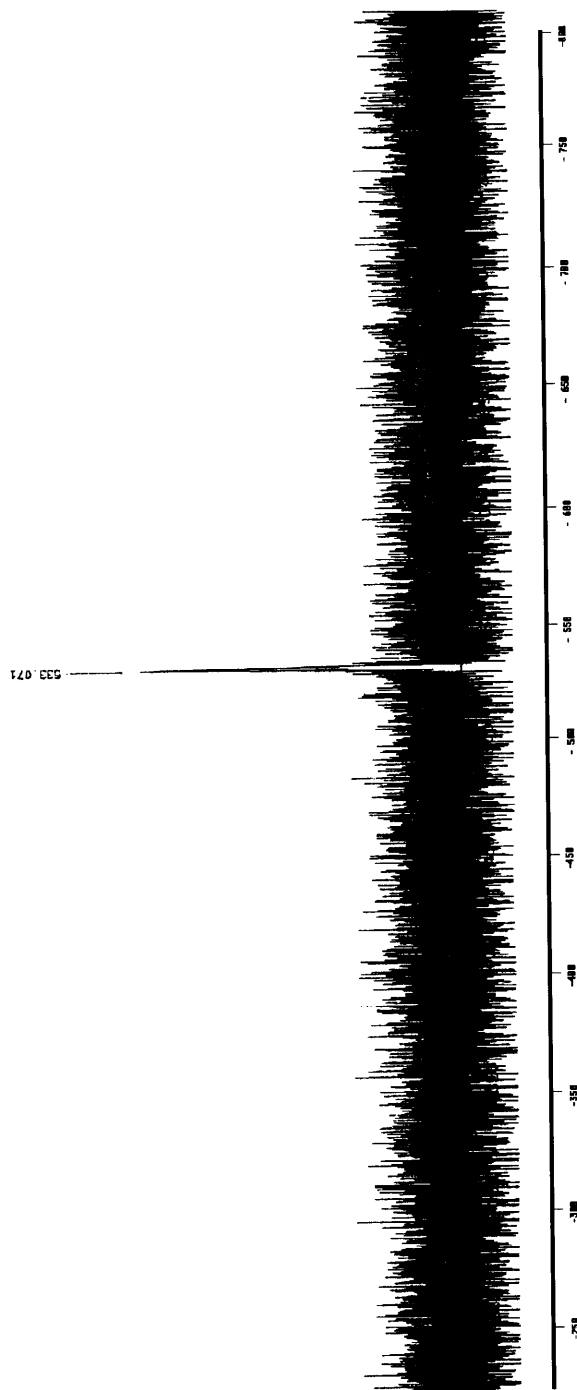
Figure 5.6: ^{13}C NMR of JWP-II-76B (d$_6$-DMSO)
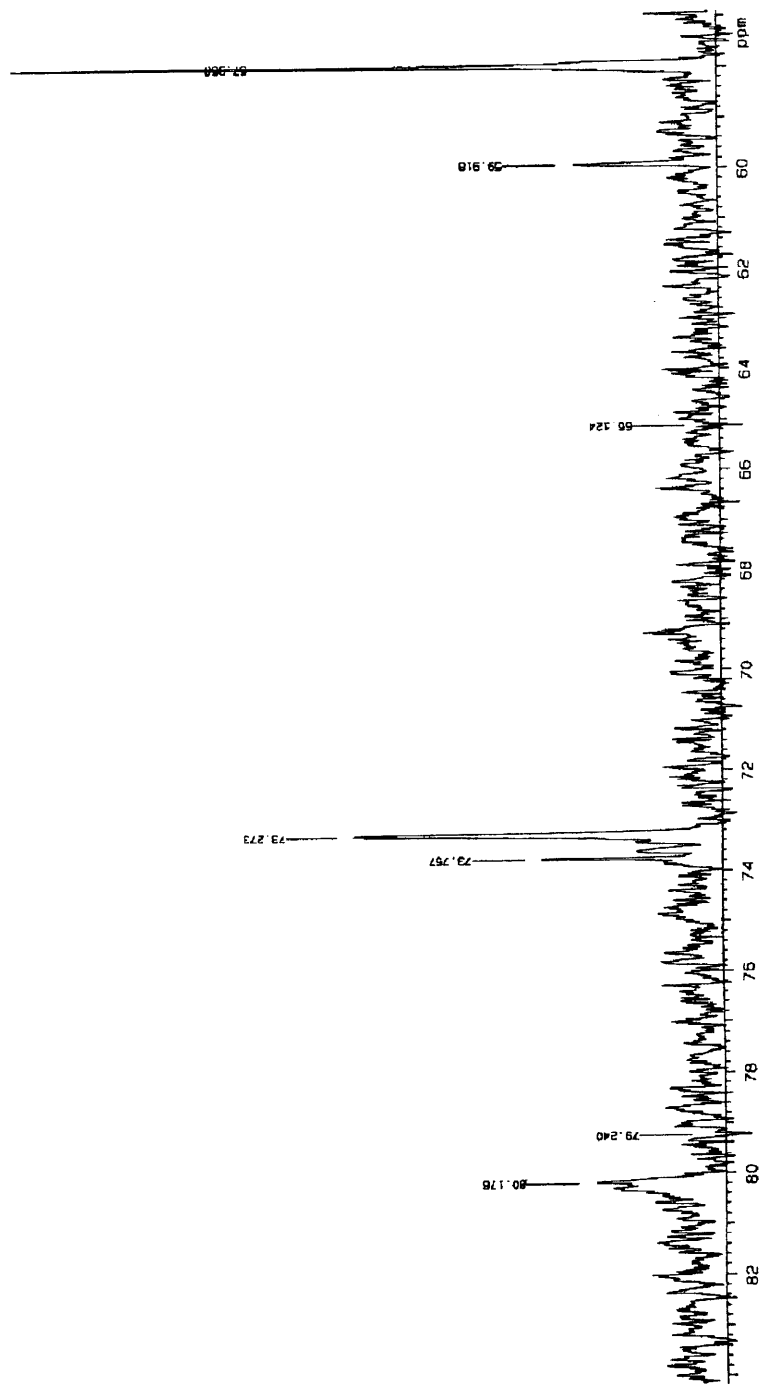
Figure 5.7: ^{1}H NMR of JWP-II-76B (d$_6$-DMSO)
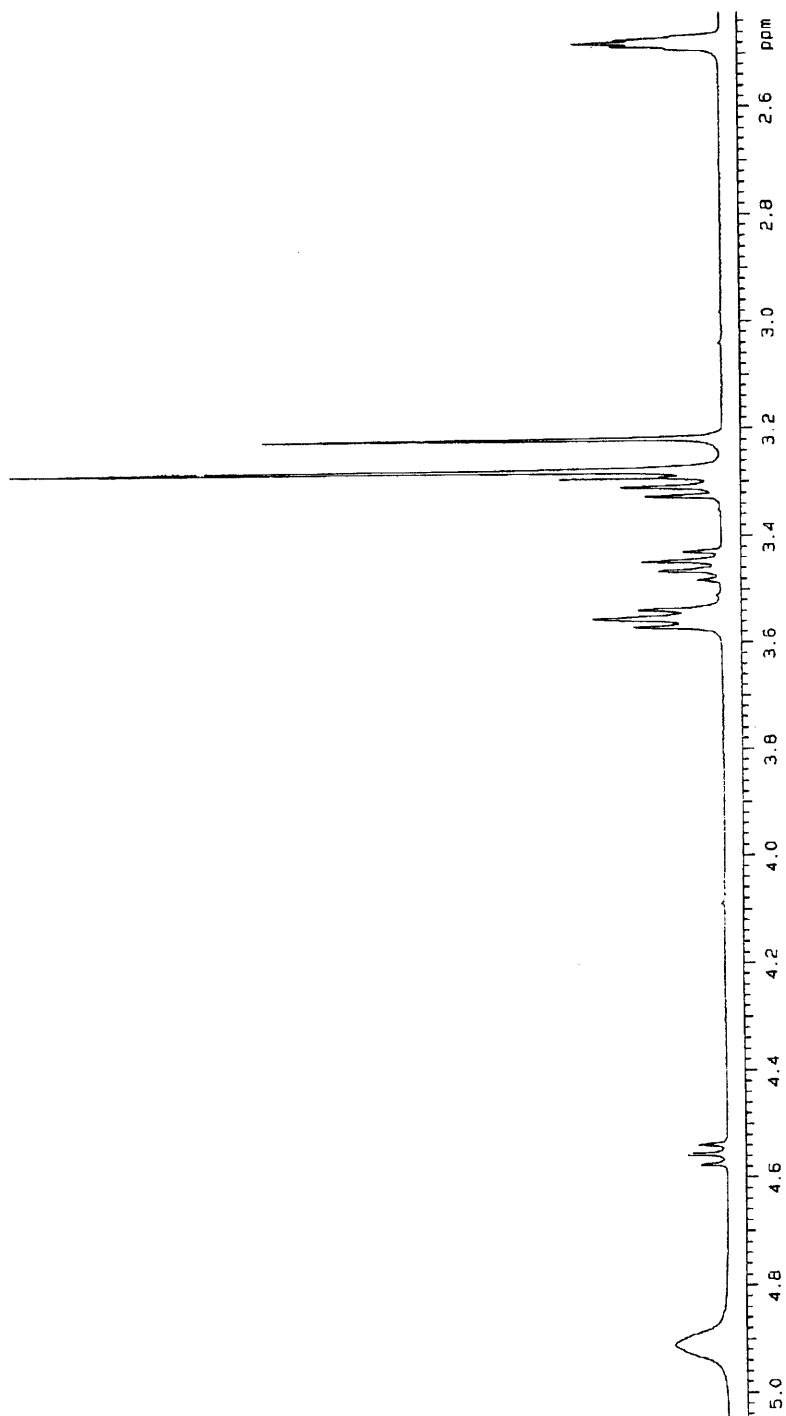
5.2.2 Experiments in Preparing Analogs of III-76B

Compound JWP-III-76A (abbreviated III-76A from here on) was synthesized by mixing V-2MOE directly with $BiCl_3$ in 2MOE solution. While III-76A was not extensively characterized, it is suspected that its structure is similar, if not identical, to that of III-76B. EDAX showed that Bi, V, and Cl were all present, although no direct elemental analysis was done on the compound. Its FTIR was identical with that of III-76B. (Compare Figures 5.2, 5.8) DTA/TGA was identical in overall shape but event locations had variations that were in some cases outside the reproducibility of the instrument (temperatures ± 2 °C). Compare Figures 5.3, 5.9. A crystal structure of III-76A was unobtainable due to the loss of solvent from the crystals during their isolation. Attempts to reproduce III-76A resulted in either oils or precipitates.

Because the precursor in the $Bi_2VO_{5.5}$ synthesis described in Chapter 4 was based on bismuth acetate, rather than the chloride, several attempts were made to isolate a Bi/V precursor (Experiments 3-11). Initial experiments centered on the literature report that the formation of a heterobimetallic alkoxide can drive precursor solubilization in polar solvents:[12] bismuth acetate and either vanadium isopropoxide or vanadium 2-methoxyethoxide were mixed in hexane solvent and stirred or refluxed (Experiments 3-5). Likewise, bismuth acetate, 2-methoxyethanol, and vanadium isopropoxide were stirred in THF solvent (Experiment 8). In these cases the persistence of the milky suspension of $Bi(OAc)_3$ in the solvent suggested no reaction had occurred; for the mixture of

Bi(OAc)$_3$ and V-2MOE in hexane without reflux, an oil formed which unfortunately could not be induced to yield crystals. It was hoped that THF would be useful in solubilizing the hoped-for product, in case hexane was too nonpolar to dissolve it after its formation. However, it is probable that the donor solvent instead blocked reaction.[12] Bismuth acetate and the vanadium alkoxides were mixed with repeated removal and replacement of 2MOE solvent, in the hopes of driving off with the evaporated solvent the acetate and isopropoxy groups. Using vanadium 2-methoxyethoxide (Experiment 6, 10, 11), this tactic gave back the reactants; on the other hand vanadium isopropoxide gave a homogenous waxy solid which, on redissolving in 2MOE, resulted in the fibrous growth associated with the alcoholysis of Bi(OAc)$_3$ rather than in crystals (Experiment 7). Since the presence of V-2MOE in solution with Bi(OAc)$_3$ had been observed to suppress the formation of the fibrous product, this result is surprising. A second attempt of the latter experiment gave a yellow oil that resulted in a precipitate after one month at -10 °C. EDX on the precipitate showed that the only metal it contained was Bi. Whatever interaction is occurring between the bismuth acetate and the vanadium 2-methoxyethoxide in solution, an intermediate did not prove isolable. Possibly partial hydrolysis of the Bi- and V- containing precursor solution would have yielded a heterobimetallic oxoalkoxide, but this experiment was not pursued.

Other attempts to synthesize analogs of III-76B were made as well. The original idea had been to take BiCl$_3$ and V-2MOE and make analogs of the III-76B complex by adding a species of the type Ë---Ë, where Ë is an element having donatable electrons. Thus

the 2MOE "analogs" used were ethanolamine ($HOCH_2CH_2NH_2$) and ethylene glycol ($HOCH_2CH_2OH$), both in diethyl ether and tetrahydrofuran solvents (Experiments 12-18). All experiments resulted in a precipitate plus yellow or orange oil (diethyl ether solvent) or a yellow-orange gum (THF solvent). $VO(OiPr)_3$ and ethanolamine gave a yellow precipitate which was possibly $VO(NHCH_2CH_2OH)_2$ (Experiment 14).[36]

It is probable that the 2MOE "analogs" used created polymeric products because both end groups were ionizable, of the type X---X,[37] while 2MOE is of the type L---X (L=neutral donor, X=ionizable donor). A donor of the type L---X, $Me_2NCH_2CH_2OH$ was tried (Experiment 19), using the N,N-dimethylethanolamine itself as the solvent. This mixture resulted in a red solution that did not yield crystals on either attempt. In hindsight, this is probably due to high solubility of any product in the N,N-dimethylethanolamine, and a different solvent should have been explored. It is also possible that the potential adduct forms a chelate-type complex with vanadium alone, as seen in the vanadium trialkanolamine complexes.[36] Bismuth alkoxides have demonstrated difficulty in terms of reproducibility where the specific product (cluster oxoalkoxide) varied with the commercial source of the reagents, the temperature, and the bismuth species' concentration at time of synthesis.[38] These factors may not have been well-controlled in the experiments described above. Most of these latter attempts at making an analogue of III-76B, due to the 1:1 metals ratio seen in III-76B, used the metals in 1:1. This may have provided too little of one or the other metal to form a stable structure. At the very least, 2:1 and 1:2 Bi:V ratios should have been tried. Also, the ligand was

consistently used in > 10-fold excess, which may have blocked potential reaction sites on the metals with a sort of "solvation." Synthesis of an analog of III-76B using $Ti(OiPr)_4$ was attempted once, but resulted in a precipitate that could not be re-dissolved and therefore was not further characterized. (Experiment 22)

As discussed in the introduction to this Chapter, one way to make heterobimetallic alkoxides is to use the alkali metal bimetallic alkoxide with the desired metal, followed by a salt metathesis (Equation 5.9). For example, the termetallic alkoxide $[\{Cd(OiPr)_3\}Ba\{Zr(OiPr)_9\}]_2$ was made by sequential salt elimination reactions (Equation 5.10a,b).

(5.9) $M_xM'(OR)_n + M''Cl_x \rightarrow M''M'(OR)_n + x\ MCl$

(5.10a) $CdI_2 + KZr_2(OiPr)_9 \rightarrow ICd\{Zr_2(OiPr)_9 + KI$

(5.10b) $ICd\{Zr_2(OiPr)_9 + KBa(OiPr)_3 \rightarrow$

$$1/2\ [\{Cd(OiPr)_3\}Ba\{Zr(OiPr)_9\}]_2$$
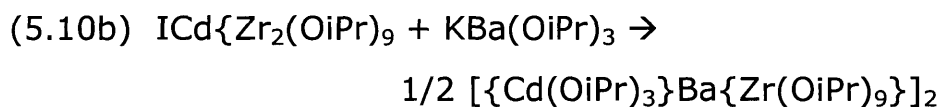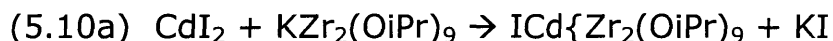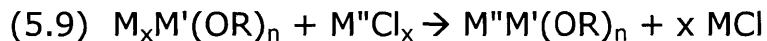
Several of the syntheses described in this Chapter were to take advantage of this. Sodium-bismuth alkoxides are known, e.g. $NaBi_3(\mu_3\text{-}O)(OR)_8(THF)$ and others.[38] One promising route, which was to give the correct stoichiometry for $Bi_2VO_{5.5}$, was based on published reactions (Equations 5.11a, b).[39]

(5.11a) $SbCl_3 + 4K + 4\ ROH \rightarrow KSb(OR)_4 + 3\ KCl$ in benzene

(5.11b) $KSb(OR)_4 + SnCl_2 \rightarrow Sn(Sb(OR)_4)_2 + 2\ KCl$ in benzene
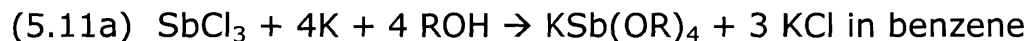
R=Me, Et, iPr, nBu, tBu, iAm

It was expected that the analogous reaction would occur with bismuth, yielding $KBi(OR)_4$; whether VX_2 could be persuaded to act as did $SnCl_2$ was more doubtful, but using VX_2 or $VOCl_3$ (even for the incorrect stoichiometry) seemed worth trying. However, as the experiments described below show, we were unable to isolate $KBi(OR)_4$ cleanly, so this route was abandoned.

Figure 5.8: FTIR of JWP-II-76A.
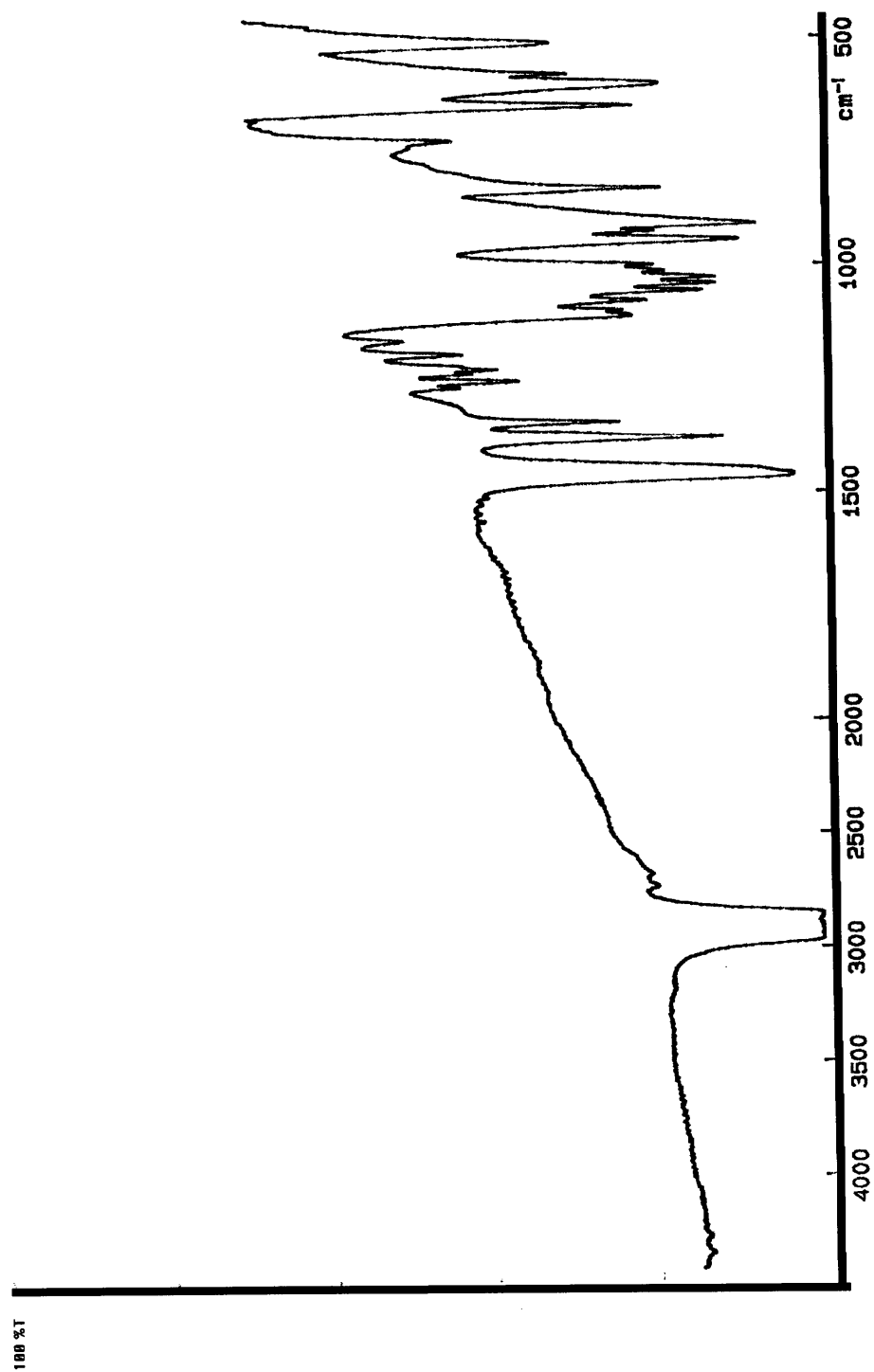
Figure 5.9: DTA/TGA of JWP-II-76A
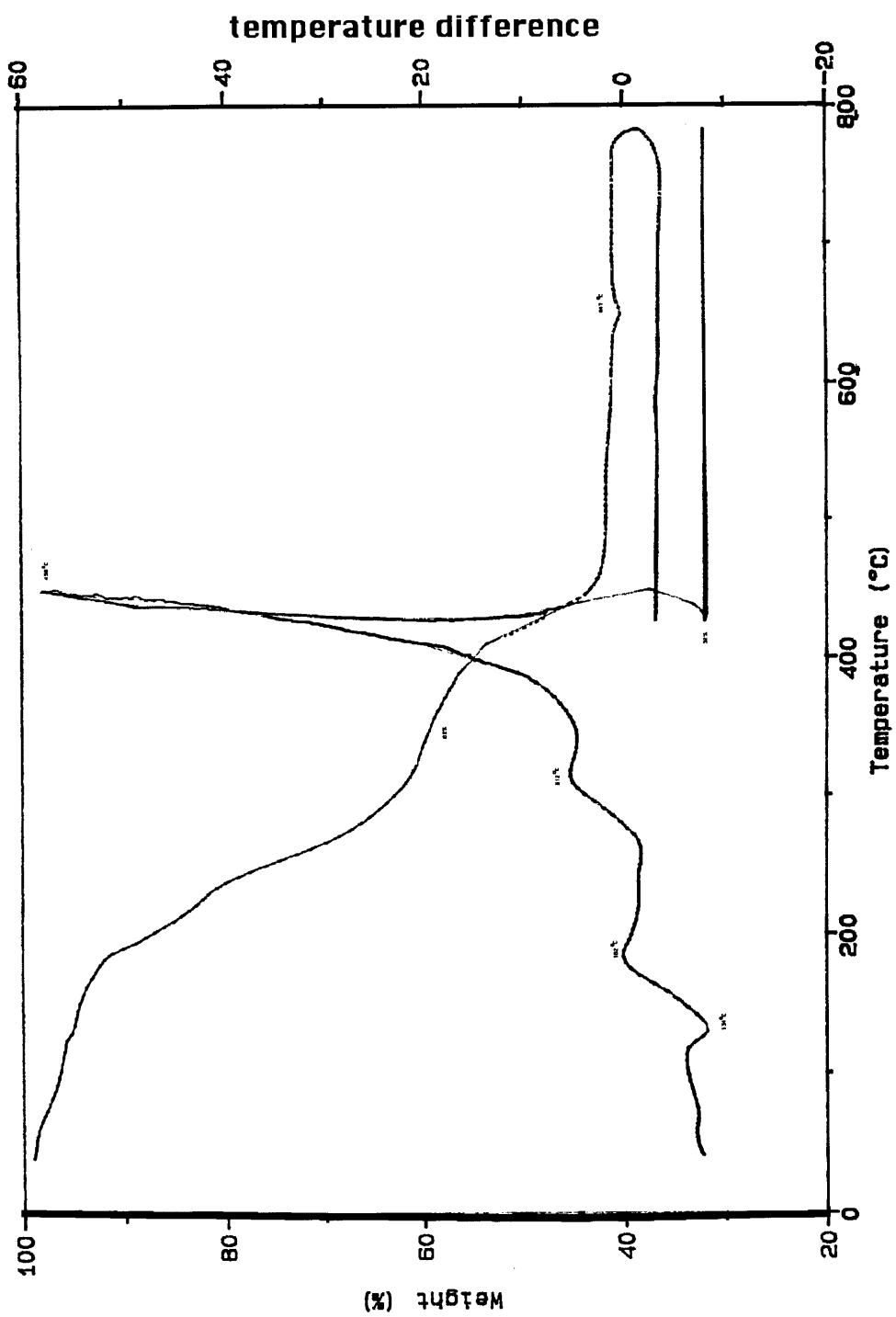
5.2.3 Precursor Characterization

The focus in precursor characterization was the exploration of the interaction between $Bi(OAc)_3$ and V-2MOE in solution. The results were somewhat confusing. UV/VIS spectra of V-2MOE alone and of a 1:2 mixture of V-2MOE and $Bi(OAc)_3$ revealed some change in the vanadium coordination sphere, as demonstrated by the 35-nm red shift of the absorption on mixing. (Figure 5.10). This shift is in the expected direction for acetate entering the vanadium coordination sphere.[32] On the other hand, ^{51}V NMR showed only a slight shift in the V-2MOE peak on addition of $Bi(OAc)_3$ (-544 ppm neat, -541 ppm in the presence of $Bi(OAc)_3$). (Repeatability $\pm$ 1 ppm; however, ^{51}V NMR is sensitive to the ionic environment,[32] and the addition of the bismuth acetate may have caused the shift in this way, rather than by actual change of the vanadium coordination sphere.)

Both standard transmission and photoaccoustic FTIR were used to characterize what changes occurred in the bonding sets of both metals. It was thought that several changes to the IR spectra could occur during the formation of a mixed Bi-V complex in solution: (1) Acetate groups on the Bi would be replaced by 2MOE groups, leaving free HOAc, which could be removed *in vacuo*, and (2) New C-O bands would appear and/or old ones would shift toward lower wavenumber (weaker bonds) due to μ1 or μ2 bridging by the 2MOE group.

288

There is some indication that some loss of acetate groups occurs in the presence of 2MOE. As expected, $Bi(OAc)_3$ (Figure 5.11) lacks the C=O stretch at 1720 cm^{-1} (location based on neat HOAc), but has bands at 1426 and 1348 cm^{-1}, the v_{as} and the v_s carbonyl peak locations expected for a carboxylate ligand. (The shift to lower-than-usual wavenumber is expected for a solid-state IR method.[40]) A solution of V-2MOE and $Bi(OAc)_3$ in 2MOE (Figure 5.12) conversely shows the free C=O peak at 1740 cm^{-1}, while the v_{as} and the v_s carbonyl peaks are overlaid on the absorptions of the 2MOE. This demonstrates at least partial alcoholysis of the acetate groups in the presence of excess 2MOE. When the solution of V-2MOE and $Bi(OAc)_3$ is placed onto a 3M Type 61 IR card and the solvent removed *in vacuo*, the C=O peak (1720 cm^{-1}) remains but is attenuated, possibly due to incomplete evaporation of the acetic acid. (Figure 5.13) This spectrum also retains the bands at 1540 and 1399 cm^{-1}, indicating the retention of acetate on the bismuth center. However, PA-FTIR of the $Bi(OAc)_3$-2MOE polymeric material and the $Bi(N(SiMe_3)_2)_3$-2MOE solid (Figure 5.14, 5.15 respectively) both show peaks in this area – e.g. they may be polymerization-broadened C-O (alcohol/ether) absorbances, so the presence of these bands in the $Bi(OAc)_3$-V-2MOE solution is not conclusive evidence of acetate-group retention. The 2MOE solvent almost certainly plays a role in breaking apart the $Bi(OAc)_3$ trimer and possibly in alcoholyzing the acetate groups from the Bi center, but it remains uncertain whether 2MOE groups bound to the vanadium also bridge to the bismuth in solution. An acetate-based analog of the bonding situation seen in III-76B is possible, however, if the positions taken by the bridging acetate groups in II-77A (Figure

5.16) are occupied instead by 2MOE groups. (Figure 5.17) Weak back-interactions from Bi-based acetate groups, or entry of liberated acetic acid into the vanadium coordination sphere, may explain the ^{51}V and UV-VIS spectra.

In an attempt to determine whether the bismuth acetate remained in solution in the gel interstices, or bonded in some way to the hydrolyzed vanadium alkoxide structure of the gel, two 2:1 Bi(OAc)$_3$: V-2MOE samples in 2MOE were hydrolyzed with excess water and permitted to gel (experiment 23). In one sample, only the syneresis fluid was removed, without breaking up the gel, and the residue from it was found to be negligible. In the other case, the gel was mechanically broken up to free trapped fluid. Again, the residue from the fluid after evaporation was found to be negligible. Thus the bismuth acetate appears not to remain as a trapped solute, but to participate chemically in the gel structure. The remnant of the gel pyrolyzed to give BiVO$_4$ and Bi$_2$VO$_{5.5}$, indicating that the bismuth was still located in the gel.

Figure 5.10: UV-VIS of V-2MOE solution with and without added Bi(OAc)₃ solution.
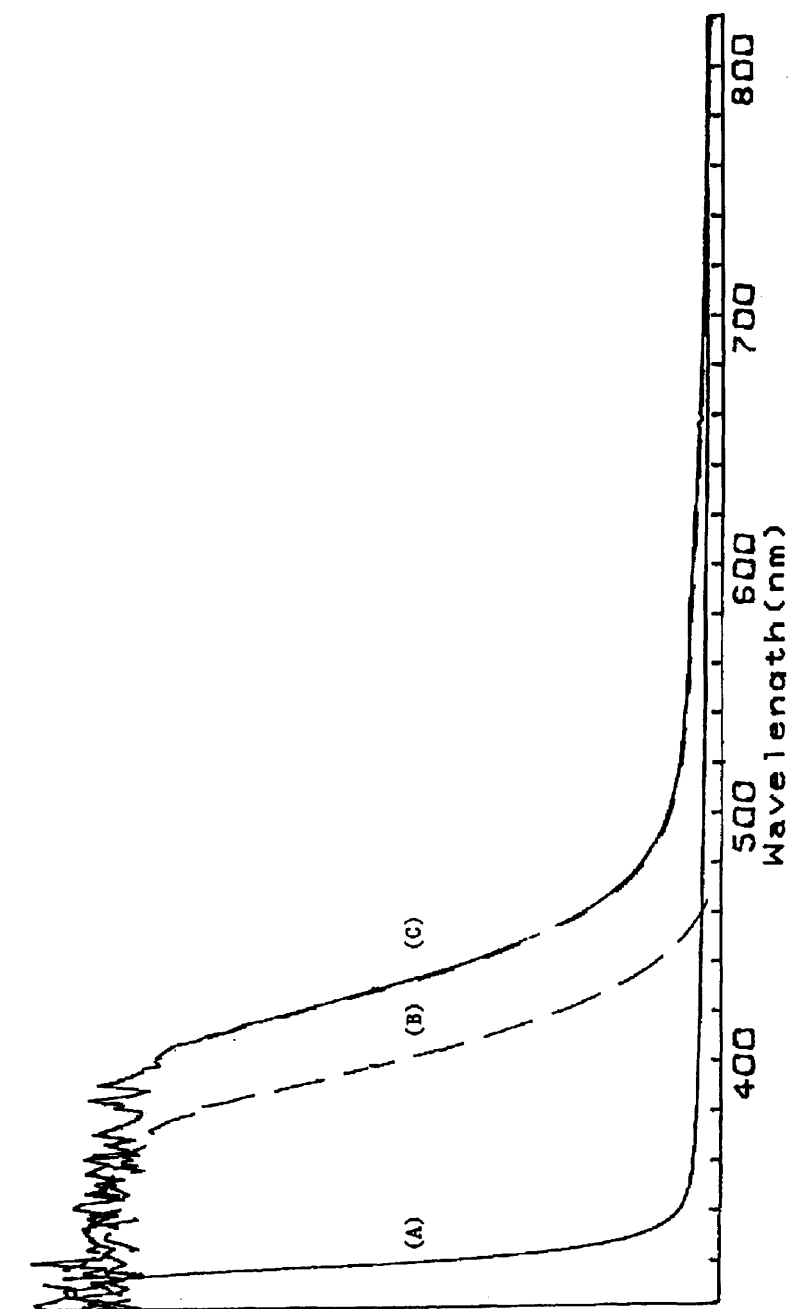
Figure 5.11: Photoaccoustic FTIR of JWP-II-77A, bismuth acetate.
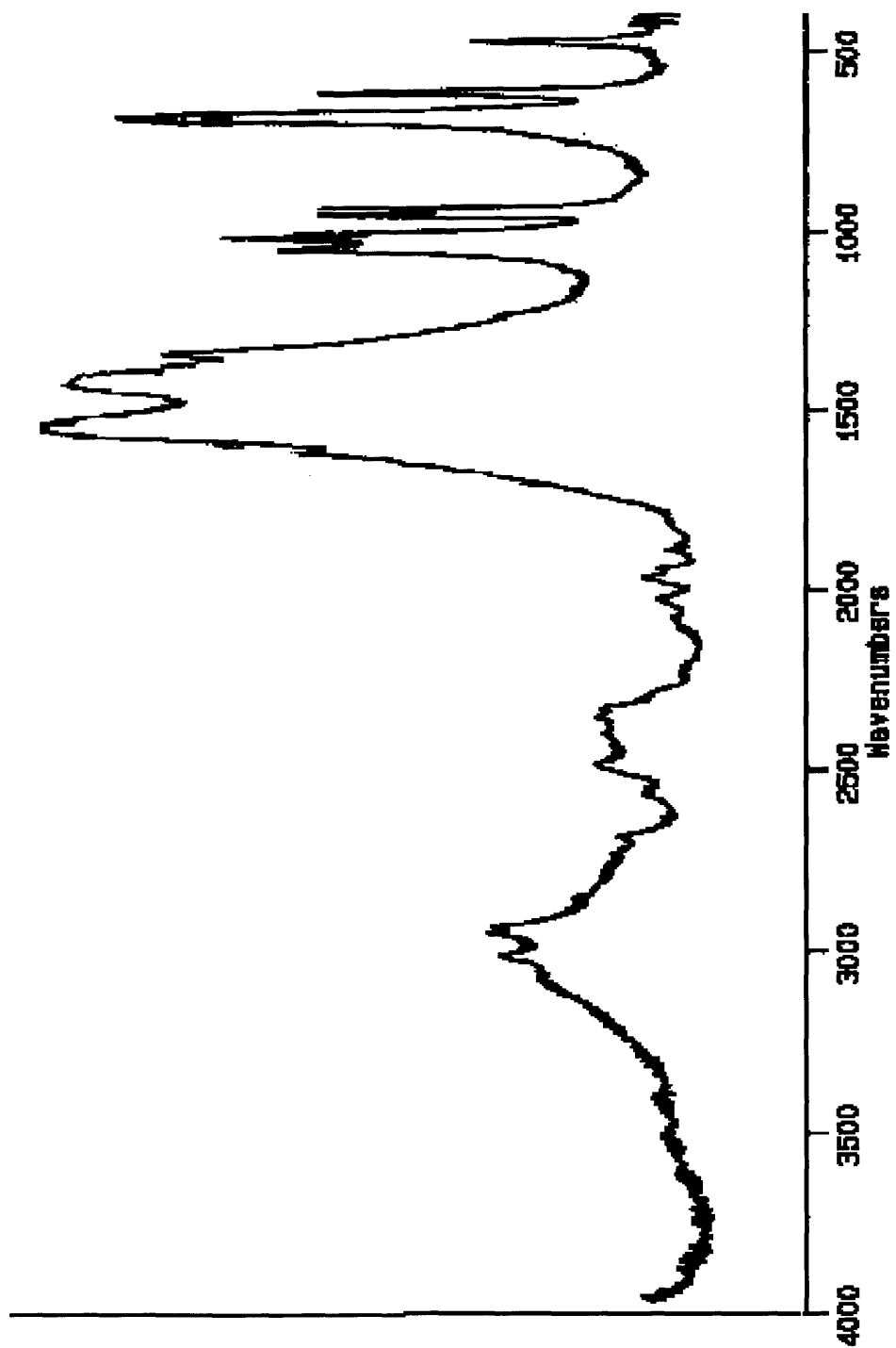
Figure 5.12: FTIR of V-2MOE/Bi(OAc)₃ mixed solution in 2MOE.
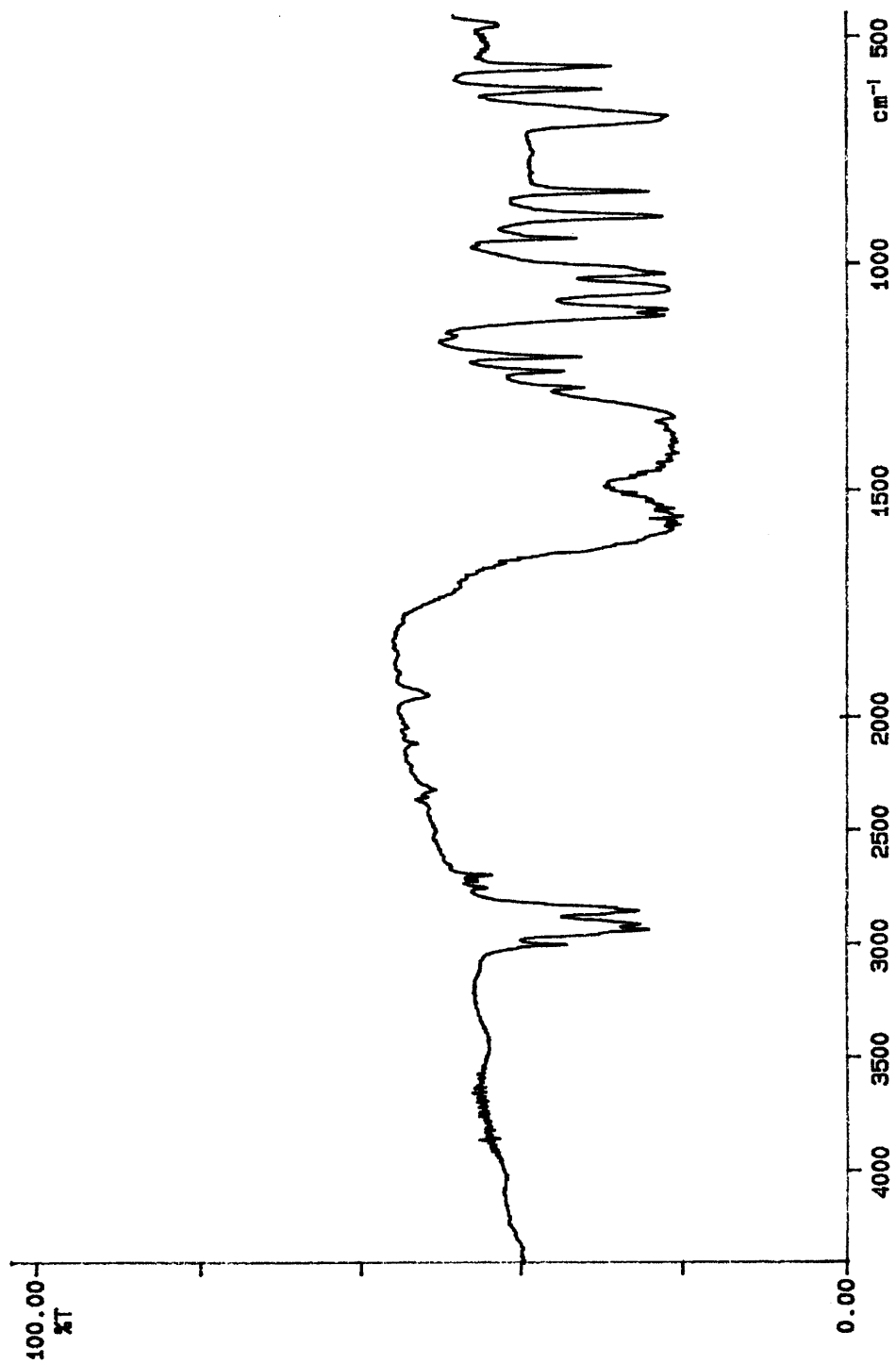
Figure 5.13: FTIR on V-2MOE/Bi(OAc)$_3$ mixed solution in 2MOE, after vacuum removal of solvent.
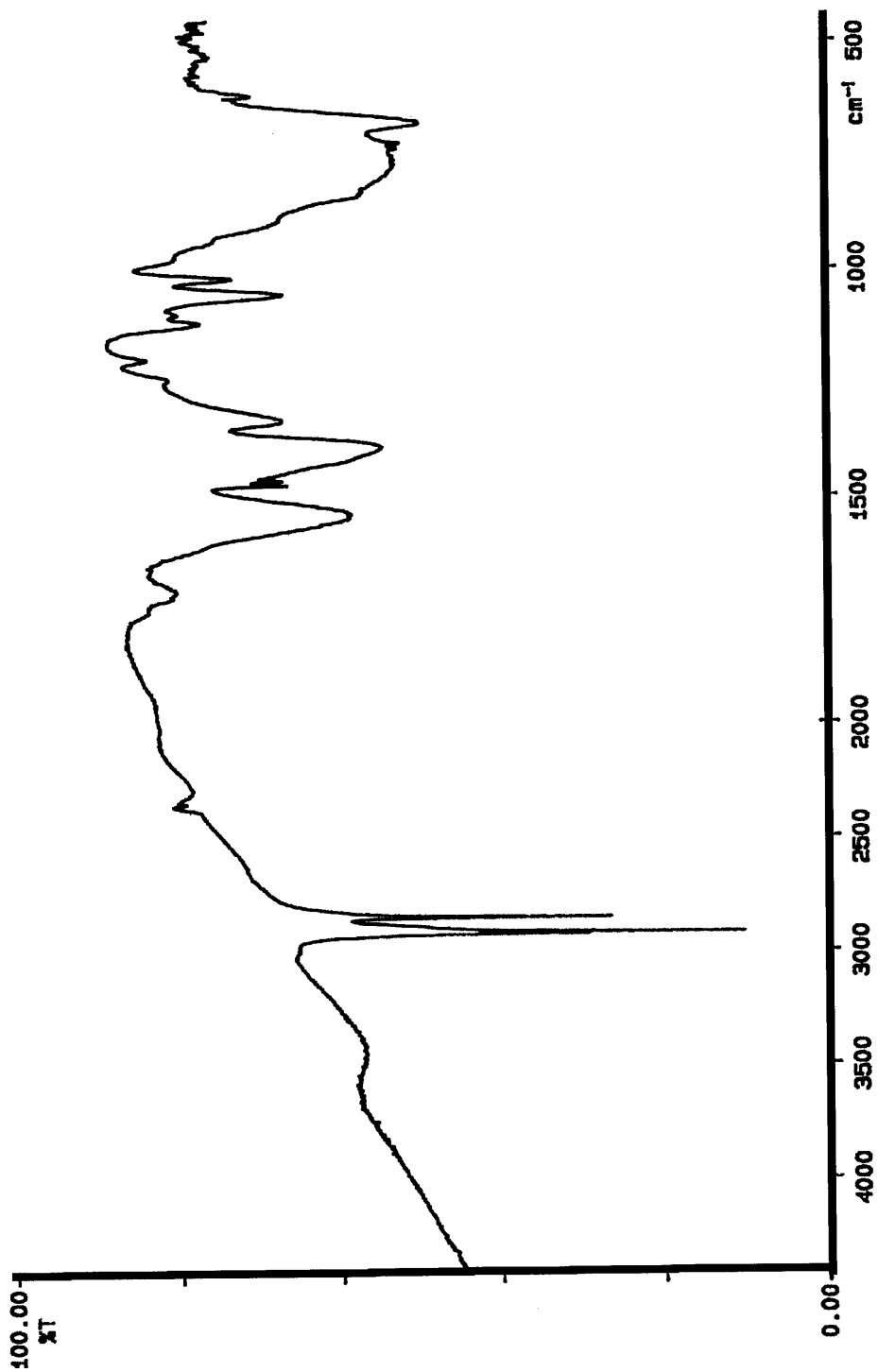
Figure 5.14: Photoaccoustic FTIR on JWP-121C, bismuth acetate/2MOE polymer.
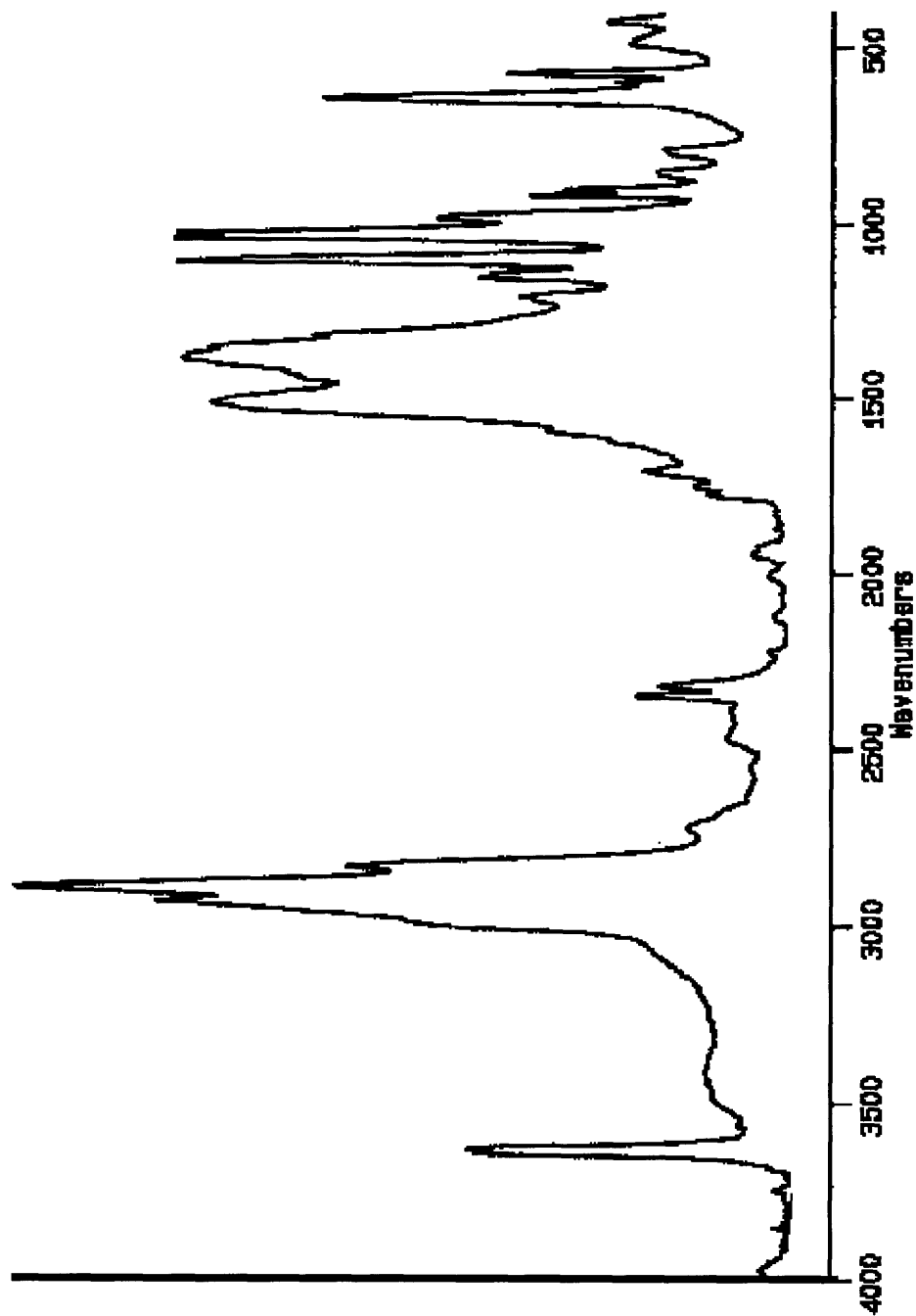
Figure 5.15: Photoaccoustic FTIR on JWP-II-24A, solid formed by alcoholyzing Bi(N(SiMe$_3$)$_2$)$_3$ with 2MOE.
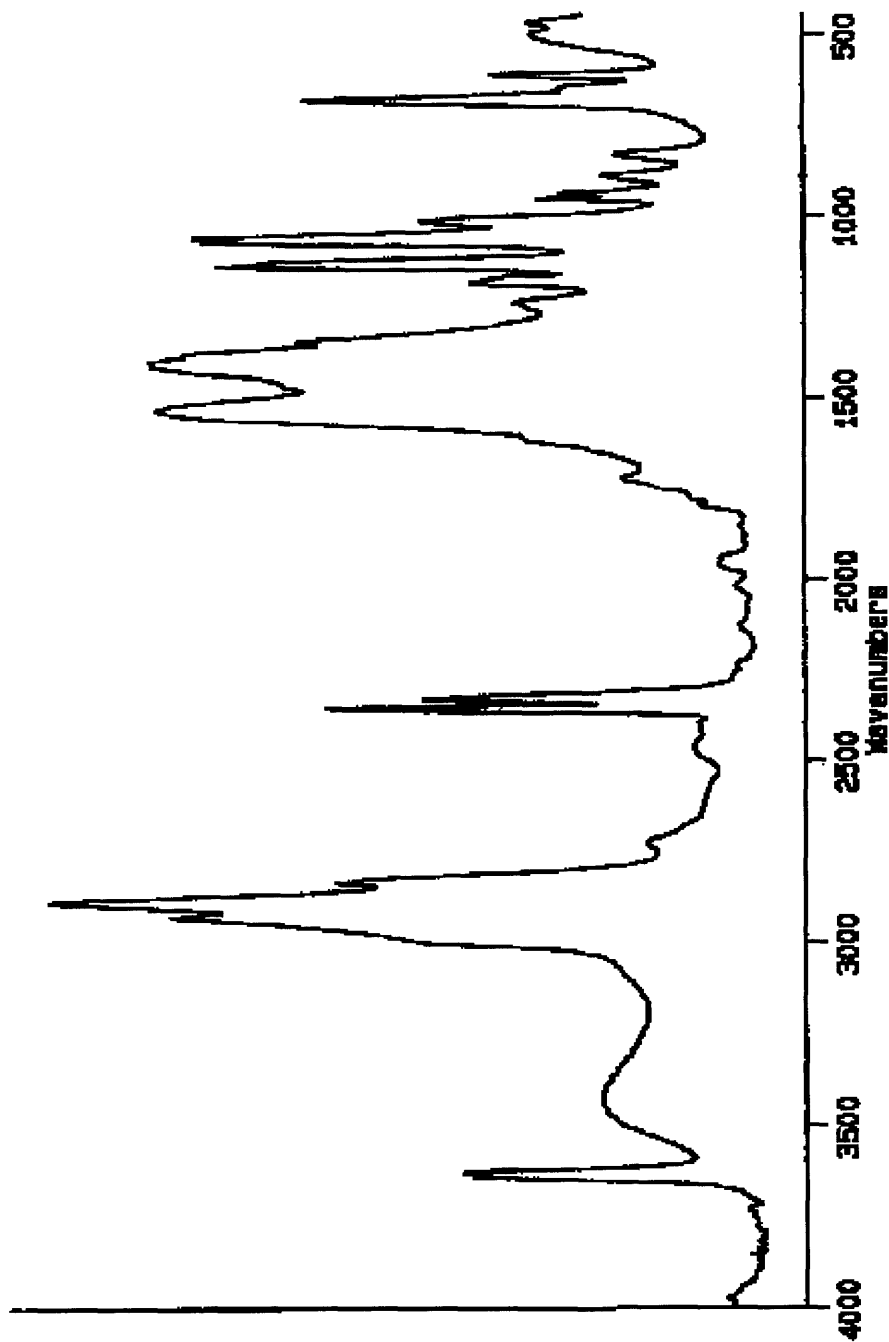
Figure 5.16: ORTEP of JWP-II-77A, bismuth acetate (see text).
Selected bond lengths (pm) and angles: Bi(3)-O(1) 254, Bi(3)-O(2) 230, Bi(3)–O(3) 267, Bi(3)-O(4) 240, Bi(3)-O(5) 252, Bi(3)-O(6) 224, Bi(3)-O(2B) 294, Bi(3)-O(4B) 283, Bi(3)-O(3A) 280; O(1)-Bi(3)-O(3) 152.5°, O(1)-Bi(3)-O(4) 117°, O(1)-Bi(3)-O(5) 80°, O(1)-Bi(3)-O(6) 74°, O(4)-Bi(3)-O(6) 80°, O(3)-Bi(3)-O(6) 79°, O(3)-Bi(3)-O(4) 50.5°, O(5)-Bi(3)-O(6) 53°, O(1)-Bi(3)-O(2) 53.4°
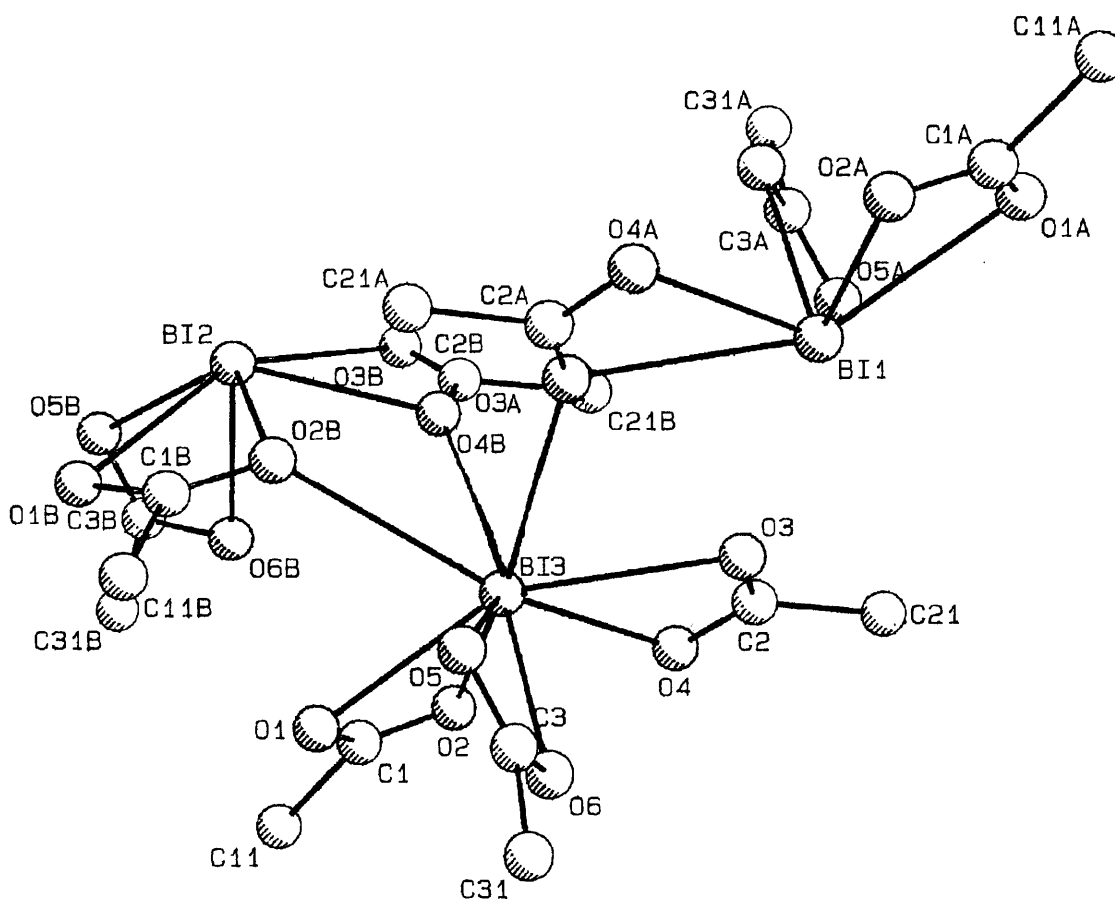
Figure 5.17: Sketch of potential Bi-V dimer in solution, showing how 2MOE bridging on the basic bismuth acetate core can occur. Compare with Figure 5.16.
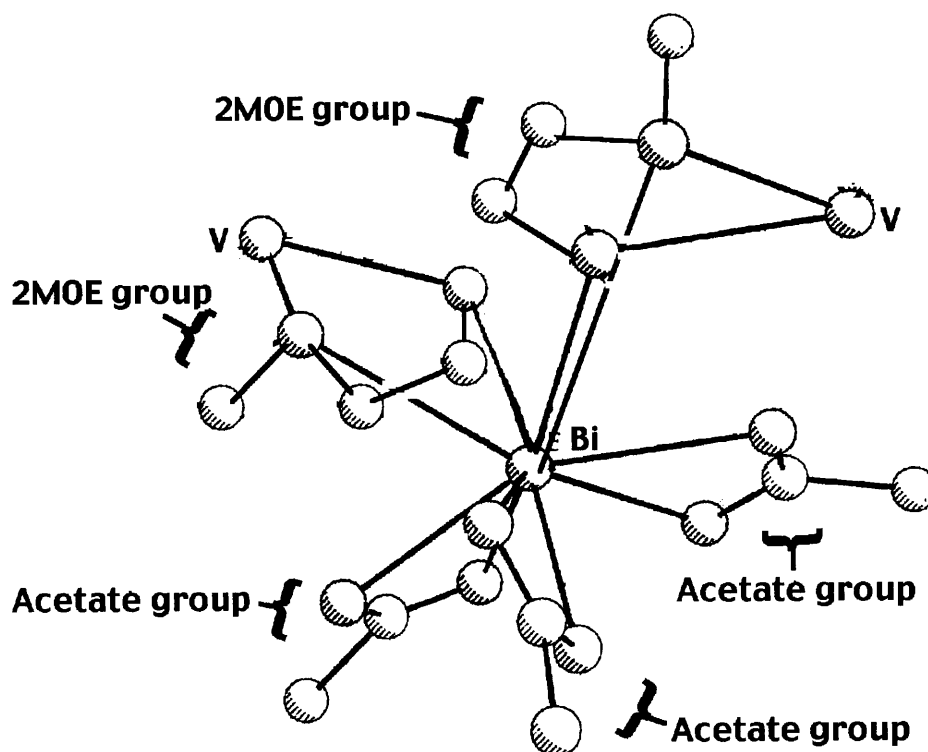
5.3 Conclusions

Overall, the isolation of one example of a μ-O Bi-V complex, synthesized starting with bismuth chloride and vanadium alkoxide, is an interesting result but one which cannot necessarily be extended to count as evidence of the formation of a single precursor complex in the bismuth acetate-vanadium alkoxide solutions used in the sol-gel synthesis of the BiMeVOx materials. The types of bridging that the 2MOE group on vanadium can perform with bismuth, however, provide a potential for interaction between the vanadium alkoxide and the bismuth acetate, and one can speculate that the sorts of inter-bismuth bridging done by the acetate groups in the bismuth acetate structure (see Figure 5.16) could potentially also be done by 2MOE groups on bismuth, with complete retention of the acetate groups. Conversely, the acetate groups on Bi(OAc)$_3$ can be lost through alcoholysis by 2MOE in forming the fibrous polymeric material. (Figure 5.14) Such substitution of 2MOE groups for acetato ligands demonstrates a second process by which 2MOE groups on the vanadium could create bridged Bi-V complexes. The suppression of the formation of the fibrous material in the presence of V-2MOE suggests of interaction between the vanadium alkoxide and bismuth compound in solution – "alcoholysis" or bonding by the 2MOE groups on V-2MOE may act to block polymer formation by free 2MOE and Bi(OAc)$_3$.[12] The shift in the visible absorption spectrum of the vanadium alkoxide in the presence of the bismuth precursor also suggests interaction between the two species in solution, though

the shift of the ^{51}V NMR peak by 3 ppm is not strong evidence of changes taking place in the vanadium coordination sphere. The UV-VIS spectral shift, is thus not adequately explained. Until a Bi-V precursor complex is obtained from the preparation actually used in the sol-gel depositions, the existence of a single Bi-V precursor complex in solution prior to hydrolysis remains speculative. In the hydrolyzed precursor solution, the bismuth appears to become bonded to the poly(vanadium oxide) gel structure, rather than remaining as a trapped solute.

A number of the experiments in this Chapter may be worth repeating under more favorable synthesis conditions and with more attention to indirect (e.g. spectroscopic) methods of characterizing what is taking place in solution, rather than relying on crystallization to provide a characterizable material. It is likely, also, that attempts to crystallize out a Bi-V complex from solutions containing vanadium alkoxide and bismuth dimethylsilamide would be fruitful.

5.4 Experimental Section

All experimental work was done in an argon-filled glove box or on an nitrogen-equipped Schlenk line. Solvents were used pre-dried by the manufacturer without further preparation.

See the Appendix to Part I of this thesis for a list of materials and instruments used in this chapter.

Experiment 1 (JWP/III/76A) V-2MOE + BiCl₃

In the glovebox V-2MOE (6.4035 g, 3.2 mmol) was mixed with 4 ml 2MOE. To this was added $BiCl_3$ (2.1047 g 6.7 mmol) and 10 ml

more 2MOE. All solids were dissolved after a brief stirring at room temperature, producing a yellow liquid. This was removed from the glove box and warmed *in vacuo* to remove the solvent. A brown oil remained. Anhydrous pentane (0.5 ml) was added and stirred with the oil, then removed by evaporation to again leave an oil. Five ml of 2MOE was added to form a yellow-brown solution, which was placed in a sealed flask at 4 °C under N_2. After four days tiny orange crystals and some white crystals had formed. After another week at 4 °C the mother liquor was removed by syringe and the orange crystals rinsed with a small quantity of cold 2MOE, then dried under vacuum. The mother liquor was concentrated and left at 4 °C for several days under N_2 with no further crystallization. The main set of crystals were orange but blackened on exposure to air. The crystals were checked for elemental content by EDAX using a backscatter detector and 15 keV exciting energy and found to contain Bi, V, and Cl. FTIR (Figure 5.8) (nujol, cm^{-1}) showed bands at 2948 s, 2364 w, 1462 s, 1377 s, 1232 m, 1197 m, 1102 m, 1084 m, 1038 m, 1010 m, 996 m, 946 m, 902 m, 827 m, 774 w, 722 s, 631 w, 560 m. None of the crystals were suitable for single-crystal XRD due to loss of solvent from them. DTA/TGA on the solid showed endotherms at 134 and 647 °C and exotherms accompanied by weight losses of 9.75%, 38%, and 68% at 182, 312, and 450 °C, respectively. (Figure 5.9) Yield (0.16g) 17% assuming identical formula to III-76B below. Elemental analysis and NMR were not performed.

Attempts to repeat the experiment in diethyl ether solvent (JWP/III/83A) resulted in a yellow-brown oil that separated from the

solvent. Isolation of this oil and refrigeration at 4 °C did not result in crystals.

Experiment 2 (JWP/III/76B) VO(OiPr)$_3$ + BiCl$_3$ in 2MOE

In the glovebox VO(OiPr)$_3$ (0.80g, 3.26 mmol) was added to BiCl$_3$ (2.0485 g, 6.5 mmol) and 10 ml 2MOE. The resulting yellow solution was stirred briefly at room temperature then removed from the glove box in a sealed flask and the solvent removed with warming *in vacuo* to leave an orange oily precipitate. This was redissolved with some warming in 5 ml 2MOE and left overnight at room temperature, then left at 4 °C for several days under N$_2$. After four days, orange crystals had appeared. These were collected one week later by removal of the mother liquor by syringe and rinsing in a small amount of cold 2MOE. The crystals were dried *in vacuo*; the mother liquor was concentrated and left again at 4 °C, but no further crystallization occurred. Yield: 35% (based on bismuth) air-sensitive orange crystals. The crystals were stable at room temperature under argon.

The crystals were checked for elemental content by EDAX using a backscatter detector and 15 keV exciting energy and found to contain Bi, V, and Cl. Analysis (Galbraith Laboratories, by ICP-EAS) found: C 17.38, H 3.36, Cl 15.67, Bi 35.03, V 8.11; expected: C 17.8, H 3.5, Cl 17.5, Bi 34.4, V 8.4.

Single crystal XRD indicated a dimeric complex of the formula [BiCl$_3$(μ-O)(μ-OC$_2$H$_4$OCH$_3$)$_2$(OC$_2$H$_4$OCH$_3$)V]$_2$ (C$_9$H$_{21}$BiCl$_3$O$_7$V, M=607.53). The crystal was monoclinic P2$_1$/n, a=10.7405(8) Å, b=14.9328(1) Å, c=11.2839(8) Å, β=97.2330(10)°. V=1795.4(2) Å^3

at T=188(2) K. $Z=4$, $D_c=2.248$ g/cm3, $\lambda=0.71073$ Å (Mo K$_\alpha$). Of the 7070 reflections collected, 2567 were independent with $I>2\sigma(I)$, yielding $R_1=0.0258$, $wR_2=0.0508$. See Figure 5.1 for ORTEP and representative bond lengths and angles.

FTIR was run in KBr and Nujol, with the following peaks: (cm^{-1}) 2930 s, 1447 m, 1341 m, 1250, 1224, 1192 broad, m, 1050 m, 944, 911, 830, 647, 600 576 507 m/w. (Figure 5.2). NMR data: ^{51}V (δ, ppm; 300 MHz, DMSO-d$_6$, VOCl$_3$=0 ppm) -553.1 (s); ^{1}H (δ, ppm, 300 mHz, DMSO-d$_6$) 3.24 (S, 3H), 3.30 (s, 6H), 3.33 (t, 3j-5.2 Hz, 2H), 3.49 (q, ^{4}J=5.2 Hz, 2H), 3.57 (t, ^{3}J=4.8 Hz, 6H), 4.58 (t, ^{3}J=5.2 Hz, 1H), 4.92-4.95 (broad, 4H); ^{13}C (δ, ppm, 300 MHz, DMSO-d$_6$) 57.95, 73.25, 80.36, 86.18, 92.09, 102.21 (high background noise). (Figures 5.5-5.7) It should be noted that the DMSO solvent was used as-received and turned out to be contaminated with a small quantity of water, which we believe protonated O(3). This gives rise to the extra splitting in the 3.49 ppm peak (to a quartet) and in the 4.58 ppm peak in the proton spectrum. See Figure 5.3 for DTA/TGA on the solid, which showed an endotherm at 144 °C with no attendant weight change, stepped exothermic weight losses up to 328 °C, and a major weight loss from 375-450 °C. The product of the thermal analysis was identified by powder XRD to be primarily BiVO$_4$ (JCPDS #14-688). (Figure 5.4)

Attempts at repeating the experiment in diethyl ether solvent (JWP/III/83B) resulted in an instant white precipitate which was not characterized further. The experiment described here was reproduced (JWP/III/107A) to give a 33.8% yield of orange crystals. These were verified by NMR and IR for authenticity.

Experiment 3 (JWP/III/78A) Bi(OAc)₃ + V-2MOE in hexane

To a suspension of Bi(OAc)$_3$ (2.0071 g, 5.2 mmol) in 15 ml of hexane was added V-2MOE solution (5.23 g, 2.6 mmol) in 2MOE. This was stirred for 5 hours at room temperature then heated 1 hour to leave a yellow-green solution and some white solid. This was permitted to cool to room temperature and filtered, and the concentrated filtrate refrigerated at 4 °C for one month. A brown oil separated out of the yellow mother liquor. No further characterization was performed.

Experiment 4 (JWP/III/79A) Bi(OAc)₃ + VO(OiPr)₃ in hexane with reflux

To a suspension of Bi(OAc)$_3$ (2.0159 g, 5.22 mmol) in 15 ml of hexane was added of VO(OiPr)$_3$ (0.65 g, 2.65 mmol). This was stirred at room temperature for 5 hours to form a milky suspension, which was refluxed for one hour. The suspension was permitted to cool to room temperature and settle. This was filtered and added to the filtrate from /79B (Experiment 5).

Experiment 5 (JWP/III/79B) Bi(OAc)₃ + VO(OiPr)₃ in hexane

To Bi(OAc)$_3$ (2.0185 g, 5.22 mmol) was added VO(OiPr)$_3$ (0.65 g, 2.65 mmol) and 15 ml hexane. This was stirred at room temperature for 5 hours to produce a milky suspension, which was warmed to give a yellow solution and a white solid. This was cooled to room temperature and filtered, and the filtrate from /79A (Expt.

4) added to it. This was refrigerated at 4 °C for two days, then the solvent volume reduced *in vacuo*. Yellow deposits were noted in the trap, indicating sublimation of a vanadium compound. The concentrated solution was again cooled to 4 °C for one month. No crystals appeared.

Experiment 6 (JWP/III/84A) Bi(OAc)₃ + V-2MOE

In the glove box Bi(OAc)$_3$ (2.0120g, 5.22 mmol) was added to V-2MOE solution (5.2249 g, 2.5 mmol), and 20 ml 2MOE added. This was warmed with stirring to dissolve, then permitted to cool overnight to room temperature, and refrigerated for two days at 4 °C. The solvent was removed *in vacuo* with warming on a water bath, resulting in a white-yellow solid in a yellow-brown oil. To this was added 60 ml hexane and the resulting mix refluxed and hot filtered. White powder appeared in the filtrate as it cooled. The solid on the filter was pyrolyzed in air at 800 °C for 2 h. Powder XRD of this material could not be matched to any Bi- and/or V-containing phase in the JCPDS database (Figure 5.18).

Experiment 7 (JWP/III/91A) Bi(OAc)₃ + VO(OiPr)₃ in 2MOE

Bi(OAc)$_3$ (0.5038 g, 1.3 mmol) and VO(OiPr)$_3$ (0.2947g, 1.20 mmol) were dissolved in 20 ml 2MOE. The solution was warmed at 45 °C for 2 h and the solvent removed *in vacuo* to give an inhomogenous white-yellow solid. 20 ml of 2MOE were again added to redissolve the solid, and the mixture was heated at 55 °C overnight. The solvent was removed *in vacuo* to yield a

homogenous yellow semisolid. This was again dissolved in 15 ml 2MOE with warming and left at room temperature overnight. Some precipitate appeared in the flask bottom. The solution was refrigerated (4 °C) two days. A yellow fibrous solid appeared which occupied the entire solvent volume. After four days more at 4 °C, the solvent was removed *in vacuo*. FTIR (Figure 5.19) in nujol gave bands at (cm^{-1}, approx.) 3500 vw, 3000-2850 m, 1949 w, 1574 s, br, 1416-1335 s, br, 1271 w, 1235 w, 1203 w, 1113 m, 1099 m, 1056 m, 1020 m, 942 w, 895 m, 840 m, 673 m, 614 w, 564 w. The experiment was repeated on JWP/III/91C. This product gave an identical IR.

Experiment 8 (JWP/III/92A) Bi(OAc)$_3$ + VO(OiPr)$_3$ in THF

Bi(OAc)$_3$ (0.25 g, 0.65 mmol) was added to 50 ml THF containing VO(OiPr)$_3$ (0.39 g ,1.59 mmol) and 0.5 ml (6.6 mmol) 2MOE. The resulting mixture was opalescent yellow. This was warmed with stirring for one week and the maize-yellow suspension permitted to settle, leaving a white solid and yellow solution. Because no reactions appeared to have occurred, no further characterization was done.

Experiment 9 (JWP/III/109A) Bi(OAc)$_3$ + VO(OiPr)$_3$ in 2MOE

Bi(OAc)$_3$ (0.7053 g, 1.83 mmol) and VO(OiPr)$_3$ (0.3681 g, 1.50 mmol) were added to 20 ml 2MOE. These were dissolved with warming then permitted to stand overnight. The solvent was removed *in vacuo* and 2MOE re-added to redissolve the material.

The volume was reduced *in vacuo* and the sample let stand at room temperature overnight. This was reduced again in volume and the clear solution decanted and left in a refrigerator at 4 °C. FTIR in KBr on the solid left from the decantation shows bands at (cm^{-1}) approx. 3500 vw, 3000-2850 w, 1578 s, 1384 s, 1336 s, 1235 w, 1204 w, 1113 m, 1100 m, 1056 s, 1020 m, 942 w, 896 m, 840 m, 675 s, 613 w, 564 w. (Figure 5.20) Over several days a yellow oil separated out from the now-colorless solution. The solvent was removed *in vacuo* and the oil redissolved in a small amount of 2MOE and left at -10 °C for one month. A yellow precipitate formed. The solvent was removed from this *in vacuo* and the solid rinsed with cold 2MOE and Et$_2$O. EDX on the solid (see JWP/III/145) showed that it contained only Bi.

Experiment 10 JWP-II-120 Bi(OAc)$_3$ + V-2MOE, evap. together

In the glovebox, Bi(OAc)$_3$ (4.0026 g, 2.6 mmol) was added to a flask and 50 ml 2MOE added. V-2MOE (7.127g, 3.53 mmol) was added with a 25 ml 2MOE wash to obtain a clear yellow solution. Some of this sample was saved for IR (JWP-II-120A). The remainder of the solution was distilled with vacuum assistance and heating to 1/3 volume, followed by addition of 2MOE back to the original volume and continued vacuum distillation to near dryness. The remainder of the solvent removal was performed *in vacuo* without heating (JWP-II-120C). The solid was kept at 30 mT vacuum over three days but remained a dark yellow-brown oily solid with white speckles. The solid could be redissolved in 2MOE, hydrolyzed, and pyrolyzed at 600 °C to yield Bi$_2$VO$_{5.5}$. PA-FTIR was done on II-120C

307

and compared with II-39-0 (this had been aged approximately 9 months prior to evaporation of the solvent and PA-FTIR). (Figure 5.21a,b) The III-120C solid's PA-FTIR is very similar to that of II-39-0, with new or more intense bands at 1740, 1100, and 1018 cm^{-1}. The III-120A FTIR, taken in 2MOE solution, is dominated by the 2MOE peaks. (Figure 5.22)

Experiment 11 (JWP-II-86A) Bi(OAc)$_3$ + V-2MOE

Bismuth acetate (II-69A) and V-2MOE were dissolved in minimum 2MOE in a 2:1 molar proportion and left in an open vial in a glove box for 5 months. Semicrystalline clear plates covered with green-black spots resulted. PA-FTIR of this material (dried and ground) was identical to that of II-39-0. (Figure 5.23)

Experiment 12 (JWP/III/88A) BiCl$_3$ + VO(OiPr)$_3$ + ethanolamine in Et$_2$O

Ethanolamine (1.5 ml, 24.8 mmol) was added to a solution of BiCl$_3$ (1.0281g, 3.3 mmol) in 50 ml of Et$_2$O. A white fluffy precipitate formed. To this was added VO(OiPr)$_3$ (0.69 g, 2.82 mmol) and the yellow slurry sonicated, then left stirring at 45 °C overnight. No change in the appearance of the mixture was noted. No further characterization was done.

Experiment 13 (JWP/III/88B) BiCl$_3$ + VO(OiPr)$_3$ + ethanolamine in THF

Ethanolamine (1 ml, 16.5 mmol) was added BiCl$_3$ to (1.0804 g, 3.42 mmol) and VO(OiPr)$_3$ (0.6477 g, 2.64 mmol) dissolved in 40 ml THF. An orange-yellow clump instantly fell out of solution. This was sonicated and left stirring on a warm (45 °C) bath overnight to give a faint green solution and a white-brown powder. No further characterization was done.

Experiment 14 (JWP/III/93A) VO(OiPr)$_3$ + ethanolamine

Ethanolamine (0.6g, 9.8 mmol) was added to VO(OiPr)$_3$ (0.5110g, 2.08 mmol) in 30 ml Et$_2$O. A yellow-white precipitate appeared, then became a deep yellow-orange over some minutes. The solution was stirred at room temperature for several hours to obtain a precipitate and a yellow oil which clung to the flask sides. The Et$_2$O/precipitate suspension was decanted off the oil and minimal acetonitrile was added with warming to dissolve the oil. This was left for several weeks at 4 °C. No crystals grew. The yellow precipitate was filtered and dried: 0.2333 g. It became purple-black on exposure to moist air. FTIR (KBr, cm^{-1}) showed bands at (Figure 5.24) 3227 s, br, 2869 s, 1596 s, 1461 s, 1389 w, 1355 m, 1304 m, 1264 m, 1192 vw, 1136 m, 1072 s, br, 908 s, br, 704 m, 623 m, 602 m, 480 m.

Experiment 15 (JWP/III/103A) BiCl$_3$ + VO(OiPr)$_3$ + ethanolamine

BiCl$_3$ (1.0648g, 3.4 mmol) dissolved readily in 75 ml Et$_2$O. VO(OiPr)$_3$ (0.83g, 3.4 mmol) was added to give a yellowish opalescent solution. On addition of 1 ml (16.5 mmol) ethanolamine a canary yellow precipitate and orange oil formed. After stirring 1 h at room temperature the solvent was removed and benzene and pyridine added sequentially to try to dissolve the solid and oil. Neither solvent would dissolve the solid or the oil. The solvents were decanted off and the solid and oil dried *in vacuo*; 2MOE was added to give a yellow paintlike suspension which settled to give a yellow solution and yellow solid. No further characterization was done.

Experiment 16 (JWP/III/89A) BiCl$_3$ + VO(OiPr)$_3$ + ethylene glycol in Et$_2$O

VO(OiPr)$_3$ (0.6496 g, 2.6 mmol) was added to BiCl$_3$ (1.0093 g, 3.4 mmol) dissolved in 50 ml Et$_2$O. A faintly yellow opalescent solution resulted. To this was added 1.5 ml (26.6 mmol) ethylene glycol. A bright yellow precipitate appeared instantly, and separated from an orange oil. After sonication, the precipitate redissolved to give an orange oil only. This was left stirring on a warm bath (30-40 °C) overnight to give a green solution with opaque orange-green oil. Concentration to approximately 10 ml Et$_2$O and cooling at 4 °C for 1 month did not yield crystals.

310

Experiment 17 (JWP/III/89B) BiCl$_3$ + VO(OiPr)$_3$ + ethylene glycol in THF

Experiment 9 was repeated as follows: BiCl$_3$ (1.012 g, 3.4 mmol) and VO(OiPr)$_3$ (0.6517g, 2.6 mmol) were mixed in 100 ml THF to give a white-yellow suspension. To this was added 1 ml (17.7 mmol) ethylene glycol. The resulting mixture became orange-juice yellow and translucent (some cloudiness). This was stirred overnight at 30-45 °C. A bright yellow precipitate was collected from the yellow liquid. This would not dissolve in any of the NMR solvents tested.

Experiment 18 (JWP/III/103B) BiCl$_3$ + VO(OiPr)$_3$ + ethylene glycol

BiCl$_3$ (1.0808 g, 2.8 mmol) was dissolved in 75 ml Et$_2$O and VO(OiPr)$_3$ (0.64 g, 2.6 mmol) added to give a yellowish opalescent solution. 1.5 ml (26.6 mmol) of ethylene glycol was added to give a fluffy yellow precipitate and an orange oil. After 1 h at room temperature the solvent was removed *in vacuo* and more ethylene glycol added to give a yellow paintlike suspension. On settling, this gave a yellow solid and an orange-yellow liquid. No further characterization was done.

Experiment 19 (JWP/III/106A) BiCl₃ + VO(OiPr)₃ + N,N-dimethylethanolamine

BiCl$_3$ (1.037g, 3.3 mmol) was added to VO(OiPr)$_3$ (0.7871g, 3.2 mmol) in 15 ml Me$_2$NCH$_2$CH$_2$OH. This was stirred for 8 h with light warming to yield a dark red solution with a clump of yellow-white solid at the bottom of the flask, and the mixture was sonicated in an attempt to break up the solid clump. After 40 min of sonication the solution has became cloudy and was discarded. The experiment was repeated on JWP/III/108C: BiCl$_3$ (1.0081 g, 3.2 mmol) was stirred in 4 ml Me$_2$NCH$_2$CH$_2$OH and VO(OiPr)$_3$ (0.6570 g, 2.7 mmol) in 5 ml Me$_2$NCH$_2$CH$_2$OH added. A dark red solution resulted; the solvent volume was reduced to approximately 7 ml. This was left at 4 °C for several months, but no crystals grew.

Experiment 20 (JWP/III/113B) KOiPr + BiCl₃

Potassium metal (2.9972 g, 77 mmol) was refluxed in 30 ml HOiPr for 2 h to dissolve all the metal. The solution was cooled BiCl$_3$ (5.99g, 19 mmol) in 75 ml THF added slowly by cannula. The resulting solution was refluxed 1.5 h, resulting in a thick green-grey precipitate. Hexane was added to aid stirring. The mixture was permitted to stand overnight at room temperature. A brown liquid and white-grey solid resulted. To this was added 5 ml more HOiPr and the mixture filtered to leave a light tan solid. XRD of the solid shows KCl. The solvent was removed *in vacuo* from the filtrate to leave a solid. ESEM one the solid showed a set of crystals (KCl?)

312

embedded in an amorphous matrix. (Figure 5.16) Elemental analysis (Oneida): 26.45 C, 4.87 H, 45.62 Bi, 18.40 K (29.8C, 5.8H, 8.07 K, 43.1 Bi expected).

Experiment 21 (JWP/III/117A) $BiCl_3$ + 4 KOiPr + VI_2

Potassium metal (0.4976g, 12.8 mmol) was dissolved with reflux in 40 ml HOiPr. After cooling, this was added slowly to a solution of $BiCl_3$ (1.007g, 3.2mmol) in 60 ml THF and the mixture refluxed 1.5 h to give a blue-grey suspension. This was cooled and a suspension of VI_2 (0.4838 g, 1.59 mmol) in 50 ml HOiPr added to give a dark purple-grey suspension. This was warmed (40 °C) overnight and filtered to yield a black solid and a brown liquid. The solid was washed with HOiPr and dried (0.9668 g found, 0.71 g KCl expected). XRD on the solid showed $BiCl_3$, KCl, KI, and VI_2 (find and check).

Experiment 22 (JWP/III/107B) $BiCl_3$ + $Ti(OiPr)_4$ in 2MOE

$BiCl_3$ (1.0083 g, 3.2 mmol) and $Ti(OiPr)_4$ (1.7068 g, 5.92 mmol) were stirred in 15 ml 2MOE at room temperature for 8 hr to dissolve all solids. The clear and colorless solution was stirred for 10 min at 45 °C and the solvent removed *in vacuo*. With warming under vacuum the solution became milky. 9 ml 2MOE was added to redissolve the precipitate, but the suspension remained milky. The experiment was discarded.

Experiment 23 (JWP-II-143) location of Bi in gel

To two flasks were added a solution of $Bi(OAc)_3$ (1 g, 2.6 mmol) and V-2MOE (1.3 mmol) dissolved in 40 ml 2MOE. The solution in each flask was hydrolyzed with 2 ml of water in 4 ml of 2MOE, resulting in a gel with syneresis in both cases. (1) From one flask, the syneresis fluid was removed and the gel rinsed several times. The rinsings were added to the syneresis fluid, which was evaporated carefully in a tared container. Residue 0.0004 g. (2) The gel in the other flask was broken up with a stirring rod and filtered gently with repeated washings with 2MOE. The filtrate was carefully evaporated in a tared container. Residue 0.000 g. The gel remaining on the filter was vacuum dried and pyrolyzed. DTA-TGA showed a monotonic weight decrease until approximately 450 °C, with exotherms at 290 and 385 and an endotherm at 830 °C. (Figure 5.25) The gel, pyrolyzed at 550 °C for 8 h in air, was identified by XRD to be $BiVO_4$ + $Bi_2VO_{5.5}$.

Experiment 24 (JWP-III-127) ^{51}V NMR and UV-VIS of precursor solutions

The V-2MOE solution prepared by dissolving V-2MOE (0.6057g, 13.2 mmol) in 25 ml 2MOE above was found to have a single ^{51}V NMR peak at -543.8 ppm. A 1:1 mix of this V-2MOE solution and a solution of $Bi(OAc)_3$ (0.994g, 2.57 mmol in 25 ml 2MOE) gave a single ^{51}V NMR peak at -541.1 ppm. A solution made by combining 1:4

glacial HOAc in the V-2MOE solution gave a single peak at -512.6 ppm.

The V-2MOE (background = 2MOE), and 1:1 Bi/V (background = Bi(OAc)$_3$ solution) solutions were scanned 300-800 nm on a HP8452A diode array spectrophotometer in a 1 cm plastic cell (cutoff 300 nm), with the backgrounds indicated for each solution subtracted. The experiment was repeated several times to ensure that the observed red-shifting of the Bi/V solution relative to the V solution was not an artifact of the instrument. The observed shift between the V-2MOE solution and that containing Bi(OAc)$_3$ averaged to 35 nm to the red; the average instrument reproducibility between two runs was +_2 nm (5 trials). (Figure 5.10)

Experiment 25 (JWP-III-111) ^{51}V NMR of precursor solutions

^{51}V NMR were run on the Varian Unity (300 MHz) NMR, using the deuterium lock off and VOCl$_3$ as an external standard (δ=0 ppm).

Table 5.1: ^{51}V NMR Results of Expt. 25.

Solution	^{51} V NMR Peaks (ppm)
VO(OiPr)$_3$ 10% in iPrOH (commercial, from Strem)	-627*
V-2MOE from V$_2$O$_5$	-544
VO(OiPr)$_3$ in 2MOE, after 1h	-627, -594, -571
VO(OiPr)$_3$ + BiCl$_3$ in THF	-628, -606, -596
V-2MOE + HOAc	-521
V-2MOE + Bi(OAc)$_3$	-541

*-629 ppm expected[32]

Experiment 26 (JWP-II-148) FTIR of precursor solutions

The 2:1 Bi(OAc)$_3$:V-2MOE precursor solution was spread onto 3M Type 61 IR cards and FTIRs run before and after the cards were dried under vacuum. The "wet" solution IR was dominated by the 2MOE solvent bands. (Figure 5.12) The dried precursor IR (Figure 5.13), however, showed a greatly reduced band and 3400 cm^{-1}, indicating the disappearance of most of the -OH groups from the material on the IR card; the 1722 cm^{-1} band shifted to 1707 cm^{-1}, indicating the weakening of the C=O groups present in the dried precursor. Bands at 1540, 1400, 1113 (ν(C-O ether)), 1052 (ν(C-O alcohol), and 1014 (ρ(OCH$_3$)?) cm^{-1} are attributable to the retained 2MOE groups according to the assignments given. The broad shoulder 980-700 cm^{-1} and moderately strong peak at 680 cm^{-1} may be assignable to the V=O and V-O bands, respectively.

316

Figure 5.18: Powder XRD of the pyrolysis product of JWP-III-84A.
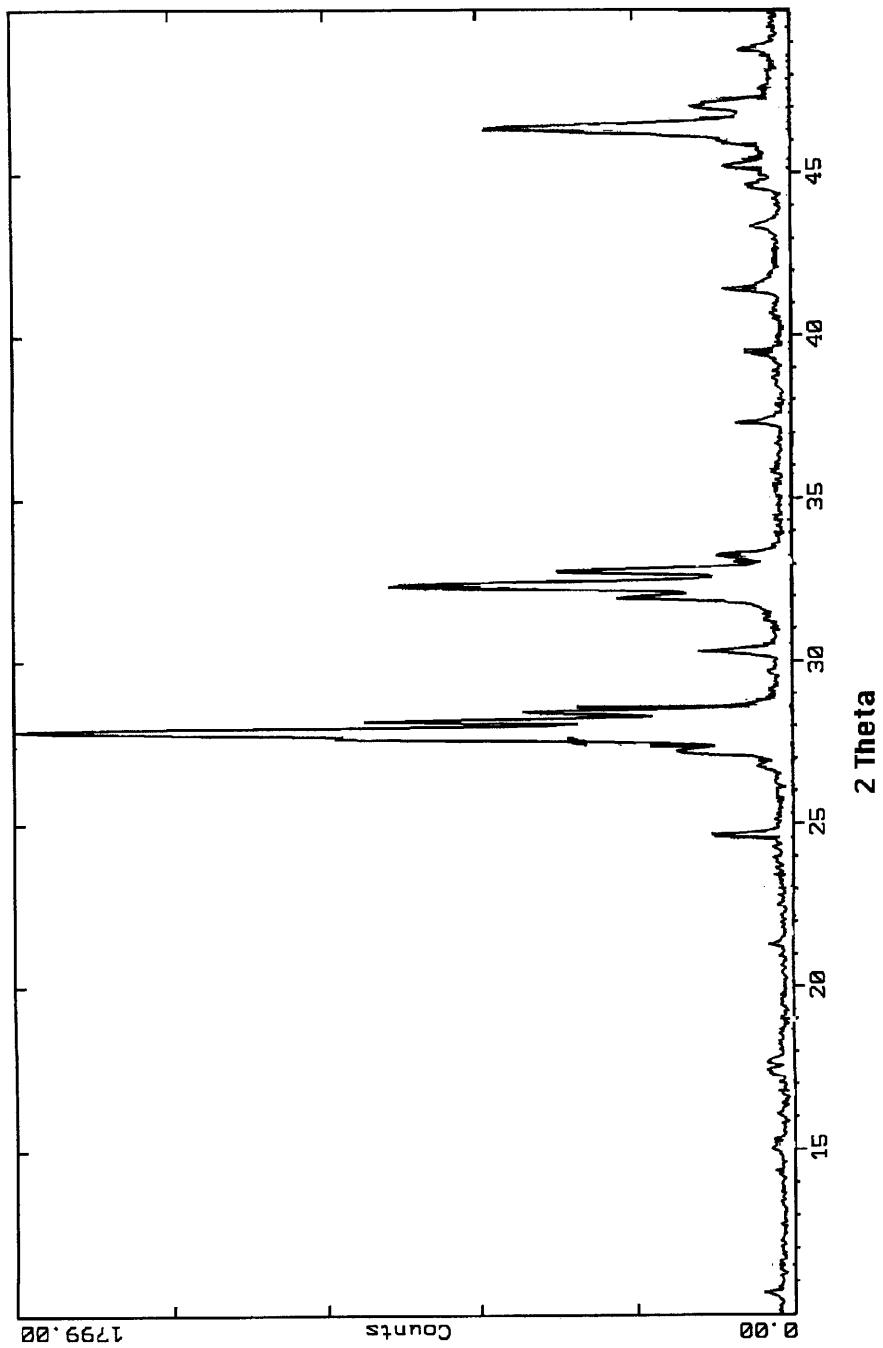
Figure 5.19: FTIR of JWP-III-91C.
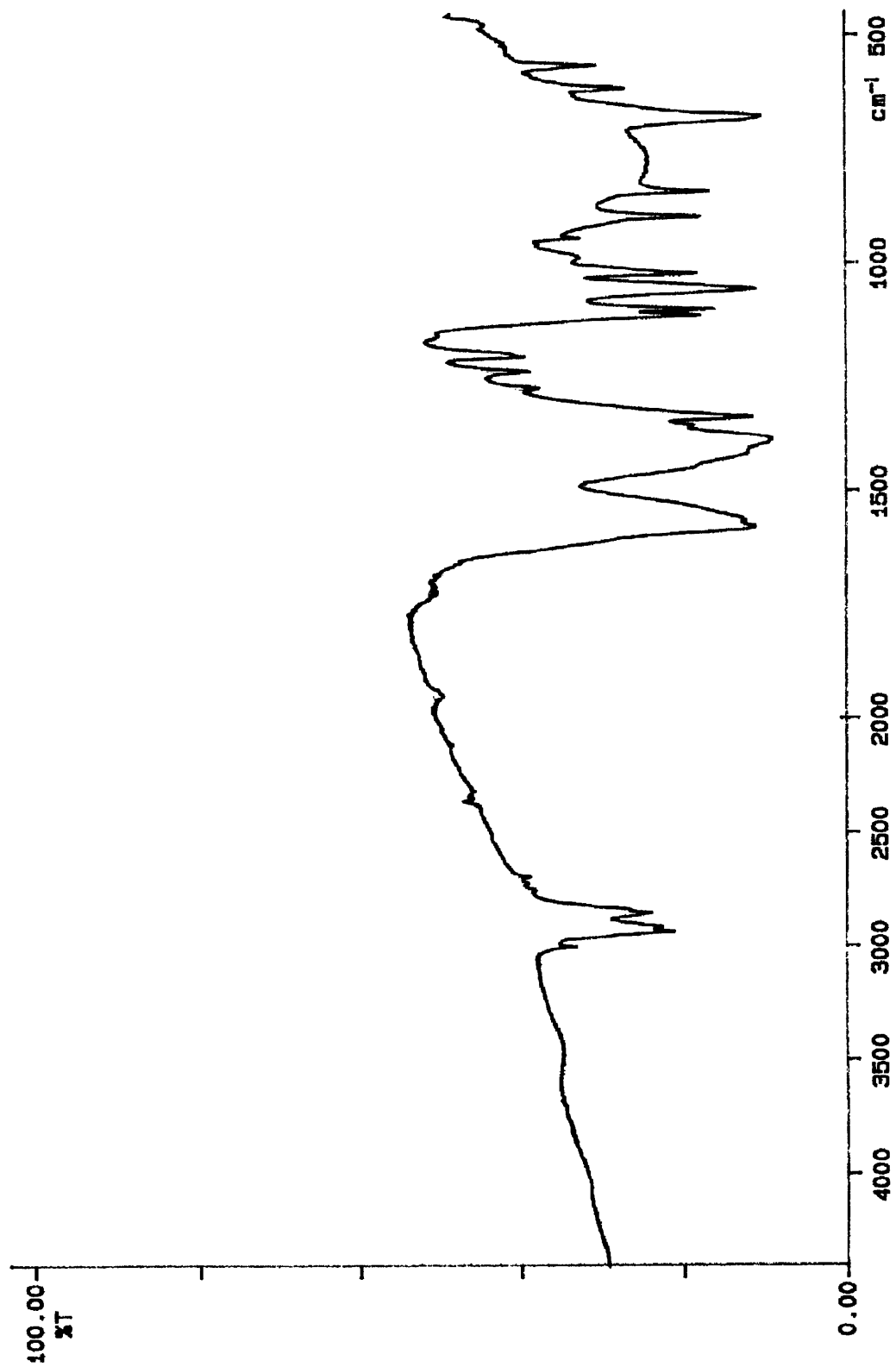
Figure 5.20: Phototaccoustic FTIR of JWP-III-109A.
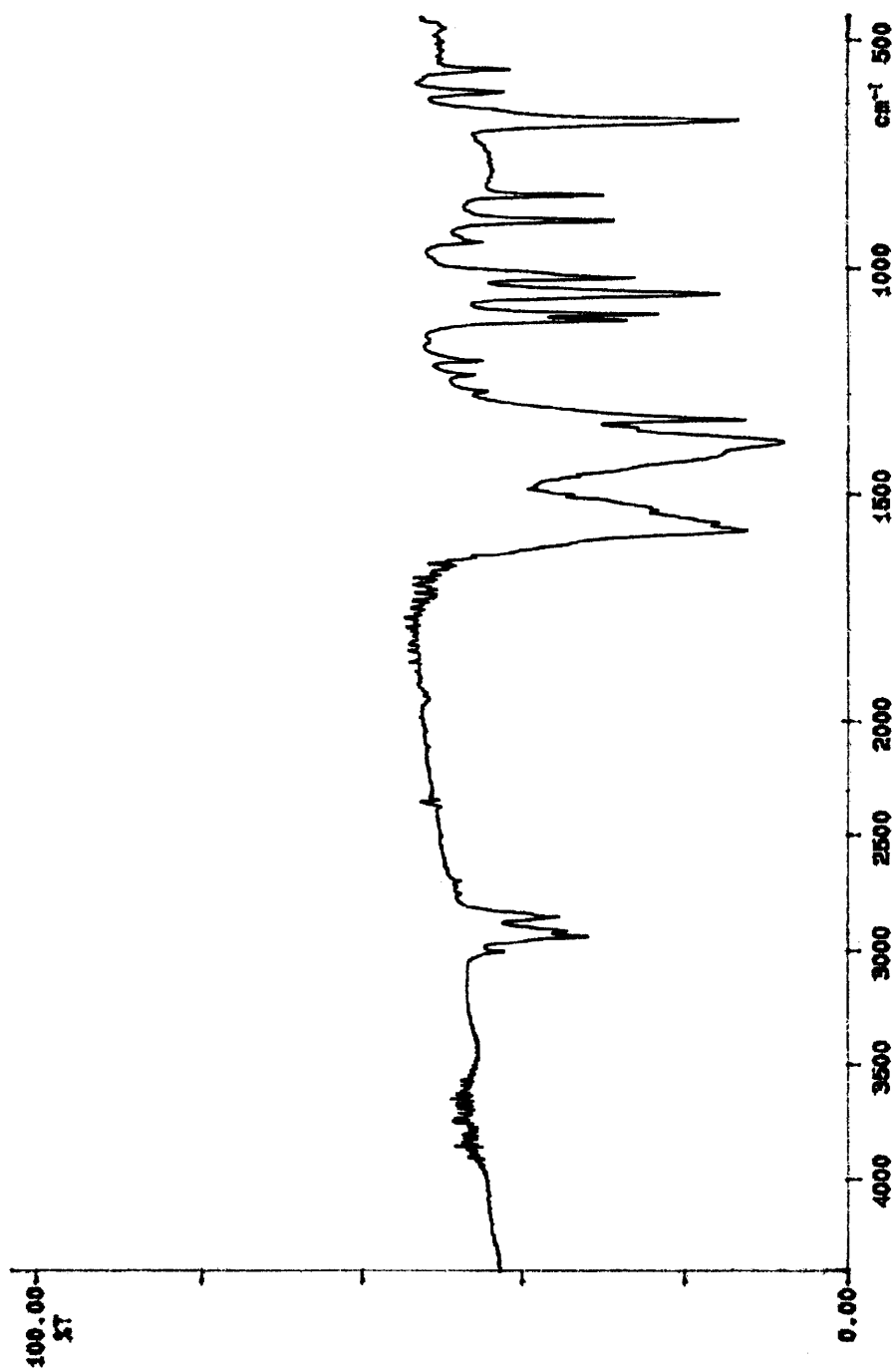
Figure 5.21a: FTIR of JWP-II-39-0.
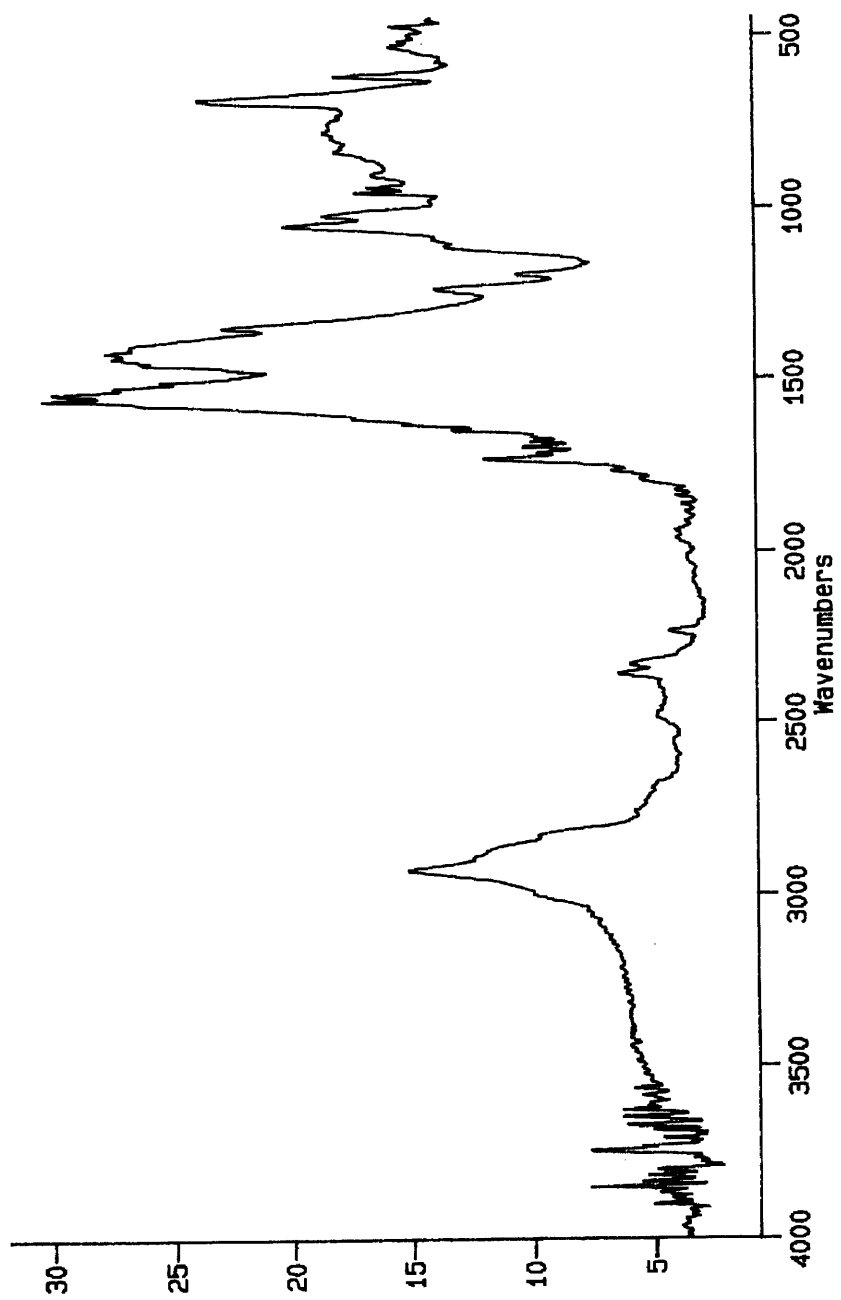
Figure 5.21b: FTIR of JWP-II-120C.
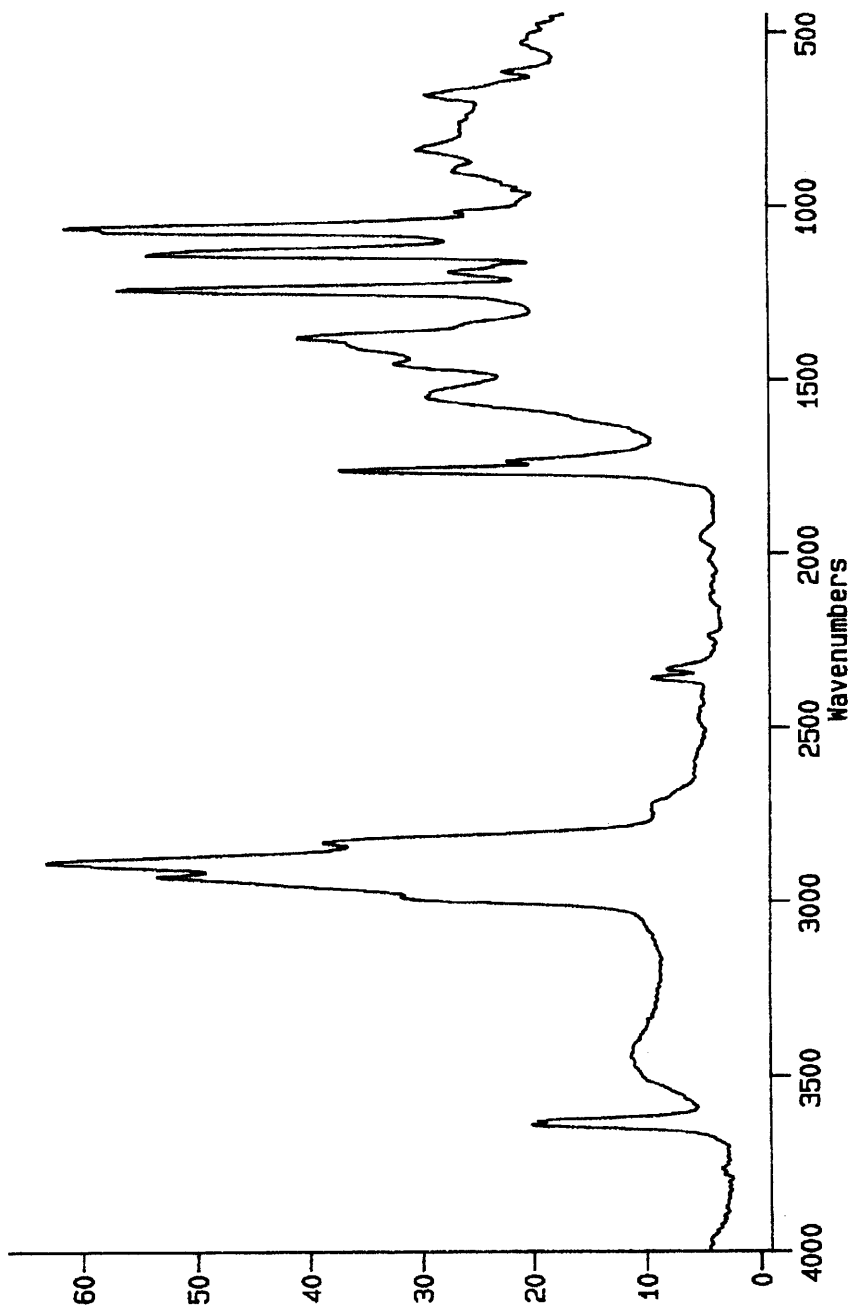
Figure 5.22: FTIR of JWP-II-120A.
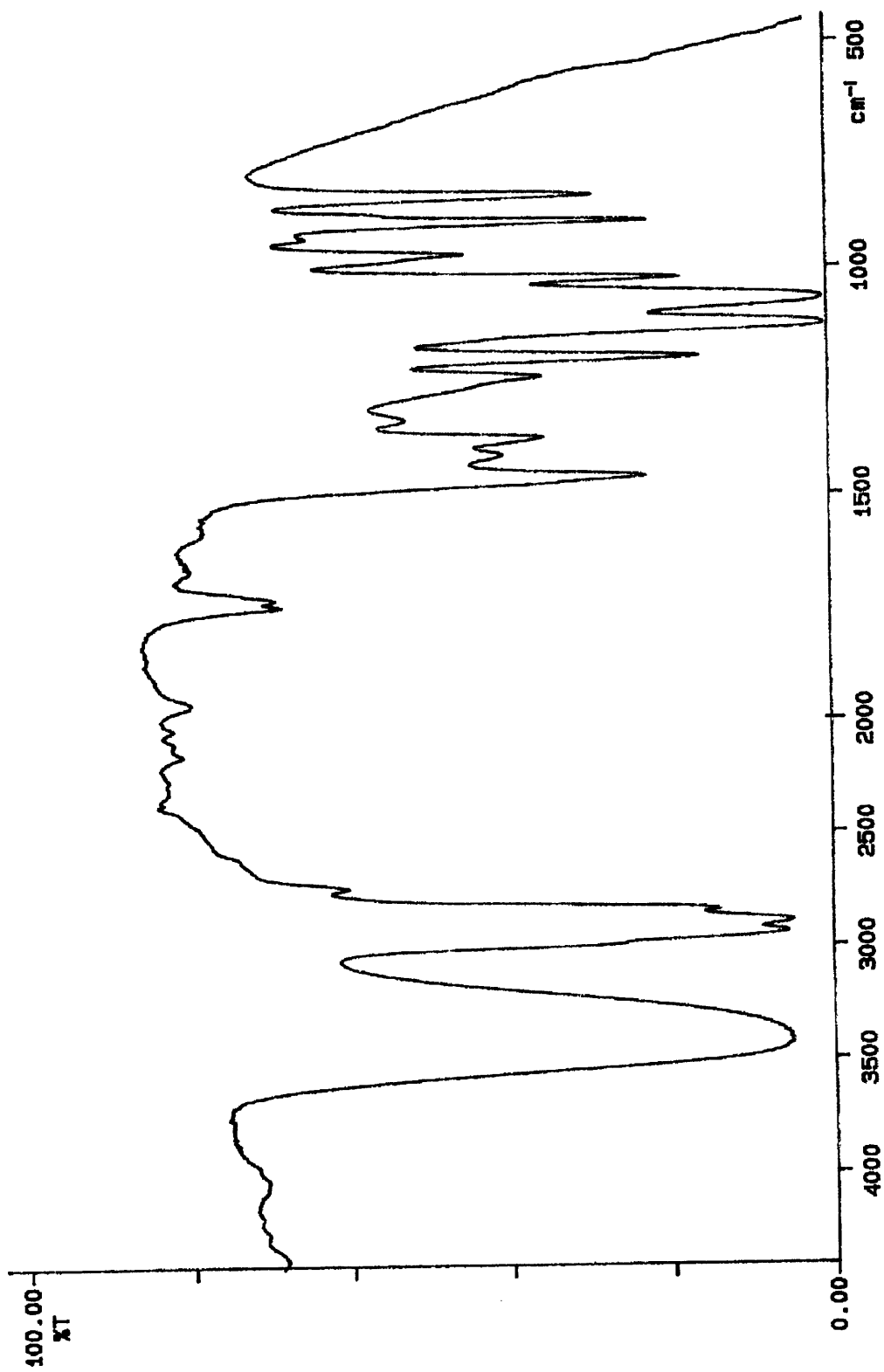
Figure 5.23: FTIR of JWP-II-86A.

323
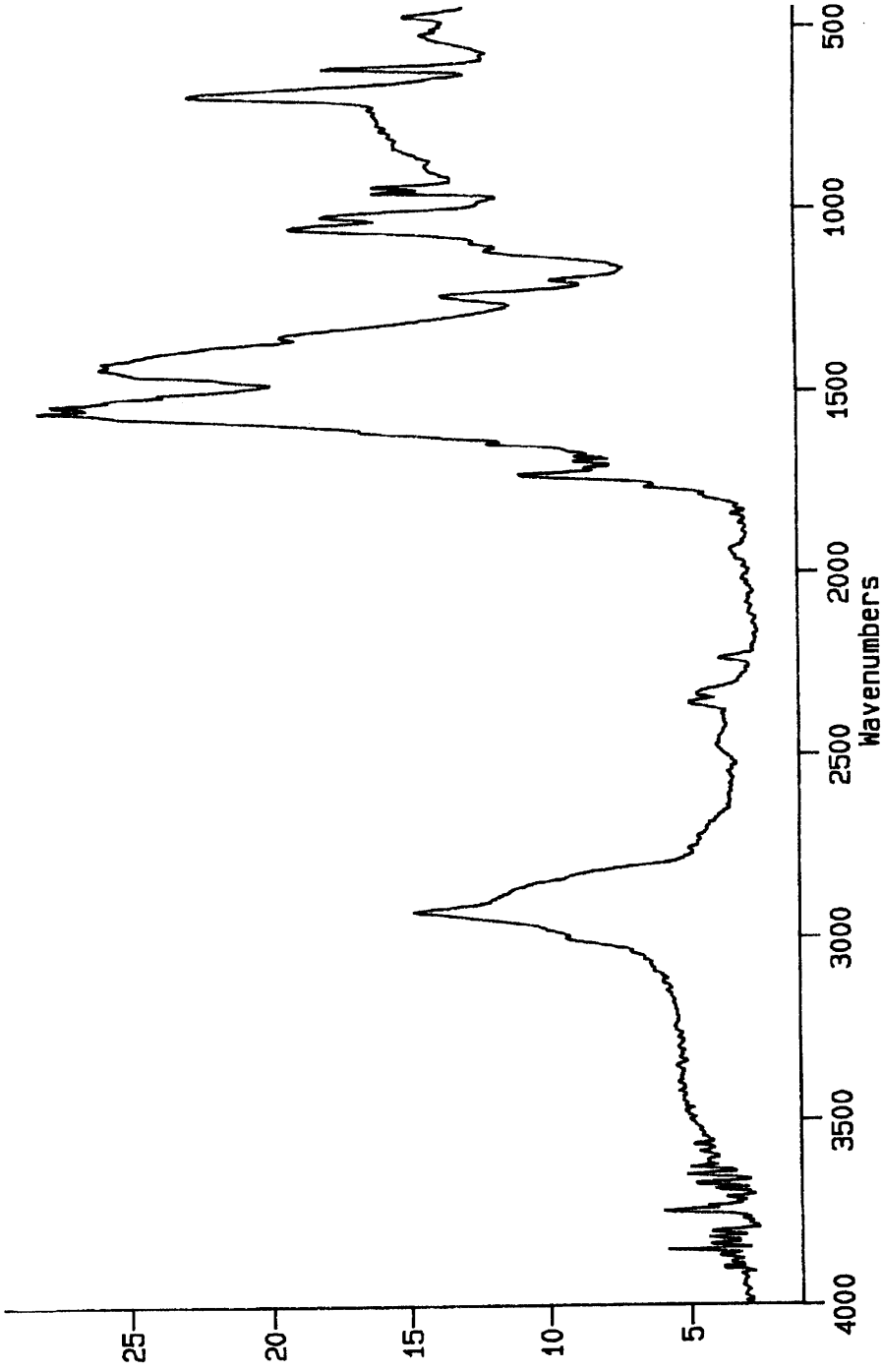
Figure 5.24: FTIR of JWP-III-93C.
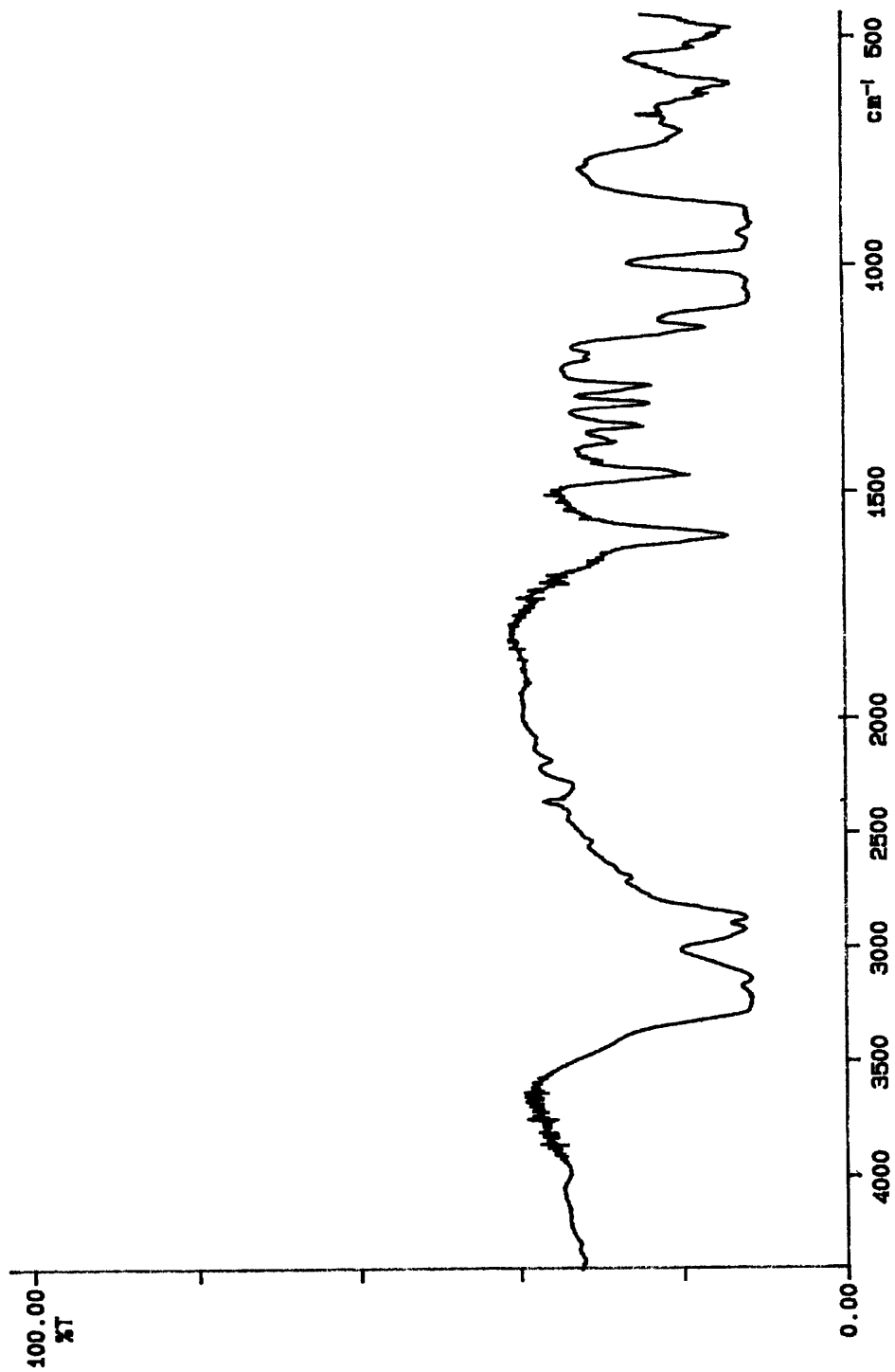
Figure 5.25: DTA/TGA of gel from experiment JWP-II-143.
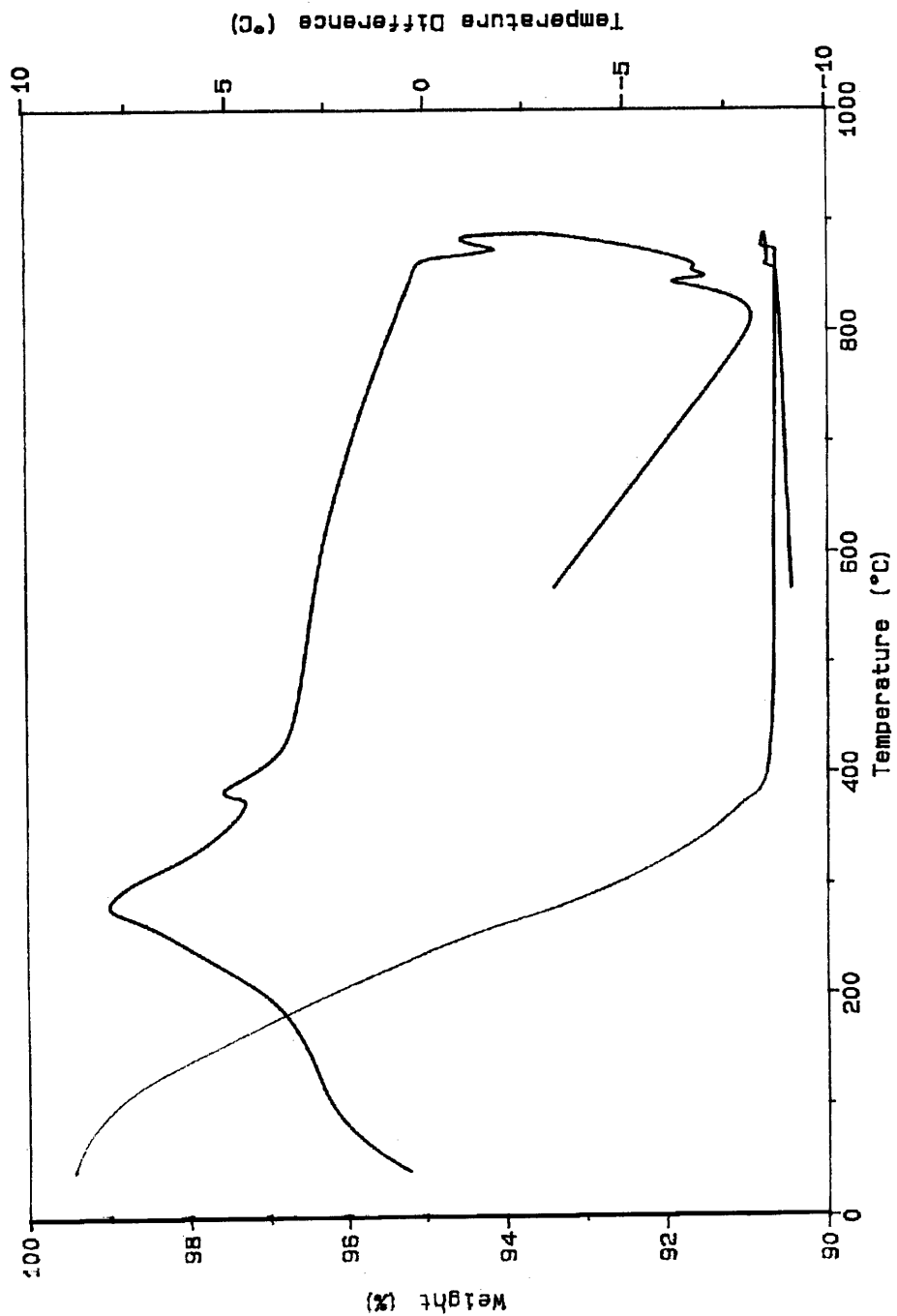
5.5 References

1) Crans, D. C.; Shin, P. K. *J. Am. Chem. Soc.* **1994**, *116*, 1305.

2) Crans, D. C.; Felty, R. A.; Chen, H.; Eckert, H.; Das, N. *Inorg. Chem.* **1994**, *33*, 2427.

3) Mondal, S.; Rath, S. P.; Dutta, S.; Chakravorty, A. *J. Chem. Soc. Dalton Trans.* **1996**, *1996*, 99.

4) Crans, D. C.; Felty, R. A.; Anderson, O. P.; Miller, M. M. *Inorg. Chem.* **1993**, *32*, 247.

5) Mehrotra, R. C.; Singh, A.; Sogani, S. *Chem. Rev.* **1994**, *94*, 1643.

6) Sauer, N. N.; Garcia, E.; Salazar, K. V.; Ryan, R. R.; Martin, J. A. *J. Am. Chem. Soc.* **1990**, *112*, 1524.

7) Campion, J.-F.; Payne, D. A.; Chae, H. K.; Maurin, J. K.; Wilson, S. R. *Inorg. Chem.* **1991**, *30*, 3244.

8) Mehrotra, R. C. *J. Non-Crystalline Solids* **1988**, *100*, 1.

9) Bartley, W. G.; Wardlaw, W. *J. Chem. Soc.* **1958**, 422.

10) Gaskins, B. C.; Lannutti, J. J. *J. Mater. Res.* **1996**, *11*, 1953.

11) Danielle, S.; Papiernik, R.; Hubert-Pfalzgraf, L. G.; Jagner, S.; Hakansson, M. *Inorg. Chem.* **1995**, *34*, 628.

12) Hubert-Pfalzgraf, L. G. *Mater. Res. Soc. Symp. Proc.*, **1992**, *271*, 15.

13) Teff, D. J.; Huffman, J. C.; Caulton, K. G. *Inorg. Chem.* **1995**, *34*, 2491.

14) Papiernik, R.; Hubert-Pfalzgraf, L. G.; Daran, J.-C.; Jeannin, Y. *J. Chem. Soc. Chem. Commun.* **1990**, 695.

15) Chandler, C. D.; Roger, C.; Hampden-Smith, M. J. *Chem. Rev.* **1993**, *93*, 1205.

16) Hirota, K.; Komatsu, G.; Takemura, H.; Yamaguchi, O. *Ceramics International* **1992**, 285.

17) Massiani, M. C.; Papiernik, R.; Hubert-Pfalzgraf, L. G.; Daran, J. C. *J. Chem. Soc. Chem. Commun.* **1990**, 301.

18) Massiani, M.-C.; Papiernik, R.; Hubert-Pfalzgraf, L. G. *Polyhedron* **1991**, *10*, 437.

19) Sauer, N. N.; Garcia, E.; Ryan, R. R. in *Better Ceramics Through Chemistry IV*; Philadelphia: Materials Research Society, 1990; Vol. 180, pp 921.

20) Tohge, N.; Fukuda, Y.; Minami, T. *Jpn. J. Appl. Phys.* **1992**, *31*, 4016.

21) Toyoda, M.; Payne, D. A. *Mater. Lett.* **1993**, *18*, 84.

22) Yamaguchi, O.; Maruyama, N.; Hirota, K. *Br. Ceram. Trans. J.* **1991**, *90*, 111.

23) Mehrotra, R. C.; Rai, A., K *Ind. J. Chem.* **1966**, *4*, 537.

24) Matchett, M. A.; Chiang, M. Y.; Buhro, W. E. *Inorg. Chem.* **1990**, *29*, 360.

25) Jones, C. M.; Burkart, M. D.; Bachman, R. E.; Serra, D. L.; Hwu, S.-J.; Whitmire, K. H. *Inorg. Chem.* **1993**, *32*, 5136.

26) Rogers, R. D.; Bond, A. H.; Aguinaga, S.; Reyes, A. *J. Am. Chem. Soc.* **1992**, *114*, 2967.

27) Rogers, R. D.; Bond, A. H.; Aguinaga, S. *J. Am. Chem. Soc.* **1992**, *114*, 2960.

28) Evans, W. J.; Hain, J. H. J.; Ziller, J. W. *J. Chem. Soc. Chem. Commun.* **1989**, 1628.

29) Toyoda, M.; Hamaji, Y.; Tomono, K.; Payne, D. A. *Jpn. J. Appl. Phys.* **1993**, *32*, 4158.

30) Turova, N. Y.; Kessler, V. G.; Kuchieko, S. I. *Polyhedron* **1991**, *10*, 2617.

31) Corriu, R.; Leclercq, D.; Lefevre, P.; Mutin, P. H.; Vioux, A. *Chem. Mater.* **1992**, *4*, 961.

32) Priebsch, W.; Rehder, D. *Inorg. Chem.* **1990**, *29*, 3013.

33) Nandra, K. K.; Sinn, E.; Addison, A. W. *Inorg. Chem.* **1996**, *29*, 3013.

34) Goel, S. C.; Kramer, K. S.; Gibbons, P. C.; Buhro, W. E. *Inorg. Chem.* **1989**, *28*, 3619.

35) Alcock, N. W. *Adv. Inorg. Chem. Radiochem.* **1972**, *15*, 1.

36) Nugent, W. A.; Harlow, R. L. *J. Am. Chem. Soc.* **1994**, *116*, 6142.

37) Cummins, C., personal communication.

38) Whitmire, K. H.; Jones, C. M.; Burkart, M. D.; Hutchinson, J. C.; McKnight, A. L. in *Mater. Res. Soc. Symp. Proc.,* **1992**; *271*, 149.

39) Athar, T.; Bohra, R.; Mehrotra, R. C. *Main Grp. Met. Chem.* **1987**, *10*, 399.

40) Bowdoin, C. *Infrared Spectroscopy: I. Interpretation of Spectra and II. Instrumentation, Polymer Spectra, Sample Handling, and Computer Assisted Spectroscopy*; Bowdoin College: Brunswick, ME, 1987; Vol. 1.

Chapter Six: Deposition of BiMeVOx Films onto Smooth and Porous Substrates

The experimental work described in this chapter was adapted, in part, from Pell, J.W., Delak, K.M., and zur Loye, H.-C., in *Polycrystalline Thin Films*, MRS Symp. Proc. **403**, 1996, 459-464; and Pell, J.W., Delak, K.M., and zur Loye, H.-C., *Chem. Mater.*, **10**, 1998, 1764-1770.

6.1 Introduction

6.1.1 Background

Air separators utilizing a thin, dense membrane of an oxygen-ion conducting material offer significant advantages over conventional methods involving repeated fractional distillation of air, both in terms of efficiency and economics.[1,2] Likewise, membrane reactors incorporating an ionic conductor can have increased conversion efficiency and selectivity over fully oxidized products in partial oxidation and ammonoxidation reactions.[3-7] The use of a thin membrane of the conducting material shortens the path that oxygen ions must traverse, effecting a corresponding reduction in the temperature required to achieve a given oxygen flux. Further decreases in operating temperature are desirable to reduce heating costs in both air separators and membrane reactors, and to broaden the range of reactants which can be used in partial oxidation or ammonoxidation reactions.

An important restriction, however, is that the membrane must be crack- and pore-free, and robust under thermal cycling. Unsupported membranes must be thick (hundreds of μm) to give reliable performance, while some supported membranes such as films of yttria-stabilized zirconia (YSZ) on porous substrates need to be on the order of 30 μm thick to be initially crack-free.[8,9] This thickness still requires operating temperatures near 1000 °C to reduce resistive losses—and these films developed gas leaks during thermal cycling. Furthermore, the use of ever-thinner membranes

330

does not guarantee a continuous increase in oxygen flux, since the kinetics of oxygen-ion recombination reactions become limiting.[2] On the other hand, a material with a conductivity greater than YSZ may be used to fabricate thicker, more reliable membranes. If the conductive material has both ionic and electronic conductivity, so that charge balance may be maintained across the membrane without having to resort to the incorporation of an external circuit in the device design, this situation is even better.

One of the most versatile techniques for producing thin films of oxide materials is the sol-gel method, which has been demonstrated to produce high-quality films of a number of materials, including YSZ[10,11] and bismuth and lead titanates.[12-15] In the sol-gel method, a solution of suitable precursors is deposited onto a substrate, followed by gelation to a homogenous solid layer, which is dried and fired (350-450 °C) to remove unwanted organic components.[16] Higher-temperature processing yields a crystalline film, and repetition of this procedure can result in films of up to several μm in thickness. The film thickness will be a function of the solution concentration and viscosity, in addition to parameters associated with the specific deposition method—e.g. dip- or spin-coating. Thinner films develop less strain during drying shrinkage, and are thus less prone to crack. Additionally, cracking may be reduced by increasing film-substrate adhesion through substrate cleaning, or by rapid solvent removal and polymer network modification aimed at preventing the extensive cross-linking which can lead to an inelastic film.[11]

Several groups have reported the sol-gel deposition of films of YSZ on a number of continuous and porous substrates. Chen et al.[17] observe that solutions with a viscosity below 50 cps will not wet a smooth glass substrate, while high viscosities (>500 cps) gave inhomogenous, cracked films. On porous substrates, on the other hand, viscosities of nearly 200 cps and multiple coatings were required to produce continuous films of 0.1 to 0.5 μm thickness.

Kueper et al.[11] use less viscous precursor solutions to prepare crack-free thin films of 0.1-0.5 μm thickness on cleaned quartz substrates. They establish a principle of rapid solvent removal after film casting to minimize polymeric cross-linking in the film, in order to provide maximum film flexibility and limit cracking. Only on substrates with the smallest-scale porosity examined (0.02 μm) could a continuous film be formed by their process; substrates with larger pores suffered from entry of the film into the pores. In addition to the solvent-removal rate, the importance of network-modifying additives in controlling the elastic properties and porosity of the green and calcined films must be taken into consideration.[18]

In this Chapter we report the deposition of BiCuVOx films onto quartz substrates from the sol-gel precursor formulations discussed in Chapter 4. The films showed poor thermal behavior, agglomerating and forming holes and hillocks on heating. The water-to-alkoxide ratio and additives used in the BiCuVOx precursor formulation were varied but found to exacerbate the defect-formation behavior of these films on quartz substrates. A number of other substrates, comprised of metal films electron beam deposited onto quartz, were tested. BiCuVOx films remained defect-free over

the entire range of temperatures on these substrates. Other BiMeVOx films were prepared on quartz and metal substrates and found to be reproducibly defect-free in several cases. Finally, BiCuVOx films were prepared defect-free on porous alumina substrates. This latter accomplishment provided supported oxide-ion conductive films ready for testing in a membrane reactor.

6.1.2 Materials and Methods

Some initial comments about what was done experimentally will make the discussion easier to follow. See Section 6.6 for the details of individual experiments.

6.1.2.1 Precursor Solutions

The standard precursor solution for BiCuVOx films was made as described in Chapter Four: bismuth acetate, vanadium 2-methoxyethoxide, and copper acetate were dissolved in 2-methoxyethanol to produce a stock solution approximately 0.05 M in BiCuVOx equivalents. This was aged some two weeks prior to its first use, then was used throughout the majority of the film casting experiments as follows: the solution was diluted 50% with methanol just prior to use, then hydrolyzed by adding slowly, with stirring, one mole of water per hydrolyzable alkoxide group (e.g. 4 H_2O/V). Solutions were then permitted to stir one hour at room temperature in a closed container prior to deposition. The pre-hydrolysis dilution with methanol was found to be necessary to produce thin, rapidly-drying films.

A similar recipe was used to make precursor solutions for other BiMeVOx films. In these, Nb was added as niobium(V) isopropoxide, Mn as manganese(II) acetate, Fe as iron(II) acetylacetonate, and Ti as titanium(IV) isopropoxide, all in appropriate amounts to deliver the required number of moles of dopant. Concentrations of the stock solutions were approximately 0.05 M in BiMeVOx equivalents; the stock solutions were again diluted 50% with methanol prior to hydrolysis and casting. The quantity of hydrolysis water was set at one mole water per mole total alkoxide groups, including those on the vanadium and on the dopant metals.

The precursor solutions were prepared and stored under inert atmosphere until hydrolysis. After hydrolysis, they were permitted to be open to air, but were kept tightly closed between withdrawal of aliquots for depositions. A hydrolyzed solution was used for a day's experiments (the maximum time before use was five hours after hydrolysis), then discarded.

6.1.2.2 Substrates

Quartz microscope slides were cut into pieces measuring approximately 1 cm square. It was found that these slides, as received, were not wet by the precursor solution described above – e.g. a drop of solution formed a very rounded bead on the surface of the quartz. Sonicating the slide in acetone or methanol permitted the solution to wet the surface to the extent that the bead became highly flattened, probably due to the removal of hydrophobic organic

residues or coatings left on the quartz from the fabrication of the slides. However, films produced by dip coating onto quartz substrates which had been prepared in this way flaked off easily.

It was thought that "roughing up" the surface of the quartz substrates by rinsing them in aqueous hydrofluoric acid would improve the precursor solution wetting as well as the film adhesion. This may operate by leaving dangling Si-O- bonds (capped with adsorbed atmospheric water) or otherwise providing a charged surface to facilitate wetting. This sort of behavior has been seen with polymeric siloxane solutions on silica substrates.[19] Therefore, quartz slides were prepared by sonication for 30 minutes in acetone or methanol to remove hydrophobic contaminants gained during fabrication and packaging, followed by immersion for one minute in 48% aqueous HF. They were then rinsed thoroughly with water and methanol and dried. Quartz slides prepared in this way were examined by environmental scanning electron microscopy (ESEM) and compared with those prepared by other methods. They were found to have no gross surface damage, unlike those which, for instance, had been sonicated in aqueous HF. (Figure 6.1) In some cases, the quartz substrates were dried at high temperature (600 °C) or on a hot plate (300 °C) and cooled in a dessicator prior to use; neither step made any discernible difference in the film adhesion or general quality.

The film's adhesion to metal substrates was also investigated. Metal substrates were initially constructed by cutting 1 cm squares pieces from thin metal sheets (0.001" Ag, 0.01" Ag, 0.005" Pt), and subsequently pressing them flat. However, wrinkles and bends in the substrates that developed during the coating process due to

the handling procedures often cracked the deposited films and made it difficult to distinguish defects arising from precursor chemistry from those arising from careless handling of the substrates. Promising results seen with the BiCuVOx coatings on platinum substrates (Figure 6.2) prompted us to find a better way of producing metal substrates.

Later metal substrates were therefore prepared by electron beam (E-beam) deposition. Quartz samples were cleaned as described above, dried, and mounted in an electron beam deposition apparatus. A 100 Å layer of titanium was first deposited to improve the 1000-Å platinum layer's adhesion to the quartz. The platinum coatings deposited in this way were adherent to the "scotch tape test." The slides were examined by ESEM and found to be smooth and defect-free. (Figure 6.3) Platinum peaks in the grazing-incidence X-ray diffraction (GIXRD) patterns were in the expected positions; the titanium underlayer could not be detected at a grazing angle of 1°. (Figure 6.4)

A number of other metals and oxides were identified as potentially able to act as substrate materials for the BiMeVOx materials, according to their ability to provide a matching lattice. (Table 6.1) Substrates were prepared with some of these coatings and used, e.g. Pt, WO_3, Al_2O_3, Ag. The silver films would not adhere to the quartz substrates, even with a Ti underlayer. The tungsten oxide films appeared adherent to the naked eye but under ESEM inspection were fraught with holes and delaminated areas. The platinum and alumina films were of good quality, and were used in deposition experiments with each of the BiMeVOx materials (M = Cu, Nb, Ti, and Mn).

Porous alumina disks (Whatman brand, Anodisc™) having a regular 0.02 μm pore size were sonicated in acetone and baked at 650 °C for one hour to remove organics left on them during their fabrication. These were examined in ESEM so that film voids could be distinguished from the original appearance of the substrate and were examined with GIXRD. Scanned in both the grazing incidence and normal modes, the anopore discs appeared amorphous due to a combination of X-ray scattering from the pores and the small material-to-void volume ratio in the discs. (Figure 6.5)

6.1.2.3 Deposition of Films onto Substrates

Two methods of depositing a sol-gel precursor onto a substrate are common: dip coating and spin coating. Both require specialized equipment to provide reproducible depositions. Because dip-coating is more appropriate for depositions onto large, non-flat pieces, we first tried dip-coating solutions by hand, then built a dip-coating apparatus.

Dip coating is a method of applying a precursor solution to a large surface area of any shape in a short time. (Figure 6.6) A single coating run may produce a film less than about 0.2 μm in thickness.[20] During dip-coating, the substrate is immersed in and withdrawn from the coating solution at a constant rate and angle. For a continuous process, e.g. a loop being pulled through the solution, the thickness h of the liquid layer adhering to the substrate can be given by Equation 6.1.

(6.1) $h = K(\eta U/\rho g)^{1/2}$

where ρ is the solution density, g the gravitational acceleration, η the viscosity, U the withdrawal speed; and K is a function of the capillary forces, which in turn depend on solution viscosity and surface tension, as well as the withdrawal speed. K is usually near 0.8 for a Newtonian liquid.[21]

For an individual piece, the thickness is parabolic with distance x from the leading edge of the substrate and the time that the leading edge left the bath (Equation 6.2):

(6.2) $h = (\eta x/\rho g t)^{1/2}$

The equation has been verified experimentally to a first approximation;[22] however, because the equation was developed for an ideal viscous liquid, where the thickness is determined solely by run-off from the substrate, it is not fully applicable to sol-gel films, where the solvent vapor pressure, humidity, substrate temperature, and other factors control the transformation of a partially polymerized metal alkoxide sol to a gel on a substrate. In the sol-gel case, the viscosity of the deposited solution is changing constantly during the dip-coating process. An empirical equation[23] to describe the thickness of a densified film produced by dip-coating a silicon alkoxide precursor solution takes K in Equation 6.1 as being a function of a dimensionless flow term J and the densities of the solution ρ, the densified film ρ_p and solvent ρ_s. (Equation 6.3):

(6.3) $h_p = J[(\rho-\rho_s)(\rho_p-\rho_s)][\eta U/\rho g]^{1/2}$

The slower the dip speed, the smaller the viscous drag force by which the substrate lifts the liquid, and the thinner the film as a result. For films under a micron in thickness, the disjoining pressure limits the thin-ness. This pressure stems from London-van der Waals forces and electric double layer forces. If the disjoining pressure varies with the film thickness such that there is some equilibrium value of the thickness, the liquid will wet the substrate perfectly and the film thickness will fall to this limit as the substrate withdrawal speed is reduced.[21] Evaporation also may set a limit on the film thin-ness, since the viscosity rises as the solvent evaporates from the film. Problems with the method include the fact that the precursor solution bath surface responds to any slight vibration with ripples that affect the film as it is deposited; the film tends to sag if left in the vertical orientation while the coating is still liquid; particulate matter can easily fall into the precursor bath; and the rate of evaporation of solvent from the substrate may fluctuate according to local conditions.

We dip-coated BiCuVOx precursor solutions onto cleaned quartz slides and pyrolyzed them to investigate the feasibility of using this method of film casting. Initial dip-coatings by hand proved irreproducible, so we assembled a crude dip-coating apparatus. (Figure 6.7) A range of withdrawal rates were tried, as were precursor solutions at different concentrations and degrees of hydrolysis.

In general, the films produced by dip-coating were badly cracked. Irregularities in the film caused by poor control of the dipping rate and vibrations from the motor may have caused the cracking. Reproducibility was an ongoing problem. However, GIXRD

showed that the films were phase-pure and highly-oriented BiCuVOx. Because of the unpromising results, in addition to the expense of designing and building a proper dip-coating apparatus, we abandoned dip-coating in favor of spin-coating.

In spin-coating (Figure 6.8), excess precursor solution is dropped onto the center of the substrate, which is then spun around its center like a record. Centrifugal force and the balance of surface tension with the tendency to wet the substrate causes the solution to flow outward radially as the substrate begins to spin. As the substrate reaches its final angular velocity, the excess liquid runs to the edges of the substrate and flies off. As the film thins, the resistance to flow increases, and the evaporation of the solvent increases the viscosity of the liquid, until viscous drag balances the centrifugal forces. This results in a uniform film. If the spin-off speed is too fast relative to the evaporation rate, the liquid will fly off rather than coat the substrate. At the point when the centrifugal force and the viscous drag are equal, the rate of film thinning may be expressed by a differential equation with solutions in thickness (h) for three stages of spin-coating, one for during the initial solution spreading (Equation 6.4), one for the period during spin-off (Equation 6.5), and one for the final thinning during solvent evaporation (Equation 6.6).[21]

(6.4) $h(t) = h_0(1+4\rho\omega^2 h_0^2 t/3\mu)^{-1/2}$

(6.5) $h = (3\mu\varepsilon/2p_A{}^\circ\omega^2)^{1/3}$

(6.6) $h = (1-p_A{}^\circ/p_A)(3\mu\varepsilon/2p_A{}^\circ\omega^2)^{1/3}$

where h_0 is the initial film thickness (after spreading, prior to spin-off), μ is viscosity, ρ is density, ω is the angular momentum, t is time, p_A is the mass

of volatile solvent per unit volume (p_A° is the initial value of this) and ε is the evaporation rate.

Complications to thickness control include the influence of the gas flow dynamics on the evaporation rate, which, if too fast, may lead to the formation of a skin on the solution surface or to premature precipitation of the contents of the precursor solution. These cause inhomogeneity and cracking of the film, and are ideally prevented by maintenance of a controlled atmosphere in the spin-coating chamber. Too-fast spin-up of the substrate can lead to a radial "spoke" pattern caused by breakup of the wave front; this pattern may persist in the way the particles are packed in the coating. As with dip-coating, contamination will damage the integrity of the film produced in a spin-coating process.

We constructed a crude spin-coater from a centrifuge using a variable transformer to control the motor speed and calibrated the spin rate stroboscopically. This equipment worked well in terms of reproducibility and per-deposition film thickness, and was used for most of the depositions described in this Chapter.

6.1.2.4 Heat Treatment

The loss of solvent or volatile decomposition products of the precursor will leave holes in an already-formed film. This problem is exacerbated when several additional layers of film have been added on top of the one from which the decomposition gases are escaping. As a result, after each layer was deposited and air-dried, the substrate was placed onto a hot plate for initial decomposition

of the organic components of the precursor. The hot plate temperature was approximately 350 °C. DTA/TGA had shown (Chapter 4, Figure 4.10, 4.17) that the $Bi_2VO_{5.5}$ precursor was completely decomposed by approximately 430 °C; powder XRD on the $Bi_2Cu_{0.1}V_{0.9}O_{5.35}$ precursor suggested that it was mostly decomposed by 350 °C. There was sufficient precedent for this procedural step in the literature that we did not look into how failure to do this would affect the film quality. To give one example, it was found for PZT ($PbZr_{0.5}Ti_{0.5}O_3$) films on platinum that more efficient removal of the organics, e.g. by heating them at 400 °C rather than 275 °C prior to annealing, resulted in more uniform films.[24]

In most experiments, we also sought to form the γ-BiCuVOx phase in steps, e.g. after every five layers were deposited. This was done by a process of rapid thermal anneal (RTA),[14] in which the substrates were placed into an already-hot furnace. The furnace temperature was 450 °C, the lowest at which the γ phase was seen in the bulk experiments. After approximately ten minutes, the samples were removed and permitted to cool slowly (thick alumina slabs served as thermal sinks to modulate the cooling rate) in air before additional layers were deposited. Samples not subjected to this treatment often had the appearance of cracks in underlayers and showed agglomeration behavior (*vide infra*, section 6.3.1).

All samples were subjected to a final annealing step, which involved their being placed in furnace initially at room temperature, then ramped at 5 °C/minute to a set temperature for 4 or 8 hours (there did not appear to be a difference in film quality with the soak

time; early experiments used the longer period). The samples were cooled at a rate of 2°C/minute. Cooling rates faster than 5 °C/minute were associated with cracked films. Slower rates did not appear to make a difference in the film quality.

6.1.2.5 General Comments

A description of the chemicals and the general instrumentation used for the experiments described in this Chapter may be found in the Appendix to Part I of this thesis.

While E-beam depositions were conducted in the CMSE Fabrication Lab cleanroom, all sol-gel depositions, whether dip- or spin-coated, were carried out in a normal laboratory hood. Some precautions were taken to prevent particulate matter from getting into the precursor solution or films. Substrates were handled with forceps after cleaning or other preparations were complete. After mounting the substrate in the spin-coater, the sample was blown with Aero-Duster™ and the cover of the spin-coater lowered; the precursor solution was drawn into a syringe, and passed through a filter disc as it was deposited onto the substrate through a hole in the spin-coater cover. This method was found to be satisfactory in preventing excessive particulate matter from getting into the films; in the absence of these precautions, ESEM revealed the films to be riddled with boulder-like dust particles and cracks around them.

Table 6.1: Lattice Parameters for various E-beam materials

Material	Lattice Type	Lattice Size (Å)	Face Diagonal (Å)	
Pt	cubic	3.923	5.548	
Al_2O_3	hexagonal	4.759x12.99	n/a	
Ag	cubic	4.086	5.779	
Au	cubic	4.079	5.769	
Al	cubic	4.049	5.726	
Ni	cubic	3.524	4.984	
WO_3	cubic	3.714	5.252	
MgO	cubic	4.123	5.831	
YSZ (15%)	cubic	5.139	7.268	
BiCuVOx	tetragonal	3.92x15.45	5.54	5.15*
BiNbVOx	tetragonal	3.91x15.75	5.53	5.25
BiTiVOx	tetragonal	3.93x15.44	5.56	5.15
BiMnVOx	tetragonal	3.92x15.49	5.54	5.16
BiFeVOx	tetragonal	3.94x15.46	5.57	5.15

* 1/3 of the **c** parameter

Figure 6.1: Effects of the preparation steps on the quartz substrates. (a) Quartz substrate cleaned with acetone and 48% HF solution as described in the text. The large white object is a dust mote. X 865. The cleaning steps used for the depositions described in the text do little or no gross surface damage to the quartz. (b) Quartz substrate sonicated 5 min. in 48% HF solution. X 940. The damage to the substrate is clear.

(a)
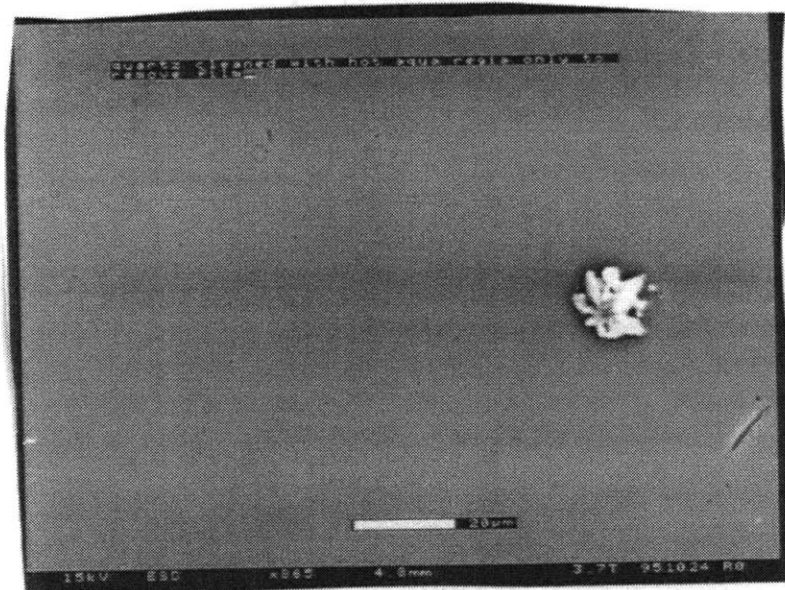
(b)
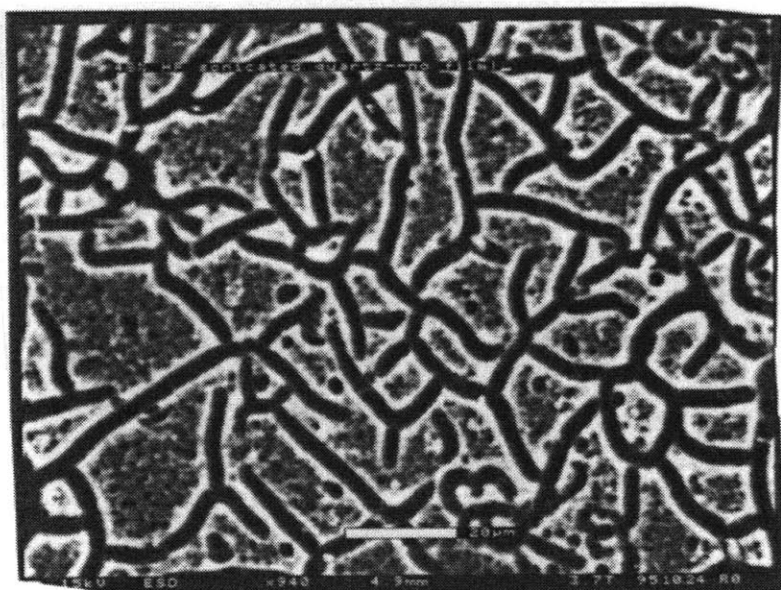
Figure 6.2: BiCuVOx film on a platinum sheet. The two objects near the top are dust motes; the "canals" are due to wrinkles on the metal sheet. X 1350.
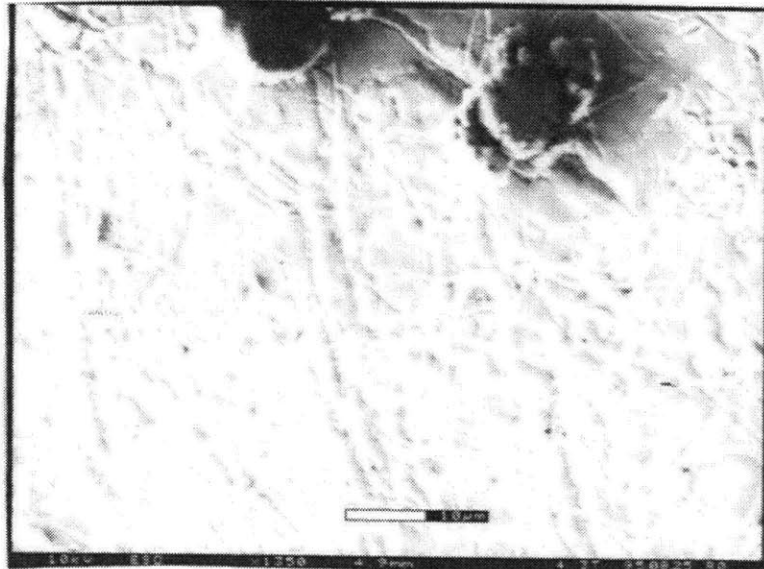
Figure 6.3: Platinum film deposited onto quartz by E-beam. The dark area is bare substrate created by masking the quartz. The large white spot at center is a dust mote. X 8050.
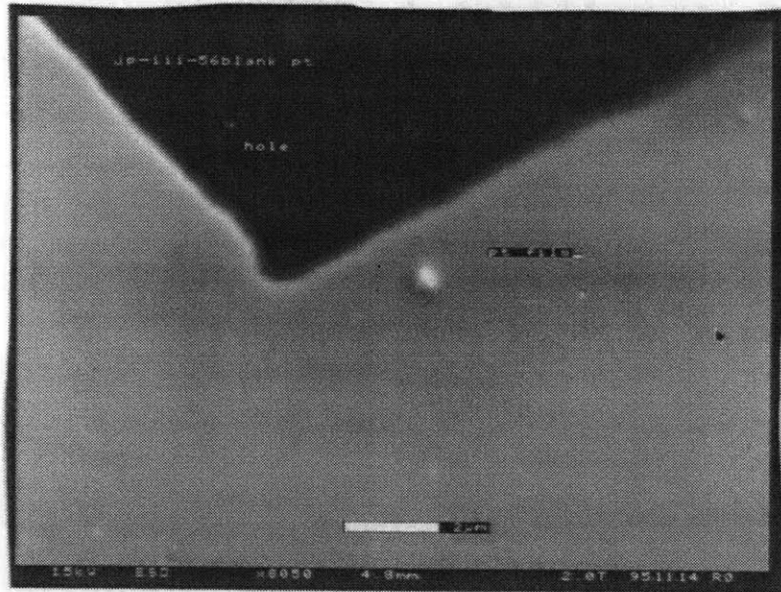
Figure 6.4: Grazing incidence X-ray diffraction pattern (GIXRD) of the E-beam deposited Pt films on quartz. Grazing angle is 1°. The Ti underlayer does not show through the 1000 Å Pt layer. Note that the Pt peaks (marked with lines) are slightly offset due to improper alignment of the sample in the X-ray beam.
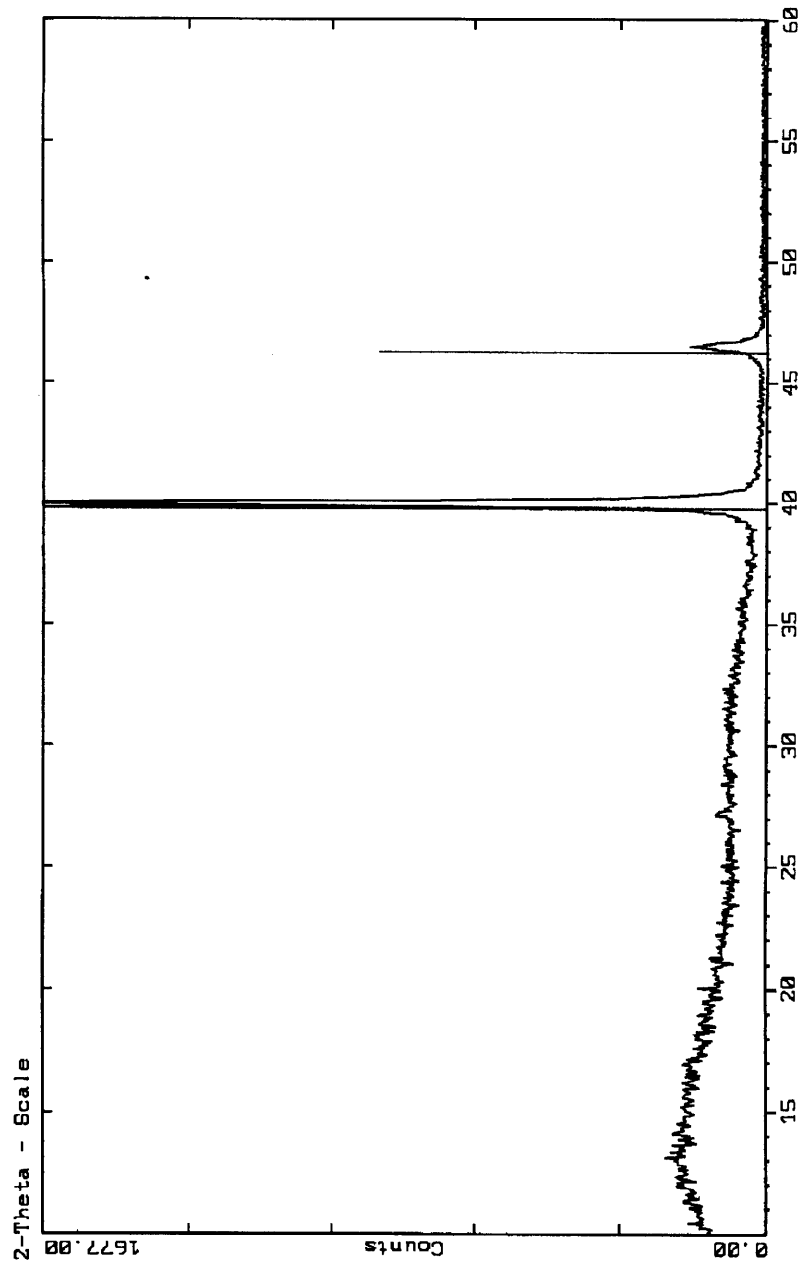
Figure 6.5: (a) Porous alumina (Whatman brand Anodisc™) filter used as a porous substrate. The white mass is dust. X 11500.
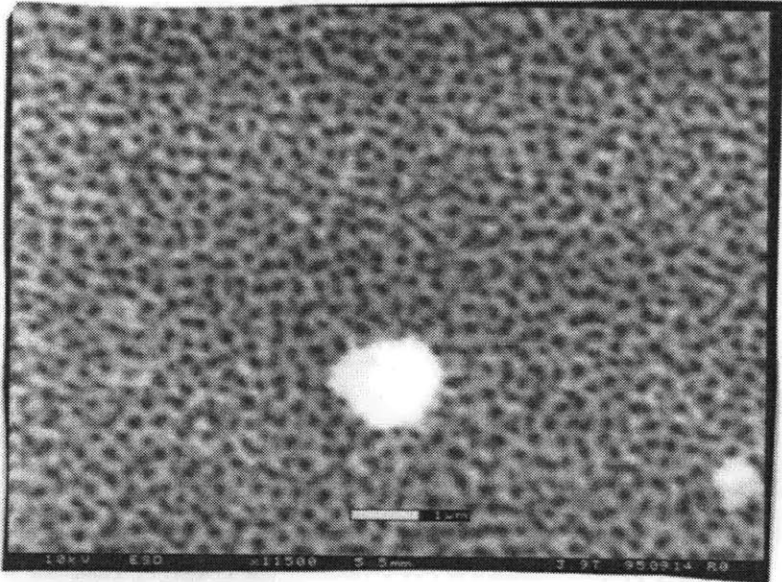
Figure 6.5, continued: (b) GIXRD of the porous alumina, with positions for Al_2O_3 (corundum) marked with lines. The amorphous appearance is due to scattering from the pores.
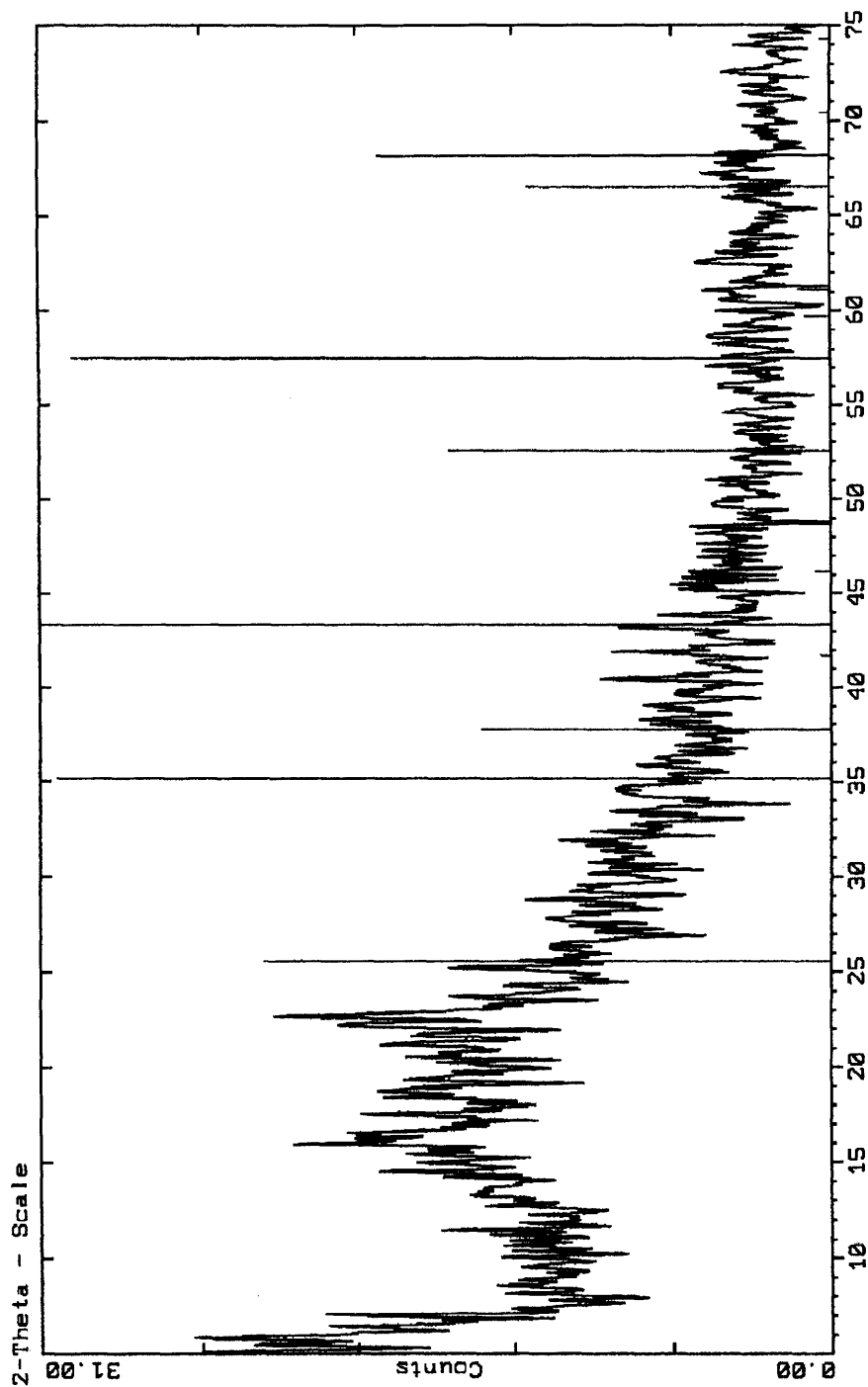
Figure 6.6: Cartoon of the dipcoating process. (a) Insertion of the sample into the precursor solution. (b) Solution begins to run off the substrate as it is withdrawn and (c) reaches a uniform thickness.

(a)   (b)   (c)
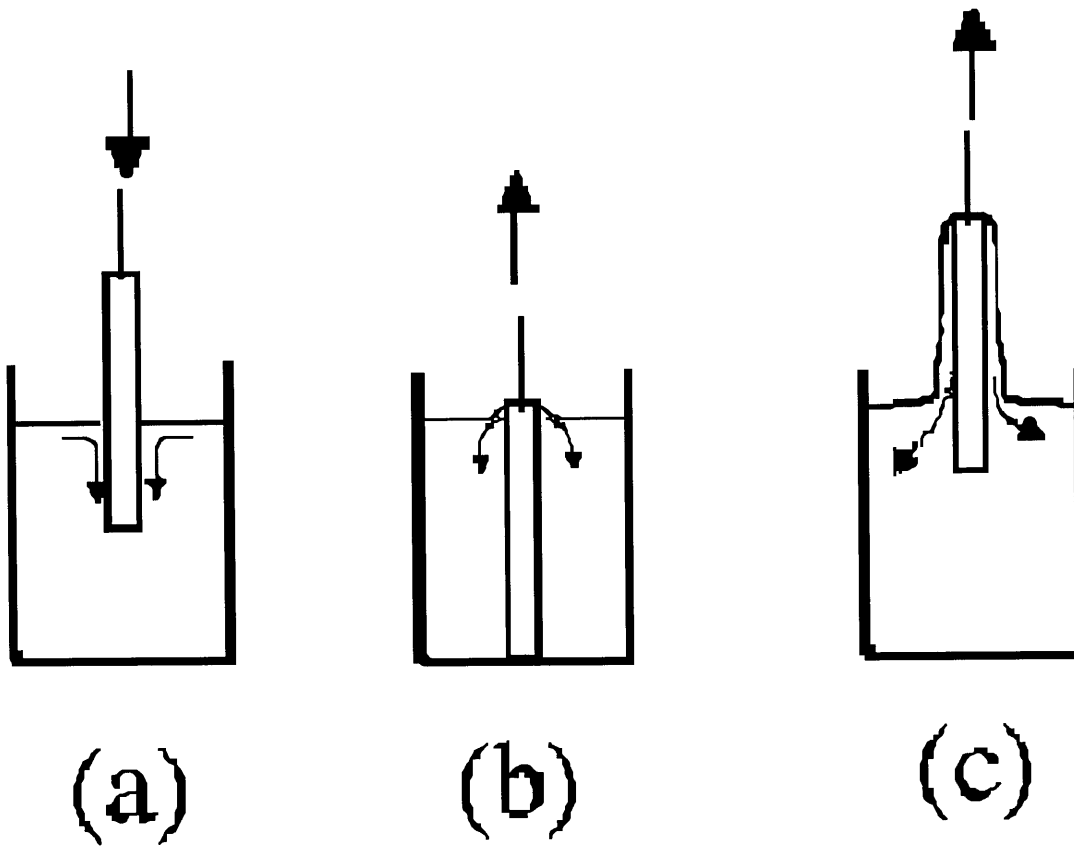
Figure 6.7: Home-made dipcoating apparatus. The switchable motor, mounted on the back wall of the housing, turns a gear. A toothed belt connects this to two other gears, which drive threaded rods. These spin freely, and a metal block with threaded holes moves up and down (depending on the motor direction) The substrate is attached to the block.
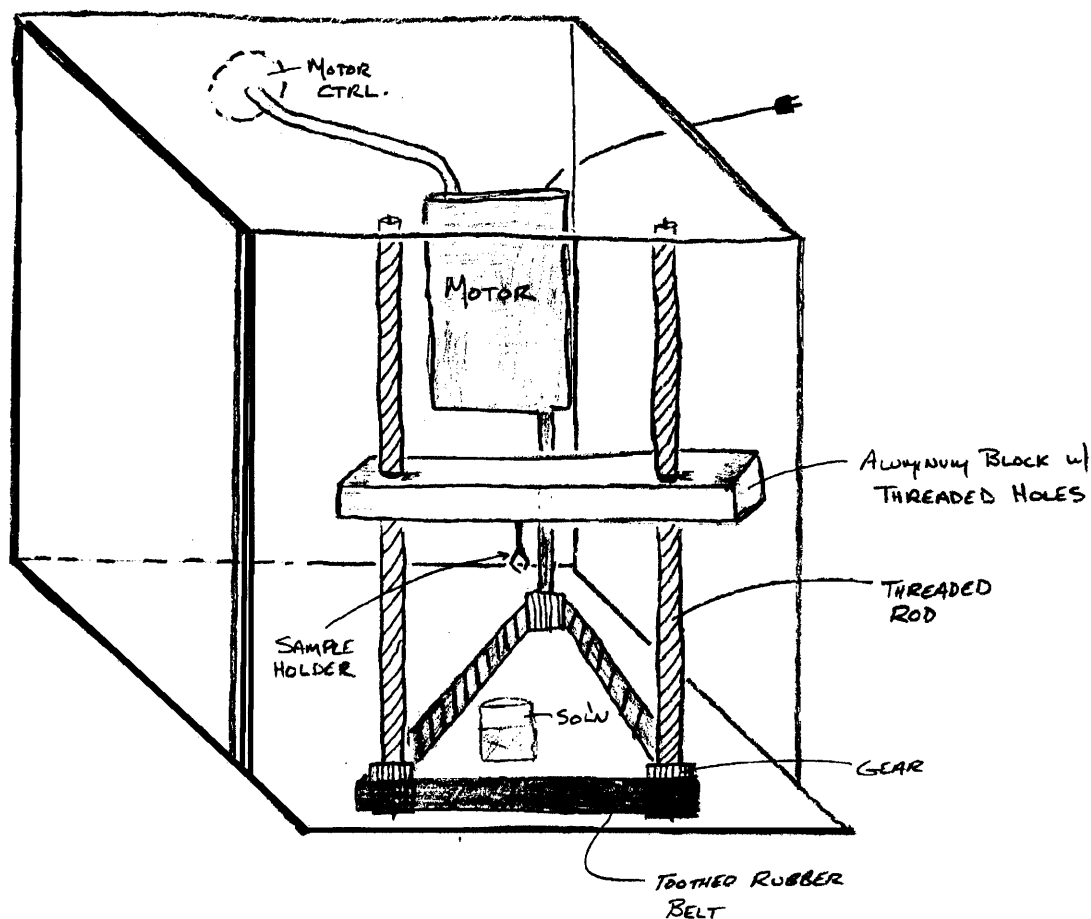
Figure 6.8: Cartoon of the spincoating process. (a) Precursor solution is dropped onto the substrate and spreads. (b) During spin-up, centrifugal forces thin the film. (c) Viscous drag balances centrifugal forces at a critical thickness to yield a uniform film, which (d) thins further as it dries.

(a)

(b)

(c)

(d)
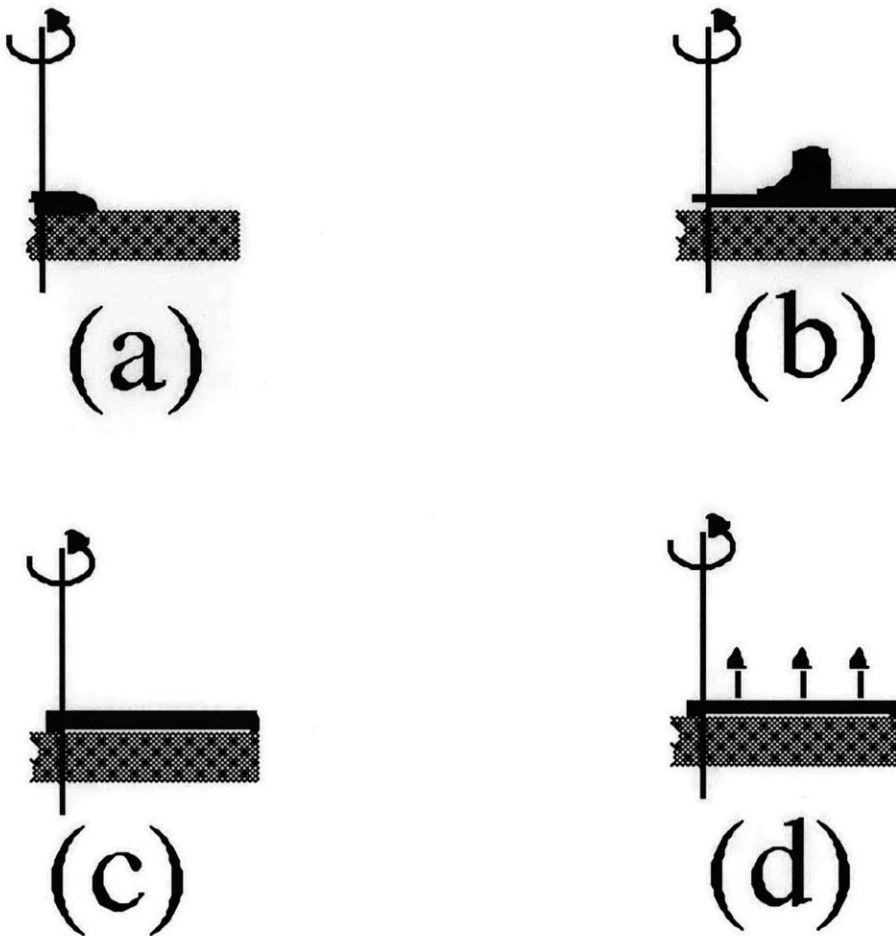
Figure 6.9: Cartoon showing the angles and dimensions for film grains on a substrate. See discussion in the text.
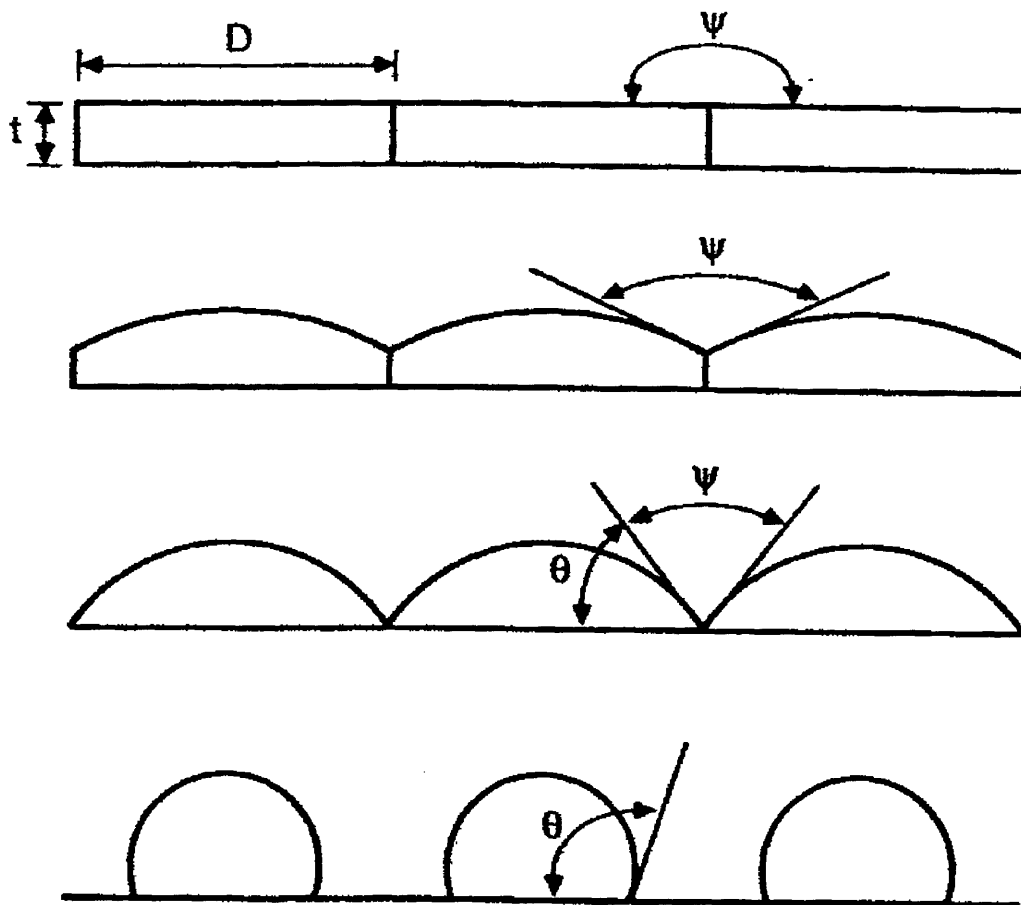
6.2 Background on Films

There is a wealth of information in the applied physics literature regarding the growth of vapor-deposited films of a variety of materials. On the other hand, there few studies of films which were deposited by the sol-gel method. Thus all of the discussion of the behaviors seen in the BiMeVOx films reported in this Chapter is based on studies of vapor-deposited films.

6.2.1 Modes of Film Growth

It is generally understood that there are three modes of crystal growth on a surface that can take place during physical or chemical vapor deposition processes.[25] In the Volmer-Weber mode, small clusters are nucleated directly on the substrate surface and grow into islands of the condensed phase; this occurs if the adatoms are more strongly bound to each other than to the substrate. In layer, or Frank-van der Merwe mode, the adatoms are more strongly bound to the substrate than to each other, so they initially form a complete monolayer on the surface, then a second layer atop that one. The Stranski-Krastanov, layer-plus-island mode, combines the two: after forming some monolayers, subsequent layer growth becomes unfavorable and islands form atop the layers below. Small imperfections in the surface of the substrate can strongly influence the binding of single adatoms or small clusters to the substrate and influence the adsorption, diffusion, and nucleation behavior of the growing film. The layer growth (Franck-van der Merwe) mode is what would be expected

for a situation where many of the adatoms are arriving at the substrate at once (high supersaturation).[25]   This is approximately what occurs in the sol-gel method.

Film growth can be considered to be a multi-stage process:[26] (1) nucleation, when clusters of solid begin to condense on the substrate at active centers (defects, impurities, etc.) on the substrate surface; (2) crystal (grain) growth as nucleated clusters join; (3) coalescence, during which the intergrain area develops and the coalescing crystals influence the reorganization of the film structure; and (4) secondary nucleation, growth, and coalescence, during which stage the channels between the grains are filled, leading to the growth of a continuous film. The coalescence stages can be treated as sintering processes, but they may be incomplete, leaving an intergranular area containing defects or high- or low-angle grain boundaries. The effects of impurities or dopants become very important when their solubility in the primary material at the given temperature is not sufficiently high. In this case they can become segregated during the crystal growth and coalescence phases and move onto grain boundaries, where they can block surface self-diffusion and may change the surface free energy.[26] Thus the presence of a dopant may result in rounded crystals with broad, deep grooves between grains. In the extreme case, islands of the primary material, separated by the bare substrate, form and remain separated by grain boundaries coated with impurity/dopant. Liquid-like coalescence tends to occur with small crystals and often leads to the development of crystal lattice orientation

("texture").[26,27] The grain size and the texture are partially controlled by the presence of impurities or dopants.[28]

6.2.2 Defects in films

As discussed in the section above, one of the major contributors to defects in thin films is the presence of contaminants or poorly-soluble dopants which may segregate to grain boundaries and prevent grain coalescence. The inhomogeneity created by surface segregation of contaminants has a high relative effect on the material properties of the film because the number of atoms at the surface of a grain is a large percentage of the total number of atoms in the grain. Thus surface segregation modifies the bulk concentration as well because there is not a large reservoir of bulk material to make up for the local inhomogeneities. Surface segregation can be predicted to some degree, and is a function of film thickness, average composition, heat of segregation, and the temperature.[29]

A more severe case of the grain boundary grooving seen with surface segregation of impurities occurs when the film agglomerates. In this instance, the initially continuous film "dewets," or uncovers, the substrate. The process is driven by the surface tension of the film material and by stresses and strains within the film. Agglomeration begins with the formation of a hole, which exposes the substrate; the hole then grows. Defects in the film are therefore critical in the inception of agglomeration. Tensile stresses (strains) within a film lead to agglomeration, while

compressive stresses lead to hillock formation; however, from a hillocked film, agglomeration may still occur as the hillock gains more and more matter from the surrounding area, leaving it bare of film. The free energy per unit area of film (g) is the energy of the film-vapor interface (γ_{fv}) plus that of the film-substrate interface (γ_{fs}). (Equation 6.7)

(6.7) $g = \gamma_{fv} + \gamma_{fs}$

If the energetics of the film agglomeration are controlled only by isotropic interface energies, the equilibrium morphology will have a constant curvature – i.e. flat or spherical cross-sections. The stability of an island morphology (spherical cross-sections) is determined by how well the film wets the substrate and measured by the contact angle θ between film and substrate. This is a function of the interface energies, so the minimum thickness for a stable film increases with decreasing wettability. The stability condition is expressed by Equation 6.8. The island radius r in this equation is determined kinetically in PVD films, while a sol-gel film's island radius may be determined by the precursor morphology.

(6.8) $r/t > (3 \sin \theta/(1-\cos \theta)$

in which r is the radius of the island (=D/2) and t is the thickness of the original film.[30] (Figure 6.9)

An initially flat surface with positive surface tension will not spontaneously form holes. The usual source for the nucleation of holes is grain boundary grooving, which is most severe where three

grains intersect. In general, grain boundary grooving and the subsequent formation of holes is a consequence of the competition of adjacent grains for the material between them. Smaller grains have a higher surface curvature (higher chemical potential) than do large grains, so polycrystalline films are nonequilibrium systems: the small grains lose matter to larger ones and thin in the direction normal to the substrate.[31] Grain boundary grooving is exacerbated when surface-segregated dopants or contaminants prevent grain coalescence. Pinholes from dust particles and other contaminants also form potential points for hole nucleation. Holes will grow only if they are larger than a critical radius r_c. (Equation 6.9)

$$(6.9) \quad r > r_c = h\gamma_{fv}/(\gamma_{fv} + \gamma_{fs} - \gamma_{sv}) = t/(1-\cos\theta)$$

The behavior of holes that do form depends therefore on the assorted interfacial energies. When $\gamma_{sv} > \gamma_{fv} + \gamma_{fs}$, r_c becomes infinite and the hole will shrink: the film wets the substrate well. When $\gamma_{sv} < \gamma_{fv} + \gamma_{fs}$, then $\theta > 0$ and the film only partially wets the surface. In this case, holes where $r > r_c$ will grow.[30]

Film stresses contribute to the initial formation and growth of holes, whether these stresses arise from lattice misfits, thermal expansion mismatches, or from the growth process, including phase changes. Misfit strains will increase the stability of islands over that of the continuous film. When hole nucleation arises through grain boundary grooving, there is an incubation time for agglomeration.[30] This incubation time depends on the film thickness. If the grain size is several times larger than the film thickness little grain growth

occurs on annealing because of grain boundary grooving. If a grain is under lower compressive stress than the surrounding grains, atoms diffuse into it, leading to hillock formation. On the other hand, a grain with lower tensile stress will lose material to grains with higher tensile stress, leading to a hole in the film. In compressively stressed samples, therefore, hillock formation often precedes agglomeration.[30] The formation of a hill around the atom source (hole) is typical. Holes, once formed, grow and collide, leading eventually to the formation of islands.

Finally, fractures may occur in films having either large-scale contamination (e.g. dust particles), or having stresses or strains arising from inhomogeneities in the film density, thermal expansion coefficient mismatch, or from mismatch between the film's crystal lattice and that of the substrate. Where radial cracking has occurred, it is centered on a dust particle or a region of higher film density. During sintering the lower density matrix surrounding the defect shrinks away from it. Circumferential cracking is seen when the central lower density region pulls inward from the higher-density matrix in order to sinter.[32] (Figure 6.10a) Strains in the film occur when the substrate lattice is larger than that of the film, or when the substrate has a higher thermal expansion coefficient than the film. The film under such strains appears to have been "pulled apart." In the opposites of these cases, stresses in the film cause an appearance of having been "pushed together," with plates of the film piling one atop the other. (Figure 6.10b)

6.2.3 Texture development

Little or no information is available in the literature regarding the development of orientation (texture) in sol-gel deposited films. This is curious, since oriented films of dielectrics, ferroelectrics, and superconductors ($Bi_3Ti_4O_{12}$, $PbZr_{0.5}Ti_{0.5}O_3$, $YBa_2Cu_3O_{7-\delta}$ etc.) are highly desirable to the electronics industry.[33,34] For vapor-deposited films, nucleation is not orientation-selective during the deposition, but grain growth may be orientation-selective. When the film wets the substrate fully, oriented or epitaxial growth is usually promoted by a substrate with a lattice matching that of the film. In this context, a "lattice match" is not necessarily a direct correspondence, say, between the film and substrate **a** and **c** parameters, but can be an overlap in the periodicity of the electrostatic charge pattern.[34] Conversely, if the substrate is amorphous, it is surface energy minimization that drives texture uniformity (all grains having the same planes parallel to that of the film). Differential thermal expansion during heating leads to high biaxial strain in a film, so strain energy minimization may occur during grain growth. Thus strain energy minimization and surface and interface energy minimization both favor the development of texture via preferred growth of grains with specific orientations; the interface energy, in particular, is a strong function of the crystallographic orientation of the grain.[27] For films that do not wet the substrate well, texture development occurs during coalescence or thickening of the films.

Slight changes in the film composition can greatly change the texture development of the film. For example, in YBCO films E-beam

deposited onto $SrTiO_3$ substrates at low temperature showed strong a-axis orientation (i.e. a-axis normal to the substrate), while those produced at high temperature gave little or no orientation. A slight change in composition (Ba-rich and Cu-poor) gave c-axis oriented films.[35]

6.2.4 Effects of Sol-Gel Precursor Variation on Film Morphology

In sol-gel films, the morphology prior to the inception of any of the film growth processes discussed above is influenced by four major factors: (1) the kinetics of the loss of organics during solidification, (2) the quantity of organics remaining in the film prior to crystallization, (3) the homogeneity of the components within the film, and (4) the structure and rigidity of the polymer prepared in solution. The first two factors are primarily controlled by choosing the ligands on the metals to be hydrolyzable into volatile components, which will evaporate out of the film at a relatively low temperature, or by the use of ligands that decompose cleanly at low temperature, leaving little carbonaceous residue. Heating steps prior to the film crystallization and annealing heat treatment can help reduce organic residues, as discussed above (Section 6.1.2.4). Aging the solution after hydrolysis also reduces the carbon formation in the pyrolyzed film.[19] Finally, the use of a thin coating and a low heating rate to permit oxygen diffusion into the film to burn off organics cleanly will also reduce the amount of carbon formation.

During sol-gel processing the metal alkoxide and/or salt components are homogeneously mixed on the molecular level; this state of affairs is maintained on hydrolysis, gelation, and pyrolysis. However, differences in hydrolysis rates, the limited solubility of one component in the others (preferential precipitation) and the separation of components during thermal processing due to the higher stability of a non-target phase at the lower temperatures, all may produce inhomogeneity. Such problems often are seen in $YBa_2Cu_3O_{7-\delta}$ sol-gel syntheses due to the insolubility of the copper alkoxides and the fast gelation rate of the yttrium alkoxides.[36] Complexing additives like carboxylic acids, amines, diols and alcohol-ethers, and acetylacetonate have been known to help maintain homogeneity in a number of sol-gel systems by coordinating to the metal centers, modulating the hydrolysis rate. However, these additives may disrupt the formation of the M-O-M network because they do not hydrolyze off the metal nor contribute to the condensation reactions.

The morphology of the precursor in solution can affect several aspects of the pyrolyzed film morphology. As noted in Chapter Three, vanadium oxide gels yielding V_2O_5 on pyrolysis have a ribbon-like microstructure.[37,38] Passerini[39] found that rapidly spin-coated V_2O_5 films (3000 RPM) tended to be amorphous, with a uniform-appearing surface that revealed agglomerates at high magnification. The ribbons in these films were randomly oriented due to the high shear forces experienced by the gel precursor during spin-coating which disrupted ribbon self-alignment. The rapid evaporation of the solvent from the freshly deposited film prevents further reorganization. The agglomeration is due to the

363

random grain orientation: the grains could not coalesce into a continuous film. Conversely, in a dip-coated film the V_2O_5 crystallites stacked with *001* perpendicular to the substrate, and films spin-coated at a slower 1750 RPM had the V_2O_5 crystallites preferentially oriented with *001* parallel to the substrate. This is opposite to what we found, i.e. that dip-coated films were less oriented than those spin-coated at approximately 3000 RPM.

The relative rates of hydrolysis and condensation of the precursors in solution may affect the film morphology – primarily the porosity – by changing the ability of the gel oligimers to pack together tightly as the gel becomes densified. Film precursor solutions are dilute, so individual species are at most weakly interacting. During deposition drying, the rapid increase in concentration forces the precursors close to each other. Evaporation (during which the structure compacts and becomes "frozen" in position) competes with continuing condensation (which stiffens the structure against further compacting). The deposition method puts a shear stress on the film and shrinkage during the removal of solvent and continued condensation puts tensile stresses on it as well.

The degree of interaction between species in the precursor solution, and the amount of compaction expected from them, has been studied at some length using fractal concepts to make sense of small-angle X-ray scattering (SAXS) data. SAXS is the X-ray scale equivalent of Rayleigh scattering, in general terms. In SAXS, the dependence of the scattered beam intensity on the scattering wavevector K, defined in Equation 6.10, leads to the fractal dimension D. This latter value relates the mass (M) of an object to

its radius according to Equation 6.11. Euclidian objects (e.g. not fractal) have D=4, but fractal structures have lower values which depend on the degree of branching in the structure. A random walk-type structure, for example, would have D=2.[18] Fractal objects are the type that come about in sol-gel precursor solutions. Those objects for which Equation 6.11 applies are mass fractals. Others, which are uniform on the interior and ramified on the surface, scatter X-rays only from the surface; for these objects, a surface fractal dimension may be defined.[40]

(6.10a) $I(K) \propto K^{-D}$

(6.10b) $K = 4\pi/\lambda \sin \theta/2$

λ = wavelength of the incident beam, θ = scattered angle

(6.11) $M \approx r^{D}$

The mass fractal dimension of the precursor oligimers in solution can be directly related to their ability to interact and pack tightly. Mandelbrot[41] shows that for two fractal structures of radius R placed next to each other, the number of times ($I_{1,2}$) an "arm" of one intersects an "arm" of the other goes according to Equation 6.12. Intersections represent a lost opportunity for mutual interpenetration by the fractal objects.

(6.12) $I_{1,2} \propto R \exp (D_1 + D_2 - d)$

D_1, D_2 = mass fractal dimensions of the structures 1, 2;
d = the dimension of space (=3)

It can be seen from Equation 6.12 that if $D_1+D_2 < 3$, the probability of intersections decreases as R increases, and there is a situation of "mutual transparency," where the two objects may interpenetrate extensively. If $D_1+D_2 > 3$, on the other hand, the probability of intersection increases with increasing R (e.g. less interpenetration). Depending on the condensation rate, there is a given probability that intersections will lead to the "sticking" of two precursor polymers. This probability depends on the chemical identities of the precursor structures. If the sticking probability is high, the structure will be more porous because the cluster interpenetration is inhibited; if the sticking probability is low, few intersections result in sticking, and the precursors interpenetrate to give denser structures. Brinker found that weakly branched, compliant structures interpenetrate and rearrange until the solvent is removed, giving an efficient packing and high density.[18] Highly branched and rigid precursor clusters, on the other hand, do not interpenetrate and do not collapse under capillary drying forces, leaving pores. Likewise, branched precursors that stick irreversibly form non-uniform rigid structures and have an associated porosity. Because individual cluster density decreases with the distance from the center of mass, the porosity of noninterpenetrating clusters increases with increasing cluster size.

Controlling the structure of the oligimers in the precursor solution is well-understood for the hydrolysis of alkoxysilane solutions. Increasing the water of hydrolysis when preparing a siloxane solution improves the wetting behavior of the solution on many substrates, and such solutions yield films that readily densify on heat treatment due to the superior wetting. Acid catalysis of

366

tetraethoxysilane (TEOS) solutions leads to a linear polymer structure.[16] Within this regime, it has been found that the ratio of hydrolysis water to TEOS is important in determining the shape of the polymers. Where $W=[H_2O]/[TEOS]$, $W=1-2$ leads to long linear polymers. At $W=5$, spherical polymer growth begins, and by $W=20$ spherical or three-dimensional growth of the polymers predominates.[20] Linear particles, therefore, were best obtained with acid catalysis and a small amount of water ($W < 4$).[42] Additives likewise may have an effect on the oligimer structure: in tetramethoxysilane (TMOS) gels, SAXS scattering developed rapidly in the presence of acid catalysts and in the absence of formamide additive.[43] Formamide acts by slowing hydrolysis and speeding condensation. In a regime where hydrolysis occurs rapidly, monomers are more likely to be hydrolyzed than are sites already on clusters, and the monomers are therefore incorporated into the clusters. Less branching occurs as the growth occurs from monomers which are partially hydrolyzed. On the other hand, as polymerization continues, eventually monomer-cluster growth shifts to cluster-cluster growth, and because clusters are somewhat mutually opaque, this leads to ramified structures.[40]

Metal alkoxides can be expected to behave similarly, though there are fewer literature reports regarding them. A diluted and unrestricted hydrolysis of metal hydroxides leads to spherical polymers with a network connectivity (c) (a smaller connectivity value corresponds to a more open network) that follows Equation 6.13.[44] The quantity of hydrolysis water affects the chemical makeup of the product by producing a higher M-O-M content. The

increase in connectivity gives a tighter network that retains its shape on the removal of organics, and therefore remains porous; less-hydrolyzed, looser networks collapse when the organic groups are removed during pyrolysis.

(6.13) $c = 4 - (36\pi/n)^{1/3}$

n is the number of hydrolyzed groups

6.2.5 The Role of Additives

The cracking of films may be controlled by the addition of drying control chemical additives (DCCAs) to the precursor solution. The DCCA is usually added in an amount comparable to the amount of silicon alkoxide when it is functioning to control capillary forces developed as solvent evaporates out of pores in the gel matrix.[16,45] To what extent this model can be transferred to the situation of a thin layer of gel that makes up a film is questionable.

DCCAs also replace alcoholic ligands on transition metals and silicon and stabilize them. Small quantities of DCCAs such as glycols or ethanolamines suppress the precipitation of oxides in metal alkoxide solutions.[46] Dimethylformamide has also been used.[45] Zirconium butoxide-containing precursors have been stabilized using acetylacetonate.[47] In synthesizing $YBa_2Cu_4O_8$ by a sol-gel procedure it was found that the homogeneity of the material was greatly dependent on the additive, which was used in a ratio of 0.44 mole additive to 1 mole copper. Tartaric acid prevented segregation of the metal acetates and gave a single 124 phase, as

did 1,2-ethanediol. The other additives tried, ascorbic acid, citric acid, poly(vinyl alcohol), and succinic acid, gave the 123 phase ($YBa_2Cu_3O_{7-\delta}$) plus $BaCuO_2$ and CuO: they failed in preventing metal segregation. EDS showed that the precursor powders were inhomogenous, and the fired samples followed suit.[48] Additives also may affect the pyrolyzed film morphology, as seen with zirconium oxide coatings: those prepared from a precursor containing acetylacetonate had 1 μm crystallites on quartz, while 0.5 μm crystallites were obtained from a solution containing triethanolamine. Only diethanolamine additive led to a hard, dense, and smooth ZrO_2 film.[49]

The DCCAs act in these instances by coordinating with the metals either alongside or by displacing the original alkoxide ligands. In zirconium oxide solutions stabilized by acetylacetone, the chelation of the additive was shown by the observation that the p-p* transition shifted to longer wavelength. Hydrolysis of the chelated ligand began when over three equivalents of water had been added; otherwise, the butoxy groups were hydrolyzed first, in accordance with the partial charge model.[47]

In this model by Livage and Henry[50,51] nucleophilic attack of a metal alkoxide by a molecule XOH (e.g. hydrolysis (X=H), condensation (X=M), or chemical modification (X=R′) is described as a three step process. (1) nucleophilic addition of XOH onto the positively charged metal (Equation 6.14), (2) proton transfer from the entering molecule to the leaving alkoxy group (Equation 6.15), and (3) departure of the positively charged protonated group. (Equation 6.16)

$$\text{(6.14)} \quad \overset{\delta-}{\text{X}}\text{-}\overset{\delta+}{\text{O}}\text{H} + \text{M-OR} \longrightarrow \overset{\delta-}{\text{X-O-M-OR}}$$

$$\underset{\overset{|}{\text{H}} \;\; \delta+}{}$$

$$\text{(6.15)} \quad \text{(product from 6.14)} \longrightarrow \overset{\delta+ \; \delta+}{\text{XO--M--ROH}}$$

$$\text{(6.16)} \quad \text{(product from 6.15)} \longrightarrow \text{XO--M + ROH}$$
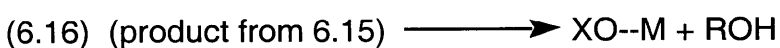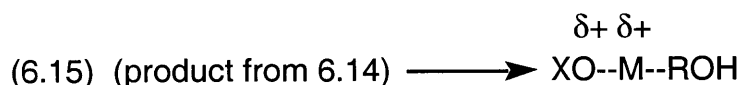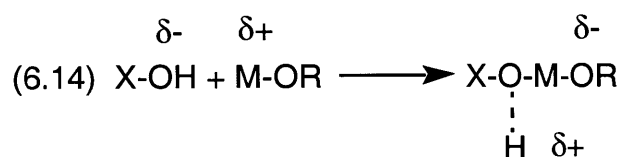
The process depends on the charge distribution in the alkoxide and in the transition state (product of Equation 6.14). In the partial charge model, the electronegativity of an atom χ_i varies linearly with its partial charge δ_i, and electron transfer ends when all electronegativities reach a mean electronegativity χ_m given by Equation 6.17. The partial charge δ_i on each atom is given by Equation 6.18. This model deals only with the enthalpy changes involved in the chemical reactions, and does not account for entropic, steric, or resonance stabilization contributions to the reactions.

$$\text{(6.17)} \quad \chi_m = \left(\Sigma_i \; p_i (\chi_i^0)^{1/2} \right) / \left(\Sigma_i \; p_i / (\chi_i^0)^{1/2} \right)$$

$$\text{(6.18)} \quad \delta_i = (\chi_m - \chi_i^0)/k(\chi_i^0)^{1/2}$$

where the molecule's atom (X_i) count is given by ($p_1 X_1 * p_2 X_2 * ... p_i X_i$) and k is a constant depending on the electronegativity scale used (k=1.36 for Pauling's scale).

These equations can be used to calculate the charge distribution on atoms of the transition state (product of Equation 6.15). Groups that remain negatively charged will remain coordinated to the metal, while those that are positively charged will be good leaving groups. This information can be used, in turn, to predict the outcome of chemical modifications (e.g. will the additive substitute for one of the alkoxy groups), as well as hydrolysis reactions (which additive will hydrolyze off first). For example, the model can be used to explain why addition of acetic acid to a TEOS solution reduces the gelation time,[52] while it prevents precipitation and increases the gelation time in Ti(OnBu)$_4$ solutions. Titanium in the tetrabutoxide, according to the model, has a high positive charge ($\delta = +0.61$). On addition of acetic acid to make a transition state Ti(OnBu)$_4$(HOAc) the HOAc becomes negatively charged ($\delta = -0.7$) while HOBu becomes positively charged ($\delta = +0.1$). One alcohol molecule is thus removed, leading to Ti(OnBu)$_3$(OAc). Experimental data confirms these predictions.[50] In Si(OEt)$_4$, on the other hand, the initial partial charge on Si is +0.32, leading to more weakly-associated transition state. The alkoxy group is only weakly positive ($\delta=+0.05$) and, though the acetic acid is negatively charged ($\delta=-0.53$), the drive toward loss of the ethoxy group is not very strong. Reflux of TEOS with HOAc does eventually provide a substituted compound.[50] On metals, acetate groups tend to act as bidentate ligands and are generally last to be removed on hydrolysis, in accordance with the partial charge model.[53]

The enol form of acetylacetonate is readily reactive with metal alkoxides and essentially inert to hydrolysis. Alkoxides of a number of transition metals, as well as of Al and Si, react with glycols, leading to glycolate derivatives in which two alcohol groups of the glycol are bound to the same metal. The chelate effect adds to the stability of such complexes against hydrolysis. The stabilization of the metal alkoxide against hydrolysis by organic additives prevents inhomogeneities from arising as one component of the precursor hydrolyses and co-condenses faster than the other(s). The additives also serve to modify the oligimer structures accessible in solution, leading to a change in the fractal dimension *versus* what would be the case in the absence of the additive. They act in this way by limiting possible sites for hydrolysis, thereby also limiting the degree of branching; furthermore, coordinated additives sterically block potential sites for condensation of hydrolyzed monomers or oligimers, again limiting the degree of branching and modifying the sticking probability.

Figure 6.10: (a) Circumferential cracking seen just to the right of the inset. Background is X 865, inset is X 6400 close-up on the grains not in the defect area. (b) Side-on view of a film showing cracking under compressive stress. x 1050.

(a)
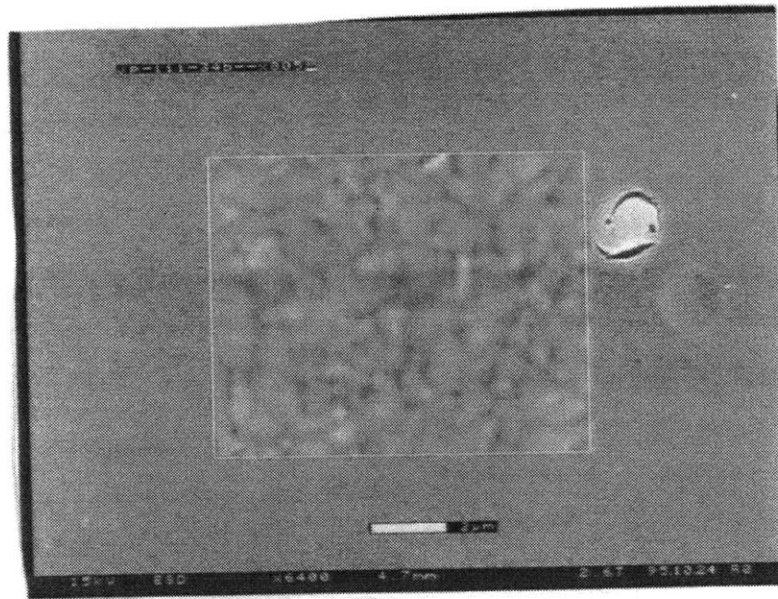
(b)
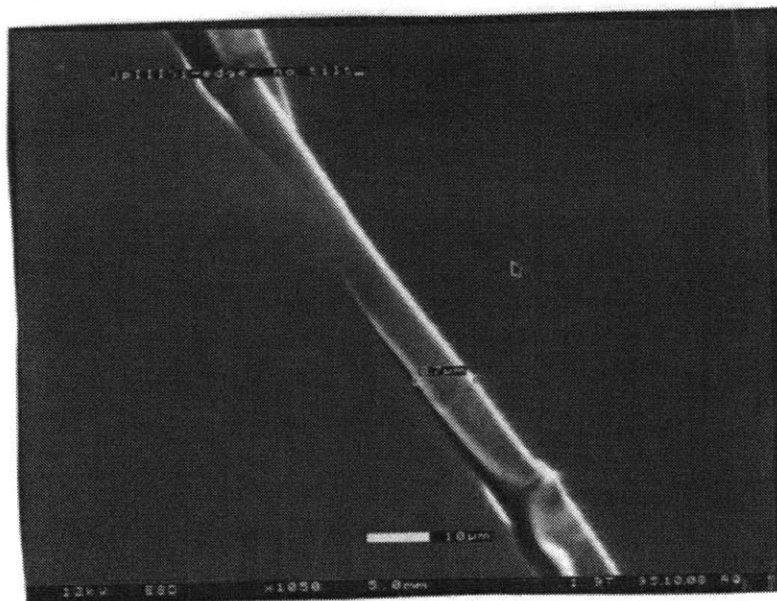
6.3 Results and Discussion – Smooth Substrates

6.3.1 Role of the substrate preparation

Initially, we attempted to deposit films of BiCuVOx onto quartz substrates as-received from the supplier. Samples which had been dip-coated showed a grainy first layer, and subsequent layers stress-cracked on heating. (Figure 6.11) Spin-coated films were also cracked or extremely grainy (Figure 6.12) for all deposition conditions examined. While the Figures show electron micrographs, the cracked nature of these films was visible under optical microscopy and in many cases to the naked eye. Later depositions were performed on quartz substrates which had been cleaned with hydrofluoric acid solution before use. Films deposited on such substrates were mainly uncracked according to electron microscopy were transparent and slightly colored, where the color was a function of the film thickness and angle of viewing. Films in excess of 1.5 µm thick were yellow in color. Those films which were of poor quality were, conversely, cloudy or opaque, and in many cases a crazing pattern could be seen under a low-power (x150) optical microscope. However, even these films appeared to be porous under ESEM.

The pores were assumed not to be due to the explosive departure of the organics from the film during pyrolysis, because if the pores had originated from a rapid departure of gas from a fully- or even partially-formed film, the edges of the pores would have been lifted out and away. However, high-resolution ESEM micrographs did not show this. (Figure 6.13) Despite this, the additional steps of pre-decomposing the film by placing freshly-

374

deposited and air-dried samples on a hot plate (350 °C), followed by a rapid thermal treatment at 500 °C (with some exceptions to the latter step) were put into the standard deposition procedure in the hope of removing a larger proportion of organics prior to film crystallization and annealing. Films produced in this way continued to have holes, according to ESEM micrographs.

We therefore considered that the pores in the films were arising from something inherent in the precursor itself. A V_2O_5 gel is composed of ribbon-like fibers, crosslinked and approximately 1 μm long. Such a cross-linked network of linear pieces densify to a porous film,[37,38,54,55] just as randomly piled sticks will form a stack with a large amount of void space. Certain other colloid particle morphologies are reported to lead to porous gels as well.[56,57] The precursor morphology may also be responsible for the film's *001* orientation as shear forces aligned the ribbons during spin-coating. Films which were spin- then dip-coated were not strongly oriented. (Figure 6.51)

We first attempted to remove the porosity by "annealing it out" – by raising the pyrolysis temperature to densify the film. BiCuVOx films were deposited onto a number of smooth metallic substrates to help determine the origin of the behavior seen on the quartz. Later work focused on changing the precursor particle morphology in the hope of getting a dense and pore-free film. BiCuVOx films were deposited onto a number of other smooth substrates to help determine the origin of the behavior seen.

It was hoped that bringing the film samples near the BiCuVOx melting point (determined by DTA/TGA) of 895 °C would increase the film grain mobility enough to close up defects in the film. BiCuVOx

precursor solutions containing no additives were spin-cast onto cleaned quartz substrates and heat-treated at 450, 550, and 650 °C. BiCuVOx films annealed at 450 °C were homogenous and defect-free, but those heated at 550 and 650 °C exhibited grain formation with the appearance of voids. (Figure 6.14) GIXRD showed formation of the desired phase at 450 °C; crystallinity, as well as a strong 00l-texturing, developed further with increasing firing temperature. (Figure 6.15) This behavior is typical of all films cast. It was hoped that heating BiCuVOx films to still higher temperatures (750, 800, and 850 °C) would cause the films to anneal and regain homogeneity. However, these films remained agglomerated. (Figure 6.16) In addition, films heated to 875 °C demonstrated a drastic loss of crystallinity according to GIXRD, with the ingrowth of unidentified new peaks. (Figure 6.17)

BiCuVOx films were deposited by dip- and spin-coating onto platinum sheet samples and appeared smooth and elastic, with a high degree of preferential orientation. (Figures 6.18, 6.19) These experiments were later reproduced using as substrates quartz samples onto which a 1000 Å layer of platinum had been deposited by E-beam. The samples were heated at a number of different pyrolysis temperatures and found to remain smooth and defect-free over the entire regime of temperatures. Samples deposited onto silver substrates, conversely, were grainy in appearance and showed mainly Bi_2O_3 in GIXRD. The poor match between the BiCuVOx lattice and that of the silver is the likely culprit for the poor quality of these films. (Table 6.1)

One cause suggested for the agglomeration seen in the BiCuVOx films is the formation of intermediate molten or semi-liquid

phases during the annealing process. However, the agglomeration temperatures were well under the temperature at which BiCuVOx (895 °C) melts without evidence of decomposition, therefore low-melting phases would not have come about through decomposition of this phase – for instance, by sublimation losses of bismuth oxide — nor were other phases seen in the GIXRDs. Also, the BiCuVOx phase is completely formed by 450 °C, well below the melting points of oxides that may be intermediates (V_2O_5—690 °C, Bi_2O_3—825 °C, $BiVO_4$—880°C). Moreover, were the agglomeration due to the formation of intermediate or decomposition phases, it should have also occurred on the platinum. There was no indication in the GIXRDs that the bismuth oxide layer of the BiCuVOx had reacted with the quartz substrate, although the small degree of reaction necessary to alter the film-substrate interactions and cause agglomeration would have fallen below the GIXRD detection limits.

BiNbVOx precursor solutions were spin-cast onto quartz substrates using a procedure similar to that for the BiCuVOx films. Those heat-treated at 450 °C were homogenous and defect-free, and GIXRD showed the desired $Bi_2Nb_{0.3}V_{0.7}O_{5.5}$ phase, with preferred *001*-orientation. These films, contrary to what was observed with BiCuVOx films, remained homogenous, phase-pure, and mainly defect-free according to ESEM (some defects could be traced to dust contamination) to the highest heating temperature of 650 °C. (Figures 6.20, 6.21) BiNbVOx films cast onto platinum substrates (Figures 6.22, 6.23) were likewise defect-free.

While there are numerous reports in the literature regarding the phenomena of grain growth, hillock and void formation, and film agglomeration for films grown by physical deposition techniques,[25-

27,30 we have seen only one[58] corresponding published report on sol-gel films. Several reports of the behavior of sol-gel films on thermal cycling have focused on cracking due to thermal stresses.[8,9] However, it may be instructive to examine our observations in light of the agglomeration seen in some films deposited by physical methods (electron-beam evaporation, ion-implantation, sputtering, PVD).

Film agglomeration, or de-wetting, is associated with stresses in the film parallel to the substrate, or with defects in the film providing nucleation points for holes.[30] Stresses are typically due to thermal expansion mismatch and lattice mismatch. Since, however, the quartz substrates are amorphous, lattice mismatch should not be at issue in our study. Likewise, thermal expansion mismatch between the quartz and the BiCuVOx film is unlikely to be the cause of the agglomeration, since the BiNbVOx films on quartz did not show agglomeration on heating to the same temperatures. BiNbVOx is expected to have a thermal expansion coefficient close to that of BiCuVOx, although no measurements of either value have been made. Finally, the fact of the non-agglomeration of the BiNbVOx films contradicts explanations of the BiCuVOx agglomeration which involve the formation of other phases or reaction with the substrate. These arguments suggest that the explanation for the agglomeration of the BiCuVOx films at temperatures where BiNbVOx films remained defect-free, lies either in the energetics of the film-substrate interaction or in the precursor morphology.

The relative energies of adhesion of the film with itself (surface tension) and the film with the substrate vary with the

378

elemental composition of the ceramic film.[25,26,30] Therefore, one reason for the difference in the annealing behavior of the 30% Nb-doped and the 10% Cu-doped films lies in the relative strengths of the films' adhesion to the substrate versus their self-adhesion. A second explanation may lie in the differences in precursor morphology due to the different methods of introducing the dopant. In the case of BiNbVOx, the dopant is added as a hydrolyzable alkoxide which is easily incorporated into the growing vanadium oxide polymer. Conversely, the $Cu(OAc)_2$ dopant may not be homogeneously distributed in the precursor material, and copper atoms are therefore more likely to segregate to grain surfaces. Segregation of impurities—either the dopant metal or organics remaining from the precursor—onto grain surfaces may block grain growth and coalescence and contribute to the formation of grooves which subsequently deepen to expose bare substrate.[26] The initial grain size—which depends on the metal-oxide polymer cluster size and morphology—can also contribute to the ease of void formation, as smaller grains lose matter to larger grains.[30] This material loss will be normal to the substrate and eventually will result in the formation of voids in the film. This occurs when the degree of spheridization (ψ) (Figure 6.9) of the grains is greater than a critical value (ψ_{crit}) which is related to the ratio of the grain size (D) and the film thickness (t) according to Equation 6.19.[58]

(6.19) $D/t = 4 (1+ \cos \psi_{crit}) / (\pi - \psi_{crit} - \sin \psi_{crit})$

(See Figure 6.9 for an explanation of the variables.)

The degree of spheridization ψ is determined by the balance of interface energies between film and vapor, film and substrate, vapor and substrate, and grain boundaries. These interface energies are a property of the film and the substrate.

Consideration of the total free energy of the surfaces and interfaces enables the location of an energy minimum as a function of the degree of spheridization ψ. Miller et al.[58] found that for grain size-to-film thickness ratios of D/t $<=$ 8/π, the continuous film is the most stable configuration for all values of ψ. For D/t $=>$ 13.3/π an island morphology is the most stable state, regardless of the value of ψ. D/t ratios between these values have metastable states whose fate depends on ψ. Further calculations permit the development of a phase diagram relating the film morphology to the D/t and the wetting angle θ.[58] (Figure 6.24)

To further investigate the behavior of BiMeVOx films on smooth substrates, BiCuVOx, BiNbVOx, BiTiVOx, BiFeVOx, and BiMnVOx films were deposited onto quartz, platinum, and alumina substrates and heated at either 450 °C or 650 °C. The lower-temperature samples, after examination by GIXRD and ESEM, were heated a second time, now at 750 °C. (Figures 6.25-6.30) The Nb- and Ti-containing films were smooth and unagglomerated on both quartz and platinum (although hillocks and pores were formed) at 650 °C, while the Cu-, Fe-, and Mn-doped films were agglomerated on the quartz slides but smooth (with hillock formation) on the platinum. The films on alumina followed a similar pattern. All films were heated again at 750 °C and showed cracking and agglomeration. GIXRD of all these films showed a strong *001*

orientation. (Figure 6.62) The experiment that would clarify the relative roles of the dopant identity and the method of adding the dopant (alkoxide or organic salt) – namely, to cast films of, say, BiNbVOx on quartz using a precursor solution made from $Nb(OAc)_5$, or of BiCuVOx on quartz using a precursor solution containing $Cu(OR)_2$ – was not done.

Figure 6.11: BiCuVOx film dipcoated onto a quartz slide as received from the manufacturer. X 545.
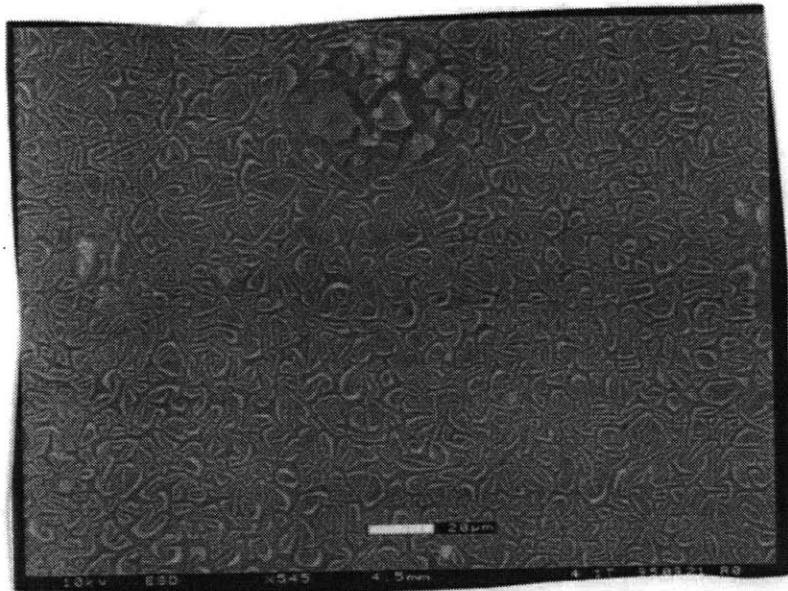
Figure 6.12: BiCuVOx films spincoated onto quartz slides as received from the manufacturer. (a) X 2200, (b) X 6250. Note the large-scale cracking due to the film's failure to adhere to the substrate.

(a)
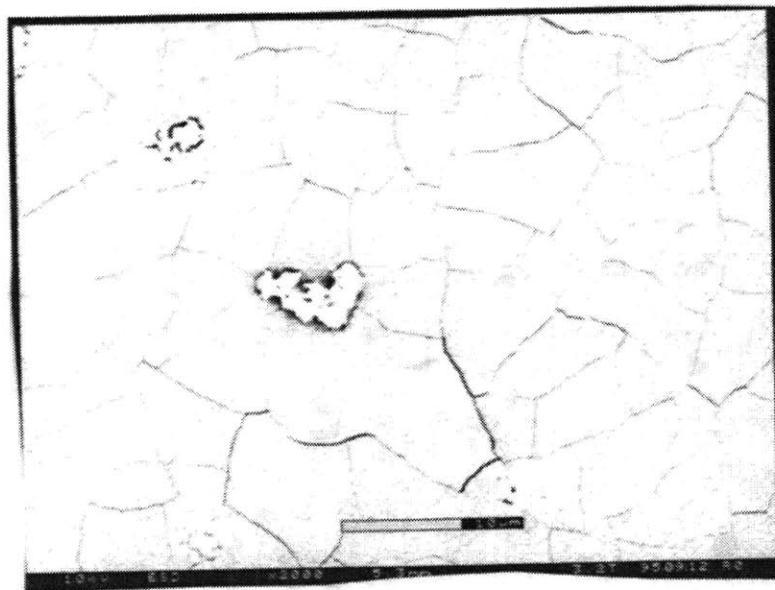
(b)
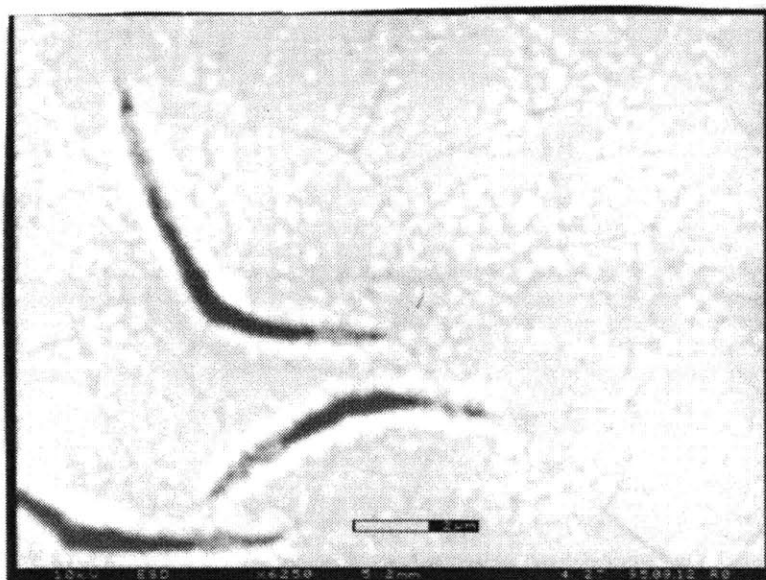
Figure 6.13: Pores in the BiCuVOx films on quartz, showing the flat pore edges. Inset: X 12000, background X 800.
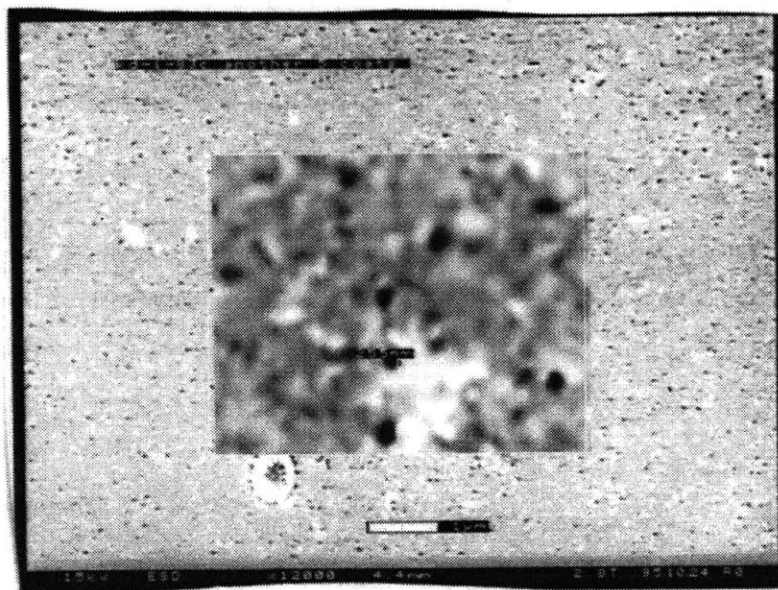
Figure 6.14: BiCuVOx films on quartz heated at (a) 450 °C, (b) 550 °C, (c) 650 °C. All are X 7500. The films show an increasing dewetting from the substrate.

(a)

(b)

(c)
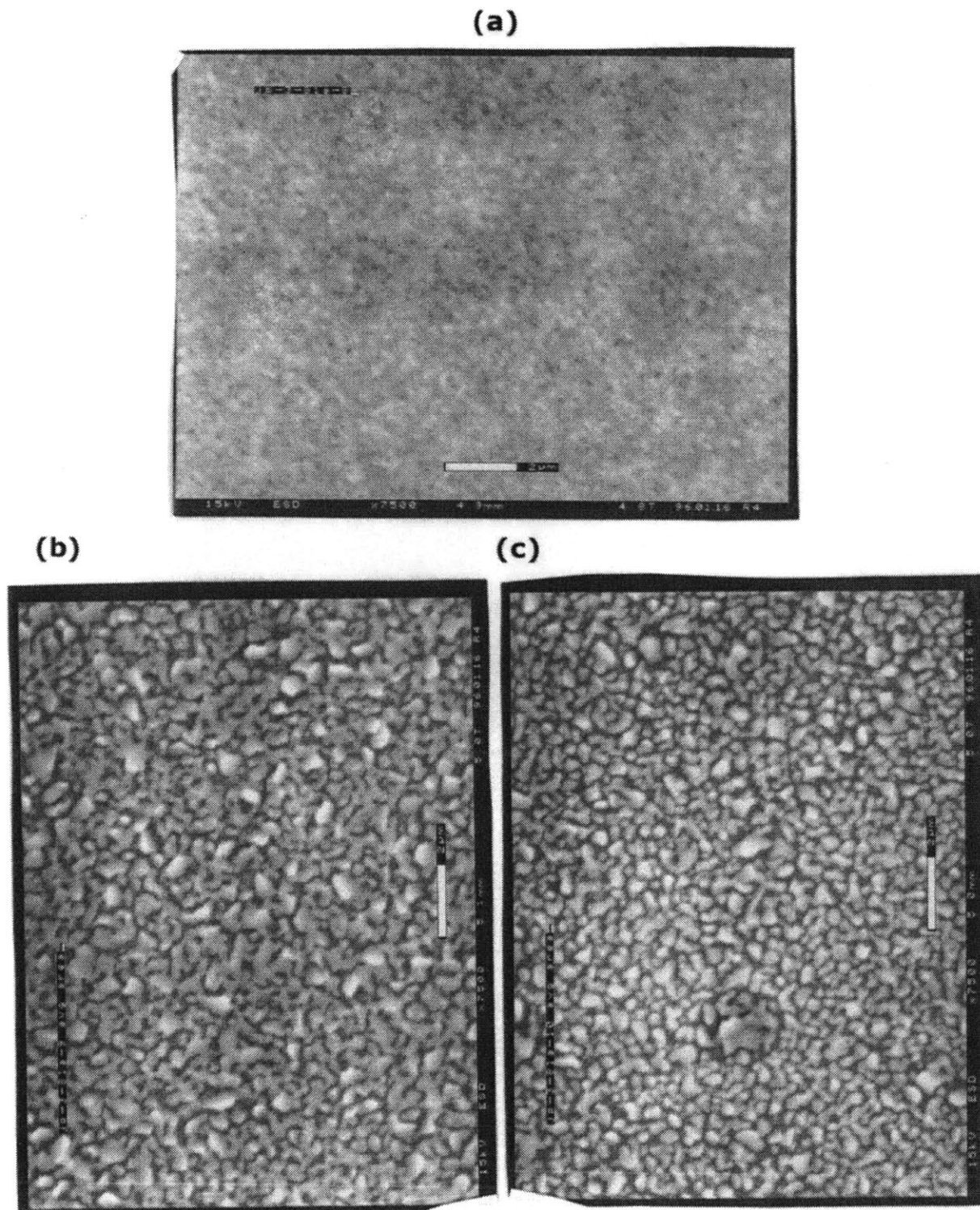
Figure 6.15: GIXRD of BiCuVOx films on quartz shown in Fig. 6.14. (a) 450 °C, (b) 550 °C, (c) 650 °C. Grazing angle 1°. The films are strongly *001*-oriented.
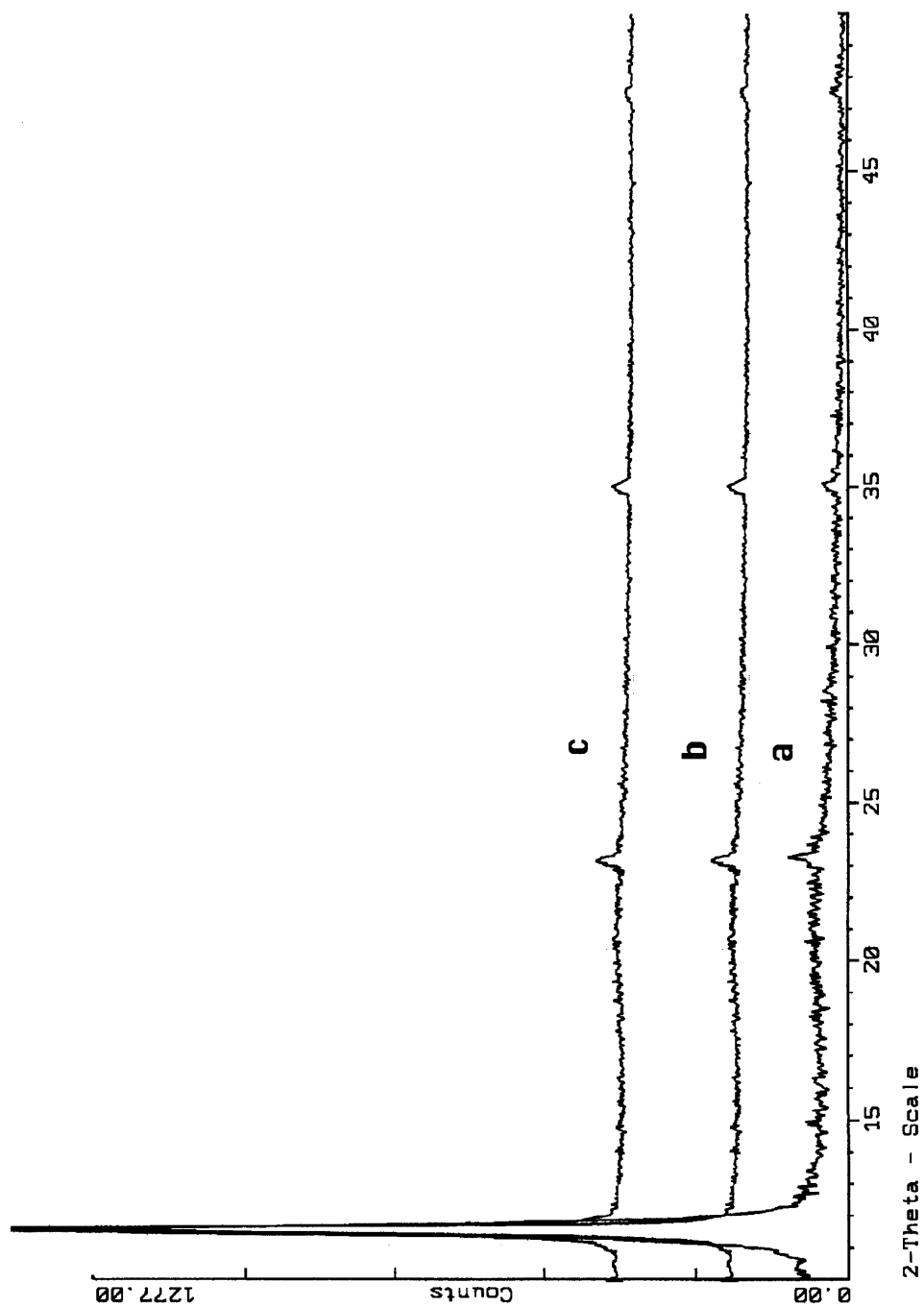
Figure 6.16: BiCuVOx films heated to (a) 750 °C (X 4700), (b) 800 °C (X 970), and (c) 850 °C (X 290). The large areas of bare substrate seen in (b) and (c) are typical of the overall appearance of the films. The film in (a) shows grain coarsening (compare with Fig. 6.14) but longer heating times at this temperature did not result in better substrate coverage.

(a)
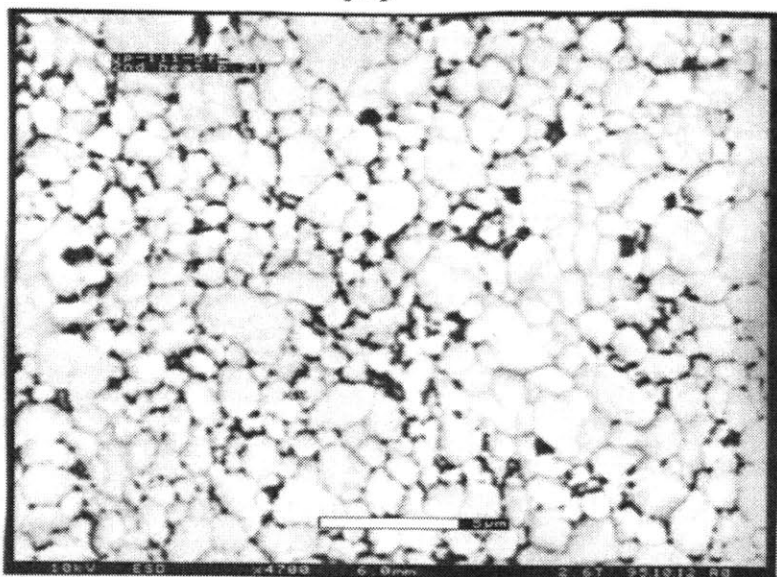
(b)
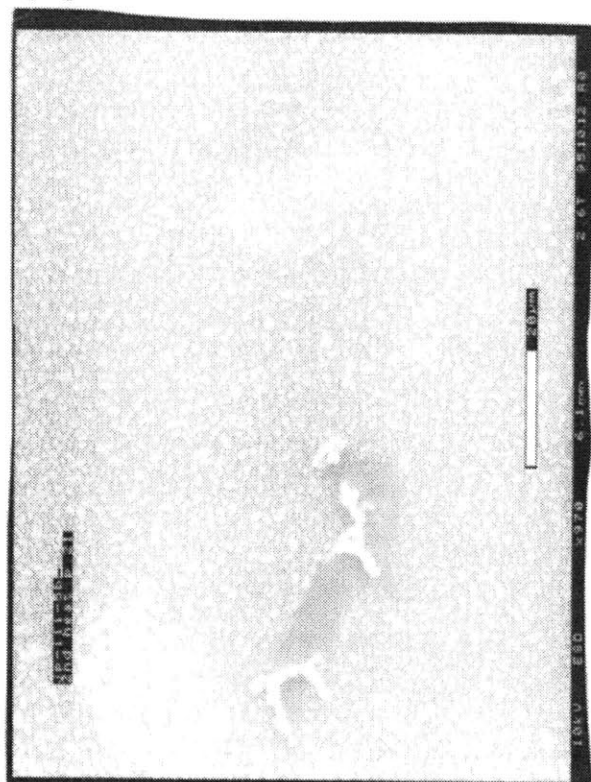
(c)

Figure 6.17: GIXRD of BiCuVOx film on quartz, heated to 875 °C. The γ phase has disappeared; the peaks do not match V_2O_5, CuO, Bi_2O_3, or any known combination of these, nor any known Bi-Si oxide. BiCuVOx melts congruently at 895 °C.
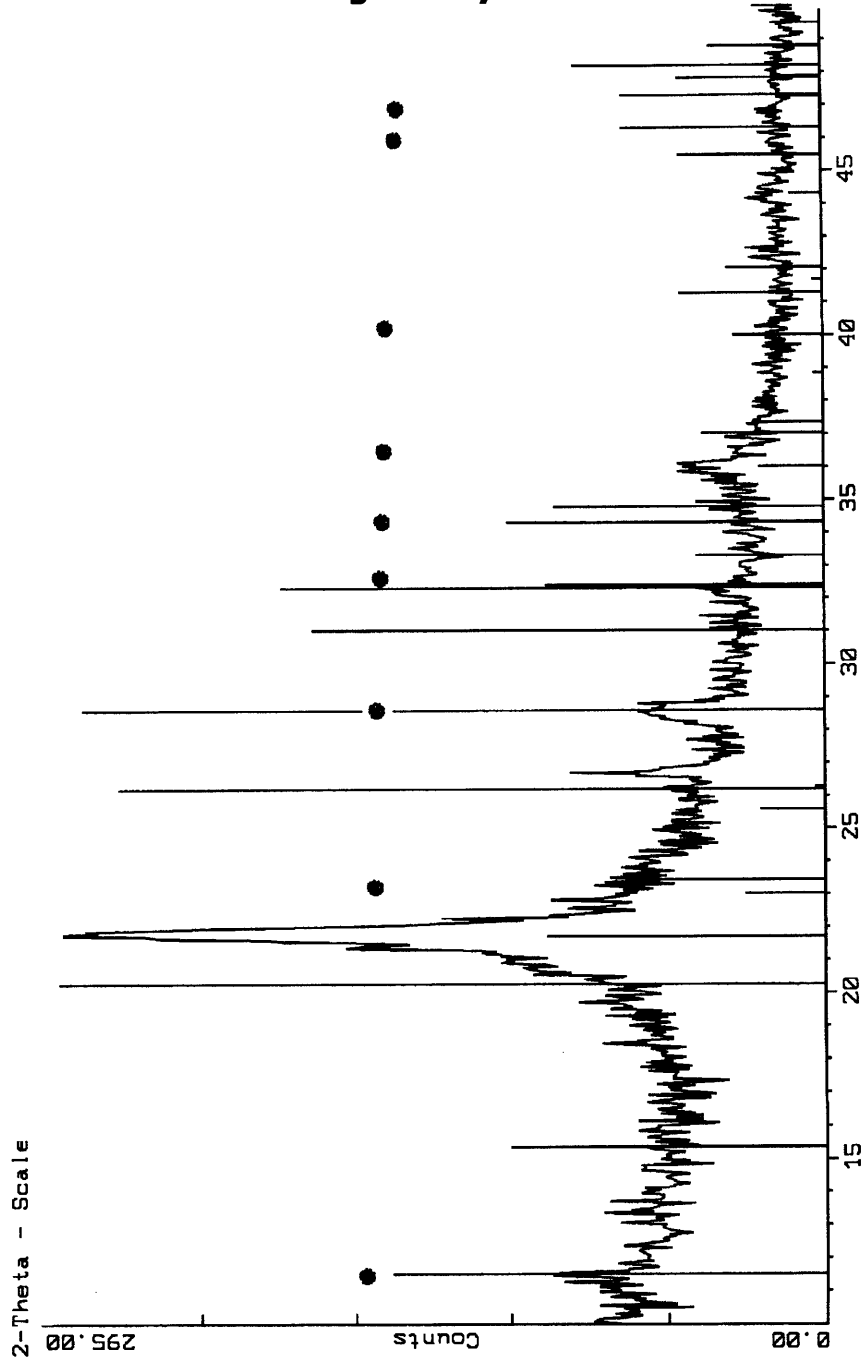
Figure 6.18: (a) BiCuVOx film dipcoated onto a platinum sheet. The tear in the film is possibly due to bending the substrate during processing, and shows the elasticity of the film (the defect heals). X 5550. (b) BiCuVOx film spincoated onto a platinum sheet. The holes (dark spots) are caused by dust motes; the light spots are hillocks. X 8250. Both films were annealed at 650 °C and show no agglomeration.

(a)
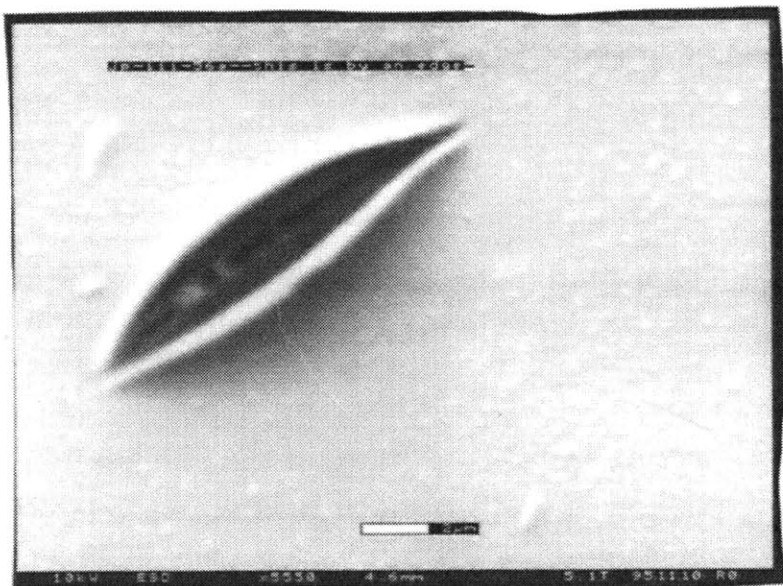
(b)
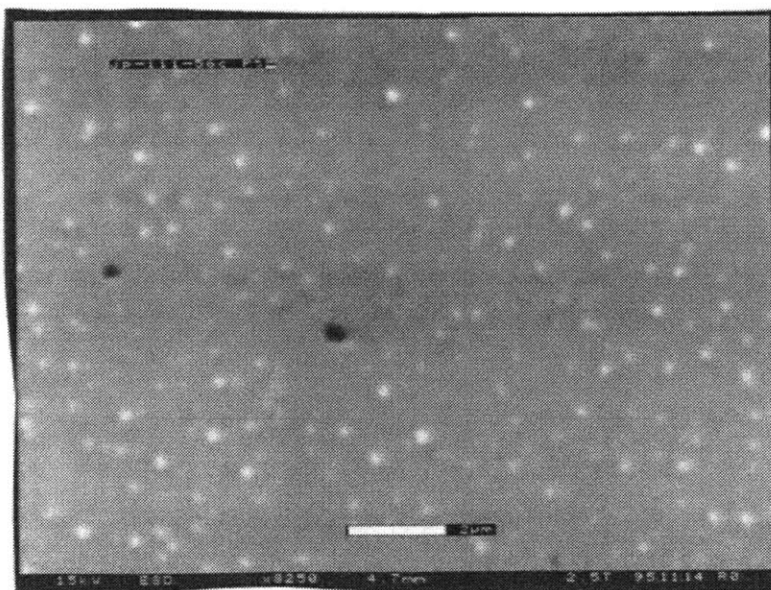
Figure 6.19: GIXRD (1°) of BiCuVOx films on platinum. (a) Dip-coated. (b) Spin-coated. Note the greater degree of orientation of the spin-coated film. Platinum peaks are marked *.
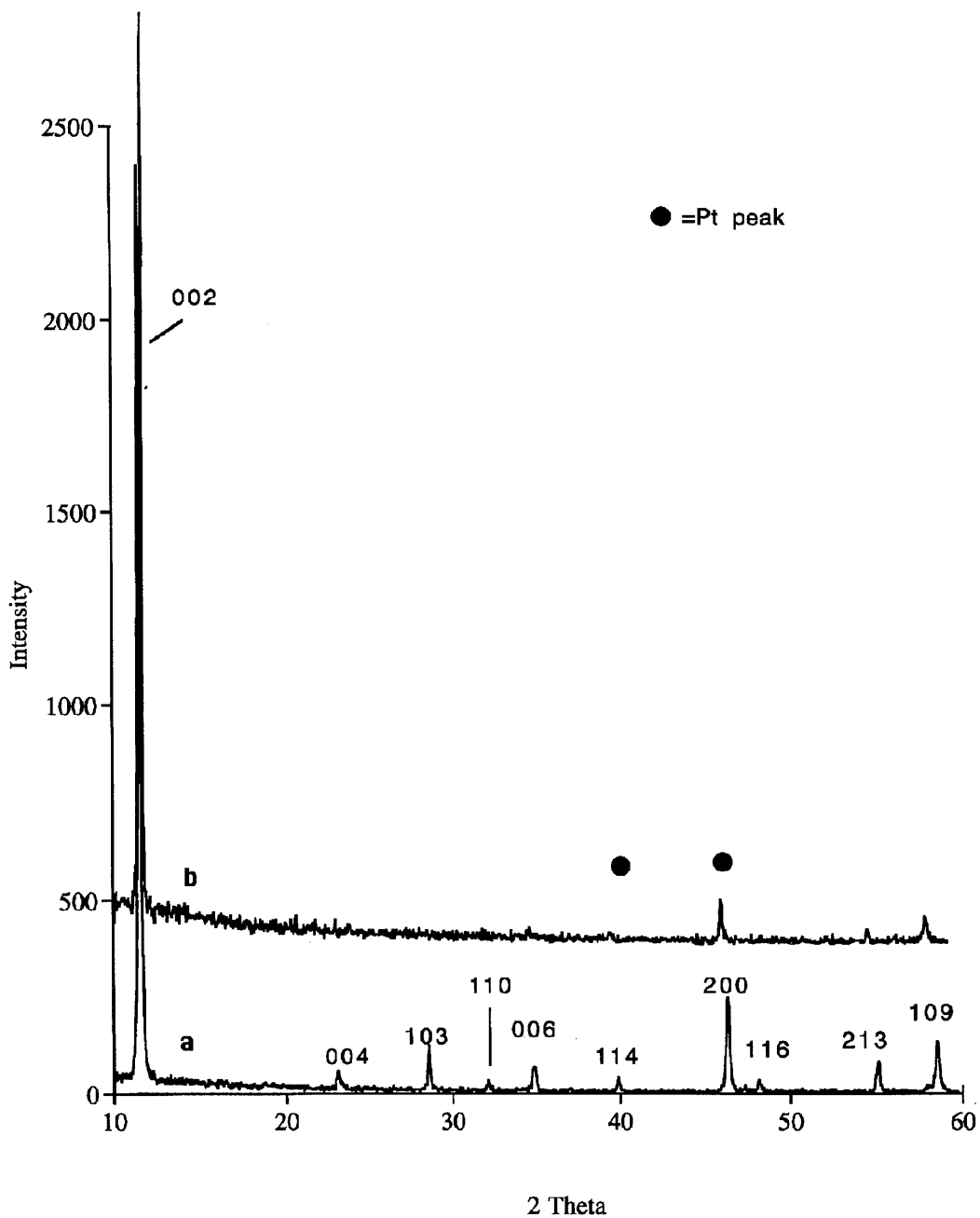
Figure 6.20: BiNbVOx films on quartz. (a) 450 °C, X 2850, (b) 550 °C, X 7600, (c) 650 °C, x7500. The films remain unagglomerated and defect-free, though hillock formation is visible in (c). Compare with Fig. 6.14.

(a)

(b)

(c)
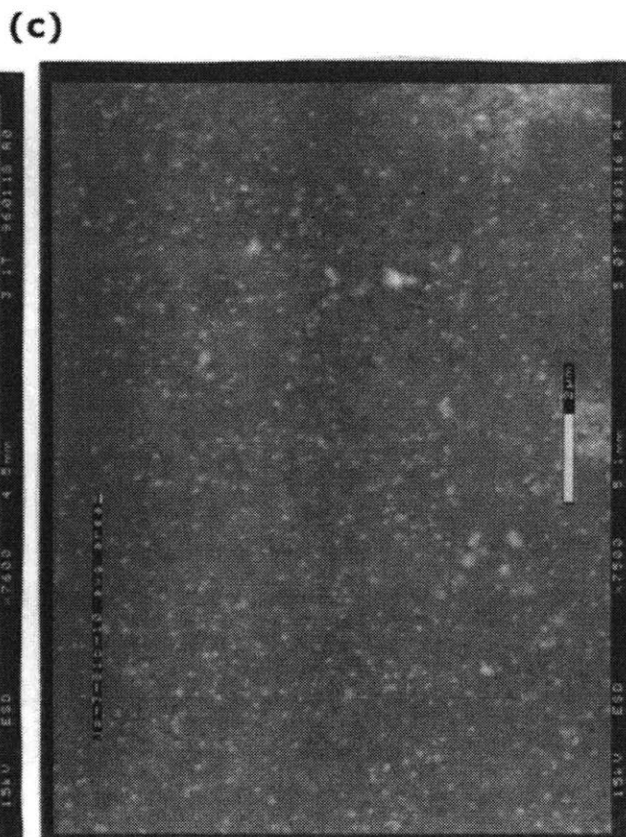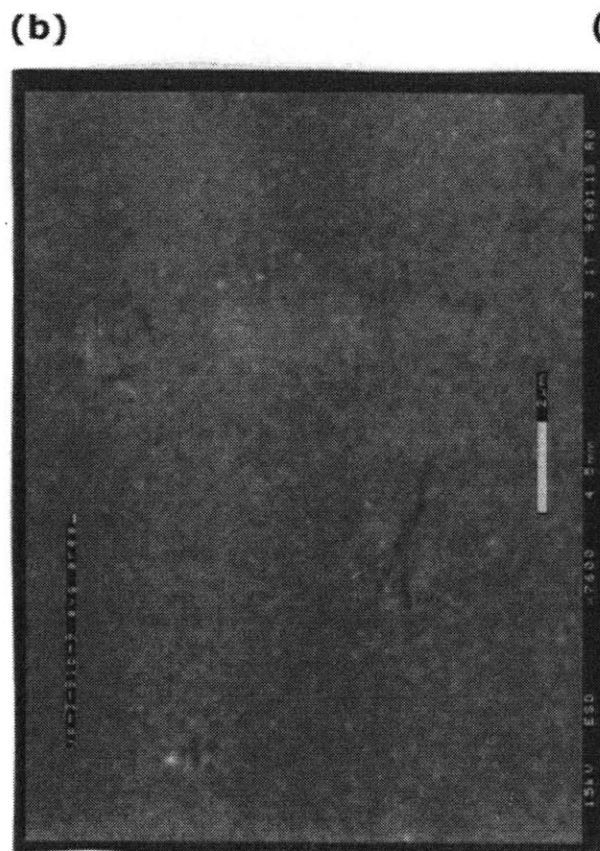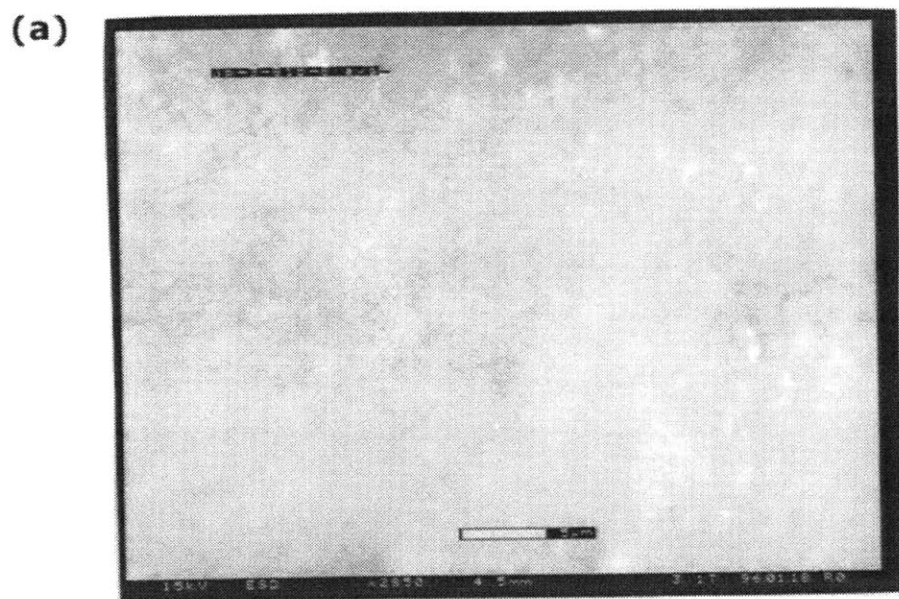
Figure 6.21: GIXRD (1°) of BiNbVOx films on quartz. (a) 450
°C, (b) 550 °C, (c) 650 °C. The films, like BiCuVOx (Fig. 6.15),
are strongly *00l*-oriented.
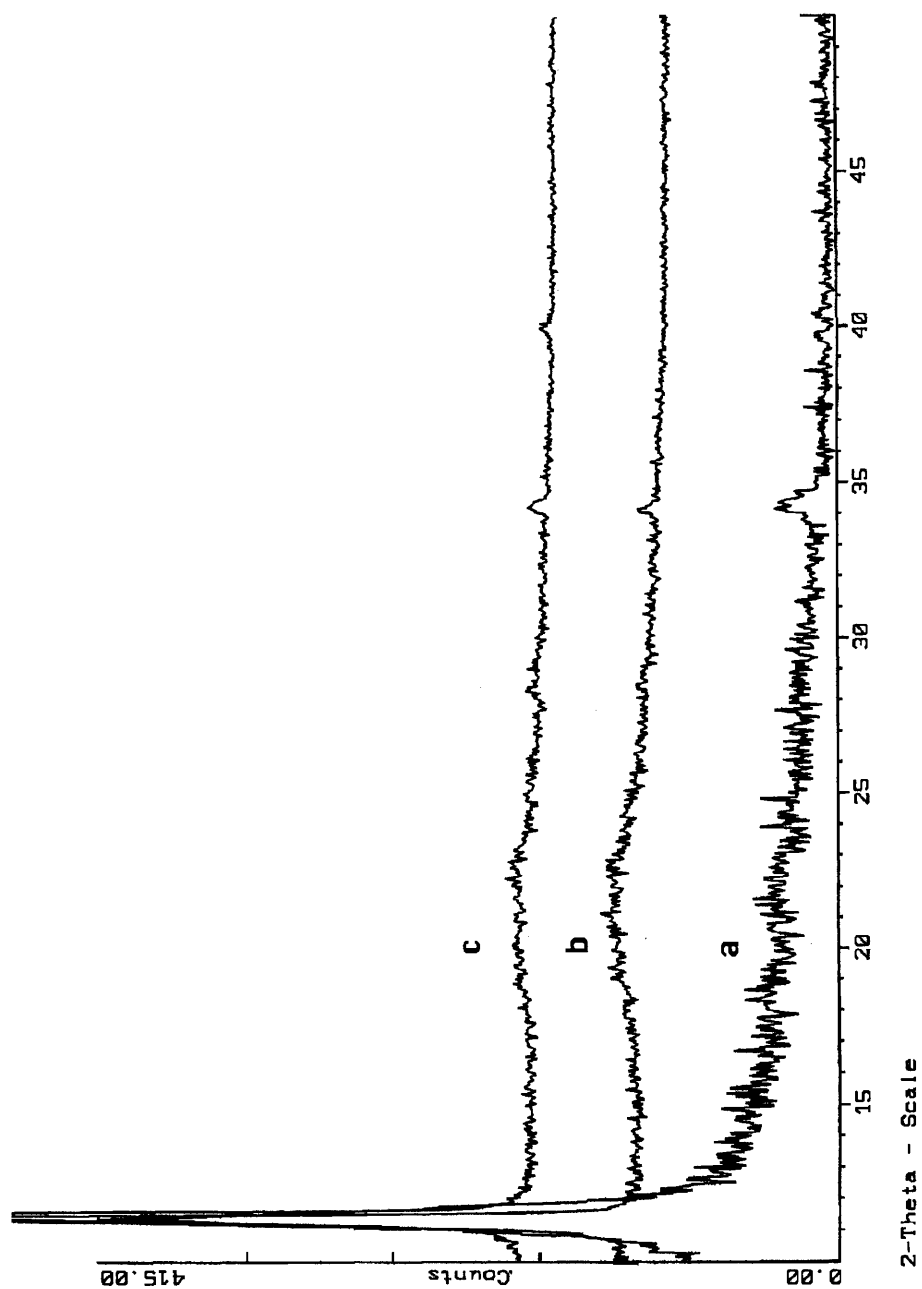
Figure 6.22: BiNbVOx on E-beam platinum substrates, heated to 650 °C. (a) X 1350. White spots are dust motes. (b) Close-up (X 10000) of the area near the dust mote in the upper left of (a). The grain morphology is visible: there is some mild hillocking but no grain boundary grooving.

(a)
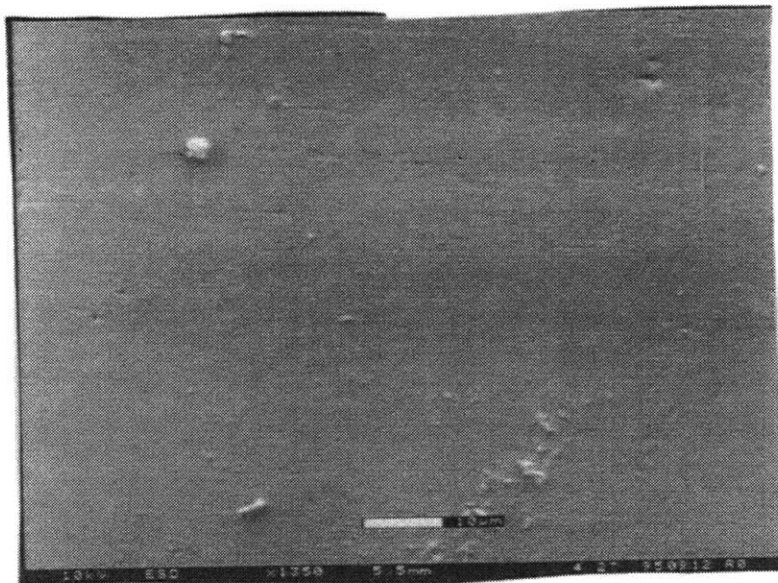
(b)

Figure 6.23: GIXRD (1°) of BiNbVOx film on Pt (650 °C). The lines mark the expected positions for γ phase peaks. The film is strongly *00l* oriented.
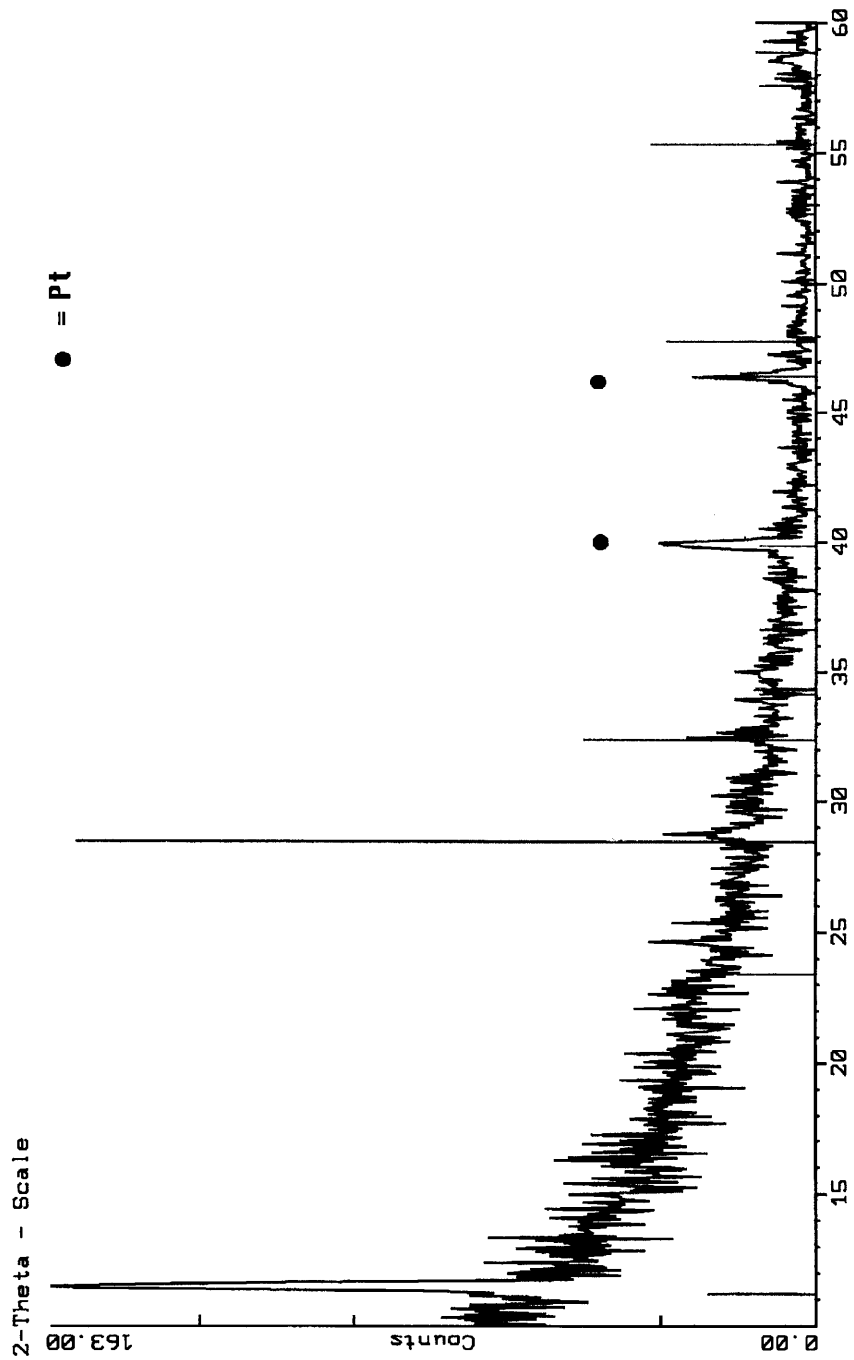
Figure 6.24: Film behavior as a function of grain size (D)-to-film thickness (t) ratio and wetting angle.[58]
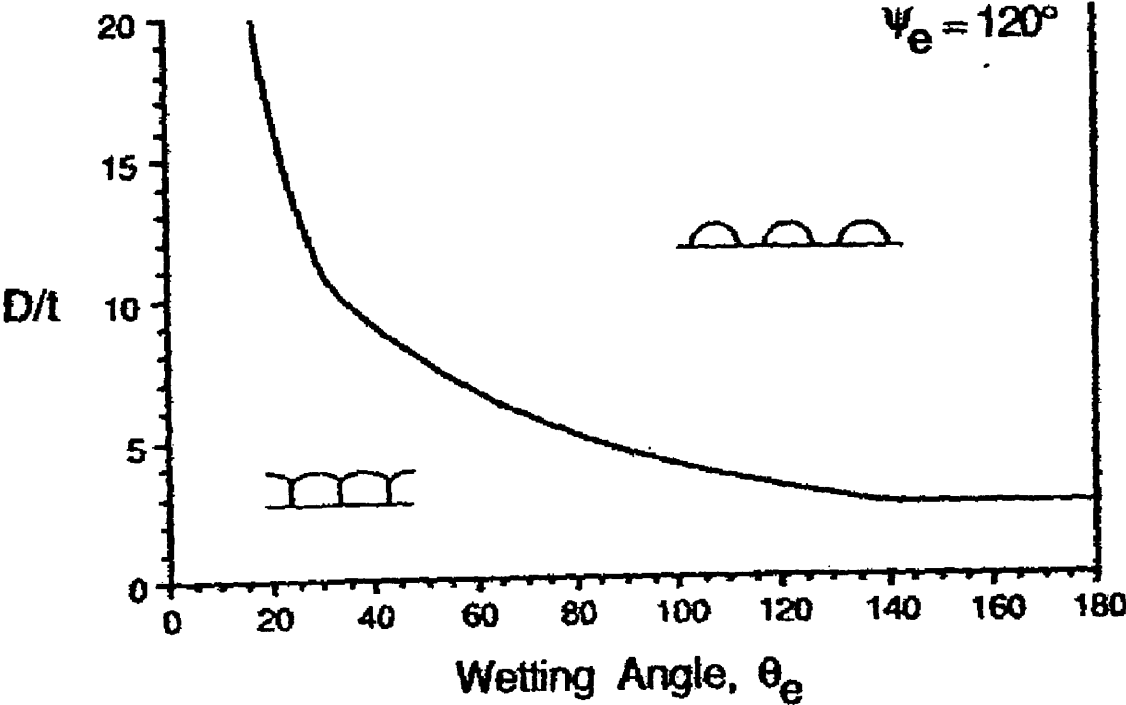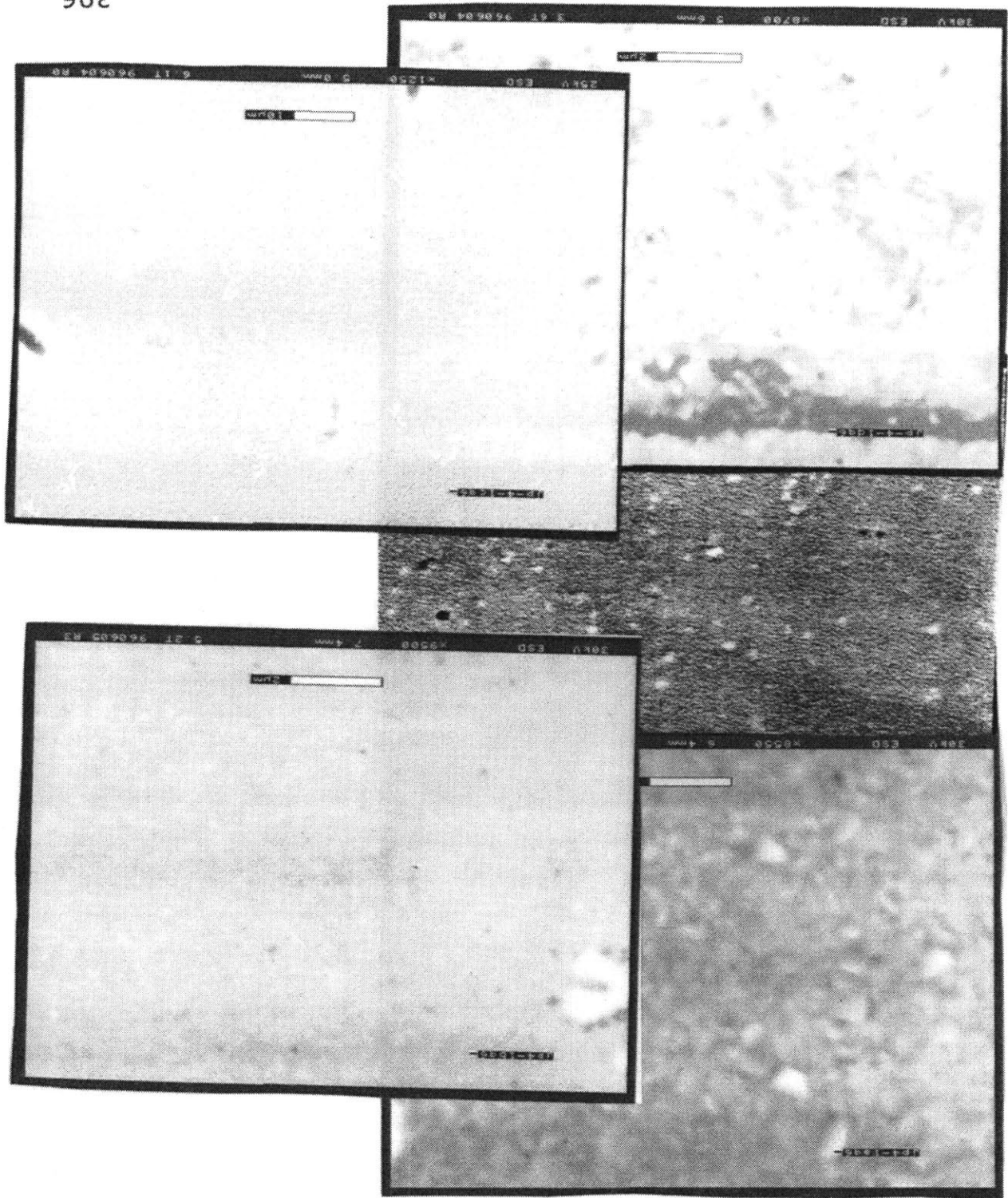
Figure 6.25: BiMeVOx films on quartz substrates, 650 °C heating temperature. 450 °C films were unagglomerated. Left, going down: BiCuVOx (X 8850), BiFeVOx (X 1450), BiMnVOx (X 8700). Right, going down: BiNbVOx (X 9500), BiTiVOx (X 1250).

Figure 6.26: BiMeVOx films on platinum substrates, 650 °C heating temperature. 450 °C films were defect-free. Clockwise from left: BiCuVOx (X 10000), BiNbVOx (X 10500), BiMnVOx (X 8800), BiTiVOx (X 9100). Dark spots are pores caused by decomposition of organics or by dust.
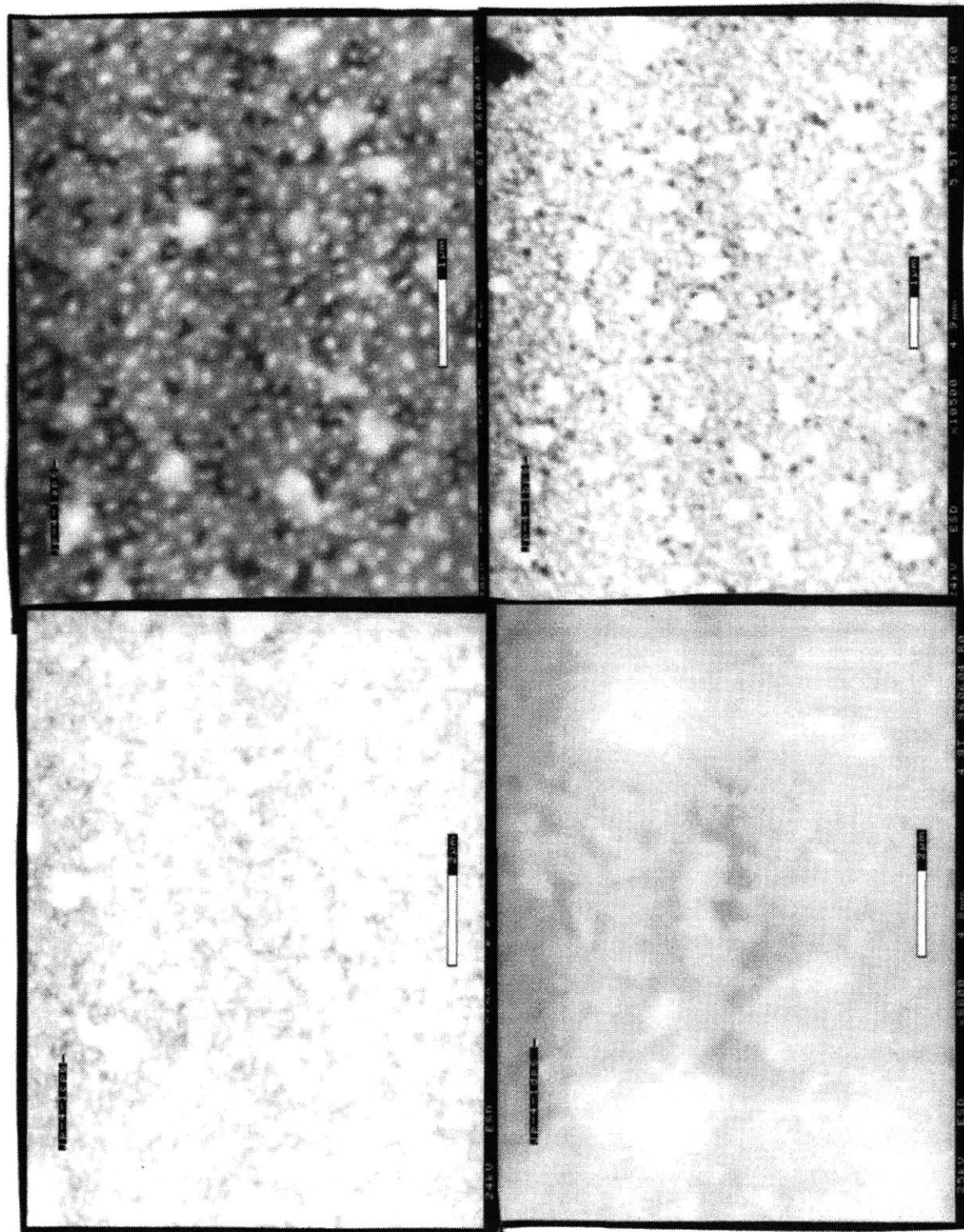
Figure 6.27: BiMeVOx films on alumina substrates, 650 °C heating temperature. 450 °C films were defect-free. Clockwise from left: BiCuVOx (X 8350), BiNbVOx (X 9200), BiMnVOx (X 7400), BiTiVOx (X 9150).
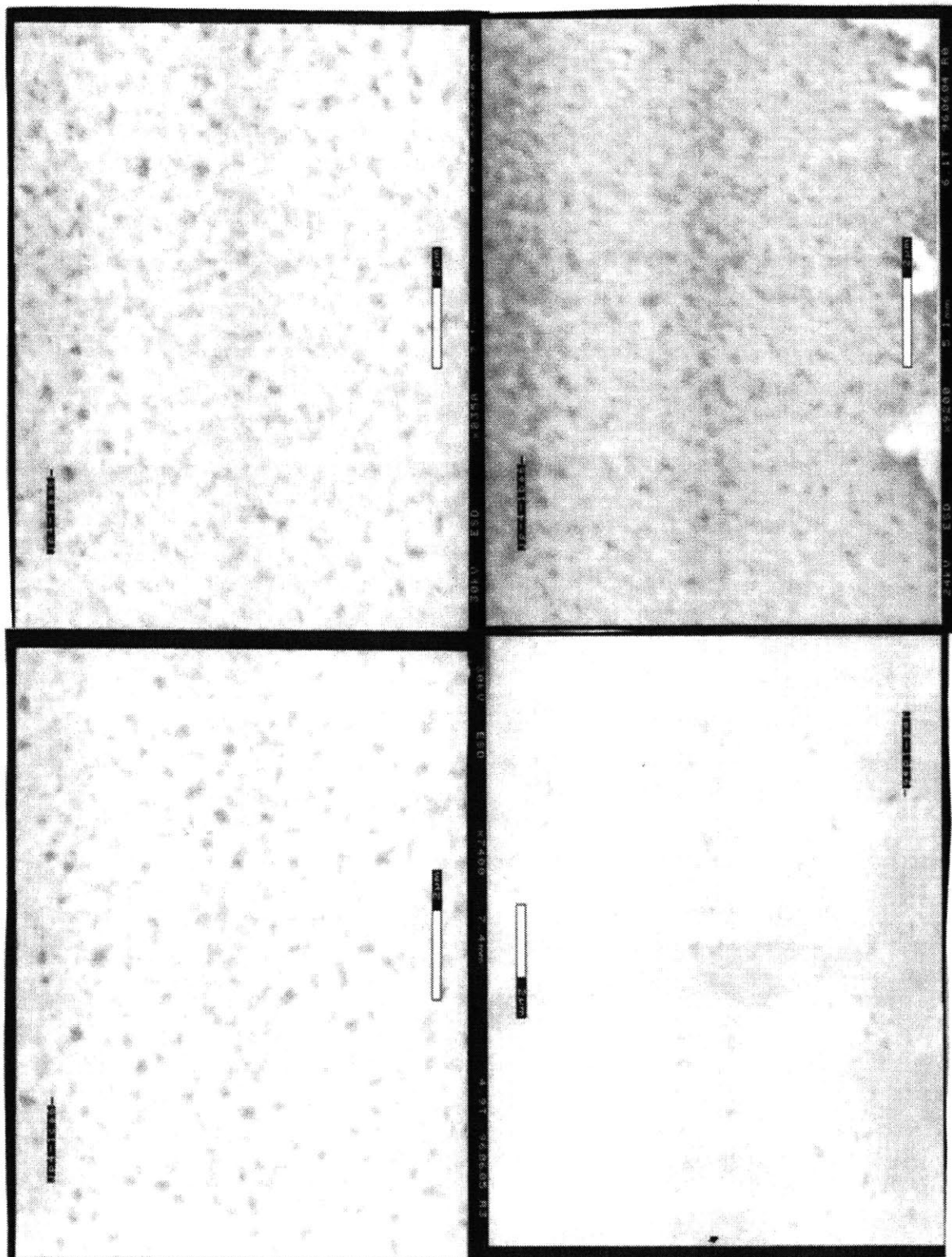
Figure 6.28: BiMeVOx films on quartz substrates, 750 °C heating temperature. Clockwise from left: BiCuVOx (X 1200), BiNbVOx (X 1100), BiMnVOx (X 6450), BiTiVOx (X 5200). The platelike grains appear to have stacked edge-on against the substrate.
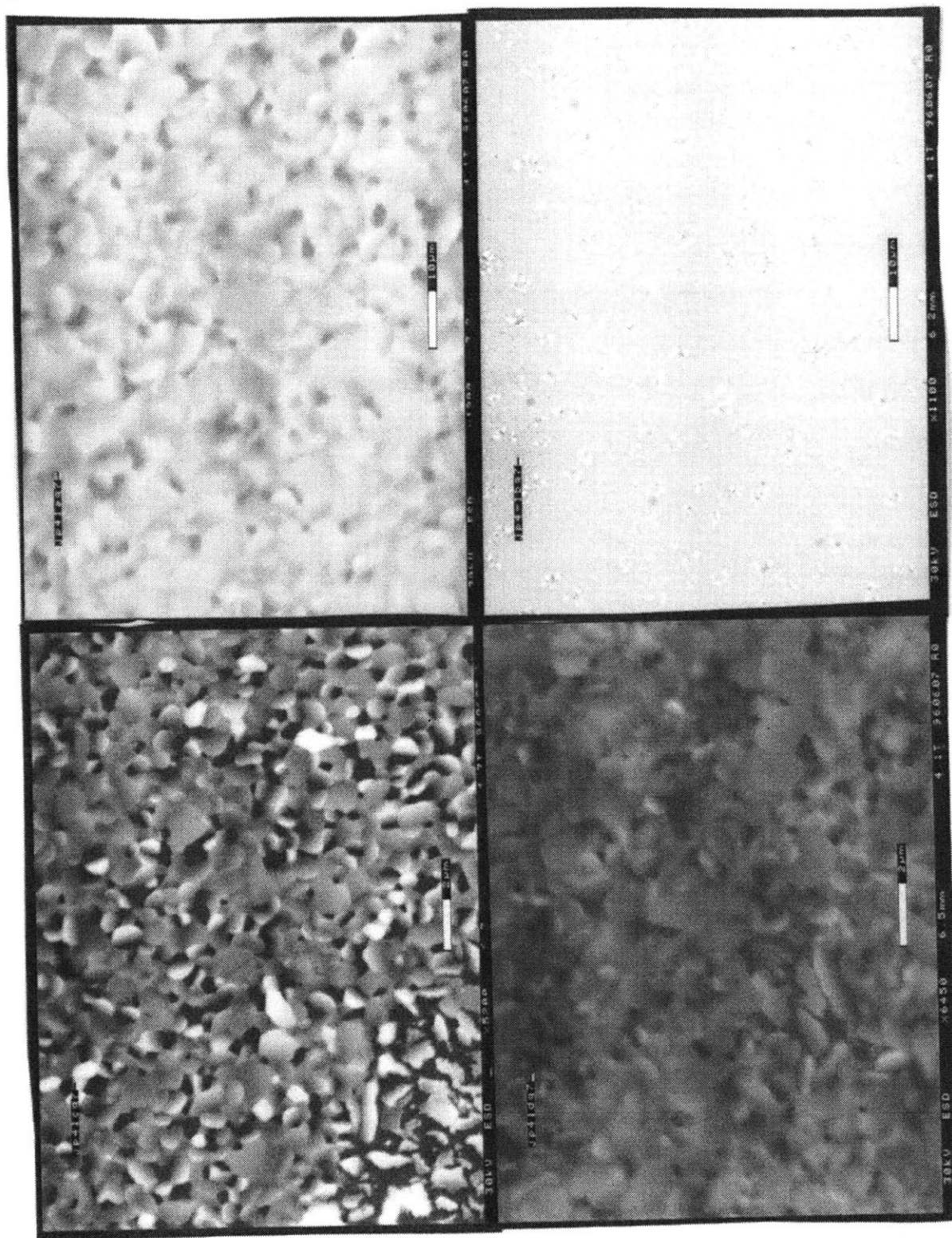
Figure 6.29: BiMeVOx films on platinum substrates, 750 °C heating temperature. Clockwise from left: BiCuVOx (X 2050), BiNbVOx (X3100), BiMnVOx (X 5100), BiTiVOx (X 3800).
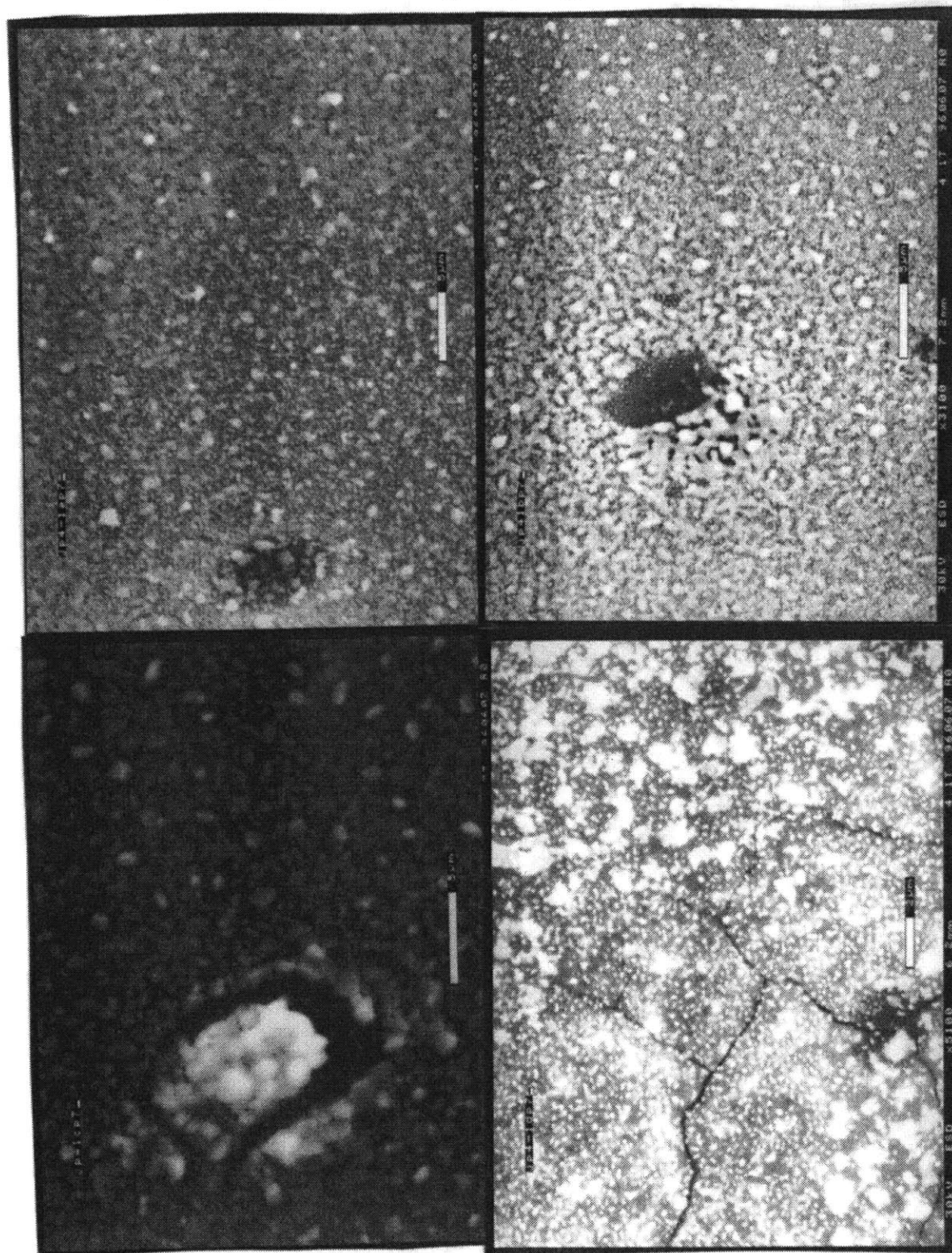
Figure 6.30: BiMeVOx films on alumina substrates, 750 °C heating temperature. Clockwise from left: BiCuVOx (X 6200), BiNbVOx (X5000), BiMnVOx (X 8100), BiTiVOx (X 10500).
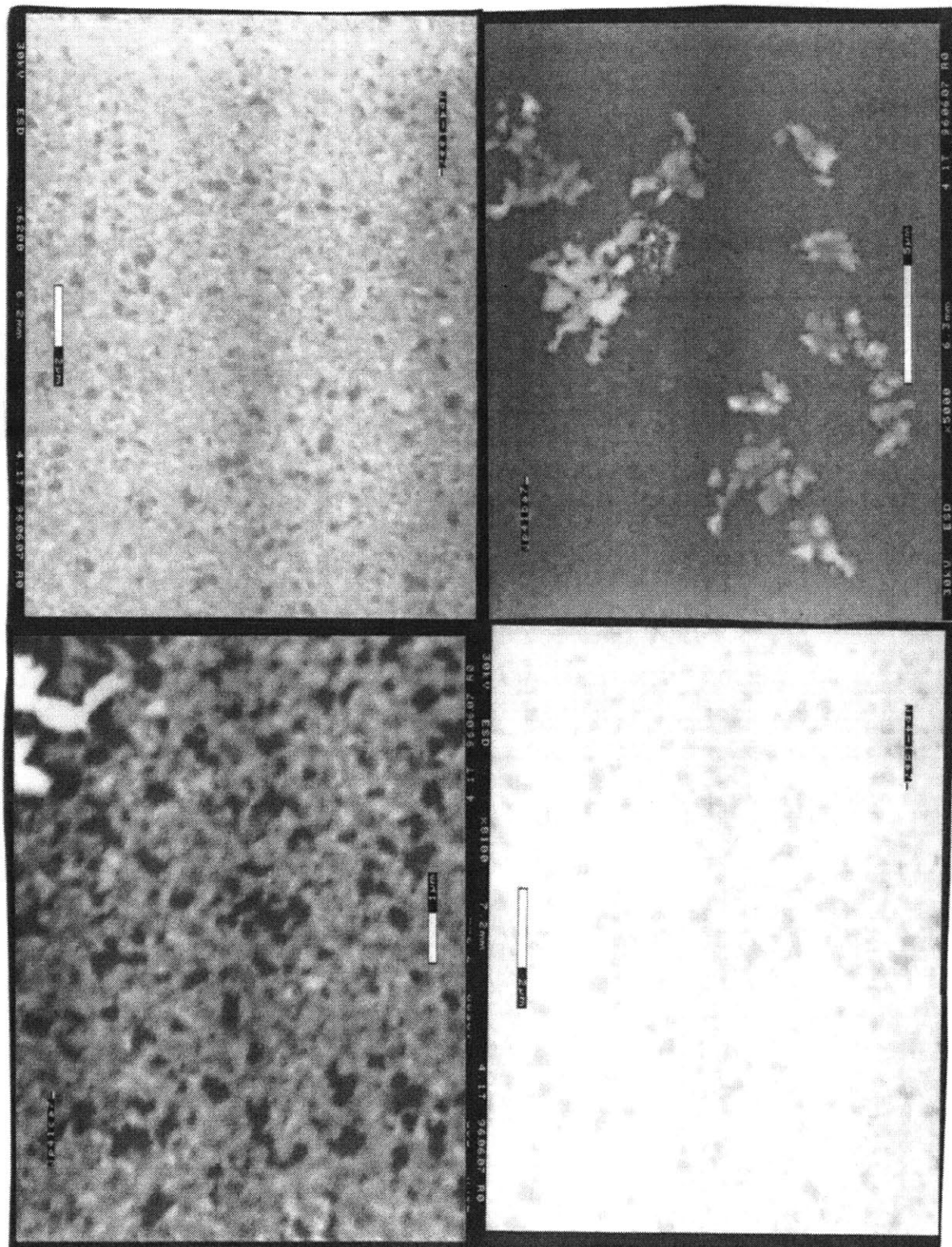
6.3.2 Role of the Precursor

Because the nature of the precursor may have been playing an important role in the morphology of the film, we turned our attention to what effect chemical modifications to the BiCuVOx precursor would have on the final quality of the film. That the grain size-to-film thickness ratio is important in determining whether a continuous film is more stable than an island morphology has been discussed above. Furthermore, the degree of branching – or the fractal dimension — of the precursor oligimers in the sol or gel determines the degree to which the oligimers can interpenetrate and densify. The fractal dimension, in turn, is determined by the relative degrees or rates of hydrolysis and condensation of the metal alkoxide precursor. Thus several experiments were undertaken to try to change the degree of branching of the precursor oligimers. The actual (average) fractal dimension of the oligimers resulting in each experiment was not found due to the unavailability of SAXS measurements.

One approach to improving the film quality was to add an acid catalyst. In TEOS gels, use of an acid catalyst during hydrolysis produces gels that collapse easily,[59,60] because the gel so produced is less branched than those made with base catalysis, where the sol particles are compact and highly branched.[16] This experiment was tried (Experiment #5) and found to give no improvement in the film quality.

Several approaches to BiCuVOx precursor solution preparation were tested to see whether the agglomeration seen in the BiCuVOx

films could be avoided. It was found that completely unhydrolyzed solutions would not wet the quartz surface completely, and the GIXRD patterns for these films showed formation of $BiVO_4$ and Bi_2O_3 in addition to the desired $Bi_2Cu_{0.1}V_{0.9}O_{5.35}$ phase. For water-to-alkoxide ratios (W) of 1, 2, and 5 there was no apparent correlation between the ratio and film quality, although a rough measure of the average pore size (25 pores, measurement using the "ruler" in the ESEM image analysis software) showed some relationship between pore size and amount of hydrolysis water. While the W = 0-1 region should have been tested for the precursor behavior and resulting film quality, the experiment was not done. (Table 6.2)

Both the addition of an acid catalyst and increased W favor the formation of small, non-branched particles in the precursor sol because the hydrolysis reactions outpace the condensation reactions. These particles would be expected to pack together on the substrate surface, yielding a dense film exhibiting little shrinkage during pyrolysis. However, increasing W or $[H^+]$ did not significantly lessen the agglomeration of the BiCuVOx films on quartz. A number of common DCCAs were next added to the precursor solutions to test whether slowing the hydrolysis reactions by complexing the vanadium alkoxide with organic ligands would improve the film quality.

BiCuVOx films made from precursor solutions with added 1,3-propanediol, N, N-dimethylformamide, diglyme, acetic acid, ethylene glycol, triethanolamine, or diethanolamine were spin-cast as usual and pyrolyzed at 550 °C. These represent a subset of the additives initially screened (Table 6.3); those which resulted in a precipitate were not used in casting films. All of these had been found by the

partial charge model (*vide supra*) to be likely to substitute for a 2MOE ligand on the vanadium alkoxide. The additives were added in the quantity of one mole additive per mole of alkoxide group, and were thus present in sufficiently small amounts that they were not expected to have affected the bulk solution viscosity.

The films made with additive-containing precursor solutions showed agglomeration or dewetting which is in some cases worse than that in the controls. (Figure 6.31, Table 6.3) A variation in the appearance of the BiCuVOx grains or islands with the identity of the additive was noted: the amount of bare substrate decreased as the identity of the additive changed, in the order (least coverage – most coverage, determined by the image-analysis software with the ESEM) 1,3-propanediol > ethylene glycol > N,N-dimethylformamide > acetic acid > diethanolamine. Films made from precursor solutions containing triethanolamine showed a mixture of BiCuVOx and $BiVO_4$ phases, but all other GIXRD patterns showed formation of *00l*-oriented, phase-pure BiCuVOx. (Figure 6.32) Film thicknesses were 0.8-1.4 μm by profilometry (10 layers).

The effects of additives in the precursor solutions on BiNbVOx film morphology was also investigated. BiNbVOx films demonstrated little variation in quality with precursor additive, and all except TEA showed formation of *00l*-oriented and phase-pure BiNbVOx by GIXRD. As with BiCuVOx, the triethanolamine-containing precursor solution gave films which were blotchy and inhomogenous; GIXRD of these films showed a mixture of BiNbVOx and $BiVO_4$. (Figures 6.33, 6.34)

The quantities of additive used (<1 vol%) would not be expected to modify significantly the bulk properties of the precursor

solution, such as the surface tension or the viscosity. Therefore it is unlikely that the effects of the different additives on the film morphology is due to a difference in the wetting behavior of the precursor solution on the substrate. The additives probably have acted by reducing the precursor homogeneity, adversely affecting the growth and coalescence of grains in the film by permitting segregation of some component of the BiCuVOx at grain boundaries. This effect would be in opposition to what has generally been seen in other sol-gel systems where additives have been used; for example, additives such as those used in our experiments greatly increased the homogeneity and improved the particle morphology in the 124 superconductors.[48] In those cases, however, the components of the sols were added as alkoxides. The additives in our experiments also have a distinct effect on the gel greenbody morphology, as shown in the ESEM micrographs. (Figure 6.35) Triethanolamine, which produced clumpy and phase-mixed films, gives a "fuzzy" precursor morphology, indicating a high degree of branching and/or inhomogeneity. The other additives give a uniform-appearing precursor. The precursor gel from diethanolamine has some elements of the triethanolamine gel and those of the other additives.

In addition to segregating some gel component to the grain boundaries, a second possible mechanism for the additive effects on the film morphology revolves around the hydrolyzability of the additive from the vanadium center. When $VO(OR)_3$, is hydrolyzed, fast condensation processes lead to the formation of intermediate decavanadate species, and the subsequent slow processes lead to different equilibrium species.[61] Since the decavanadate species

lead to the ribbonlike morphology,[37,38] steric limits on the fast condensations can prevent the usual oligimer form from taking shape. The oligimers with the resulting morphology pack less well in the film than the ribbonlike ones.

Double-donor additive ligands may also act by cross-linking the metal centers, effectively forcing a more open structure in the unpyrolyzed film by increasing the sticking probability and decreasing the interpenetration of growing oligimers. Bridging of 1,2-diols in aqueous complexes of vanadium(V) is common;[62] for example, ethylene glycol can be used to create a bridged dinuclear vanadium (V) complex.[63] The additives which gave the lowest-quality films, namely ethylene glycol, propanolamine, and triethanolamine, replace some or all of the 2MOE ligands on the vanadium center, producing a bridged complex. These bridging ligands are unlikely to hydrolyze off, according to the partial charge model, IR data, and the literature. Work by Crans et al.[64] shows that triethanolamine, as well as tripropanolamine, is bound by the central N and only two alcohol arms, leaving the third dangling. This seems to be true of $\alpha-\omega$ difunctional molecules in general. Ligands of the form $HO(CH_2)_xOH$, $HO(CH_2)_xNHR$, and $HO(CH_2)_xC(O)OMe$ can be attached to $\{VO(OR)_2\}$ via the hydroxyl and carboxyl functions, respectively, to give a species $VO(OR)_2OR'$, where R' has a terminal "dangling" function.[65] This is likely to be true of the propanolamine also: it will be bound only on the amine end, leaving a dangling -OH group. Ethylene glycol also has the potential for a dangling alcohol group. On the other hand, diethanolamine is bound by the amine nitrogen and both alcohol arms, even in aqueous solution;[64] this

additive gave a fairly dense, albeit defected, film. These correlations suggest that the dangling alcohol group is key: it represents an opportunity for the ligand to coordinate to more than one metal center. In the vocabulary of the fractal model, the dangling -OH group provides an increased sticking probability for approaching branched oligimers, and limits interpenetration.

The additives, as unhydrolyzed groups, also place a steric constraint on the packing of the metal oxide polymer chains. They are, however, removed during pyrolysis of the films, possibly expelling membrane from the path of the decomposition gas, leaving voids which can become nucleation points for hole formation.[19,44]

Several experiments were undertaken to characterize the chemical basis for the effects of the additives on BiCuVOx films. A mixture of $Bi(OAc)_3$ and V-2MOE, aged overnight, spread on an IR card, hydrolyzed and vacuum dried, gives the IR spectrum shown in Figure 6.36a. Peaks at 1540 and 1400 cm^{-1} are evidence of bridging acetate groups[66] which remain bound after hydrolysis. (For monodentate carboxylate the expected bands would be at 1320 cm^{-1} (symmetric) and 1660 and 1630 cm^{-1} (asymmetric).[62]) The -OH stretch is greatly reduced; the remnant is probably due to still-bound 2MOE (which is also responsible for the stretches in the 1000-1100 cm^{-1} region). The broad band from 600-1000 cm^{-1} arises from extended V-O and ν(V=O) bonding.[67-69] Normally the ν(V=O) band falls in the 990-950 cm^{-1} region. Bi-O bands should appear near 500 and 350 cm^{-1} , below the range of the instrument.[70] IR spectra for $Bi(OAc)_3$/V-2MOE/additive mixtures

treated similarly show, for example, retention of ethylene glycol (Figure 6.36b). The presence of the bands attributable to the additive, even after vacuum drying overnight, suggests that it has complexed with one of the metals. The strong -OH band, as well as the v(C-O) bands in the 1000-1100 cm^{-1} region, are due to the retention of the ethylene glycol and/or 2MOE. The band at 1650 cm^{-1} may arise from a monodentate acetate group (the other expected bands are swallowed in the alcoholic ones). The broad band 850-500 cm^{-1} is again from extended V-O bonding, and the band at 880 cm^{-1} may arise from a stronger-than-usual v(V=O).

A direct indication of the interaction level between the additives and the vanadium center in V-2MOE is found in the ^{51}V NMR data. (Table 6.4) Solutions of 0.02 M [V-2MOE] in 2MOE were prepared and one mole equivalent of additive per mole of alkoxide group was added. (^{1}H and ^{13}C NMR spectra were dominated by the solvent and additive peaks and were therefore uninformative.) Triethanolamine and 1,3-propanediol induce immediate precipitation of an insoluble complex when added directly to the V-2MOE solution. This behavior has been seen with other vanadium alkoxides[45,62,64,68,71] and points to the reason for these additives' negative effects on the gel and film quality. Trialkanolamines (L), in particular, replace -OnPr in VO(OnPr)$_3$ to give LV=O.[71] These complexes were poorly soluble in ethereal solvents and precipitated as white solids. Presumably a similar mechanism is responsible for what was seen in our experiments. Multiple peaks appearing in the ^{51}V NMR of the diethanolamine and ethylene glycol samples indicate the presence of several vanadium-containing

species with differing degrees of condensation and/or ligand substitution. For comparison (Table 6.4), published experiments show that the addition of one equivalent of $VO(OEt)_3$ to two of ethylene glycol give a precipitate which has the ^{51}V NMR signals -496 and -515 ppm; the solution gives peaks at -463, -474, -503, -506, and -515 ppm, representing the precipitate species (complete substitution of the ethoxy groups) plus some partially-substituted species.[64] The high upfield shifts of the V signal in these solutions indicates strong binding. It should be noted in interpreting these results, however, that the $\delta(^{51}V)$ depends strongly on concentration for smaller R in $VO(OR)_3$, where the shift becomes less negative with increasing concentration.[69]

The identity of the precursor solution additive has little or no effect on the BiNbVOx film morphology. The change in the elemental composition versus BiCuVOx may be sufficient to stabilize the flat film against any tendency for grain coarsening, hillock formation, or agglomeration. Also, the additional interconnection potential realized by the extremely hydrolyzable $Nb(OiPr)_5$ dopant in relatively high proportion (0.3 Nb:2 Bi) may have counteracted the effects additives may otherwise have had on the precursor morphology or on elemental segregation during grain growth.

Table 6.2: Effect of Changing Water-to-Alkoxide Ratio on Film Quality

H_2O/-OR Groups	Time to Gel (h)	Film Avg. Pore (nm)
0	stable sol'n	will not wet substrate
1	stable sol'n	290
2	48	300
3	6-8	320
5	4-6	340
10	ppte. after 1 h	not measured

Table 6.3: Effects of Additive on Gel and Film Quality

Additive	Gel Behavior	Film Morphology
Diisopropanolamine	ppte	not tested
Ethanolamine	ppte	not tested
Diethanolamine	cracked gel	nearly continuous
Triethanolamine	gel (ppte at high conc.)	needlelike structures
N, N-dimethylformamide	gel	liquidlike coalescence
Acetylacetone	gel + ppte.	not tested
ethylene glycol	gel	excess: liquidlike coalescence; equivalent: homogenous film
di(glycol) methyl ether (diglyme)	cracked gel	grainy, large pores
1,3-propanediol	cracked gel	small round islands
acetic acid	gel	excess: no pores equivalent: grainy, large pores
nitric acid	stable sol'n	no wetting
ammonium hydroxide	ppte	not tested

Table 6.4: ^{51}V NMR of V-2MOE + additives (δ, VOCl$_3$= 0 ppm)

Additive	^{51}V NMR Peak Positions
none	-541 ppm
diethanolamine	-437, -461
triethanolamine	pale green ppte., no NMR done
ethylene glycol	-471, -479, -541
dimethylformamide	-544
acetic acid	-521
methanol	-532
1,3-propanediol	yellow fibrous ppte., no NMR

Figure 6.31: BiCuVOx films on quartz spin-cast from precursors containing additives. All films shown have been heated to 550 °C and are X 7500. (a) ethylene glycol, (b) triethanolamine, (c) N, N-dimethylformamide.

(a)
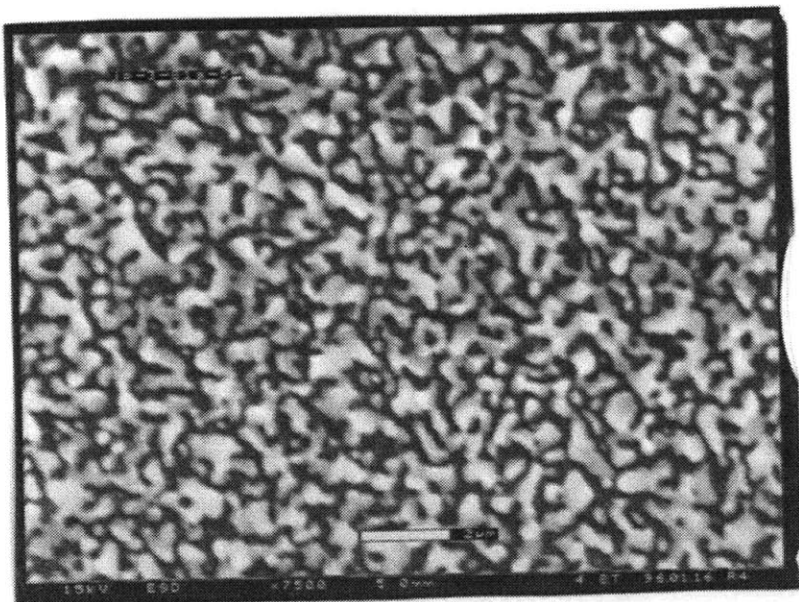
(b)
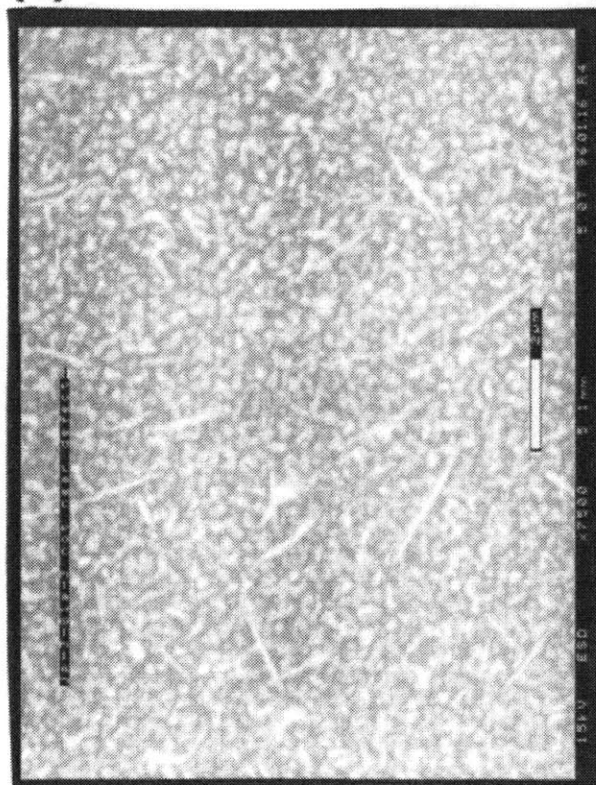
(c)
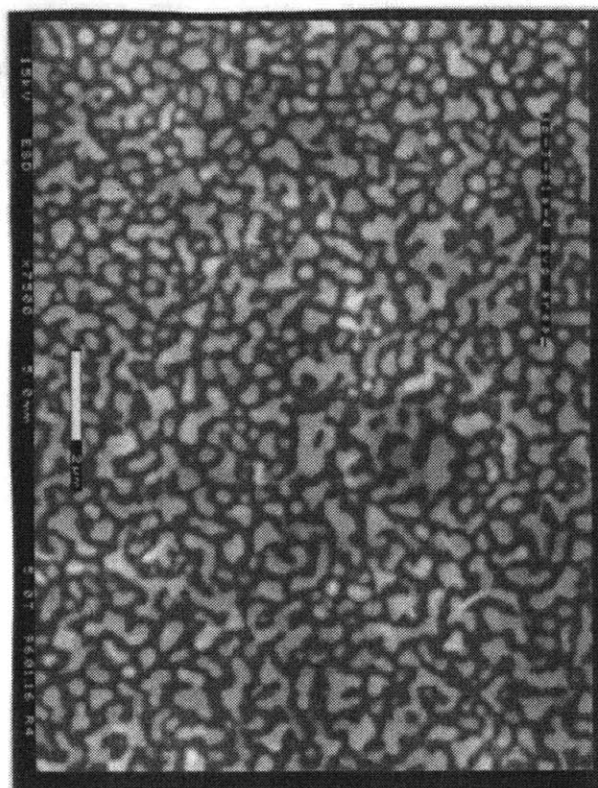
Figure 6.31, continued: (d) diethanolamine, (e) acetic acid, (f) 1,3-propanediol. See Fig. 6.14b for a "control" film with no additive.

(d)
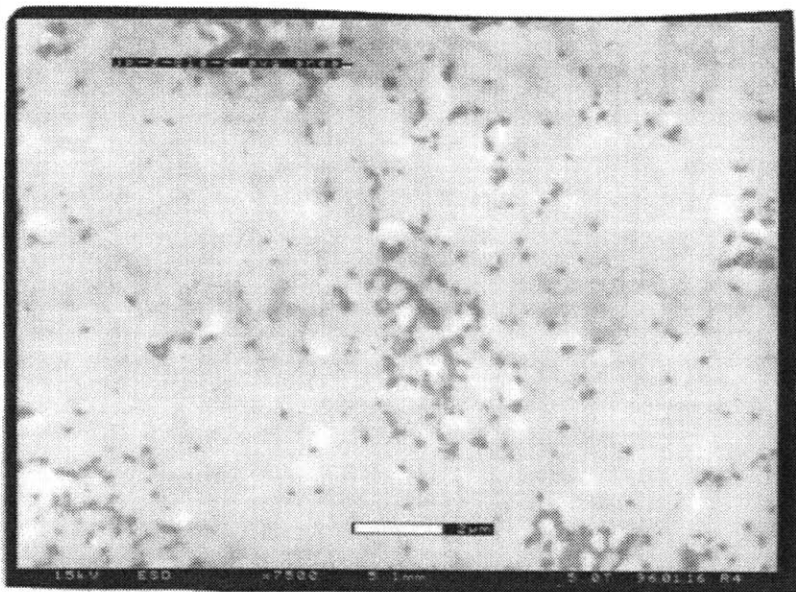
(e)
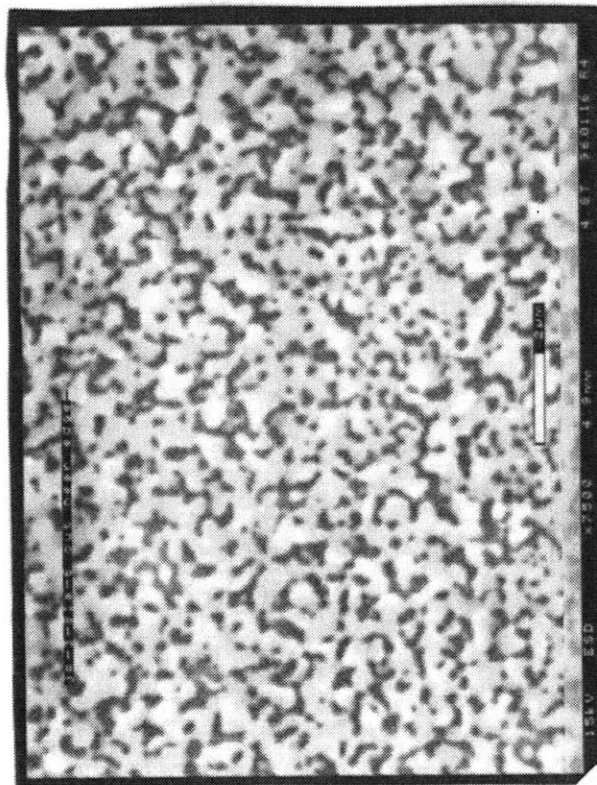
(f)
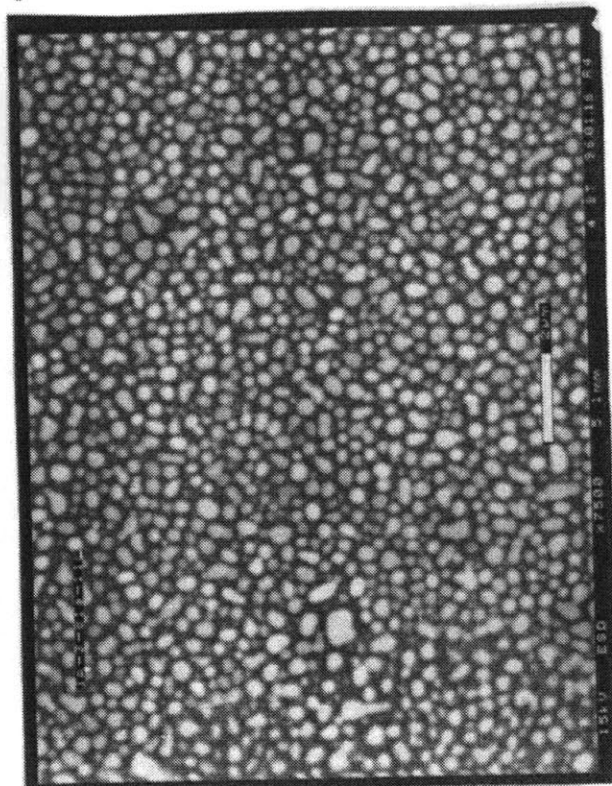
Figure 6.32: GIXRD (1°) of BiCuVOx films on quartz made from precursor solutions containing additives. (a) no additive, (b) ethanolamine (N, N-dimethylformamide, ethylene glycol, acetic acid same), (c) 1,3-propanediol
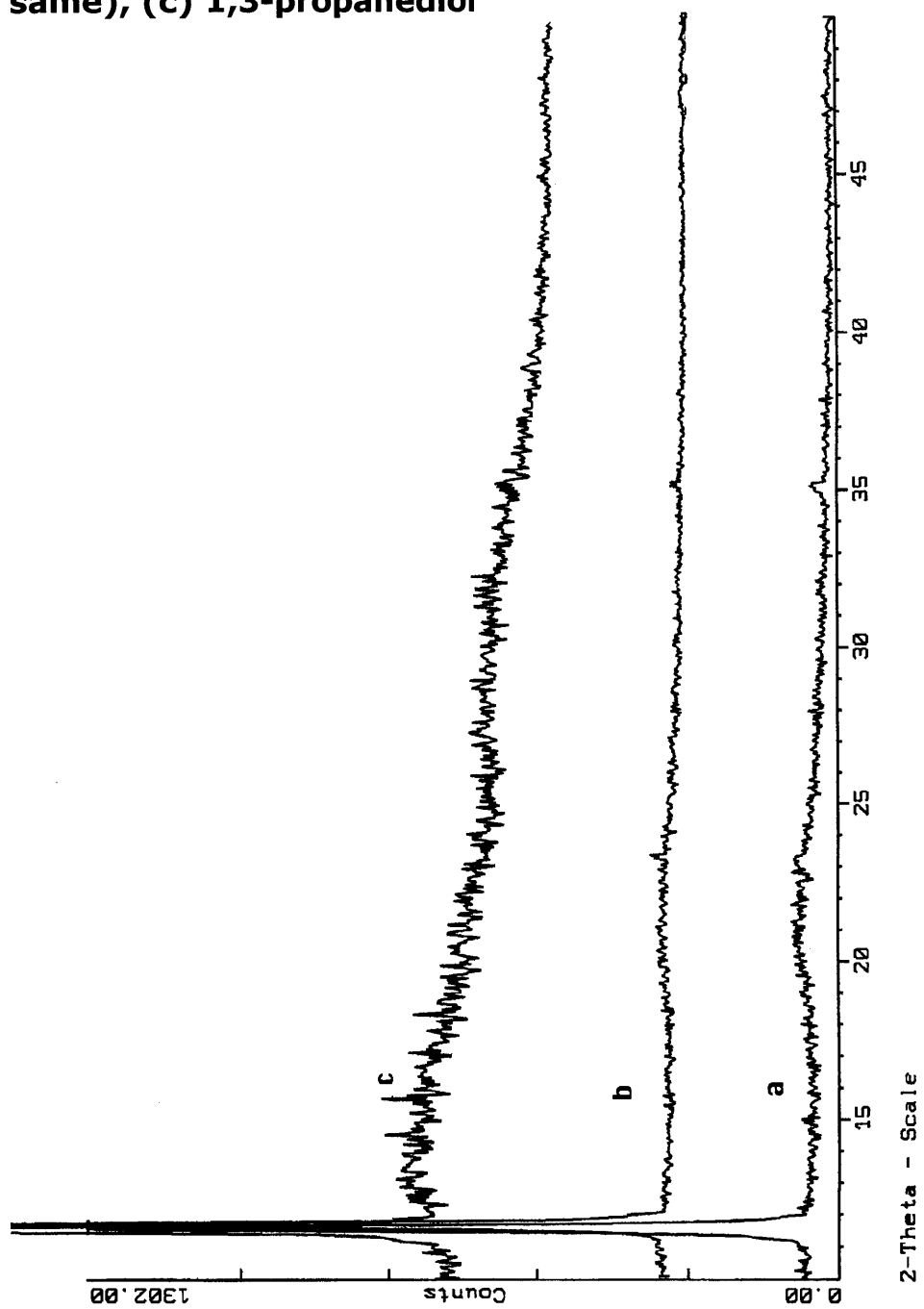
Figure 6.32, continued: (d) triethanolamine.
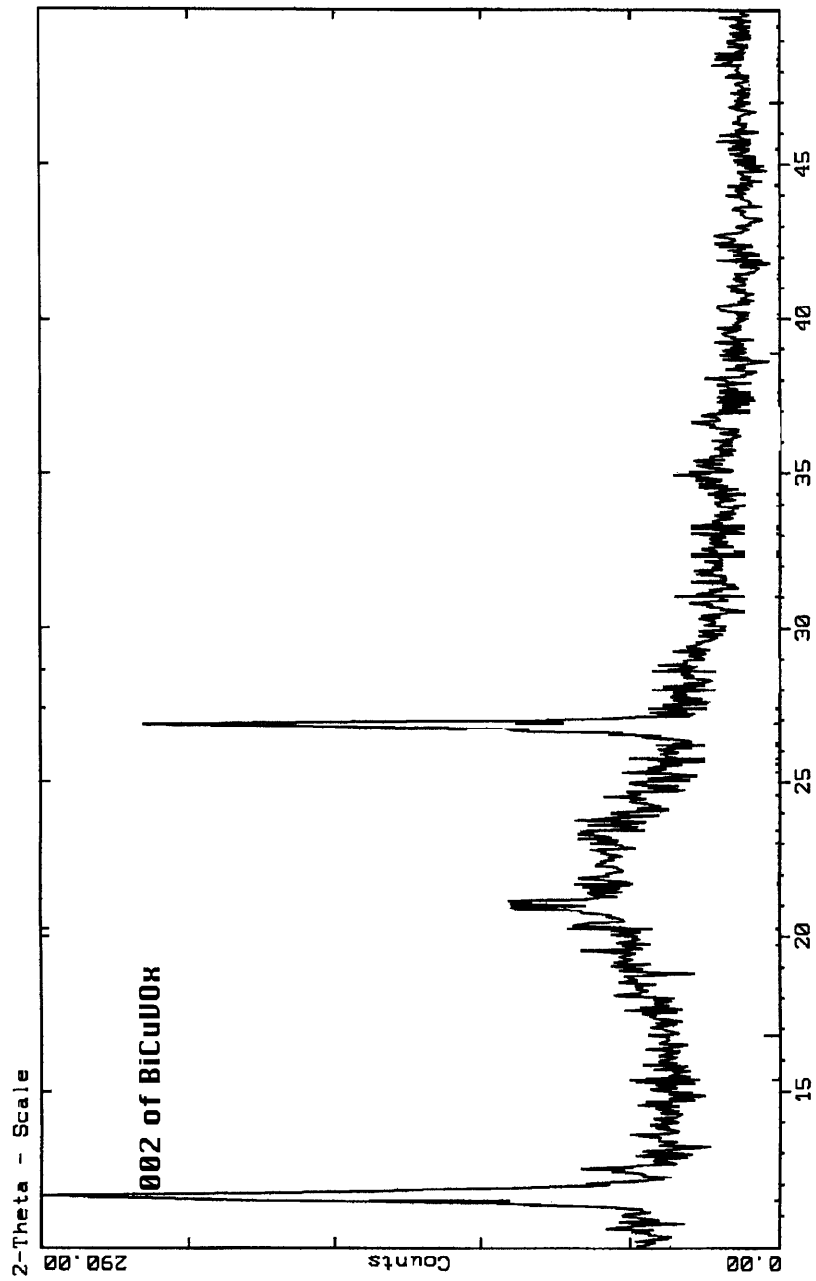
Figure 6.33: BiNbVOx films on quartz spin-cast from precursors containing additives. All films shown have been heated to 550 °C and are X 7500. (a) ethylene glycol, (b) triethanolamine, (c) N, N-dimethylformamide.

(a)
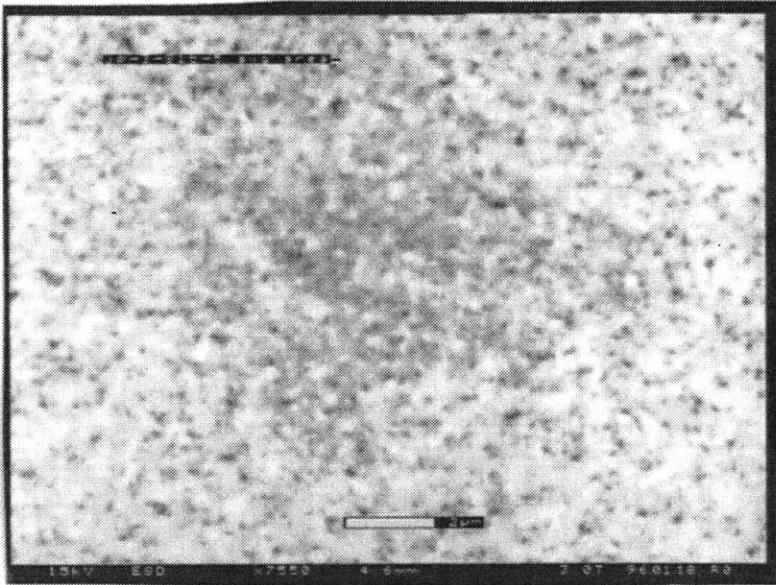
(b)
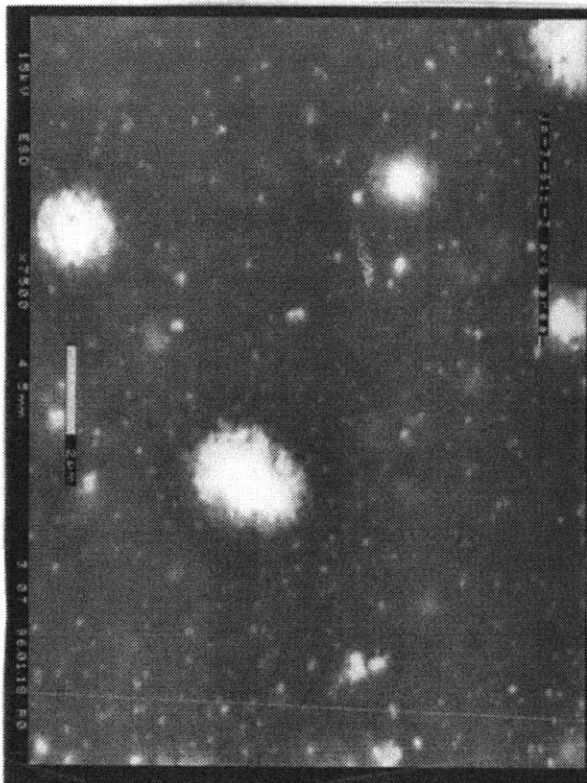
(c)
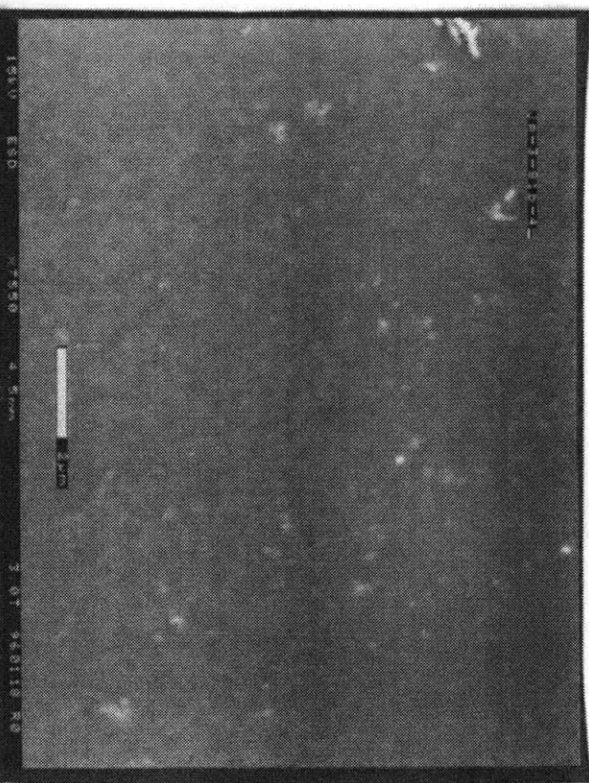
Figure 6.33, continued: : (d) diethanolamine, (e) acetic acid, (f) 1,3-propanediol. See Fig. 6.20b for a "control" film with no additive.

(d)
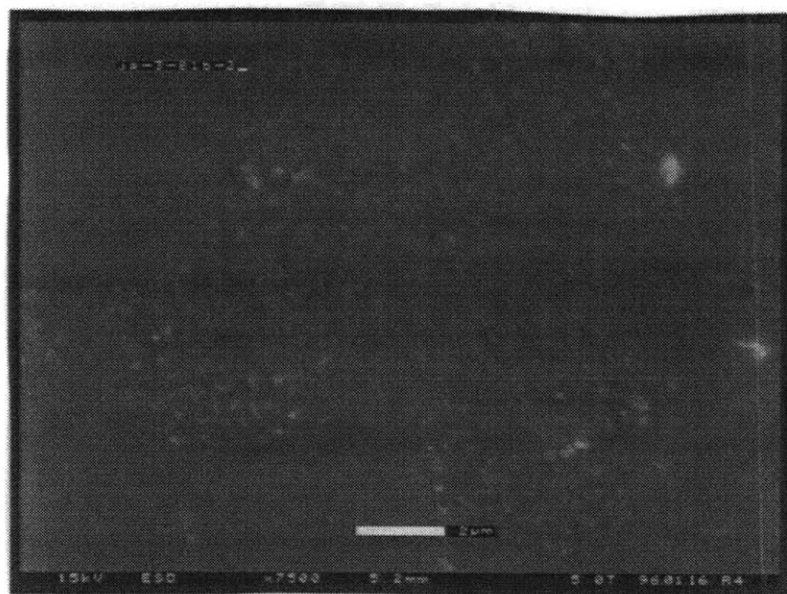
(e)
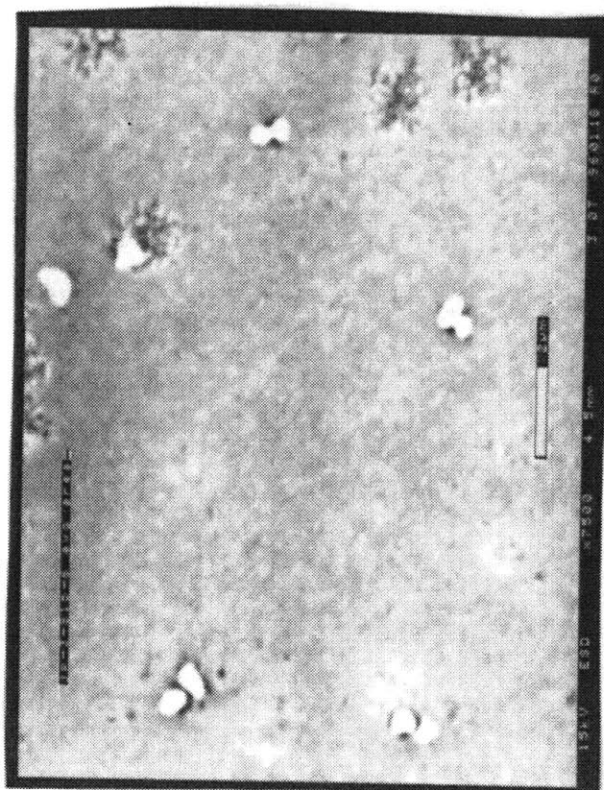
(f)
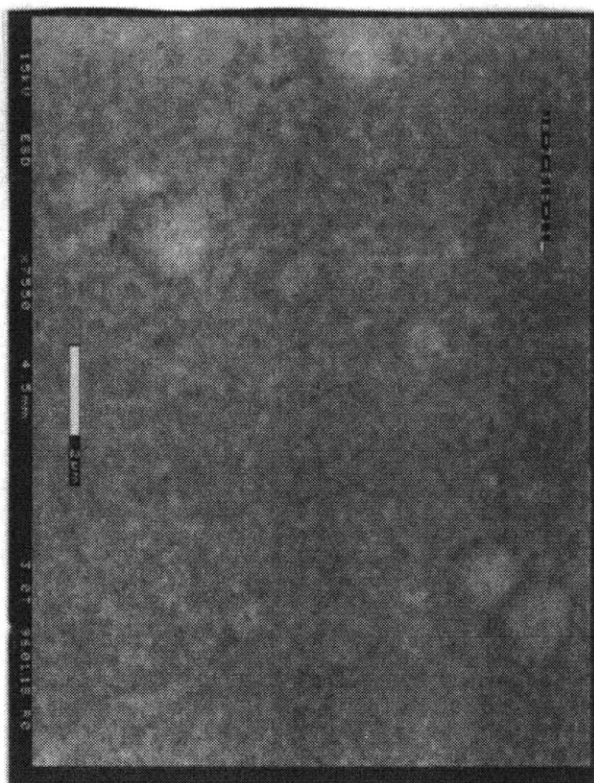
Figure 6.34: GIXRD (1°) of BiNbVOx films on quartz made from precursor solutions containing additives. (a) no additive, (b) ethanolamine (diethanolamine, N, N-dimethylformamide, ethylene glycol, acetic acid same), (c) 1,3-propanediol. The film produced using triethanolamine is completely amorphous to XRD.
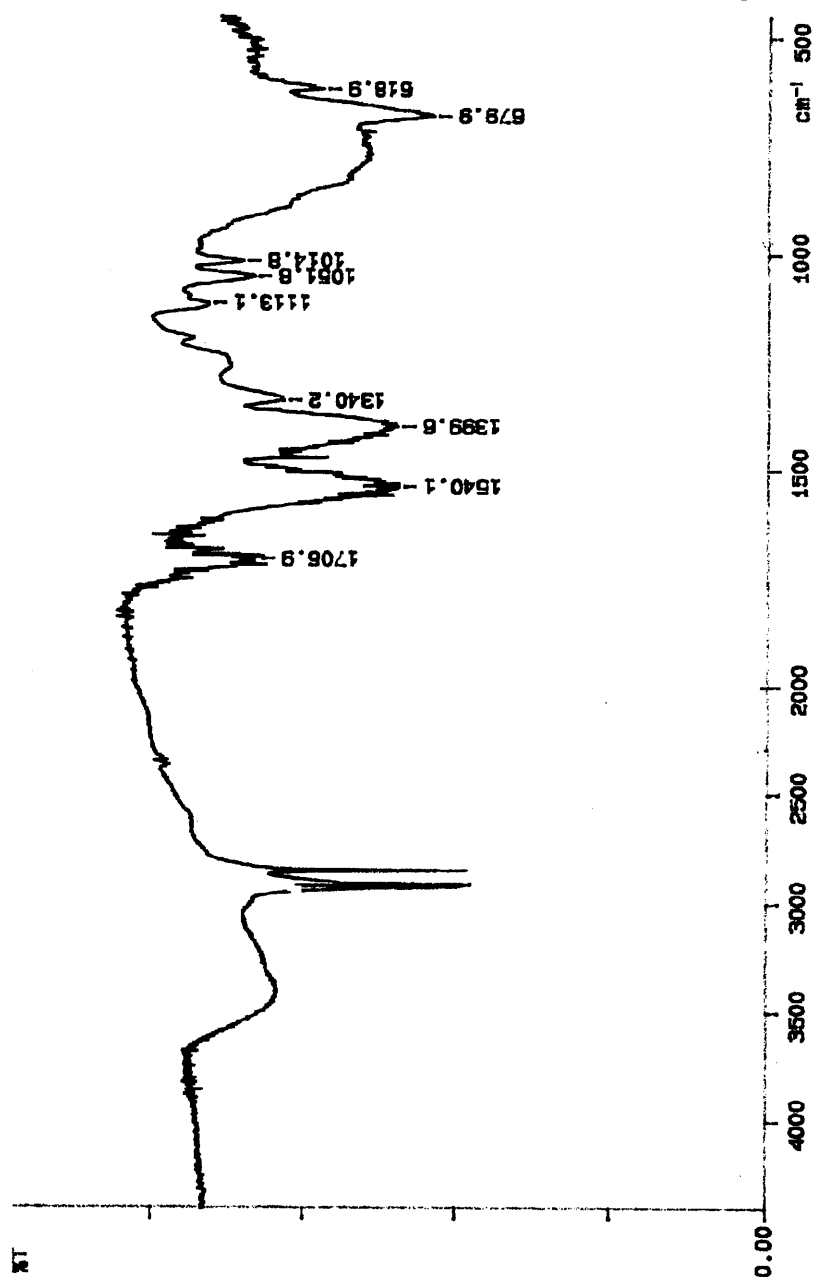
Figure 6.35: Effect of additives on the precursor gel morphology. Clockwise from left: no additive (X 160), 1,3-propanediol (X 865, ethylene glycol, dimethylformamide same), diethanolamine (X 175), triethanolamine (X 235).
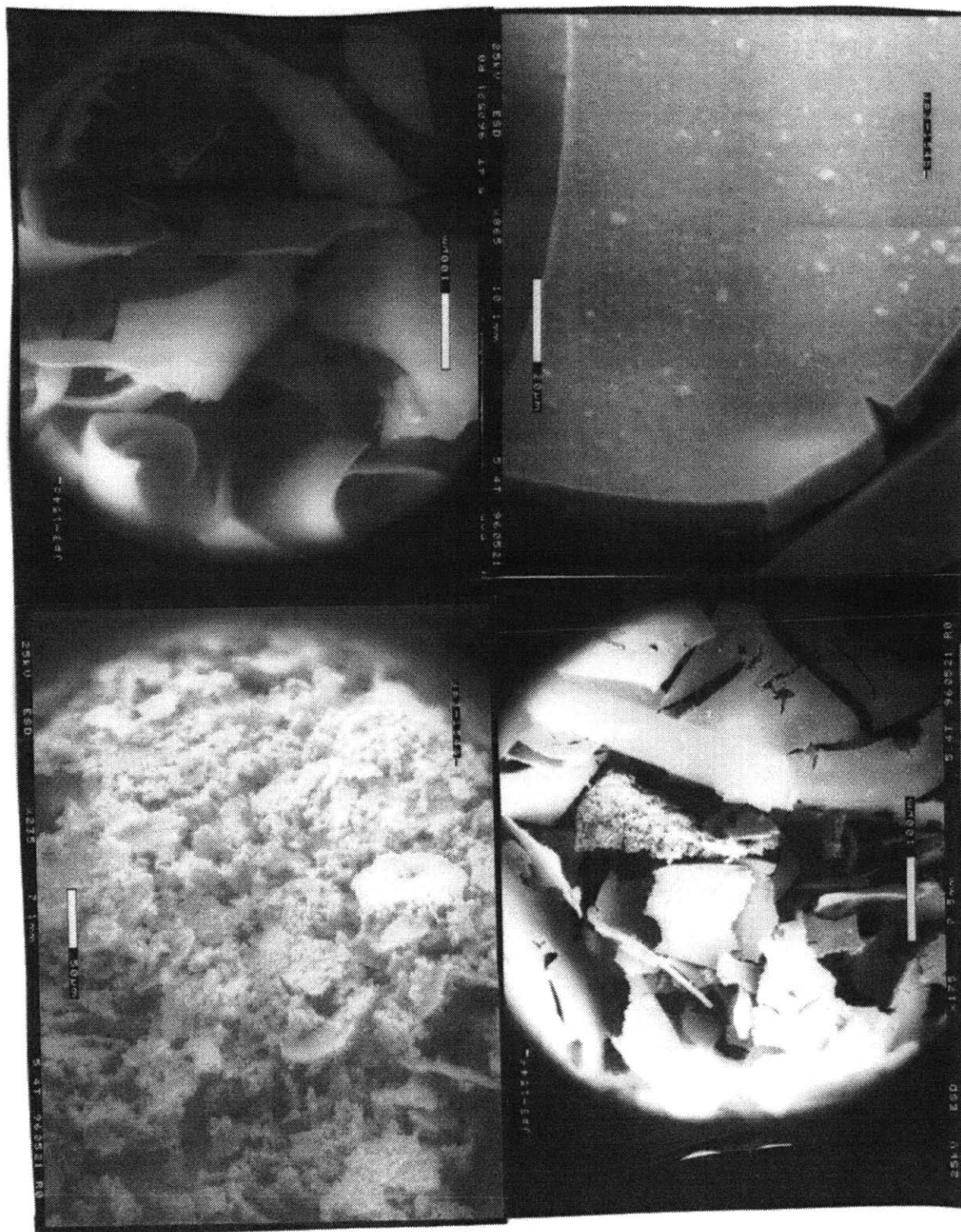
Figure 6.36: (a) FTIR of Bi$_2$VO$_{5.5}$ precursor hydrolyzed and dried _in vacuo_ overnight on an IR card (background subtracted).
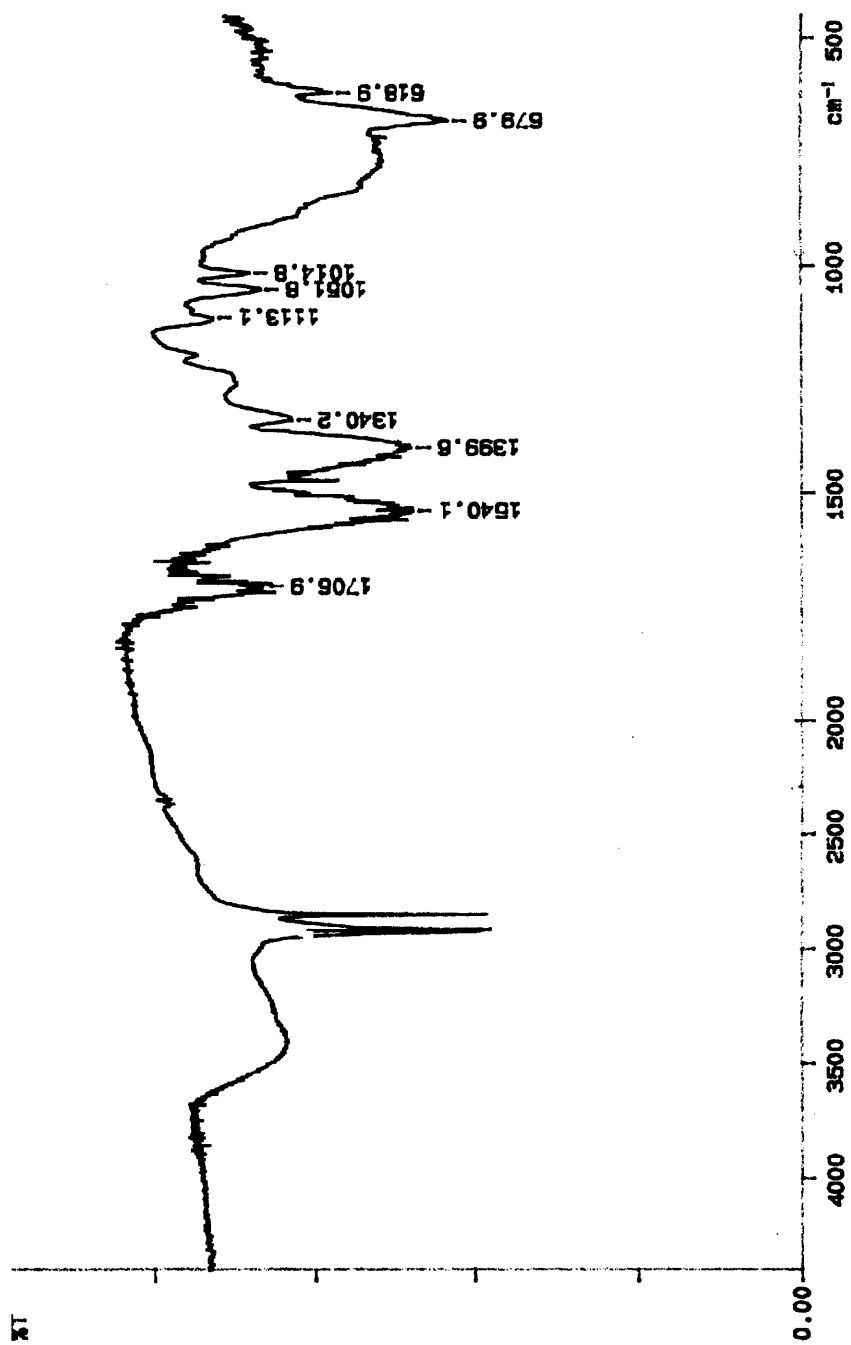
Figure 6.36, continued: (b) FTIR of $Bi_2VO_{5.5}$ precursor plus ethylene glycol, hydrolyzed and dried *in vacuo* overnight on an IR card (background subtracted).
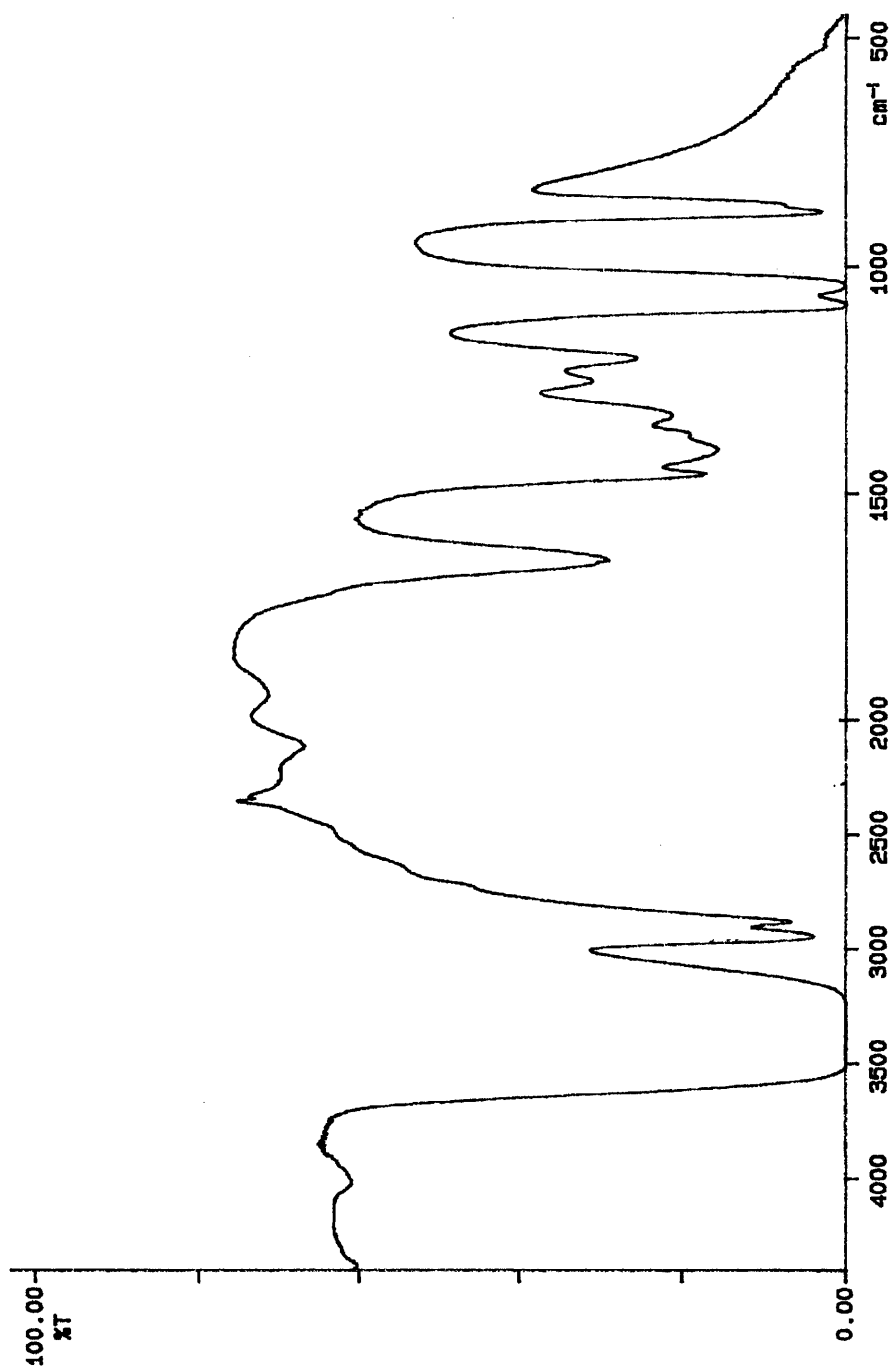
6.4 Results and Discussion – Porous Substrates

To date, CIMR components have been fabricated by extruding or otherwise forming a tube of the oxygen-ion conducting ceramic, usually YSZ.[72] The degree to which the wall thickness can be reduced is limited by the strength of the ceramic. Forming the conductor as a membrane on a porous support is an alternative, and was the ultimate goal of this project. The porosity of the support is necessary for gas permeability. One method of depositing such a film is disclosed in the patent literature:[73] electrochemical chemical vapor deposition (ECVD) is used to deposit an oxygen-ion conductor into a porous support. The conductor fills the pores, blocking them and providing semipermeability. In this case, the length of the conducting path is at least equal to the thickness of the support, and is more likely to be greater than the support's thickness because of the various twists and turns the pores in the support may take. Furthermore, the ECVD process does not lend itself to rapid or large-scale fabrication. We wanted to deposit a film of BiCuVOx *atop* the pores via, ultimately, a dip-coating process; and our original choice for a support was porous Vycor glass. However, due to the severe agglomeration seen with BiCuVOx films on the smooth quartz used as a model system for Vycor, porous alumina was chosen instead. This substrate was available with a highly monodisperse 0.02 μm pore size from Whatman.

The first step was to deposit films of BiCuVOx on porous alumina substrates having the pores plugged with BiCuVOx

material. This was done to provide a way of seeing whether the agglomeration seen on quartz substrates would also be an issue on the alumina (the results for BiCuVOx deposited on E-beam alumina were ambiguous due to questions about the adherence of the alumina film itself on the quartz (Figure 6.27)); the pores were plugged so that agglomeration effects could be distinguished from those arising from the porosity of the substrate. Aliquots of each of the stock solutions, made as described above, were diluted 50% with anhydrous methanol as usual and one of the following network modifiers was added in a ratio of one mole of additive per mole of alkoxide groups present: diethanolamine, triethanolamine, N,N-dimethylformamide, ethylene glycol, 1,3-propanediol, or acetic acid. One sample was left additive-free as a control. Each of the resulting precursor solutions was hydrolyzed with deionized water in an amount equivalent to the moles of alkoxide groups present.

Each precursor solution was permitted to soak into an Anopore disc, which was then dried and heated rapidly to 375 °C to remove solvents and most organics. One surface of each disc was swabbed quickly with dilute HCl to remove surface film (leaving BiCuVOx in the pores) and dried, then fired at 400 °C for 2h. This was expected to remove organics from the material in the pores and prevent production of volatiles which would damage the spin-cast film overlayers. After this initial preparation, 5 layers of film were deposited for each precursor solution as described above. The final thermal treatment was at 550 °C in air.

The samples were examined in ESEM and were found to be cracked. (Table 6.5) This was probably due to incomplete removal of the surface oxide by the HCl swab, leaving a thick and inelastic

film in some areas of each substrate. The appearance of pores in many of the films indicates the failure of the precursor to cover the substrate surface, in addition to the expulsion of ceramic material from the pores as organics not removed during the 400 °C heating step decomposed. (Figure 6.37) In most films, this appears to be the case, with many of the pores filled with film, while others remain empty. GIXRD on these films shows the presence of *00l*-oriented BiCuVOx. (Figure 6.38) Identification of other phases remained uncertain due to the excessive noise in the diffraction pattern caused by X-ray scattering off the pores of the substrate. This occurred at all angles within the diffractometer's range. Despite the poor quality of the films, it was apparent that the gross agglomeration seen with the BiCuVOx films on quartz was not occurring on the alumina substrates. We therefore went on to try to deposit films of BiCuVOx directly atop the substrate by spin-coating.

Five layers of BiCuVOx film were spin-coated onto a fresh Anopore disc for each additive-containing precursor solution described above. The final heating step was at 550 °C in air. The results for these samples are summarized in Table 6.5.

Several precursor solutions gave homogenous, pore-free films, though these had pinholes which were most likely due to dust contaminants. The area around these holes was uncracked, indicating a high degree of elasticity in the film. (Figure 6.39) The roughness in the surface morphology of the defect-free films reflects the texture of the substrate. The films were 0.3-0.5 μm thick according to measurement of the fracture-surface cross-sections in ESEM. GIXRD patterns tended to show a poor signal/noise ratio

due to the small quantity of diffracting material present, and a highly amorphous background which is due to the small effective crystallite size of the BiMeVOx ceramic on the alumina disc combined with X-ray scattering off the substrate pores. Lower incident angles did not improve the pattern. Due to the background, the phase purity of the films is uncertain. While the lattice of alumina (see Table 6.1) does not fit that of BiCuVOx in any direction – which may explain extreme graininess of the films on the E-beam alumina – the porosity of the Anopore discs may interfere with the regularity of the alumina lattice so that the substrate is in fact virtually amorphous. Films on E-beam alumina were phase-pure and *00l*-oriented. If so, there is no reason to expect that the film is not phase-pure BiCuVOx.

As with the precursor solutions used on smooth (poreless) substrates, it is unlikely that the small volume of the additives acted to produce continuous films by modifying the surface tension or viscosity of the precursor solutions. Instead, the difference between the film-producing behavior of the solutions containing various additives is in their hydrolysis behavior. The "control" solution, containing no additive, and dimethylformamide, diethanolamine, and 1,3-propanediol gave continuous films on the porous substrates. These gave varied results for films on smooth quartz. It may be that the additives which failed to give continuous films were those that tend to chelate rather than bridge,[74] and in failing to be removed on hydrolysis prevented formation of large precursor oligimers in the sol that could maintain structural integrity over the 0.02 μm span across the pores.

426

Table 6.5: Effects of Additives on BiCuVOx films on porous alumina

Additive	Pore-Plugged	No Plug
N,N-dimethylformamide	cracking & pores	pore-free
1,3-propanediol	pores visible	pore-free
Ethylene glycol	cracking & pores	cracking & pores
none	cracking & pores	pore-free
Acetic acid	cracking & pores	cracking & pores
Diethanolamine	pores visible	pore-free
Triethanolamine	pores visible	pores visible

Figure 6.37: BiCuVOx films deposited on pre-plugged Anopore porous alumina substrates. Additive: 1, 3-propanediol. (a) X 5900, (b) X 10000. Covered and non-covered parts are clearly visible.

(a)
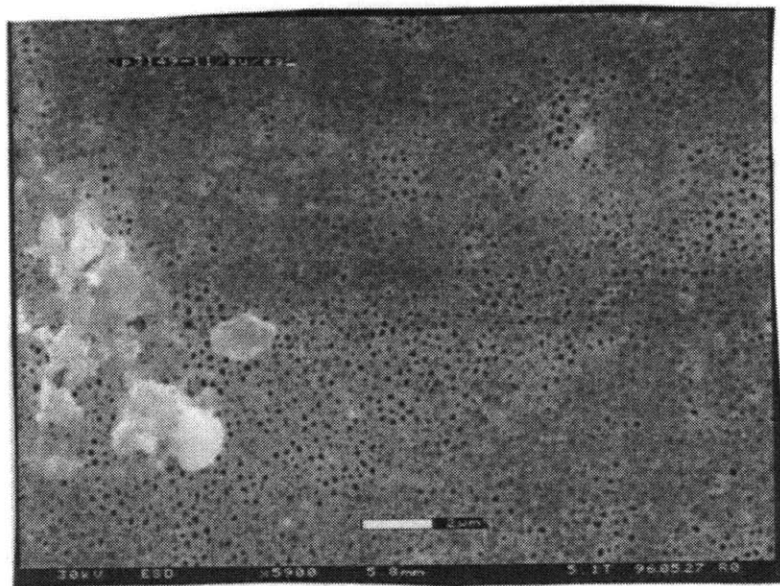
(b)
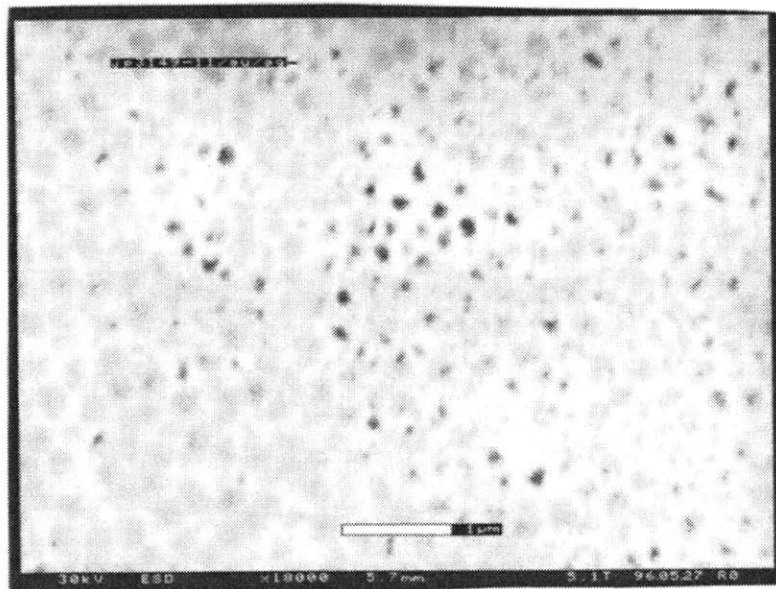
Figure 6.38: GIXRD (1.5°) of the film shown in Fig. 6.37. The gold peaks are due to the 100 Å layer of Au added to improve ESEM imaging. The marked lines are BiCuVOx.
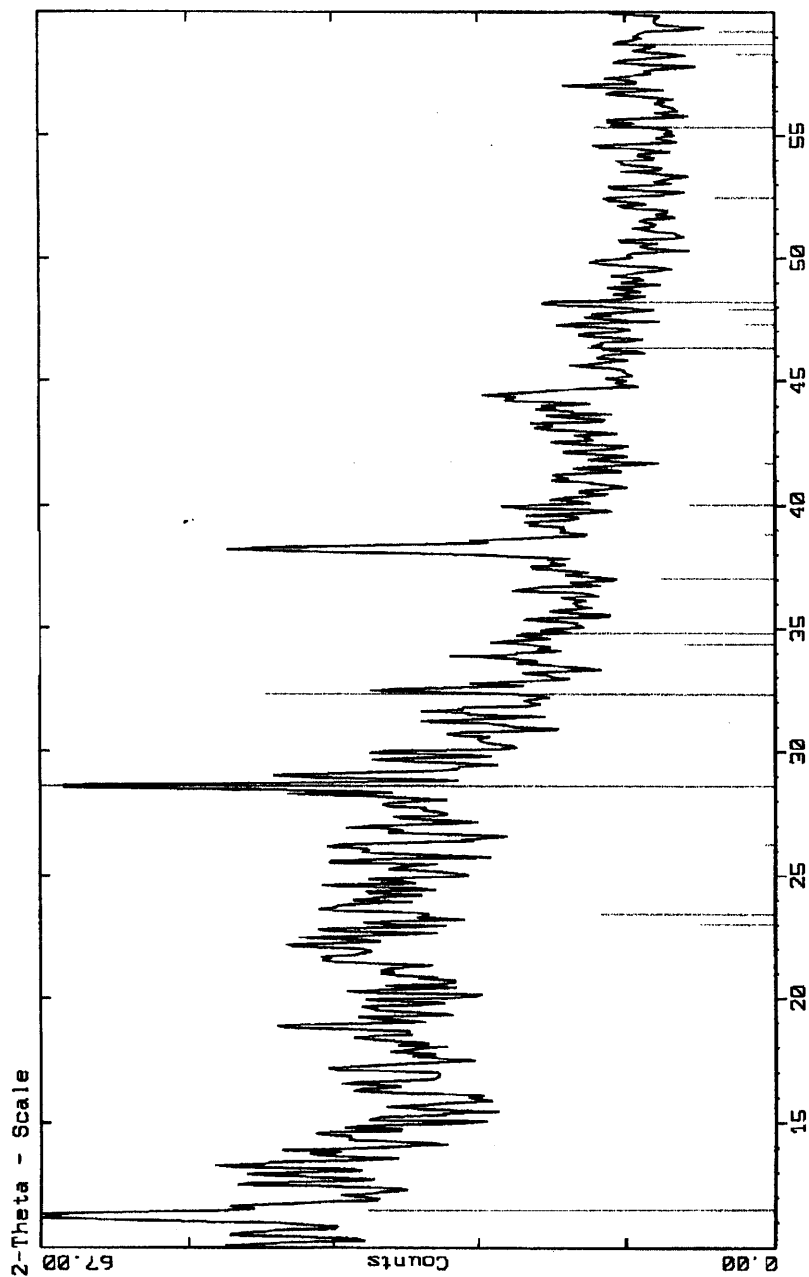
Figure 6.39: BiCuVOx films deposited on Anopore porous alumina substrates. (a) diethanolamine, X 17000. The dark areas are gouges deliberately made on the sample. (b) methanol, X 10000. The film has no defects.

(a)

(b)
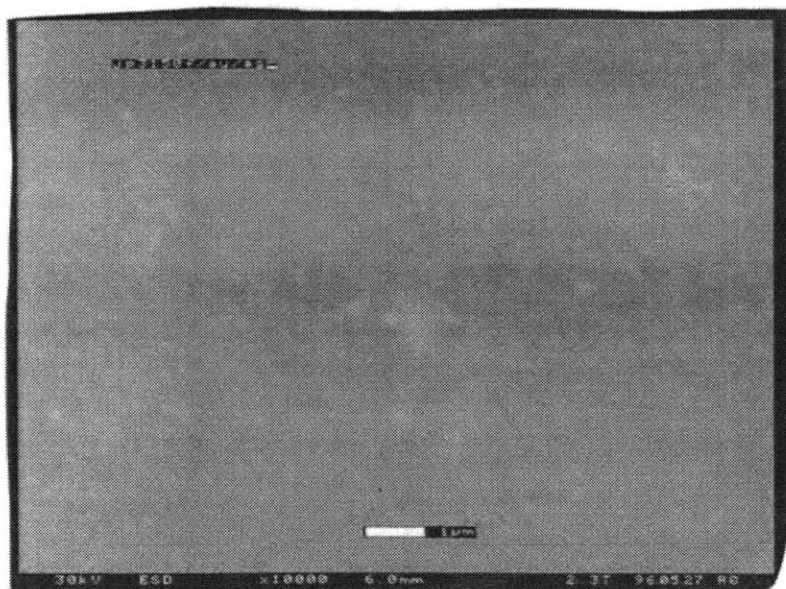
Figure 6.39, continued (clockwise): (c) 1,3-propanediol X 1350 and (d) X 12500, a close-up of the pore in the center of (c). This was probably made by a dust-mote. Note that the film is uncracked around the hole. (e) diethanolamine, X7950, fracture surface viewed at 25° to horizontal. The topography of the film is seen to be rough (the large raised areas are the clots of scraped film seen in (a)).
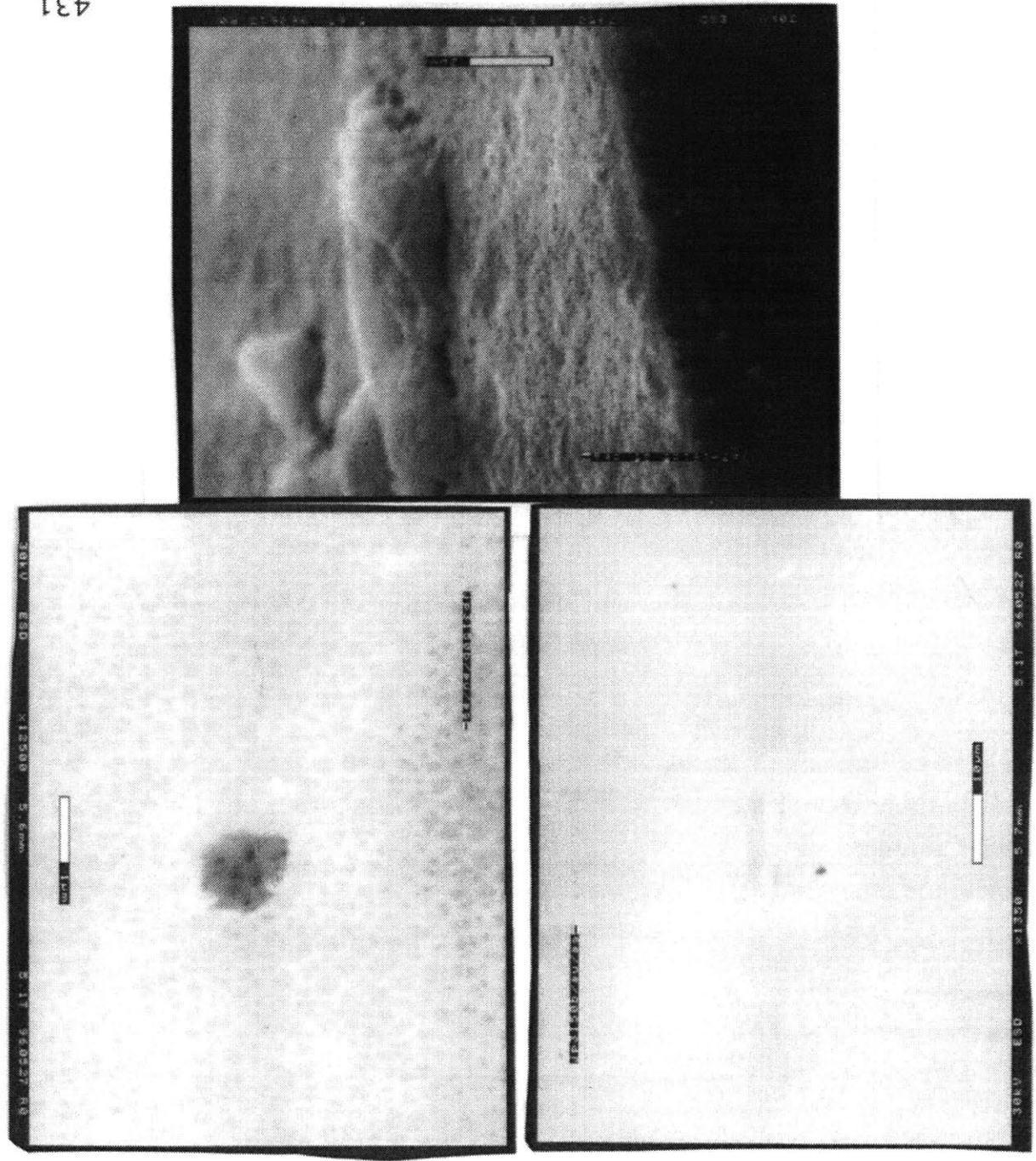
6.5 Conclusions

See Table 6.6 for a summary of key experiments and results described in this Chapter. Defect-free BiNbVOx films were cast onto smooth (poreless) quartz substrates, while films of BiCuVOx on quartz substrates were initially homogenous but showed agglomeration with increasing annealing temperatures. The film-substrate interaction energies are partly responsible for the difference between how these films behave on quartz. However, the higher number of hydrolyzable groups in the BiNbVOx precursor leads to a more highly connected and densifiable gel network and possibly mitigates the grain boundary segregation of dopants, which causes grain-boundary grooving and dewetting of the film from the substrate. Several gel-network modifying compounds were added to the BiCuVOx precursor solutions and did not significantly improve the quality of the resulting films, and in several cases had a deleterious effect on film quality due to interactions between the additive and the vanadium alkoxide. Films of BiMeVOx on quartz also had agglomeration behavior that followed the number of alkoxide groups. (Table 6.7)

Films of BiCuVOx were successfully cast onto porous alumina substrates. While GIXRD identification of these films was impossible, it is assumed that the change of substrate did not negatively affect the formation of the desired phase. Some BiCuVOx films deposited onto the porous alumina substrates were sufficiently thick to give a readable diffraction pattern, and appeared to contain only BiCuVOx. ESEM examination revealed these films to be on the whole defect-free and elastic, as evidenced by the behavior of the films around the occasional holes caused, apparently, by adventitious dust contaminants.

432

Table 6.6: Summary of key experiments and results

Experiment Class	Detail	Result Summary
basic parameters	spin vs. dip	dip-coat equipment gives poor reproducibility; use spin-coating
	substrate preparation	quartz slides must be cleaned with acetone and 48% $HF_{(aq)}$ rinse
	spin rate	best films at 3500 RPM
	heat treatment	require heating on hot-plate between layers; final anneal T>450 °C
BiCuVOx on quartz	final anneal temp.	defect free at 450 °C but develop agglomeration at higher temperature
	"anneal out" bare areas	severe agglomeration/ islanding to 850 °C
	change hydrolysis ratio	increased water gives no change in agglomeration, increases pore size
	additives	worsen agglomeration; variation among additives connected to presence of dangling -OH group?
	use copper aminoalkoxide	still agglomerated

Table 6.6, continued.

Experiment Class	Detail	Result Summary
BiCuVOx on other substrates	platinum	defect-free for control and all additives
	alumina	defect-free but very grainy
other BiMeVOx on quartz	BiNbVOx	defect-free on Pt and quartz for control and all additives
	BiFeVOx	agglomeration on quartz substrates
	BiMnVOx	agglomeration on quartz substrates
	BiTiVOx	defect-free on quartz substrates
BiCuVOx on porous substrates	plug pores	overlayer film destroyed by decomposition from pores
	pores not plugged	defect-free for control and some additives

Table 6.7: Effect of Alkoxide Groups on Film Behavior on Quartz

Film	# OR from V alkoxide	# OR from M dopant	-OR / Bi	Film Quality
BiMnVOx	3.4	0	1.7	agglomerated
BiFeVOx	3.6	0	1.8	agglomerated
BiCuVOx	3.6	0	1.8	agglomerated
BiCuVOx (aminoalkoxide)	3.6	0.2	1.9	agglomerated
BiTiVOx	3.6	0.4	2.0	defectless
BiNbVOx	2.8	1.5	2.15	defectless

6.6 Experimental Section

General comments regarding experimental procedures may be found in Sections 6.1.2 and in the Appendix to Part I of this thesis.

6.6.1 Dip coating experiments

Experiment 1 (JWP-II-161) Dip Coating BiCuVOx on Quartz and Pt

A precursor solution was made by dissolving $Bi(OAc)_3$ (5.000 g, 12.95 mmol) V-2MOE (16.54 g, 5.827 mmol), and $Cu(OAc)_2$ (0.1176 g, 0.6475 mmol) in 150 ml 2MOE as described in Chapter Four to produce a 0.0432 M BiCuVOx solution. The solution was split into two samples. One of them was hydrolyzed with water (0.1 ml to 18.5 ml solution, 2 mol H_2O per alkoxide group). Quartz slides were cleaned in acetone and 48% aqueous HF solution, rinsed with water, then heated on a hotplate (350 °C) for 15 minutes. They were then cooled to room temperature in a dessicator. These substrates were dipped by hand with an approximate withdrawal rate of 1 cm/sec, into either the hydrolyzed or unhydrolyzed precursor solution twice, with intermediate drying in air or under vacuum (vacuum dessicator, approximately 1 torr) followed by 5 min. on a 300 °C hotplate or in a 550 °C furnace. (Table 6.8) Samples were heated in a furnace at 350, 450, 550, or 650 °C for 3 hours followed by slow cooling and examination under light microscope, GIXRD, and ESEM. (Figure 6.40)

Table 6.8: Parameters and Results Summary for Experiment 1

Table codes: hyd = sample was hydrolyzed; air or vac = method of drying, hp = sample placed on hot plate; rta = sample put in and out of 550 °C furnace; T = temperature of final annealing; in GIXRD Results column: g, other = phases seen; pref = $00l$-oriented.

Sample	hyd	air OR vac	hp	rta	T (°C)	Appearance	GIXRD Results
161HAQ	Y	air	N	N	550	translucent, crazing	γ, other, pref
161HBQ	Y	vac	N	N	550	opaque	γ
161HCQ	Y	vac	Y	Y	550	translucent, cracks	γ,pref
161HDQ	Y	vac	Y	N	550	translucent / opaque, cracks	γ, other, pref
161HEQ	Y	air	Y	Y	550	opaque	γ
161HFQ	Y	air	Y	N	550	opaque	γ
161UAQ	N	air	N	N	550	crazing	γ, other
161UBQ	N	vac	N	N	550	crazing	γ, other
161UCQ	N	vac	Y	Y	550	cracked	γ, pref
161UDQ	N	vac	Y	N	550	smooth, islands	γ, amorph
161UEQ	N	air	Y	Y	550	cracked	γ, other
161UFQ	N	air	Y	N	550	islands, cracked	γ, other
161HQ3	Y	air	Y	N	350	crazing, voids	amorph
161HQ4	Y	air	Y	N	450	crazing, opaque	γ

Table 6.8, continued.

Sample	hyd	air OR vac	hp	rta	T (°C)	Appearance	GIXRD Results
161HQ5	Y	air	Y	N	550	crazing, voids	γ, other
161HQ6	Y	air	Y	N	650	crazing, voids	γ, slight pref
161UQ3	N	air	Y	N	350	crazing, voids	amorph
161UQ4	N	air	Y	N	450	crazing, voids	γ
161UQ5	N	air	Y	N	550	crazing, voids	γ
161UQ6	N	air	Y	N	650	crazing, voids	γ, other

Experiment 2 (JWP-II-168) Dipcoating with a more dilute solution

The unhydrolyzed precursor solution described in Experiment 1 was diluted 50% with anhydrous methanol and hydrolyzed with 2 moles of water per mole of alkoxide group. The precursor was dip-coated three times onto quartz substrates prepared as described in Experiment 1. Between coatings, the substrates were left horizontal to dry then rapidly heated in a 600 °C furnace. (Five samples were treated identically.) The resulting films was examined by GIXRD (1°) and ESEM. Figure 6.41 shows a typical result, with large-scale voids in the films and on the smaller scale, cracking and voids between grains. GIXRD shows oriented BiCuVOx with an amorphous background.

6.6.2 Spin coating experiments

Experiment 3: Construction and calibration of spin-coater

We constructed a spin-coating apparatus by removing from a Beckman #152 Microfuge Centrifuge the tube-holding arms and the switch. Switching and motor speed was instead handled via the voltage setting on a Staco Energy Products #3PN1010 Variable Autotransformer variac. The apparatus was placed on thick, soft rubber pads to damp vibrations. A hole was cut in the cover, directly over the rotating center stud, through which precursor solution could be dropped onto the rotating substrate. The

substrate was mounted on the rotating center stud with red clay initially, and later with Fun-Tak™ adhesive. The spin-coater was calibrated using a Strobotac Type 1531 (General Radio Co.) strobe light. A line was marked on the rotating center stud and the variac set at the desired voltage setting. After 5 sec, the strobe light was set to make the red line appear to stand still. The setting was read directly from the strobe light; for RPM of the hub center, these numbers are to be divided by 2 due to the sampling method used.

It was noted that the rotation rate varied somewhat with the time the centrifuge had been running, becoming constant approximately 20-30 s after the switch had been turned to the "on" position. The calibration plot is reported below; points very far off, and those for variac setting > 40, at which the speed reached a plateau, where discarded. (Figure 6.42)

Experiment 4 (JWP-II-169) optimization of spin coat speeds

A number of different spin rate settings and times were tried and an "optimum" setting chosen according to what gave the most consistent and best results for the same solution. It should be noted that the optimum spin rate varies with the solution viscosity; however, since we sought to optimize the solution itself, the initial tests were used to obtain a convenient set of spin coater settings for what was believed to be a reasonably standard solution. Because the spin-coater required some 30 s of spin time before its rate became constant, some tests were done comparing films where the precursor solution was dropped on, then the sample spinning started, with those where the solution was dropped onto

the spinning sample. Those where the solution was dropped onto a non-spinning sample had a ring of film near the center of the sample, where apparently additional film was deposited due to rapid evaporation of the solvent from the precursor prior to its distribution in spin-up.

The precursor solution JWP-II-168, described in Experiment 1, was dropped onto a spinning quartz substrate which had been prepared as in Experiment 1. Several variac settings were used, each for 15 s of spin. Each of the samples was coated three times with intermediate drying, baking on a hot plate (300 °C), then heating 10 min in a 600 °C furnace before final annealing at 650 °C/2 h with cooling at 2°/min. Results are summarized in Table 6.9.

A sample of the precursor solution, diluted 50% with methanol, was spun onto the substrate at setting 30 for a total of 20 coatings with intermediate heatings as described. It was noted that the apparent color of the film changed with increasing layer number when the film was viewed at a slight angle: e.g. < 12 coats, completely transparent and colorless; 14 coats blue-violet; 16 coats green; 18 coats reddish; >20 coats yellow when viewed normal to the substrate (e.g. natural color of the ceramic). This observation was used as an on-line estimate of film thicknesses. (Figures 6.43, 6.44)

The general procedure for use of the spin coater involved spinning the substrate for approximately 15 seconds at 30V on the variac (3500 RPM), then dropping on the solution and spinning an additional 2-5 seconds (timings were by observation of a stopwatch). The sample was permitted to stop rotating slowly by simply shutting off the current to the spin coater.

Because dust particles were expected to cause problems in the film quality, dust was kept to a minimum in the region of the spin-coating by (1) keeping the centrifuge cover down, (2) using a low-particulate Aero-Duster™ spray to clean the immediate area of the depositions before spin-coating, and (3) passing the precursor solutions through a filter (Gelman Sciences Acrodisc™ 0.2 μm syringe filter) as they were dropped onto the spinning substrate.

Table 6.9: Results of Varying the Spin Rate

Variac Setting/ Speed (RPM)	GIXRD	Appearance
20/1100	*001* oriented	translucent, cracked
25/2600	*001* oriented	translucent, cracked
30/3500	*001* oriented	transparent, grainy in ESEM
40/5500	amorphous	not covered with film?

6.6.3 Deposition of BiCuVOx on Quartz Substrates

Experiment 5 (JWP-III-17) BiCuVOx Precursor with Catalyst, Different Anneal Temperatures

A precursor solution was made to approximately 0.05 M BiCuVOx by adding $Bi(OAc)_3$ (9.653g, 25 mmol), V-2MOE (22.695g at 4.96×10^{-4} mol/g, 11.3 mmol), and $Cu(OAc)_2$ (0.227g, 1.3 mmol) to 250 ml 2MOE. Ten ml of this solution was diluted with 10 ml of a

mixture of MeOH and acid or base, as described in the table below. These solutions were then hydrolyzed with water (0.25 ml, 13.9 mmol, 1.25 equivalents relative to vanadium; the water content of the acids/bases was ignored). Samples were spin-coated as described above for 6 coats, with intermediate heating, first on a hot plate (300 °C), then in a furnace at 550 °C for 10 minutes with rapid heating and medium cooling. (The cooling rate was moderated by handling the samples on a thick block of alumina which was placed in the oven and removed with the samples on it, and which cooled to room temperature fairly slowly when placed on an insulated pad.) Samples were then final-annealed at 600 °C or 875 °C for 8 h, with cooling to RT at 1.5 °/min. (Table 6.10) The acid catalysis alone made no improvement in the film quality.

Table 6.10: Effect of Acid/Base and Heating Temperature

Sample	Temp (°C)	Added to 10 ml precursor	Optical Microscope	ESEM result location
III-18A	875	10 ml MeOH	some cracking	Figure 6.45d
III-18B	600	10 ml MeOH	cracking	Figure 6.45a
III-18C	875	5 ml MeOH + 5 ml HOAc	cracked areas	Figure 6.45e
III-18D	600	5 ml MeOH + 5 ml HOAc	smooth with porosity	Figure 6.45b
III-18E	875	8 ml MeOH + 2 ml HOAc	cracking, beading	large-scale cracking
III-18F	600	8 ml MeOH + 2 ml HOAc	spotty coverage	not done
III-18G	875	9 ml MeOH + 1 ml NH_4OH	"molten" spots, peeled areas	not done
III-18H	600	9 ml MeOH + 1 ml NH_4OH	spotty coverage (inst. blue gel in precursor sol'n)	not done
III-18I	875	9.75 ml MeOH + 0.25 ml HNO_3	severe cracking	not done
III-18J	600	9.75 ml MeOH + 0.25 ml HNO_3	grainy; crazed areas	Figure 6.45c

6.6.4 Variation of hydrolysis water

Experiment 6 (JWP-III-34) BiCuVOx Films, Varying Water

The precursor solution made in Experiment 5 above was diluted 2/3 with methanol and split into several 25-ml samples. One sample was left unhydrolyzed, while the others were or hydrolyzed with, respectively, 68 µl, 136 µl, 0.34, or 0.68 ml of water (1, 2, 5, 10 equivalents relative to the number of alkoxide groups). These were spin-coated under the usual conditions onto quartz substrates (prepared as described above) with intermediate heating on a hotplate, followed by 5 min. at 550 °C, for a total of 9 coats. Unhydrolyzed precursor solution would not wet the quartz sufficiently to deposit a film. The samples were pyrolyzed at 575 °C for 8 hours with cooling at 5 °/min, then examined by GIXRD and ESEM. All GIXRD showed highly oriented films (002, 004, 006 only); ESEM showed high porosity in all cases. See Table 6.2 above. (Figure 6.46)

Experiment 7 (JWP-III-43) Additional layers to "fill in" pores

Films produced in Experiment 6 above were spin-coated again according to the same procedure, placing on an additional 4 layers of film. These were heated again at 575 °C/8h with 5°/min cooling, and re-examined under an ESEM. Figure 6.47.

6.6.5 Variation of annealing temperature

Experiment 8 (JWP-III-5) BiCuVOx, Variation of Annealing Temperatures

Quartz substrates were spin-coated with a precursor solution made by diluting 15 ml of the precursor solution made in Experiment 1 with 25 ml MeOH and hydrolyzing with 0.5 ml (12 equivalents relative to the number of alkoxide groups) of water. Five layers were spin-coated (setting 30, 3 sec) onto the samples, with intermediate time on a hot plate (300 °C). Some samples were dipped one time in the precursor solution after the spin layers were deposited. Samples were heated 1 hour in each of 450, 550, and 650 °C and examined by GIXRD and ESEM. (Figure 6.48, 6.49) One sample was not heated in a furnace at all; after the final layer it was left on the hot plate at its highest setting (approx. 350 °C) for 1 hour. GIXRD (1°) shows increasing crystallinity and orientation of the BiCuVOx phase with rising temperature. The samples which had been dipped for their final coat were less oriented. (Figure 6.50)

Experiment 9 (JWP-III-21) Higher temperature to anneal out pores

The samples from Experiment 8 were reheated for 1 hour (ramp 5°/min, cooling 1°/min) in 750, 800, and 850 °C furnaces. The ESEMs show "beading" of the film into islands and increased voiding between grains. Figure 6.51. The samples were subjected to a 3rd heating at 750 °C for 8 hours and were found to have still increased

446

voiding between grains, as well as agglomerated areas.   Figure 6.52.

Experiment 10 (JWP-III-81) Varying temperature, less water

Stock solution was produced by adding $Bi(OAc)_3$ (2 g, 5.2 mmol), V-2MOE (4.7g at 4.96×10^{-4} mol/g, 2.3 mmol), and $Cu(OAc)_2$ (0.0485 g, 3 mmol) to 2MOE to make a 100 ml total volume. This was diluted 50% with methanol and hydrolyzed with 0.17 ml water (1 equivalent relative to alkoxide groups). This solution was deposited by spin-coating (variac at 30%) for 3 s, followed by placement on a hot plate (300 °C) between layers. Eight layers of film were deposited in this manner. The films were heated in air for 2 h at 450, 550, and 650 °C with cooling at 2 °/min then were examined by GIXRD and ESEM. (Figures 6.14, 6.15).

6.6.6 Behavior of Bulk Gels in Presence of Additives

Experiment 11 (JWP-II-122) Additive effects on phase formation, gel quality

Precursor solutions containing $Bi(OAc)_3$ (4 g, 10.4 mmol), V-2MOE (7.125 g, 3.53 mmol), and $Cu(OAc)_2$ (0.094 g, 5 mmol) in 30 ml 2MOE were mixed with diisopropanolamine (0.47 g, 3.5 mmol), acetylacetone (0.35 g, 3.5 mmol), or ethylene glycol (0.22 g, 3.5 mmol), in the amount of 1 mol additive per mol vanadium. The sample containing diisopropanolamine showed no change at first, but overnight had a fluffy white sediment in a deep green liquid.

The sample containing acetylacetone became milky blood red and on heating, green; standing overnight produced a bright yellow precipitate. The solution containing ethylene glycol showed no immediate change but had some white precipitate after overnight standing. These were stirred again and diluted to 150 ml with 2MOE, then hydrolyzed with water (0.25 g, 1 equivalent relative to the number of alkoxide groups). After standing overnight, the one containing diisopropanolamine gave a pale green gelatinous solid and green supernatant; acetylacetone one gave a beige and orange precipitate and orange-green supernatant; ethylene glycol one gave a firm green gel with no syneresis. All were heated 12 h at 550 °C in air and characterized by XRD. All three showed γ phase BiCuVOx with a distinct $BiVO_4$ impurity.

Experiment 12 (JWP-II-137) Additive effects on gel and phase quality II

Precursor solutions were made as in Experiment 11, and additives dimethyl succinate (0.51 g, 3.5 mmol), 1,3-propanediol (0.27 g, 3.5 mmol), ethanolamine (0.21 g, 3.5 mmol), diethanolamine (0.37 g, 3.5 mmol), and triethanolamine (0.52 g, 3.5 mmol) added in the amount of 1 mol additive per mol of vanadium. Each solution was hydrolyzed with water (0.25 g, 1 equivalent relative to the number of alkoxide groups). See results in Table 6.11.

The solids were pyrolyzed 550 °C for 12 hours and characterized by XRD; all gave clean γ phase BiCuVOx, except

diethanolamine and triethanolamine, which gave BiCuVOx
contaminated with $BiVO_4$.

Table 6.11: Results for Experiment 12, effects of some additives on bulk gels.

Additive	Solution, pre-hydrolysis	After hydrolysis + 12 hours	behavior on quartz slide, hydrolyzed
dimethyl succinate	clear green	inhomogenous gelatinous liquid	uniform wetting
1,3-propanediol	milky green	firm gel	uniform wetting
ethanolamine	yellow-green milky	blue liquid & ppte	beading, particles
diethanolamine	yellow-green clear	blue liquid & milky gel	wetting, particles
triethanolamine	clear bright yellow	infirm gel	uniform wetting

Experiment 13 (JWP-II-162) Effects of additives on gel III; initial dip-coating experiments

A precursor solution was made by dissolving $Bi(OAc)_3$ (5.000 g, 12.95 mmol) V-2MOE (16.54 g, 5.827 mmol), and $Cu(OAc)_2$ (0.1176 g, 0.6475 mmol) in 150 ml 2MOE as described in Chapter Four to produce a 0.043 M BiCuVOx solution. Three 10-ml samples (5 mmol V) of this solution were set aside and ethanolamine (0.684 g, 11.2 mmol), diethanolamine (1.052 g, 10.0 mmol) or triethanolamine

(1.661 g, 11.1 mmol) were added to three 10-ml samples of this solution, and the solutions hydrolyzed with 0.1 ml (5.6 mmol) water. In the samples containing ethanolamine and diethanolamine a milky appearance occurred immediately, and the solution turned blue-green; the one containing ethanolamine gelled almost instantly, but the gel was broken up easily by agitation. The triethanolamine-containing solution remained yellow and clear. Quartz slides were dipped into each precursor twice with intermediate heating on a hot plate, then heated for 3 h at 550 °C with cooling at 3°/min. All three films were cracked under optical microscope inspection, and while the ethanolamine- and diethanolamine-containing samples were γ-BiCuVOx according to GIXRD, the triethanolamine-containing solution gave an amorphous film.

Experiment 14 (JWP-III-31) Effects of additives IV

A precursor solution was made by dissolving $Bi(OAc)_3$ (5.000 g, 12.95 mmol) V-2MOE (16.54 g, 5.827 mmol), and $Cu(OAc)_2$ (0.1176 g, 0.6475 mmol) in 150 ml 2MOE as described in Chapter Four to produce a 0.043 M BiCuVOx solution. Six 10-ml samples (5 mmol V) of this solution were diluted with 4 ml MeOH and set aside some of the additives listed below added. In all cases, the additive was added in 1 mol/mol V to a precursor solution; each solution was hydrolyzed with 0.1 ml (5.6 mmol) of water.

Table 6.12: Effects of additives on gel quality, Experiment 14

Additive	Am't (g)	Instant Result	Overnight Result
pyridine	0.40	milky blue color	opaque green gel
acetylacetone	0.50	clear red-brown color	transparent green gel, brown particles
triethanolamine	0.75	clear green color	no gelation
diglyme	0.68	clear green color	transparent gel, cracked
1,3-propanediol	0.38	clear green color	transparent gel, uncracked
ethylene glycol	0.31	clear green color	transparent gel, dense

Experiment 15 (JWP-III-129) ^{51}V NMR of solutions with additives

Several of the additives used in the experiments above were added to 10-ml V-2MOE solutions 2.2×10^{-3} mol/g in V, at 1 mol alkoxide per mole of additive. ^{51}V NMR spectra were taken on a Varian Unity 300 MHz instrument using $VOCl_3$ as an external standard ($\delta=0$ ppm). See Table 6.13 for results.

Table 6.13: ^{51}V NMR of V-2MOE solutions containing some additives

Additive	Amount (g)	^{51}V NMR Peaks (ppm)
none (control)	0	-541
diethanolamine	0.0023	-437, -461
triethanolamine	0.0033	ppte; not done
ethylene glycol	0.0014	-471, -479, -541
N,N-dimethylformamide	0.0016	-544
acetic acid	0.0011	-521
methanol	0.0007	-532
1,3-propanediol	0.0015	ppte; not done

6.6.7 Film Quality when Additives Were Used

A number of the above experiments using additives included dip-coating of films on slides; however, the films were thick and cracked, and not further investigated. It is uncertain whether the cracking is the fault of the additive, experimenter, or the dip-coating process. The following experiments spin-coated the precursor solution-plus-additive onto the substrate.

Experiment 16 (JWP-III-57) BiCuVOx on quartz, with additives

A precursor solution was made with Bi(OAc)$_3$ (1 g, 2.6 mmol), V-2MOE (2.35 g at 4.96x10-4 mol/g, 1.2 mmol), and Cu(OAc)$_2$ (0.024 g, 0.13 mmol) in 40 ml 2MOE. From this stock solution, 10 ml was taken and diluted with 25 ml MeOH. This was hydrolyzed with 21 μl of water (1 mol water/mol alkoxide) and spin-coated onto quartz slides, 8 layers with intermediate heating on a hot plate and at 550 °C (10 min). Other precursor solutions were made using 20 ml of the stock BiCuVOx solution, diluting 50% with MeOH, and adding N,N-dimethylformamide (0.2 g, 2.6 mmol), ethylene glycol (0.16 g, 2.6 mmol), diethanolamine (0.27 g, 2.6 mmol), or triethanolamine (0.39 g, 2.6 mmol) (1 mol additive/mol alkoxide). These precursor solutions were hydrolyzed (47 μl water, 1 mol H$_2$O/mol alkoxide group) and deposited as above onto quartz substrates, 8 layers. All samples were pyrolyzed 600 °C/4h with cooling at 3°/min and were examined by GIXRD and ESEM. The films were pure but strongly oriented (Figure 6.53) and showed agglomeration and porosity. (Figure 6.54)

Experiment 17 (JWP-III-81) BiCuVOx on quartz, with additives

Experiment 16 was repeated to verify the results. A precursor solution was made of Bi(OAc)$_3$ (2.0036 g, 5.2 mmol), V-2MOE (4.7004 g, 2.3 mmol), and Cu(OAc)$_2$ (0.0485 g, 0.27 mmol) in 100 ml 2MOE, diluted 50% in methanol, and split into 8 portions. Likewise, a precursor solution was made to the same base concentration using Bi(OAc)$_3$ (2.0024 g, 5.2 mmol) V-2MOE (3.68 g, 1.8 mmol) and

Nb(OiPr)$_5$ (2.44 g, 0.8 mmol) diluted 50% in methanol, and split into 8 portions. Each portion received 1 mol additive/mol alkoxide present (see Table 6.14), and was hydrolyzed using 16.8 μl water for the BiCuVOx solutions and 20 μl water for the BiNbVOx solutions (1 mol water/mol alkoxide present). Eight layers were deposited by spin-coating onto quartz substrates for each solution, with intermediate heating on a hot plate followed by 5 minutes in a 550 °C furnace. The slides were pyrolyzed at 550 °C/2 h with cooling at 2°/min and examined by GIXRD and ESEM. Surface coverage was determined using the image analysis software of the ESEM. (Figures 6.31 - 6.34)

The solutions were left over the weekend to be gelled. Diethanolamine gave a viscous milky liquid and triethanolamine an ungelled yellow liquid. The solvent was evaporated out of all samples and some of the precursor solids inspected under ESEM. Figure 6.35. The bulk gels were pyrolyzed at 550 °C for 8 h. XRD showed clean γ phase in was produced from all precursor solutions except that containing triethanolamine. This solution produced g-BiCuVOx, BiVO$_4$, and unidentified peaks. (Figure 6.55)

Table 6.14: Amounts of additive used for Experiment 17

Sample #	Additive	Amt. for BiCuVOx (g)	Amt. for BiNbVOx (g)
81x-1	ethanolamine	0.0570	0.0715
81x-2	diethanolamine	0.1009	0.1237
81x-3	triethanolamine	0.1530	0.1660
81x-4	dimethylformamide	0.0739	0.0832
81x-5	ethylene glycol	0.0592	0.0719
81x-6	acetic acid	0.0563	0.0701
81x-7	methanol (also samples 8-10)	0	0
81x-11	1,3-propanediol	0.0723	0.089

Experiment 6.18 (JWP-III-58) Addition of Cu as hydrolyzable substance

A precursor solution was made by mixing Bi(OAc)$_3$ (2 g, 5.18 mmol), V-2MOE (4.700 g at 4.957×10^{-4} mol/g, 2.33 mmol), and copper dimethylaminoethoxide (0.0621 g, 0.259 mmol) in 80 ml of 2MOE. Twenty ml of this mixture was diluted with 30 ml of methanol and hydrolyzed with water (84 µl, 4.67 mmol). A precipitate formed and the sample was discarded. This was repeated, adding the water slowly together with the methanol, but a precipitate formed again. Ten ml of the precursor solution was diluted with 10 ml of methanol and the unhydrolyzed solution used to spin-coat 8 layers, with intermediate heating, onto quartz slides. These were heated

at 550 °C for 4 h according to the usual procedure. ESEM showed agglomerated films, and GIXRD showed a strongly *001*-oriented but phase-pure BiCuVOx film.

6.6.8 BiCuVOx Films on Metal Substrates

Experiment 19 (JWP-II-170) BiCuVOx films on Pt sheets

A precursor solution was made by dissolving $Bi(OAc)_3$ (5.000 g, 12.95 mmol) V-2MOE (16.54 g, 5.827 mmol), and $Cu(OAc)_2$ (0.1176 g, 0.6475 mmol) in 150 ml 2MOE as described in Chapter Four to produce a 0.0432 M BiCuVOx solution. The solution was split into two samples. The solution was diluted 50% with methanol and hydrolyzed (100 ml solution) with 0.16 ml water (1 mole of water per mole of alkoxide group). Substrates made from platinum sheet as described in Section 6.1.2.2 above were dipcoated once or twice, or spincoated once or twice, with intermediate heating on a hotplate, then pyrolyzed at 650 °C for 2h with cooling at 2°/min. Samples were examined by GIXRD (Figure 6.18) and showed a high degree of preferential orientation, and in ESEM showed smooth coatings. (Figure 6.19) The experiment was repeated on JWP-II-181, with the same results.

Experiment 20 (JWP-III-34) BiCuVOx on Pt, varying water

The precursor solutions described in Experiment 6 were also deposited by dip-coating onto platinum sheets and by spin coating

onto platinum sheets with intermediate drying and heating on a hot plate. They were characterized by GIXRD (Figure 6.58) and found to be phase-pure, with less-than-complete preferential orientation. ESEM showed the films were smooth and defect-free. (Figure 6.59)

Experiment 21 (JWP-III-56) BiCuVOx on Pt, varying additive

Platinum coatings were deposited by E-beam on quartz substrates (Ti adhesion layer). (Table 6.15) A 0.039 M stock precursor solution was made by dissolving $Bi(OAc)_2$ (1 g, 2.59 mmol), $Cu(OAc)_2$ (0.0251 g, 0.14 mmol), V-2MOE (2.355 g at 4.95×10^{-4} mol/g ,1.17 mmol) in 25 ml of 2MOE; a second one was made by diluting 10 ml of the first with methanol to a 0.016 M level. They were hydrolyzed with 42 μl and 14 μl of water, respectively (1 mol water per mol alkoxide). Precursor solutions from Experiment 16, containing ethylene glycol and diethanolamine additives, were also used. These solutions were spin-coated, 7 layers with intermediate heating on a hot plate followed by 10 minutes at 550 °C, onto the platinum-on-quartz substrates. Samples were pyrolyzed at 600 °C/4 hours with 2 °/minute cooling and examined in GIXRD and ESEM. All had strong but not total preferential orientation. (Figures 6.60, 6.61)

Table 6.15: E-beam deposition parameters for substrates made

(Ti adhesion layer used with Pt, Ag, parameters are for this adhesion layer)

Parameter	Ti	Pt	Al_2O_3	Ag	WO_3
rise time	0.5	0.5	0.3	1	1
soak time	0.5	0.5	0.3	1	1
soak power	15	35	12	15	10
rate	3	3	3	3	5
thickness2	50	100	200	500	1000
fall time	0.3	0.3	0.3	0.3	0.3
idle power	0	0	0	0	0
max power	30	55	25	25	20
gain/damp	5.4	5.4	5.4	4.5	4.3
Z factor	0.628	0.245	0.336	0.929	1
tool factor	086	086	086	086	086
density	4.5	21.45	3.79	10.49	7.16
thickness (Å)	59	107	616	496	1200

6.6.9 Preparation of films on porous substrates

Experiment 22 (JWP-III-149) BiCuVOx on pore-plugged substrates

Whatman Anopore™ 0.02 μm porosity alumina membranes were prepared as described in Section 6.1.2.2 above. Solutions from Experiment 17 containing additives, were permitted to soak into the membranes, which were then lightly swabbed with dilute

458

HCl to remove the surface coating and heated for 2 h at 400 °C to decompose organics. The wetting behavior of each solution was monitored during this process. (Table 6.15) After the heating, the precursor solutions were spin-cast onto these "pre-clogged" and onto some new (no prior coating) Anopore membranes, 5 s at setting 30V, with intermediate hotplate (2 min) and furnace (500 °C/5 min). GIXRD proved impossible due to interference from the porous alumina. The films were examined in ESEM (Figure 6.37) and the results are described in Table 6.16.

Table 6.16 Effects of Additives on Wetting Behavior and Film Quality on Porous Substrates

Additive	Wetting Behavior *	Pore-Plugged	Not Pore-Plugged
diethanolamine	beads	pores	pore-free
triethanolamine	soaks	pores	pores
dimethylformamide	beads	cracking, pores	pore-free
ethylene glycol	soaks	cracking, pores	cracking, pores
acetic acid	soaks	cracking, pores	cracking, pores
methanol (control)	soaks	cracking, pores	pore-free
1,3-propanediol	soaks	pores	pore-free

*Here, "soaks" means the solution moved rapidly into the pores of the membrane, while "beads" means the solution sat on the surface in a bead during the pre-clogging step.

6.6.10 BiMeVOx Films on Assorted Substrates

Experiment 23 (JWP-IV-1) BiMeVOx on quartz, Pt, Al_2O_3

Four precursor solution were made according to Table 6.17, dissolving the materials listed there in 50 ml 2MOE and 25 ml MeOH to create precursor solutions 0.052 M (in Bi_2) delivering

$Bi_2Cu_{0.1}V_{0.9}O_{5.35}$, $Bi_2Nb_{0.3}V_{0.7}O_{5.5}$, $Bi_2Ti_{0.1}V_{0.9}O_{5.5-\delta}$, and

$Bi_2Mn_{0.15}V_{0.85}O_{5.5-\delta}$, respectively. These solutions were hydrolyzed with water equivalent to the number of alkoxide groups present in each precursor solution.

Precursor solutions were spin-coated (30V, 3500 RPM) onto quartz substrates prepared as usual. Part of each were masked for profilometry. Between each of the seven coatings, the sample was dried on a hot plate (300 °C) then left in a furnace at 400 °C for 5 minutes. The same procedure was followed to deposit films on Pt substrates (E-beam on quartz) and Al_2O_3 substrates (E-beam on glass). One of each sample was heated at 450 °C/8h with cooling at 2 °C/min, while the other was heated at 650 °C/8h with cooling at 2 °C/min. Films were characterized by GIXRD and ESEM. (Figures 6.62, 6.25 - 6.27) Then, all samples that had been heated at 450 °C were again heated, now at 750 °C/8 h with cooling at 2 °C/min and re-examined by GIXRD and ESEM. (Figures 6.28 - 6.30) GIXRD showed all remained phase-pure and oriented.

Table 6.17: Preparation of BiMeVOx precursor solutions

Dopant Identity	Bi(OAc)₃ g	V-2MOE g (mmol)*	Dopant g (mmol)	H₂O μl (mmol) **
Cu(OAc)₂	2.0013	6.9254	0.0482	42
Nb(OiPr)₅	2.0023	5.3799	2.4444	56
Ti(OiPr)₄	2.0005	6.9145	0.0865	48
Mn(OAc)₂*4H₂O	2.0009	6.5352	0.0672	40

*3.37×10^{-4} mol/g
**used on 1/3 of the solution

461

Experiment 24 (KD-83) BiFeVOx on quartz

Bi(OAc)$_3$ (0.4999g, 1.3 mmol), V-2MOE (2.685 g at 2.235x10^{-4} mol/g (from vanadium isopropoxide), 0.58 mmol), and Fe(acac)$_2$ (0.0187g, 0.07 mmol) were mixed in a total of 25 ml of 2MOE to produce a 0.052 M solution. This was added to 50 ml methanol and hydrolyzed with 40 μl of water (1 mol H$_2$O/ mol alkoxide). The solution was spin cast in the usual manner to deposit 10 coatings onto quartz slides, prepared in the usual manner. All samples were heated to 450 °C/8 hours with 1 °/min cooling; two of them were given 5 more coats after the first pyrolysis and heated at 550 °C/8 h with 2°/min cooling. ESEMS (Figure 6.63) indicated some agglomeration in the films, but no cracking or pore formation. GIXRD indicated poorly crystalline phase-pure but oriented films. (Figure 6.64)

(b)

(a)

Figure 6.40: BiCuVOx on quartz, dip-coated and annealed at 550 °C. (a) X 2650, (b) X 4850.
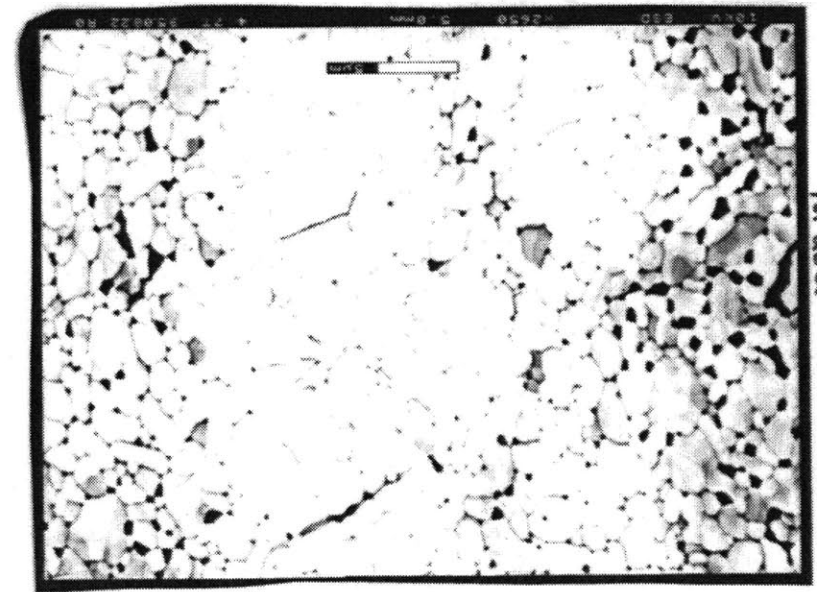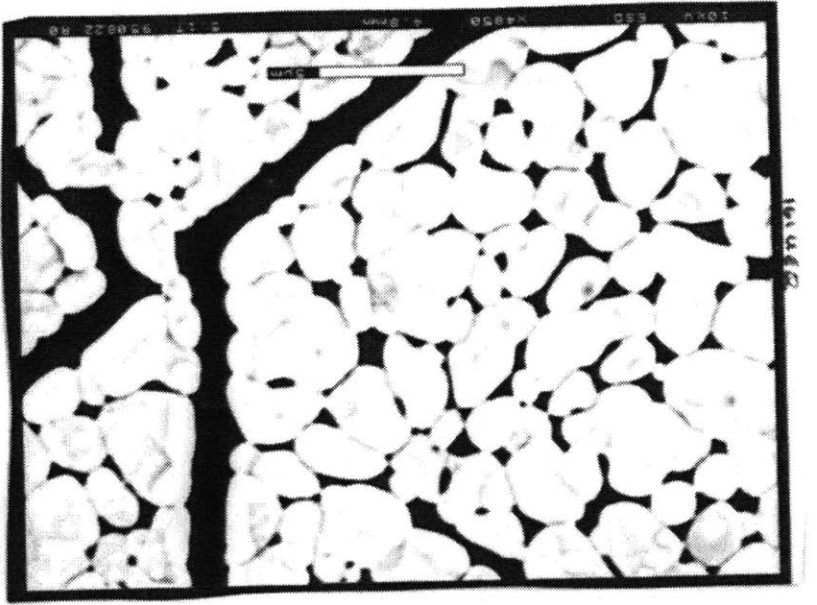
Figure 6.41: BiCuVOx on quartz, dip-coated and annealed at 550 °C, using a more dilute solution than in Fig. 6.40. Patchy areas in (a) may be due to irregularities in the dipping. The blowup of one area (b) shows a cracked top layer plus a grainy underlayer. (a) X 665, (b) X 10500.

(a)
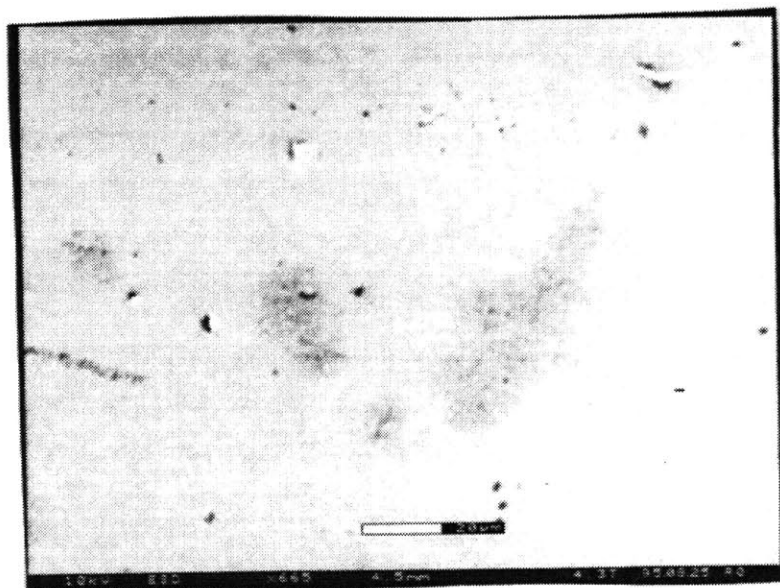
(b)
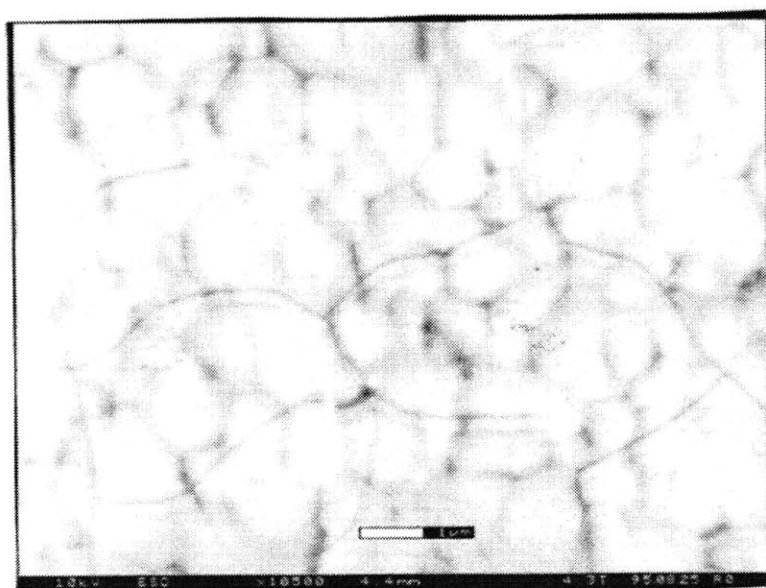
Figure 6.42: Calibration curve for the spin-coater.
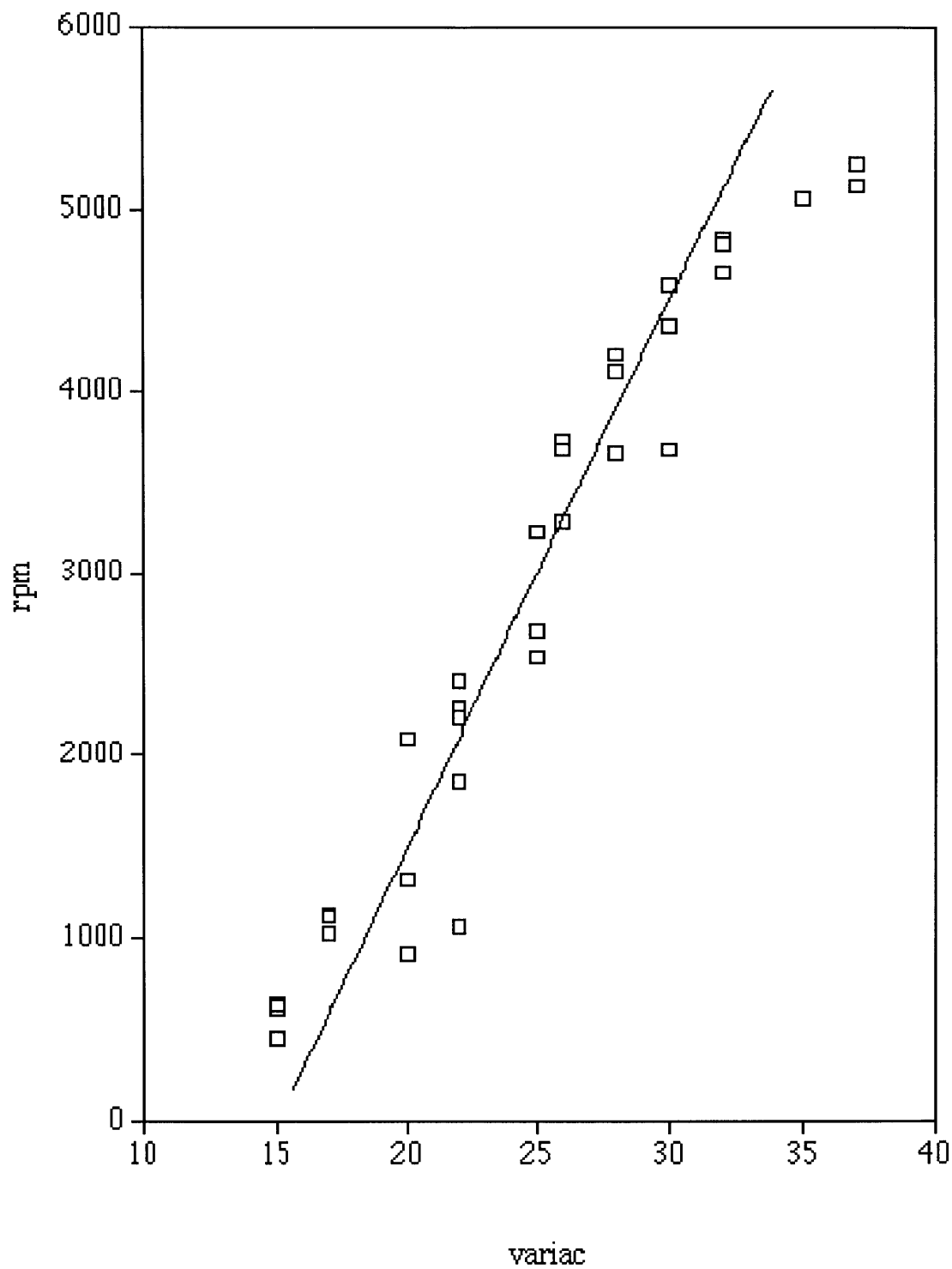
Figure 6.43: Optimization of spin-coater setting for BiCuVOx films. (a) Coating produced at variac setting 30 V (3500 RPM), X 1250. (b) Coating produced at variac setting 20 V (1100 RPM), X 230.

(a)

(b)

Figure 6.44: Effects of different spin-coater speeds on GIXRD. All are at 1° grazing angle. (a) Setting 20 V (1100 RPM), (b) Setting 30 V (3500 RPM). The GIXRD for setting 40 V showed an amorphous material. The lines marked are for BiCuVOx.
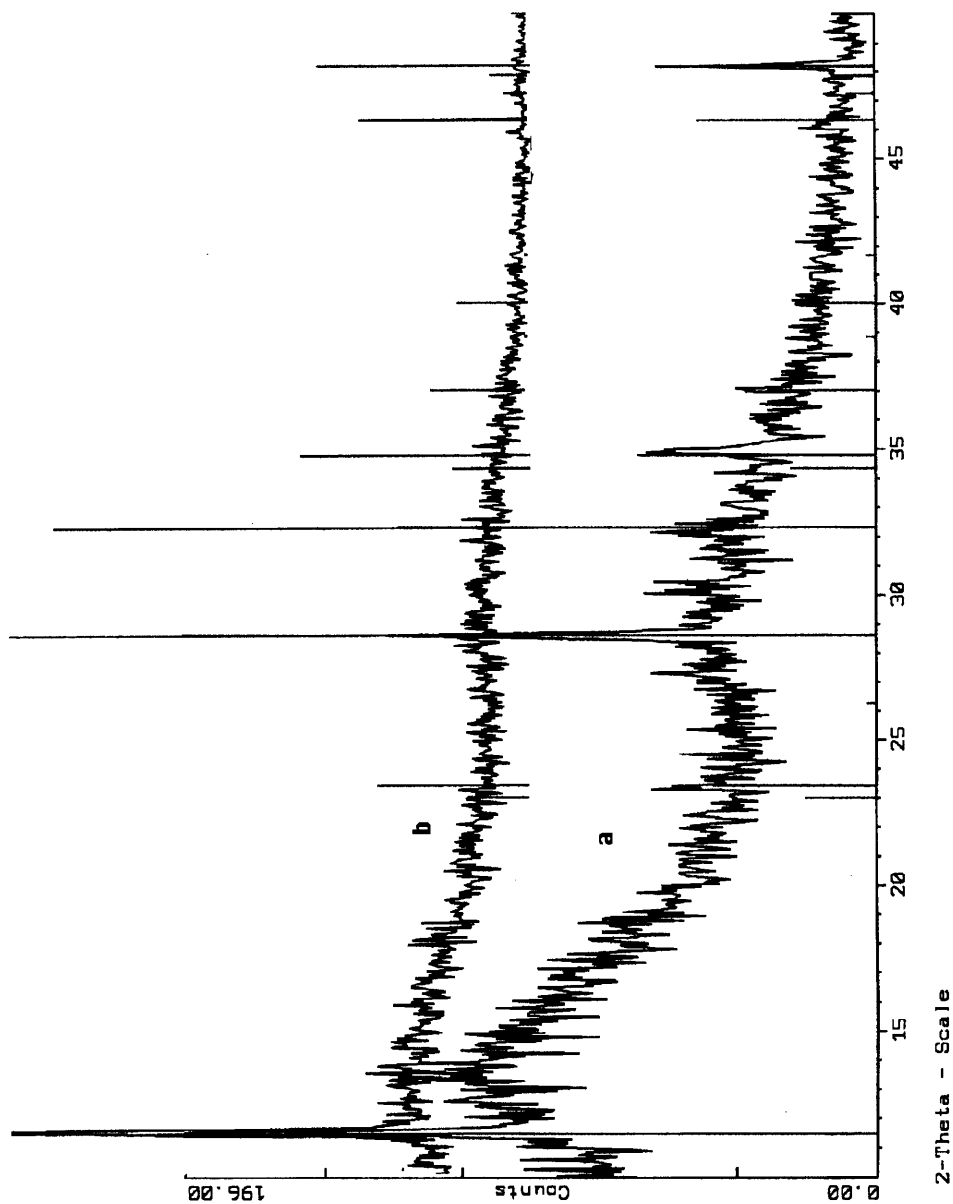
Figure 6.45: BiCuVOx on quartz, acid catalysts. (a) control (no catalyst), 600 °C annealing, X 5250. (b) acetic acid, 600 °C annealing, X 2250. (c) nitric acid, 600 °C annealing, X 2300.

(a)
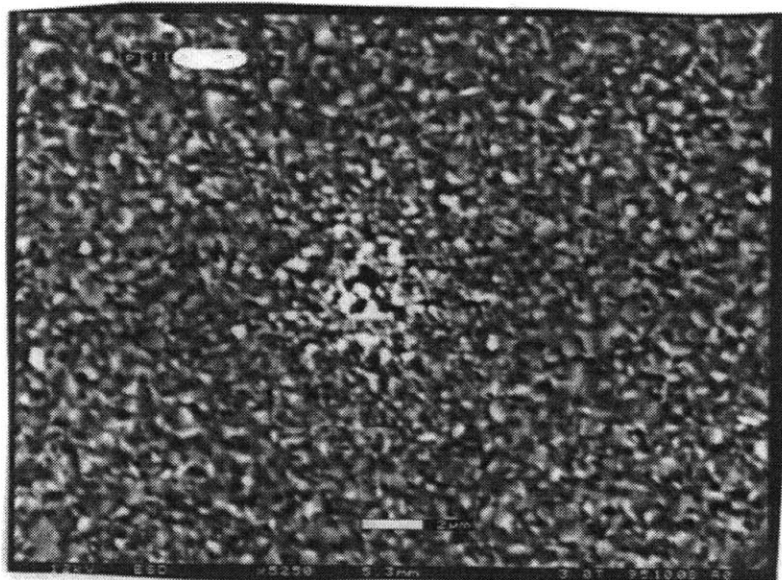
(b)
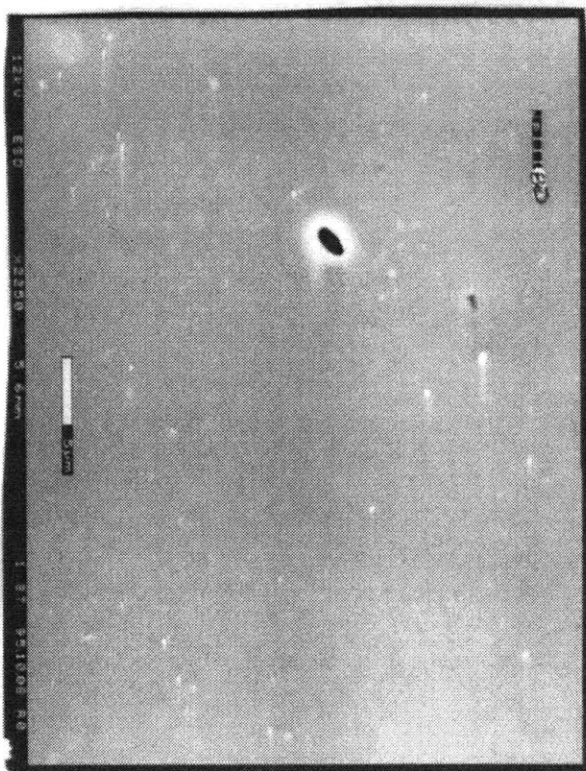
(c)
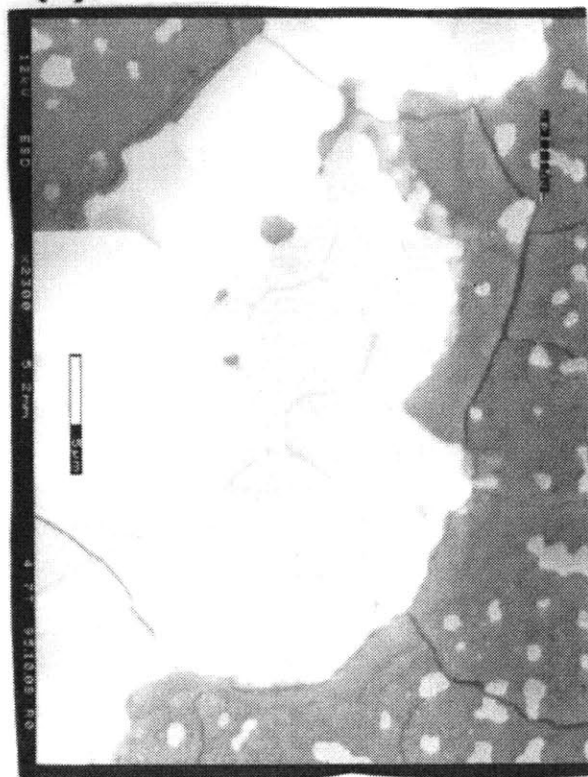
Figure 6.45, continued: **(d) control (no catalyst), 875 °C annealing, X 2950. (e) acetic acid, 875 °C annealing, X 540.**

(d)
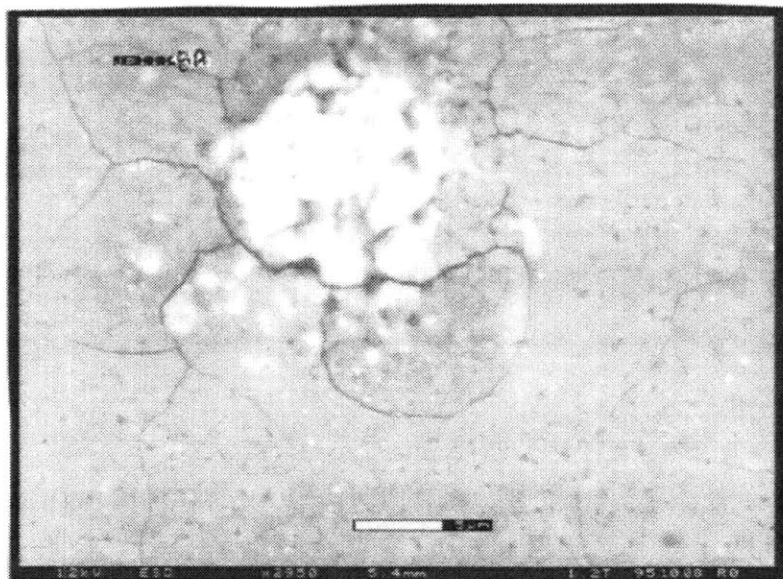
(e)
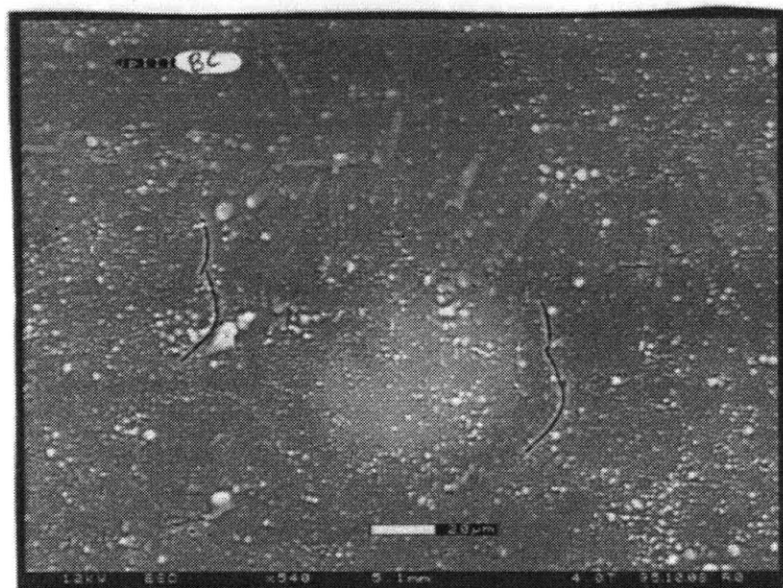
Figure 6.46: BiCuVOx on quartz, varying water-to-alkoxide ratio (W). (a) W=1, X 4350, (b) W=2, X 7200, (c) W=5, X 4400.

(a)
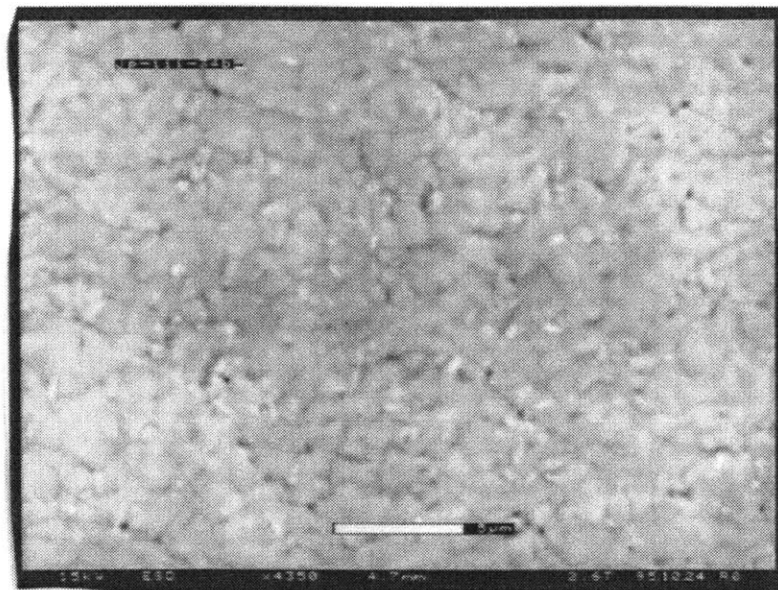
(b)
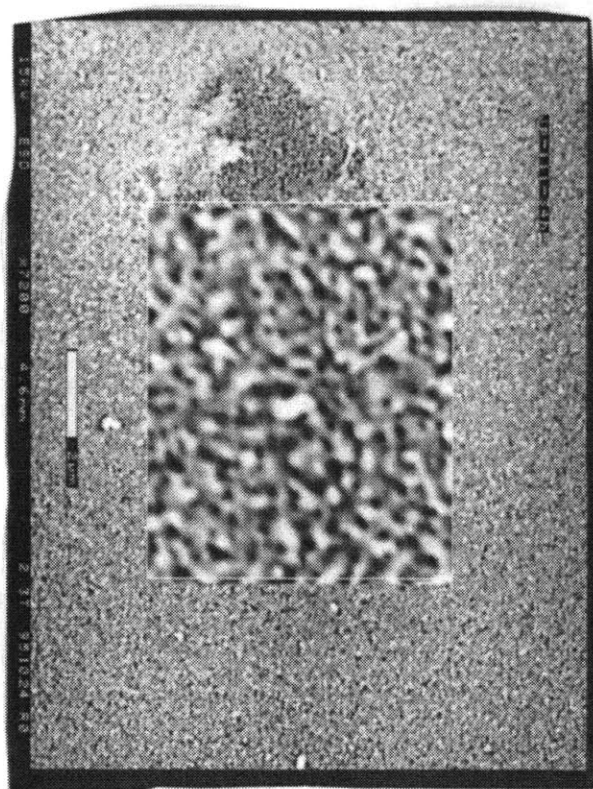
(c)
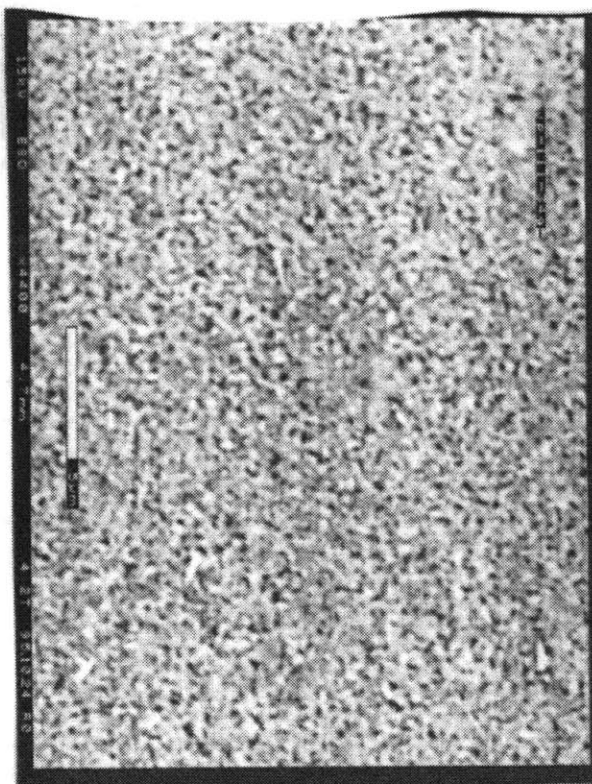
Figure 6.47: BiCuVOx on quartz, varying water-to-alkoxide ratio (W), 5 layers added to samples in Fig. 6.46. (a) W=1, X 2150, (b) W=2, X 5500 (inset X 9050), (c) W=5, X 5400.
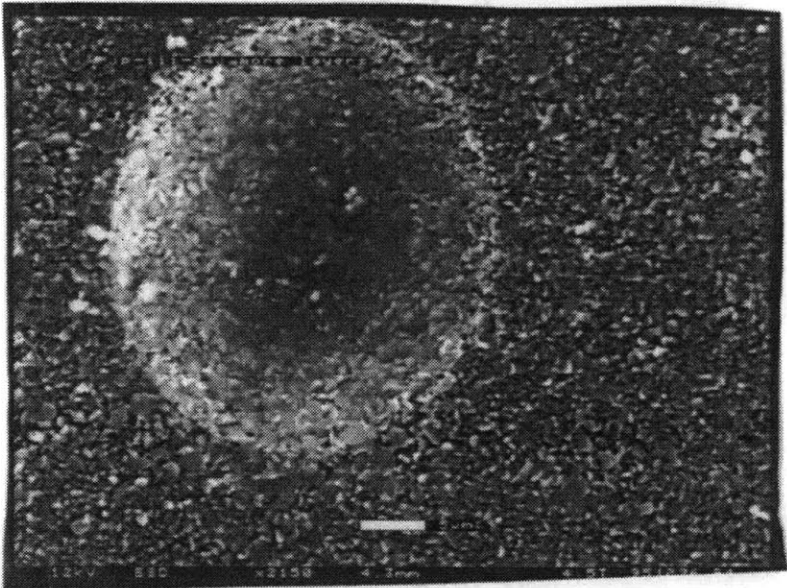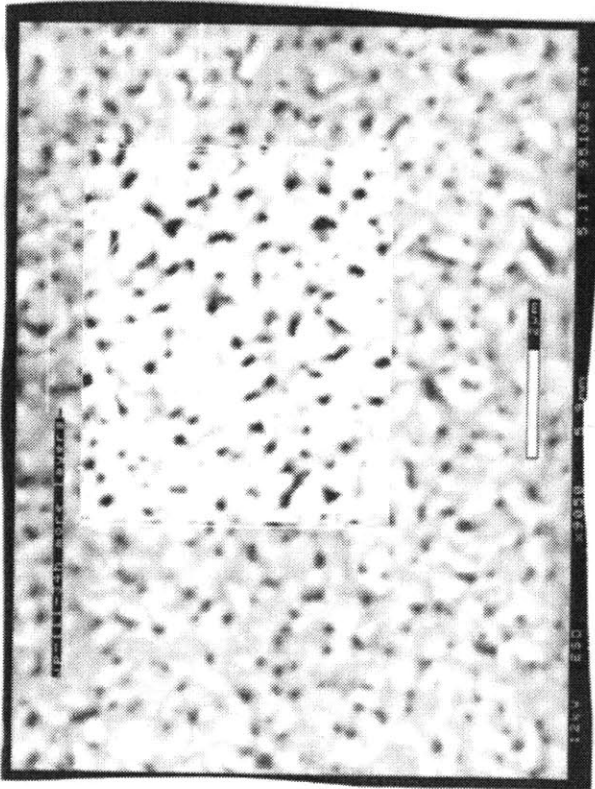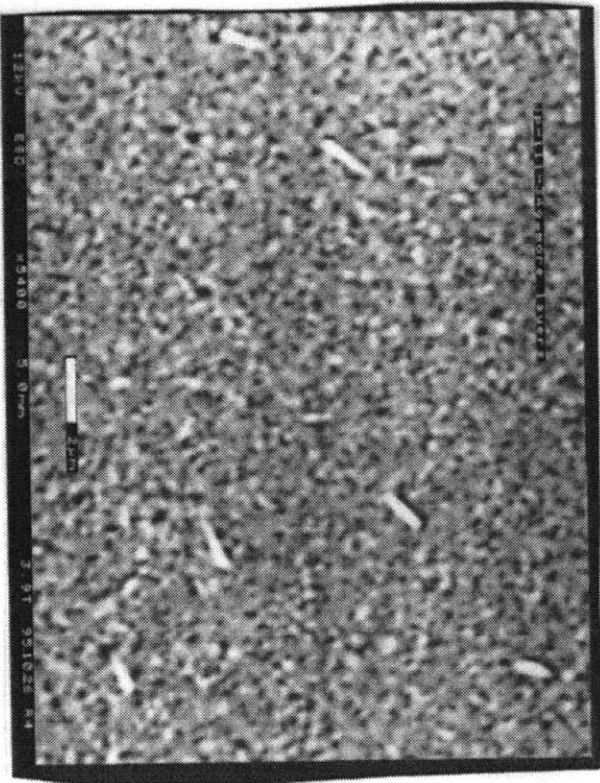
Figure 6.48: BiCuVOx on quartz, varying temperature of final annealing step. (a) 450 °C, X 3550, (b) 550 °C, X 6600, (c) 650 °C, X 5650 (inset).

(a)
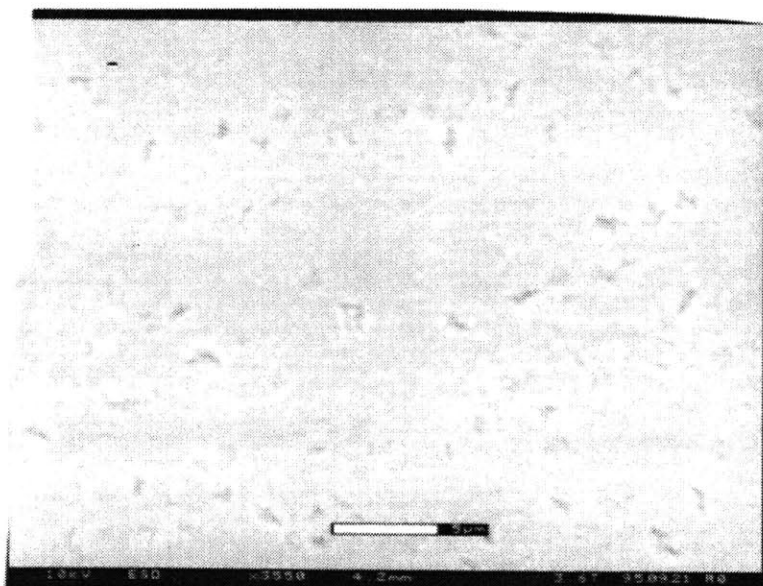
(b)
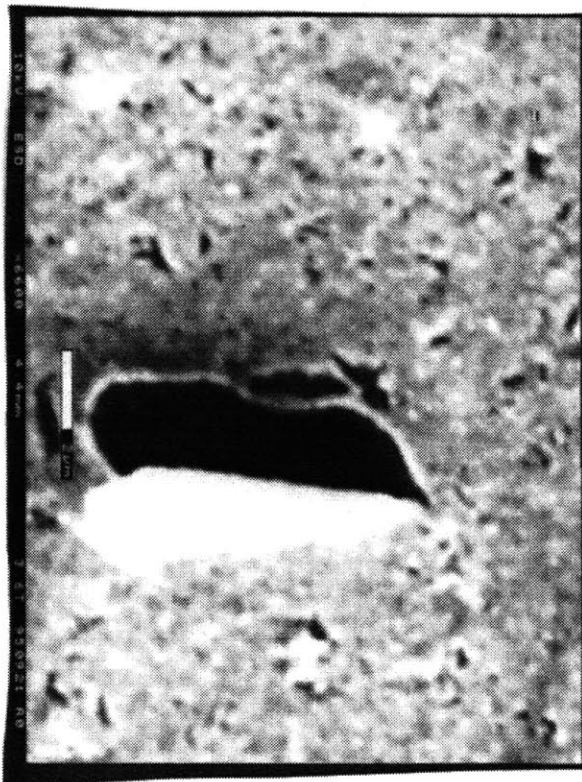
(c)
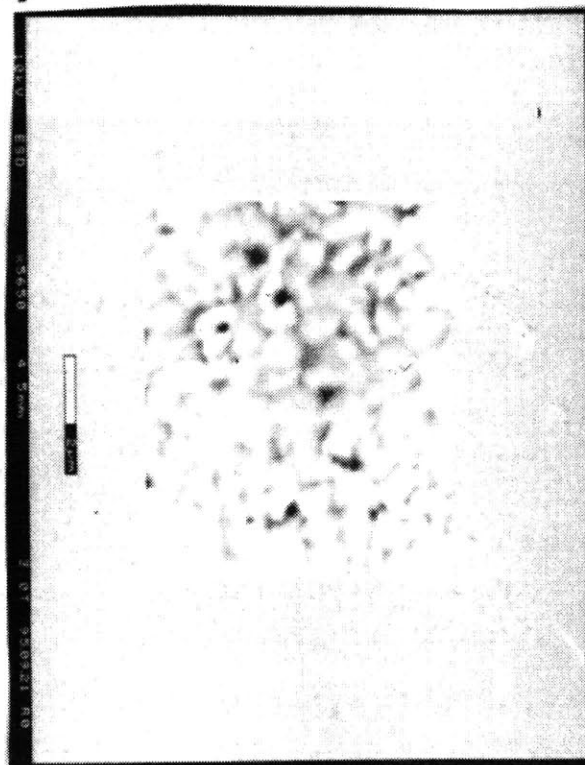
Figure 6.49: BiCuVOx on quartz, varying temperature of final annealing step. Grazing angle 1°. (a) 450 °C, (b) 550 °C, (c) 650 °C.
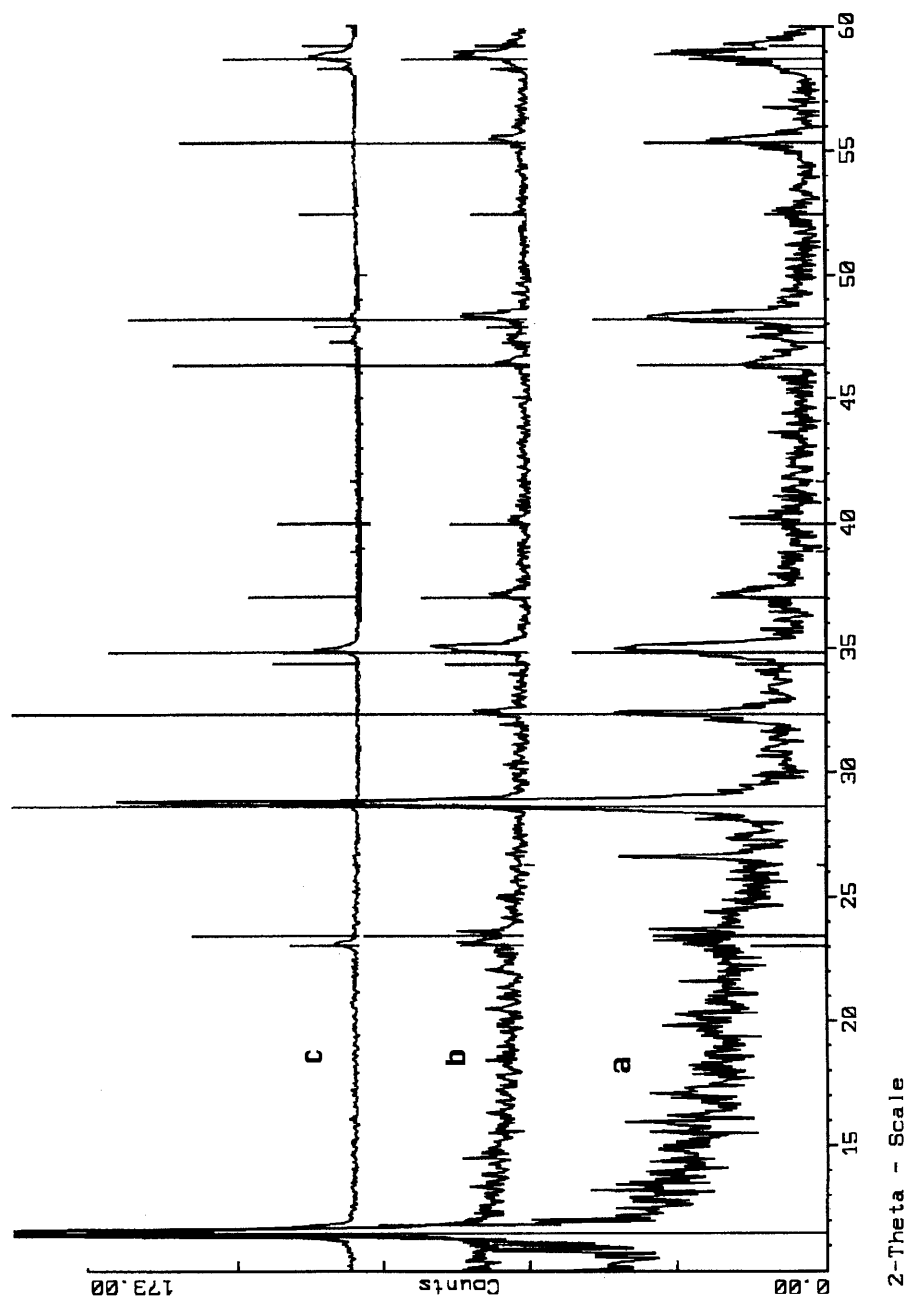
Figure 6.50: BiCuVOx on quartz, sample dipcoated after 5 layers deposited by spin coating, heating 550 °C. Grazing angle 1°. The film is considerably less oriented than those which had been only spincoated.
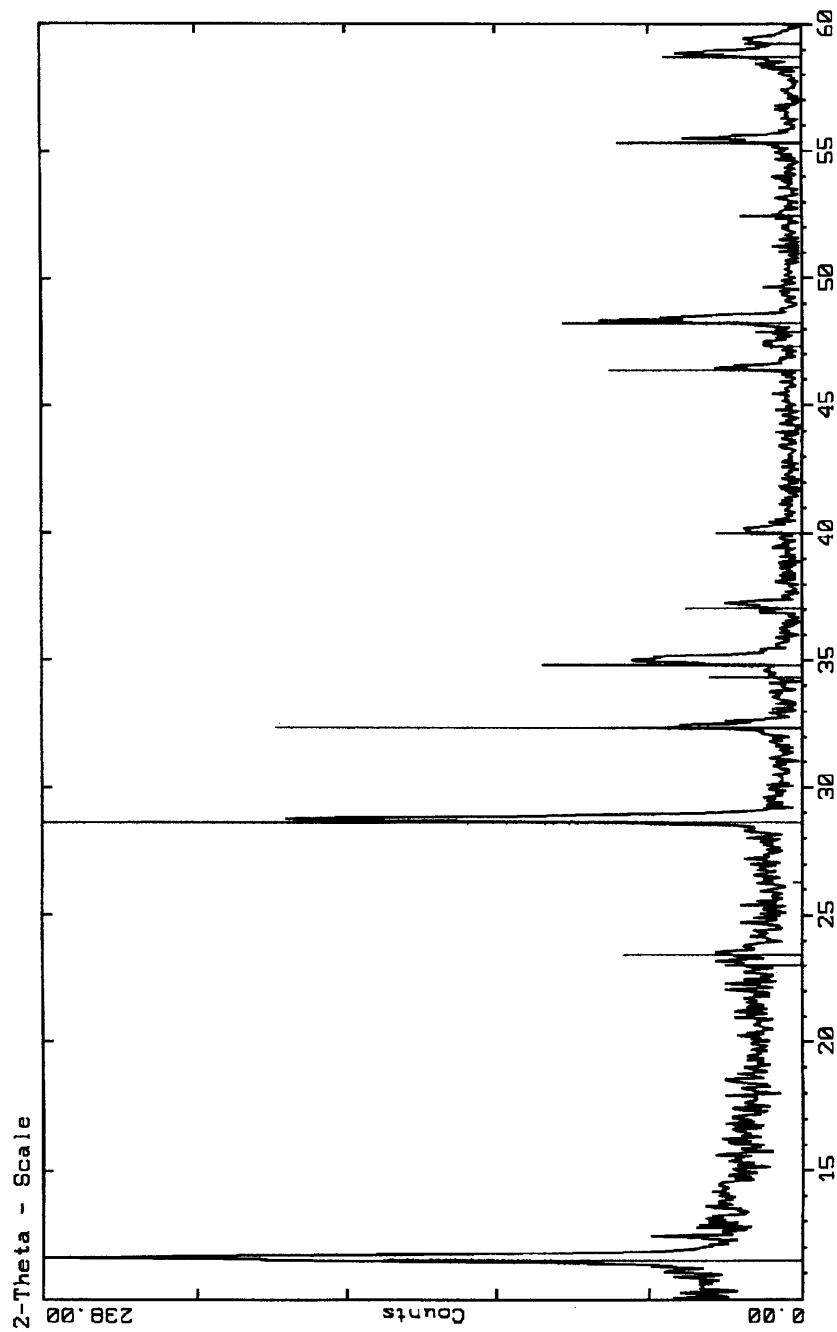
Figure 6.51: BiCuVOx on quartz, heated a second time to anneal out pores. (a) 750 °C, X 2900, (b) 800 °C, X 1100.

(a)
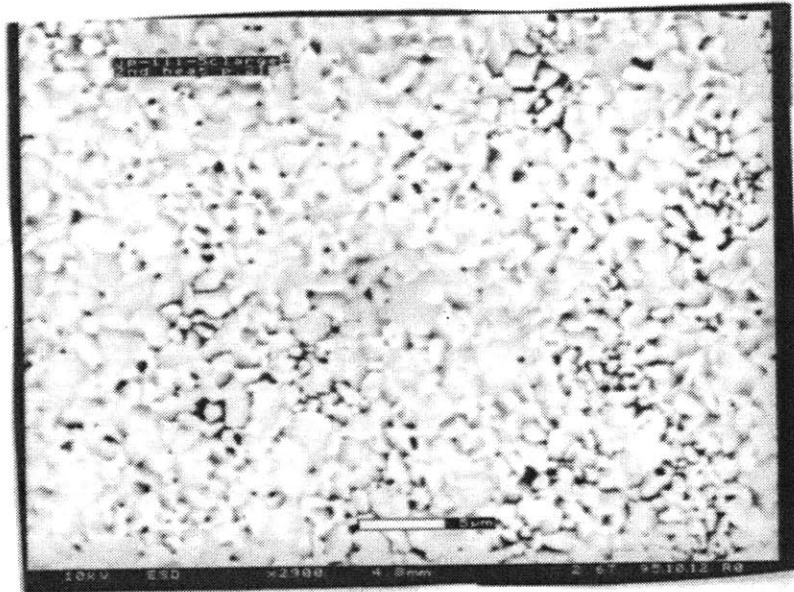
(b)
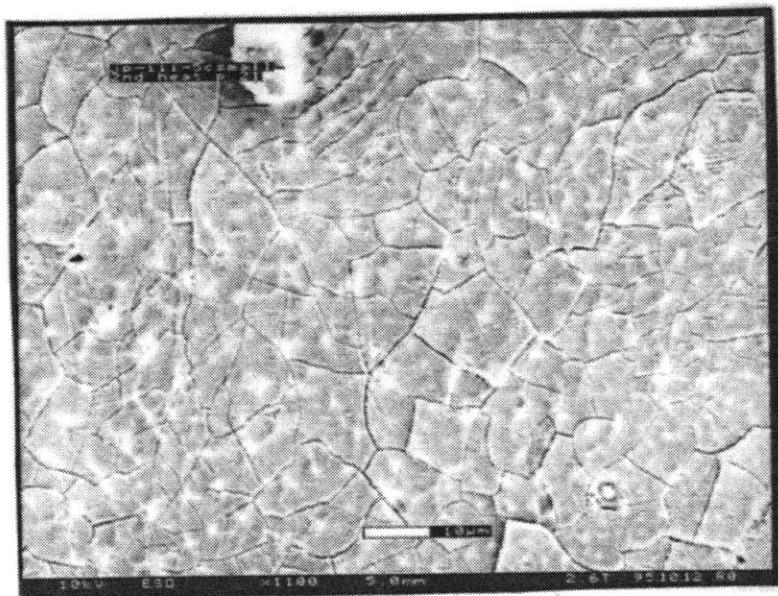
Figure 6.52: BiCuVOx on quartz, heated a third time to anneal out pores, at 750 °C for 8 hours. (a) X 470, (b) X 9050.

(a)
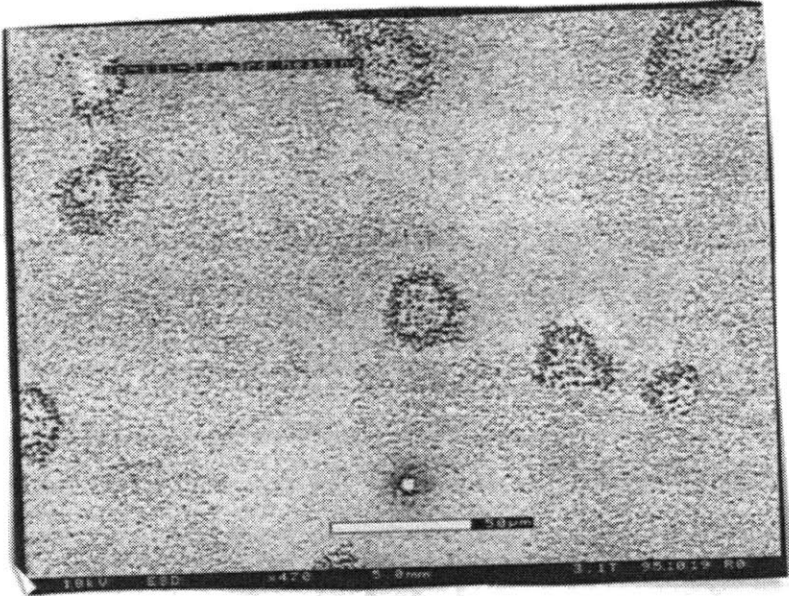
(b)
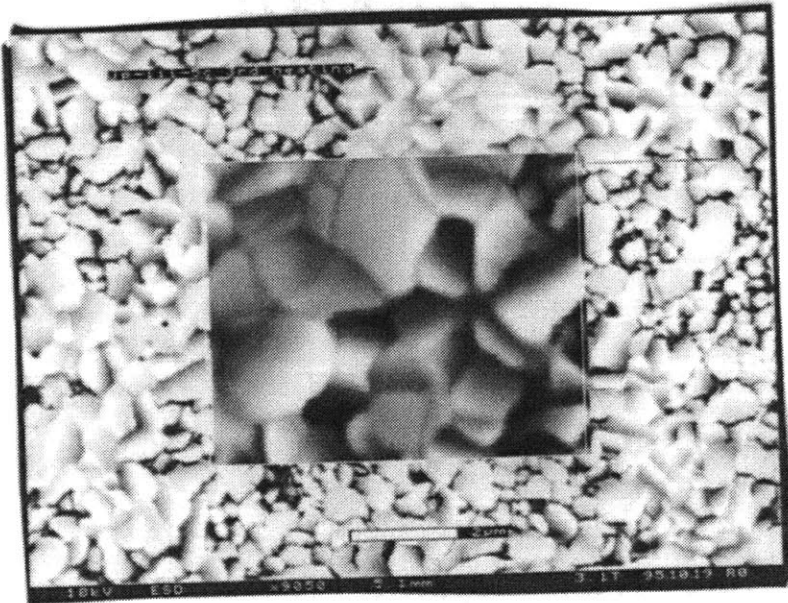
Figure 6.53: BiCuVOx on quartz, varying additives. Samples heated at 550 °C. Grazing angle 1°. (a) control (no additive), (b) diethanolamine, (c) N, N-dimethylformamide. The triethanolamine-containing sample was amorphous to GIXRD.
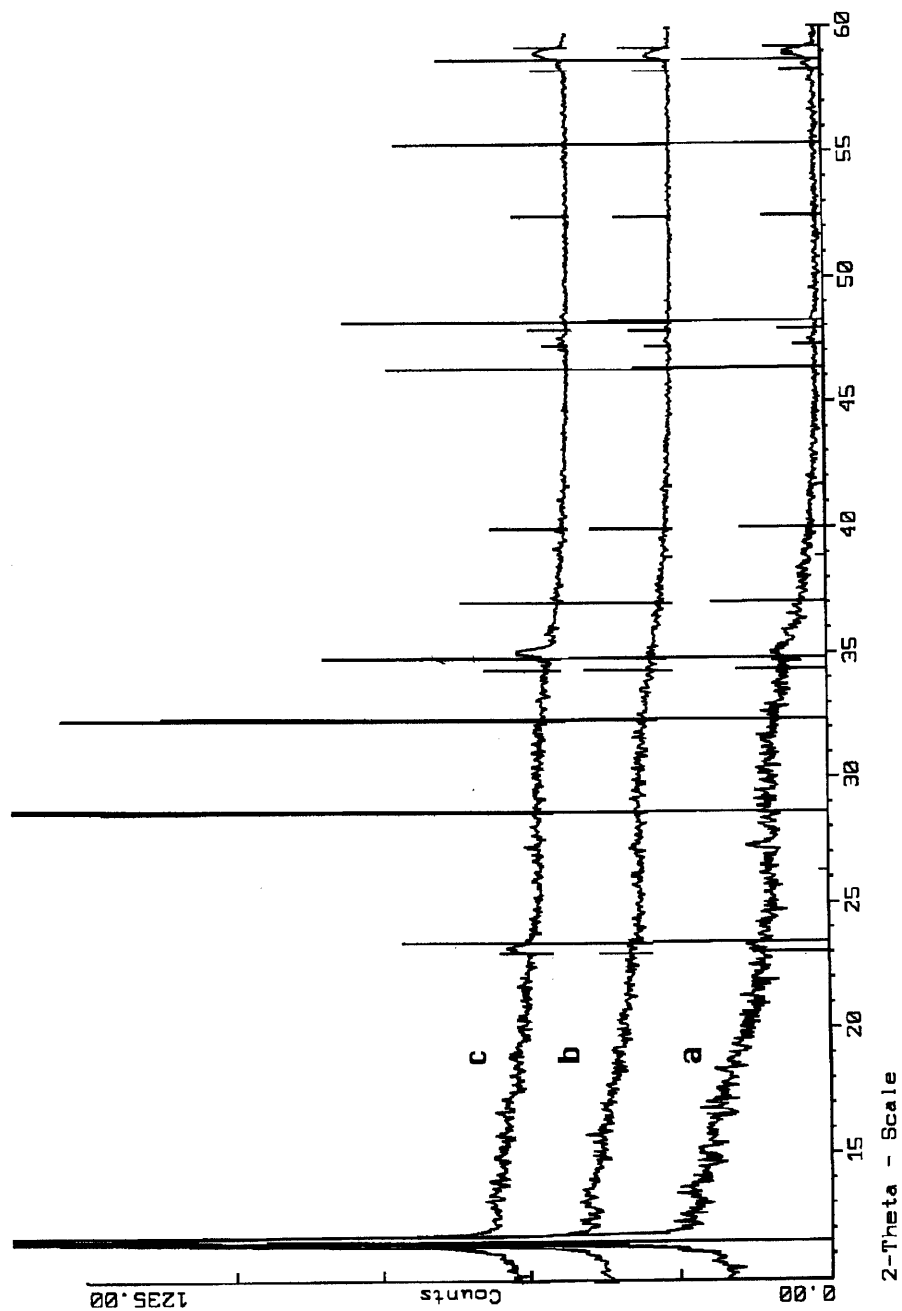
Figure 6.54: BiCuVOx on quartz, varying additives. Samples heated at 550 °C. (a) control (no additive), (b) N, N-dimethylformamide, (c) ethylene glycol. All X 8000.

(a)
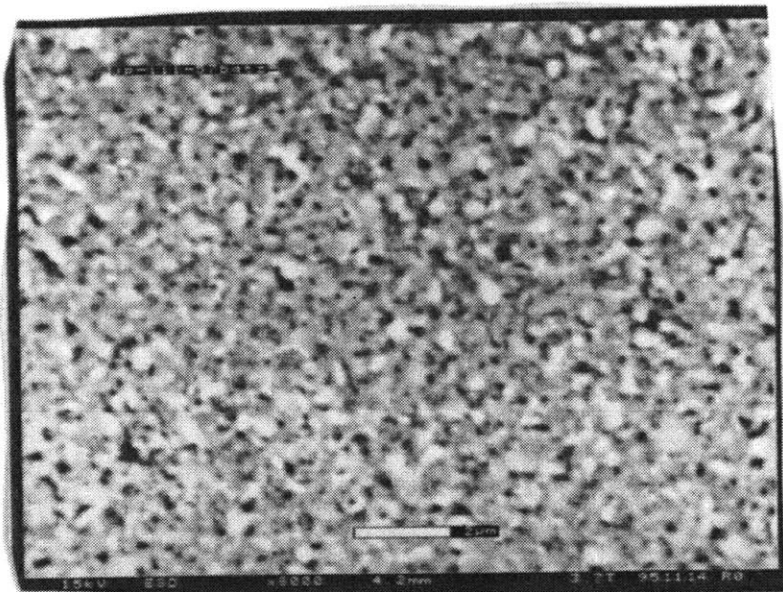
(b)
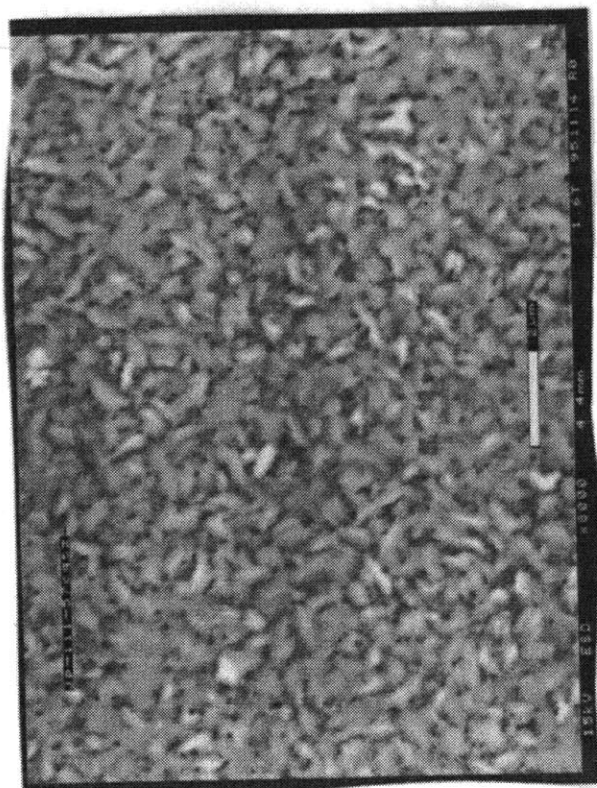
(c)
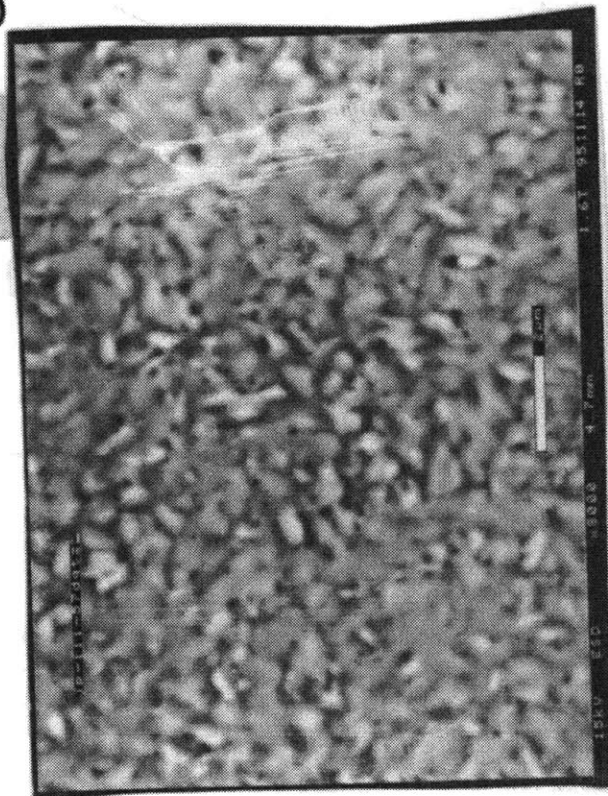
Figure 6.54, continued: (d) diethanolamine (X 1350), (e) triethanolamine (X 8050)

(d)
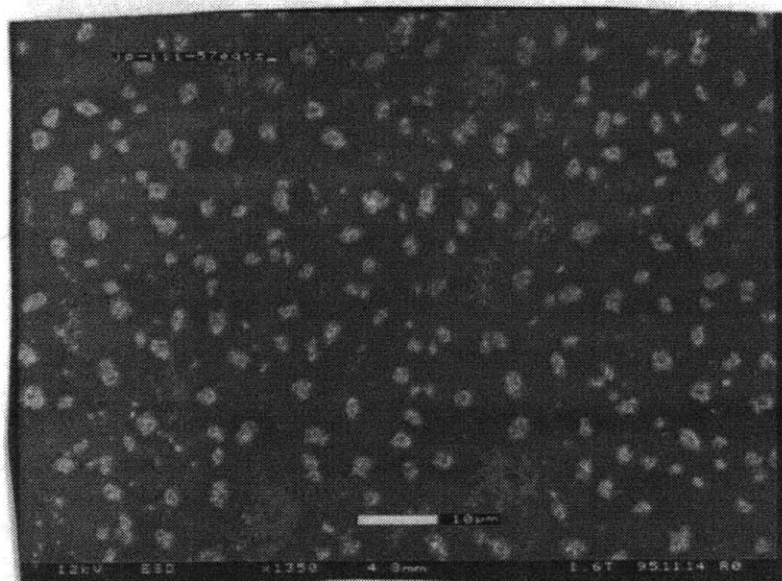
(e)
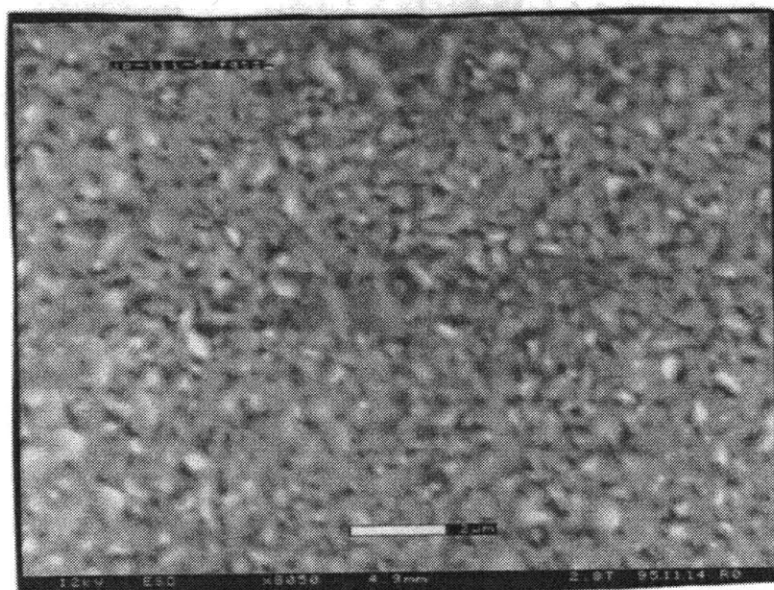
Figure 6.55: Bulk BiCuVOx made from a precursor solution containing triethanolamine. Pyrolyzed at 550 °C.
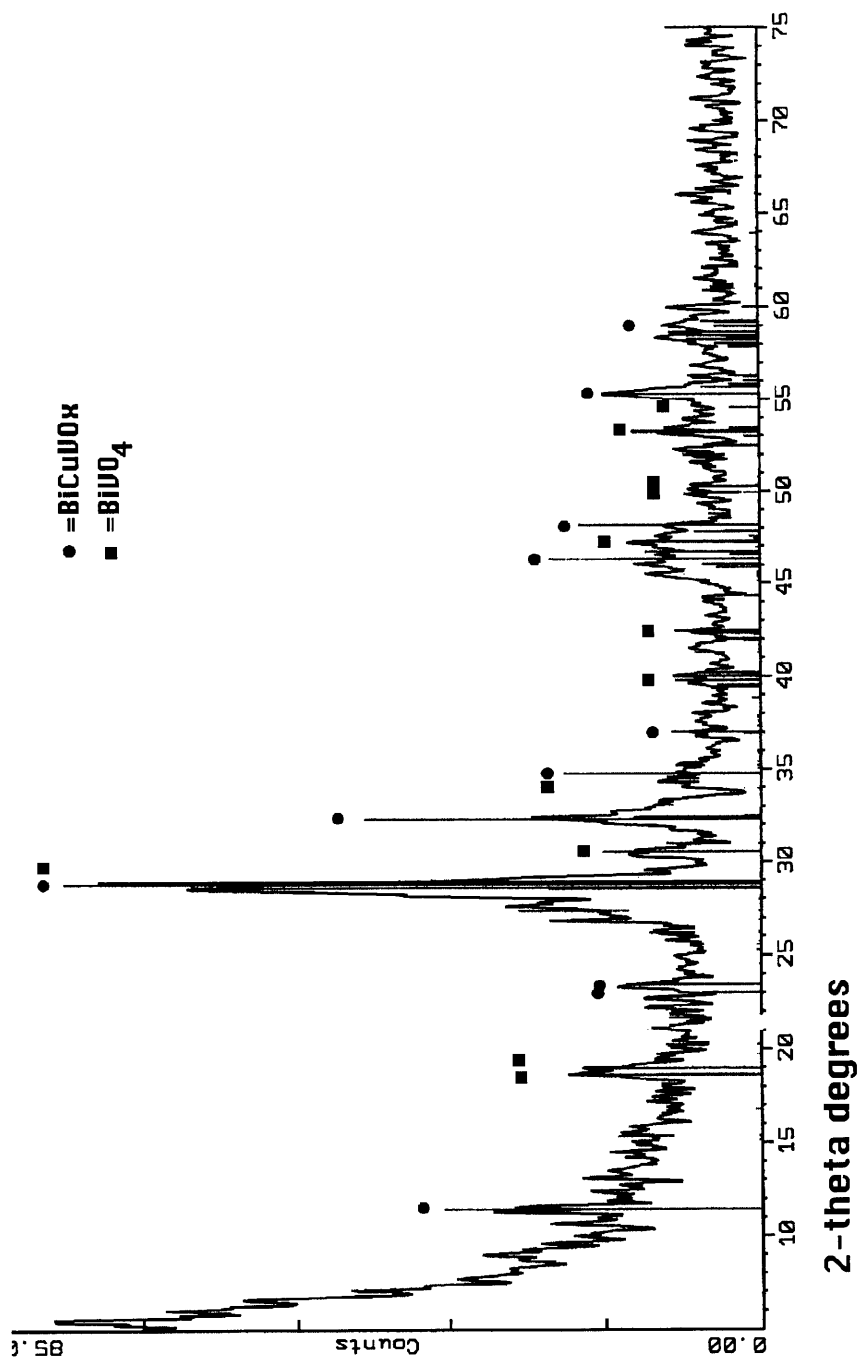
Figure 6.56: BiCuVOx on quartz, with copper dopant added as dimethylaminoethoxide. (a) X 325, (b) X 8050.

(a)
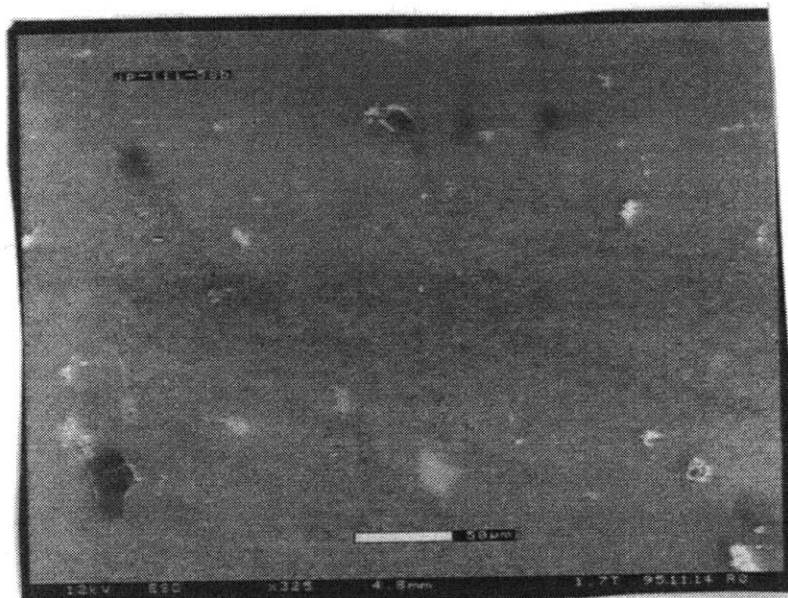
(b)
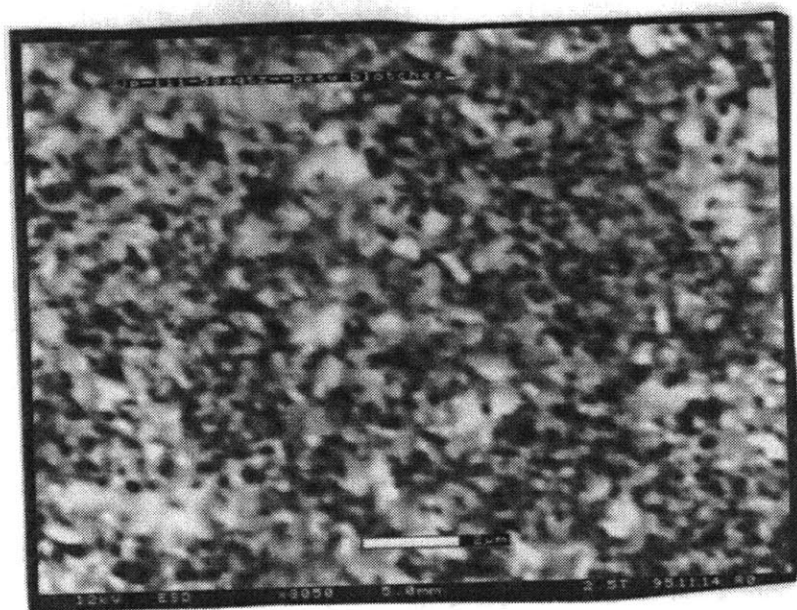
Figure 6.57: BiCuVOx on quartz, with copper dopant added as dimethylaminoethoxide. Grazing angle, 1°.
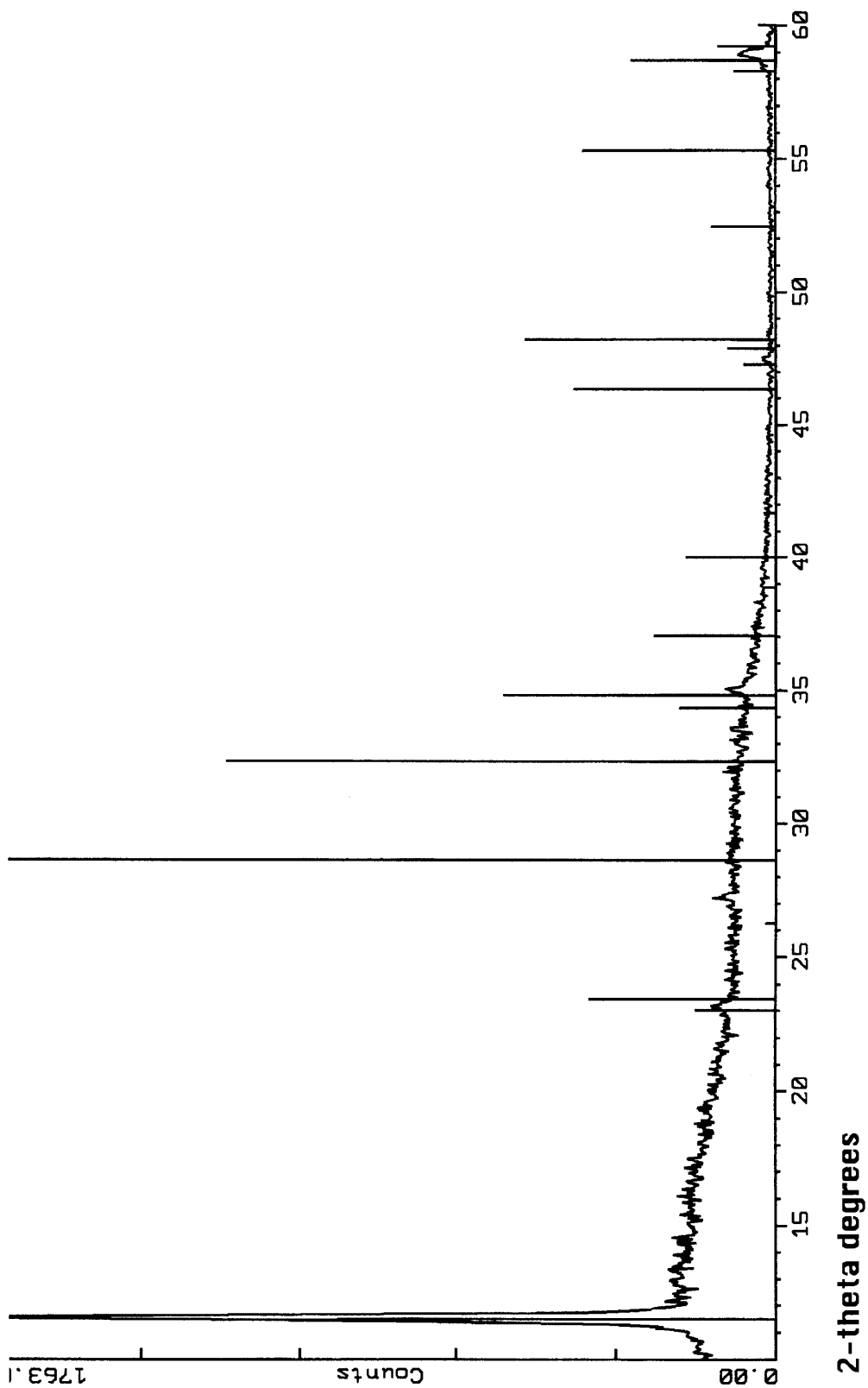
Figure 6.58: BiCuVOx on E-beam platinum. Platinum peaks are marked with *. The lines marked are BiCuVOx. Grazing angle 1°. Sample was heated at 550 °C.
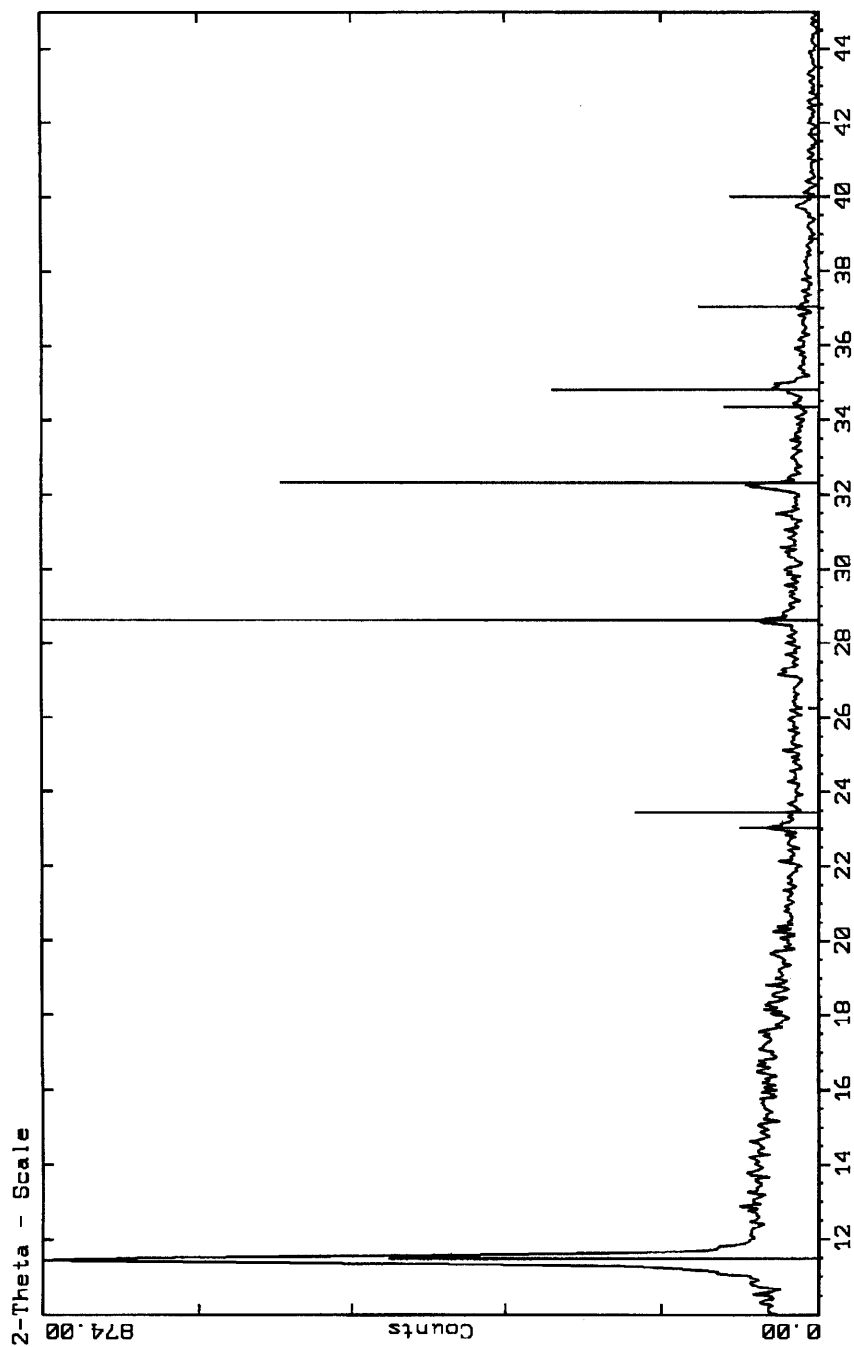
Figure 6.59: BiCuVOx on E-beam platinum. Sample is same as the one in Fig. 6.58.

Figure 6.60: BiCuVOx on E-beam platinum, varying the additive. Heating temperature 600 °C. (a) control (no additive) X 8050, (b) ethylene glycol, X 8050, (c) diethanolamine, X 8000. The light spots are hillocks.

(a)
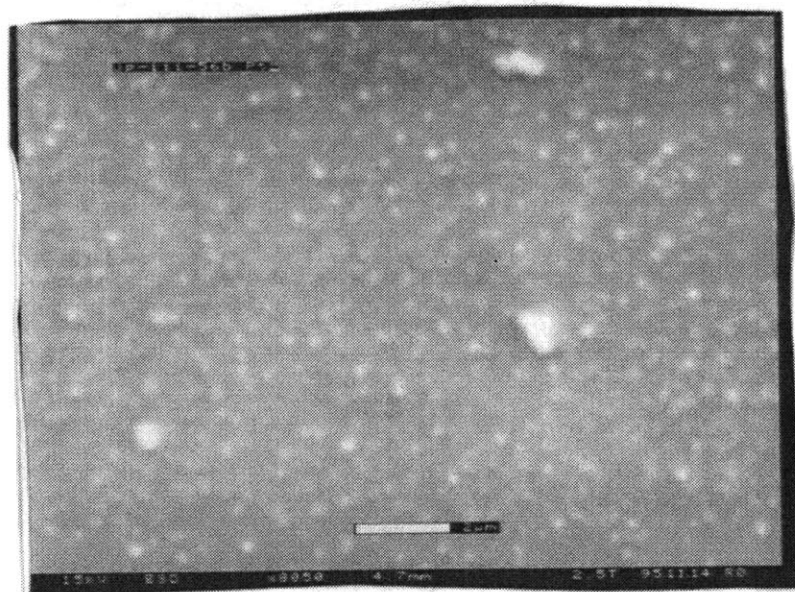
(b)
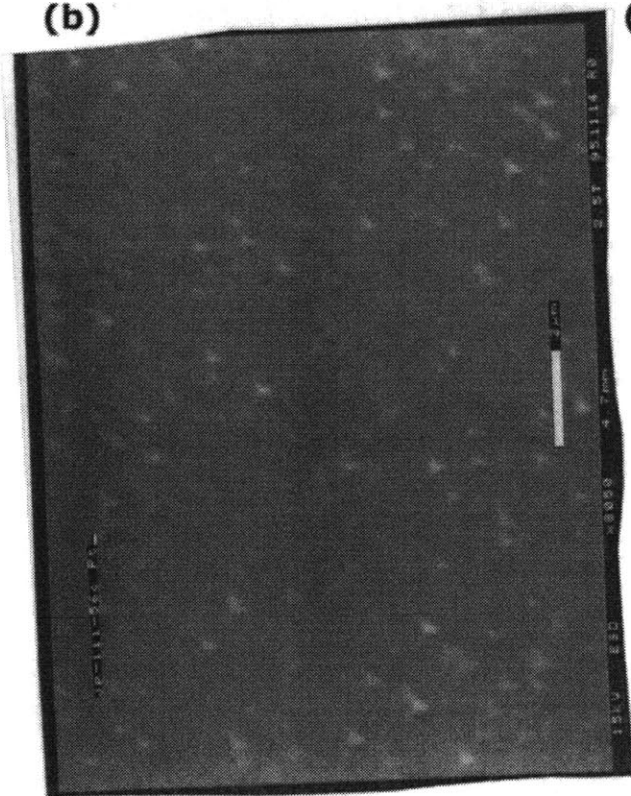
(c)
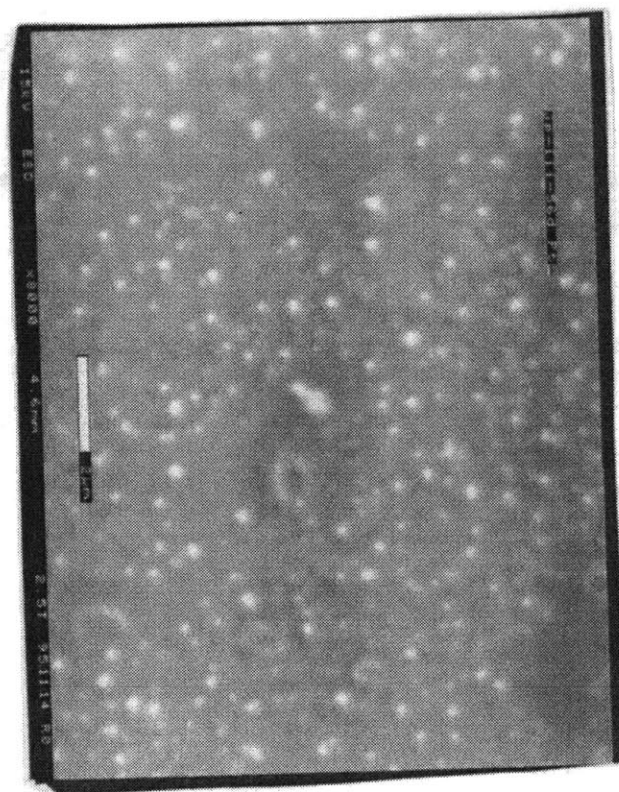
Figure 6.61: BiCuVOx on E-beam platinum, varying the additive. Heating temperature 600 °C. (a) control, (b) ethylene glycol, (c) diethanolamine.
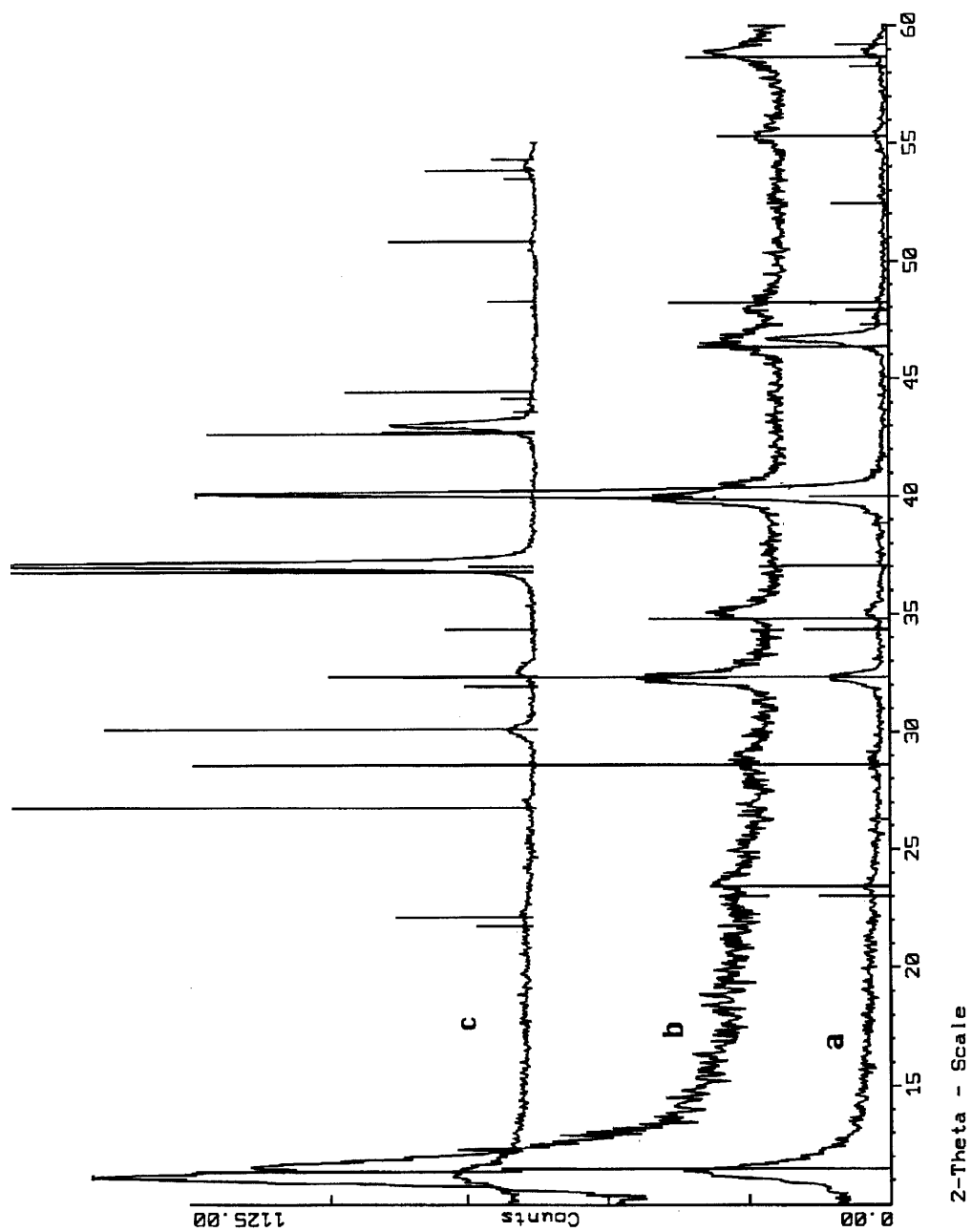
Figure 6.62: BiMeVOx on platinum substrates. Heated to 600 °C. (a) BiCuVOx, (b) BiMnVOx. Other dopants similar.

487
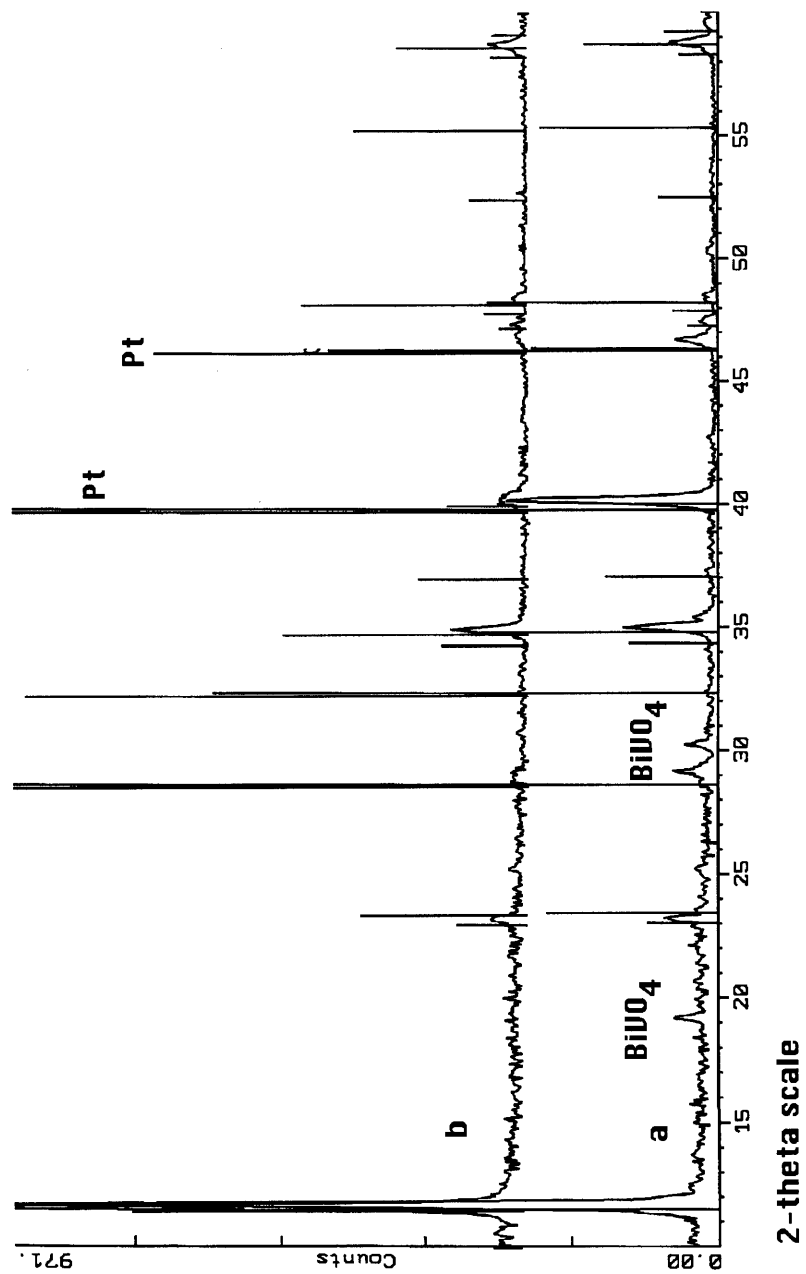
Figure 6.62, continued: BiMeVOx on alumina substrates. Heated to 600 °C. (c) BiCuVOx, (d) BiTiVOx. Other dopants similar.
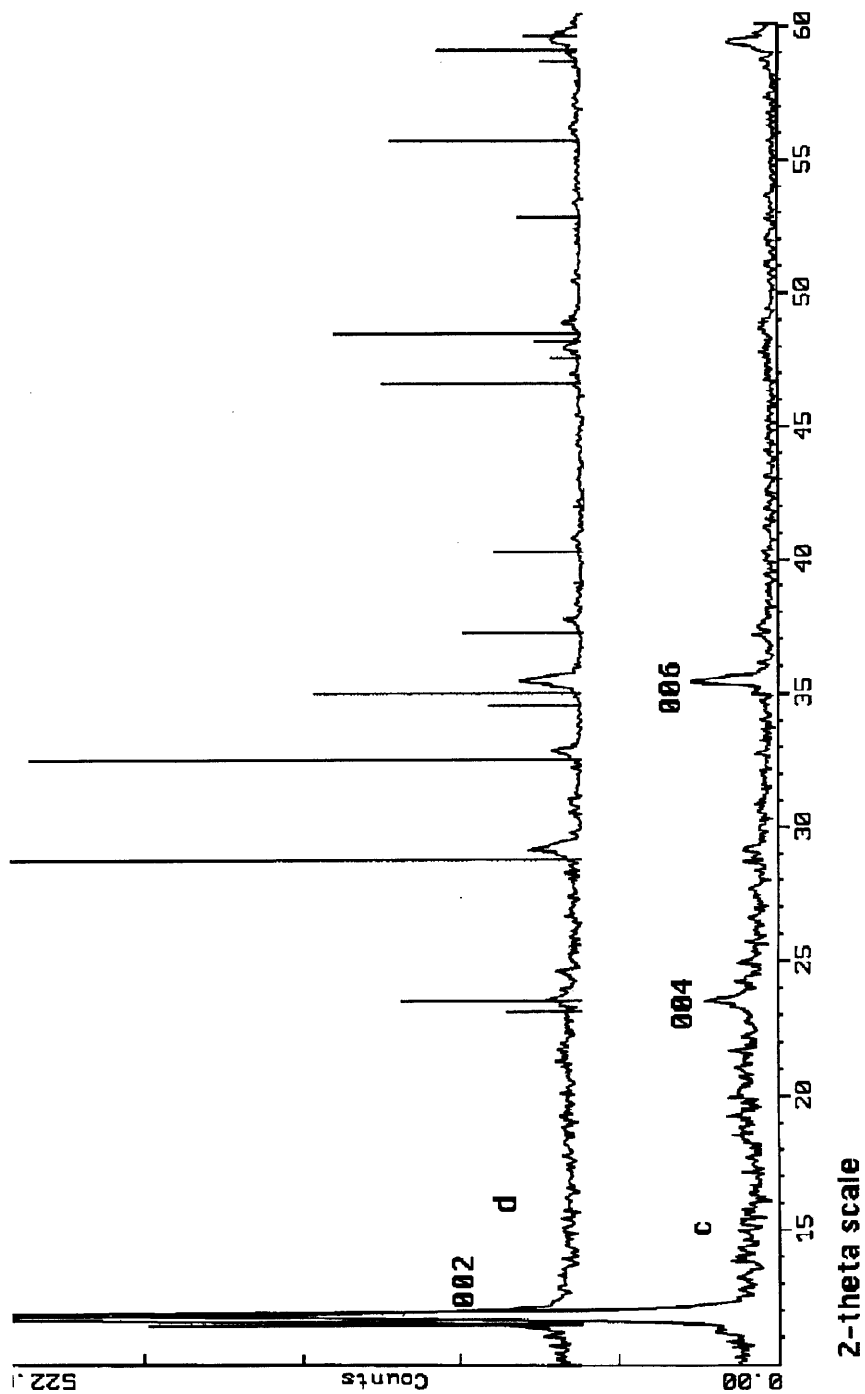
Figure 6.62, continued: BiMeVOx on quartz substrates. Heated to 600 °C. (e) BiCuVOx, (f) BiTiVOx. Other dopants similar.
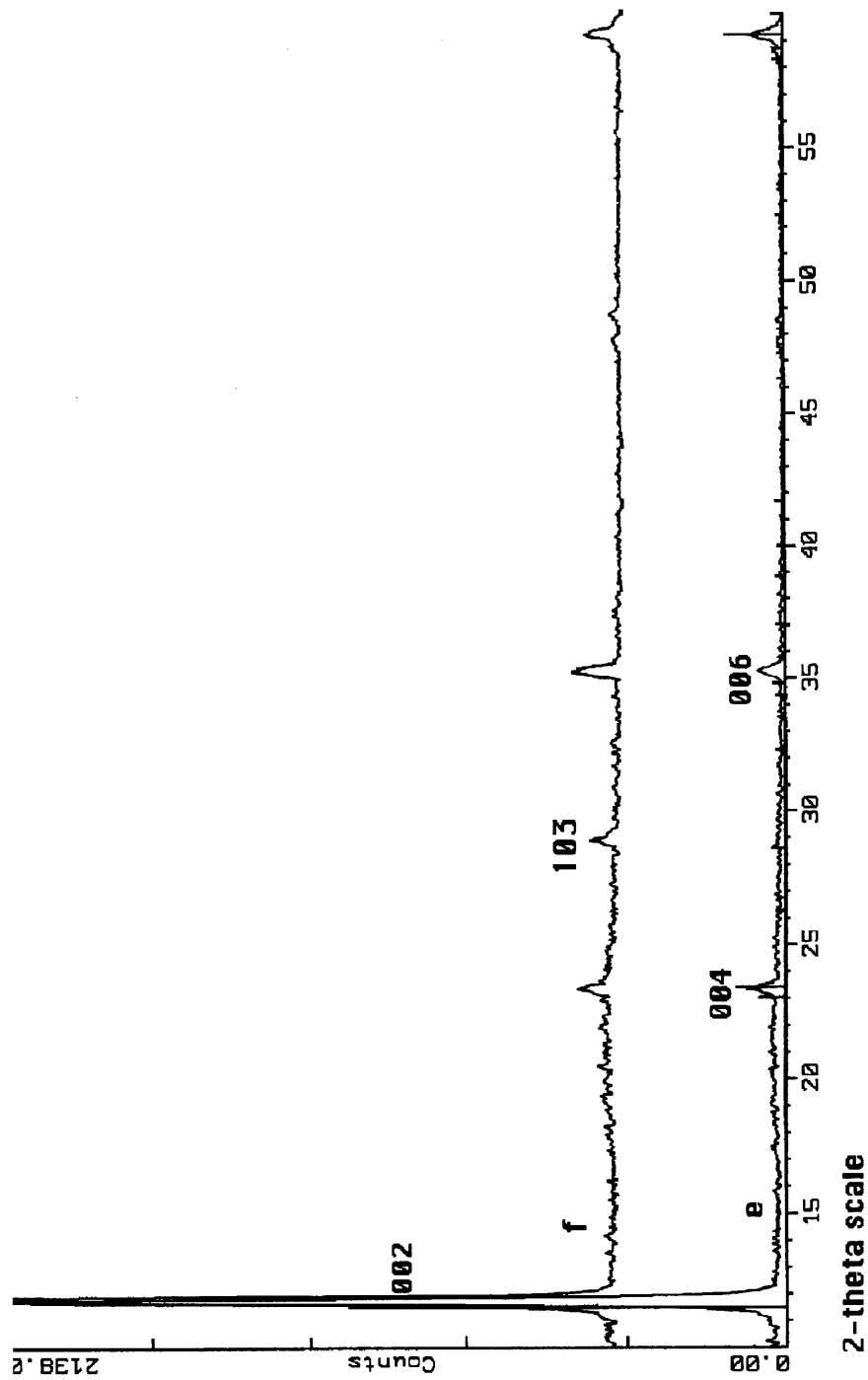
Figure 6.63: BiFeVOx on quartz. Heated to 550 °C. X 7900.
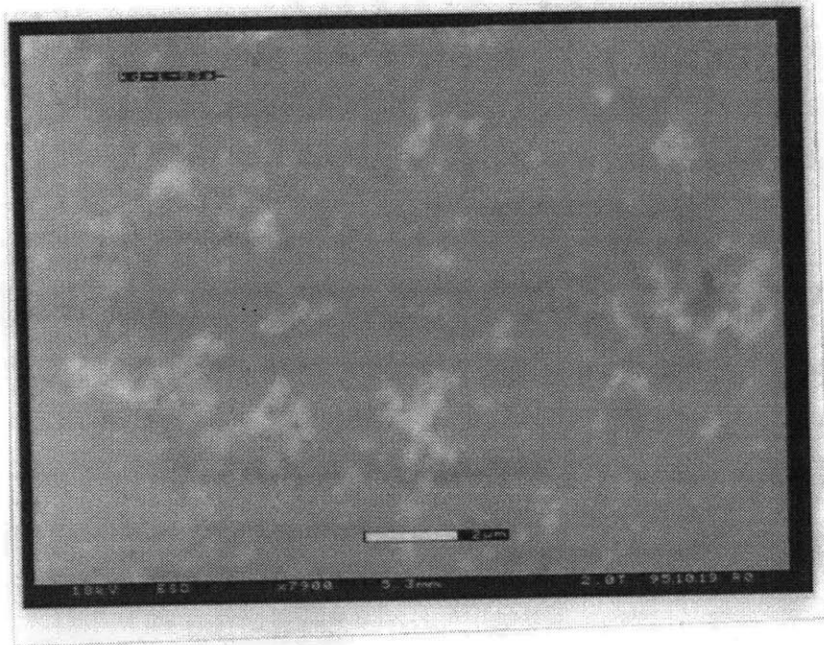
Figure 6.64: BiFeVOx on quartz, heated to 550 °C. Grazing angle 0.75°. Background noise has been subtracted. Only the 002 peak is visible beyond the noise.
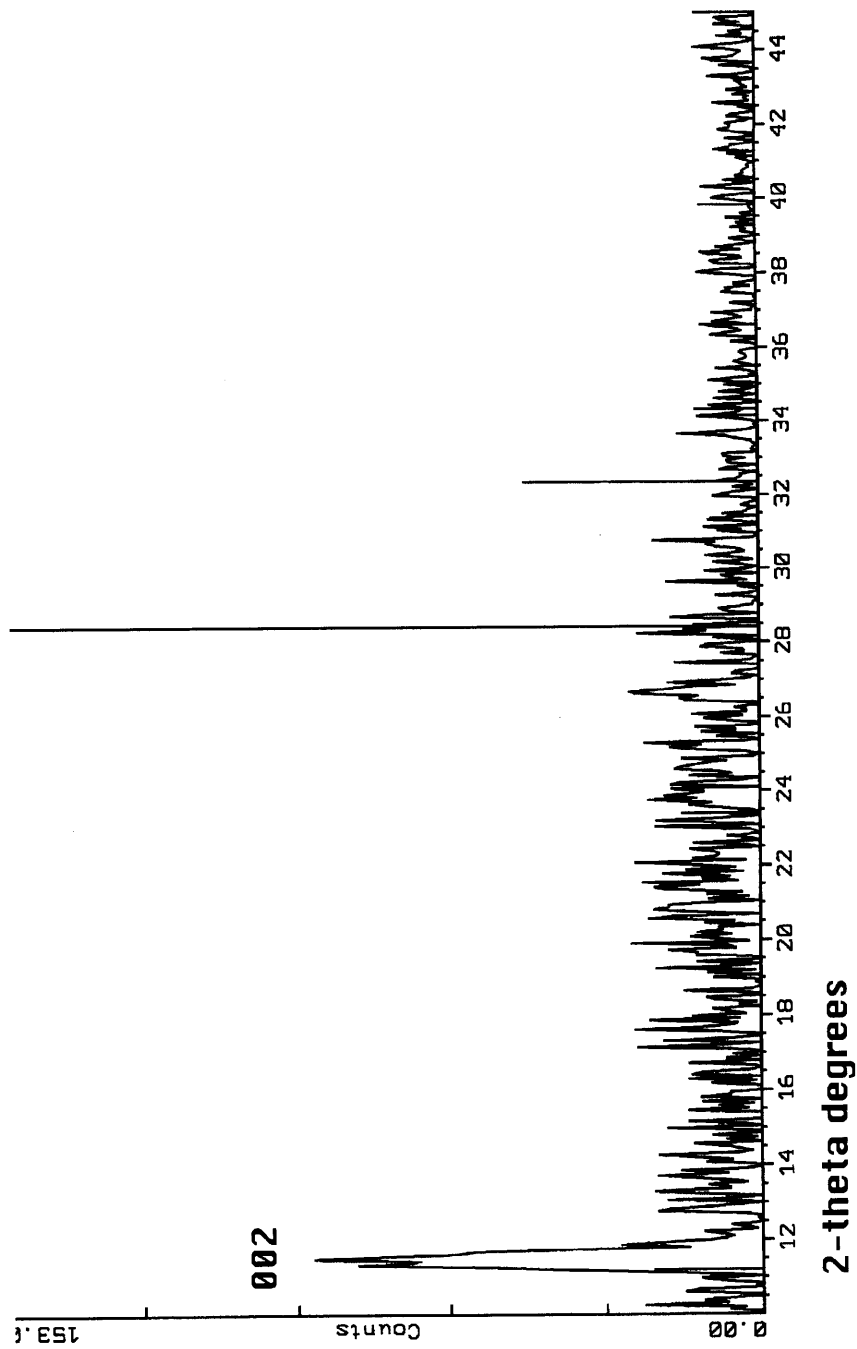
6.7 References

1) Chen, M. S.; Hegarty, W. P.; Steyert, W. A., Air Products and Chemicals, Inc.: US Patent No. 5,118,395, 1992.

2) Thorogood, R. M.; Srinivasan, R.; Yee, T. F.; Drake, M. P., Air Products and Chemicals: US Patent No. 5,240,480, 1993.

3) Rincon-Rubio, L. M.; Nguyen, B. C.; Mason, D. M. *J. Electrochem. Soc.* **1985**, *132*, 2919.

4) Minh, N. Q. *J. Am. Ceram. Soc.* **1993**, *76*, 563.

5) Harold, M. P.; Lee, C.; Burggraaf, A. J.; Keizer, K.; Zaspalis, V. T.; de Lange, R. S. A. *MRS Bulletin* **1994**, *April*, 34.

6) Hsieh, H. P. *Catal. Rev. - Sci. Eng.* **1991**, *33*, 1.

7) Dumelie, M.; Nowogrocki, G.; Boivin, J. C. *Solid State Ionics* **1988**, *28-30*, 524.

8) Isenberg, A. O. *S. S. Ionics* **1981**, *3/4*, 431.

9) Sekiguchi, T.; Sawano, M.; Eguchi, K.; Arai, H. *S. S. Ionics* **1990**, *40/41*, 502.

10) Chen, C. C.; Nasrallah, M. M.; Anderson, H. U. *Solid State Ionics* **1994**, *70/71*, 101.

11) Kueper, T. W.; Visco, S. J.; DeJonghe, L. C. *Solid State Ionics* **1992**, *52*, 251.

12) Selvaraj, U.; Prasadarao, A. V.; Komarneni, S.; Roy, R. *Mater. Lett.* **1995**, *23*, 123.

13) Joshi, P. C.; Mansingh, A.; Kamalasanan, M. N.; Chandra, S. *Appl. Phys. Lett.* **1991**, *59*, 2389.

14) Joshi, P. C.; Krupanidhi, S. B. *J. Appl. Phys.* **1992**, *72*, 5827.

15) Toyoda, M.; Payne, D. A. *Mater. Lett.* **1993**, *18*, 84.

16) Brinker, C. J.; Scherer, G. W. *Sol-Gel Science: The Physics and Chemistry of Sol-Gel Processing*; Academic Press: New York, 1990.

17) Chen, L.-C. in *Pulsed Laser Deposition of Thin Films*, Chrisey, D. B. and Hubler, G. K., Ed.; John Wiley and Sons: New York, 1994, pp 167-198.

18) Brinker, C. J.; Hurd, A. J.; Ward, K. J. *Fundamentals of Sol-Gel Thin-Film Formations*; Mackenzie, J. D. and Ulrich, D. R., Ed.; Wiley: New York, 1988, pp 223-239.

19) Yoldas, B. E.; Partlow, P. *Thin Solid Films* **1985**, *129*, 1.

20) Sakka, S.; Kozuka, H. *J. Non-Crystalline Solids* **1988**, *100*, 142.

21) Scriven, L. E. *Physics and Applications of Dip Coating and Spin Coating*; Mat. Res. Soc., 1988; Vol. 121, pp 717.

22) Mukherjee, S. P. in *Ultrastructure Processing of Advanced Ceramics, Glasses, and Composites;* Hench, L. L. and Ulrich, D. R., Eds., New York: Wiley, 1988, pp 178.

23) Strawbridge, I.; James, P. F. *J. Non-Crystalline Solids* **1986**, *82*, 366.

24) Lipeles, R. A.; Coleman, D. J. in *Ultrastructure Processing of Advanced Ceramics, Glasses, and Composites,* Mackenzie, J. D. and Ulrich, D. R., Ed.; Wiley: New York, 1988, pp 919-924.

25) Venables, J. A.; Spiller, G. D. T.; Hanbucken, M. *Rep. Prog. Phys.* **1984**, *47*, 399.

26) Barna, P. B. in *Diagnostics and Applications of Thin Films;* IOP Publishing Ltd.: London, 1992, pp 295.

27) Thompson, C. V.; Carel, R. *Mat. Sci. and Eng.* **1995**, *B32*, 211.

28) Chopra, K. L. *Thin Film Phenomena*; McGraw-Hill: New York, 1969.

29) Swaminarayan, S.; Srolovitz, D. J. *Acta Mater.* **1996**, *44*, 2067.

30) Srolovitz, D. J.; Goldiner, M. G. *JOM (Journal of Metallurgy)* **1995**, *March*, 31.

31) Hackney, S. A. *Scripta Metall.* **1988**, *22*, 1273.

32) Lange, F. F.; Claussen, N. E. in *Ultrastructure Processing of Advanced Ceramics, Glasses, and Composites* Hench, L. L. and Ulrich, D. R., Ed.; Wiley: New York, 1984, pp 493-505.

33) Lakeman, C. D. E.; Payne, D. A. *Mater. Chem. and Phys.* **1994**, *38*, 305.

34) Guo, R.; Bhalla, A. S.; Cross, L. E.; Roy, R. *J. Mater. Res.* **1994**, *9*, 1644.

35) Oh, B.; Naito, M.; Arnason, S.; Rosenthal, P.; Barton, R.; Beasley, M. R.; Geballe, T. H.; Hammond, R. H.; Kapitulnik, A. *Appl. Phys. Lett.* **1987**, *51*, 852.

36) Houk, C. S.; Burgoine, G. A.; Page, C. J. *Chem. Mater.* **1995**, *7*, 649.

37) Legendre, J.-J.; Livage, J. *J. Colloid and Interface Sci.* **1983**, *94*, 75.

38) Legendre, J.-J.; Aldebert, P.; Baffier, N.; Livage, J. *J. Colloid and Interface Sci.* **1983**, *94*, 84.

39) Passerini, S.; Chang, D.; Chu, X.; Le, D. B.; Smyrl, W. *Chem. Mater.* **1995**, *7*, 780.

40) Schaefer, D. W.; Martin, J. E.; Hurd, A. J.; Keefer, K. D. *Structure of Random Materials*; Boccara, N. and Daoud, M., Ed.; Springer-Verlag: New York, 1985.

41) Mandelbrot, B. B. *The Fractal Geometry of Nature*; Freeman: San Fransisco, 1982.

42) Kozuka, H.; Kuroki, H.; Sakka, S. *J. Non-Crystalline Solids* **1988**, *100*, 226.

43)Orcel, G.; Gould, R. W.; Hench, L. L. *Mater. Res. Soc. Symp. Proc.,* **1986**; *73*, 289.

44)Yoldas, B. E. "Modification of Oxides by Polymerization Process" in *Ultrastructure Processing of Advanced Ceramics, Glasses, and Composites,* Hench, L. L. and Ulrich, D. R., Ed.; Wiley: New York, 1984.

45)Uchida, N.; Ishiyama, N.; Kato, Z.; Uematsu, K. *J. Mater. Sci.* **1994**, *29*, 5188.

46)Calzada, M. L.; Sirera, R.; Carmona, F.; Jimenez, B. *J. Am. Ceram. Soc.* **1995**, *78*, 1802.

47)Yamada, K.; Chow, T. Y.; Horihata, T.; Nagata, M. *J . Non-Crystalline Solids* **1988**, *100*, 316.

48)Kareiva, A.; Bryntse, I.; Karppinen, M.; Niinisto, L. *J. S. S. Chem.* **1996**, *121*, 356.

49)Selvaraj, U., *et al.*, *Mater. Lett.* **1991**, *12*, 311.

50)Sanchez, C.; Livage, J.; Henry, M.; Babonneau, F. *J. Non-Crys. Solids* **1988**, *100*, 65.

51)Livage, J.; Henry, M. in *Ultrastructure Processing of Advanced Ceramics, Glasses, and Composites*, Mackenzie, J. D. and Ulrich, D. R., Ed.; Wiley: New York, 1988, pp 183-195.

52)Pope, E. J. A.; Mackenzie, J. C. *J. Noncrystalline Solids* **1986**, *87*, 185.

53)Gugliemi, M.; Carturan, G. *J. Non-Crystalline Solids* **1988**, *100*, 16.

54)Bullot, J.; Cordier, P.; Gallais, O.; Gauthier, M. *J. Non-Crystalline Solids* **1984**, *68*, 123.

55)Gharbi, N.; R'Kha, C.; Ballutaud, D.; Michaud, M.; Livage, J.; Audiere, J. P.; Schiffmacher, G. *J. Non-Crystalline Solids* **1981**, *46*, 247.

56) Xu, Q.; Anderson, M. A. *Mater. Res. Soc. Symp. Proc.*, **1989**; *132*, 41.

57) Anderson, H. U.; Pennell, M. J.; Guha, J. P. in *Ceramic Powder Science,* New York: American Ceramic Society, 1987; Vol. 21, pp 91-98.

58) Miller, K. T.; Lange, F. F.; Marshall, D. B. *Mater. Res. Soc. Symp. Proc.,* **1988**; *121*, 823.

59) Hirashima, H.; Kamimura, S. in *Better Ceramics Through Chemistry III,* Brinker, C. J., Clark, D. E. and Ulrich, D. R., Ed.; Mater. Res. Soc.: Pittsburgh, 1988, pp 779-784.

60) Hirashima, H.; Sato, A.; Yoshida, T. *Yogyo-Kyokai-shi* **1986**, *94*, 875.

61) Langbein, H.; Polte, A.; Lang, R.; Grossmann, G. *Z. Naturforsch* **1991**, *49b*, 1509.

62) Mondal, S.; Rath, S. P.; Dutta, S.; Chakravorty, A. *J. Chem. Soc. Dalton Trans.* **1996**, *1996*, 99.

63) Crans, D. C.; Felty, R. A.; Anderson, O. P.; Miller, M. M. *Inorg. Chem.* **1993**, *32*, 247.

64) Crans, D. C.; Shin, P. K. *J. Am. Chem. Soc.* **1994**, *116*, 1305.

65) Hillerns, F.; Rehder, D. *Chem. Ber.* **1991**, *124*, 2249.

66) Nakomoto, K. *Infrared and Raman Spectra of Inorganic and Coordination Compounds*; 4th ed.; Wiley: New York, 1986.

67) Crans, D. C.; Chen, H.; Felty, R. A. *J. Amer. Chem. Soc.* **1992**, *114*, 4543.

68) Crans, D. C.; Felty, R. A.; Chen, H.; Eckert, H.; Das, N. *Inorg. Chem.* **1994**, *33*, 2427.

69) Priebsch, W.; Rehder, D. *Inorg. Chem.* **1990**, *29*, 3013.

70) McDevitt, N. T.; Baun, W. L. *Spectrochim. Acta* **1964**, *20*, 799.

71)Nugent, W. A.; Harlow, R. L. *J. Am. Chem. Soc.* **1994**, *116*, 6142.

72)Mazenek, T., talk given to zur Loye group.

73)Burggraaf, A. J. *J. Eur. Cer. Soc.* **1991**, *8*, 59.

74)Chandler, C. D.; Roger, C.; Hampden-Smith, M. J. *Chem. Rev.* **1993**, *93*, 1205.

Chapter Seven:

Conclusions and Outlook

We set out in this research project to produce thin films of oxide ion conducting ceramics on porous supports. On the whole, we were successful in doing so.

The family of Aurivillius structures known as the BiMeVOx materials, with the general formula $Bi_2M_xV_{1-x}O_{5.5-\delta}$, have the highest oxide-ion conductivities known among ceramics. The parent structure is $Bi_2VO_{5.5}$, an oxygen-deficient layered structure comprised of alternating $(Bi_2O_2)^{2+}$ layers and perovskitic $(VO_{3.5}\square_{0.5})^{5-}$ layers. Its highest-temperature, highest-conductivity phase may be stabilized to room temperature by the addition of a dopant metal M, which also may introduce extrinsic oxygen vacancies, increasing the oxide ion conductivity still further. Thin films of oxygen ion conductors such as the BiMeVOx materials are potentially useful because the reduced length of the conduction path in a film permits a greater oxide ion flux at a given temperature than do more traditionally fabricated bulk forms of the materials. Potential commercial uses of the such films include air separation units and catalytic inorganic membrane reactors. The BiMeVOx materials may be expected to have some catalytic properties with respect to partial oxidation reactions. This would be a further benefit to using these materials in a partial oxidation CIMR, in addition to the high oxygen flux achievable with films of this ceramic.

Films of the parent (undoped) $Bi_2VO_{5.5}$ and the doped $Bi_2Cu_{0.1}V_{0.9}O_{5.35}$ were deposited by pulsed laser deposition (PLD) onto lattice-matched $SrTiO_3$ substrates. The undoped parent ceramic cracked and delaminated as the sample was cooled down from the deposition temperature, due to the need for the lattice to

shift 45° to match the substrate lattice as the phase went from high-temperature γ to room-temperature α. The initially crack-free doped (BiCuVOx) films were subjected to a second thermal treatment and found to have cracked due to thermal expansion mismatch. However, the direction of the cracking highlighted the oriented nature of the film on the lattice-matched substrate. Magnesium oxide and YSZ were also tried as substrates, but both $Bi_2VO_{5.5}$ and BiCuVOx films cracked and delaminated severely, due to the complete lack of lattice match. This section of the project pointed out the importance of obtaining substrates with good lattice and thermal expansion coefficient matches to the BiMeVOx film.

The sol-gel method is a wet-chemical process for depositing films of oxide ceramics onto substrates. It can be low-cost in terms of capital equipment needed for film deposition, and in many cases, in terms of the precursor chemicals needed to form the solution from which the films are to be cast. Our initial attempts to produce a precursor solution to the doped BiMeVOx materials centered on the use of vanadic acid with a number of different bismuth compounds. While vanadic acid will gel spontaneously under many conditions, the highly acidic conditions necessary for dissolving the bismuth species used in these experiments were detrimental to the polycondensation of the vanadic acid, and film-castable solutions were never produced.

Vanadium 2-methoxyethoxide was therefore used in place of the vanadic acid, and a way of producing bismuth acetate that would dissolve in 2-methoxyethanol was found. This bismuth acetate, on examination by single-crystal XRD, was found to be very similar (there were small discrepancies in the lattice parameters) to

the structure published already in the literature. However, all previous reports of the compound's behavior, including those regarding commercial materials, said that bismuth acetate was insoluble. The bismuth acetate, when left in 2-methoxyethanol solution, produced a fibrous material thought to have formed through alcoholysis and polymerization. The vanadium 2-methoxyethoxide and bismuth acetate were successfully combined to form a precursor solution which gelled on hydrolysis and which formed bulk $Bi_2VO_{5.5}$ at temperatures low relative to those needed for solid-state synthesis. Dopant metals Cu, Mn, Fe, Ti, and Nb were added as the alkoxides or acetates, and bulk BiMeVOx materials were also formed phase-pure at low pyrolysis temperatures. The precursor solutions were determined to be film-castable. In the course of this research, a bismuth-vanadium alkoxide complex, possibly analogous to the precursor structure in solution, was isolated and structurally characterized. It is to our knowledge the first bismuth-containing heterobimetallic alkoxide to be so characterized.

Films of BiCuVOx were cast initially defect-free onto quartz substrates but found to agglomerate on heating at higher temperatures. Addition of a variety of coordinating compounds decreased the film quality, while use of acid catalysts and increasing the water-to-alkoxide ratio for hydrolysis had little effect on the quality of the films. BiCuVOx films on platinum substrates, however, remained defect-free over all temperatures examined, suggesting that the quartz substrate had a major role in the agglomeration observed. On the other hand, BiNbVOx films remained defect-free over all temperatures on both quartz and platinum substrates.

Films of other BiMeVOx materials (M=Fe, Ti, Mn) on quartz were examined. The quality of these appeared to vary with the method of adding the dopant: BiTiVOx and BiNbVOx (dopant added as alkoxide) did not agglomerate, while BiCuVOx, BiMnVOx, and BiFeVOx (dopant added as acetate or acac) did. The relative importance of how the dopant was added, *versus* the role of the identity of the dopant, was not carefully examined. Since the BiMeVOx examples that did not agglomerate on quartz were those whose dopants were added as alkoxides, it is suggested that the precursor structure – in particular, the greater gel network connectivity available where there are more hydrolyzable groups – also was important in enabling some films to remain defect-free at temperatures where others agglomerated.

All films cast were *00l*-oriented, e.g. **c**-axis perpendicular to the substrate. This is 90° to the direction necessary for the highest conductivity available in the material to be achieved. The orientation was influenced by the deposition method to some extent – e.g. spin coating gave more strong texturing than did dip coating for many samples – and to some degree by the substrate. Both sol-gel and pulsed laser deposited films were oriented, however, on widely different substrates. Some films on platinum were less oriented, possibly because platinum's lattice is 1/3 the **c**-axis of BiMeVOx. (Table 6.1) Methods of producing nonoriented films or films with the **c**-axis parallel to the substrate, are worth exploring.

BiCuVOx films were successfully cast defect-free onto porous alumina substrates (pore size 0.02 μm). The use of the complexing additives with the films on porous substrates had either no effect or

502

a detrimental one, relative to the quality of the film produced by the additive-free precursor solution.

The ultimate test of the process would be to prepare the BiCuVOx films onto the porous alumina substrates under cleanroom conditions, then test them in a permeation cell for gas-tightness. Following that, their conductivity would be examined by impedance spectroscopy. Furthermore, the principle of increased oxygen flux with decreased conduction path hits a point of diminishing returns when the kinetics of oxide ion recombination become large relative to the rate of conduction through the membrane. Another issue with the membrane conductivity is whether the large proportion of surface species, relative to the bulk, affects the oxide ion conductivity. Since the location (random distribution) of vacancies and the energy surfaces over which a moving O^{2-} ion must travel in hopping from site to site during conduction are bulk properties which are subject to distortion by proximity to the surface, the ionic conductivity of the thin film cannot be assumed to be necessarily identical to that of the bulk. Early termination of the project made it impossible to make any permeation cell or conductivity measurements on the films deposited in this project.

The process of depositing BiMeVOx films onto porous substrates requires several more development steps before the question of commercial viability can be addressed. The work described here was successful only with spin-coating depositions, while large-scale processes (in terms of the size of the pieces, not the throughput) require the precursor solutions to be optimized for dip-coating. It may well be that with a proper dip-coating apparatus this goal would be achievable with no or few

modifications to the precursor solutions reported in this work. (We realized after the project had ended that a potential solution to the problem of the vibrations from the motor (or an unsteady hand), and the inconsistent and irreproducible withdrawal rate, could have been solved by draining the solution out away from the substrate. This could be done crudely but reproducibly with an assembly of standard laboratory equipment, and the precursor solution could be kept protected from moisture and evaporation, and recycled to minimize waste.) A better synthesis of the vanadium 2-methoxyethoxide is necessary to make the process cost-effective, as the methods used in this work were wasteful in a way that was unimportant on the laboratory scale but would be prohibitive on even a pilot scale. It may be worth investigating the use of $Na(OCH_2CH_2OCH_3)$ with $VOCl_3$ as a synthetic route. The sodium alkoxide will be less susceptible to oxidation than is the alcohol. Another issue is that 2-methoxyethanol is associated in industry – particularly the silicon chip industry – with human reproductive toxicity. Substituting ethoxyethanol or 2-ethoxyethanol, or an even larger alcohol-ether, would increase the safety of the process, but this substitution will require re-optimization of the precursor formulation, including, possibly, modification of the vanadium alkoxide synthesis. Were these issues addressed, however, we believe that the sol-gel deposition of films of BiMeVOx, particularly BiCuVOx, onto porous supports could be a cost-effective process and lead to improvements in air separation and CIMR technology.

A number of interesting tangents arose in the course of this project, and may be worth pursuing. There are to date no studies of the mechanism of film growth and defect formation for films

produced in a wet deposition process, despite the great wealth of publications regarding films produced by any of a great range of physical and vapor deposition processes. In all of these latter processes, the arrival of film material at the substrate surface can be modeled as a one-adatom-at-a-time process, with building-up of either monolayers or of islands that later coalesce. Reports in the PLD literature refer to the difficulty of modeling the situation where a large flux of ceramic atoms appear at the substrate surface nearly all at once; but even in PLD the Volmer-Weber, Frank-van der Merwe, or Stranski-Krastanov growth models can be used with some modification. In the sol-gel film case, however, the adatoms must considered to be all nearly in place – i.e. several monolayers' worth – *simultaneously* prior to the start of the model time. What steps occur next in the mechanism of film formation from the gel network is an open field for investigation and modeling.

A second area of investigation that remains to be spun off this project is the question of the precursor chemistry. The exact nature of the interactions between the partially- or fully-alcoholyzed bismuth acetate species with the vanadium alkoxide were examined only cursorily in the work reported here because it was tangential to the project goal. However, the isolation of the bismuth-vanadium chloroalkoxide is tantalizing: can a bismuth-vanadium acetate-alkoxide be isolated and characterized? Can standard metatheses be performed on the chloroalkoxide to add more metals, perhaps increase the Bi-to-V ratio to that needed for the BiMeVOx materials? Extension of the precursor chemistry into Bi-Ti combinations would be even more interesting from a practical point of view, since

bismuth-titanium oxides are of great interest in the electronics industry.

The project described in Part I of this thesis achieved its main goal of producing defect-free films of $Bi_2Cu_{0.1}V_{0.9}O_{5.35}$ on porous supports. The further work necessary to "tie up loose ends," both from the scientific perspective and with an eye towards eventual commercialization of the process was left undone due to the early termination of the project.

Appendix to Part I:

Materials and Methods

A1. Chemicals used

The reagent compounds used in Part I of this thesis are listed below. "Homemade" refers to a compound made by the author. "JM/AA" refers to a compound from Johnson-Matthey Alfa-Aesar or any of its subsidiaries prior to 1999. Purities listed typically refer to the metals purity and not to the compound purity.

Table A1: Compounds Used

Compound	Manufacturer	Purity (%)	Chapter Used
V_2O_5	JM/AA	99.995	2
Bi_2O_3	JM/AA	99.99	2
CuO	JM/AA	99.99	2
Dowex 50Wx2-100 strongly acidic cation exchanger	Aldrich		3
$NaVO_3$	JM/AA	98% (99% found to be wrong phase)	3
$Bi(NO_3)_3 \bullet 5H_2O$	JM/AA	technical	3
NH_4VO_3	JM/AA	99.99	3
gum arabic	Aldrich	n/a	3
glycine	Aldrich	98	3

Table A1, continued.

Compound	Manufacturer	Purity (%)	Chapter Used
2-methoxyethanol	Aldrich	99 anhydr.	3
ethylene glycol	Aldrich	95	3
glacial acetic acid	Malinkrodt	technical	3
ethanol	Malinkrodt	95	3
nitric acid, conc.	Malinkrodt	technical	3
$Bi(OAc)_3$	Strem	99	3
$Bi(OAc)_3$	JM/AA		3
V-2MOE	homemade	n/a	4, 5, 6
$Bi(OAc)_3$	homemade	n/a	4, 5, 6
V_2O_5	JM/AA	99.5	4
$VOCl_3$	Strem	99	4
BuOH	Malinkrodt	technical	4
benzene	Aldrich	98	4
iPrOH	Malinkrodt	technical	4
$VO(OiPr)_3$	Strem	10% in HOiPr	4
EtOH	Aldrich	100%	4
NH_3 gas	Matheson	anhydr.	4
tetreethylene glycol	Aldrich	99	4
$BiCl_3$	Strem	99.999	4
$BiCl_3$	JM/AA	99.95	4
$NaN(SiMe_3)_2$	United Technologies	95	4
MeOH	Malinkrodt	technical	4

Table A1, continued.

Compound	Manufacturer	Purity (%)	Chapter Used
acetonitrile	Malinkrodt	technical	4
diethyl ether	Aldrich	anhydr., 99.5	4
sodium	Aldrich	n/a	4
pentane	Aldrich	anhydr., 99.5	4
tetrahydrofuran	Aldrich	anhydr., 99.5	4
2-methoxyethyl ether (diglyme)	Aldrich	anhydr., 99.5	4
acetic anhydride	Malinkrodt	technical	4
d_4-tetrahydrofuran, $CDCl_3$, d_{10}-dimethoxyethane	Cambridge Isotope Labs	standard NMR purity	4
$V(OnBu)_4$	homemade	n/a	4
P_2O_5	Aldrich	technical	4
NH_4OH, conc.	Malinkrodt	technical	4
copper 2-ethylhexanoate	Strem	solvent-free	4
bismuth 2-ethylhexanoate	Strem	72% in mineral spirits	3, 4
$Cu(OAc)_2$	Strem	anhydr.	4
$Nb(OiPr)_5$	Strem	10% in HOiPr/pentane	4
$NbCl_5$	Strem	99.99	4
acetylacetone	Aldrich	99.5	4

Table A1, continued.

Compound	Manufacturer	Purity (%)	Chapter Used
$Mn(OAc)_2*4H_2O$	Strem	99+	4
$Fe(OAc)_2$	Strem	anhydr., 97	4
$Fe(acac)_2$	Strem	99	4
$Ti(OiPr)_4$	Aldrich	99	4
ethanolamine	Aldrich	99.5	5
N,N-dimethylethanolamine	Aldrich	99.5	5
VI_2	Cerac		5
hexane	Aldrich	anhydr., 99.5	5
potassium	Aldrich	n/a	5
diisopropanolamine	Aldrich	95	6
acetylacetone	Aldrich	99+	6
dimethyl succinate	Aldrich	98+	6
1,3-propanediol	Aldrich	98	6
ethanolamine	Aldrich	99.5	6
diethanolamine	Aldrich	98.5	6
triethanolamine	Aldrich	98	6
pyridine	Aldrich	99	6
N,N-dimethylformamide	Aldrich	99.8	6
copper dimethylaminoethoxide	Strem	n/a	6

A2. Instrumentation

FTIR: Transmission IR measurements were made on a Perkin-Elmer model 1610 FTIR, with the background subtracted out of the final spectrum. Spectra were run from 4000 to 400 cm^{-1} at a resolution of 4 cm^{-1}, and 16-32 scans were collected and summed to give the resultant spectrum. Samples were prepared either as KBr disks or as nujol mulls, when solids, or were used neat when liquids, as indicated in the text. Some samples were deposited as liquids onto 3M Type 61 IR cards, and spectra were taken with the sample either wet or after drying.

PA-FTIR: Photoaccoustic fourier transform infrared spectroscopy[1] measurements were made on a Bio-Rad FTS-60A at room temperature.

P-XRD: Powder X-ray diffraction data was collected on two diffractometers. The first, used during the early part of the research, was a Rigaku RU300 rotating anode $\theta/2\theta$ diffractometer with Cu $K\alpha$ radiation, $\lambda(K\alpha_1)$ = 1.5406 Å, $\lambda(K\alpha_2)$ = 1.54439 Å, unresolved $\lambda(K\alpha)$=1.54184 Å.[2] The diffractometer was equipped with a graphite monochromator. The generator was operated at 50 kV and 200 mA and the slits used were DS 0.5°, SS 0.5°, RS 0.15°. Samples were generally run as a continuous scan (20°/min) from 5-75°, though in some cases shorter 2θ ranges were used.

The second diffractometer used was a Siemens D5000 theta/theta diffractometer using a stationary copper vacuum tube to produce the Cu X-radiation. The diffractometer was operated at 40 kV and 45 mA and was equipped with a monochromator. X-ray patterns were measured with a rotating sample stage to ensure uniform sample exposure. The slits used were SS 1 mm, DS 1 mm, RS 0.6 mm. Samples were generally run as a stepped scan from 5-75°, with step size 0.05° and 1 sec/step data collection.

The Siemens diffractometer was also equipped with a grazing incidence attachment, where the incident beam arm was kept at a constant settable incident angle (usually 1°) and the detector arm moved through diffracted angles theta. The grazing incidence attachment permitted detection of the diffracted beam.

In both cases, samples were prepared by grinding to a fine powder and suspending the powder in a Collodion/amyl acetate (1:3 ratio) binder, then applying the suspension to a glass slide. The solvent in the binder was removed in a drying oven (ca. 120 °C). The glass slide was then mounted on the sample holder (aluminum for the Rigaku, plastic for the Siemens) with clay. For grazing incidence measurements, the substrate holding the film was mounted directly onto the sample holder using clay.

Lattice parameters were determined using the computer software PPLP in the NRCVAX package.[3] Theoretical powder patterns were also calculated using the NRCVAX package. The JCPDS database was used to find matching powder patterns for known compounds, using the matching and searching utilities of the resident software on the Rigaku and Siemens instruments.

SC-XRD: Single-crystal X-ray diffraction data collection and analysis was performed in the chemistry department facility by Dr. William C. Davis.

ESEM: Environmental scanning electron microscopy was performed on an Electro-Scan unit (CMSE Microscope Facility). Except where indicated, samples were mounted on aluminum studs using carbon tape and the water vapor level was set at 2-4 mTorr; no other sample preparation was performed. Where indicated, a thin layer of gold was evaporated onto the sample surface to relieve charging effects. Stigmation was performed at 8000 X or at the magnification level used, whichever was higher. The unit was equipped with a Link Analytical energy dispersive spectroscopy (EDS) analyzer, and it and the attached software were used in some experiments.

NMR: ^1H and ^{13}C NMR were performed on a Brucker AC250 250 MHz NMR, or on a Varian Unity UN300 300 MHz NMR. For measurements on both instruments, deuterated solvents (Cambridge Isotope Laboratories) to provide a lock signal. ^{51}V NMR were performed on a Varian Unity UN300 300 MHz NMR equipped with a tunable broadband probe.

Thermal analysis: Simultaneous differential thermogravimetric analysis and thermogravimetric analysis (DTA-TGA) data were obtained using a TA Instruments SDT 2960. Samples were run under atmospheres of oxygen, nitrogen, or air. The furnace was generally ramped up and down at 25 °C/min unless otherwise noted.

Profilometry: A Dektak[3] profilimeter equipped with 12.5 μm stylus was used to detect the height of the drop between the area of the substrate covered with film and that which was not. Uncovered areas were produced by masking the substrate. After approximately 5 measurements on samples produced with a given set of deposition parameters, all samples deposited with the same parameters were assumed to have the same thickness. Sample thicknesses were rechecked when changes were made to the deposition parameters.

E-beam: Electron-beam deposition of platinum, alumina, and other materials was performed using an E-beam unit built by the Microfabrication Lab in CMSE, with electron gun control by a PAK-8 Programming unit. Deposition parameters for various substrates are listed in Chapter 6.

Substrates: Smooth (non-porous) substrates were quartz microscope slides obtained from Finkenbeiner, Inc. (Waltham, MA), in some cases used as a support for a film of platinum (1000 Å) atop a titanium adhesion layer (100 Å), or a film of alumina, both applied by E-beam. Porous substrates were Whatman Anopore (aluminum oxide) filter disks, porosity 0.02 μm.

Solid state synthesis: Stoichiometric amounts of the starting materials were weighed and combined in an agate mortar. Acetone was added as a mixing aid and the powders were ground for 15-30 minutes, then the acetone was permitted to evaporate. Powders

were pressed into a pellet to increase reactivity by decreasing the intergrain distances. The powder was placed into a 1/2-inch pellet die and pressed uniaxially to 5000-8000 pounds. The pellet was removed from the press and placed on platinum foil in an alumina tray or crucible.

Heating: Samples, prepared by solid state or by precursor methods, were placed in alumina trays or crucibles and heated in a Lindberg® box furnace (max. T 1050 °C) or a Lindberg® tube furnace (max. T 1150 °C). Ramp rates for solid state syntheses were generally 10 °C/minute unless otherwise noted; cooling rates were generally 5 °C/minute. For films, ramp rates were 5 °C/minute up and 2 °C/minute down; some samples were placed into an already-hot furnace (See Chapter 6). For samples produced by the solid-state method, the pellets usually needed to be re-ground and re-pressed, followed by another heating period, before samples were phase-pure. Film samples were heated (See Chapter 6) after deposition of each layer on an alumina plate atop a standard laboratory hot plate, maximum surface temperature approximately 350 °C.

Conductivity measurements: For solid state syntheses, pellets made in a 1/2 inch pellet die were sintered for 8-12 hours 25 °C higher than the synthesis temperature. For sol-gel samples, pellets were merely pressed from the powder. The dimensions of the pellets were measured with calipers (±0.02 mm) followed by weighing the samples to determine their density. The faces of the sintered pellets were sanded and painted with platinum ink

(Engelhard) to form electrodes. The paint was baked onto the surface of the pellet at 850 °C for 1 hour to remove the binder, in the case of solid state samples, and was baked at the pyrolysis temperature of the sample for 1 hour for sol-gel samples. The platinum tended to flake off the samples on cooling, so complete coverage of both faces was difficult to obtain.

The sample holder consisted of nested nickel metal and ceramic tubes, both open at both ends. The nickel tube was grounded to eliminate noise in the impedance plots, though spikes at 60 Hz were still occasionally observed. Inside the nickel tube was a mullite tube (3/4" OD) with Cajon® Ultra-torr connectors at each end; inserted into this mullite tube was a smaller diameter (1/2" OD) mullite rod with two small holes bored through the rod along the long axis. The platinum electrode lead and the thermocouple were inserted into these bores. The end of the thermocouple was positioned approximately 2mm away from the sample at the end of the tube. The electrodes were made of platinum foil and were attached to the platinum lead. BNC connectors were soldered to the platinum leads and to the nickel ground. Ultra-torr fittings were used to align the tubes inside each other and to help apply pressure on the electrodes; springs attached to the end of the double-bore rod and the nickel tube also kept pressure on the electrodes to ensure maximum contact. (Figure A.1)[4]

The sample holders were placed in a hinged tube furnace equipped with a programmable controller connected to a thermocouple placed directly outside of the nickel tube. The

517

temperature settings were changed by resetting the set point on the controller.

AC impedance measurements were performed using a Solartron 1260 Impedance/Gain-Phase analyzer interfaced to a PC computer driven by Z-plot software. Frequency was varied between 5 MHz to 1 Hz, with a waveform amplitude of 10 mV and zero mV bias, with integration over 100 cycles and a 10 sec. measurement delay. Frequencies were swept by logs, downward, at increments of 10. Measurements were made between 300 °C and 975 °C in 50, 25, or 10 °C increments, except where noted. Heating or cooling rates between intervals was not varied. Pellets were allowed to equilibrate for 4-6 hours at each temperature interval before the conductivity was measured. The overall temperature range was limited by the resolution and the sample holder: at low T, the resistance was too high (Z>2-3 MΩ) for interpretation, and at high T the resistance would become sufficiently low that the Solartron could not measure the impedance.

Air-sensitive procedures were done in either an argon-filled glove box or using oven-dried glassware on a double-manifold supplied with vacuum and nitrogen gas.

UV-VIS measurements were performed on an Hewlett-Packard HP5245A spectrophotometer using plastic cells.

Figure A.1: Schematic of the pellet holder used for oxygen ion conductivity measurements.[4]
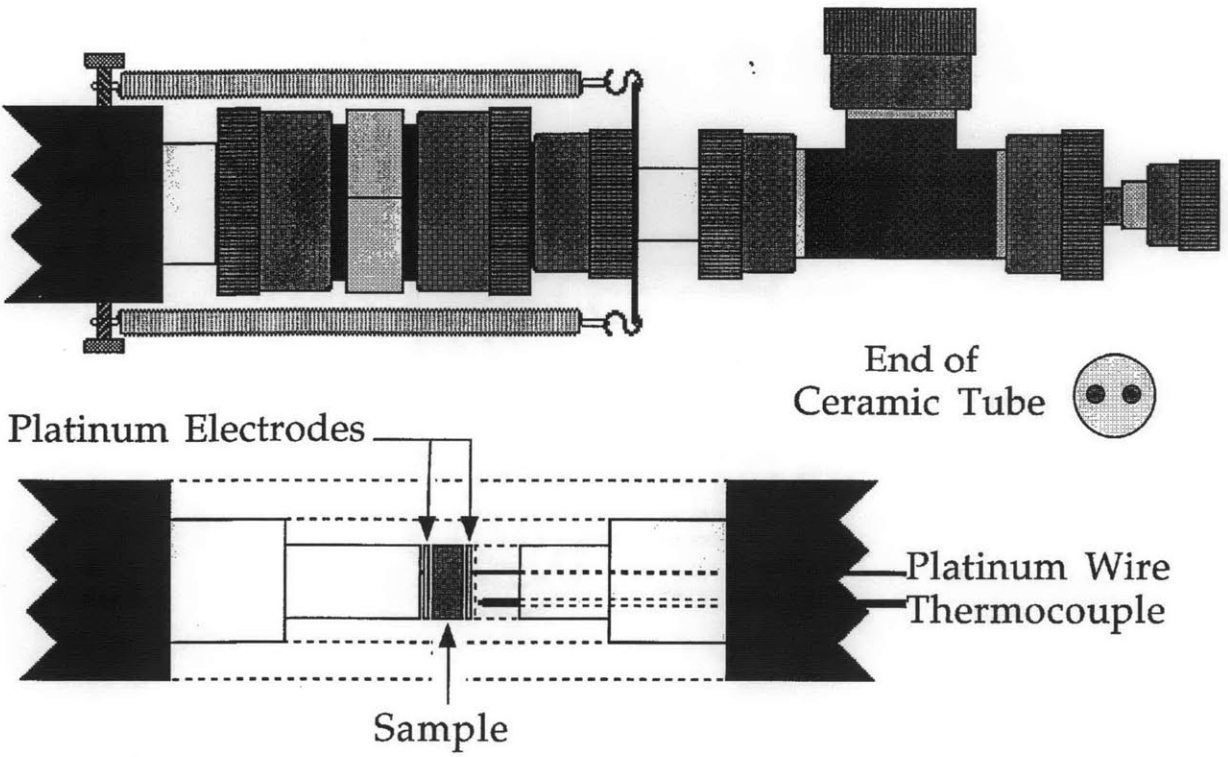
A3. References

1) Ying, J. Y.; Benziger, J. B.; Navrotsky, A. *J. Am. Ceram. Soc.* **1993**, *76*, 2571.

2) Klug, H.; Alexander, L. *X-ray Diffraction Procedures*; 2nd ed.; John Wiley & Sons: New York, 1974.

3) Gabe, E. J.; Page, Y. L.; Charland, J.-P.; Lee, F. L.; *et al. NRCVAX -- An interactive program system for structure analysis*, 1989; Vol. 22, pp 384.

4) Kendall, K. R., Ph.D. Thesis, Massachusetts Institute of Technology: Cambridge, MA, 1996.

Chapter Eight

Introduction and Background on Transition Metal Carbides

8.1 Technological Uses of Transition Metal Carbides

8.1.1 Structural/refractory uses[1,2]

The carbides of the transition metals in Groups IV - VI have extremely high melting points (Table 8.1) and are therefore referred to collectively as the "refractory carbides." In addition to their stability at high temperatures, these compounds are extremely hard (Table 8.2), finding industrial use in cutting tools and wear-resistant parts. Their hardness is retained to very high temperatures, and they have low chemical reactivity – they are attacked only by concentrated acid or base in the presence of oxidizing agents at room temperature, and retain good corrosion resistance to high temperatures. The refractory carbides are strong, with Young's modulus values – a measure of elastic deformation resistance – rivaling those of SiC at room temperature. In addition, they have good thermal shock resistance and good thermal conductivity, permitting heat to be drawn away from the working surface of the tool. This gives them a benefit over other refractory materials, which do not conduct heat so well. (Table 8.3)

Tungsten carbide, WC, is the most commonly used for fabrication as "cemented carbide" tools for cutting steel, in which the carbide is bonded in a metal matrix, usually cobalt. Cobalt is used because it wets the carbide particles and therefore behaves as a good binder without having significant ability to dissolve the carbide, so that the carbide is left pure in the bound form. However, pure WC-Co cemented carbides tend to weld locally with the steel being cut. TiC, TaC, and NbC are often used in conjunction

with WC because TiC locally forms a layer of TiO^2 or $TiO_2{}^3$ which protects the tool from wear, and TaC and NbC raise the melting temperature and oxidation resistance of the tool.

For high-temperature applications, the carbides are used as pure-material sintered parts or in a Co/Mo/W/carbide sintered composite. They outperform the standard alloys and so-called "superalloys" in such applications as rocket nozzles and jet engine parts, where erosion resistance at temperatures of 2500 °C and up is crucial. TiC_{1-x} and VC_{1-x} in particular maintain high strengths up to 1800 °C and therefore can be used as high temperature structural materials, provided that internal and surface flaws, such as stress cracks and pores introduced during fabrication and sintering, are removed. Such defects lead to a high room-temperature brittleness; plastic flow relieves internal stresses caused by defects and leads to reduced brittleness at high temperatures. Plastic deformation occurs particularly via a mechanism of dislocation glide along {111} planes.

It must be noted that there is some variation in the literature with respect to the reports of assorted mechanical and thermodynamic properties of the refractory carbides. The transition metal carbides show a range of nonstoichiometries and possibilities for vacancy ordering, so the precise phases being tested for a given property are often unclear. Furthermore, small concentrations of oxygen present as metal oxide are famously difficult to remove – or even detect – and can be expected to affect the properties of the material.

Mixed-metal carbides have been examined for their melting point and hot-hardness behavior as well. The hardness arc-cast or

zone-melted samples of $(Ta_{0.8}Hf_{0.2})C_{1+x}$ was tested (by indentation using diamond or B_4C tips) and compared with that of the similarly-prepared pure-metal carbides TaC_{1-x} and HfC_{1+x} over the temperature range 800 - 2000 °C.[4] In all cases the hot hardness decreased with increasing temperature. For temperatures up to 1400 °C the hardness order increased as HfC_{1+x} < $(Ta_{0.8}Hf_{0.2})C_{1+x}$ < TaC_{1-x}, but over 1400 °C the mixed carbide began to outperform the tantalum carbide. Hardnesses varied from 600 kg/mm^2 to 150 kg/mm^2 over the temperature range tested.

The melting points of the mixed-metal carbides outperform those of the pure-metal carbides, as well. Samples prepared by vacuum reduction of the mixed oxide powders at 2000 °C, followed by sintering at 2200 °C and 2500 °C in good vacuum were tested for their melting behavior.[5] 8TaC·ZrC and 4TaC·HfC had melting points 3890 °C and 3990 °C, respectively, somewhat higher than those of the pure-metal carbides (measured at 3470, 3750, and 3840 °C for Zr, Hf, and Ta carbides, respectively). The higher melting points in the mixed-metal carbides was attributed to composition changes due to the selective evaporation of carbon during melting.

Table 8.1: Melting points of the carbides of Groups IV-VI

Metal Name	Metal MP (°C)[2]	Carbide (MC) MP (°C)*[2]	Carbide (MC) MP (°C)**[6]
Ti	1677	3067	2940
Zr	1852	3420	3420
Hf	2222	3928	3820
V	1917	2648	
Nb	2487	3600	
Ta	2997	3983	
Cr	1900	1810 (Cr_3C_2)	
Mo	2610	2600	
W	3380	2776	

* Values listed in Toth (see Ref. 2)

** Values listed in *Kirk-Othmer Encyclopedia of Chemical Technology* (See Ref. 6)

Table 8.2: Properties of Group IV - VI Carbides[2]

Phase	Struct.	Lattice (Å)	Young's Modulus x 10^6 psi	Micro-hardness (kg/mm^2)	Therm. Exp. Coef. x 10^{-6}	Color
TiC	B1	4.328	39-67	2900	7.4	grey
ZrC$_{0.97}$	B1	4.698	56	2600	6.7	grey
HfC$_{0.99}$	B1	4.640	46-61	2700	6.6	grey
VC$_{0.97}$	B1	4.166	63	2900	--	grey
NbC$_{0.99}$	B1	4.470	49-74	2400	6.6	lavender
TaC$_{0.99}$	B1	4.456	53-78	2500	6.3	gold
Cr$_3$C$_2$	ortho-rhombic	a: 11.47, b: 5.545, c: 2.830	56	1300	10.3	grey
Mo$_2$C	ortho-rhombic	a: 7.244, b: 6.004, c: 5.199	33	1500	4.9//a, 8.2//c	grey
WC	hexa-gonal	a: 2.906, c: 2.837	97	2100 (basal plane)	5.0//a, 4.2//c	grey

Table 8.3: Properties of other Refractory Materials[6]

Material	Melting Point (°C)	Microhardness (kg/mm^2)
SiC	2300 dec	2580
C, diamond	3800 dec	7600
Al$_2$O$_3$	2050	2080

8.1.2 Catalytic uses

In addition to the technological uses of transition metal carbides which exploit their high hardness and stability at high temperatures, certain carbides have been examined for their catalytic properties in a number of reactions. This is in addition to their being potential supports for more traditional catalytic materials (Ni, Pt, Rh, etc.) due to their high heat stability.

The observation has been made that tungsten was active as a catalyst and showed good selectivity toward xylene formation during the isomerization and hydrogenolysis of 1,1,3-trimethylcyclopentane, but only after an induction period, as is also characteristic of platinum and paladium.[7] Base transition metals do not behave this way. The behavior was explained by invoking the formation of tungsten carbide on the surface of the metal; WC is similar to Pt in selectivity for neopentane isomerization as well.[8] Mo_2C has been found to behave similarly to Ru in $CO-H_2$ reactions.[9] These are merely two examples: in fact, carbides of the Group IV-VI metals have been studied for their activity in oxidation, hydrogenation/dehydrogenation, isomerization, hydrogenolysis, and $CO-H_2$ reactions, and in many cases have been found to rival the performance of the less economic Group VIII metals. While the refractory carbides do not show high activity for oxidation reactions (for example, the rate of H_2 oxidation follows the order metal >> carbide > oxide for Group V and VI metals[10], and the rate of NH_3 oxidation over refractory carbides is lower than that over Group VIII metals[11]), they are as active as the transition metals themselves

527

for hydrogenation and dehydrogenation reactions. In isomerization reactions, WC, Pt, and Ir are unique in their high activity and selectivity.[12] However, it is not necessary for the refractory carbides to be more or even equally active in catalyzing given reactions compared with the noble metals, because the lower cost of the carbides will in many cases offset the losses in catalytic activity.

The Group IV-VI metal carbides are, however, difficult to prepare as high purity (e.g. free of surface oxide or graphitic and amorphous carbon contamination) and high surface area powders. There have been a number of approaches to synthesizing the carbides in a way that produces a high specific surface area, including carburization of a spray of the oxide powder using a CH_4/H_2 gas mixture,[13] reaction of the metal oxide vapors with activated carbon,[14] ultrasound irradiation of the metal carbonyl,[15] carburization of a precursor deposited onto a support such as alumina,[16,17] and similar approaches.[18] The problem of surface contamination has been addressed as well, with most solutions centering on the idea of activation of the surface of the carbide via a thermal treatment prior to catalytic use. The thermal treatment includes heating in vacuum, which has been found to activate TaC, TiC, and WC for hydrogenation of ethylene,[19,20] or reduction in flowing hydrogen gas.[14,21] These methods, of course, are for removing surface oxygen; surface carbon (amorphous or graphitic) is difficult to remove.

The catalytic uses of the transition metal carbides are mentioned in the context of this project because the low-temperature precursor methods reported in Chapter 9 have the potential for yielding high-surface area carbides possibly useful for catalytic applications. However, the structural and refractory

characteristics of the carbides were the focus of the project reported in Part II of this thesis, and no exploration of the catalytic potential, even characterization as basic as finding the surface area via BET analysis, was considered.

8.2 Structures of Transition Metal Carbides

Most of the transition metal monocarbides form in the *B1* (NaCl) structure, *fcc* metal with carbon occupying the octahedral interstitial sites. The shortest M-M distance is about 30% greater in the *B*1 carbide than in the pure metal for the Group IV and V carbides, but drops to less than 10% greater for the Group VI or VII carbides.[18] At 100% site occupancy, the stoichiometry of the carbide is $MC_{1.0}$, though this situation is rarely realized. The concentration and ordering, if any, of the vacancies that result from a nonstoichiometric M-C ratio have a great effect on the thermodynamic, mechanical, electronic, and magnetic properties of the metal carbides; however, the details of these effects are a matter of some debate in the literature, due to the difficulties inherent in synthesizing pure compounds and in measuring the exact details of the crystal structure of a given sample. The metal carbides share many characteristics with the metals themselves, having a plastic deformation like the *fcc* metals which, while lowering the high-temperature hardness, protects parts fabricated from the carbides from catastrophic failure in response to stresses.

Most of the Group IV-V metal carbides conform to the Hägg rules, which were developed empirically to "predict" the structures of the transition metal borides, carbides, halides, and nitrides.[22] The structure adopted by the metal carbide is determined by the ratio of the radius of the nonmetal atom (r_x) to that of the metal atom (r_m). For $r = r_x / r_m < 0.59$, the structures adopted are the

simple $A1$, $A2$, $A3$, and hexagonal lattices. For r > 0.59, more complex structures form to prevent the expansion of the lattice – which would have been required for the simple structure to accommodate the large nonmetal atom – from taking the metal atoms beyond the distance for favorable metal-metal interactions. The monocarbides take on an fcc metal lattice with carbon atoms on the octahedral interstitial sites, while random occupation of half of the O_h sites in M_2C or M_3C leads to the $L3'$ (anti-NiAs) structure, and carbon occupation of the trigonal prismatic sites in the hcp lattice formed by the tungsten atoms leads to the CdI_2 structure.[2] Non-Hägg structures are known among the carbides as well, a major example being Cr_2C_3. Specific phases available to each metal will be discussed in Section 8.4 below.

One much-noted feature of the structure of the transition metal carbides is that the lattice adopted by the metal in the carbide is never that of the parent metal. That is to say, if the metal has an hcp lattice, its carbide has the metal on an fcc lattice; the fcc parent metal occupies a non-cubic lattice in the daughter carbide; and bcc parent metals have both fcc and hcp lattices available in the daughter carbides. This has been explained using Engel-Brewer theory of metals,[23,24] in which the structure adopted by a metal or alloy depends on the s-p electron count.[18] With increasing s-p electron count the metal structure progresses from bcc to hcp to fcc across the transition series. Likewise, the Group IV and V metal carbides MC form in the $B1$ structure rather than a hexagonal form because the incompletely filled bands of the host metals can accommodate a high ratio of sp-electron-rich carbon to metal. In Group VI the stoichiometry M_2C occurs often, while Groups VII and

VIII, when they form carbides at all, take on metal-rich stoichiometries M_3C and M_4C, consistent with an attempt to avoid filling antibonding levels in the metal bands.[25]

The nature of the bonding in the monocarbides is a matter of some debate, although all agree that the simple ionic model (M^+C^- or M^-C^+) is not consistent with the properties of the carbides. Ionic materials will not typically slip on the {111} planes due to the strong repulsive (coulombic) interactions across the shear plane in the half-glide position; instead, they will slip on the {110} or {100} planes.[2] The catalytic behavior of WC is similar to that of Pt, as noted in Section 8.1.2, and this is explained according to the addition of the carbon valence electrons to those of tungsten to give a count equal to that of platinum. However, the exact direction of electron transfer is the subject of some controversy. X-ray photelectron spectroscopy (XPS) and electronegativity considerations suggest simple M → C electron donation, but the XPS data is questionable due to the possibility for backdonation or screening effects.[25] Furthermore, simple M → C donation would result in ionic compounds such as the alkali and alkaline earth metal carbides. However, these materials are resistors with low optical transparency or reflectivity, and readily hydrolyze to the metal oxide and hydrocarbon. In contrast, the transition metal carbides are conductors with a shiny metallic and colored appearance and are hydrolytically stable. Band occupation suggests C → M electron transfer. Carbon appears to combine its *sp* electrons with the metal *spd* bands, leading to the similarity between the crystal structures, reactivities, and catalytic activities of the refractory carbides and the Group VIII metals. Such a donation scheme may be used to explain,

if crudely, the trend in melting point maxima, which occurs in Group VI for the metals, Group V for the carbides, and Group IV for the analogous mononitrides: the maxima may be associated with the half-filled d shell.[25]

The Group IV-V carbides are able to form continuous solid solutions with each other over a wide range of compositions, but are only partially miscible with the carbides of the Group VI - VIII metals.[18] Ceramic materials of mixed C, N, and O composition are also common, with oxycarbides of definite stoichiometry having been reported for a number of the early transition metals. Even "pure" metal carbides tend to contain small amounts of dissolved oxygen.

8.3 Synthesis and Characterization

The distinction between "traditional" methods and "precursor" methods made in this section is admittedly somewhat arbitrary, since any starting material besides the elements themselves could be considered to be "precursors." However, the separation has been made so that simple starting materials are included with "traditional" methods, and starting materials requiring some high degree of design and synthetic effort have been designated "precursor" methods.

8.3.1 Traditional Methods[2]

The usual method of preparing polycrystalline transition metal carbides on the research scale entails the direct reaction of metal or metal hydride powders with carbon. Pure materials with a homogenous composition are difficult to achieve, however, requiring high-purity gases or good vacuum in combination with very high tempertures. The methods are summarized in Equations 8.3-8.6.

(8.3a) $M + C \rightarrow MC$

(8.3b) $MH + C \rightarrow MC + H_2$
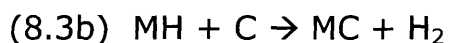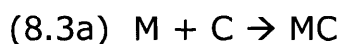
Direct reaction by melting or sintering the starting material with carbon in vacuum or inert atmosphere.

(8.4) $M_xO_y + C \rightarrow MC + CO$
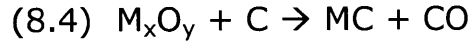
Reaction of the metal oxide and excess carbon in inert or reducing atmosphere.

(8.5a) $M + C_xH_{2x+y} \rightarrow MC + H_2$

(8.5b) $M + CO \rightarrow MC + O_2$
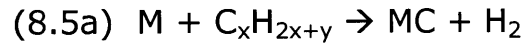
Reaction of the metal with a carburizing gas.

(8.6a) $MCl_n + C_xH_{2x+y} \rightarrow MC + HCl + (C_qH_r)$

(8.6b) $M(CO)_n + H_2 \rightarrow MC + (CO, CO_2, H_2, H_2O)$
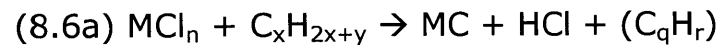
Reaction of the metal halide or carbonyl vapor with hydrogen.

The reaction temperatures for synthesis of the refractory carbides according to Equations 8.3a, b are listed in Table 8.5. However, most carbide systems must be heated for several hours at temperatures over 2000 °C to ensure compositional homogeneity. With good vacuum, such treatment also will remove oxygen contamination from many of the metal carbides. Reports regarding the range of temperatures required to form the carbides according to other reaction schemes give variable numbers.

Table 8.5: Reaction temperatures for direct formation of metal carbides[2]

Metal	Reaction	Temperature Range (°C)
Ti	8.3a, b	1700 - 2100
Zr	8.3a, b	1800 - 2200
Hf	8.3a, b	1900 - 2300
V	8.3a	1100 - 1200
Nb	8.3a	1300 - 1400
Ta	8.3a	1300 - 1500
Cr	8.3a	1400 - 1800
Mo	8.3a	1200 - 1400
W	8.3a	1400 - 1600

8.3.2 Precursor Methods

Many of the reported precursor methods for making high-temperature carbides focus on the synthesis of α- or β-SiC rather than on the carbides of the early transition metals. In addition the solid-state reaction between silica and carbon (Acheson process),[6] β-SiC has been made by pyrolysis of high-Si rice hulls (a carbothermal reduction of SiO_2 collected by the rice plant and locallized in the hulls). This process is commercially practiced. It has also been synthesized, more notably, by the pyrolysis of polymers such as poly(dimethylsilane) or poly(phenylmethylsilane).[26] These polymers are synthesized via the Würtz-type coupling of appropriate chlorosilanes, e.g. coupling in the presence of sodium or

potassium metal (M) with loss of MCl driving the polymerization. Linear polycarbosilanes produce nearly zero ceramic yield: branching on the silicon backbone is crucial. The presence of Si-H and Si-vinyl functionalities lead to the potential for hydrosilation cross-linking and a still-higher ceramic yield.

Similar work has been done to give organometallic precursors for the transition metal carbides. This work is dogged by the relatively few compounds of the Group IV - V metals which are stable, have a low C/M ratio (so that excess free carbon is avoided), and which do not contain oxygen. Those which do fulfill these criteria tend to be sublimable, leading to a low ceramic yield, since the opportunities for polymerization or cross-linking of these materials are few. Seyferth and Tracy attempted to couple dimethyltitanocene with methyldichlorosilane in the presence of sodium metal to produce a copolymer precursor for (Si, Ti)C, but little of the product was soluble in toluene and the ceramic yield was low.[3] Dichlorobis(2,4-pentanedionato)titanium(IV) was reacted similarly with methyldichlorosilane in the presence of Na, but the products were soluble only in THF and contained chlorine. Finally, dimethylmetalloocene, which decomposes in ultraviolet light to Cp_2M and 2 $\cdot CH_3$ (M=Ti, Zr, Hf), was used with the polysilane made by the Würtz coupling of $HMeSiCl_2$ to produce air-sensitive metal-containing polysilanes with ceramic yields ranging from 44% (Hf) to approximately 80% (Ti). The polymers were at least sparingly soluble in aromatic or ethereal solvents, sometimes more soluble, depending on the specific reaction conditions.

Unpublished research performed in the Seyferth labs polymerized zirconium and hafnium metallocene methacrylates for

use as precursors for ZrC and HfC. The precursors were solids or viscous polymers. Liquid precursors were obtained when substituted metallocene dichlorides were polymerized with n-butyllithium and a diyne. These gave ceramic yields near 60%, but the process suffered from the inability to scale it up.

Most other research involving organometallic precursors for the refractory carbides has centered on the small-molecule, monomeric metallocene compounds for use with various forms of chemical vapor deposition of films of these the carbide materials.

Precursors for the refractory carbides have been made from the metal alkoxides transesterified with polyhydroxyl alcohols and mixed with phenolic resins or furfuryl alcohol to provide excess carbon. In most of these cases the precursor was a solid, though some soluble precursor polymers resulted. Past work along this line will be discussed in more detail in Chapter 9.

8.3.3 Characterization

Complete characterization of the refractory carbides is difficult. Since many of the important mechanical and catalytic properties are sensitive to a number of factors which tend to vary widely among samples, there is a variation in literature reports regarding measurement of these properties. These factors include (1) the crystal structure and lattice parameters, including the presence of vacancy ordering; (2) the chemical composition, including not only the overall carbon-to-metal ratio present in the bulk sample, but the amount of free carbon *versus* combined (lattice) carbon; (3) the impurity concentration, particularly that of oxygen; (4) the overall

defect structure, including grain size, dislocations, and porosity; and (5) the sample homogeneity.

The crystal structure can be found and the lattice parameters measured by X-ray and neutron diffraction experiments. Sample homogeneity may be deduced from X-ray diffraction (XRD) data by noting the sharpness of the splitting the $K_{\alpha 1}$ and $K_{\alpha 2}$ lines, and crystalline impurity phases present in concentrations over approximately 5% may often be detected using XRD. Even large oxygen impurity concentrations, however, may escape notice due to the formation of a solid solution with the carbide. The effects of medium-to-large oxygen impurity concentrations on lattice parameters are not well-described. Very careful XRD analysis may also detect ordering of carbon atoms or vacancies in the structures of the carbides of the lighter metals, when such ordering is accompanied by a distortion of the lattice. The specific details of the ordering would not be easy to determine even using modelling techniques such as Rietveld analysis;[27] ordering without an accompanying symmetry or lattice parameter change would only be detectable using a complex Fourier analysis of the XRD peak intensities.[28] Neutron or electron diffraction experiments, on the other hand, would give unambiguous information regarding the ordering of carbon atoms on the interstitial sites, however, electron diffraction sample preparation is made difficult by the need to make a thin section of the brittle and possibly porous carbide material, and neutron diffraction is not immediately available to most researchers.

Chemical analysis of the bulk material primarily yields information about the quantity of carbon in the sample. The total

539

carbon content may be found by heating the carbide in a stream of oxygen, completely converting it to the metal oxide. The CO_2 generated is captured and measured by weight or by the conductivity of a combusted CO_2-O_2 mixture in a commercial Leco unit. This process is complicated by the high temperatures tolerated by the refractory carbides, since it relies on all of the carbon's being driven off as CO_2. Diffusion of carbon and/or oxygen through the metal carbide and/or oxide is slow even at very high temperatures. Free carbon (graphite) may be determined by dissolving the carbide in a mixture of hydrofluoric and nitric acids (warning: the dissolution reaction is violent and exothermic). The unbound carbon does not dissolve; it is collected, washed, and analyzed as CO_2.

Oxygen analysis is extremely difficult because once the solid solution M(C,O) has formed the oxygen is nearly impossible to remove. This is particularly true in the case of nonstoichiometric carbides MC_{1-x}, where empty octahedral interstitial sites are very inviting to the stray oxygen atom. Vacuum-fusion techniques, e.g. heating the refractory carbide to 2400-2800 °C in a graphite mold or platinum bath under vacuum, followed by determination of the oxygen removed as CO_x, are the major methods available, but are often only partially successful. This is particularly true of the carbides of the Group IV metals. Neutron activation analysis, in which oxygen is activated by the reaction $^{16}O(n,p)^{16}N$, then monitoring the 6.1 and 7.1 MeV γ-radiation from ^{16}N, has proven useful.

Sample homogeneity and local compositions may be measured by microprobe analysis, in which the X-ray emission of elements on

irradiation with an electron beam, as in an electron microscope, is measured and correlated with the concentration of the element. The microprobe must be equipped with a thin detector window to give good quantitative information regarding light elements ($Z< 10$), however. Electron energy loss spectroscopy (EELS), on the other hand, can sensitively detect elements in the $Z < 10$ region.[29] Both of these methods are extremely locallized, however, and multiple areas of several samples must be examined for conclusions regarding the bulk material to be validly made.

Vacancy concentration is likewise difficult to measure due to the ambiguities in chemical composition measurements. Where the composition is well-known, comparison of X-ray density with a physically-measured density will give a good estimate of the vacancy concentration. Likewise, density measurements can give information regarding larger-scale defects such as porosity. Electron microscopy can give reasonable estimates of the grain size.

8.4 Tour of the Group IV - V Carbides

The material in Section 8.4 is primarily based on E.K. Storms' *The Refractory Carbides*.[1]

8.4.1 General Trends

Approximate preparation of the transition metal carbides is straightforward, but ensuring a given stoichiometry and purity against oxygen contamination is famously difficult. Variations in the quantity of vacancies on the carbon (or, less frequently, the metal) lattice, as well as variations in the amount of dissolved oxygen, lead to a wide range of claims regarding even basic thermodyanmic, mechanical, and electromagnetic data for the early transition metal carbides. Removal of the oxycarbide phases, which can be considered to be solid solutions of MO and MC, depends on the partial pressure of CO over the sample to be purified. At the high-carbon end of the stoichiometric range, Equation 8.7 leads to additional dissolved oxygen in the lattice if CO is removed. At the low-carbon end, Equation 8.8 occurs independently of the CO partial pressure. Thus if excess graphite is present, a high CO partial pressure leads to more nearly stoichiometric carbide as Equation 8.7 is forced left; but the success of this approach in purifying a given metal carbide depends on the stability of the oxycarbide, the annealing temperature and time, and, clearly, the partial pressure of carbon monoxide.

(8.7) $M_xO_y + C$ (dissolved in MC) = MO (dissolved in MC) + $CO_{(g)}$

(8.8) $M_xO_y + M$ (dissolved in MC) = MO (dissolved in MC)
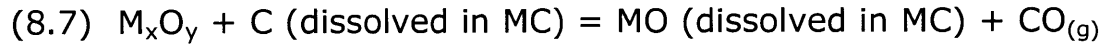
Group IV carbides are difficult to purify without melting; heating up to 2000 °C will result in increased oxygen contamination if the vacuum is not better than 10^{-6} torr. Moreover, as noted in the previous section, few straightforward chemical methods exist for finding the oxygen level in the Group IV carbides MC_{1-x} bulk materials; none are reliable. The Group V and VI carbides purify readily at temperatures over 1800 °C.

Slow diffusion of carbon in all of the refractory carbides results in stoichiometry gradients which are difficult to detect in bulk materials but which may compromise the material strength, hardness, and high-temperature behavior. The lattice parameter and the sharpness of the XRD pattern can give some rough indication of the homogeneity, however.

Group IV metals tend to form in a single cubic phase with a limiting stoichiometry near $MC_{1.0}$, but which normally varies from $MC_{0.5}$ to $MC_{0.97}$ depending on the synthesis conditions. Group V metals form an M_2C phase in addition to the monocarbide. The composition range of the M_2C phase is narrow at room temperature, with decomposition into the cubic phase plus liquid at high temperatures. The V-C system has a cubic phase extending to $MC_{0.88}$, while NbC and TaC approach $MC_{1.0}$ and melt congruently even at carbon-deficient stoichiometries. The Group VI metals have a more complex M-C phase diagram, forming a number of distinct compositions. The chromium carbides behave uniquely, while the Mo-C and W-C systems have common features, with the MC and

M_2C phases stable at high temperatures. (Table 8.4) The trends in melting points indicate that the Group IV, V, and lower two Group VI metals have strong M-C and M-M bonds, distinct from the Groups IA - IIIB metals, which form acetylenic M-C bonds, and from the Groups VIII - IIB metals, which form unstable carbides, if at all.

Removal of bound carbon causes the lattice parameter to decrease in most of the refractory carbides, but to increase in TiC and ZrC. The behavior of HfC on decrease of the lattice carbon-to-metal ratio is uncertain due to the variation in this behavior among reports. For several metal carbides, the variation of lattice parameter with carbon content is linear. Removal of carbon from the lattice also is associated with reductions in hardness, at least for the Group IV carbides. Dissolved oxygen lowers the lattice parameter in Group IV carbides, while it increases it in Group V carbides, and has an uncertain effect for carbides of Group VI metals. The effect of oxygen contamination on mechanical properties is not clearly reported in the literature.

The refractory carbides show high chemical resistance but will react under certain conditions. At high temperatures, the high-carbon compositions form hydrocarbons in the presence of hydrogen. The reactions with oxygen have been indicated above (Equations 8.7, 8.8), and are complex. The carbides will form the nitrides at high temperatures and in the presence of N_2, NH_3, or N_2/H_2 mixtures; however, the cubic carbides and nitrides are completely miscible.

8.4.2 Group IV

The conversion of TiO_2 to TiC occurs via the intermediates Ti_3O_5, Ti_2O_3, and TiO in the temperature range 1000 - 1500 °C. The carbide closest to $TiC_{1.0}$ forms at 1600-1700 °C under 1-10 torr of CO. Titanium hydride and carbon form $TiC_{1.0-x}$ after 1 hour in vacuum at 1200 °C. TiC has also been formed by heating a tungsten wire or carbon filament in an atmosphere of $TiCl_4$, H_2, and hydrocarbon, or by reaction of CaC_2, $TiCl_4$, and H_2 at 800 °C (CaC_2 and $CaCl_2$ are removed by washing with water after the reaction is complete). The last traces of oxygen are difficult to remove, and have a significant effect on the material properties. Later heating may recontaminate even a "pure" sample of titanium carbide if the vacuum is not sufficiently good; a nonprotecting, non-adherent TiO_2 (anatase) layer forms at about 450 °C. The Ti-C system has one cubic compound of formula TiC, although other phases have occasionally been claimed. TiC is metallic and grey, and is stable to most concentrated acids or bases. It will dissolve completely in HNO_3 and combinations of HNO_3 with HCl (aqua regia), HF, and H_2SO_4.

The reduction of ZrO_2 proceeds via Zr_2O_3 and ZrO to the carbide between 950-1200 °C. It has also been formed using ZrH plus graphite or from $ZrCl_4$ in the presence of hydrogen and hydrocarbon vapor. Attempts to remove oxygen completely are generally unsuccessful except under melting conditions. "Pure" ZrC heated at temperatures under 1800 °C tends to gather oxygen up to several percent. The Zr-C system contains one cubic compound, ZrC, and the lattice parameter varies with oxygen contamination

noticibly at levels of 1000 ppm. ZrC is somewhat more susceptible to acid attack than is TiC and oxidizes rapidly above 500 °C.

HfO_2 forms an oxycarbide of constant composition between 1743 - 2033 °C and under 70-1000 torr of CO, with Hf_2O_3 forming at 1000-1200 °C and the HfC-HfO solid solution between 1300-1800 °C. HfC forms a carbon-deficient lattice between 1800 - 2000 °C, but can be made stoichiometric by repeated heating at 1900 °C. HfC has also been formed from $HfCl_4$ + H_2 + CH_4 in the presence of a hot tungsten wire and from hafnium hydride and carbon. It is one the most difficult carbides to rid of its oxygen, only becoming "pure" when melted or heated at temperatures in excess of 2500 °C in good vacuum. The Hf-C system has one cubic phase HfC, but the composition can range to a low of $HfC_{0.52}$. Its melting point increases with increasing carbon content up to a maximum, then HfC forms a eutectic with carbon. There has been no study of lattice parameter variation with either oxygen or carbon content.

8.4.3 Group V

Vanadium carbide has been formed by heating V_2O_5 or V_2O_3 with carbon for two hours at 1800 °C in 1-10 torr of CO. V_2O_5 begins reacting with carbon at 435 °C, and the oxygen concentration is relatively easily reduced to below detectable limits by higher-temperature treatments or by the reaction of vanadium metal or hydride with carbon. Loss of vanadium at high temperatures and low carbon content presents a difficulty, but nearly-saturated VC can be heated to 2000 °C without loss of vanadium. The carbide has been made by treatment of VCl_4 in an

atmosphere of hydrogen and methane at 1500 - 2000 °C. The two main phases are cubic VC, available over the range $VC_{0.78}$-$VC_{1.0}$, and the hexagonal β-V_2C, available for C/V atom ratios of 0.4-0.5 between approximately 1500 - 2000 °C, but presenting a very narrow range of stable compositions at room temperature. Reports of V_5C and V_4C_3 have been discredited. VC will react with dry HCl gas at 750 °C to produce VCl_2, methane, and hydrogen, and has a high rate of oxidation in air, with powdered VC and V_2C being attacked slowly by air even at room temperature. V_2C is soluble in hot 50% HCl solution, leaving a carbon residue, but VC is inert under these conditions; both of the vanadium carbides are attacked by concentrated nitric, sulfuric, and perchloric acids.

Niobium (V) oxide begins to react with carbon at 675 °C, forming NbO_2 and NbC_x below 1200 °C and forming an NbC_xO_y solid solution between 1450 and 1500 °C. Pure NbC is accessible by heating the metal and carbon powders directly, but high temperatures and heating times are required to complete the reaction and drive off oxygen and nitrogen contaminants. The conditions are made less stringent by the presence of an H_2 atmosphere. $NbCl_5$ heated in the presence of hydrogen and methane forms the pure carbide at 900 -1000 °C. The Nb-C system has the cubic phase NbC and two crystal forms (α, room temperature, with a very narrow composition range and β, existing between 2300-3000 °C and over the C/Nb ratio range 0.4-0.5) of Nb_2C. A third, ζ phase of Nb_2C (C/Nb range 0.5-0.7) has been suggested to exist on the basis of a single weak powder pattern line, but has not been verified. The lattice parameter increases as the C/Nb atom ratio approaches unity, and is increased as well by

the presence of oxygen and nitrogen. NbC is inert even to boiling aqua regia but will dissolve in HNO_3/HF mixtures; it is severely corroded in air at temperatures above 1100 °C. Its color ranges from grey ($NbC_{0.9}$) to lavender ($NbC_{0.99}$).

The tantalum carbide system is relatively easy to free of oxygen impurities, but due to the slow rate of carbon diffusion it tends to have inhomogeneities in its bulk composition. Evaporation of carbon at temperatures above 2400 °C renders the use of high temperatures to establish a uniform composition problematic. Reaction from the elements in vacuum begins at approximately 1000 °C but is slow to reach completion. Use of hydrogen or methane atmospheres increases the reaction rate but requires a post-synthesis vacuum annealling step to remove dissolved hydrogen. TaC cannot be made from $TaCl_5$ in a hydrocarbon/hydrogen atmosphere due to the formation of metallic tantalum, but has been made with varying success by heating Ta wire in methane. Arc-melting tends to produce C-deficient, inhomogenous carbides. The Ta-C system has the cubic phase TaC and a hexagonal compound Ta_2C (actually the $C6$ anti-CdI_2 structure type due to ordering of the carbon atoms) with an α–β transition near 2000 °C. A ζ phase has been claimed at 2000 - 3000 °C over the C/Ta atom ratio 0.70-0.75 but its existence remains a point of debate. The cubic phase persists over a wide temperature and composition range, possibly as low as $TaC_{0.58}$ and verified down to at least $TaC_{0.74}$. The composition $TaC_{0.89}$ is the highest-melting substance known. Very small amounts of carbon ($Ta_{64}C$) result in a tetragonal distortion to the normally *bcc* Ta parent lattice. The TaC lattice varies linearly with composition, with the equation C/Ta = -25.641 + 5.9757*a*. It is

grey and metallic in appearance up to about $TaC_{0.85}$, then becomes increasingly brown with rising carbon content until the golden $TaC_{0.99}$ is reached. It is the most acid-stable of the refractory carbides, dissolving in a nitric/hydrofluoric acid mix, and reacts with pure oxygen above 800 °C. Loss of carbon results from lower-temperature reactions with oxygen in air.

Table 8.4: Range of Melting Points for Group IV-VI Carbides[1]

Metal	Element MP (°C)	Maximum MP (°C)	MP in the presence of C (°C)	Atom Ratio at Max MP
Ti	1668	3067	2776	0.8
Zr	1855	3420	2850	0.83
Hf	2222	3950	3180	0.95
V	1888	2700	2700	0.85
Nb	2467	3600	3300	0.82
Ta	3014	4000	3400	0.88
Cr	1915	1875	1875	0.68
Mo	2620	>=2580	2580	0.72
W	3410	>=2780	2780	0.75

8.5 Goals of the Part II Project

The specific goals of Part II of this thesis were the synthesis of a industrially-useful liquid precursor for tantalum and hafnium carbides, TaC and HfC. As indicated in Section 8.3.2 above, most precursor methods have resulted in solid or at best soluble polymeric materials. Liquid precursors were preferred in this project so that removal of solvent during fabrication of HfC or TaC monoliths could be avoided. The liquid precursors were to be used in conjunction with proprietary technology owned by Foster-Miller, Inc., of Waltham, Massachusetts, to fabricate high-performance parts of solid TaC or HfC. Factors of concern included (1) ease of synthesis, particularly of scale-up; (2) ease of handling (e.g. room-temperature stability, reasonable air-stability); (3) clean decomposition to the target carbide without undue contamination by metal oxide or by excess graphitic carbon; (4) low volatility – e.g. the material should decompose *in situ* during pyrolysis, rather than distill; (5) low gas production on decomposition, so that bubbles in the solid would not become points of structural weakness; (6) low viscosity over a temperature range near or just above room temperature (e.g. the precursor was to be a liquid or low-melting solid). Cost was an addtional concern but was left to be addressed in later phases of the project.

Early work on the project focused on the use of organometalic precursors for TaC and for HfC. The main idea behind this approach was that the precursor was best formed by putting the M-C bonds

in place during the synthesis, eliminating any need to remove heteroatom bonds (particularly oxygen) from the metal center via carbothermal reduction during the pyrolysis step. Large, waxy groups or smaller, symmetry-destroying groups, would enforce the liquid form of the precursor. Efforts first focused on using $CpTaCl_4$ or Cp_2TaCl_2 as starting materials, and using organolithium or Grignard reagents to add alkyne groups based on 1-hexyne, trimethylsilylacetylene, and triethylsilylacetylene by a salt metathesis; however, the products consistently decomposed, possibly due to reduction of the tantalum by the organolithium or - magnesium reagent. A similar approach using hafnocene and substituted hafnocenes (e.g. bis(methylcyclopentadienyl)hafnium dichloride, bis(vinyldimethylsilylcyclopentadienyl) hafnium dichloride) gave liquid precursors which pyrolyzed to HfC, and which were obtained in pure form. Stirring pentakis(dimethylamido)tantalum with alkynes, with loss of $\geq$ 2 dimethylamine groups, gave liquid precursors which pyrolyzed to TaC but which defied purification and characterization attempts. Thus this work showed some success, but was dogged by the sensitivity of the organometallic compounds made. The organometallic approach has not been discussed in detail in this Thesis.

Practical concerns of scalability were a major factor in the abandonment of this approach in favor of a sol-gel-type route in which the alkoxide in alcohol solution would be hydrolyzed to form the precursor, which would be reduced carbothermally during pyrolysis. This route was superior in ease of synthesis, scale-up, handling, and cost, but was found to give a too-low mass-of-carbide-per-gram-of-precursor. It also formed a glassy, bubble-

ridden solid which was high in excess carbon. The work is discussed in Chapter 9, and has been continued by researchers at Foster-Miller, Inc.

It should be noted by the reader that the work described in Chapter 9 involved a practical challenge to the academic chemist. Traditional methods of purifying chemical materials for characterization include primarily crystallization and distillation or sublimation. However, the materials synthesized in these chapters were designed *not* to crystallize, and were expected to decompose on heating rather than to distill. Therefore, purification for the sake of getting NMR, MS, or elemental analytic evidence of the structure claimed was rarely possible. Production of a formulation with reproducible properties and pyrolysis behavior was given priority over isolation and characterization of an exact precursor molecule.

8.6 References

1) Storms, E. K. *The Refractory Carbides*; Academic Press: New York, 1967.

2) Toth, L. E. *Transition Metal Carbides and Nitrides*; Academic Press: New York, 1971.

3) Tracy, H. J., Ph.D. Thesis, Massachusetts Institute of Technology: Cambridge, MA, 1990.

4) Koester, R. D.; Moak, D. P. *J. Am. Ceram. Soc.* **1967**, *50*, 290.

5) Andrievskii, R. A.; Strel'nikova, N. S.; Poltoratskii, N. I.; Kharkardin, E. D.; Smirnov, V. S. *Porosh. Met.* **1967**, *7*, 85.

6) Mark, H. F.; Othmer, D. F.; Overberger, C. G.; Seaborg, G. T. *Kirk-Othmer Encyclopedia of Chemical Technology*; 3rd ed.; John Wiley & Sons: New York, 1978; Vol. 4, pp 480, 492, 497.

7) Muller, J. M.; Gault, F. G. *Bull. Soc. Chim. Fr.* **1970**, *2*, 416.

8) Boudart, M.; Levy, R. *Science* **1973**, *181*, 547.

9) Leclerq, L.; Imura, K.; Yoshida, S.; Barbee, T.; Boudart, M. ; in *Preparation of Catalysts III*, Delman, B. *et al.*, Eds.; Elsevier: Amsterdam, 1978, pp 627.

10) Il'chenko, N. I. *Kinet. Katal.* **1977**, *18*, 153.

11) Il'chenko, N. I.; Chevotareva, N. P.; Shvidak, N. V. *React. Kinet. Catal. Lett.* **1976**, *4*, 343.

12) Ptak, L. D.; Boudart, M. *J. Catal.* **1970**, *16*, 90.

13) Lee, J. S.; Oyama, S. T.; Boudart, M. *J. Catal.* **1987**, *106*, 125.

14) Ledoux, M. J.; Huu, C. P.; Guille, J.; Dunlop, H. *J. Catal.* **1992**, *134*, 383.

15) Suslick, K. S.; Hyeon, T.; Fang, M.M.; Cichowlas, A.A. *Mat. Sci. Eng. A.* **1995**, *204,* 186.

16) Lee, J. S.; Yeom, M. H.; Park, K. Y.; Nam, I.-S.; Chung, J. S.; Kim, T. G.; Moon, S. H. *J. Catal.* **1991**, *128*, 126.

17) Brenner, A.; Burwell Jr., R. L. *J. Am. Chem. Soc.* **1975**, *97*, 2566.

18) Oyama, S. T. *Catal. Today* **1992**, *15*, 179.

19) Vidik, B.; Lemaitre, J.; Leclercq, L. *J. Catal.* **1986**, *99*, 439.

20) Kojima, I.; Miyazaki, E.; Inoue, Y.; Yasumori, I. *J. Catal.* **1982**, *73*, 128.

21) Ledoux, M.-J.; Guille, J.-L.; Pham-Huu, C.; Maria, S., Pechiney Recherche: U.S. Patent No. 5,139,987, 1992.

22) Hagg, G. *Z. Phys. Chem, Abt..* **1931**, *B12*, 33.

23) Engel, N. *Ingenioren* **1939**, *N101*.

24) Brewer, L. *Science* **1968**, *161*, 115.

25) Oyama, S. T. *J. Solid State Chem.* **1992**, *96*, 442.

26) Schilling Jr., C. L. *Brit. Polymer J.* **1986**, *18*, 355.

27) Young, R. A. *The Rietveld Method*; Oxford University Press: New York, 1993.

28) Klug, H.; Alexander, L. *X-ray Diffraction Procedures*; 2 ed.; John Wiley & Sons: New York, 1974.

29) Cheetham, A. K.; Day, P. *Solid State Chemistry: Techniques*; Oxford University Press: New York, 1987.

Chapter Nine

Sol–Gel Approaches To TaC and HfC

9.1 General Comments

9.1.1 Previous Work

In addition to looking at organometallic tantalum and hafnium compounds as precursors for TaC and HfC, a second route was developed for synthesizing liquid precursors for tantalum and hafnium carbides. Reduction of metal oxides to the carbides, known as carbothermal reduction, takes place at elevated temperatures under inert atmosphere or good vacuum for all of the transition metals. This route to particulate formulations of metal carbides has been used traditionally, either as a single-step process, in which high-surface area metal oxides are mixed with finely-divided carbon black, then heated, or as a two step process, where the metal oxides are first reduced to the metals with hydrogen, then are heated together with carbon.[1,2] Firing temperatures required are in excess of 1500 °C, and particles with high surface area cannot be made by this method due to sintering during the high-temperature treatment. In addition, monolithic ceramic pieces cannot be produced directly; they must be hot-pressed or otherwise fabricated from the pre-synthesized powder. Fibers are also inaccessible by this route. A number of alternatives to the traditional powder method have appeared in the literature and/or in industrial use. In particular, polymer precursors for silicon carbide have been a popular area of research.[3-5]

One alternate route to transition metal carbide materials is the carbothermal reduction of oxygen-containing polymeric transition metal compounds. Such precursors can be made in reactions of the sol-gel type. This section reviews briefly the U.S. patents and articles in the open literature regarding polymeric precursors for refractory ceramics. It is not intended to be a complete review.

Birchall et al. in 1989 received a patent for a process for making refractory borides and silicides by reacting together the metal alkoxide (or halide) with silicon or boron alkoxides and glycerol or another polyalcohol.[6] Polymerization of the mixture, leading to a solid powder, occurs on the removal by distillation of the alkoxide groups, and their replacement with the polyalcohol. The reaction could be seen as a process in which the metal oxide reacts with the boron or silicon oxide and with excess carbon present due to the "coking" reduction of the organics present in the alcoholic groups. Because of the atomic-scale mixing that occurs in the solution of liquid precursors, the purity is high and the reaction temperatures and times are lower than would be necessary for mechanically-mixed samples of the same metal and nonmetal oxides. Follow-up patents were issued to Birchall and his co-workers, which reveal processes for the production of refractory carbides and nitrides. One uses trace quantities of aluminum chloride to increase the proportion of carbon retained in the coked product.[7] Others use furfuryl alcohol, in addition to the glycerol or other polyalcohol, to provide excess carbon to bring about the carbothermal reduction.[8-10] Dispersant (polyhydroxystearic acid derivatives of polymethyl methacrylate) is used in another case to

provide for small precipitate particles.[11] Several produce polymeric (gel) products which are soluble in water, acetone, ethanol,[7] 1,1,1-trichloroethylene, N-methylpyrollidone,[8] and other solvents, while others specify the insolubility of the polymeric precursor.[11] Other researchers also patent processes involving the reaction of metal or nonmetal alkoxides or chlorides with furfuryl alcohol in an inert solvent, leading to fine powder precursors which may be pyrolyzed to carbides (or nitrides, in nitrogen or ammonia atmospheres).[12] Thus the production of SiC, AlC, and transition metal carbides, as well as the analogous borides, nitrides, and silicides, are accomplished by the mixture of compounds of the metal or nonmetal which are reactive with hydroxyl groups (halides, alkoxides), with polyhydroxyl compounds (glycerol, ethylene glycol), in the presence of materials (furfuryl alcohol, aluminum) which provide for the retention of sufficient carbon in the "coked" (pyrolyzed) product to effect the carbothermal reduction of the M-O bonds.

Rhine and Jiang used furfuryl alcohol in direct reaction with titanium n-butoxide in tetrahydrofuran, with hydrolysis, to produce soluble solid or liquid precursors for TiC.[13,14] Use of acid catalyst increased the carbon retention during removal of the solvent and during pyrolysis by catalyzing the polymerization of furfuryl alcohol; however, this approach gave less soluble solid precursors. For making SiC, Rhine and Jiang compared furfuryl alcohol, polyphenylpropylsilsesquioxane, and polyphenylvinylsilsesquioxane as sources of carbon, and found very different morphologies of the pyrolyzed products, with more excess carbon and less homogeneity of the SiC/C composite resulting from pyrolysis.[15]

Other solution-derived precursors for transition metal carbides include the use of soluble molybdenum or tungsten compounds (peroxo acids or ethylene glycolates) with carbonaceous gel or saccharose as carbon sources;[16] these sources of carbon are also used with niobium or tantalum alkoxides.[17] Cellulose triacetate and titanium or zirconium alkoxide undergo a transesterification reaction to form a gel, which pyrolyzed leads to the metal carbide.[18] Preiss *et al.* reported a study of the polymeric precursors for TaC, NbC, and Mo_2C in which reaction between the alkoxide, acetylacetone, and a polyalcohol "bridging group" was studied. They found that tantalum n-butoxide reacted with ethylene glycol, saccharose, tartaric acid, catechol, and resorcinol gave a soluble and fiber-spinnable precursor that on pyrolysis gave little excess carbon (weight% carbon ranged from 5.2-7.1%).[19] TiC/C composite fibers were produced by reaction of titanium isopropoxide with phenolic resin fibers.[20] Transesterification of titanium isopropoxide with o-xylene-α-α'-diacetate led to a polymeric TiC precursor which was soluble and fiber-spinnable, and formed TiC at 800 °C. Other bifunctional acetates $(H_3CCOO)_2R$ (R= $(CH_2)_3$, $(CH_2)_4$, m,p,o-xylenes) were tested and found to give either insoluble products or precursors which failed to form TiC, or which required high temperatures (1600 °C) to do so.[2,21] Fibers and films were accessible using any of these precursor methods.

In this Chapter we report the formulation of liquid and gelatinous precursors for TaC, HfC, ZrC, TiC, and NbC, using the metal alkoxides in combination with hydrolysis-rate modifying 2-methoxyethanol, furfuryl alcohol to provide a high carbon retention

on pyrolysis, as well as the potential for polymerization during heat treatment. Unlike the work reported in the patent literature to date, the hydrolytic removal of alkoxide groups is performed in order to provide for a M-O-M network.

9.1.2 Background

The chemistry of the transition metal alkoxides has already been discussed extensively in Part I of this thesis, and the reader is referred to the relevant Chapters there. The properties of metal alkoxides taken advantage of in this chapter are their facile exchange of ligands – e.g. the original ethoxide, propoxide, butoxide, etc. for a furfuryl alcohol group – and their hydrolyzability. In all cases we attempted to produce either a liquid state precursor directly by substitution of the original ligands on the metal alkoxide for larger ones that would block crystallization and oligomerization, or by production of a sol of the hydrolyzed metal alkoxide. Furfuryl alcohol was the substitute alkoxide ligand chosen due to its polymerization reaction and its high conversion to carbon during pyrolysis.

Furfuryl alcohol[22] (Figure 9.1a) is derived from the basic furan ring, and is obtained by reduction of furfural (2-furancarboxylaldehyde), which in turn may be synthesized from vegetable resources such as rice hulls, corncobs, and wood. Most of the furan derivatives, including furfuryl alcohol, cross-link on heating, particularly in the presence of an acid catalyst. They therefore fall under the rubric of the "thermosetting resins." Furfural gives a black cross-linked product on heating at 100 - 250 °C in inert atmosphere, and on treatment with Lewis or Bronsted acids in the absence of water. Furfuryl alcohol polymerizes in the presence of air or acid catalyst by condensation of the methylol group with the C-5 hydrogen atom, leading to linear chains. (Figure

9.1b) Condensation between methylene groups in a chain and the methylol group of a furfuryl alcohol molecule lead to cross-linking. When the crosslinking is carried out at pH 3-5, quick cooling followed by neutralization of the acid will stop the condensation reactions at the desired viscoscity.[23] When heated at temperatures up to 320 °C, the resin cross-links further, but over 380 °C it tends to release hydrogen and produce paramagnetic centers. Pyrolysis above 450 °C gives high yields of glassy and porous carbon. The intense red-brown to black coloring of the resin comes about when the "homoconjugated" system of methylene-linked furan rings broadens the range of UV absorbtion and shifts it toward lower frequencies.[23]

Another furfural derivative, 2,5-bis(hydroxymethyl)furan, made from reaction of furfuryl alcohol with formaldehyde, was considered for use in these experiments. It polymerizes and cross-links at lower temperatures than does the monoalcohol.

Jiang and Rhine found that furfuryl alcohol substitutes for one of the butoxide groups in titanium tetra(n-butoxide),[13] and that the Ti-OFu bond was more resistant to hydrolysis than the Ti-OnBu bond. This can be expected to be the case also with the tantalum and hafnium alkoxides. Despite this hydrolysis resistance, they found that FuOH was lost from the system when the hydrolyzed alkoxide/furfuryl alcohol mixture was distilled; a catalytic quantity of sulfuric acid was added to assist in the retention of the FuOH through its polymerization. However, addition of the acid decreased the solubility of the precursor. The precursor, when acid-free water was used, was a soluble solid or viscous liquid, depending on the quantity of water used. XRD showed that their TiC was phase-pure

after 12 h heating in argon at 1150 °C or more; lower temperature treatments led to TiO_2 and an unidentified oxycarbide phase. However, elemental analysis suggested that temperatures of 1300 °C were required to effect complete conversion. Most of their products analyzed to be high in carbon, however. They calculated that each furfuryl alcohol molecule gave a carbon yield of approximately 45%, so that for the Equation 9.1 to go completely, a metal-to-furfuryl alcohol ratio of 0.8 would be required. For Equation 9.2, the same ratio would need to be nearly 1.9.

(9.1) $MO_2 + 3 C + x C \rightarrow MC + 2 CO + x C$

(9.2) $M_2O_5 + 7 C + x C \rightarrow MC + 5 CO + x C$
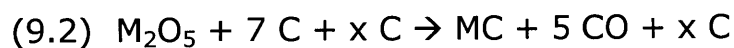
x C = moles of excess carbon

While Jiang and Rhine used a low heating rate of 3 °C/min. for pyrolysis, since slow heating rates lead to maximum carbon yield, other work has found that precursor polymers similar to those used by Jiang and Rhine, and by us, had a post-pyrolysis carbon content which was independent of the heating rate used.[10] In all of our experiments, it should be noted, we used a high heating rate due to the expectation that we would have plenty of excess carbon. Stanley et al. noted that the quantity of carbon yield in the coked (heated to approximately 450 °C) precursor was obtained from the amount of aliphatic *versus* unsaturated organic groups in the polymer, but that there seemed to be a secondary effect of the identity of the metal.[10] This effect also has been reported regarding burnout of polymer binders from ceramic greenbodies: addition of metal oxide powders to the greenbodies decreases the

amount of carbonaceous residue in the pyrolyzed product. It was found that highly acidic or basic metal oxide powders were associated with a higher carbon residue because they lead to dehydration and formation of additional unsaturation in the organic polymer. The trend for the Group IV metals is Ti< Zr < Hf in increasing carbon residue expected.

We investigated briefly the behavior of furfuryl alcohol and an acid catalyst in the absence of the metal alkoxide (Experiment 23) As the temperature increased, the viscoscity increased, particularly over 100 °C. By 115 °C the mixture had become a brown-black gum and by 120-125 °C it had become a brittle brown-black solid. It pyrolyzed with a 44% weight retention to X-ray amorphous material, presumably carbon. This behavior is also what was observed for precursor mixtures containing furfuryl alcohol and metal alkoxide.

Figure 9.1 (a) furfuryl alcohol and (b) poly(furfuryl alcohol), non-crosslinked.

(a)

(b)
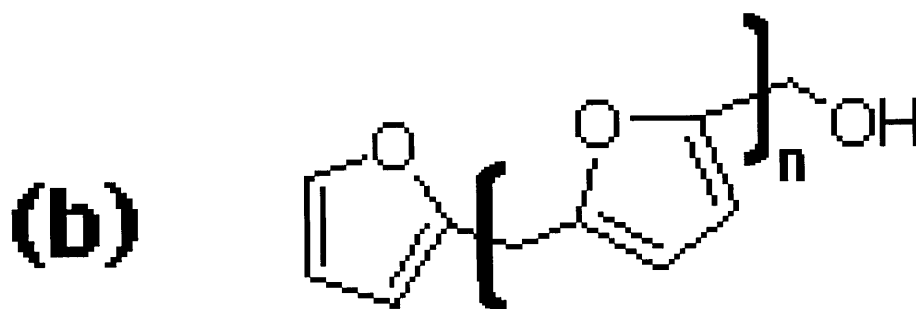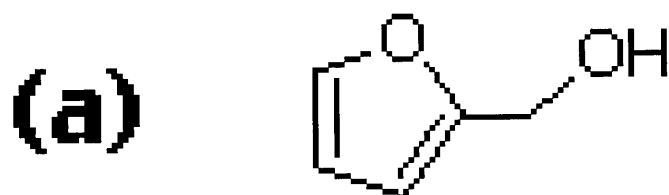
9.2 Results and Discussion

9.2.1 Tantalum Carbide Precursors

Initial attempts at using a tantalum alkoxide as a liquid precursor for tantalum carbide centered on the TiC precursor prepared by this method and reported in the literature by Jiang and Rhine.[13] These preparations (Experiments 1-3) were based on refluxing tantalum ethoxide with furfuryl alcohol in tetrahydrofuran, followed by hydrolysis with water equivalent to one mole of tantalum ethoxide. In the initial experiment, gelatinous solids appeared immediately on hydrolysis; these pyrolyzed to a combination of tantalum carbide and oxide, with a 50% weight retention. Later experiments of this series added 2-methoxyethanol (2MOE) as a hydrolysis rate modifier and increased the furfuryl alcohol-to-alkoxide ratio. In these trials, the addition of less than two equivalents of water provided a precursor that remained liquid until heating to 120 °C, at which point it gelled; four equivalents of water added, however, led to an immediate gellation. Both samples, however, pyrolyzed to TaC.

Because it was undesirable for the precursor to be diluted by the inert solvent THF, due to the requirements of the application, the remaining experiments omitted this solvent. Use of seven equivalents each of 2MOE and FuOH, plus 1.2 equivalents of water, led to a liquid precursor that gelled on extended heating at 90 °C, after removal of some solvent in vacuo. (Experiment 4) It produced TaC (30% weight retention) on pyrolysis. A smaller FuOH- and 2MOE-to-alkoxide ratio (five and three, respectively), combined with

567

hydrolysis with 1.2 equivalents of a 1M sulfuric acid solution, also gave a solution which was concentrated under vacuum and heating to an orange-brown viscous liquid. This gave a 56% weight retention on pyrolysis to phase-pure TaC. (Experiment 5) Mixing tantalum ethoxide with furfuryl alcohol directly, with distillation of liquid between 80-83 °C (presumably be ethanol) and no hydrolysis, gave an increasingly concentrated liquid which suddenly became a black solid at 140 °C heating temperature. (Several previous attempts at this experiment led to a rapid reaction that blew apart the apparatus and left a glassy black solid.) This solid pyrolyzed to TaC under several heating conditions with a 55-65% weight retention. (Experiment 6, see Table 9.1) The FuOH-to-Ta(OEt)$_5$ ratio was further reduced in Experiment 7 to 2.5, the ratio of 2MOE to tantalum ethoxide increased to 5, and the amount of hydrolysis water (acid solution) increased slightly, still leading to a liquid precursor. On heating to 130 °C, however, with loss of solvent permitted, the precursor became a rubbery gel. The gel was insoluble in a range of solvents. It was pyrolyzed by researchers at Foster-Miller, Inc. to TaC at 1600 °C in 2 h, but weight retention was not reported by them.

In all cases the pyrolyzed materials were assumed to contain excess carbon, and this problem was addressed in Experiment 8, which looked at the effect of varying amounts of FuOH on the hydrolysis and pyrolysis behavior of the precursor solutions. In these experiments the 2MOE was left out, and THF used as a solvent. It was found that ratios of FuOH-to-tantalum ethoxide of less than 2 gave solid precipitates which persisted when the ratio became less than 1.5. Solvent THF and in some cases ethanol were

distilled from the samples, and they gelled as heating continued. For higher FuOH:Ta(OEt)$_5$ ratios the "cured" gel was darker and more brittle; those containing little FuOH were light-colored and resinous. Samples having an FuOH:Ta(OEt)$_5$ ratio of at least 1.5 pyrolyzed to TaC, while those containing less FuOH gave an oxide and carbide mixed-phase product.

Obtaining a liquid precursor for TaC was, therefore, reasonably straightforward. Tantalum ethoxide, a liquid, was used neat with two mole equivalents of furfuryl alcohol and in most cases up to five equivalents of 2-methoxyethanol. Up to 1.2 equivalents of 1 M aqueous sulfuric acid as a solution in 2MOE or THF, provided slowly to the stirred alkoxide solution, could be used to hydrolyze the alkoxide and provide for polymerization of the FuOH present. It was not clear from the experiments performed, however, whether the acid was actually necessary for obtaining a good yield of metal carbide; it may merely have served to increase the amount of free carbon in the samples. Due to the difficulties involved with getting reliable elemental analyses on the refractory carbides, few of these experiments had their pyrolyzed products analyzed for carbon. For those that did (see Table 9.4) the carbon analysis was approximately 20 wt% (6.2 wt% expected for TaC) for the hydrolyzed samples (pyrolysis time 57 h at 1400 °C) and 40% for the unhydrolyzed one (pyrolysis time 12 h at 1400 °C). Extended heating can be expected to remove the excess carbon, but it is preferable to avoid such a step.

The key to the behavior of the precusor is the replacement of one or more ethoxide groups on the tantalum center with furfuryl alkoxide groups. The latter ligands hydrolyze more slowly than

ethoxide ligands, and therefore modulate the hydrolysis behavior. The retention of unsaturated groups on the tantalum center ensures that material for carbothermal reduction of the Ta-O bonds will be nearby during pyrolysis. A distillation step was introduced into the final formulation of the tantalum carbide precursor (Experiment 9) to help this substitution take place, by providing for the removal of substituted ethanol from the system. The hydrolyzed precusor that results from this formulation remains a liquid until over 100 °C, continued heating and loss of solvent permits the gelation of the hydrolyzed alkoxide and the polymerization of the furfuryl alcohol. The reactions that take place at that temperature are rapid and may take place with release of gas (see Experiment 6A). Pyrolysis at a ramp rate of 25 °C/min. to 1400, with a 2-hour soak at this temperature, led to phase-pure TaC in at least one case, but use of temperatures nearer to 1490 °C and soak times near 12 h, were more typical. Extensive work to determine minimum heating temperatures and times for formation of the TaC phase was not done, partially due to the concern regarding excess free carbon and the difficulties involved in the elemental analysis, which would have led to slow feedback of information regarding the effects of the heating regimes.

In the formulation given, however, there is still quite a bit of excess solvent that could possibly be removed from the system. The present recommendation, based on how the precursor behaved on heating, is to perform the curing step (100 °C heating) with vacuum-assisted solvent removal. However, it is perhaps possible to synthesize a tantalum alkoxide already containing heavy -OFu substitution, which would be a liquid and could be used, therefore,

neat (possibly without hydrolysis). The experiments described in this Chapter provide one method of such a synthesis: e.g. distillation of $Ta(OEt)_5$ with FuOH to produce the substitution of 2-3 ethoxide groups, followed by careful purification of the mixed-ligand alkoxide by vacuum distillation. An alternative would be to synthesize the furfuryl alkoxide directly from $TaCl_5$, or via the pentakis(dimethylamide) as an intermediate.[24,25] Steric constraints may limit the substitution to some number less than five, yielding a chloroalkoxide; but this could be substituted in a second step with a smaller alcohol such as ethanol.[26] An approach via furfuryl acetate may also be possible.[27,28]

A solution to the problem of excess carbon in the pyrolyzed product may be to hydrolyze the alkoxide with more than the 1-1.5 equivalents which were used in the experiments described. This is, of course, in addition to decreasing the excess furfuryl alcohol. Use of a chelating agent such as acetylacetone will help to prevent precipitation, should that be necessary.

A number of pyrolysis conditions were also tested in the course of these experiments. Pyrolysis under CO and under non-flowing argon did not appear to affect the product (although this was not the case for the hafnium precursors, see below). (Experiments 17-18)

9.2.2 Hafnium Carbide Precursors

Because hafnium ethoxide is commercially available as a solid, which is probably considerably oligomerized,[29] formulation of a hafnium carbide precursor by the alkoxide method presented an additional challenge.

In the initial test (Experiment 10), the a high (10-fold) excess of FuOH and 2MOE were used. The hafnium ethoxide dissolved with stirring at reflux, but a gel formed on hydrolysis with a single equivalent of acid solution. The gel broke down with stirring and heating to 85 °C. A second equivalent of acid solution , plus distillation of the volatiles, led to a brown viscous gel. Several pyrolysis conditions were tested (see Table 9.3). Soak times of 10-12 h over 1400 °C were required to get HfC; some of those samples, where the temperature ramp rate was 10 °C/min. or less, were contaminated with HfO_2. For both fast (25 °C/min) and slow (5 °C/min) heating rates, however, a 20-h soak at 1490 °C was sufficient to get HfC, phase-pure according to XRD.

While Jiang and Rhine found that furfuryl alcohol substitutes for one of the butoxide groups in titanium tetra(n-butoxide),[13] distillation of hafnium ethoxide with five equivalents of furfuryl alcohol dissolved all the solids; measurement of the distillate gave a formula for the substituted alkoxide as $Hf(OEt)_{1.6}(OFu)_{2.4}$. This hydrolyzed in acid solution (1 equivalent) to a loose gel, which pyrolyzed to HfC. (Experiment 11) The unhydrolyzed liquid was not pyrolyzed, however. A single equivalent of furfuryl alcohol, plus

three equivalents of 2MOE, were sufficient to dissolve the hafnium ethoxide with stirring overnight (warming sped the process). Hydrolysis with slightly over one equivalent of acid solution in 2MOE gave some gel formation, but this re-dissolved and the mixture appeared to be a homogeneous liquid after stirring and heating. The liquid was heated, in fact, to some 195 °C (volatiles were refluxed, rather than being permitted to vent) without solidification. A second equivalent of acid solution and heating led to an insoluble gel, which was pyrolyzed to HfC by heating at 1600 °C for 2 hours by researchers at FMI, Inc.; the weight retention was not reported by them. (Experiment 12)

Later preparations (Experiments 13 and 15) used a high excess of FuOH and 2MOE to attempt to suppress any solids or gel formation. While these mixtures did in fact behave in the desired manner with respect to hydrolysis, they were insufficiently concentrated to satisfy the requirements of the application.

Hafnium ethoxide (Experiment 14) was stirred with ethanol overnight before mixing with excess furfuryl alcohol, in the hopes of being able to thereby improve the solubility and alcohol-exchange reactivity of the ethoxide. The volatiles were distilled off at 76-80 °C and the distillate, identified by NMR as ethanol, was weighed to give a presumptive formula of $Hf(OEt)_2(OFu)_2$ in a furfuryl alcohol solution. This liquid was pyrolyzed directly, giving HfC; however, the morphology of the pyrolyzed product suggested that a large quantity of gas had caused foaming during some stage of the pyrolysis. Mixing the liquid with glycerol, then pyrolyzing, also gave HfC, but this sample was relatively dense, probably due to alcohol exchange between the hafnium alkoxide in solution and the

polyalcohol, which has the potential for cross-linking. Use of polyalcohols with simple alkoxides to provide solid polymer precursors for carbides is known from the patent literature.[6-9,11,12]

Finally, the isopropanol adduct of hafnium isopropoxide was tested in the hopes of providing improved solubility (due to a smaller degree of oligomerization expected with the bulkier alkoxide ligand and due to the alcohol adduct) and slower hydrolysis (as expected for a larger and more ramified alkoxide group). (Experiments 16, 18) Even in high excess furfuryl alcohol, however, hydrolysis with only one equivalent of acid solution led to gelation.

Hafnium ethoxide was chosen as the starting material for these experiments because only very small samples of other alkoxides were available commercially, and there were long (6-8 week) lead times for delivery of orders. Other alkoxides were, in addition, more expensive. Hafnium isopropoxide monoisopropylate was tested because it was expected to have improved solubility and slower hydrolysis, relative to the ethoxide. The butoxide would have been a superior starting material, as it is a liquid, but cost and availability issues prevented its being tested. A possible solution to the solubility and hydrolysis problem is to synthesize the desired hafnium alkoxides directly. While many metal alkoxides are synthesized from either metal chloride plus the alkali metal salts of, say furfuryl and alcohols (two equivalents of each), or from the chloride and alcohol directly, in the presence of an ammonia to act as an HCl trapping agent, it is questionable whether this approach will work well with hafnium. Bradley et al. first convert the hafnium tetrachloride into the pyridinium hexachloride, then react with

alcohol in the presence of ammonia.[30] A synthesis of hafnium alkoxides starting from the tetrachloride and an ester also looks promising, but does not appear to be in wide use.[27,28]

A further point is that all the experiments described in this section involved acid hydrolysis of the alkoxide/furfuryl alcohol mixture. It is possible that hydrolysis with neutral water would have not led to the gelation and solids that were seen in these experiments; on the other hand, the acid was added to improve retention of the furfuryl alcohol, to ensure its availability for the carbothermal reduction. While many of the experiments here had furfuryl alcohol in such high excess that "running out" of it was unlikely to be a problem, that consideration would become important as further work reduced the quantity of excess alcohol required to dissolve the hafnium alkoxide.

Pyrolyses under a number of conditions were explored. Pyrolysis under CO yielded hafnium oxide, as did pyrolysis under non-flowing argon. Pyrolysis under a very slow argon flow, with a 33 h soak at 1490 °C, led to HfC (20% weight retention) with a 7.3 wt% carbon analysis. The use of a graphite crucible led to a pyrolyzed product with a soft, greasy feel, suggesting that it was extremely high in graphitic carbon. Slow heating rates did not appear to affect the results; for 25 h soaks at 1490 °C, a 5 °C/min. ramp rate gave HfC with 11.93 wt% carbon, while the 25 °C/min ramp rate gave 12.19 wt%. Experiments involving shorter soak times at these temperatures and ramp rates were not performed, due to time constraints. See Table 9.5 for a summary of experimental conditions used.

9.2.3 Precursors for Other Metal Carbides

Because the major goals of this project only referred to the production of precursors for tantalum and hafnium carbide, exploration into using the alkoxide approach as a route to other carbides was at best cursory. Of course, a process for making titanium carbide has been reported in the literature.[13] A more or less direct substitution of Ti(OiPr)$_4$ in the tantalum carbide precursor recipe, however, also gave a liquid precursor for TiC. Use of titanium tetrabutoxide was successful as well in giving a liquid precursor for TiC. (Experiments 25, 27)

Niobium carbide was tried only once due the limited quantity of niobium alkoxide that was immediately available. In this case, hydrolysis led to a gelatinous solid, possibly due to the hexane present in the starting material (Nb(OiPr)$_5$ 10 w/v% in 50-50 iPrOH-hexane). The extremely fast hydrolysis of niobium alkoxides, in general, contributed to the formation of solid on hydrolysis; the large quantity of parent alcohol in the starting material preparation would have acted to suppress substitution of the -OiPr groups with the slower-hydrolyzing -OFu or -2MOE. However, the solid pyrolyzed to give NbC plus some other phases tentatively identified as other niobium carbides (Nb$_5$C$_6$). The peaks did not match any niobium oxides in the JCPDS database. (Experiment 25)

Zirconium carbide was tried several times using in all cases a 70 wt% solution of the n-propoxide in the parent alcohol as a starting material. A sample with 5 equivalents of FuOH and 1.5 equivalents of sulfuric acid solution, gave a gelatinous solid which

576

pyrolyzed to ZrC. (Experiment 25) In another experiment, the propanol was distilled off to give a solution of $Zr(OFu)_{2.4}(OPr)_{1.6}$ in furfuryl alcohol, but hydrolysis with 1 equivalent of acid solution gave a suspension of gelatinous clots. A second equivalent of acid solution led to a gel, which became ZrC on pyrolysis. (Experiment 26) A variation on this experiment led to a viscous liquid that remained liquid to 210 °C until vacuum was applied: because gel was present when the hydrolysis was done, however, it is uncertain whether this preparation could be considered to be a "liquid precursor" – i.e. whether it would have passed completely through, say, a filter medium. A third variation on this experiment, with a higher quantity of 2MOE than had previously been used, gave wisps of solid on hydrolysis, but these redissolved when the mixture was heated. (Experiment 27) The mixture remained liquid to 210 °C. The viscous liquid was pyrolyzed to ZrC and ZrO_2 contamination, and the morphology of the pyrolyzed material suggested that the precursor had produced a large quantity of gaseous material, as it appeared that a foam had been produced before the organics became charred in the furnace. A second sample of this precursor, which had been left open to air for several weeks and became a dense amberlike solid, pyrolyzed to ZrC. Finally, a preparation containing a large excess of 2MOE and FuOH (Experiment 28) was hydrolyzed without appearance of solids; after heating and being permitted to stand in a closed container for several weeks, however, this became a crumbly tarlike solid.

In all of the ZrC precursor experiments, it appears that the too-fast rate of hydrolysis of the zirconium propoxide was a stumbling block. Further experimentation, using the butoxide

and/or more carefully removing the excess parent alcohol to ensure substitution of the alkoxide ligands, needs to be done.

These preliminary results demonstrate that the alkoxide route outlined for the tantalum and hafnium carbide precursors can readily be adjusted to formulate precursors for other metal carbides. The problem of too-fast hydrolysis leading to the formation of a gel or precipitate can be addressed by changing to a less-hydrolyzable starting material at the outset (where these are easily available) or by use of a chelating agent (acetylacetone, for instance) or other materials to modify the hydrolysis and condensation rates. Such methods are well-known in the sol-gel field, and are cited in Part I of this thesis. By the same basic strategies, mixed-metal carbides can be synthesized simply by mixing appropriate starting ratios of the metal alkoxides with furfuryl alcohol and adjusting the hydrolysis rates using the methods cited in Part I so that one metal alkoxide does not react significantly faster than the other(s).

9.3 Conclusions and Outlook

Using metal alkoxides and furfuryl alcohol as starting
materials, we were able to formulate liquid or soluble precursors for
metal carbides. The precursors, in most cases, underwent
polymerization to gums or glassy solids on heating with removal of
solvent during a 125-150 °C curing step, then were pyrolyzed to the
metal carbides with a 30-50% weight retention compared with the
cured solid. Generally this pyrolysis step was performed at
temperatures of at least 1400 °C and heating times of 10-12 h.
Because the ability to produce metal carbide at lower temperatures
was not a goal of the project, however, a study of which phases
appeared at what heating temperatures and times was not
performed. The pyroylzed solids contained some 20 percent carbon
by weight, on average, compared with the 6% carbon expected for
a pure metal carbide sample. The alkoxide-based precursors for
metal carbides have the benefit of ease of preparation at even the
multikilogram scale.

There are several difficulties that remain to be addressed with
this route, however. Those metal alkoxides which are not liquid
require an excess of furfuryl alcohol to dissolve them. This
contributes to a low carbide production per gram of *liquid* starting
material, because the excess furfuryl alcohol solvent must be
removed at some point during the fabrication step; and any excess
furfuryl alcohol that is not removed contributes to the free carbon
excess in the pyrolyzed solid. This issue was not a major concern

for the tantalum carbide precursor, where the neat tantalum ethoxide starting material is a liquid. However, the low solubility of the hafnium ethoxide starting material made the excess solvent a real problem. For the other metal carbides produced in this Chapter, the starting alkoxides were available as more or less concentrated solutions in the parent alcohols, so while less furfuryl alcohol was required in these cases, the precursor liquid was still more dilute than it ideally should be.

One solution, mentioned above, is to synthesize liquid hafnium and zirconium alkoxides directly as starting materials. Larger alcohol groups will deter the oligomerization that leads to insolubility of these alkoxides; if the furfuryl alcohol is directly used as an alkoxide ligand, this will save on the quantity of solvent required. An ideal situation would be to produce a homoleptic metal alkoxide using unsaturated alcohols with an unsymmetrical substitution to prevent crystallization. The unsaturation will provide sufficient carbon on pyrolysis to force the carbothermal reduction of the metal-oxygen bonds. Such metal alkoxides could be made via the usual methods of alkoxide synthesis.

Hydrolysis of the precursor solutions was carried out in this formulation for three reasons. First, it provided the acidic environment required for catalyzing the polymerization of the furfuryl alcohol. Second, the hydrolysis and condensation reactions of the metal alkoxides led to a M-O-M network which safeguarded against evaporative metal loss during thermal treatment and removed the most hydrolyzable alkoxide ligands, *viz*. ethoxide, propoxide, butoxide (leaving the furfuryl alkoxide ligands) from the bonding sphere of the metal. This reduced the amount of excess

carbon in the pyrolyzed product. Finally, the hydrolysis step may make a significant difference between the processes already patented and the one designed here.

However, the hydrolysis step comes with the risk of precipitation or gelation of the precursor material prior to the curing step. This can be avoided in some cases by using less than or equal to one equivalent of water in the hydrolysis step. In other cases, a compound added to slow the hydrolysis further can be added. Here, we used 2-methoxyethanol, which had shown success in the work on vanadium alkoxides presented in Part I of this thesis. However, other compounds may be more beneficial, particularly acetylacetone or alkanolamines. These will, at least in theory, substitute the more hydrolyzable alkoxide groups first, so that the furfuryl alkoxide ligands will remain intact on the metal despite the addition of these materials.

Many of the precursor samples produced a brittle, glassy pyrolyzed material. While this morphology may have been partially due to the excess carbon, gas production during the pyrolysis is a concern. Samples which were loaded into the furnace as a liquid, rather than as a densified post-cured solid, appeared to have foamed up with gas during the heat treatments. It is unclear to us how to eliminate this difficulty via the chemistry, although some of the concepts regarding the fractal dimension of the hydrolyzed and condensed alkoxides, discussed in Part I of this thesis, may be applied. In particular, tweaking the hydrolysis chemistry to give a more linear M-O-M polymer by adjusting the acidity of the hydrolysis water could help. Also, using slow, multistage heat treatments and vacuum-assisted removal of the solvent vapors and decomposition

gases produced during heating, will maximize densification and minimize pore production.

While the process discussed in this Chapter specifically uses furfuryl alcohol as the source of carbon for the reduction of the M-O bonds, metal alkoxides can be used with a number of other materials reactions with the same basic concept to produce liquid precursors for metal carbides. There was not sufficient time during this project to explore these possibilities, but they will be mentioned here for completeness.

Copolymerization of metal (Ti, Nb, Ta) alkoxides with ethyl cellulose (the ethyl ether of cellulose) led to a material with M-O-cellulose bonds. The copolymerization was effected by heating equal weights of the alkoxide and ethyl cellulose in toluene for two hours, followed by removal of the solvent by distillation.[31] While the products were solids, it is possible that using a higher metal-to-cellulose ratio could lead to a liquid. Vanadium alkoxide has been reacted with acetoacetoxyethylmethacrylate (AAEM) in the presence of azobis(isobutyronitrile) (AIBN) and water, leading to the simultaneous development of inorganic (metal alkoxide-based) and organic (AAEM-based) polymers. The resulting material was a film-castable sol.[32] The analogous reaction for hafnium or zirconium alkoxides may be worth exploring. Other possibilities may arise by examining the optical coating literature for promising inorganic-organic polymers. A final suggestion is the mixture of poly(vinyl alcohol) with the alkoxides: the unsaturation on the PVA will possibly provide for sufficient carbon retention on coking for the carbothermal reduction to take place.

9.4 Experimental

All of the experiments were done in pre-dried glassware on a Schlenk line equipped with vacuum and oxygen-scavenged argon. Solid samples were loaded into glassware in a nitrogen-filled glovebox. Solvents were distilled from Na/benzophenone or CaH_2 prior to use. Except where indicated, reagents were used as-received from the indicated manufacturer.

NMR and XRD characterizations were performed on same instruments as those described in the Appendix to Part I. Pyrolyses were carried out in Lindberg(R) 1500 °C tube furnaces using mullite tubes joined gas-tightly at the ends with quartz fittings. A thick-walled rubber tube led from an argon tank, through a tube containing an oxygen scavenger, and into the mullite tube via the quartz fitting. The quartz fitting on the downstream end was directed to a thinner-walled rubber tube leading to a mineral oil bubbler and into a fume hood. The mullite tube was flushed rapidly for 30 minutes prior to the insertion of a tared sample; the sample was inserted into the approximate center of the furnace under rapid argon counter-flow, then the furnace tube closed up and flushed for 15-30 minutes further. The gas flow rate was then reduced to approximately 1 bubble/minute and left at that rate during the furnace's heating and cooling cycle. Due to problems with the furnace controllers, the furnace was checked often and adjustments made during a run if the final temperature had not been reached appropriately. Samples were pyrolyzed in graphite or alumina boats

and were ground and examined by XRD as described in the Appendix to Part I of this thesis. It should be noted that for a number of the XRD experiments, the monochromator was not in place, leading to a set of peaks arising from the Cu Kβ line. These peaks have been positively identified, and are marked on the relevant figures; they do not arise from a second phase. (Figure 9.2)

TGA/DTA was performed on a Perkin-Elmer TGS-1 under Ar. Simultaneous differential thermogravimetric analysis and thermogravimetric analysis (DTA-TGA) data were obtained using a TA Instruments SDT 2960 under He in the lab of Dr. H.-C. zur Loye, at the University of S. Carolina.

Compounds used include: furfuryl alcohol (Aldrich, 98%), 2-methoxyethanol (Aldrich, 99.8% anhydrous), Ta(OEt)$_5$ (Strem, 99.99+%), Hf(OEt)$_4$ (Strem, 99%), Hf(OiPr)$_4 \bullet$HOiPr (Strem 99%), Zr(OPr)$_4$ (Aldrich, 70 wt% in propanol), Ti(OiPr)$_4$ (Aldrich 97%), Ti(OBu)$_4$ (Strem 98%), Nb(OiPr)$_5$ (Aldrich, 10% w/v in 1:1 iPrOH/hexane).

In the experimental descriptions below, the quantity of moles listed beside sulfuric acid solutions is that of the water, not of the acid. The following abbreviations are used: FuOH = furfuryl alcohol, 2MOE = 2-methoxyethanol.

9.4.1 Tantalum Carbide Precursors

Experiment 1: JP-I-285 Ta(OEt)₅ + FuOH/THF + H₂O

In a 100 ml 3-neck flask equipped with a stir bar and a condensor were placed furfuryl alcohol (used as-received, 2.2 ml, 25.4 mmol) and 30 ml tetrahydrofuran, to give a pale yellow solution. $Ta(OEt)_5$ (10 g, 24.6 mmol) was added, making the solution a darker shade of yellow. The mixture was refluxed briefly, then water (0.45 ml, 25 mmol, 1 equiv.) added at 40 °C. White-yellow chunks of solid instantly appeared. The mixture was refluxed overnight to give a milky tan suspension. The solvent was removed in vacuo, leaving approx. 6 g of solid which would not redissolve in any common solvent.

A 2.4694 g sample was pyrolyzed in an alumina boat under argon, heating at 10 °C/min to 350 °C, hold for 1 hour, then ramping 25 °C/min to 1450 °C, hold for 30 min., then cooling. After this heat treatment, there were 1.2401 g (50.2%) recovered of a chunky blue-black shiny solid. XRD showed poorly crystalline TaC, Ta_2O_5, and other materials. (Figure 9.3)

Experiment 2: JP-I-286-1 Ta(OEt)₅ + 2MOE + FuOH/THF + H₂O

$Ta(OEt)_5$ (5.5 g, 13.5 mmol), 2-methoxyethanol (5 ml, 63 mmol), 10 ml of tetrahydrofuran, and furfuryl alcohol (5 ml, 56 mmol, used as-received) was added to a 50-ml 3-neck flask equipped with a stir

bar and a condensor to give a yellow-brown solution. To this solution, stirring vigorously, a suspension of H_2O in 15 ml tetrahydrofuran (0.45 ml, 25 mmol, 1.85 equiv.) was added dropwise. No immediate reaction was apparent; the mixture was set to reflux and became a viscous gel at 120 °C bath temperature. It was cooled and the solvent removed in vacuo to give 5.190 g of solid.

A 2.1738 g sample was pyrolyzed in an alumina boat under argon, heating at 10 °C/min to 350 °C, hold for 1 hour; ramping 25 °C/min to 1450 °C, hold for 30 min.; then cooling. After this heat treatment, there were 0.8613 g (39.6%) recovered of a chunky blue-black shiny solid. XRD showed TaC, but no Ta_2O_5. In a second pyrolysis trial, the sample (0.6637 g) was pyrolyzed, ramping from room temperature at 10 °C/min. to 200 °C, held for 10 h, then ramped at 20 °C/min to 1400 °C and held for 57 h, all under flowing argon. This left a mixture of dull grey and brown-gold solid, 0.4265 g (64.3%), identified by XRD as TaC. (Figure 9.4)

Experiment 3: JP-I-286-2 Ta(OEt)₅ + 2MOE + FuOH/THF + H₂O

Ta(OEt)₅ (5.5 g, 13.5 mmol) was added to a 50-ml 3-neck flask equipped with a stir bar and a condensor with 2-methoxyethanol (5 ml, 63 mmol), 10 ml of tetrahydrofuran, and furfuryl alcohol (5 ml, 56 mmol, used as-received), to give a yellow-brown solution. A suspension of H_2O (1 ml, 55.6 mmol, 4 equiv.) in 15 ml tetrahydrofuran was added dropwise to the rapidly stirred mixture at room temperature; within approximately 2 mintues an opalescent gel immobilized the stir bar. The gel became opaque over 10-15

min. The solvent was removed in vacuo to give 6.704 g of amber-like glassy chunks.

A 2.0616 g sample was pyrolyzed in an alumina boat under argon, heating at 10 °C/min to 350 °C, hold for 1 hour; ramping 25 °C/min to 1450 °C, hold for 30 min., then cooling. After this heat treatment, there were 1.5722 g (76.3%) recovered of a chunky blue-black shiny solid. XRD showed TaC, Ta_2O_5, and possibly other phases. In a second pyrolysis attempt the sample (0.4342 g) was pyrolyzed, ramping from room temperature at 10 °C/min. to 200 °C, held for 10 h, then ramped at 20 °C/min to 1400 °C and held for 57 h, all under flowing argon. This left a dull brown-gold/grey solid, 0.2447 g (56.3%), identified by XRD as TaC.

Experiment 4: JP-I-291 Ta(OEt)$_5$ + 2MOE + FuOH + H$_2$O

Ta(OEt)$_5$ (5 g, 12 mmol) was added to 2 ml of 2MOE (25.4 mmol) and 2 ml of FuOH (23.1 mmol, vacuum distilled 70-75 °C/10-12 mm) in a 3-neck flask. This mixture became yellow over approximately 10 min. A solution of 0.25 ml H_2O (13.8 mmol, 1.2 equiv.) in 4 ml 2MOE (50 mmol) and 3 ml FuOH (34.8 mmol) was added dropwise to the vigorously-stirred mixture, and the color became greenish. It was stirred at room temperature for 2 h, becoming bright yellow, then was heated to reflux. Vacuum was applied for approximately 5 minutes at 60 °C heating temperature, then the flask was returned to atmospheric pressure under argon. At 90 °C the mixture became a dark brown gel (18 hours after hydrolysis). The solvent was removed under vacuum and 4 g of brown obsidian-like solid was obtained. Elemental analysis: 31.59% C, 2.85% H.

The sample (3.9482 g) was pyrolyzed under gently flowing argon, ramping from room temperature at 10 °C/min. to 200 °C, held for 10 h, then ramped at 20 °C/min to 1400 °C and held for 57 h. This left a black glassy solid, 1.1882 g (30%), identified by XRD as TaC. (Figure 9.5) The sample was also pyrolyzed in a TGA/DTA under helium, ramp rate 25 °C/min., and showed decomposition in three main steps, at 200 °C (exothermic), 450 °C (exothermic), and 1100 °C (endothermic). The last step probably represents the carbothermal reduction of the M-O bonds. The TGA yield was approximately 56%. (Figure 9.6)

Experiment 5: JP-I-292 Ta(OEt)$_5$ + FuOH + H$^+$/H$_2$O

Ta(OEt)$_5$ (5 g, 12 mmol) and FuOH (5 ml, 57.8 mmol) were mixed in a vial to give a yellow solution. A solution of 1 M H$_2$SO$_4$ (0.25 ml, 13.8 mmol, 1.2 equiv.) in 3 ml 2MOE (38 mmol) was injected slowly into the Ta alkoxide solution with vigorous shaking. There was an exotherm. Half of the sample was taken into a second vial and concentrated under vacuum with heating. It was left under vacuum over 2 days and became orange-brown and viscous liquid. Elemental analysis: 24.27% C, 2.69% H. The other part was left undisturbed over 2 days and remained unchanged.

The viscous sample (1.5366 g) was pyrolyzed under gently flowing argon, ramping at 20 °C/min to 400 °C, holding for 10 min., then ramping at 25 °C/min. to 1400 °C and holding for 2 h. This left 0.8682 g (56%) of dense chunky solid. XRD identified the phases present as TaC; Ta oxides were not seen. (Figure 9.7). TGA was run under argon, ramp rate 10 °C/min., and showed a two

decomposition steps at approximately 160 °C and 460 °C. TGA yield was 72%, however, this represents only the removal of the organics present to approximately 900 °C. (Figure 9.8)

Experiment 6: JP-I-298B Replacement of EtOH by FuOH

A. Ta(OEt)$_5$ (7.67 g 19 mmol) of was placed in a 100-ml schlenk flask equipped with a stir bar and a short-path distillation head. 10 ml (111 mmol) FuOH was added to give a yellow solution. The mixture was heated to distill off ethanol. Yellowish liquid distilled 72-90 °C. When the bath temperature reached 150 °C the apparatus blew apart leaving a solid black residue. The experiment was repeated once with the same result.

B. Ta(OEt)$_5$ (10.9 g, 26.8 mmol) was placed in a small flask and 10 ml FuOH (116 mmol) added. Distillation of yellowish liquid occurred between 81-83 °C. Continued heating was performed very slowly. When the bath temperature reached 140 °C the material in the flask became a gummy black solid. Elemental analysis 47.42 % C 3.30% H. The sample was pyrolyzed several times under flowing argon using different heating regimes: see Table 9.1 below.

Experiment 7: JP-II-73A Ta(OEt)$_5$ + FuOH + H$^+$/H$_2$O

Ta(OEt)$_5$ (8.5 g, 20.9 mmol) and FuOH (5 ml, 57.8 mmol, used as-received) were added to a vial and hydrolyzed with a solution of 0.5 ml 1 M H$_2$SO$_4$ solution (27.8 mmol, 1.32 equiv.) in 5 ml 2MOE (63.4 mmol) and 2 ml FuOH (23.1 mmol). The vial was shaken and left sealed overnight and found to be still liquid. It was heated at 130 °C with venting to a bubbler, leading to a mix of liquid and gel. This

was left to cool overnight, producing a hard red-brown gel. The solvent was removed in vacuo and 14.41 g rubbery black chunks collected. These were insoluble in tetrahydrofuran, toluene, and heptane. Three samples were heated on the premises at Foster-Miller, ramp rate 25 °C/min to 1600 °C, 1800 °C, or 2000 °C, hold for 2 h under argon. All three samples were identified as TaC by XRD, and increased in crystallinity with increasing temperature, as expected. The 2000 °C sample also showed an XRD peak for graphite. (Figure 9.9) Weight retention was not reported by FMI for any of the samples. ESEM examination of the 1600 °C sample particles showed dense and smooth surfaces, suggesting that either little gas production had occurred during pyrolysis. (Figure 9.10)

Experiment 8: JP-II-78 Ta(OEt)₅ + varying FuOH + H⁺/H₂O in THF

In each of 7 vials 2.5 g (6.15 mmol) of Ta(OEt)$_5$ was stirred with FuOH as listed below (Table 9.2) and 10 ml of tetrahydrofuran for 1 hour. The samples were then hydroyzed with 0.11 ml (6.11 mmol) 1M H$_2$SO$_4$ solution in 5 ml tetrahydrofuran and stirred over 2 days. The samples were transferred to small flasks equipped with stir bars and short-path distillation heads and the distillate collected. For vials #1-3 the first fraction was collected 65-68 °C (clear and colorless liquid) and the second from approximately 80-90 °C (yellow liquid). In these samples the material became a brown solid. Vials # 4-7 distilled only at approximately 64-70 °C, with no yellow liquid collected. Gels were produced in these samples with continued

heating. The collected distillates were identified by NMR as being THF with a very small amount of ethanol, so it is expected that little or no ethanol was driven off the alkoxide. The solids were darker and more brittle for higher amounts of FuOH; smaller amounts of FuOH gave yellow resinous solids. The solids were held under vacuum overnight and found that the solids were more powdery/crumbly with decreasing FuOH. They were pyrolyzed under argon, ramp rate 10 °C/min. to 1490 °C, hold for 4 h then cooling. Results can be found in Table 9.2. (Figure 9.11 a-c)

Experiment 9: Formulation for TaC precursor

In the glovebox add to an oven-dried 500 ml schlenk flask equipped with a stir bar 50 g tantalum ethoxide (250 mmol) and 40 ml (400 mmol) furfuryl alcohol (FuOH). The solution becomes yellow (or more yellow, if the FuOH was used undistilled). Stir for 2 hours at room temperature, then heat the stirred flask on an oil bath to 80 °C for 4 hours under a gentle inert gas sweep directed in the gas inlet tub and out the schlenk arm to a trap (cool in ice water) which is vented to an oil bubbler. Cool to room temperature, still with inert gas sweep, and slowly add a solution of 4.5 ml 1M sulfuric acid (H_2SO_4) (250 mmol) solution in 40 ml (500 mmol) 2-methoxyethanol (2MOE) with rapid stirring. You may see some wisps of semisolid form: if so, increase the stirring rate and slow the addition rate of the hydrolysis solution. Close up and stir overnight.

591

9.4.2 Hafnium Carbide Precursors

Experiment 10: JP-I-296 Hf(OEt)$_4$ + 2MOE + FuOH + H$_2$O/H$^+$

Hf(OEt)$_4$ (6.04 g, 16.8 mmol) was mixed with 10 ml FuOH (116 mmol, distilled) to give a yellow milky suspension. This was warmed to try to dissolve the solids. 5 ml of 2MOE was added, then, after 2 h of stirring, 5 ml more 2MOE was added (total 10 ml, 126.8 mmol). After an additonal hour of stirring, the solution was heated to reflux, dissolving all solids. The mixture was cooled and a solution of 0.3 ml 1 M H$_2$SO$_4$ (16.7 mmol) in 1 ml 2MOE (12.7 mmol) added. Gelatinous chunks appeared instantly. The mixture was shaken and stirred vigorously for 10 minutes but the gel would not break up. The mixture was heated to distill off the liquid; at 85 °C it became a clear brown solution. An additional 0.3 ml of 1 M H$_2$SO$_4$ (16.7 mmol) solution in 1 ml FuOH (11.6 mmol) was added at 110 °C, giving white and brown-black solid chunks. It was stirred for 45 minutes at 110 °C with distillation of volatiles, leaving a brown viscous gel containing brown semisolid chunks. The mixture was placed under vacuum overnight, leaving 13.72 g of sticky brown semisolid.

The sample (3.2764 g) was pyrolyzed under gently-flowing argon, under several different heating schemes. Results are summarized in Table 9.4. (Figure 9.12 a-b) DTA/TGA on the sample was performed under helium. Heating at 25 °C/min. showed a four-stage weight loss 50-200 °C (solvent loss, slight endothermic), 250 °C (exothermic), 500 °C (exothermic), 600 °C-1200 °C (endothermic,

carbothermal reaction). Weight loss is essentially complete at 1250 °C. The TGA yield was 68%. (Figure 9.13)

Experiment 11: JP-I-298 Replacement of EtOH by FuOH

A. $Hf(OEt)_4$ (7.27 g, 20.2 mmol) was placed in a 100 ml schlenk flask with a short-path distillation head. 10 ml (110 mmol) FuOH was added to give a yellow solution and white suspended powder. The sample was heated to try to distill off the ethanol. At bath temperature 105 °C all solids had dissolved to give a cloudy brown solution; distillation occurred at vapor temperature 75-77 °C. At vapor temperature 80 °C the distillation was stopped and the mixture cooled. 2.23 g (48 mmol) of clear and colorless liquid (identified as containing only ethanol by NMR), suggesting that solution of a material of approximate formula $Hf(OEt)_{1.6}(OFu)_{2.4}$ in FuOH had been obtained.

Approximately 1/2 the volume of the sample (10 mmol Hf) was hydrolyzed with 0.2 ml (11.1 mmol) of 1M H_2SO_4 solution in 1 ml 2MOE (12.7 mmol), leading to a chunky gel. Solvent was partially removed by placing the gel under vacuum for 2 h at room temperature, leaving a sludgy gel plus a liquid. 0.1 ml (5.5 mmol) of H_2O was added directly and the sample left overnight, during which time it solidified completely. Elemental analysis of the precursor was 41.9 % C, 4.99% H. This precursor was pyrolyzed under flowing argon at a ramp rate of 25 °C/min to 1490 °C, holding for 25 h then cooling, to give a glassy black solid (2.2192 g before, 0.5212 g after, 23.5%) which was HfC according to XRD. Heating to 1490 °C at 5 °C/min, holding for 25 h, then cooling, led to a glassy black

solid identified as HfC (2.4638 g before, 0.5619 g after, 22.8%). A sample heated at 25 °C/min to 1490 °C was examined under ESEM, and found to be comprised of porous particles, indicating that a large amount of has production had occurred on pyrolysis. (Figure 9.15)

Experiment 12: JP-II-74 Hf(OEt)$_4$ + FuOH + 2MOE + H$^+$/H$_2$O

Hf(OEt)$_4$ (4.2 g, 11.7 mmol) and 10 ml (11.6 mmol) FuOH were stirred together overnight. Most solids dissolved. 3 ml 2MOE (38 mmol) were added to dissolve the small amount of remaining solid. The mixture was hydrolyzed by dropwise addition of 0.25 ml (13.9 mmol) of 1 M H$_2$SO$_4$ solution in 3 ml (38 mmol) 2MOE. Some semisolid appeared but the sample homogenized to a murky brown viscous liquid after 2.5 h of stirring at room temperature. The sample was heated with venting to an oil bubbler. At bath temperature 145 °C brown liquid began to reflux in the flask (the liquid refluxing earlier had been clear and colorless). The bath temperature was brought to 195 °C, with the sample remaining liquid. It was cooled and left overnight. The dark brown liquid was hydroyzed with an additional 0.25 ml (13.9 mmol) of 1 M H$_2$SO$_4$ solution in 3 ml (38 mmol) 2MOE and again heated. Gelation began at 100-110 °C and solid separate from a boiling liquid phase had formed by 145 °C. The volatiles were removed *in vacuo* and 17.5 g of gummy brown solid collected. The solid was insoluble in tetrahydrofuran, heptane, and toluene. Three samples were heated on the premises at Foster-Miller, ramp rate 25 °C to 1600 °C, 1800 °C, and 2000 °C, hold for 2 h under argon. Crystallinity

increased with increasing pyrolysis temperature; all had XRD patterns matching HfC. The 2000 °C pattern did not show cyrstalline graphite. Weight retention was not reported by FMI for any of the samples. (Figure 9.16). ESEM of the 1600 °C sample showed a large, smooth grains covered with "fuzzy" particles, which may have been free carbon. (Figure 9.17)

Experiment 13: JP-II-81 Hf(OEt)$_4$ + FuOH

Hf(OEt)$_4$ (6.80 g, 19 mmol) was stirred in 25 ml (290 mmol) FuOH over two days to give a clear brown solution. This was hydrolyzed by slow addition of 0.35 ml (19.4 mmol) of a 1 M H$_2$SO$_4$ solution in 3 ml (38 mmol) of 2MOE. Some gelatinous chunks appeared. The sample was shaken for 15 minutes and became homogenous; the sample was heated and a yellow distillate collected, leaving 15.90 g of glassy black residue (some sample was unrecoverable from the flask). The precursor elemental analysis was 57.4% C, 3.87% H. The sample was pyrolyzed in a graphite boat under flowing argon, heating at 10 °C/min to 750 °C, hold for 20 min. then heating at 25 °C/min to 1490 °C, hold for 6 h before cooling. The black-grey solid (1.9930 g before, 1.11499 g after, 57.7%) was identified by XRD as HfO$_2$ plus some HfC. It was re-pyrolyzed (0.7576 g before, 0.7522 g after, 99.3%) by heating at 25 °C/min to 1490 °C, then holding for 4 h before cooling, and while it increased in crystallinity it remained a mixture of HfC and HfO$_2$. (Figure 9.18) ^{1}H NMR of the precursor solution (C$_6$D$_6$) shows peaks at (ppm) 7.12 (s, FuOH, free), 6.10/6.08 (d, FuOH, free), 4.99 (s, polyFuOH), 4.44 (s, FuOH), 3.1-

3.8 (broad, with structure, polyFuOH), 3.06 (m, EtOH), 3.05 (s, FuOH), 1.07 (t, EtOH). (Figure 9.19)

Experiment 14: JP-II-99 Hf(OEt)$_4$ + EtOH + FuOH

Hf(OEt)$_4$ (6.52 g, 18.2 mmol) was stirred with 15.45 g (335.4 mmol) of ethanol (Sigma, water content < 0.1%) overnight, but remained a milky white suspension. 14 g (143 mmol) of FuOH was added and stirring continued overnight, during which the suspension became yellow but remained milky. A distillation head and tared receiver was attached and the sample heated. By bath temperature 80 °C the solids were all dissolved and a clear and colorless liquid distilled at 76-80 °C. The bath temperature was run to 145 °C, leaving a brown liquid. The distillate was identified as ethanol by NMR, and 1.66 g (36 mmol) more was collected than was put into the flask originally. The formula of the brown liquid was concluded to be Hf(OEt)$_2$(OFu)$_2$ dissolved in excess FuOH.

The sample was pyrolyzed in a graphite boat under gentle argon flow, heating at 10 °C/min to 1000 °C, hold for 1 h, then ramp at 25 °C/min to 1490 °C and hold for 8 h before cooling. A shiny black "puff" of solid was recovered (1.2823 g before, 0.4056 g after, 31.6%) and identified by XRD as HfC.

7.22 g of the sample, containing approximately 7.4 mmol of Hf and 44 mmol of FuOH, was mixed with 3 ml of glycerol, producing a milky suspension at first, but clearing to a viscous dark brown liquid over three days' stirring. It was pyrolyzed in a graphite boat under gentle argon flow, heating at 10 °C/min to 1000 °C, hold for 1 h, then ramp at 25 °C/min to 1490 °C and hold for 8 h before cooling.

596

A grey solid (1.7754 g before, 0.3299 g after, 18.6%) was recovered and identified by XRD as HfC. ^{1}H NMR of the precursor (C_6D_6) showed peaks at (ppm) 7.06 (s, FuOH), 5.97/5.94 (d, FuOH), 4.24 (s, FuOH), 3.72 (t, unidentified), 3.33 (q, EtOH), 1.42 (s, broad, EtOH), 0.94 (t, EtOH). (Figure 9.20)

Experiment 15: Generalized formulations

A. JP-II-121 Hf(OEt)$_4$ + FuOH

Hf(OEt)$_4$ (50 g, 139.6 mmol) was added to a 500-ml schlenk flask and FuOH (used as-received, 200 ml, 2310 mmol) were added to give a red-orange suspension. This was warmed on an oil bath to 50 °C under argon with venting to an oil bubbler, and dissolves within 15 minutes to give a murky dark brown liquid. 1 M H_2SO_4 solution (2.5 ml, 138 mmol, 1 equiv.) was added in 40 ml 2MOE (50 mmol) with stirring. The solution became slightly darker. It was stored at room temperature in an airtight container for four days, then shipped, still liquid, to FMI.

B. JP-II-122 Hf(OEt)$_4$ + FuOH

Hf(OEt)$_4$ (100 g, 280 mmol) was placed in a 1000-ml schlenk flask with 300 ml FuOH (3471 mmol, used as-received) and the mixture stirred at room temperature for several hours. To assist in dissolving the alkoxide, 2MOE (50 ml, 630 mmol) was added. The mixture was stirred overnight to give a dark brown clear solution. It was heated on an oil bath at 80 °C under a gentle Ar sweep to an oil bubbler for 8 h, then was cooled and stirred at room temperature overnight. 1 M H_2SO_4 (5.2 ml, 289 mmol) was added in 20 ml of

2MOE (254 mmol) slowly with vigorous stirring overnight. There was no change apparent. It was shipped to FMI.

Experiment 16: JP-II-123 Hf(OiPr)$_4$•HOiPr + FuOH

In a 200 ml schlenk flask 25 g Hf(OiPr)$_4$•HOiPr (60 mmol) was stirred in 100 ml of FuOH (1157 mmol) and 20 ml 2MOE (254 mmol) overnight. The solution was dark brown with some solids settling. It was heated to 100 °C under argon sweep for 3 h, then to 70 °C under argon sweep for 6 h, then cooled to room temperature. 1.2 ml of 1M H$_2$SO$_4$ solution (67 mmol) in 10 ml 2MOE (127 mmol) was added slowly, giving white wispy solids. This was stirred overnight, vented to an oil bubbler, at 65 °C. The resulting gel was shaken with 100 ml 2MOE (1.27 mol) to produce a pourable opaque viscous liquid. It was stirred over 2 days at room temperature, leading to a viscous milky brown liquid/gel. The gel did not appear to change on storage at room temperature for 8 months.

Experiment 17: JP-II-126 Hf(OEt)$_4$ + FuOH

Hf(OEt)$_4$ (100 g, 280 mmol) was placed in a 1000-ml schlenk flask with 300 ml FuOH (3471 mmol, used as-received) and the mixture stirred at room temperature for several hours. To assist in dissolving the alkoxide, 2MOE (50 ml, 630 mmol) was added. The mixture was stirred over three days to give a dark brown clear solution. It was stored for 8 months in an airtight container at room temperature and remained clear and dark brown. 1 M H$_2$SO$_4$ (6.5 ml, 360 mmol) was added in 20 ml of 2MOE (254 mmol), and the

mixture darkened and formed gelatinous chunks which redissolved on vigorous stirring. The solution was permitted to stand (after 10 min. of stirring) for 1 h and settled out gelatinous chunks from a dark brown liquid.

Experiment 18: JP-II-127 Hf(OiPr)$_4$•HOiPr

Hf(OiPr)$_4$*HOiPr (25 g, 60 mmol) was dissolved in 100 ml (1157 mmol) FuOH in a 300 ml schlenk flask and stirred at room temperature for 2 weeks, then was stored at room temperature in an airtight container for 8 months. It remained a viscous brown liquid, wetting the glass container, and with no settling. 1 M H$_2$SO$_4$ solution (1.10 ml, 60 mmol) was added with 10 ml 2MOE (127 mmol) slowly, leading to the appearance of gelatinous chunks but no precipitate. Vigorous shaking kept the mixture liquid but on being permitted to stand for approximately 1 min. it became a solid, resinous brown gel.

9.4.3 Pyrolysis Condition Tests

Experiment 19: JP-I-303/4 Varying the Furance Heating Rate/Time

Tests of two different ramp rates, e.g. 5 °C and 25 °C per minute, and of different heating times, were performed on TaC and HfC samples 1/296, 1/298, and 1/300. The results are reported in the experiments describing the preparation of those precursors.

Experiment 20: JP-II-75 Pyrolyses under CO[33]

A. Sample 1/296 (HfC precursor) was pyrolyzed in a furnace flushed with CO for 45 min., ramping 25 °C/min to 1490 °C, hold for 20 h, then cooling. A finely-divided grey-and-black solid was recovered (1.6619 g before, 0.4387 g, 26%) and identified as HfO_2 by XRD.

B. Sample 1/291 (TaC precursor) was pyrolyzed in a furnace flushed with CO for 45 min., ramping 25 °C/min to 1490 °C, hold for 20 h, then cooling. Black glassy chunks of solid with tan-gold areas was recovered (1.7345 g before, 1.0294 g after, 59.3%) and identified as TaC.

Experiment 21: JP-II-75 Pyrolyses under still Ar

All pyrolyses to date have been under flowing gas, argon or CO. Here, the furnace was flushed with Ar 1 hour then shut off (vent to bubbler to handle heating expansion) during the heating. The vent to the bubbler was closed off during the cooling to prevent air suck-back.

C. Sample 1/291 (TaC precursor) was pyrolyzed in a furnace with gas flow as described, ramping 25 °C/min to 1490 °C, hold for 20 h, then cooling. Black glassy chunks of solid with tan-gold areas was recovered (1.2658 g before, 0.7603 g after, 60.1%) and identified as TaC.

D. Sample 1/296 (Hf) was pyrolyzed in a furnace flushed with CO for 45 min., ramping 25 °C/min to 1490 °C, hold for 20 h, then cooling. A crumbly black solid was recovered (1.5107 g before, 0.3871 g, 25.6%) and identified as HfO_2 by XRD.

Experiment 22: JP-II-80 Pyrolyses using graphite crucibles, slow Ar

Samples II-73A (TaC precursor) and II-74 (HfC precursor) were placed in graphite crucibles in a furnace and flushed for 1 h with argon. The argon flow was switched to barely-flowing (1 bubble/min. in an oil bubbler) and the furnace heated at 25 °C/min to 1490 °C, held for 20 h, then cooled. The pyrolyzed sample II-73A

(Ta) was grey-white on the top, glassy black on the bottom, weight retention 53.5%; the pyrolyzed sample II-74 (Hf) was soft and "greasy" black, 20.4% weight retained. The pyrolyzed samples were identified as phase-pure TaC and HfC, respectively, by XRD.

Experiment 23: JP-II-94 FuOH + H$^+$/H$_2$O

15 ml FuOH (173.5 mmol) and 0.25 ml of 1M H$_2$SO$_4$ (13.9 mmol H$_2$O, 0.25 mmol H$^+$) solution were stirred and heated under argon to observe the behavior of FuOH absent a metal alkoxide. Temperatures given are the bath temperatures. At 50 °C the solution became brown and frothed, and a clear and colorless liquid began to reflux. As the temperature increased, the viscoscity increased, particularly over 100 °C. By 115 °C the mixture had become a brown-black gum and by 120-125 °C it had become a brittle brown-black solid. It was heated under argon at a ramp rate of 10 °C/minute to 1000 °C, soak for 2 h, then ramp at 25 °C/min. to 1490 °C and soak for 4 h before cooling. The resulting solid (44% weight retention) was in the form of white-coated lumps and was amorphous to XRD.

Experiment 24: JP-II-106 Slow heating rate

TaC precursor sample 1/298 (1.6268 g) and HfC precursor sample 1/300 (1.6156 g) were heated in graphite boats under argon, temperature ramp rate 3 °C/min to 1400 and hold for 12 h before cooling. For 1/298, black solids with a brown surface tint, 1.0553 g (64.9%) were identified as TaC. (Figure 9.21) For 1/300, black

solids, 0.4837 g (29.9%) were identified as HfC. (Figure 9.22) The HfC sample was examined by ESEM and found to consist of particles with mostly smooth surfaces, with some "fuzzy" particles which may be free carbon. (Figure 9.23)

9.4.4 Expansion of the Alkoxide Route to Other Carbides

Experiment 25: JP-II-84 Precursors for Ti, Zr, Nb carbides

A. $Ti(OiPr)_4$ (9.5 g, 36.9 mmol) was placed in a 100 ml schlenk flask and 16 ml (186 mmol) of FuOH added, giving a dark red-brown solution, some transient white vapor, and an exotherm. The solution was stirred overnight and a little white solid noted the next day. It was hydrolyzed by slow addition of 1 ml of 1 M H_2SO_4 solution (55.6 mmol, 1.5 equiv.) in 5 ml of 2MOE (63.4 mmol), giving a darker red color. The solvent was distilled off (clear and colorless at first, then yellow), leaving a black residue, which was left under vacuum overnight. NMR of the distillate showed ethanol and furfuryl alcohol (minor part). Approximately 15 g of black solids were collected, Elemental analysis 57.02% C, 4.26 %H. The sample was pyrolyzed in a graphite boat under argon flow, with heating at 10 °C/min to 750 °C, hold for 20 min., then heating at 25 °C/min to 1490 °C, hold for 6 h before cooling, to give a bluish solid, (2.3272 g before, 1.1941 g after, 51.3%), identified by XRD as TiC. It was re-pyrolyzed (0.5892 g before, 0.5776 g after, 98.0%) by heating at 25 °C/min to 1490 °C, then holding for 4 h before cooling, XRD showed TiC. (Figure 9.24)

B. Zr(OPr)$_4$ (9.60 g, 22.7 mmol) was placed in a 100 ml schlenk flask and 10 ml (115.7 mmol) of FuOH added, giving a darker yellow solution. The solution was stirred overnight, then hydrolyzed by slow addition of 0.61 ml of 1 M H$_2$SO$_4$ solution (33.9 mmol, 1.5 equiv.) in 5 ml of 2MOE (63.4 mmol), giving a gelatinous white/yellow solid. The solvent was distilled off (faintly yellow distillate), leaving a black residue, which was left under vacuum overnight. NMR of the distillate showed propanol and furfuryl alcohol (minor part). 8.14 g of black solids were collected, Elemental analysis 44.85% C, 3.15 %H. The sample was pyrolyzed in a graphite boat under argon flow, with heating at 10 °C/min to 600 °C, hold for 20 min., then heating at 25 °C/min to 1490 °C, hold for 12 h before cooling, to give a solid, (1.4930 g before, 0.8907 g after, 59.7%), identified by XRD as ZrC. (Figure 9.25).

C. Nb(OiPr)$_5$ (28.07 g, 7.23 mmol) was placed in a 100 ml schlenk flask and 3.2 ml (37.2 mmol) of FuOH added, giving a darker yellow solution. The solution was stirred overnight, then hydrolyzed by slow addition of 0.2 ml of 1 M H$_2$SO$_4$ solution (11.1 mmol, 1.5 equiv.) in 5 ml of 2MOE (63.4 mmol), giving a gelatinous white/yellow solid. The solvent was distilled off (clear and colorless distillate), leaving a black residue, which was left under vacuum overnight. 5.87 g of black solids were collected, Elemental analysis 52.61% C, 5.22 %H. The sample was pyrolyzed in a graphite boat under argon flow, with heating at 10 °C/min to 600 °C, hold for 20 min., then heating at 25 °C/min to 1490 °C, hold for 12 h before cooling, to give a bluish

solid, (1.4867 g before, 0.6574 g after, 44.2%), identified by XRD as NbC. (Figure 9.26)

Experiment 26: JP-II-114 ZrC Precursor

A. Zr(OPr)$_4$ (9.31g, 22 mmol) was added to a flask with 5.7 ml FuOH (66.2 mmol), making a red solution. A short-path distillation head was added to the flask and the sample distilled with liquid collection 97-100 °C. The clear and colorless distillate was identified as PrOH by NMR; 6.25 g was collected, 3.157 g (52 mmol) in excess of that which was calculated as having been provided by the alkoxide preparation. Thus the formula of the resulting brown liquid was deduced to be Zr(OFu)$_{2.4}$(OPr)$_{1.6}$ in FuOH solution.

To this sample was added 2 ml 2MOE (25.4 mmol) and 0.4 ml (22.2 mmol, 1 equiv.) of 1 M H$_2$SO$_4$ solution in 3 ml 2MOE (38 mmol), slowly with stirring. Gelatinous clots appeared and did not homogenize despite heating at 80 °C overnight. This was permitted to cool and stand for 2 weeks with no change noted. 0.4 ml of 1 M H$_2$SO$_4$ solution (22.2 mmol) in 5 ml 2MOE (63.4 mmol) was added to this, and the mixture became a solid gel within 30 minutes. The sample was pyrolyzed (solvent was not removed by vacuum), ramp rate 5 °C/min to 750 °C (5.0933 g sample before, 0.7044 g after, 13.8%), then was put back into the furnace and heated at 25 °C/min to 1320 °C for 4 h (0.6667 g, 13% of original, 94.6% of 1st step). The sample was identified by XRD as ZrC. (Figure 9.27)

B. Zr(OPr)$_4$ (14.00 g, 30 mmol) was added to a flask with 5.2 ml FuOH (60.4 mmol), making a red solution. 0.54 ml of 1M H$_2$SO$_4$

solution (30 mmol, 1 equiv.) in 2 ml 2MOE (25.4 mmol) was added dropwise, producing a white/yellow semisolid. Heating at 80 °C with stirring clarified the suspension a little. Half of the liquid was saved and half heated to 210 °C (bath temperature) vented to an oil bubbler. This did not solidify; once vacuum was applied at this temperature the sample became a viscous black tar, 4.31 g. This was pyrolyzed in a graphite boat, ramp rate 5 °C/min to 1480 °C, hold for 6 h, then coolled to collect a black solid (1.8126 g before, 0.6333 g after, 35%). The sample was identified by XRD as ZrC.

Experiment 27: JP-II-116 Synthesis of ZrC and TiC precursors

A. Zr(OPr)$_4$ (9.04 g, 19.3 mmol) was mixed with 6 ml (76.1 mmol) of 2MOE and 3.4 ml FuOH (39.5 mmol) to give an orange solution. This was stirred several days, and went from a light orange to a dark red-brown color. 0.35 ml of 1 M H$_2$SO$_4$ solution (19.4 mmol) in 3 ml 2MOE (38 mmol) was added with stirring. Wisps of solid appeared and redissolved after 15 minutes of stirring at room temecrature. The liquid was heated with venting to a bubbler and was a liquid still at bath temperature 210 °C. The liquid pyrolyzed in an alumina boat under argon, ramping at 5 °C/min to 1000 °C, hold for 30 min, then ramping at 25 °C/min to 1490 °C for 4 h. The original 3.3804 g of precursor produced approximately 1.29 g of black "puffy" solid on top of approximately 0.2 g of white solid (39% total solids); white-green solid "growths" appeared on the boat. Both the black and the white material were identified as mixtures of two phases of ZrO$_2$, plus ZrC. After several weeks in air the precursor had become a brown glassy translucent solid. This was pyrolyzed at 20

°C/minute to 600 °C, hold for 30 min., ramp at 25 °C/min to 1490 °C and hold for 8 h before cooling (1.6004 g before, 0.5945 g after, 37.1%), and identified by XRD as ZrC + ZrO_2. (Figure 9.28)

B. Ti(OBu)$_4$ (13.64 g, 40 mmol) was mixed with 3.2 ml of 2MOE (40.6 mmol) and 6.9 ml FuOH (80.2 mmol) to give a burgundy red solution which darkened over several days' stirring. 0.72 ml of 1 M H_2SO_4 solution (40 mmol) in 4.5 ml 2MOE (57.1 mmol) was added with stirring. No solid formation was noted. The sample was heated with venting to an oil bubbler and became solid by bath temperature 230 °C. The black glassy precursor was pyrolyzed in an alumina boat under argon, ramping at 5 °C/min to 1000 °C, hold for 30 min, then ramping at 25 °C/min to 1490 °C for 4 h. Black glassy chunks were recovered (1.5116 g before, 0.7504 g after, 49.6%), identified as TiC.

Experiment 28: JP-II-124 ZrC precursor

Zr(OPr)$_4$ (11.41g, 24.4 mmol) was added to a 100 ml schlenk flask with 20 ml FuOH (232 mmol) to produce an orange solution. 5 ml 2MOE (63.4 mmol) were added and the mixture stirred overnight to produce a clear dark brown liquid. This was heated at 100 - 110 °C under argon sweep, then left at 60 °C vented overnight, leaving a dark brown liquid. After standing 1 week, the liquid had become more viscous and some solids were present in the flask. 2 ml FuOH (23.2 mmol) and 3 ml 2MOE (38 mmol) were added; this did not dissolve the solids. 0.45 ml of 1M H_2SO_4 solution (25 mmol) in 5 ml 2MOE (63.4 mmol) was slowly added to the stirred solution. This

607

was stirred at room temperature with no solids noted, and after 2 h was heated with venting to an oil bubbler at 100 °C. It was permitted to cool and stand. After several days it became a dark brown crumbly resin.

Table 9.1: Pyrolyses of JP-I-298B

Heating Scheme	% Wt. Retention	Appearance	XRD identity
RT>1490 °C @ 25 °C/min, hold 20h	63.5	black & grey glassy chunks	TaC
RT>1490 °C @ 25 °C/min, hold 25h	62.5	glassy black	TaC
RT>1490 °C @ 5 °C/min, hold 20h	54.5	grey chunks	TaC
RT>1490 °C @ 25 °C/min, hold 25h	58.7	glassy black	TaC

Table 9.2: Experimental Conditions and Results for JP-II-78

Vial #	ml FuOH	mmol FuOH	FuOH/ Ta(OEt)$_5$	hydrolysis behavior	Precursor solid (g)	Phases found	Wt. Ret'n after pyr. (%)
1	2.70	31.0	5	clear	3.82	TaC	55.9
2	2.15	24.8	4	clear	3.26	TaC	57.8
3	1.10	12.4	2	clear	2.42	TaC	59.4
4	0.80	9.3	1.5	ppte. rediss.	2.19	TaC	57.6
5	0.40	4.7	0.75	yellow ppte.	1.63	TaC + Ta$_2$O$_5$	65
6	0.27	3.1	0.5	yellow ppte.	1.56	TaC + Ta$_2$O$_5$	70.7
7	0.13	1.6	0.25	yellow ppte.	1.69	TaC + Ta$_2$O$_5$	>19 *

*sample dropped on removal from furnace

Table 9.3: Pyrolyses of JP-I-296

Heating Scheme	% Wt. Retention	Appearance	XRD identity
RT>1400 °C @ 10 °C/min, hold 6h; 1400>1450 °C @ 25 °C/min, hold 4 h; 1450 > 1500 @ 25 °C/min, hold 0.5 h.	21	black, some grey areas	HfC
RT>1495 °C @ 10 °C/min, hold 1 h	28.2	grey solid	HfO$_2$
solid from above re-heated RT>900 °C @ 5 °C/min., hold 1 h., 900 > 1490 °C @ 10 °C/min, hold 12 h.	88	grey solid	HfC, some HfO$_2$ EA 5.32 C, <0.1 % H
repeat above on new sample	25	grey-black solid	HfC + HfO$_2$ Figure 9.12a
RT>1490 @ 5 °C/min, hold 20 h	21	black-grey powder	HfC
RT>1490 @ 25 °C/min, hold 20 h	20.6	black-grey powder	HfC Figure 9.12b

Table 9.4: Tantalum Precursor Experimental Conditions

sample #	alkox/FuOH/ 2MOE/H₂O (acid?) mmol*	(Prec. state) Prec. EA	Heat Cond.	XRD/%	Ceram. EA	Notes
I-285	25/25/0/25/N	(milky susp.)	RT@10>350(1), @25>1450(0.5)	TaC, Ta₂O₅/ 50%		
I-286-1	14/56/63/25/N	(visc. gel)	RT@10>350(1), @25>1450(0.5)	TaC/39.6%		Δ FuOH
			RT@10>200(10), @20>1400(57)	TaC/64.3%	19.25 C	Δ heat
I-286-2	14/56/63/56/N	(visc. gel)	RT@10>350(1), @25>1450(0.5)	TaC, Ta₂O₅/ 76.3%		Δ H₂O
			RT@10>200(10), @20>1400(57)	TaC/56.3%	22.51 C	Δ heat
I-291	12/23/25/14/N	(liq. to 90 °C) 31.6 C, 2.9 H	RT@10>200(10), @20>1400(57)	TaC/30		Δ all para-meters
I-292	12/58/38/14/Y	(liq.) 24.3 C, 2.7 H	RT@25>1400 (2)	TaC/56		H⁺, Δ all parameters
I-298B	27/116/0/0/N	(liq. to 140 °C) 47.4 C, 3.3 H	RT@5>1490(20, 25)	TaC/54.5, 58.7		no hydrolysis
			RT@25>1490(20, 25)	TaC/63.5, 62.5		
			RT@3>1400(12)	TaC/64.9	40.3 C	slow heat

Table 9.4 (continued)

sample #	alkox/FuOH/ 2MOE/H$_2$O (acid?) mmol*	(Prec. state) Prec. EA	Heat Cond.	XRD/%	Ceram. EA	Notes
II-73A	21/81/63/28/Y	(liq. to 130 °C)	RT@10>1490(12)	TaC/53.5		
			RT@25>1600(2)	TaC/no info.		
II-78	6.2/vary/0/6.2/Y	(liq. to 90 °C)	RT@10>1490(4)	TaC for high FuOH, Ta$_2$O$_5$ for low		vary FuOH
II-108	20/20/0/30/Y	(liq. initially, gel over days)	not pyr.			THF, no 2MOE used

* in rounded numbers

Table 9.5: HfC Precursor, Experimental Conditions

Sam. #	Alkox./ FuOH/ 2MOE/H₂O (acid?) mmol	(Prec. State) Prec. EA	Heat Cond.	XRD/%	Ceram. EA	Note
I-296	17/116/ 127/ 17/Y	(liq. to 85, gel when add 17 more H₂O)	RT@10>1400 (6)>1450(4)>1500 (0.5)	HfC/21%		Hf(OEt)₄ = alkox.
			RT@10>1495 (1)	HfO₂/28.2%		new sample
			RT@25>1490 (12)	HfO₂+HfC/ 88%	5.32 C	reheat above
			RT@5>900(1)@10> 1490(12)	HfO₂+HfC/ 25%		new sample
			RT@25>1490(21)	HfC/96%	7.25 C	reheat above, slow Ar flow

Table 9.5, continued.

Sam. #	Alkox./ FuOH/ 2MOE/H$_2$O (acid?) mmol	(Prec. State) Prec. EA	Heat Cond.	XRD/%	Ceram EA	Note
			RT@5>1490(21)	HfC/21%		new sample, slow Ar flow
			RT@25>1490(20)	HfO$_2$/ 26.4%		CO atmos.
			RT@25>1490(20)	HfO$_2$/ 25.6%		no Ar flow
I-298 A	10/31/13/ 11/Y; 5.5/Y	(gel on hyd.) 49.1 C, 5 H	RT@25>1490(25)	HfC/23.5%	12.2 C	Hf(OEt)$_{1.6}$(OFu)$_{2.4}$
			RT@5>1490(25)	HfC/22.8%	11.9 C	slow heat
			RT@3>1400(12)	HfC/29.9%	17.2 C	slower heat
II-74	12/12/76/ 14/Y	(liq. to 195 °C)	not pyr.			

Table 9.5, continued.

Sam. #	Alkox./ FuOH/ 2MOE/H$_2$O (acid?) mmol	(Prec. State) Prec. EA	Heat Cond.	XRD/%	Ceram EA	Note
	add 38/14/Y	(gel at 110 °C)	RT@25>1600(2)	HfC/no info.		
II-81	19/290/38/ 19/Y	(liq. to 80 °C) 57.4 C, 3.9 H	RT@10>750, @25>1490(6)	HfO2+HfC/ 57.7%		
			RT@25>1490(4)	HfO2+HfC/ 99.8%	61.11 C	reheat sample
II-99 A	18/107/0/0 /N	(liq.)	RT@10>1000(1), @25>1490(8)	HfC/31.6%		used EtOH Hf(OEt)$_2$(OFu)$_2$
II-99 B	7.4/44/-- 39 g	(liq.)	RT@10>1000(1), @25>1490(8)	HfC/18.6		added glycerol to II-99 A

Table 9.5, continued

Sam. #	Alkox./ FuOH/ 2MOE/H₂O (acid?) mmol	(Prec. State) Prec. EA	Heat Cond.	XRD/%	Ceram EA	Note
II-108	10/45/9/ 15/Y	(liq., gel after days)	not pyr.			
II-121	140/2310/ 50/138/Y	(liq.)	shipped to FMI			
II-122	280/3471/ 884/289/Y	(liq.)	shipped to FMI			
II-123	60/1157/ 381/67/Y	(liq. to 65 °C)	not pyr.			used Hf(OiPr)₄•HOiPr
II-126	280/3471/ 884/289/Y	(liq.)	shipped to FMI			
II-127	60/1157/ 127/60/Y	(gel)	not pyr.			used Hf(OiPr)₄•HOiPr

Table 9.6: Other Ceramics, Experimental Conditions

sample #	alkox/FuOH/ 2MOE/H₂O (acid?) mmol	Prec. EA	Heat Cond.	XRD/%	Notes
II-84 A	37/200/63/56/Y	(liq. til heat) 57 C, 4.3 H	RT@10>750, @25>1490(6)	TiC/51.3%	used Ti(OiPr)$_4$
			RT@25>1490(4)	TiC/98%	reheat sample
II-116B	40/80/100/40/Y	(liq. to 230 °C)	RT@5>1000, @25>1490(4)	TiC/49.6%	used Ti(OBu)$_4$
II-84 C	7/36/63/11/Y	(gel) 52.6 C, 5.2 H	RT@10>600, @25>1490(12)	NbC/44.2%	used Nb(OiPr)$_5$
II-84 B	24/264/164/25/Y	(gel) 44.9 C, 3.2 H	RT@10>600, @25>1490(12)	ZrC/59.7%	used Zr(OPr)$_4$
II-114 A	22/66/63/22/Y	(gel clots)			Zr(OFu)$_{2.4}$(OPr)$_{1.6}$
	add 63/22/Y	(gel)	RT@5>750	13%	Solvent not removed

Table 9.6, continued.

sample #	alkox/FuOH/ 2MOE/H₂O (acid?) mmol	Prec. EA	Heat Cond.	XRD/%	Notes
			@RT@25>1320(4)	ZrC/94.6%	reheat sample
II-114 B	30/60/25/30/Y	(liq. til 210 °C + vac.)	RT@5>1480(6)	ZrC/35%	
II-116 A	19/77/80/19/Y	(liq. til 210)	RT@5>1000, @25>1490(4)	ZrC + ZrO₂/ 39%	
		(solid after 2 wks. in air)	RT@20>600,@25 >1490(8)	ZrC/ 37.1%	

Figure 9.2: XRDs of the same sample of HfC, (a) monochromator absent; (b) monochromator present. This demonstrates that some of the peaks seen in many of the XRDs in this Chapter arise from Kβ radiation, rather than impurities.
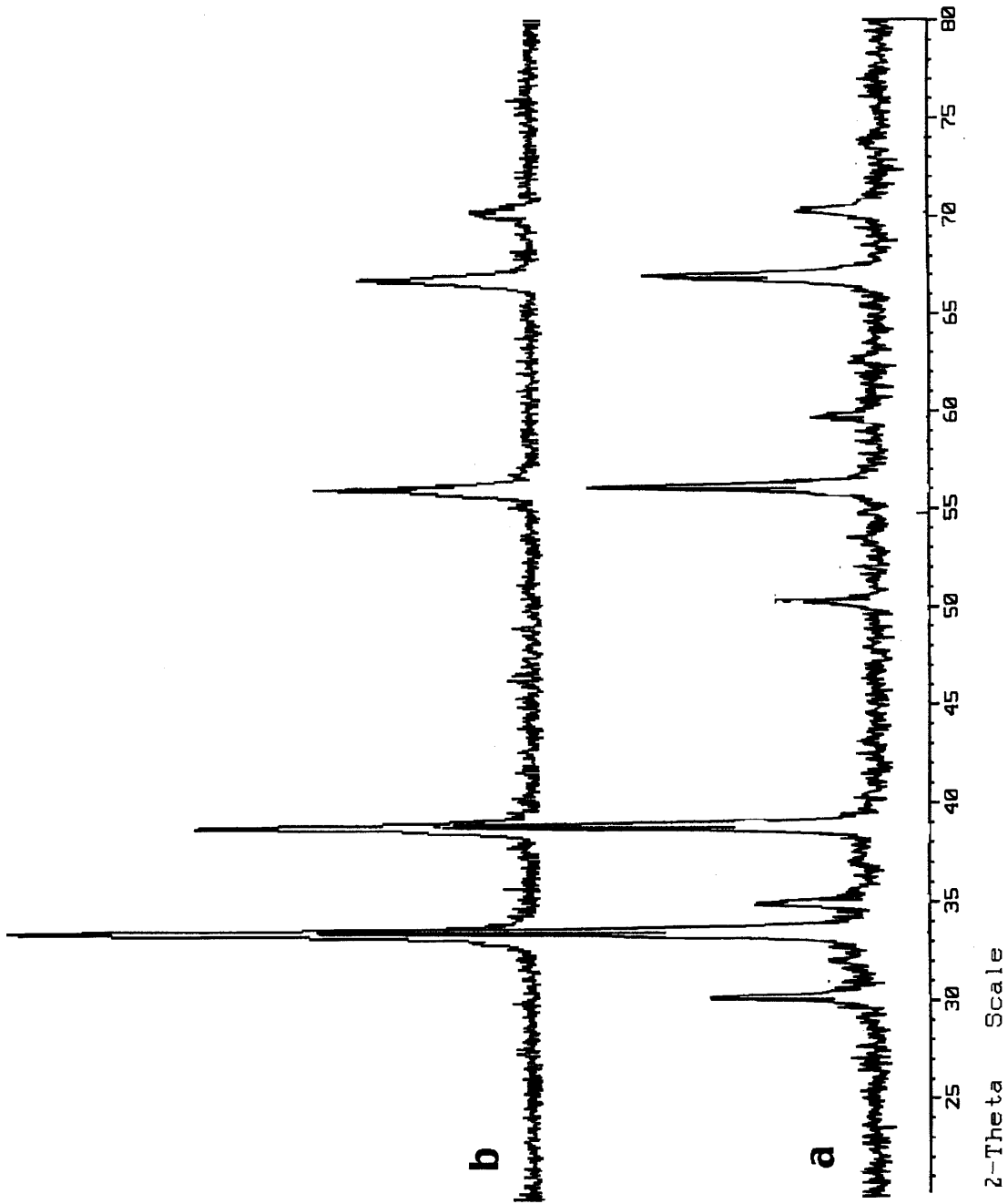
Figure 9.3: XRD of I-285. Circles indicate TaC (JCPDS 35-801), lines indicate Ta_2O_5 (JCPDS 35-922).
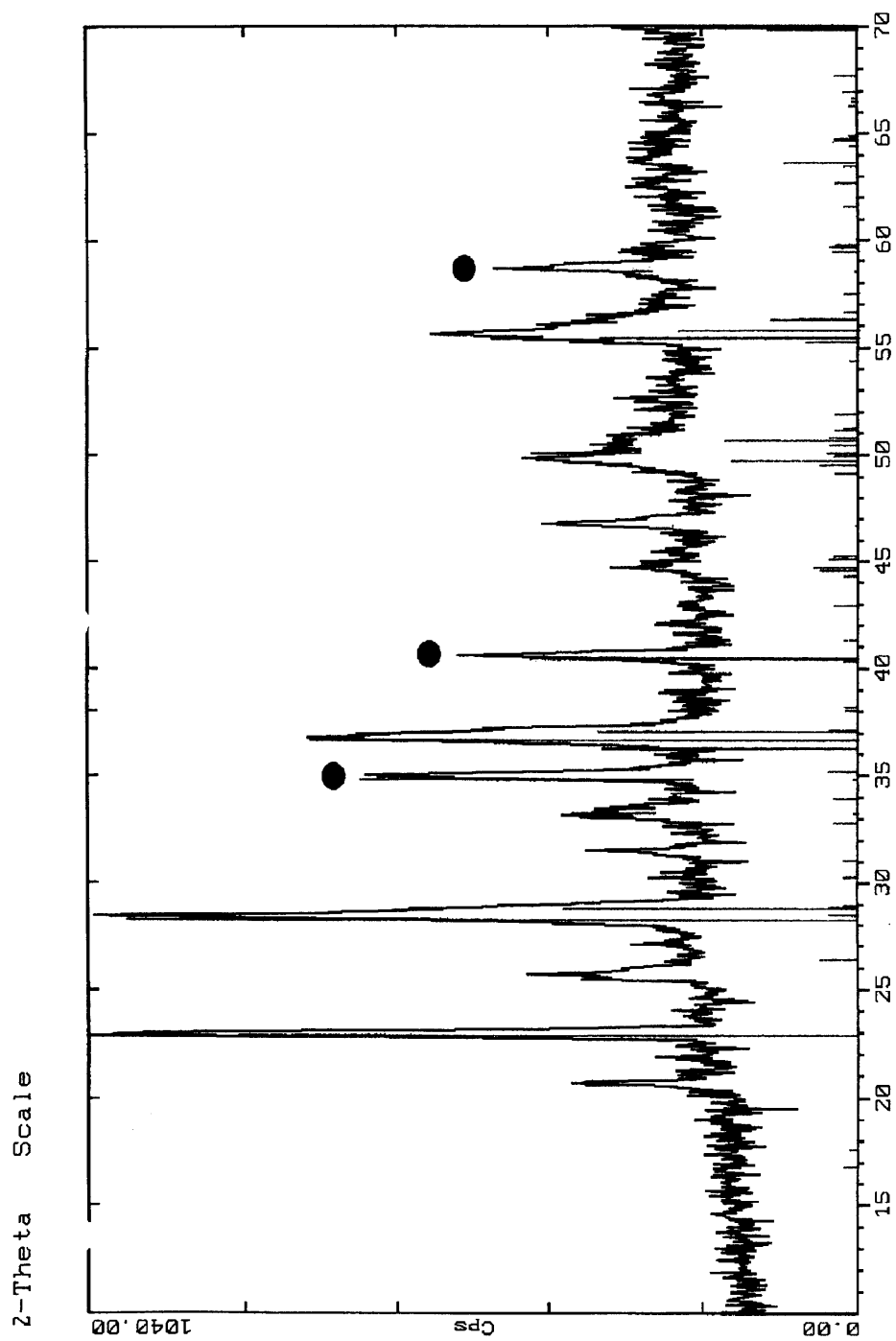
Figure 9.4: XRD of I-286-1. Lines indicate TaC (JCPDS 35-801), other peaks are from Kβ.
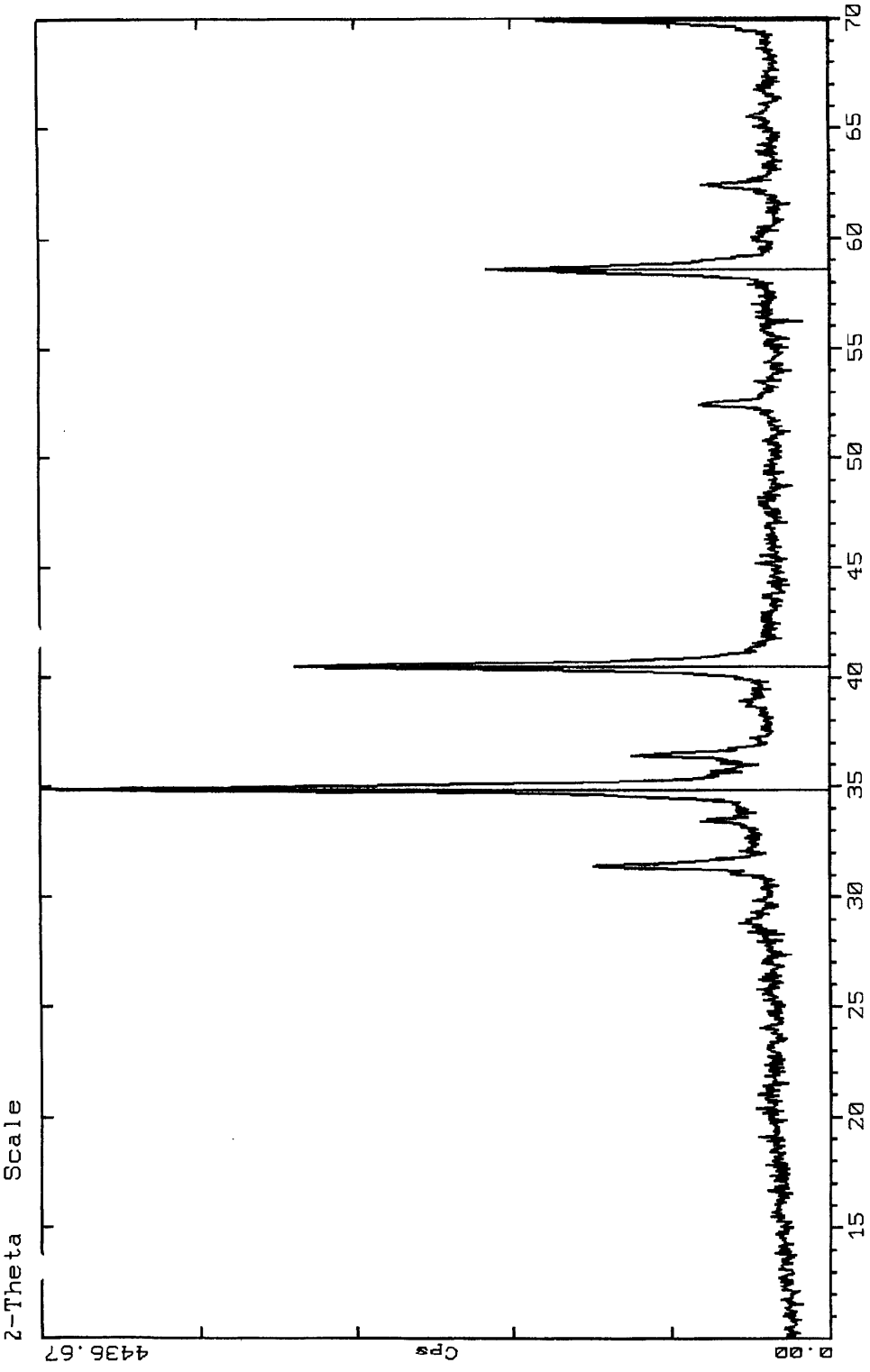
Figure 9.5: XRD of I-291. Circles indicate TaC (JCPDS 35-801), other peaks are from Kβ.
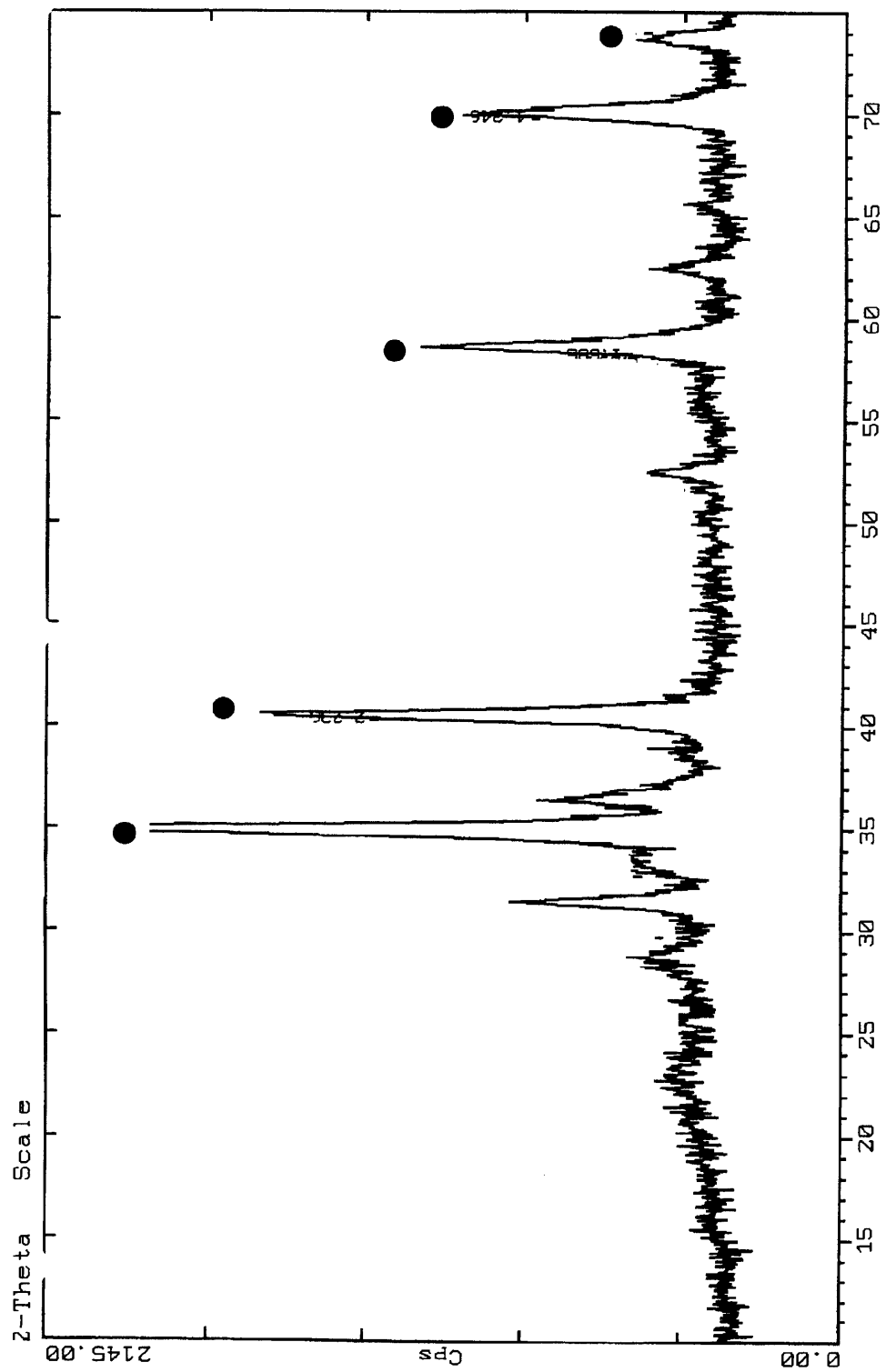
Figure 9.6: TGA/DTA of I-291.
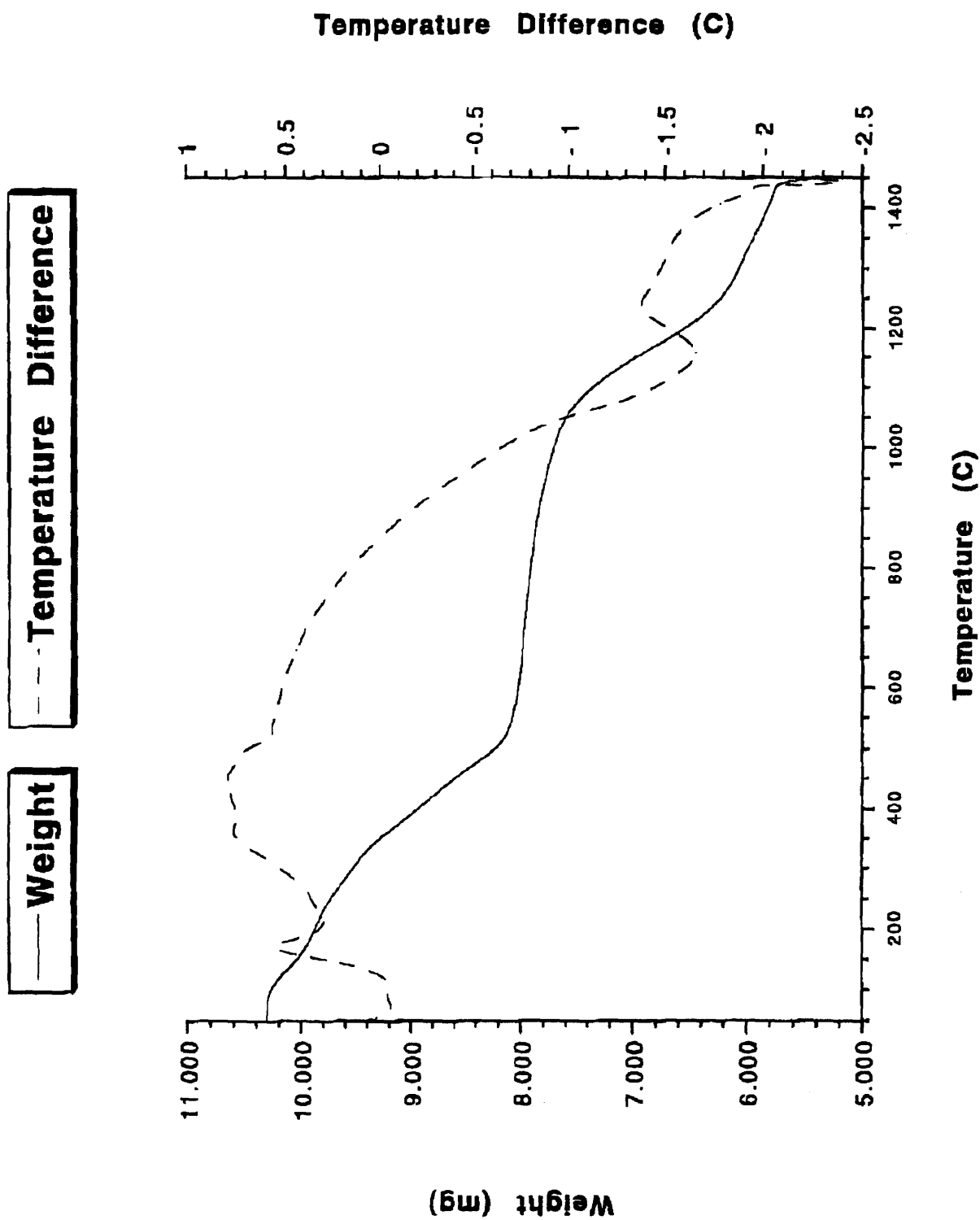
Figure 9.7: XRD of 1-292. Circles indicate TaC (JCPDS 35-801), other peaks are from Kβ.
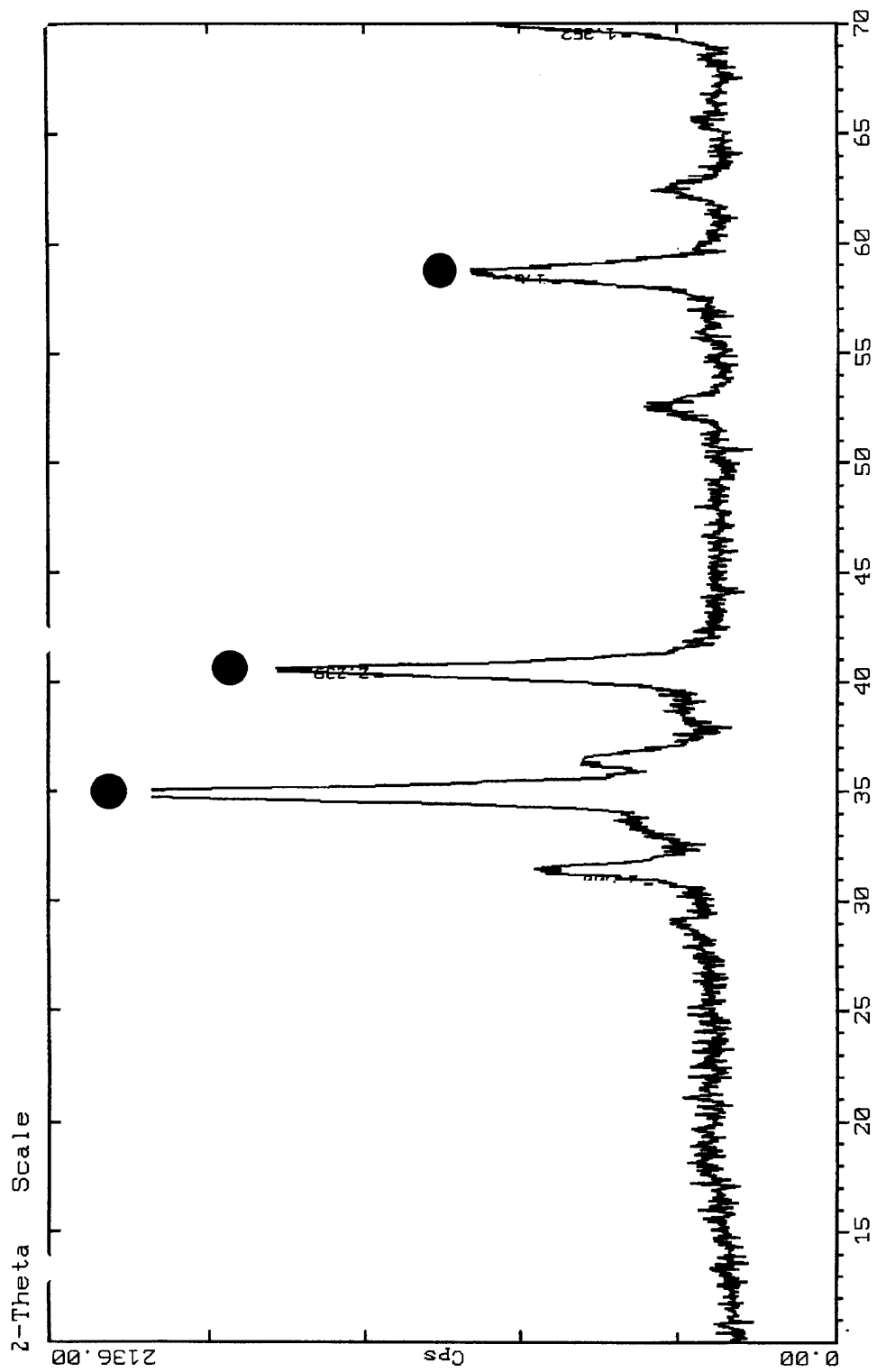
Figure 9.8: TGA of I-292.
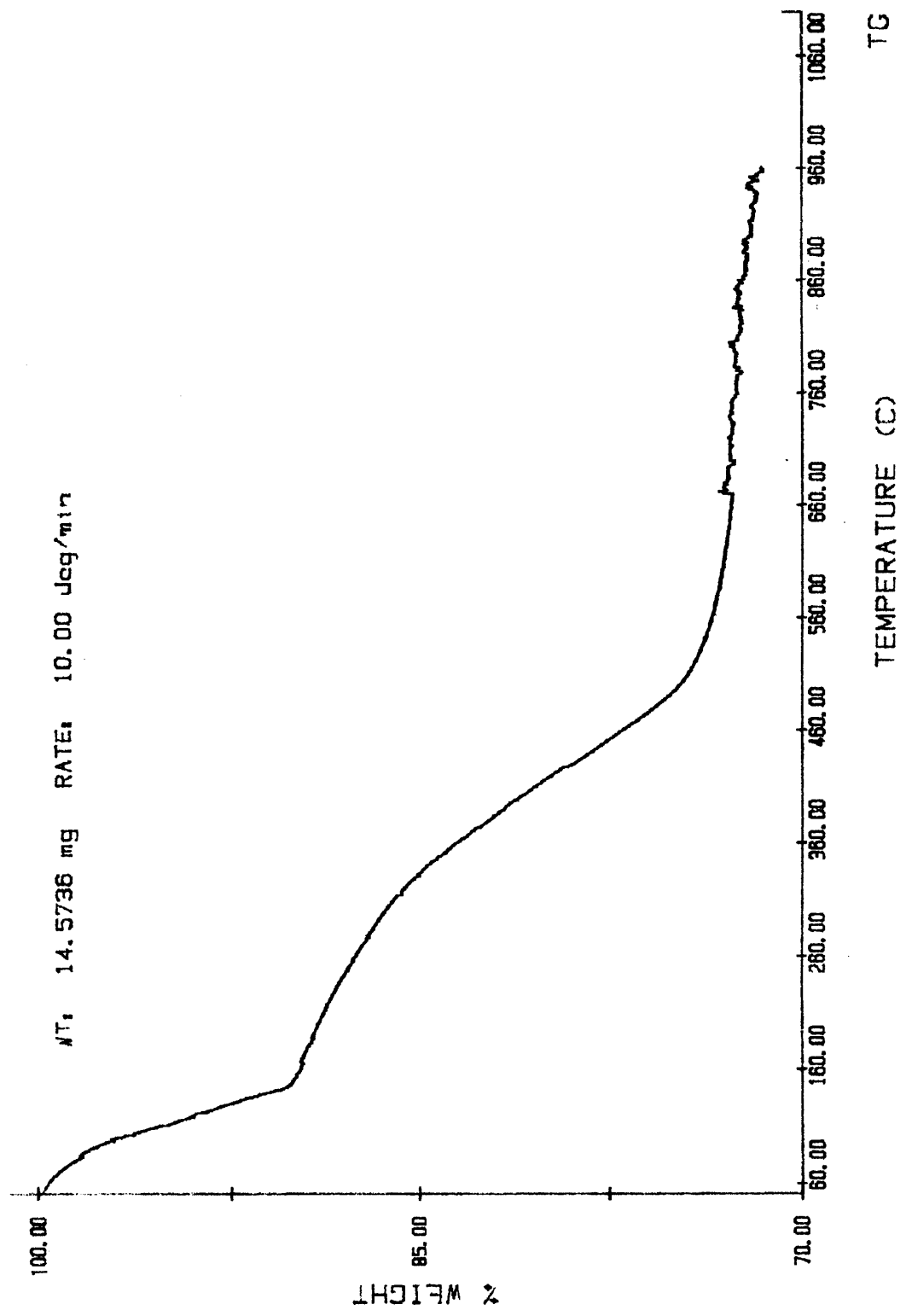
Figure 9.9: XRD of II-73 (2000 °C). Lines indicate TaC (JCPDS 35-801), circle indicates graphite (JCPDS 25-284).
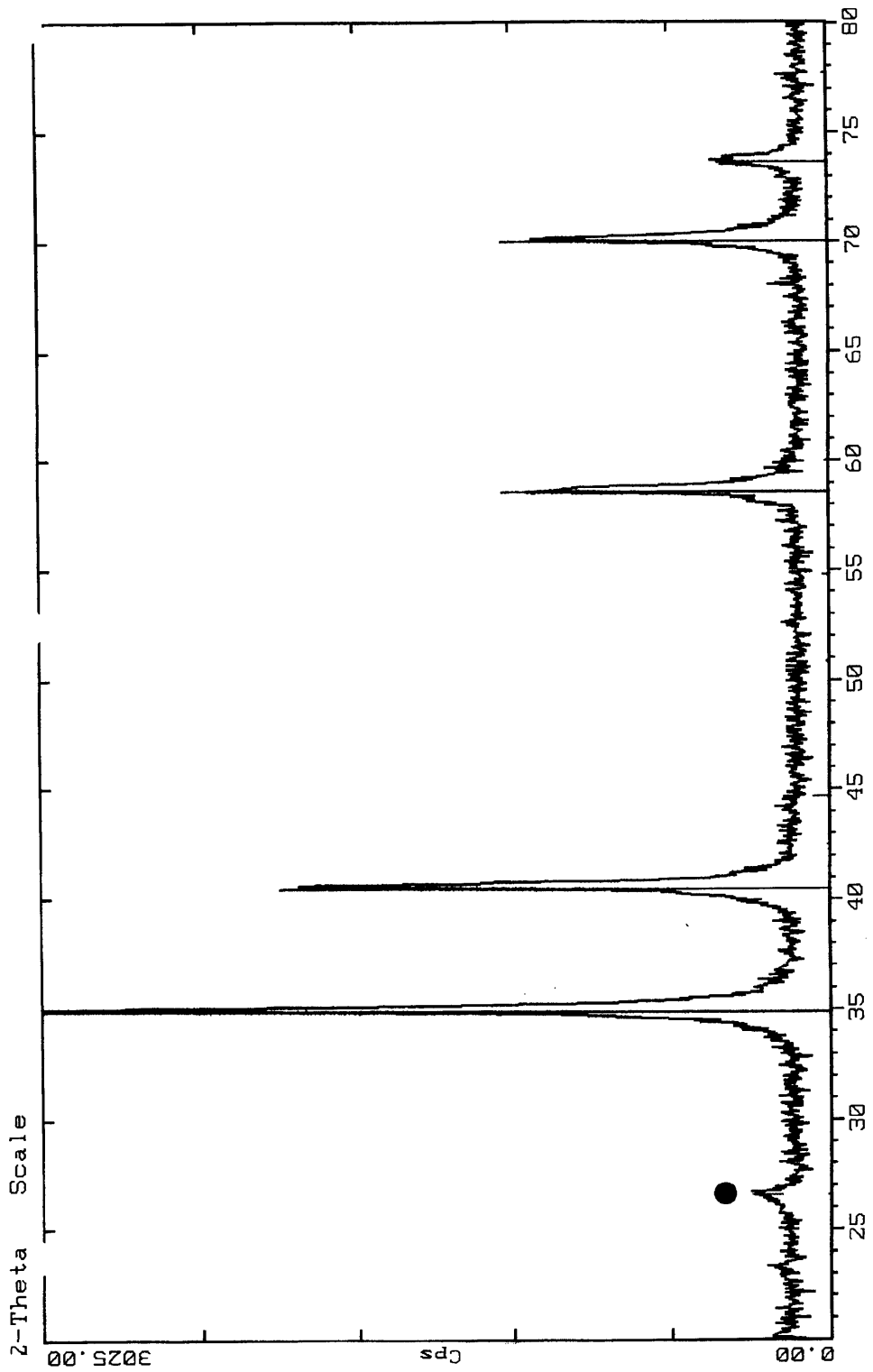
Figure 9.10: ESEM of II-73 (1600 °C). X 615.
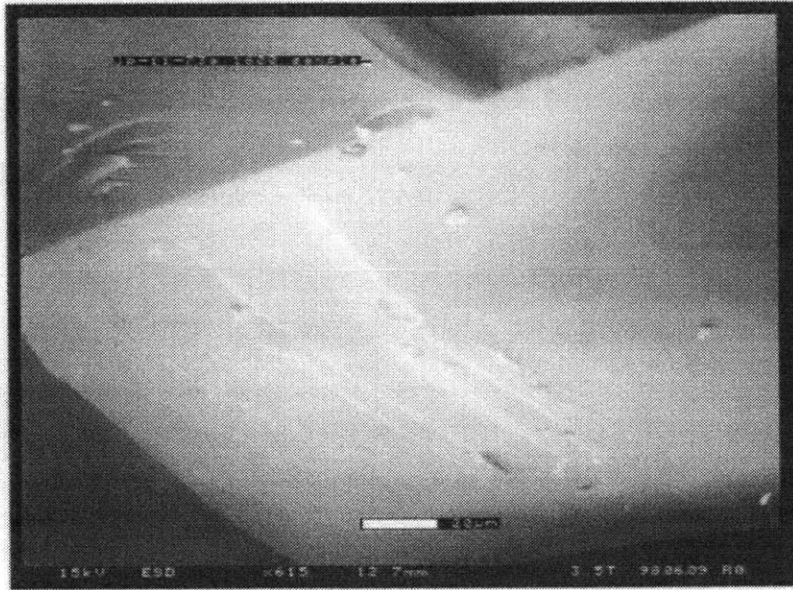
Figure 9.11: XRD of (a) II-78-1, (b) II-78-3, (c) II-78-5.
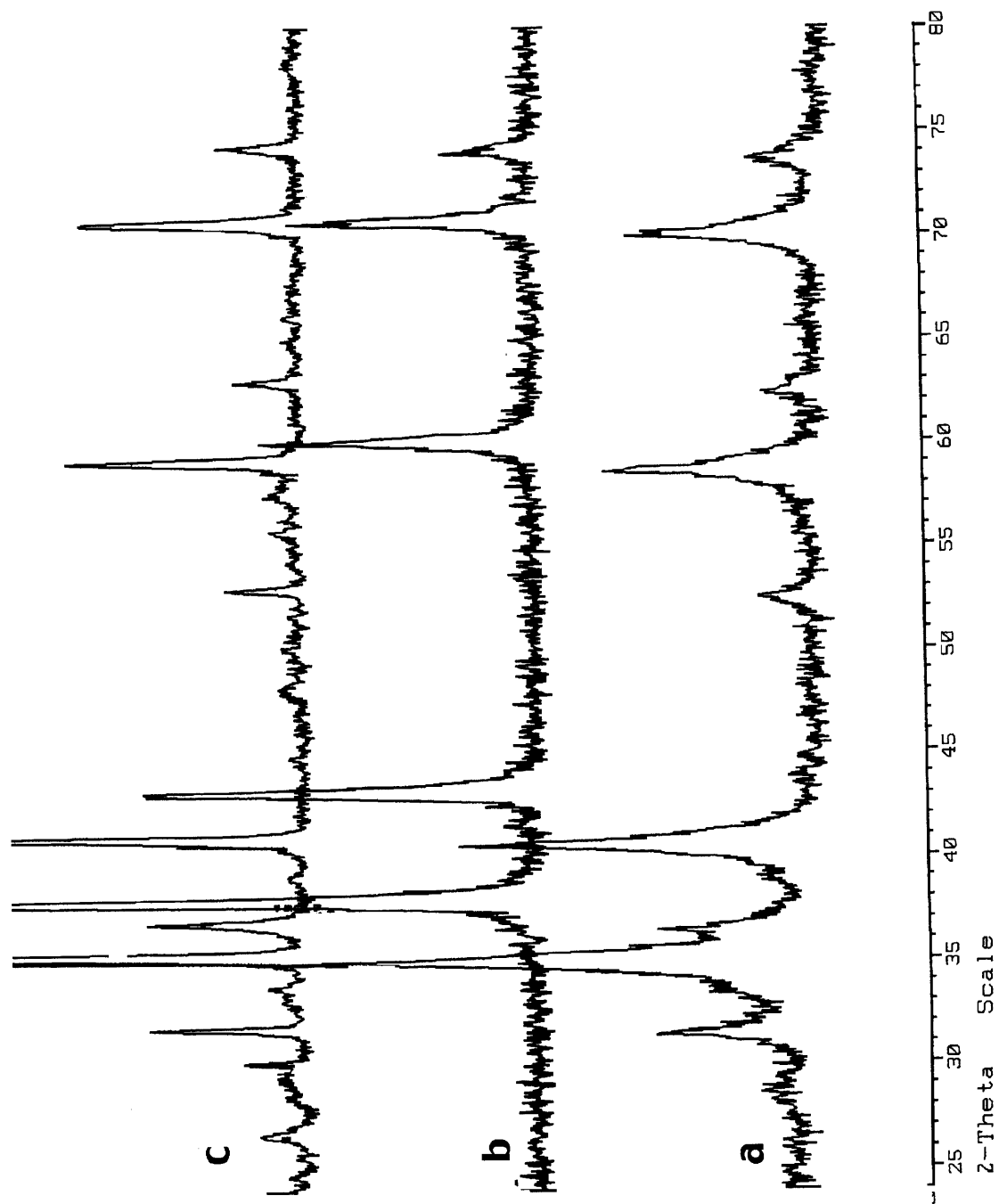
Figure 9.12 a: XRD of I-296, see Table 10.3.
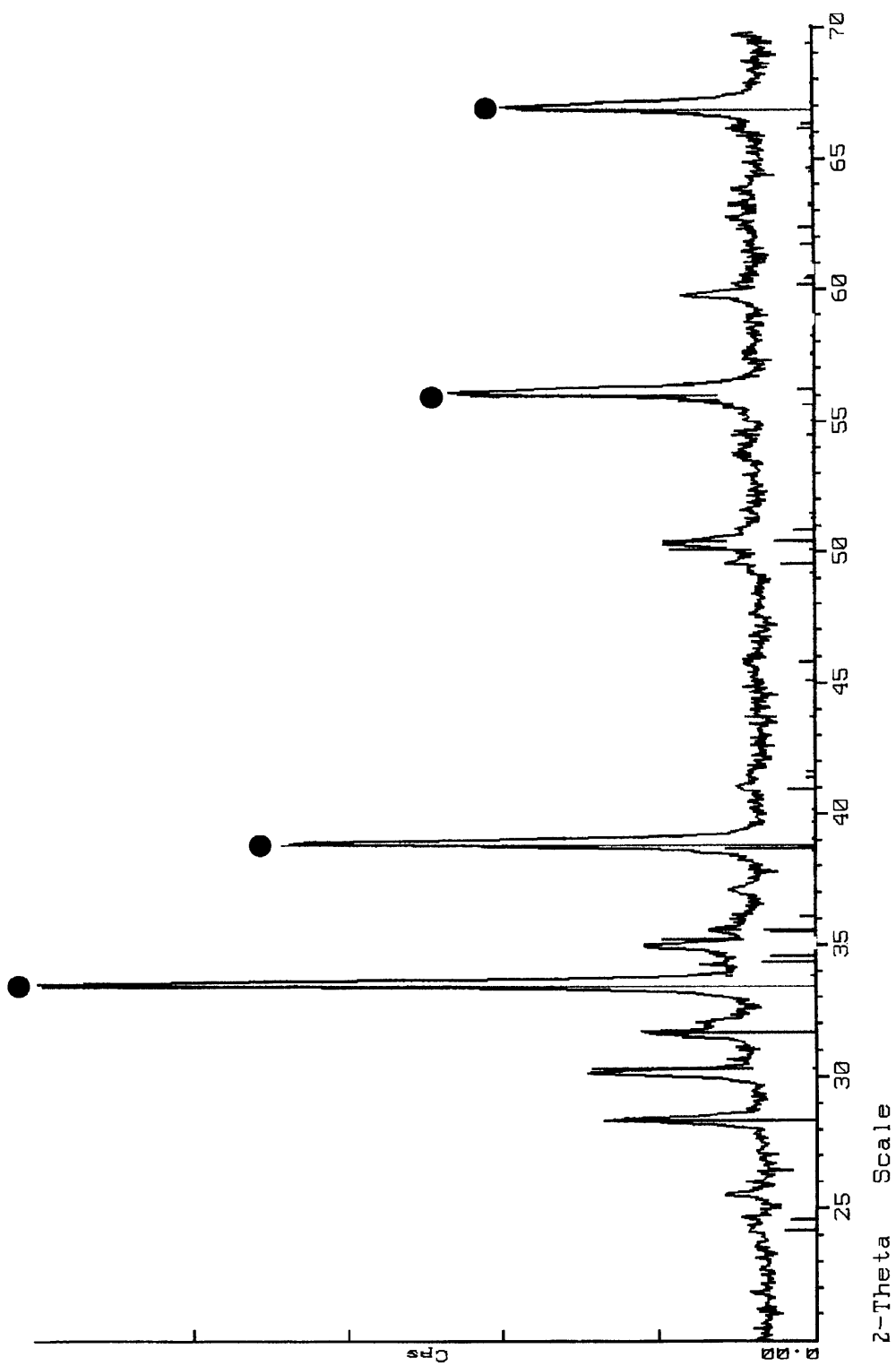
Figure 9.12 b: XRD of I-296, see Table 10.3.
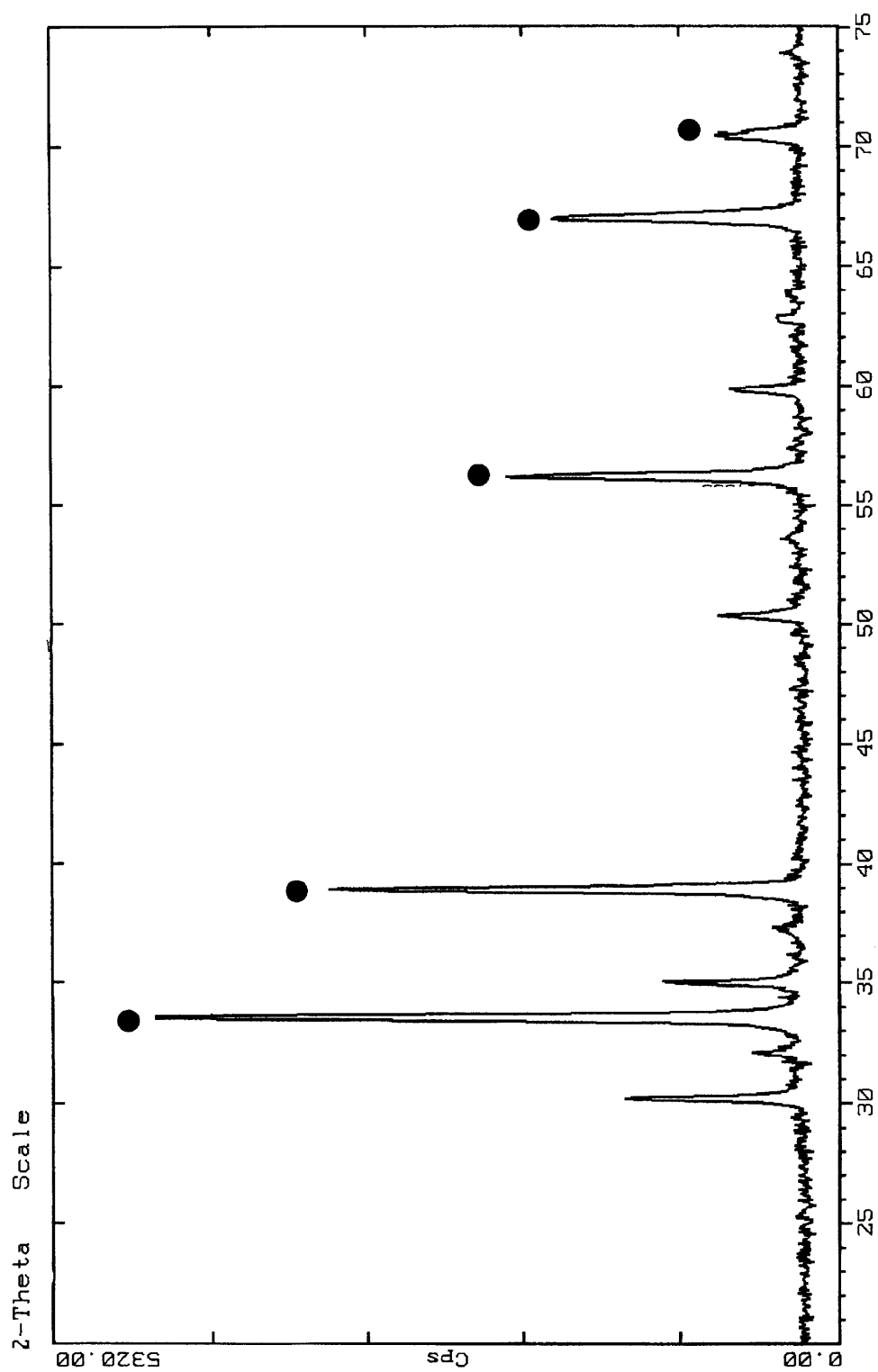
Figure 9.13: TGA/DTA of I-296.
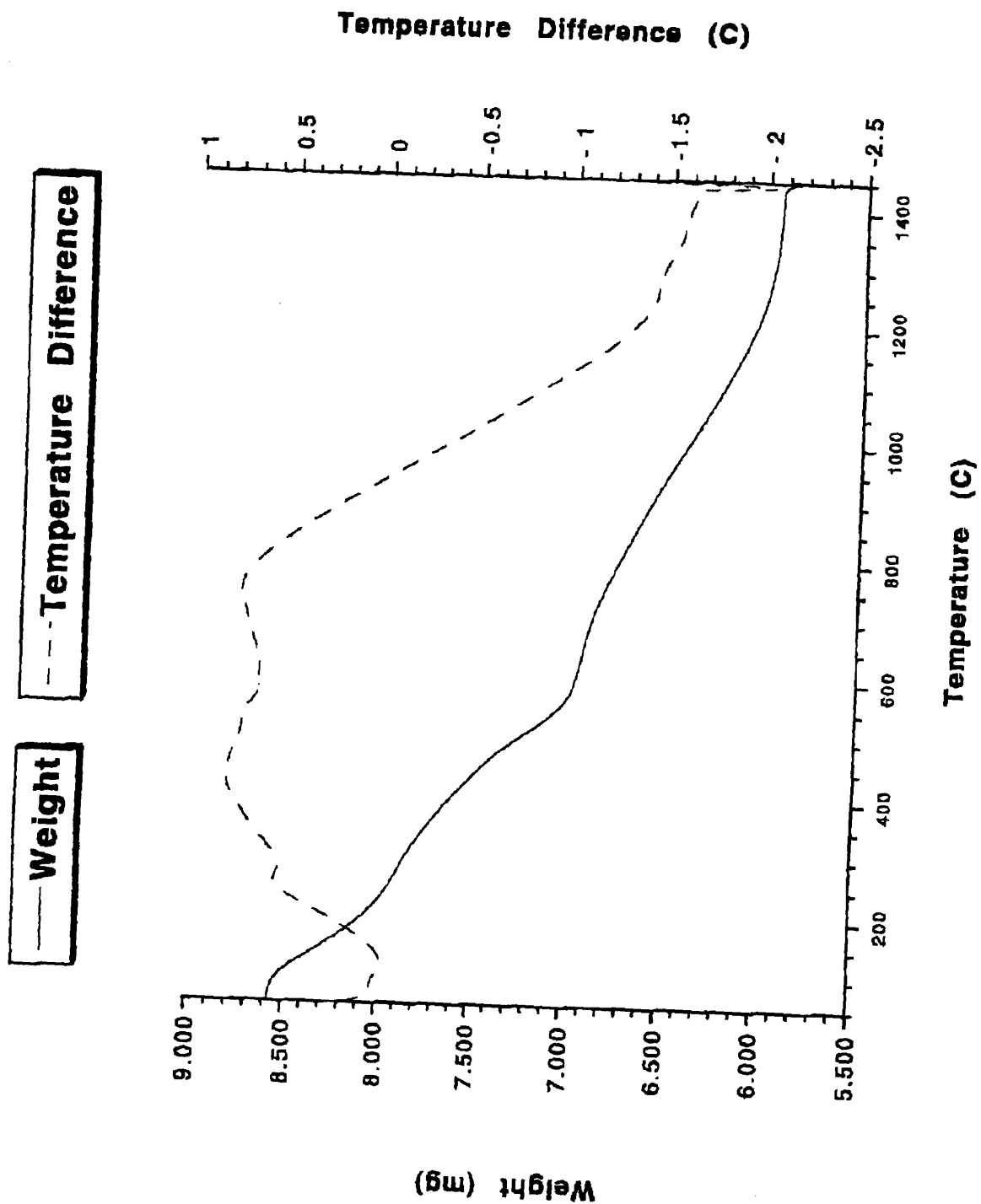
Figure 9.14: XRD of I-296.
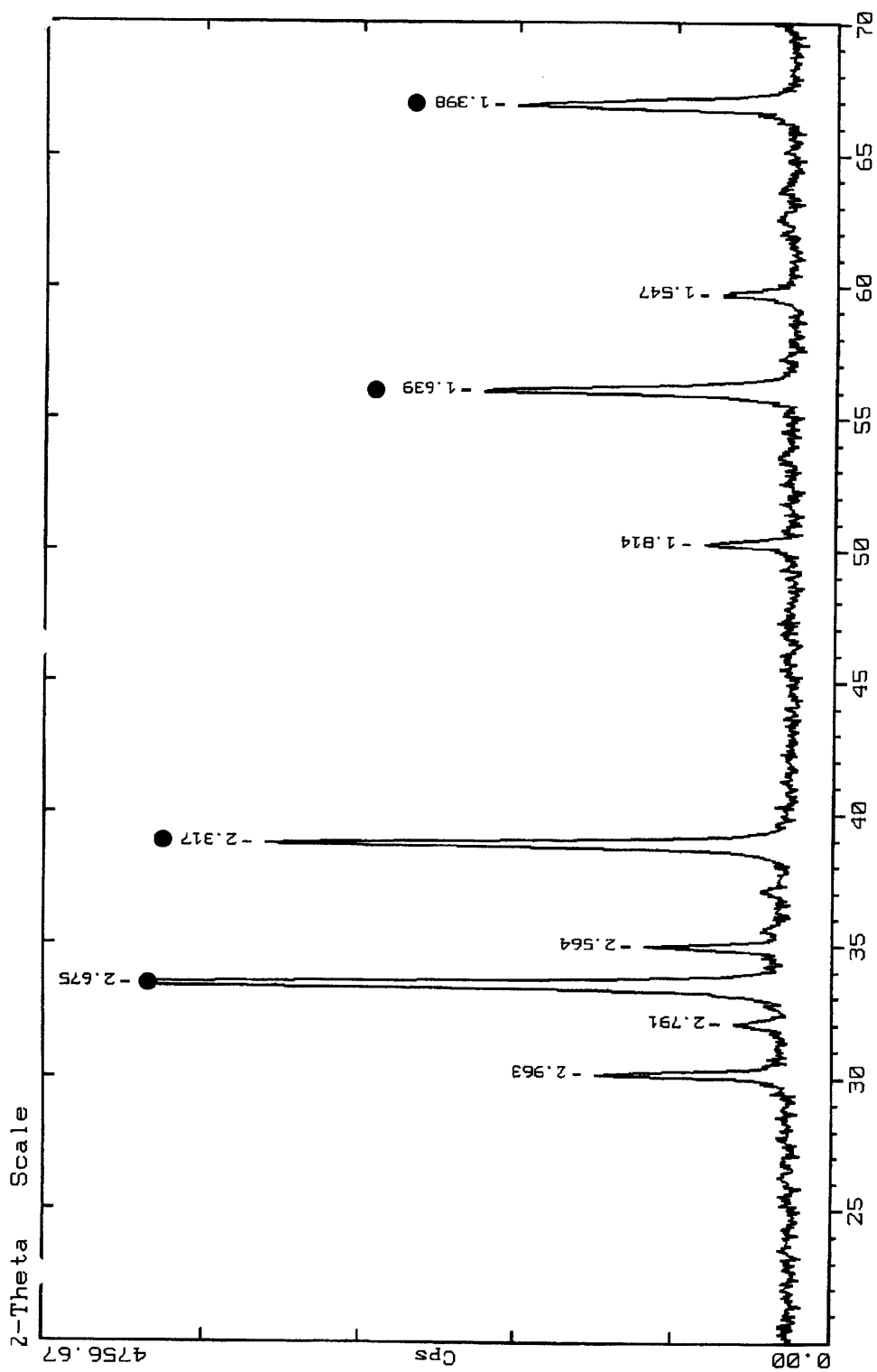
Figure 9.15: ESEM of I-296, pyrolyzed at RT>1490 @ 25 °C/min, hold 20 h. X 2100.
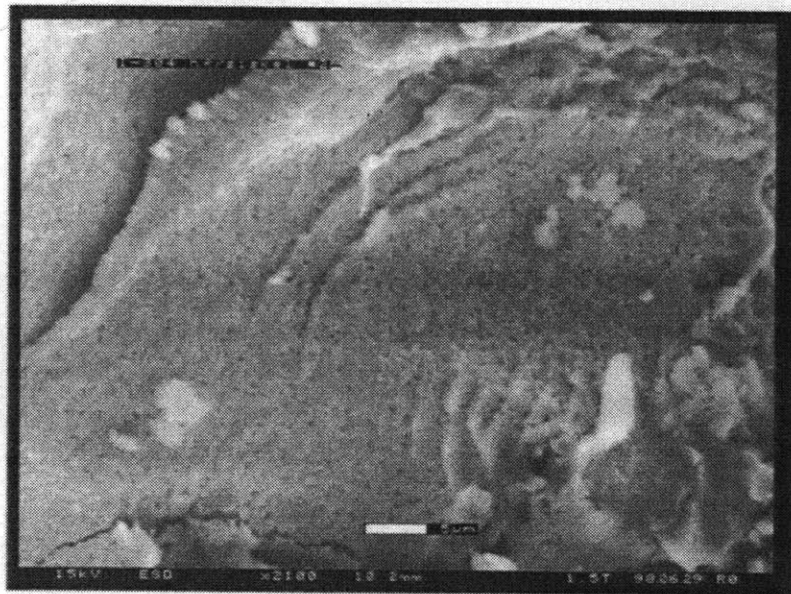
Figure 9.16: XRD of II-74, 1600 °C.
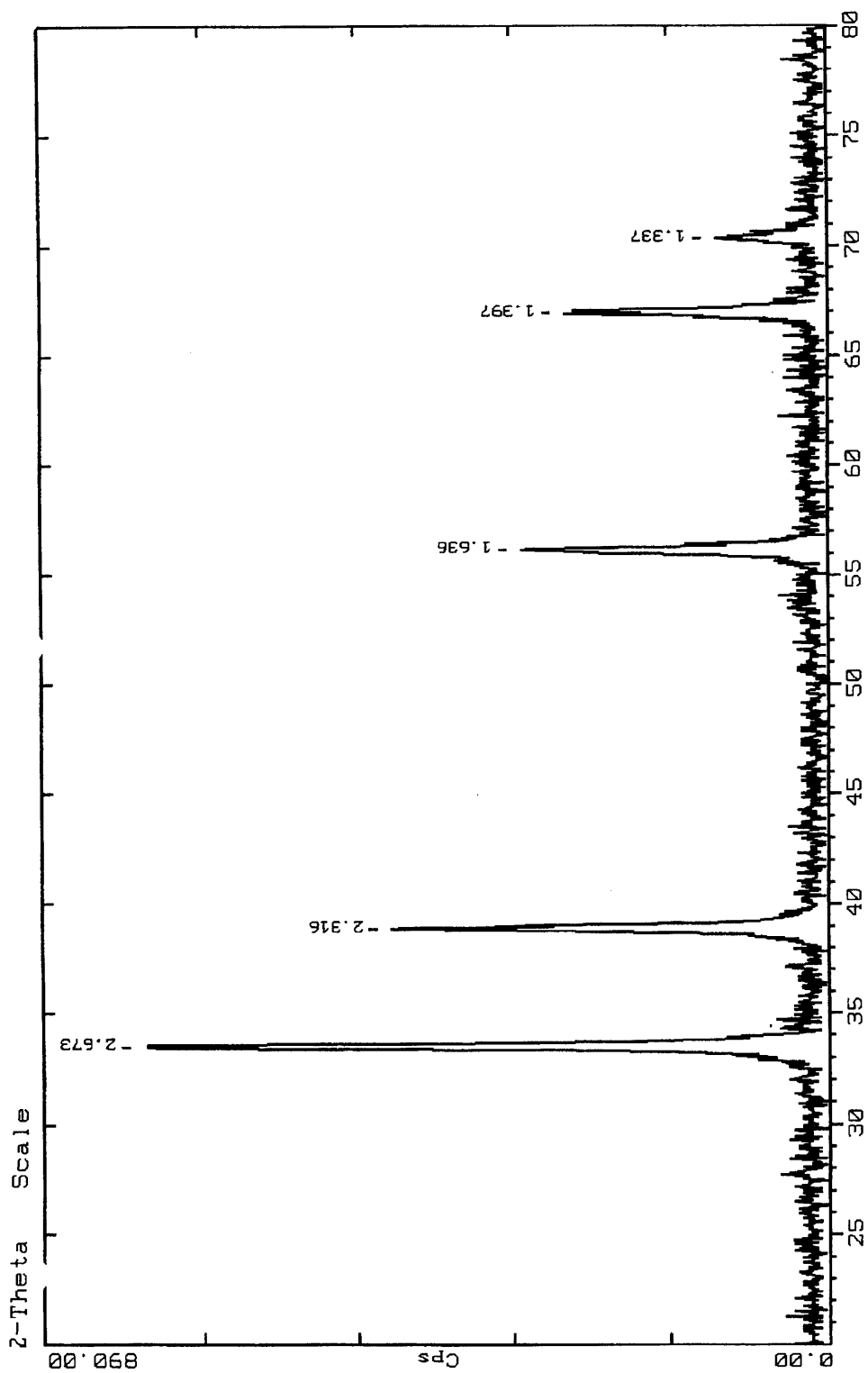
Figure 9.17: ESEM of II-74, 1600 °C. X 850.
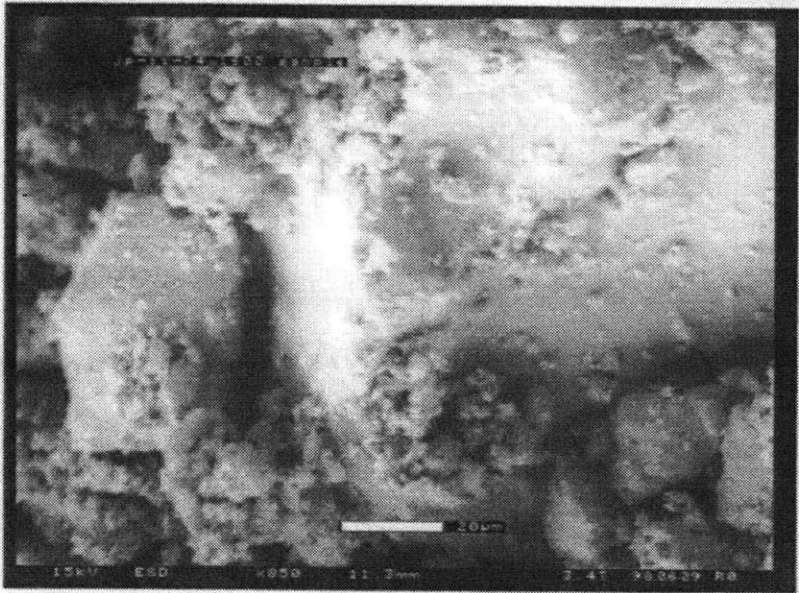
Figure 9.18: XRD of II-81, 2nd pyrolysis. Circles indicate HfC (JCPDS 39-1491), other peaks are HfO$_2$ (JCPDS 31-904)
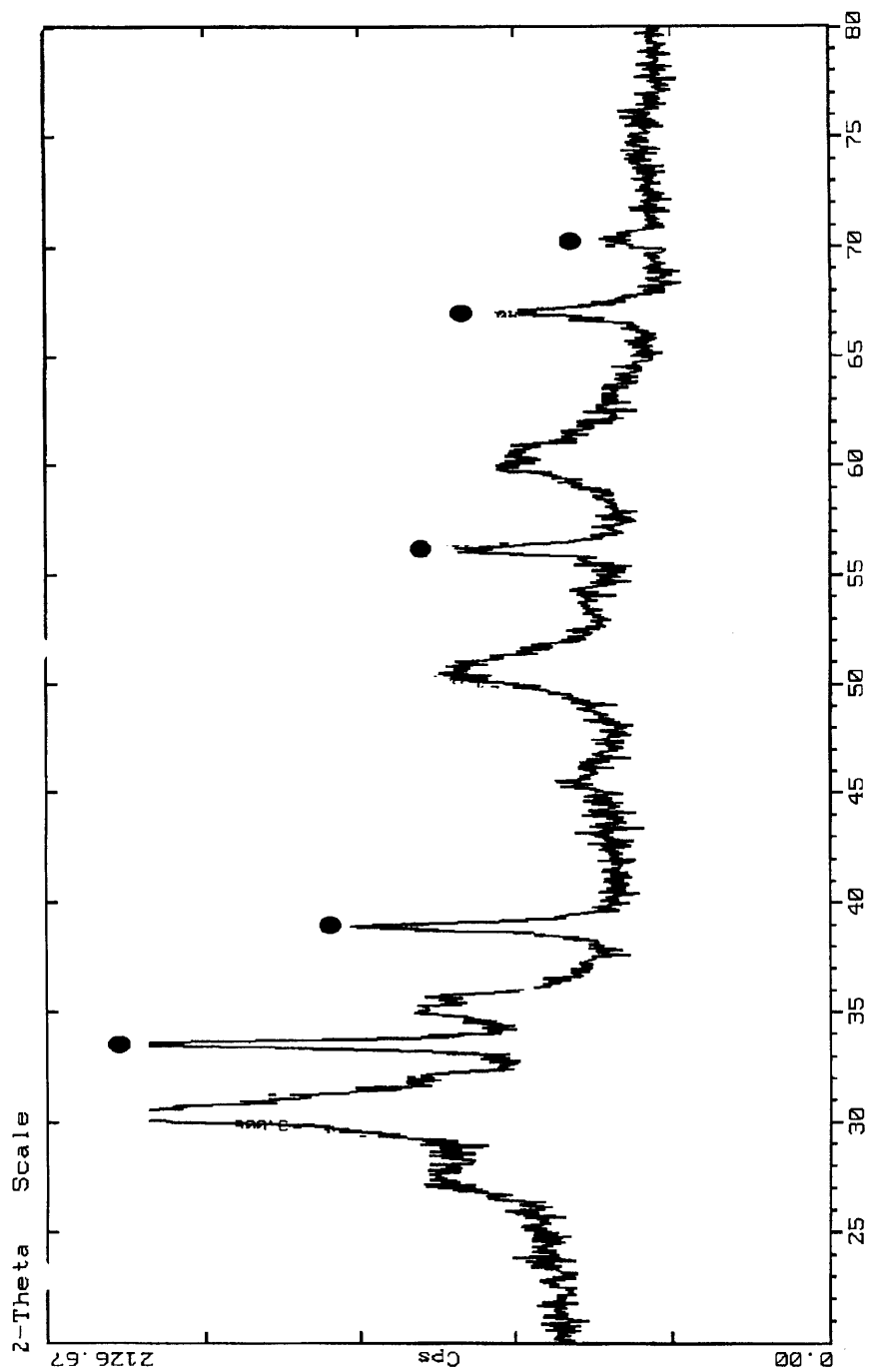
Figure 9.19: ^{1}H NMR of II-81 precursor. See Expt. 13 for peak assignments.
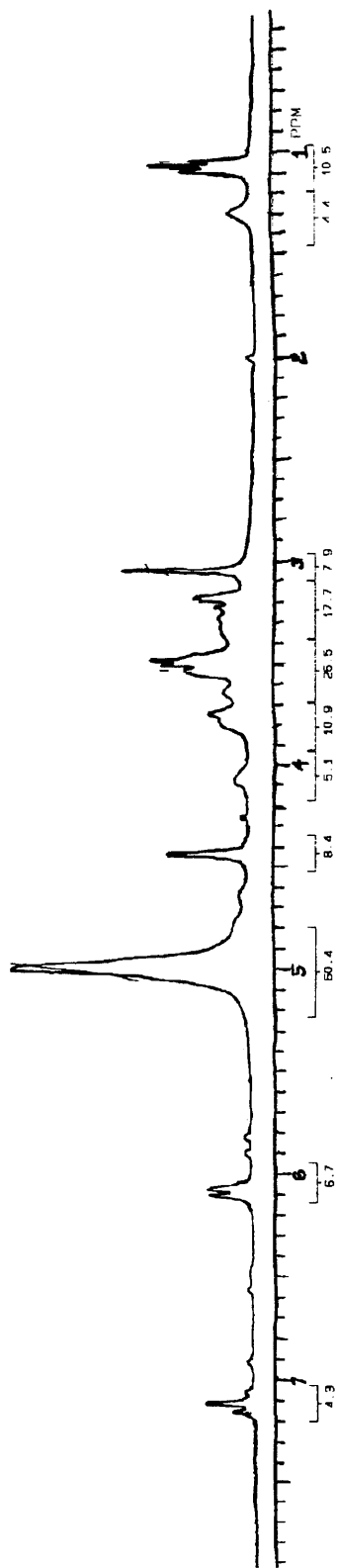
Figure 9.20: ^{1}H NMR of II-99 precursor. See Expt. 14 for peak assignments.
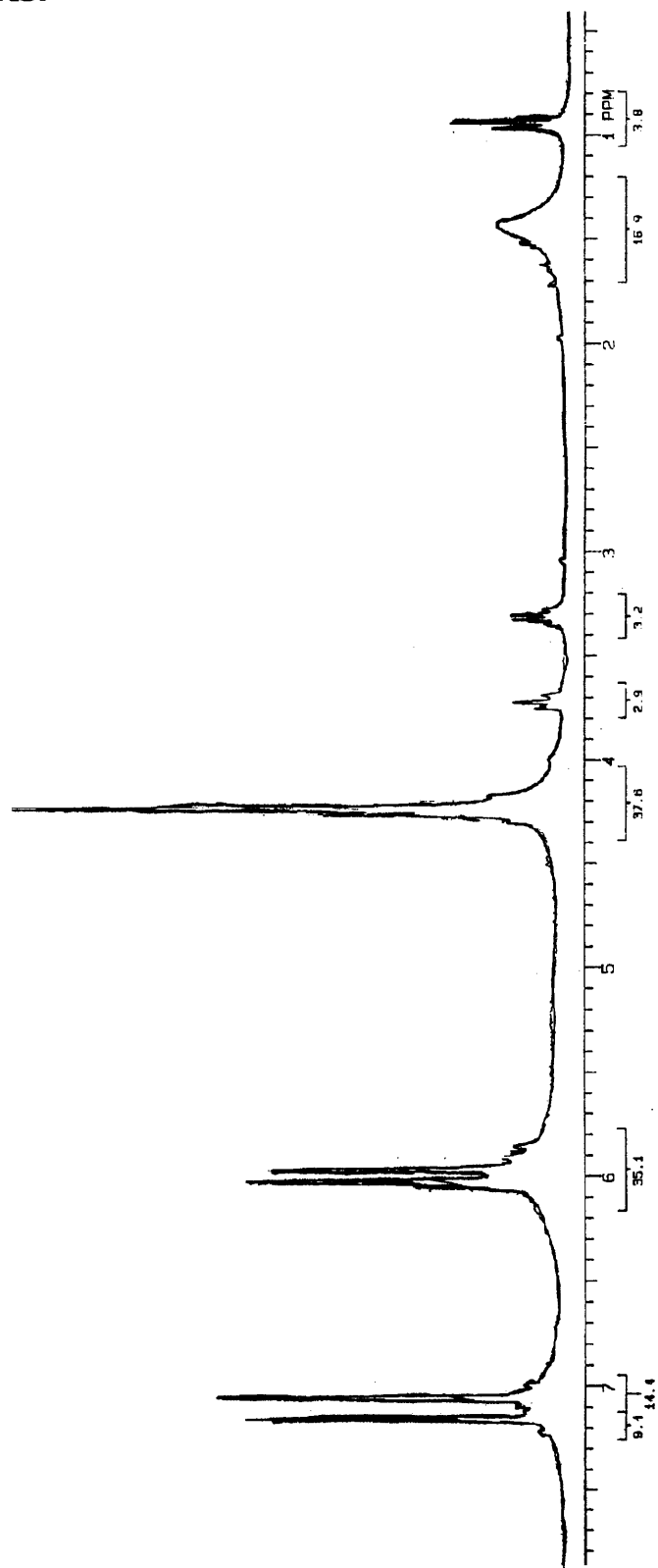
Figure 9.21: XRD of II-106 (TaC). Data has been smoothed.
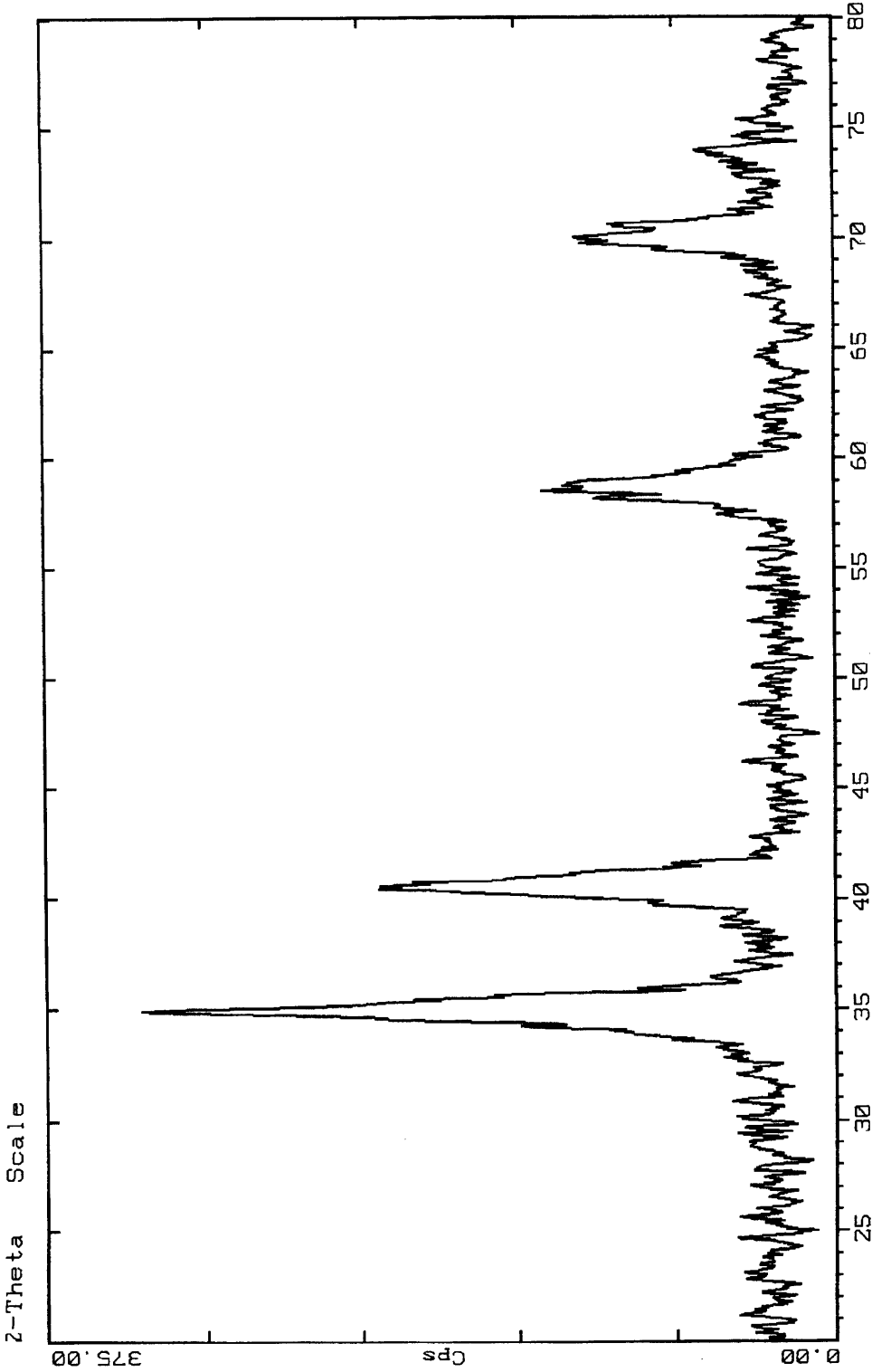
Figure 9.22: XRD of II-106 (HfC).
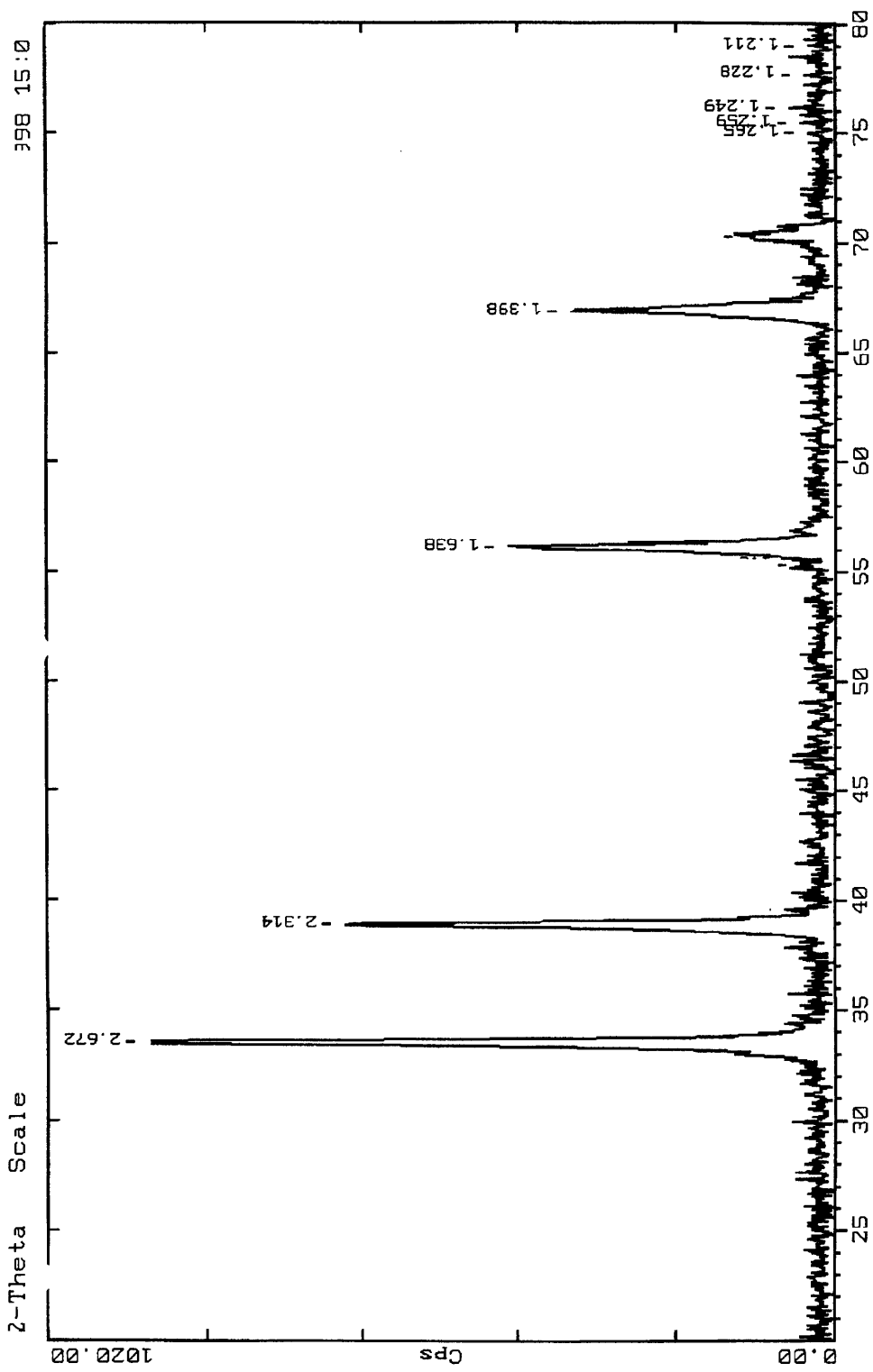
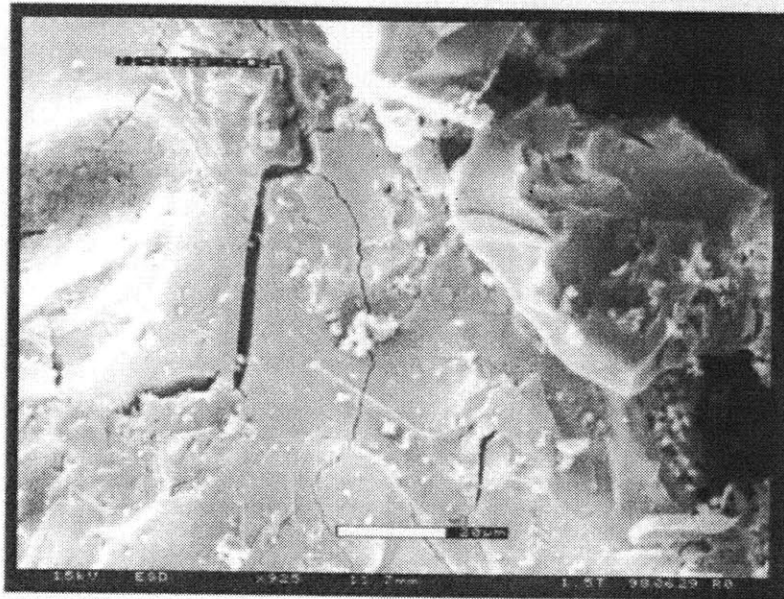Figure 9.23: ESEM of II-106 (HfC). (a) X 580, (b) X 925.
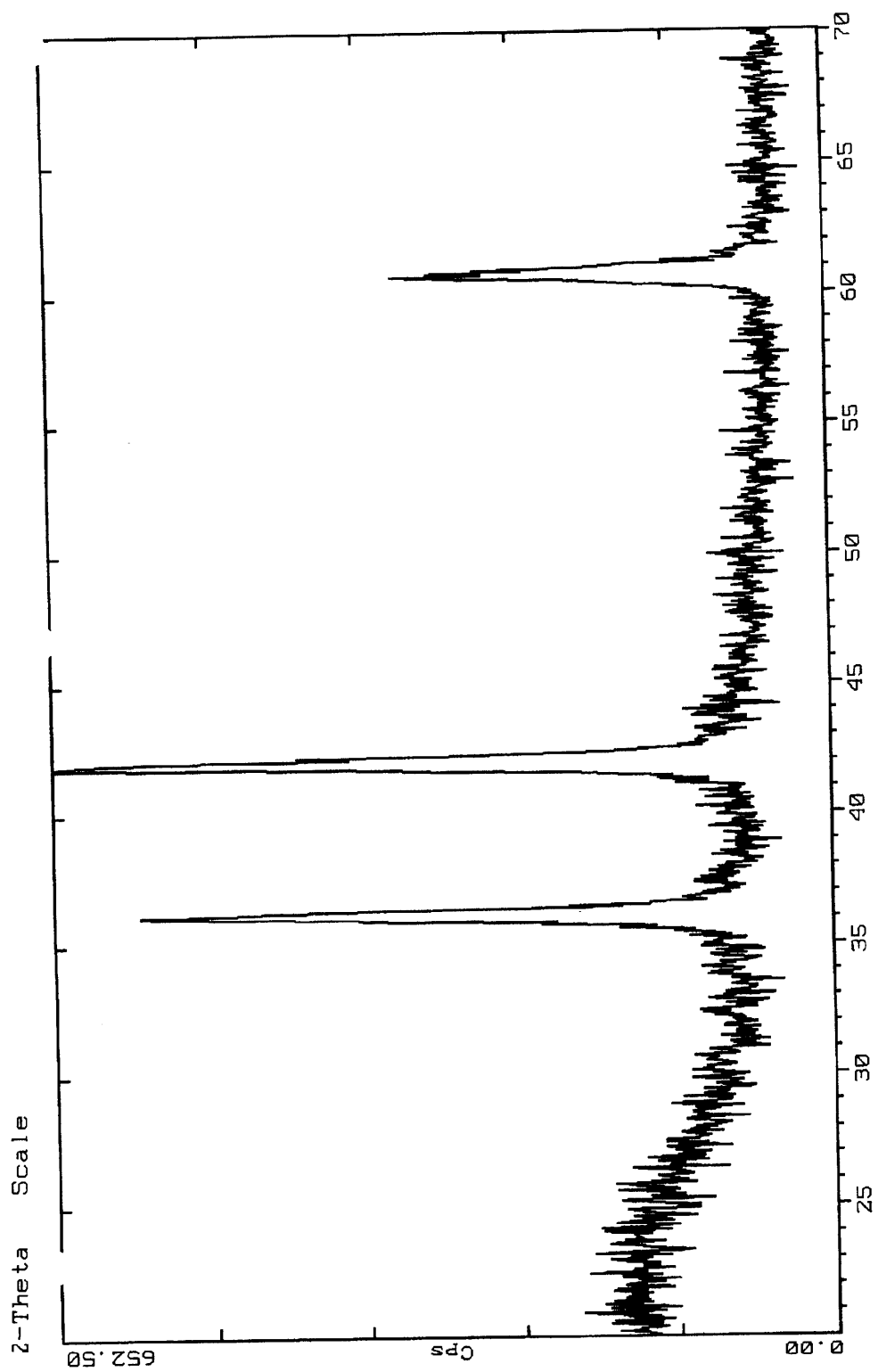
(a)
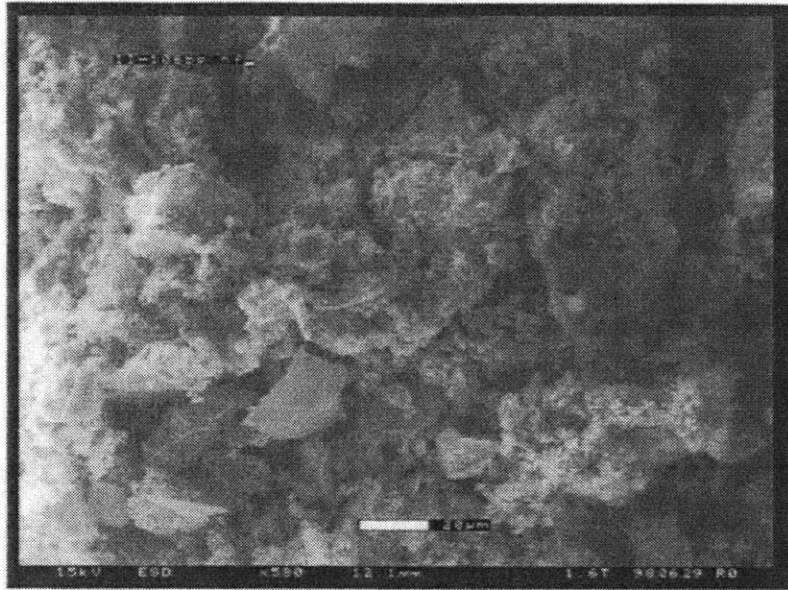
(b)

Figure 9.24: XRD of II-84a (TiC).
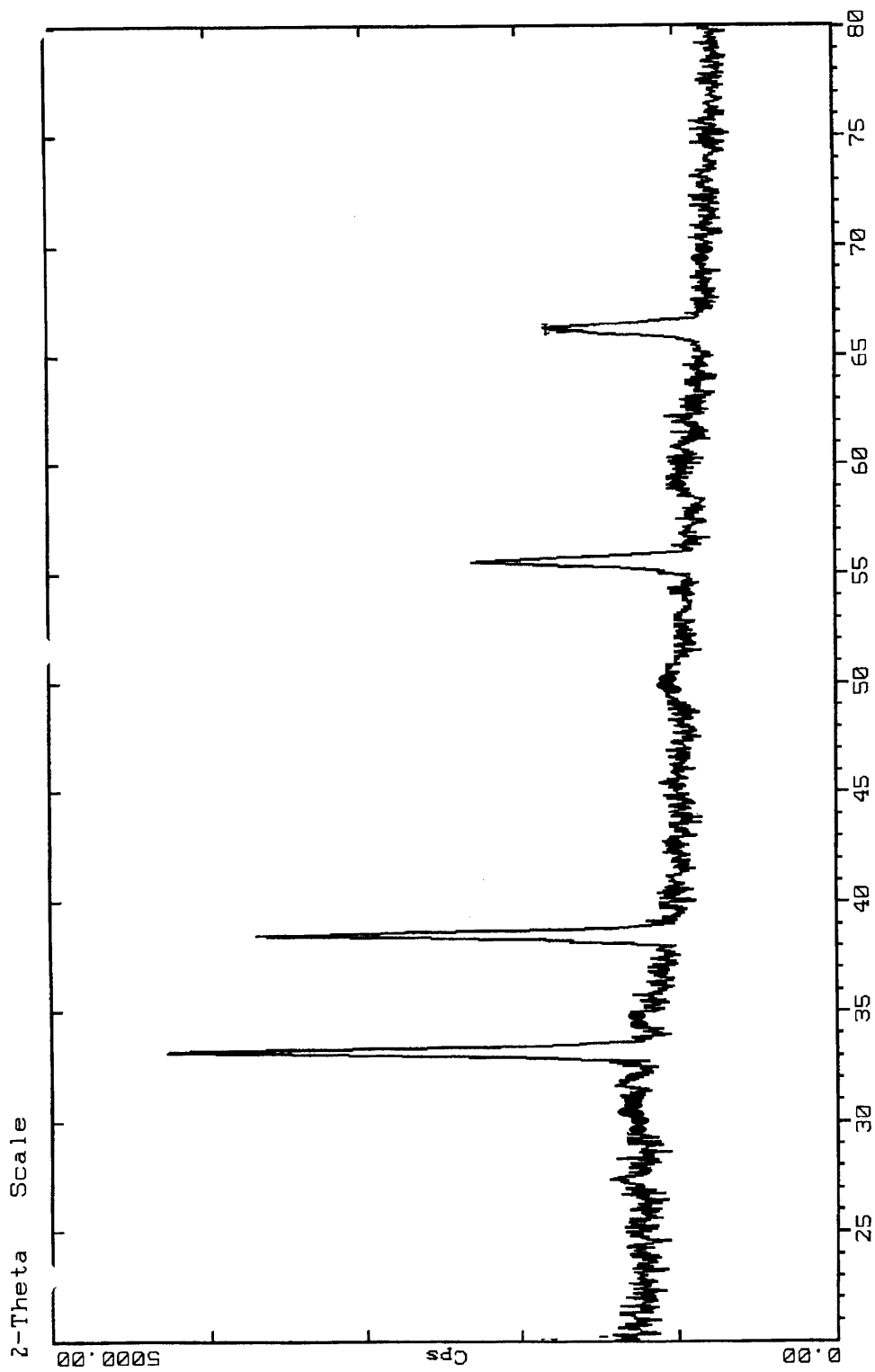
Figure 9.25: XRD of II-84b (ZrC).

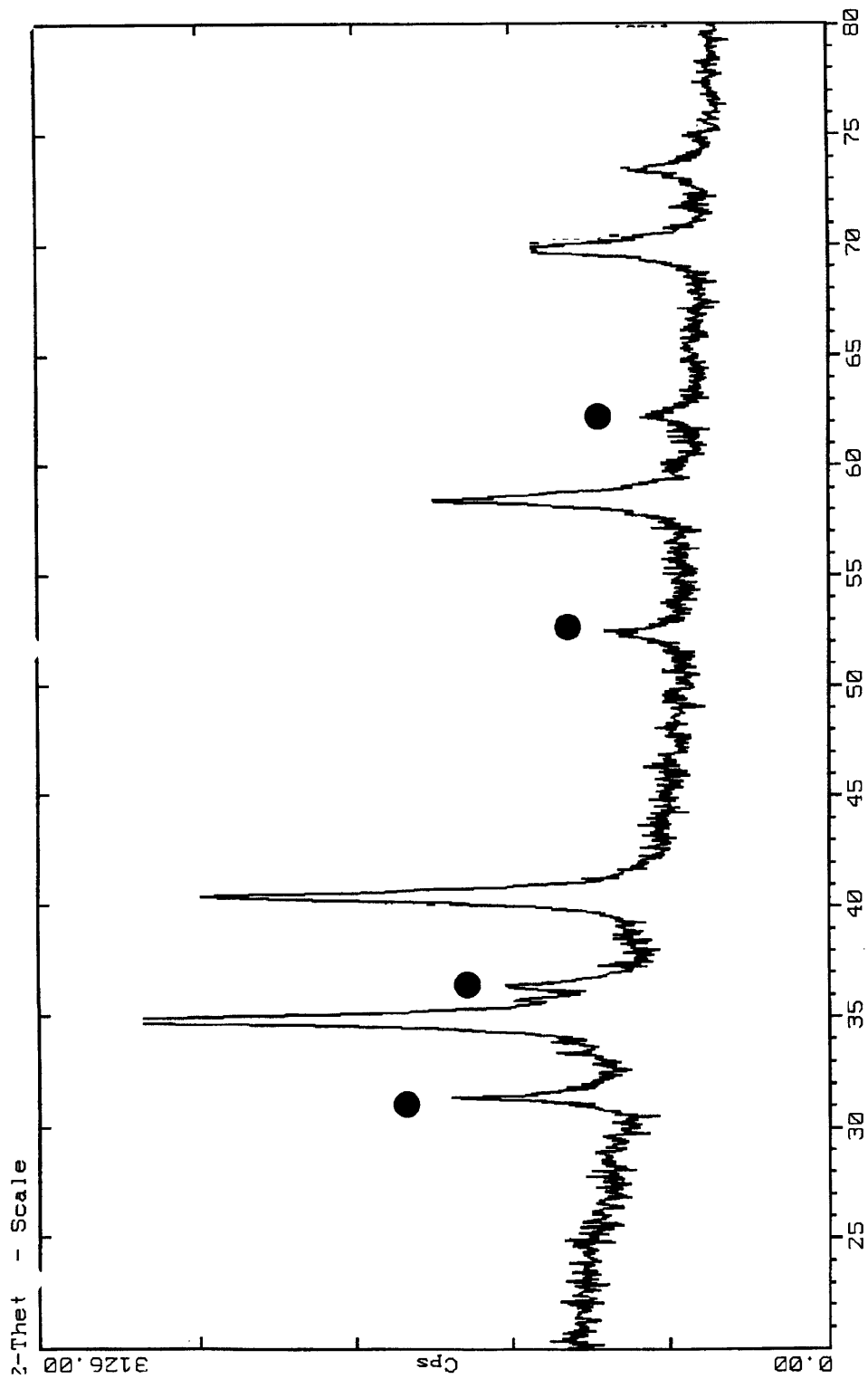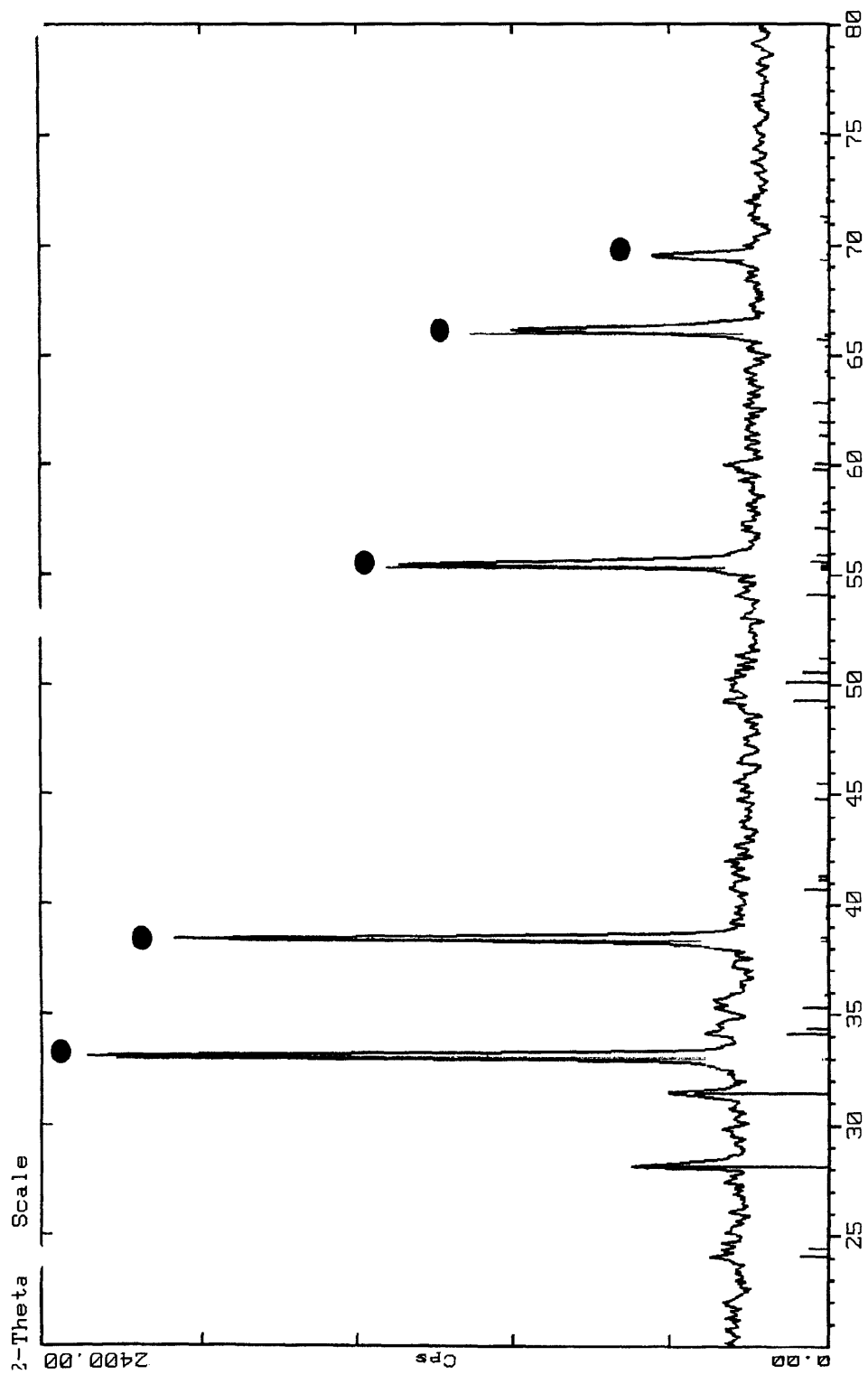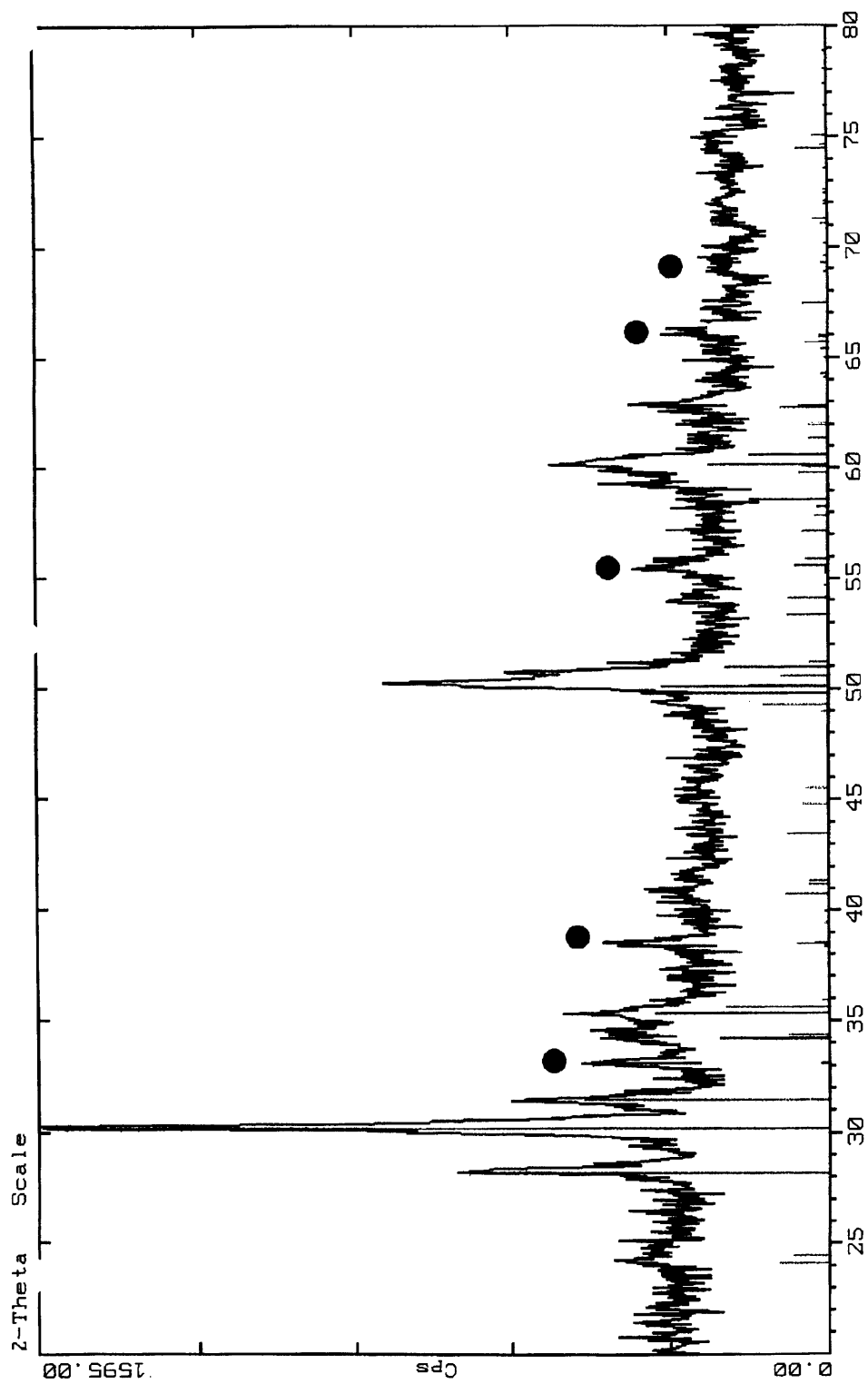**Figure 9.26: XRD of II-84c (NbC).**

Figure 9.27: XRD of II-114a. Circles indicate ZrC, lines indicate ZrO$_2$ (JCPDS 37-1484).

Figure 9.28: XRD of II-116b. Circles indicate ZrC, lines indicate ZrO₂ (JCPDS 37-1484 and 37-1413).

9.5 References

1)Preiss, H.; Meyer, B.; Olschewski, C. *J. Mater. Sci.* 1998, *33*, 713.

2)Thorne, K.; Ting, S. J.; Chu, C. J.; Mackenzie, J. D.; Getman, T. D.; Hawthorne, M. F. *J. Mater. Sci.* 1992, *27*, 4406.

3)Schilling Jr., C. L. *Br. Polymer J.* 1986, *18*, 355.

4)Okamura, K. *Adv. Compos. Mater.* 1999, *8*, 107.

5)Livage, J.; Sanchez, C.; Babonneau, F. in *Chemistry of Advanced Materials: An Overview*; Interrante, L. V. and Hampden-Smith, M. J., Ed.; Wiley-VCH: New York, 1998.

6)Birchall, J. D.; Mockford, M. J.; Stanley, D. R., Imperial Chemical Industries PLC: U.S. Patent No. 4,861,735, 1989.

7)Birchall, J. D.; Mockford, M. J.; Stanley, D. R. Imperial Chemical Industries PLC: U.S. Patent No. 4,950,626, 1990.

8)Birchall, J. D.; Mockford, M. J.; Stanley, D. R., Imperial Chemical Industries PLC: U.S. Patent No. 4,996,174, 1991.

9)Birchall, J. D.; Mockford, M. J.; Stanley, D. R., Imperial Chemical Industries PLC: U.S. Patent No. 5,120,689, 1992.

10)Stanley, D. R.; Birchall, J. D.; Hyland, J. N. K.; Thomas, L.; Hodgetts, K. *J. Mater. Chem.* 1992, *2*, 149.

11)Birchall, J. D.; Mockford, M. J.; Stanley, D. R.; Asher, P. M.; McCarthy, W. R., Imperial Chemical Industries PLC: U.S. Patent No. 5,017,525, 1991.

12)Krumbe, W.; B., L.; Franz, G., Bayer Aktiongeschellschaft: U.S. Patent No. 4,948,762, 1990.

13)Jiang, Z.; Rhine, W. E. *Chem. Mater.* 1991, *3*, 1132.

14)Jiang, Z.; Rhine, W. E. *Mat. Res. Soc. Symp. Proc,* **1992**, *249*, 45.

15)Jiang, Z.; Rhine, W. E. *Mat. Res. Soc. Symp. Proc,* **1992**, *249*, 25.

16)Preiss, H.; Meyer, B.; Olschewski, C. *J. Mater. Sci.* 1998, *33*, 713.

17)Preiss, H.; Schultze, D.; Klobes, P. *J. Eur. Ceram. Soc.* 1997, *17*, 1423.

18)Kurokawa, Y.; Ota, H.; Sato, T. *J. Mater. Sci. Lett.* 1994, *13*, 516.

19)Preiss, H.; Schultze, D.; Schierhorn, E. *J. Mater. Sci.* 1998, *33*, 4687.

20)Narisawa, M.; Kida, S.; Simoo, T.; Okamura, K.; Kurachi, Y. *J. Sol-Gel Sci. Tech.* 1995, *4*, 31.

21)Ting, S. J.; Chu, C. J.; Limatta, E.; Mackenzie, J. D.; Getman, T. D.; Hawthorne, M. F. *Mat. Res. Soc. Symp. Proc.*, **1990**, *180*, 457.

22)Mark, H. F.; Korschwitz, J. I. *Encyclopedia of Polymer Science and Engineering*; 2nd ed.; Wiley: New York, 1985; Vol. 7.

23)Laszlo-Hedvig, Z.; Szesztay, M. in *Polymeric Materials Encyclopedia*; Salamone, J. C., Ed.; CRC Press: New York, 1996; Vol. 4, pp 2691-2695.

24)Bradley, D. C.; Wardlaw, W.; Whitley, A. *J. Chem. Soc.* 1955, 726.

25)Thomas, I. M. *Can. J. Chem.* 1961, *39*, 1386.

26)Chamberlain, L. R.; Rothwell, I. P.; Huffman, J. C. *Inorg. Chem.* 1984, *23*, 2575.

27)Anand, S. K.; Singh, J. J.; Multani, R. K.; Jain, B. D. *Isr. J. Chem.* 1969, *7*, 171.

28)Anand, S. K.; Singh, J. J.; Multani, R. K.; Jain, B. D. *Bull. Chem. Soc. Jpn.* 1969, *42*, 554.

29)Bradley, D. C.; Mehrotra, R. C.; Gaur, D. P. *Metal Alkoxides*; Academic Press: New York, 1978.

30)Bradley, D. C.; Mehrotra, R. C.; Wardlaw, W. *J. Chem. Soc.* 1953, 1634.

31) Yoshinaga, I.; Yamada, N.; Katayama, S. *Mat. Res. Soc. Symp. Proc.,* **1996**; *435*, 481.

32) Campero, A.; Soto, A. M.; Jaquet, J.; Sanchez, C. *Mat. Res. Soc. Symp. Proc.,* **1996**; *435*, 527.

33) Storms, E. K. *The Refractory Carbides*; Academic Press: New York, 1967.

Chapter Ten:

Assorted Projects in Functionalizing Dendrimers

10.1 Introduction and Background on Dendrimers

Dendrimers are a unique type of "starburst" polymer having a regular generationally branched three-dimensional structure and a uniform molecular weight.[1-3] (Figure 10.1) The number of branches grows exponentially with the generation number n ($n=0$ is the core molecule, $n=1$ is the 1st layer outside the core, etc.). These polymers have a high degree of symmetry and a large number of functionalizable surface sites per polymer unit, and therefore have captured the imaginations of chemists and materials scientists. Some of the applications proposed include drug delivery,[4,5] vehicles for diagnostic imaging and radiotherapy agents,[6] building blocks for nanostructured materials,[7] supports for liquid crystals,[8], redox-active materials,[9] and catalyst supports.[10,11] Dendrimers have also been examined as "hosts," trapping "guest" molecules in the internal cavities.[12]

Dendrimers may be constructed either in a divergent manner, starting from the core molecule and building outward simultaneously on all (nonprotected) arms, or convergently, constructing the dendrimer from the outside inward. (Figure 10.2) In either case, the regularity of the structure depends on having quantitative yield and full selectivity at each generation's growth step.   Where for small molecule chemistry a 99% conversion means that one out of a hundred molecules is unreacted and must be separated from the product, for dendrimers this means that one out of a hundred *arms* – of which there may be many on a single dendrimer unit – is unreacted. However, this erroneous arm is attached to the rest of

the dendrimer unit, and the property differences between a dendrimer unit with one or two errors and a unit with no errors may be insufficient to effect separation. Random distribution of the errors among all the available arms means that a high percentage of the dendrimer units will have at least one error. Moreover, this effect is multiplied by the number of generations in the dendrimer unit, particularly as the crowding of arms sterically hinders access of reactants to the necessary sites. While for small inclusion errors (e.g. one or more arms has a $-SiMe_3$ termination rather than a -$SnBu_2H$ termination) this may be irrelevant, in other cases unreacted sites may make available side reactions that greatly affect the bulk properties of the dendrimer collection (e.g. two units have an unreacted -SiCl termination which become hydrolyzed and an -Si-O-Si- bond between the units forms, effectively doubling the new unit's molecular weight ruining the product monodispersity).

A number of dendrimer classes have been synthesized, including the poly(amidoamine) (PAMAM) "starburst" dendrimers reported by Tomalia,[1] now available commercially, hydrocarbon dendrimers (iptycenes),[13] polyethers,[14] phosphorus-based dendrimers, poly(siloxanes), and carbosilane dendrimers, to name a few.[3] The carbosilane dendrimers, in particular, have been sucessfully synthesized using hydrosilylation reactions with substituted chlorosilanes followed by reduction of the Si-Cl bond with $LiAlH_4$, in alternation with alkenylations using Grignard reagents.[15-19] Surface functionalization may be carried out, in all cases, by reacting the final generation of arms with the functional molecule – for instance, a cyclopentadienyl ring may be placed on each arm by reacting lithium cyclopentadienide with the SiCl-

terminated arms of a carbosilane dendrimer. The carbosilane dendrimers, in particular, have the benefit of a relatively chemically inert backbone, making them useful in a number of applications.

The experiments discussed in this Chapter describe some very brief work done to continue the work begun by a previous graduate student, Shane Krska. The interested reader is referred to his thesis for a more expansive treatment.[20] In those studies, dendrimers terminated with (chloromethyl)silyl groups were synthesized and used as nucleophiles, by forming lithium or magnesium reagents, and as electrophiles, participating in a number of reactions.

One of the principal tools used in synthesizing these dendrimers is the hydrosilylation reaction, in which the Si-H bond of an alkylsilane is added across the double bond of an alkene. Platinum-compounds, particularly chloroplatinic acid (Speier's catalyst, $H_2PtCl_6 \cdot 6H_2O$) and Karstedt catalyst (a platinum complex of $(ViMe_2Si)_2O$) catalyze the reaction, and some are activated by oxygen.[21] The hydrosilylation reaction also takes place under free-radical conditions, initated by UV radiation and peroxides.[22] Facilitated by the presence of electronegative groups on Si, the reaction is somewhat regiospecific, with the proton of the Si-H bond usually going to the olefinic carbon with the lower electron density. For $Si-CH_2=CH_2$ (Si-Vi) groups, this is generally the carbon β to the silicon, but α substitution does sometimes occur. (Figure 10.3) Formation of the α isomer is suppressed in the presence of bulky coordinating groups, including tetrahydrofuran solvent and triphenylphosphine.[23]

654

The dendrimers used in the work described in this chapter were built up by reacting $HSi(Me)_2CH_2Cl$ with tetravinylsilane; the resulting 4-arm dendrimer could be freed readily of any α isomer by careful recrystallization in ethanol. Later-generation dendrimers were constructed by adding a chlorosilane onto the tetravinylsilane core via a hydrosilylation reaction, then substituting at the Si-Cl bond with vinyl Grignard (vinylmagnesium bromide), and repeating the hydrosilylation step to continue building. Side reactions included incomplete hydrosilylation (depending on steric crowding), coupling of dendrimer units due to hydrolysis of the Si-Cl bonds by adventitious moisture and α substitution reactions.

The (chloromethyl)silyl group is known for its ready formation of Grignard reagents due to what has become known as the α-silicon effect,[24,25] and Krska used this to place a number of substituents onto the dendrimer surfaces, including organotin, -mercury, -platinum, and boron groups. However, he found that this was only do-able for first-generation (4-arm dendrimers), due to the slow (heating times over 1 week) and often incomplete reaction of the dendrimer with the magnesium metal to form the Grignard reagent.[20] In this Chapter we tested a number of reaction conditions that we hoped would improve and simplify the nucleophilic reaction chemistry of the (chloromethyl)silyl-terminated dendrimers.
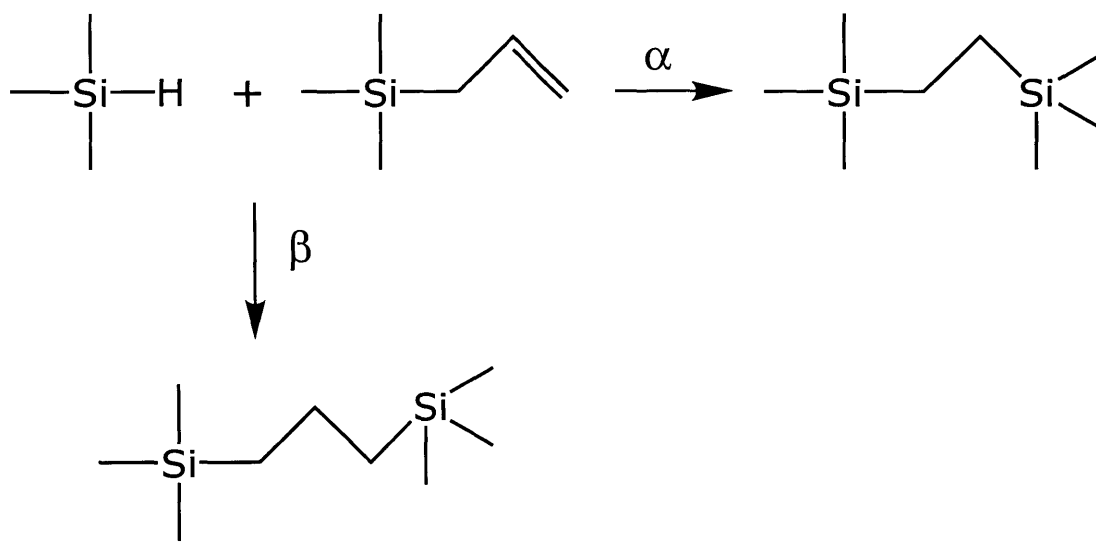
Figure 10.1: Schematic of a dendrimer.
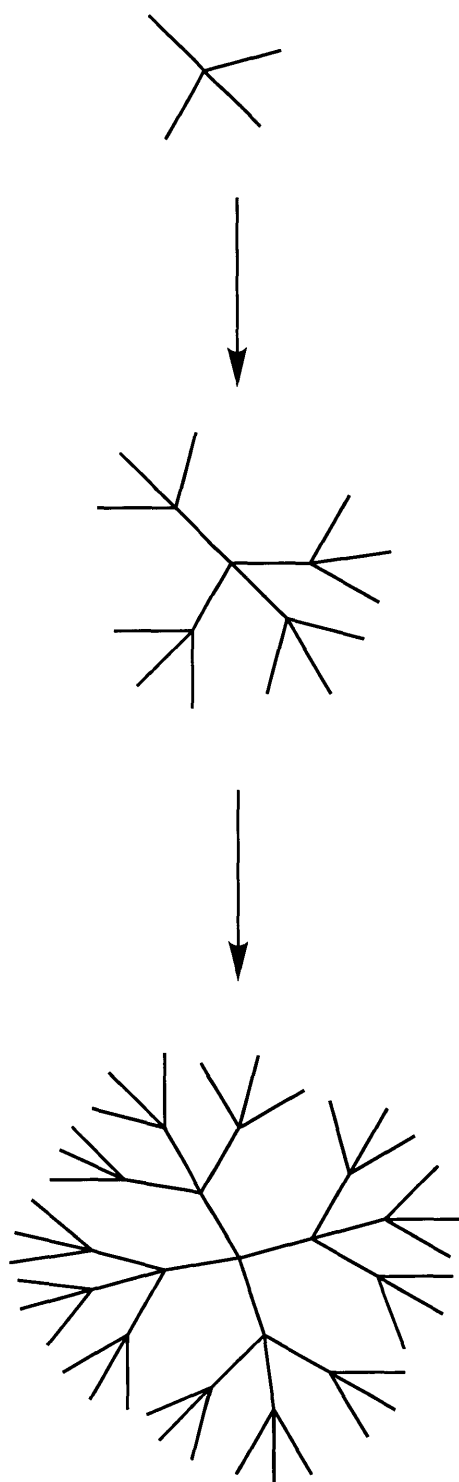
Figure 10.2: Convergent synthesis (a) *versus* divergent synthesis (b) of dendrimers.
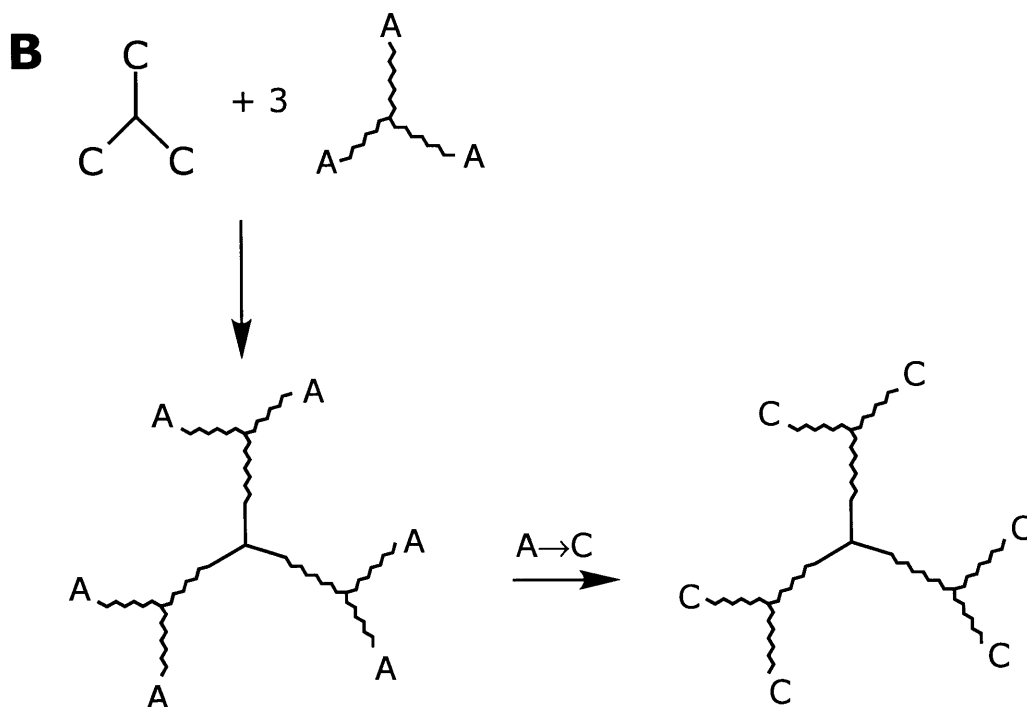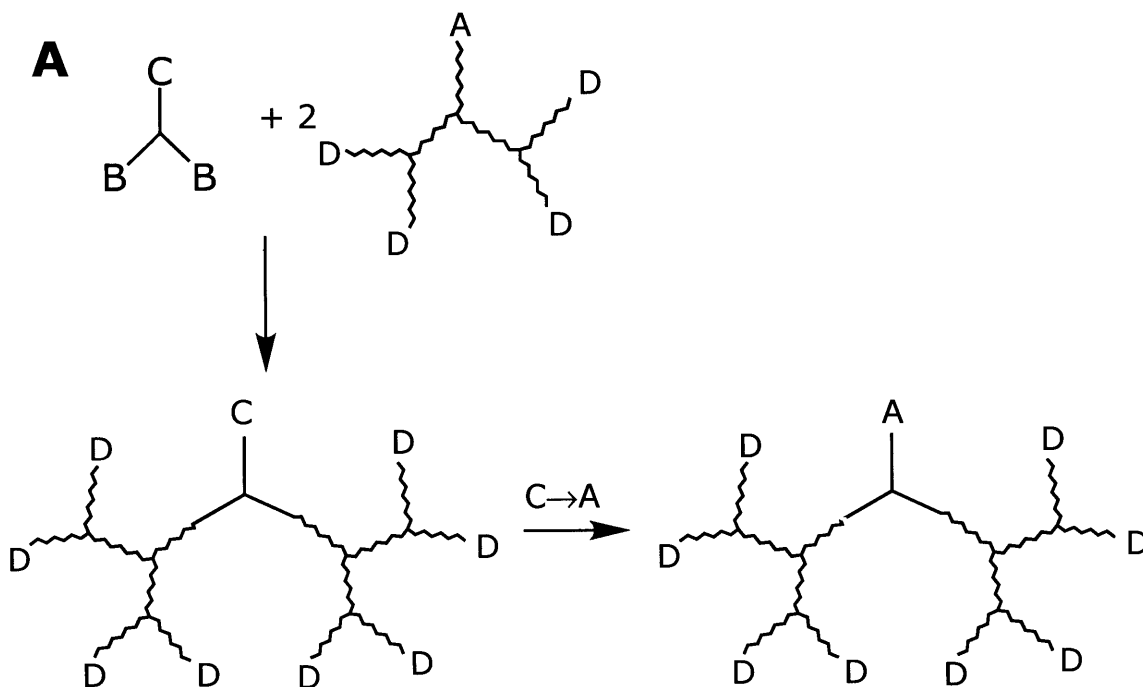
Figure 10.3: Structure of α- and β- substituted Si(CH₂CH₂Si(Me)₂CH₂Cl).

10.2 Results and Discussion

10.2.1 Grignard Reactions to Functionalize Dendrimers

The (chloromethyl)silyl group is reputed to form Grignard reagents easily, but on the dendrimers complete reaction of the arms with magnesium turnings in dry THF was sluggish, requiring a week's reflux and repeated addition of 1,2-dibromoethane. The reaction was monitored by hydrolyzing aliquots of the reaction mixture and looking for the disappearance of the chloromethyl proton signal near 2.1 ppm in the NMR spectra. The usual pattern was for the disappearance of this peak to be rapid at first, but then to "stall" after approximately 24 h of reaction time. Later reaction with a organometal halide (in these experiments, Me_2SiHCl and R_3SnCl) gave, of course, incomplete substitution. Often hydrolysis by adventitious water (glassware was dried thoroughly, and THF freshly distilled from sodium benzophenone was used) or from cleavage of the THF itself led to a high proportion of the dendrimer arms' being terminated by $-SiMe_3$ groups. Triphenylmethyl-magnesium bromide is reported to cleave tetrahydrofuran, making triphenylmethane within 24 h at room temperature or 5 h at reflux.[26] Several different approaches were taken to improve this situation.

Reversed addition order (Barbier reaction), so that the $ClSiMe_2H$ would be available immediately for reaction with magnesium-substituted arms, was not helpful; the complete reaction of chloromethyl groups occurred after several days' reflux,

659

but the product was highly contaminated with -SiMe$_3$ groups. Activation of the magnesium using 1,2-dibromoethane, usually a superior Grignard initiator, was unhelpful, even when larger quantities were used.[27] 1,2-dibromoethane reacts with the magnesium to give 2-bromoethylmagnesium bromide, which eliminates ethylene to give magnesium bromide, which dissolves away to provide a clean and active magnesium metal surface.

Finely-divided (Rieke) magnesium was tried. This form of magnesium is prepared by reduction of anhydrous magnesium chloride with potassium in refluxing THF, and is made even more active by the presence of potassium iodide.[28,29] Despite this, the reaction in one case did not go to completion, and in a second trial consumed all the chloromethyl groups but the product was contaminated with SiMe$_3$ groups.

The iodomethyl-terminated dendrimers were used in the hope of getting more facile formation of the Grignard reagent. The substitution was carried out by taking advantage of the solubility difference between NaI and NaCl in acetone.[30] A similar conversion may have been possible to obtain the bromomethyl-terminated dendrimers, but this was not tried.[31] The consumption of the iodomethyl groups was complete after a 3-h reflux, but the product was again contaminated with trimethylsilyl-terminated arms.

Small quantities of cyanide ions are catalytically active for the reaction between Grignard reagents and chlorosilanes,[32] and as that latter reaction was also suspected as a contributor to the contamination of the product, copper cyanide was added in one

trial. However, reaction of the chloromethyl groups was found to be incomplete.

The high-boiling dibutyl ether was used as a solvent in one trial, both to increase the formation of the Grignard reagent,[27] and to remove the possibility of THF cleavage as a source of the -SiMe$_3$ groups. However, a white precipitate, presumably Grignard reagent, formed during the reaction, and after quenching with Me$_2$SiHCl it was found that the consumption of the chloromethyl groups had not been complete. Diglyme and dimethoxyethane should have been tried as well, but unfortunately they were not.

The organolithium reagent was briefly examined as an alternative to the Grignard reagent for effecting the reaction. Finely-divided lithium powder, handled under argon, was used in hexane, first at low temperature (-78 °C), then with warming, and finally, with sonication. The final product contained unreacted chloromethyl groups and some -SiMe$_3$ groups, which probably came about through cleavage of the THF added[33] (in an attempt to coax the reaction to completion) by what organolithium-substituted arms had formed. The yellowing of the solution on addition of the THF may have indicated that cleavage. It is possible that the lithium used (99.9% pure) failed to react because of insufficient sodium content. It has been reported that sodium-free lithium is unreactive towards organic halides, while 1-2% Na-containing lithium is optimum.[33] An attempt to use *tert*-butyllithium to metallate the dendrimer arms, despite the use of the more reactive iodomethyl dendrimer, failed to give any consumption of the iodomethyl group. This was done in pentane at low temperature (-30 °C maximum) over a short time period, the recommended procedure for avoiding

side reactions,[33] but the poor solubility of the dendrimer under these conditions may have been a hindrance.

The product, pure to elemental analysis but having a small -SiMe$_3$ peak, was finally produced using magnesium metal which had been activated by reaction with dilute hydrochloric acid, followed by grinding in a mortar under argon.[34] This reaction was assisted by 1,2-dibromoethane and involved reflux overnight. The success, however, did not prove transferrable to the addition of -SnR$_3$ (R= Me, Bu) to the dendrimer.

The notable thing about these reactions is the unexpected difficulty in getting complete reaction of the dendrimer arms to form the Grignard reagent. The (chloromethyl)silyl group is reportedly a facile former of organomagnesium compounds, but in this case the reaction was sluggish at best. Formation of organomagnesium halides is not a quantitative reaction under the best of circumstances. However, the effect of a small impurity is multiplied in the case of the dendrimers (*vide supra*). By-products, particularly those formed by hydrogen abstraction from the solvent, are common.[34] Trace quantities of water or oxygen often may assist in the formation of the organomagnesium halide,[34] but in these syntheses, great care was taken to use thoroughly dry glassware and solvent in order to avoid the formation of the -SiMe$_3$ group via hydrolysis of the Grignard reagent.

Finally, steric issues may have played a role in the sluggish reaction of the dendrimers. In order to form an organomagnesium complex, the alkyl halide part of the molecule must adsorb onto the magnesium metal surface, undergo reaction, then leave. For small molecules, the number of available surface sites simultaneously

reachable by the molecules is large, but for the dendrimer, while one arm is adsorbed, the other arms are sticking out in the direction opposite the metal surface. This is particularly the case for the 4-arm dendrimer, where the tetrahedral shape at the core Si atom still controls the dendrimer structure; but even for higher-generation dendrimers, there are still many arms pointing opposite the reactive metal surface. The dendrimer units, due to their steric bulk, also will tend to block one another from accessing the metal surface: one can imagine packing ball bearings onto a tabletop, and compare the surface area of the ball bearings in contact with the table with the contact area that could be reached by, say, pencil-shaped objects. This treatment, of course, assumes that the dendrimers are mutually opaque, using a term from the discussion found in Chapter Six of this Thesis. Certainly this becomes the case when the charge separation in the R-Mg-X species increases the potential for electrostatic repulsions.

A further steric concern that would tend to limit the complete conversion of the dendrimer arms to organomagnesium complexes involves the demands of the organomagnesium complex itself. In addition to the metal itself, the Grignard reagent brings with it two coordinated solvent molecules.[35] These may further block unreacted arms from having access to the magnesium metal surface.

The same reactions were examined to put a tin-containing group on the dendrimer surfaces. Use of the Grignard reaction consumed the chloromethyl groups, if sluggishly, but there were -SiMe$_3$ decomposition peaks in the product NMR spectra. Hydrosilylation of trialkyl- and triphenylvinyltin onto an Si-H

terminated dendrimer was similarly unsuccessful, with some evidence (*viz.* the shiny mirror deposited in the sealed-tube reactions) that one of the metals was completely reduced. Use of radical initiator AIBN gave no better result, either in the presence of or absent the platinum hydrosilylation catalyst. Radical initiators have had some success in effecting hydrosilylation and hydrostannylation reactions.[36,37] However, the compound which was reasonably pure according to the ^{1}H NMR spectrum became milky on standing at room temperature in light and air, and subsequent ^{1}H NMR spectrum suggested that some decomposition had taken place, despite the presumed stability of the Si-CH$_2$-Sn bond.

10.2.2 Dendrimeric of Ziegler-Natta Catalysts

Another functionality which may be added to the dendrimer, and which may take advantage of its large number of active sites available, is the alkene polymerization (*i.e.*, Ziegler-Natta[38]) catalyst. Attachment of zirconium-based catalysts, e.g. zirconocene and its relatives, has been effected via the attachment of a Si-vinyl group to the cyclopentadienyl ring of the catalyst, followed by a hydrosilylation reaction in which the catalyst is attached to an Si-H terminated dendrimer. Research into this has been done by R. Wyra and B. Lungwitz under the direction of Professor D. Seyferth.[10,11] While some of their work was reproduced by the author of this thesis, it will not be reported here.

Literature evidence suggested that the use of indenyl and fluorenyl (Fl) ligands on the zirconium catalyst would lead to greater activity and stereoselectivity. While nonbridged and *meso-ansa* metallocenes are not stereoselective and are relatively inactive as catalysts, bridged metallocenes, with their rigidly-held bulky and electron-donating ligands, are both active and stereoselective.[39] In particular, silylene-bridged systems with one fluorene ring and one cyclopentadiene ring are extremely active, although they gave nonstereospecific propylene polymerization.[40] However, *ansa-*cyclopentadienyl fluorenyl complexes are efficient catalysts for syndiospecific polymerization of propylene.[41] In addition to the role of the bridging, the special nature of the bonding in fluorenyl ligands is key to the activity of catalysts containing them: there is facile ring slippage ($\eta^5 \rightarrow \eta^3 \rightarrow \eta^1$ bonding mode change), opening up new coordination sites during the catalytic cycle.[42]

We looked into the attachment of fluorenylzirconium catalysts to dendrimers. While we were able to synthesize the two ligands, ViSiMe$_2$Fl and the bridged ViSiMeFl$_2$ (Figures 10.4), we were never able to obtain a pure sample of the zirconium catalysts ViSiMe$_2$Fl(Cp)ZrCl$_2$ and ViSiMeFl$_2$ZrCl$_2$, respectively (Figures 10.5), for attachment to the dendrimer. Synthesis of the ligands was dogged by incomplete deprotonation of the fluorene starting material, and the difficulty of separating the resulting unreacted fluorene from the product. Cleavage of the THF solvent by the fluorenyllithium may explain some of the many byproducts that needed to be separated from the main product by careful chromatography and recrystallization.[26]

The zirconium catalysts with larger substituents are notoriously difficult to isolate.[42] This is partially due to the low solubilities of the compounds, particularly those with highly annelated ligands. Some complexes are known to decompose in THF and ether, and even in chlorinated solvents such as chloroform and dichloromethane.[43,44] The decomposition of *ansa*-bis(fluorenyl)zirconium dichlorides, and their low solubility, makes it difficult to obtain NMR spectra for these compounds; one solution that has been used is to substitute out the chloride ligands using methyllithium.[45] Steric crowding, which in Fl_2ZrCl_2 is claimed to cause one fluorenyl group to be coordinated η^5, while the other is coordinated η^3, contributes to the instability of the complex.[46] Ring slippage from one bonding mode to the other is encouraged by traces of THF left from the synthesis; therefore, noncoordinating solvents such as diethyl ether and toluene were used.

Fluorenyllithium is known to cleave tetrahydrofuran, as well.[26] This may explain some of the behavior seen in our experiments, particularly the appearance of sticky solids in the crystallization tubes. Small amounts of impurities, including those introduced as by-products of the use of butyllithium to deprotonate the fluorenyl ligand, prevent the crystallization that was our sole method of purification; the symmetry-breaking Si-vinyl pendant did not help matters. As a result, we found only oils even after concentration of the solvents, cooling to -30 °C, and slow evaporation of the solvents (in a glove box) were tried.

In hindsight, the difficulties in purifying these zirconium catalysts may have been avoided by using the zirconium

tetrakis(dimethylamide) as a starting material, and using the acidity
of the fluorene or cyclopentadiene proton and the loss of
dimethylamine to drive the reaction. Treatment of the substituted
metal amide with $Me_2NH \cdot HCl$ would give the zirconium chloride back.
This method has been found to be useful in synthesizing a number
of zirconium sandwich compounds.[47,48]

10.2.3 Other comments

Two other dendrimers, $PhSi(CH_2CH_2SiEt_3)_3$ and
$PhSi(CH_2CH_2Si(Me)_2CH_2Cl)_3$ were synthesized and intended for use
in a project in which "dumbell" shaped dendrimers, with different
functionalities on each half of the dumbell, were to be made. The
phenyl-Si serves to block reaction at one site on the dendrimer
core; this bond is readily cleaved by trifluoromethanesulfonic acid,
creating the opportunity for later substitution at this site.
Specifically, the $PhSi(CH_2CH_2SiEt_3)_3$ was to form the hydrophobic part
of the dumbell, and the $PhSi(CH_2CH_2Si(Me)_2CH_2Cl)_3$ was to be
substituted at the chloromethyl group by amphiphilic groups as in
the work by Krska.[20]

Formation of the $PhSi(CH_2CH_2Si(Me)_2CH_2Cl)_3$ went smoothly via
the standard hydrosilylation reaction, but the
$PhSi(CH_2CH_2Si(Me)_2CH_2Cl)_3$ had a high degree of α-substitution and
could not be completely purified as a result. The greater-than-usual
α substitution is due mainly to the small size of the phenyl
substituent, which provided a more open structure to accommodate

the α isomer. The project was terminated before the use of triphenylphosphine to force β-substitution during the hydrosilylation reaction could be explored.

Figure 10.4: **Vinylsilyl-substituted fluorene ligands.**
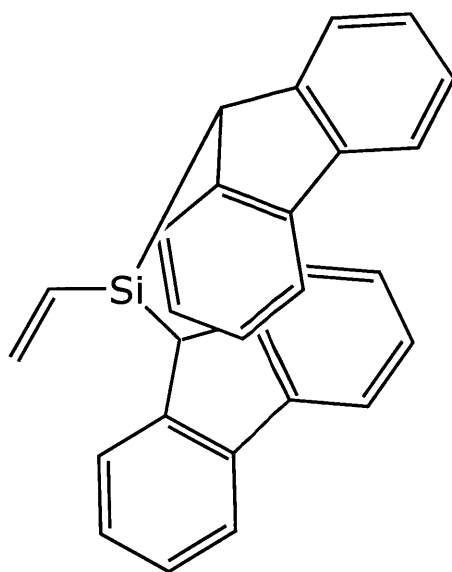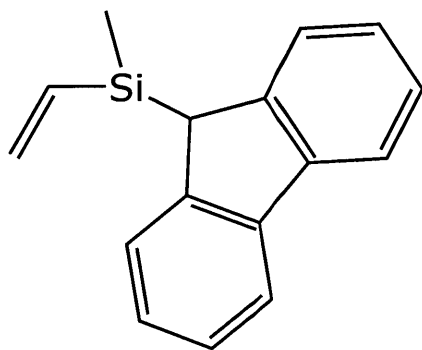
Figure 10.5: **Fluorenylzirconium compounds targeted in this work.**
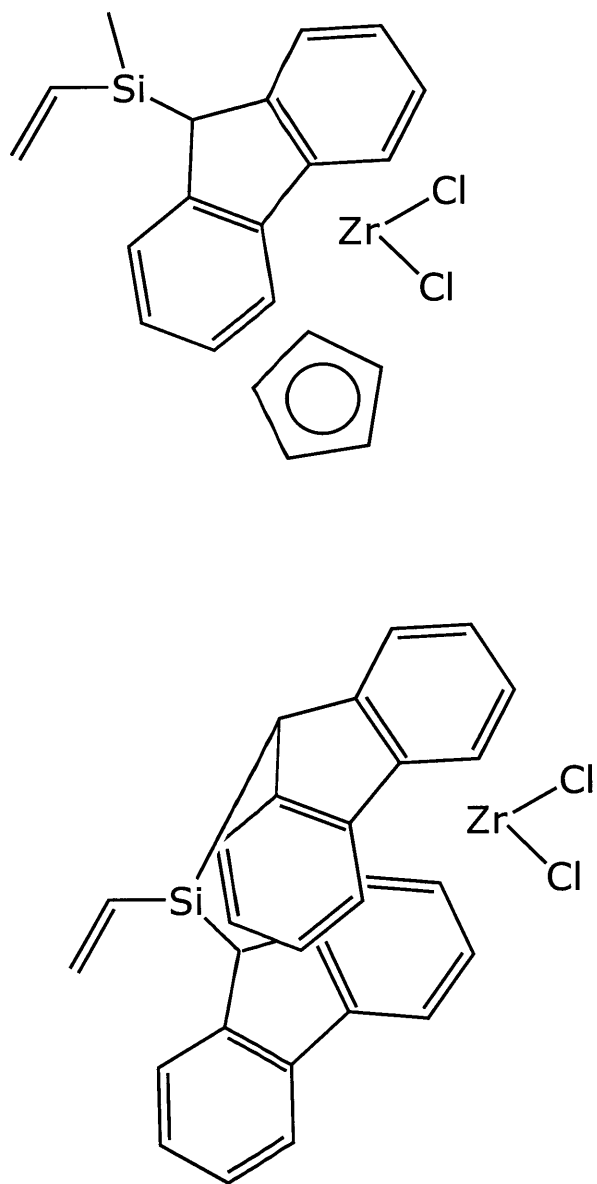
10.3 Experimental

All work was performed using standard inert-atmosphere techniques. Glassware was dried at least overnight at 120 °C. Solvents were dried over CaH_2 or Na-benzophenone and distilled from these reagents immediately before use. NMR spectra were taken on the instrumentation described in the Appendix to Part I of this Thesis; chemical shifts are reported relative to the residual proton in the deuterated solvents used, while ^{29}Si NMR spectra are reported relative to an external Me_4Si standard and ^{119}Sn NMR spectra are reported relative to an external Me_4Sn standard. Where not otherwise indicated, the term "NMR spectrum" refers to a ^1H NMR spectrum. GPC measurements were performed on a Millipore-Waters 150C HPLC/GPC system using toluene as a solvent. The Karstedt catalyst referred to below is a solution of a Pt(II) complex of $(ViMe_2Si)_2O$, approximately 2% in xylene, and was supplied by either Hüls or Gelest.

Certain starting materials were synthesized according to literature preparations: Me_2HSiCH_2Cl,[49] $Si(CH_2Si(Me)_2CH_2Cl)_4$,[20] $Si(CH_2CH_2SiVi_3)_4$,[19] $Si(CH_2CH_2Si(Me)_2CH_2I)_4$,[20] $Si(CH_2CH_2Si(Me)_2H)_4$,[10] and $PhSiVi_3$.[50] For other reagents, the commercial source is noted in the description of the experiment.

10.3.1 Synthesis of assorted dendrimers

Experiment 1 JP-I-123 Synthesis of Si(CH₂CH₂Si(CH₂CH₂SiCH₂Cl)₃)₄

$Si(CH_2CH_2Si(CH_2CH_2SiCH_2Cl)_3)_4$

$Si(CH_2CH_2SiVi_3)_4$ (6.28 g, 9 mmol, I-103) was dissolved in 10 ml THF in a roundbottom flask. A small amount of chloromethyldimethylsilane (total 20 ml, 166 mmol, I-20) was added, followed by 0.05 ml Karstedt catalyst (Hüls), and the reaction was heated to reflux to initiate it. Reflux was maintained by adding the remainder of the chloromethyldimethylsilane in small batches. The reaction was maintained at reflux overnight and monitored by NMR spectroscopy. More chloromethyldimethylsilane and chloroplatinic acid (0.5 ml of a 0.07 g/1 ml THF solution) were added when it was clear that unreacted vinyl groups remained. After two days at reflux the reaction was cooled and filtered on a celite pad using a isopropanol/hexane rinse. The filtrate was stripped of solvent to leave a grey sludge. This was dissolved in hot ethanol and hot-filtered, and the clear yellow filtrate stripped of solvent to leave a brown oil and white solid. The oil was chromatographed on silica (1:10 ethyl acetate: hexane eluant); the fractions, stripped of solvent, gave a brown powder. This was recrystallized from hot ethanol to give 1.64 g (10%) white crystals.

^{1}H NMR (CDCl₃, ppm): 0.08 (s, 4.9 H, SiMe), 0.45 (m, 5.4 H, SiCH₂CH₂Si), 2.77 (s, 2 H, SiCH₂Cl); the peak areas include the α-addition peaks.

Elemental analysis: expected 43.42 %C, 8.57 % H, 22.62% Cl; found 43.11% C, 8.89% H, 22.27% Cl.

Experiment 2 JP-I-156 Synthesis of Si(CH₂CH₂Si(CH₂CH₂Si(Me)₂CH₂I)₃)₄

Si(CH$_2$CH$_2$Si(CH$_2$CH$_2$SiCH$_2$Cl)$_3$)$_4$ (0.52 g, 0.28 mmol, I-123), NaI (0.77 g, 2.8 mmol, Malinkrodt), and 25 ml acetone (HPLC grade) were added to a 50 ml 3-neck flask equipped with a stir bar and reflux condensor. The flask was covered with aluminum foil to block light. The mixture was heated at reflux for 48 h, then the acetone was removed under vacuum. Pentane (50 ml) and water (25 ml) were stirred with the solid and the water phase removed; methylene chloride was added to the pentane phase to dissolve the solids remaining there. The organic phase was washed with additional water and dried over Na$_2$SO$_4$. Removal of the solvent left white needlelike crystals and a yellow oily residue, 0.73 g crude yield. This was recrystallized from isopropanol/methylene chloride to give 0.65 g of fine white powder, ^{1}H NMR (CDCl$_3$, ppm): 0.12 (s, 4.7 H, SiMe), 0.45 (m, 4.3 H, SiCH$_2$CH$_2$Si), 2.02 (s, 2 H, SiCH$_2$I); the peak areas include the α-addition peaks.

Elemental analysis: Expected 27.4% C, 5.42% H, 51.13% I; found 26.95% C, 5.27% H, 51.44% I.

Experiment 3 JP-I-177 Synthesis of PhSi(CH₂CH₂SiEt₃)₃

Phenyltrivinylsilane (2.66 g, 14.28 mmol, II-51) and 100 ml THF were placed in a 3-neck flask equipped with a stir bar and reflux

condensor. A small amount of triethylsilane (total 5.82 g, 50 mmol, Gelest) and 5 drops of a 5% chloroplatinic acid/isopropanol solution were added and the mixture heated to 50 °C. When the reaction started, the remainder of the HSiEt$_3$ was added in several increments. The reaction mixture was refluxed overnight, then the solvent stripped off and the remaining yellow liquid was taken up in hexane and run twice through 2-cm silica pads. The solvent was removed, leaving 6.92 g (91%) water-white oil.

^{1}H NMR (CDCl$_3$, ppm): 0.35 (m, 5.2 H, SiCH_2CH$_2$Si), 0.5 (q, 15.3 H, SiCH_2CH$_3$), 0.7 (m, 5.4 H, SiCH$_2$CH_2Si), 0.9 (t, 22 H, SiCH$_2$CH_3), 7.3, 7.45 (m, 5 H, Ph ring).

Elemental analysis: Found: 67.58% C, 11.50% H, expected 67.33% C, 11.68% H.

Experiment 4 JP-I-178 Synthesis of PhSi(CH$_2$CH$_2$Si(Me)$_2$CH$_2$Cl)$_3$

PhSiVi$_3$ (2.06 g, 11.1 mmol, II-51) and 75 ml THF were placed in a 250 ml 3-neck flask equipped with a stirbar and condensor. HSi(Me$_2$)CH$_2$Cl (5.12 g, 44.8 mmol, I-20) was added in 1-ml intervals; after the first interval 5 drops of a 5% chloroplatinic acid/isopropanol solution was added and the flask heated to 60 °C, then the rest of the reactant was added. The reaction was kept at 60 °C for 3 h, then the proton NMR spectra were checked for peaks arising from unreacted vinyl groups. The mixture was taken up in hexane and run through a silica pad; the solvent was removed by rotary evaporation and the sample kept in vacuum overnight, 5.23 g (73%) It was chromatographed on a 50-g silica gel column, using

1:250 ethyl acetate/hexane eluant. The first fraction, 3.72 g of a water-white oil, had an NMR spectrum that showed the expected product plus some α-addition.

^{1}H NMR (CDCl$_3$, ppm): 0.089 (s, 11.7 H, SiMe, β), 0.113 (s, SiMe, α), 0.5 (m, 4.2 H, SiCH$_2$CH$_2$Si), 0.75 (m, 4.0 H, SiCH$_2$CH$_2$Si), 1.11 (d, α), 2.79 (s, 7.6 H, SiCH$_2$Cl, β), 2.80 (s, SiCH$_2$Cl, α), 7.36, 7.45 (m, 5 H, Ph ring). Some of the α-addition peaks were not integrated.

10.3.2 Attempts at Functionalization of Dendrimers via Grignard Reagents

Experiment 5 JP-I-29 Attempted Synthesis of Si(CH$_2$CH$_2$Si(Me)$_2$CH$_2$Si(Me)$_2$H)$_4$ (Mg turnings)

Si(CH$_2$CH$_2$Si(Me)$_2$CH$_2$Cl)$_4$ (3.135 g, 5.5 mmol, I-27) was dissolved in 40 ml THF in a small flask. Magnesium turnings (0.83 g, 34 mmol) were dried for 1 week in an oven and placed in a hot 500 ml 3-neck flask equipped with a stir bar and condensor; this was cooled under vacuum, then sufficient THF to cover the metal was added. Dimethylchlorosilane (12 ml total, 127 mmol, Hüls, distilled from Mg) was added in small batches while the mixture was heated to 60 °C. No reaction was noted over 4 h. The dendrimer solution was added and the mixture refluxed overnight. As no reaction was evident in the morning, a small amount of 1,2-dibromoethane was added. Reaction progress was followed by ^{1}H NMR spectroscopy over the next several days, with increments of Me$_2$SiHCl added occasionally to replace losses during the reflux. (Table 10.1) After several days,

additional Mg (0.52 g, 20 mmol) was added and the reaction mixture sonicated for 60 min., but this treatment gave no change in the -CH_2Cl/product ratio. It was stirred for an additional 4 days, over which time a new -$SiMe_3$ peak was seen to be growing in. The reaction was eventually quenched and found by NMR spectroscopy to contain approximately 10% unreacted -CH_2Cl groups and -$SiMe_3$ groups.

Table 10.1 Reaction progress*

Hours after mixing	Chloromethyl/ outer methylene (of product) ratio
20	2.13
24	0.19
48	0.11
52	0.17
70	0.12
75	0.095
117	0.13

*Based on ^1H NMR spectra of aliquots of the reaction mixture, quenched and taken in $CDCl_3$. Ratios compare the area under the peak from the chloromethyl group to the areas under the peaks from the outer methylene protons. Variations among the last few readings are probably due to instrumental effects (using different NMR spectrometers, shimming differences, etc.).

Experiment 6 JP-I-38 Attempted Synthesis of Si(CH₂CH₂Si(Me)₂CH₂Si(Me)₂H)₄ (Mg turnings, opposite addition order)

Magnesium turnings (0.735 g, 30.2 mmol) were dried in an oven and cooled under vacuum in a similarly-dried 50 ml 3-neck flask equipped with a stir bar and condensor; 20 ml THF was added. $Si(CH_2CH_2Si(Me)_2CH_2Cl)_4$ (2.758 g, 4.8 mmol, I-27) was dissolved in 30 ml THF and 1/3 of this added to the magnesium turnings with heating. After 10 min. no reaction appeared to have started, so 0.2 ml 1,2-dibromoethane was added. As this appeared to have begun the reaction, the remainder of the dendrimer solution was added and the mixture refluxed for about 3 h. Attack on the Mg was noticeable. Me₂SiHCl (2.15 ml, 19.2 mmol, Hüls) was added at once; there was an exotherm and the pot contents became a murky yellow-black. This was refluxed overnight. In the morning, Mg remained; the proton NMR spectrum of an aliquot showed no peaks assigned to -CH₂Cl groups but a large number of -SiMe₃ groups. An additional 2 ml of Me₂SiHCl was added and the solution stirred at 50 °C for another half-hour. The dark yellow solution was again checked by NMR spectroscopy. There were no chloromethyl groups evident but approximately 10% of the proton area were accounted-for by -SiMe₃ groups.

Experiment 7 JP-I-45 Attempted Synthesis of Si(CH₂CH₂Si(Me)₂CH₂Si(Me)₂H)₄ (Rieke magnesium)

Si(CH$_2$CH$_2$Si(Me)$_2$CH$_2$Cl)$_4$ (2.007 g, 3.52 mmol, I-27) was dissolved in 75 ml THF in a small flask. Magnesium chloride (2.22 g, 23.3 mmol, Alfa 99% anhydrous) and KI (0.34 g, 2.05 mmol, MCB Reagents) were placed in a 250 ml 3-neck flask equipped with a stir bar and a condensor and dried in an oven overnight. They were cooled under vacuum and 125 ml THF added. Potassium metal (1.52 g, 38.8 mmol) was cut into small pieces and kept under hexane, and added piece-by-piece to the milky suspension of MgCl$_2$ in THF at 80 °C. After refluxing for three hours the reaction mixture was a murky black suspension. The dendrimer solution was added slowly at 80 °C, then refluxed overnight. The NMR spectrum of an aliquot, quenched in water, shows a significant -CH$_2$Cl peak, though the expected product is -SiMe$_3$. Me$_2$SiHCl (2 ml, 18.3 mmol) was added anyway and the solution refluxed for two days. The ^{1}H NMR spectrum of the product (after quenching and removal of solvent under vacuum) shows no -SiH or -SiCH$_2$Cl peaks, only -SiMe$_3$.

Experiment 8 JP-I-49 Attempted Synthesis of Si(CH₂CH₂Si(Me)₂CH₂Si(Me)₂H)₄ (Rieke magnesium)

Si(CH$_2$CH$_2$Si(Me)$_2$CH$_2$Cl)$_4$ (1.004 g, 1.75 mmol, I-27) was dissolved in 15 ml THF in a small flask. Separately, MgCl$_2$ (1.5 g, 15.8 mmol, Alfa,

anhydrous) was suspended in 70 ml THF in a 100 ml 3-neck equipped with a stir bar and condensor. Potassium (1.09 g, 27.9 mmol), was added to this suspension. There was an exotherm and the suspension became grey. It was stirred over 4 h, giving a uniformly black suspension. The dendrimer solution was added slowly to this, and there was an exotherm at each addition. The mixture was refluxed overnight, but remained murky black. Me_2SiHCl (1 ml, 9.17 mmol, Hüls) was added slowly and the mixture refluxed 8 h. An aliquot was taken; its NMR spectrum showed little or no reaction. 1,2-dibromoethane (0.1 ml) was added and the mixture stirred for 10 days. The NMR spectrum of an aliquot showed complete disappearance of the $-CH_2Cl$ peaks. The mixture was quenched in saturated aqueous ammonium chloride and the organic layers separated, washed with water, and dried over magnesium sulfate, leaving 1.02 g of yellow, viscous oil. This was taken up in hexane and chromatographed on a silica column (30 g). All fractions taken have ^1H NMR spectra showing no $-CH_2Cl$ peaks but a large $-SiMe_3$ peak.

Experiment 9 JP-I-55 Attempted Synthesis of Si(CH₂CH₂Si(Me)₂CH₂Si(Me)₂H)₄ (BrCH₂CH₂Br, powdered Mg)

$Si(CH_2CH_2Si(Me)_2CH_2Cl)_4$ (1.016 g, 1.75 mmol, I-27) in 75 ml THF was added to magnesium turnings (0.22 g, 9.05 mmol, oven-dried) and 0.05 ml 1,2-dibromoethane added. No reacton was evident. The mixture was stirred for 24 h at 50 °C, but there was no evidence of reaction. Some 30 drops of 1,2-dibromoethane were added, with

heating, but no reaction was evident. Me$_2$SiHCl (0.5 ml, 5.3 mmol) was added at 55 °C, and after a minute or so the metal blackened and there was a violent bubbling. The mixture was stirred overnight at reflux, during which time all of the Mg was consumed. The NMR spectrum of an aliquot showed totally unreacted dendrimer. (Exposure of the solution to air gave an orange color.) Since it was thought that the Mg had been consumed by the 1,2-dibromoethane, magnesium powder (0.7074 g, 29 mmol, Alfa 99.8%, 10-20 mesh) was added under argon flow. Some exotherm occurred and the suspension became a murky green-brown color. Additional Me$_2$SiHCl (5 ml) was added and the mix heated for 2 h. The NMR spectrum of an aliquot showed reduction of the area of the -CH$_2$Cl peak and the growth of product peaks, as well as a -SiMe$_3$ peak. The mixture was heated for 3 days with aliquots taken every 24 h and checked by NMR spectroscopy. Eventually there was no further change in the -CH$_2$Cl peak, and the reaction was quenched with a mixture of saturated ammonium chloride solution and hydrochloric acid. The organic phase was extracted with ether, washed with water, and dried over sodium sulfate. Removal of the solvent left a yellow oil, which was chromatographed on 20 g of silica using hexane. The NMR spectra of all fractions showed approximately 7% contamination with -SiMe$_3$ groups, as well as a -CH$_2$Cl peak.

Experiment 10 JP-I-67 Attempted Synthesis of
Si(CH$_2$CH$_2$Si(Me)$_2$CH$_2$Si(Me)$_2$H)$_4$
(lithium metal used)

Lithium powder (0.51 g, 73.5 mmol, Aldrich 99.9%, 325 mesh) and 25 ml hexane were added to a roundbottom flask equipped with a stir bar. This was cooled to -78 °C and a solution of Si(CH$_2$CH$_2$Si(Me)$_2$CH$_2$Cl)$_4$ (5.19 g, 9.1 mmol, I-27) in 100 ml hexane added slowly. There was no reaction apparent, so the mixture was warmed, then sonicated for 1 h. Since no reaction was apparent, the remainder of the dendrimer solution was added and the mixture sonicated for an additional 2 h, then left overnight at room temperature. The hexane was removed under vacuum and 25 ml THF added; this mixture was sonicated for 2 h. The solution became yellow. Me$_2$SiHCl (7.6 g, 80 mmol) was added and the mixture refluxed overnight. Some white precipitate formed. The solvent was decanted off and the solids washed with ether; the combined organic portions were washed with water (some fizzing occurred) and dried on sodium sulfate. Removal of the solvent left a pale yellow oil; this was chromatographed on a 20-g silica column using hexane eluant, 1.36 g. The ^{1}H NMR spectrum showed some unreacted -CH$_2$Cl peak and a large SiMe$_3$ peak.

Experiment 11 JP-I-69 Attempted Synthesis of
Si(CH$_2$CH$_2$Si(Me)$_2$CH$_2$Si(Me)$_2$H)$_4$
(use of CuCN catalyst)

Magnesium turnings (0.17 g, 7 mmol) were dried in an oven and added hot to a hot 3-neck flask equipped with a condensor and stir bar; they were cooled with stirring, dry, under vacuum. To this was added 10 ml THF and 0.1 ml 1,2-dibromoethane; after a few minutes the formation of bubbles indicated the start of the reaction. When the reaction became vigorous, the solution was removed from the magnesium by cannula and some of a solution of Si(CH$_2$CH$_2$Si(Me)$_2$CH$_2$Cl)$_4$ (0.98 g, 1.75 mmol, I-27) in 15 ml THF added immediately. This mixture was heated for 3 h at reflux, but no consumption of the magensium was evident. CuCN (0.1 g, 1.12 mmol, Aldrich) was added, and the stirring at reflux continued overnight. The resulting solution was brown-black and the Mg was consumed; the remainder of the dendrimer solution was added. After 2 h of reflux, Me$_2$SiHCl (1 ml, 9.17 mmol, Hüls) was added, and there was a violent frothing. This was stirred for 4 h at reflux, then left to cool overnight; a black solid settled out. The mixture was quenched in saturated ammonium chloride solution and the organic phase washed with water, dried on sodium sulfate, and stripped of solvent, leaving a brown oil. The ^{1}H NMR spectrum of the oil showed unreacted -CH$_2$Cl groups and a large -SiMe$_3$ peak.

Experiment 12 JP-I-83 Attempted Synthesis of Si(CH$_2$CH$_2$Si(Me)$_2$CH$_2$Si(Me)$_2$H)$_4$ (using activated Mg)

Magnesium turnings were placed in a schlenk frit and rinsed with 10% v/v HCl, then acetone, then ether. They were placed under vacuum over two days, and stored under argon. Some of this magnesium (1.1 g, 45.2 mmol) was ground in a mortar in the glove box, then placed into a 3-neck flask equipped with a stir bar, condensor, and dropping funnel, along with 15 ml THF. Two ml of a solution of Si(CH$_2$CH$_2$Si(Me)$_2$CH$_2$Cl)$_4$ (3.0194 g, 5.29 mmol, I-27) in 25 ml THF were added to the Mg and heated to reflux, with periodic additions of dendrimer solution, over 3 h. 1,2-dibromoethane (0.2 ml) was added to encourage the reaction, and when bubbling began, more dendrimer solution was added. An exotherm occurred and was maintained as the remainder of the dendrimer solution was added. The mixture was refluxed overnight, giving a dark brown solution. Me$_2$SiHCl (3 ml, 27.5 mmol) was added slowly, leading to an exotherm. The mixture was stirred for 4 h at 50 °C. The proton NMR spectrum of an aliquot showed complete consumption of the -CH$_2$Cl peaks and approximately 11% -SiMe$_3$ contamination. The mixture was quenched with saturated ammonium chloride solution, extracted with hexane, and the organic portions washed with water and dried on sodium sulfate. After removal of solvent by rotary evaporation there was 3.16 g yellowish oil. This was taken up in hexane and run through a 1-cm silica gel

pad to decolorize it; removal of solvent left 2.93 g (82%) clear and colorless liquid.

^{1}H NMR (C_6D_6, ppm): -0.22 (d, 2.2 H, SiCH$_2$Si), 0.10 (s, SiMe), 0.16 (s, SiMe) (total SiMe peak area 13.8 H), 0.75 (m, 6.6 H, SiCH$_2$CH$_2$Si), 4.30 (m, 1 H, SiH).

^{13}C NMR (C_6D_6, ppm): -0.70 (SiCH$_2$Si), 0.09 (SiMe), 0.85 (SiMe), 4.71 (SiCH$_2$CH$_2$Si), 11.37 (SiCH$_2$CH$_2$Si)

^{29}Si NMR (C_6D_6, ppm): -16.89 (*Si*CH$_2$Si), 2.95 (SiCH$_2$*Si*), 9.09 (Si-H). Elemental analysis: found 50.85% C, 11.44% H; expected 50.52% C, 11.51% H. (Figure 10.6 a-c)

Experiment 13 JP-I-174 Attempted Synthesis of Si(CH$_2$CH$_2$Si(Me)$_2$CH$_2$SnMe$_3$)$_4$ (use of iodomethyl-terminated dendrimer)

Magnesium turnings (0.093 g, 3.83 mmol) were ground in a mortar in the glovebox and placed in a 100 ml 3-neck flask equipped with a condensor, stir bar, and dropping funnel; 5 ml of THF was added. Si(CH$_2$CH$_2$Si(Me)$_2$CH$_2$I)$_4$ (0.51 g, 0.54 mmol, I-157) was dissolved in 5 ml of THF and 0.5 ml added to the Mg turnings. The mixture was heated, but no reaction occurred, so 0.05 ml 1,2-dibromoethane was added and the mixture heated more. The reaction was initiated, so the remaining dendrimer solution was added over the next hour and the mixture refluxed for 3 h. The suspension was somewhat milky white. Me$_3$SnCl (0.61 g, 3.06 mmol, Strem, freshly sublimed) was dissolved in 15 ml of THF and added all at once to the Grignard reagent. The mixture became clear yellow; it was refluxed overnight. It was cooled to room temperature, then

quenched with 50 ml saturated ammonium chloride solution. The combined organic phases were dried on magnesium sufate and the solvent removed under vacuum. The resulting water-white oil was left under vacuum for two days. The ^{1}H NMR spectrum indicated no -CH_2I groups, but multiple -$SiMe_3$ and -$SnMe_3$ groups.

Experiment 114 JP-I-107 Attempted Synthesis of $Si(CH_2CH_2Si(Me)_2CH_2SnBu_3)_4$

Magnesium turnings (1 g, 41 mmol, activated as described in Experiment 18), were ground in a mortar in the glove box, then placed in a 100 ml 3-neck flask equipped with a stir bar and condensor; 5 ml THF was added. 0.1 ml of 1,2-dibromoethane was added to the magnesium, with heating, and a reaction began after 2-3 min., then died out after 10-12 min. Some (5 ml) of a solution of $Si(CH_2CH_2Si(Me)_2CH_2Cl)_4$ (1.5 g, 2.63 mmol, I-27) in 20 ml THF was added, and there was an exotherm. The remainder of the dendrimer solution was added, washing with 10 ml THF. Additional amounts (0.1 ml each) of 1,2-dibromoethane were added at intervals, and the reaction was refluxed overnight with no apparent change or additional consumption of the magnesium. It was cooled and Bu_3SnCl (3 ml, 6.18 mmol, Aldrich, 99%, freshly distilled 158-160 °C/12 mm) added. A precipitate formed; the mixture was refluxed 1 h, becoming black, and was quenched in saturated aqueous ammonium chloride. The organic layers were collected, washed with water, dried over sodium sulfate, and stripped of solvent, leaving 4.15 g of yellow milky oil. This was chromatographed on 40 g of silica using hexane eluant. 2.66 g (92%) of clear and colorless liquid

found. The ^{1}H NMR (CDCl$_3$) spectrum showed butyl groups, methylene protons, and Si-methyl protons as expected; and the ^{119}Sn NMR spectrum had one peak at -84.47 ppm Left open to air, the sample became milky; the ^{1}H NMR spectrum indicated multiple methylene and Si-methyl peaks, and the ^{119}Sn NMR spectrum showed three peaks, at -43.82, -84.47, and -151.91 ppm. Mass. Spec. (m/e): 523, 467, 41, 355, 297, 235, 177, 121, 41 (parent ion expected at 1108). (Figure 10.7 a, b)

Experiment 15 JP-I-155 Attempted Synthesis of Si(CH$_2$CH$_2$Si(Me)$_2$CH$_2$SnBu$_3$)$_4$ (in dibutyl ether)

Si(CH$_2$CH$_2$Si(Me)$_2$CH$_2$Cl)$_4$ (0.5243 g, 0.92 mmol, I-27) was dissolved in 25 ml dibutyl ether. Magnesium turnings (0.1203 g, 4.95 mmol) were ground in a mortar in the glove box and placed with 5 ml dibutyl ether in a 250 ml 3-neck flask equipped with a stir bar and a condensor. 0.5 ml 1,2-dibromoethane was added and the mixture heated, but there was no reaction evident. The dendrimer solution was added to the magnesium and the mixture stirred at reflux (142 °C) for 9 h. The mixture became cloudy white; more solvent was added, but the solution did not clear. Reflux was continued overnight, during which time the solution became increasingly milky and a white precipitate had collected on the sides of the flask; unreacted Mg was present. The mixture was cooled to 100 °C and Bu$_3$SnCl (6 ml, 24.6 mmol, distilled) added; this was stirred at room temperature for 2 days, then at 70 °C overnight. The reaction was quenched with saturated aqueous ammonium chloride solution; this

was extracted with hexane, and the combined organic parts were washed with water, then dried over sodium sulfate. The solvent was removed under vacuum, and the remaining yellow oil was left on vacuum for 10 days to remove any excess tributyltin chloride. The ^{1}H NMR spectrum (C_6D_6) showed butyl peaks and the peaks for the starting dendrimer, where the ratio of the peak area for the SiMe peak (0.06 ppm) to that of the -CH_2Cl peak (2.60 ppm) was the same as for the unreacted dendrimer, indicating that no reaction had taken place.

Experiment 16 JP-I-165 Attempted Synthesis of Si(CH₂CH₂Si(Me)₂CH₂CH₂SnPh₃)₄

Si($CH_2CH_2Si(Me)_2CH_2I)_4$ (0.51 g, 0.54 mmol, I-157) was added to a 50 ml 3-neck flask and dissolved in 20 ml hexane. This was cooled to -80 °C (the dendrimer precipitated). 1.5 ml of *tert*-butyllithium (2.55 mmol, Aldrich, 1.7 M in pentane) were added dropwise, and the mixture was permitted to warm to -30 °C for 5 min. It was then cooled to -45 °C and a solution of Ph_3SnCl (0.837 g, 2.17 mmol, Strem) in 10 ml benzene added. The mixture was permitted to warm to room temperature, and was stirred overnight. The NMR spectrum of an aliquot indicated that no reaction had occurred.

10.3.3 Attempts at Functionalization of Dendrimers via Hydrosilylation Reactions

Experiment 17 JP-I-125 Attempted Synthesis of $Si(CH_2CH_2Si(Me)_2CH_2CH_2SnPh_3)_4$

$Si(CH_2CH_2Si(Me)_2H)_4$ (1.65 g, 4.4 mmol, I-119) was added to a 3-neck flask equipped with a stir bar and condensor, and 50 ml THF added. Triphenylvinyltin (7.03g, 18.6 mmol, lab-synthesized, purity checked by ^{1}H and ^{119}Sn NMR) was added to make a yellow-brown suspension. 0.1 ml of Karstedt catalyst (Gelest) was added and the mixture was heated to reflux; no reaction was evident. More catalyst was added as the NMR spectra of aliquots indicated no reaction had taken place during the 48-h reflux. 0.5 ml of a solution of 0.1 g of chloroplatinic acid (Strem) in THF was added at reflux; the reaction mixture became dark brown and frothed. The NMR spectra of subsequent aliquots showed decrease of SiH and Sn-Vi peaks relative to the Si-Me peaks. The mixture was left at reflux over two days more, and became black. Another aliquot was taken for NMR spectometry and showed no decrease in the Si-H peak area.

Experiment 18 JP-I-131 Attempted Synthesis of Si(CH₂CH₂Si(Me)₂CH₂CH₂SnPh₃)₄, sealed tube, AIBN

In an ampoule were placed Si(CH$_2$CH$_2$Si(Me)$_2$H)$_4$ (0.51g, 1.35 mmol, I-119), Ph$_3$SnVi (2.04 g, 9.15 mmol), and 3 ml benzene to dissolve all the solids. 0.1 ml of Karstedt catalyst (Hüls) was added and the mixture was sealed in the tube. It was held for 3 days at 165 °C, and became dark brown in color. The NMR spectrum of an aliquot showed that no reaction had occurred.

The mixture was transferred to a 3-neck flask with a stir bar and condensor and 100 mg AIBN (Alfa) added. Benzene was added to make a total of 8 ml of solvent, and the mixture heated at 90 °C overnight. The NMR spectrum of an aliquot showed no reaction. Further additions of AIBN and continued heating gave no further reaction.

Reaction using AIBN was repeated (I-139) on a fresh sample of dendrimer and tin compound, now with no platinum catalyst present, with much the same result.

Experiment 19 JP-I-127 Attempted Synthesis of Si(CH₂CH₂Si(Me)₂CH₂CH₂SnEt₃)₄

Si(CH$_2$CH$_2$Si(Me)$_2$H)$_4$ (1.55 g, 4.1 mmol, I-119) was added to a 3-neck flask equipped with a stir bar and condensor, and 50 ml THF added. Triethylvinyltin (4.07, 17.5 mmol, lab-synthesized, purity checked by ^{1}H and ^{119}Sn NMR spectroscopy) was added to make a yellow-brown suspension. 0.1 ml of Karstedt catalyst (Gelest) was

added and the mixture was heated to reflux; no reaction was evident. More catalyst was added as the NMR spectra of aliquots indicated no reaction had taken place during the 48-h reflux. 0.5 ml of a solution of 0.1 g of chloroplatinic acid (Strem) in THF was added at reflux; the reaction mixture became dark brown and frothed. The NMR spectra of subsequent aliquots showed decrease of SiH and Sn-Vi peaks relative to the Si-Me peaks. The mixture was left at reflux over two days more, and became black. Another aliquot was taken for NMR spectroscopy and showed no decrease in the Si-H peak area.

Experiment 20 JP-I-133 Attempted Synthesis of Si(CH$_2$CH$_2$Si(Me)$_2$CH$_2$CH$_2$SnEt$_3$)$_4$, sealed tube, then AIBN

In an ampoule were placed Si(CH$_2$CH$_2$Si(Me)$_2$H)$_4$ (0.52 g, 1.36 mmol, I-119), Et$_3$SnVi (1.29 g, 7.38 mmol), and 3 ml benzene to dissolve all the solids. 0.1 ml of Karstedt catalyst (Hüls) was added and the mixture was sealed in the tube. It was held for 3 days at 165 °C, and became dark brown in color. A silvery mirror lined the sides of the ampoule. The NMR spectrum of an aliquot showed that no reaction consuming vinyl or Si-H groups had occurred.

The mixture was transferred to a 3-neck flask with a stir bar and condensor and 100 mg AIBN (Alfa) added. Benzene was added to make a total of 8 ml of solvent, and the mixture heated at 90 °C overnight. The NMR spectra of aliquots showed no reaction; the mixture was left at 75-90 °C for four days with intermittent addition of AIBN. The fnial aliquot showed loss of the vinyl and Si-H groups,

and the volatiles were removed under vacuum. The ^{1}H NMR spectrum suggested decomposition.

Reaction using AIBN was repeated (I-139) on a fresh sample of dendrimer and tin compound, now with no platinum catalyst present, with much the same result.

10.3.4 Zirconium-based catalysts

Experiment 21 JP-II-17 Synthesis of ViSiMe₂Fl

Fluorene (5.34g, 32.12 mmol, Aldrich, 98%) was added to a 250 ml Schlenk flask equipped with a magnetic stirrer and dissolved in 200 ml toluene and 20 ml THF. Butyllithium (13 ml, 32.5 mmol, Aldrich, 2.5 M in hexane) was added dropwise at room temperature. The solution became increasingly red as the butyllithium as added, and there was a mild exotherm. A condensor was added and the solution was refluxed 2.5 h, leading to a brown solution. This was cooled to room temperature and stirred overnight, then cooled to -78 °C. Freshly-distilled vinyldimethylchlorosilane (10 ml, 83.6 mmol, Gelest, distilled from Mg) was added to the flask slowly, and the resulting exotherm was accompanied by a color change to milky yellow-orange. The mixture was refluxed overnight, then cooled to room temperature and hydrolyzed with water. The aqueous phase was extracted with 2 x 20 ml of hexane and the organic phases combined and dried on MgSO₄. Volatiles were removed by rotary evaporation, leaving 7.72 g (96%) orange needles.

^{1}H NMR (CDCl$_3$,ppm) -0.1 (s, 5.6 H, Si-Me), 3.87 (s, 1 H, on Fl ring), 5.5 - 6.2 (pairs of doublets, 3.8 H, Si-Vi), 7.2 - 7.4 (m, 5 H, Fl ring (peak area includes solvent peak), 7.45 (d, 2.4 H, Fl ring), 7.80 (d, 2.2 H, Fl ring).

^{13}C NMR (CDCl$_3$, ppm) 41.98 (Fl ring), 120 (Fl ring), 124.36 (Fl ring), 125.42 (Fl ring), 125.95 (Fl ring), 126.04 (Fl ring), 133.41 (SiCHCH_2), 137.05 (SiCHCH$_2$), 140.58 (Fl ring), 145.33 (Fl ring); the SiMe peak was not detected.

Mass. Spec. (m/e): Peaks at 250 (parent ion), 233, 195, 165 (loss of -SiMe$_2$Vi), 139, 115, 85 (loss of Fl), 59 (SiMe$_2$ group), 43.

Elemental: Found 80.94% C, 7.37 % H; expected 81.54 % C, 7.24 % H.

Experiment 22 JP-II-28 Synthesis of Fl$_2$SiMeVi

Fluorene (10.0467 g, 60.4 mmol, Aldrich 98%) was added to a 500 ml 3-neck flask equipped with a magnetic stir bar and condensor and dissolved in 250 ml of toluene. Butyllithium (25 ml, 62.5 mmol, Aldrich 2.5 M in hexane) was added slowly, leading to a yellow solution. This was refluxed for 2.5 h, and became cloudy orange. It was permitted to cool to room temperature, and the orange solution was removed from the solid by filter cannula. The solid was stirred with 100 ml of toluene and permitted to settle, and the liquid part again removed by filter cannula. Fifty ml of toluene and 200 ml of ether was added and the orange suspension stirred; ViSiMeCl$_2$ (4 ml, 30.8 mmol, Gelest, distilled from Mg) was added slowly at room temperature. There was an exotherm and the mixture became milky yellow. It was refluxed overnight and cooled to room temperature, then hydrolyzed with water and the water layer

extracted 2 x 50 ml with ether; the organic layer was similarly extracted with water. Organic portions were combined and dried over $MgSO_4$. Solvent was removed by rotary evaporation, leaving an orange-yellow solid; this was dissolved in hexane and the white insoluble material filtered off. Removal of the hexane left 11.63 g yellow solid (crude, GC/MS shows 3.5% contamination with unreacted fluorene plus other contaminants). Use of column chromatography (2 g of sample, 30 g silica gel, CH_2Cl_2 eluant) did not effect purification. The remaining crude material was ground in hexane and filtered to leave a beige solid and yellow filtrate; the filtrate appeared by NMR to be mostly unreacted fluorene. GCMS on the solid showed contamination with unreacted fluorene still; the solid was recrystallized from hot hexane-ethyl acetate. 2.82 g yellow brown rhombohedral and white rhombohedral crystals were collected by cooling to 0 °C. The mother liquor was further concentrated and cooled to -10 °C, and 2.32 g (18.8%) tan plates collected.

^{1}H NMR (CD_2Cl_2, ppm): -0.4 (s, 3 H, SiMe), 4.3 (s, 1.5 H, Fl ring), 5.0 - 5.7 (sets of doublets, 2.9 H, SiVi), 7.25 (t, Fl ring), 7.4 (t, Fl ring), 7.55 (m, Fl ring), 7.9 (d, Fl ring) (Fl ring total area 12.0 H).

Mass. Spec. (m/e): Peaks at 400 (parent ion), 235 (loss of one Fl), 205 (loss of Fl, 2 Me groups) 165 (Fl group), 139, 115, 70 (SiMeVi group), 43.

Elemental: Expected 86.95% C, 6.04 % H ; found 86.92% C, 6.20 % H.

Experiment 23 JP-II-21 Attempted Synthesis of ViMe$_2$SiFl(Cp)ZrCl$_2$

CpZrCl$_3$ (0.85 g, 3.24 mmol, Strem, base-free) was placed in a 100 ml schlenk flask in the glove box and suspended in 200 ml toluene. Fluorenylvinyldimethylsilane (0.827 g, 3.30 mmol, II-17) was added to a 300 ml schlenk flask equipped with a magnetic stir bar and dissolved in 25 ml toluene and 5 ml THF. Butyllithium (1.5 ml, 3.75 mmol, Aldrich 2.5 M in hexane) was added slowly, turning the solution dark brown. This was refluxed 2 h, then cooled to -78 °C. The CpZrCl$_3$ suspension was transferred into this by cannula and washed in with another 10 ml of toluene. The mixture was permitted to warm to room temperature and stirred overnight. The solvent was removed, leaving a yellow-brown oil. Pentane was stirred with the product, then removed by vacuum; the product was dissolved in toluene again and filtered on celite. Solvent was stripped from the filtrate and the resulting brown oil dissolved in 10 ml of dichloromethane It was left at -30 °C for a week, but only sticky whitish solids were found. The ^{1}H NMR spectrum (CDCl$_3$) shows multiple fluorenyl rings' worth of peaks, as well as multiple Si-vinyl peaks, arising from unreacted fluorenyl starting material and product. Small peaks in the alkane region suggest residues from the butyllithium.

Experiment 24 JP-II-34 Attempted Synthesis of ViMe$_2$SiFl(Cp)ZrCl$_2$

Fluorenylvinyldimethylsilane (4.02 g, 16.1 mmol, II-17) was dissolved in 100 ml toluene in a 3-neck flask equipped with a condensor and a magnetic stir bar. Butyllithium (6.4 ml, 16 mmol, Aldrich 2.5 M in hexane) was added slowly and the solution refluxed overnight. It was cooled and CpZrCl$_3$ (4.09 g, 15.6 mmol, Strem, base-free) was added under argon counterflow. A orange-yellow precipitate formed. The mixture was refluxed for an hour, then left stirring at 40 °C overnight. It was hot-filtered through celite to leave a red-brown filtrate and a yellow solid on the frit. The solvent was partially removed and the solution left at -30 °C over 2 days. No solid appeared; the solvent was removed under vacuum to leave a caramel-like oil. This was ground in pentane and the pentane removed by filter cannula; the remaining tar was dissolved in dichloromethane and filtered, then stored at -30 °C over two days. Repeated incremental removal of solvent *in vacuo* and cooling to -30 °C did not lead to crystals. Solid which appeared in the flask seemed to be decomposition product.

The ^{1}H NMR spectrum indicated Zr-bound Si-vinyl and fluorenyl ligand, as well as some unreacted fluorenyl ligand; other organic contaminants were present.

Experiment 25 JP-II-37 Attempted Synthesis of ViMe$_2$SiFl(Cp)ZrCl$_2$

Fluorenylvinyldimethylsilane (0.99 g, 3.95 mmol, II-17) was dissolved in 100 ml ether and methyllithium (2.8 ml, 3.92 mmol, Aldrich 1.4 M in ether) added slowly. This was stirred at room temperature for 45 min. after gas production stopped, and CpZrCl$_3$ (1.03 g, 3.92 mmol, Strem base-free) added under argon counterflow. The solution became orange and milky. This was stirred overnight at room temperature and the solvent removed in vacuo; pentane was stirred in the product and removed by filter cannula (yellow filtrate). The remaining semisolid was vacuum-dried, then dissolved in dichloromethane; this was filtered to remove undissolved material. It was left at -30 °C for two days. Repeated incremental removal of solvent and cooling at -30 °C did not lead to crystal formation.

Experiment 26 JP-II-47 Attempted Synthesis of ViMe$_2$SiFl(Cp)ZrCl$_2$

Fluorenylvinyldimethylsilane (1.007 g, 4.02 mmol, II-17) was added to a schlenk flask and dissolved in 50 ml of toluene. Methyllithium (2.87 ml, 4.02 mmol, Aldrich 1.4 M in ether) was added at room temperature. The mixture was stirred overnight. CpZrCl$_3$ (1.055 g, 4.02 mmol, Strem base-free) was added under argon counterflow. The resulting orange cloudy suspension was stirred at room temperature for two days, then filtered on ceilte to give a yellow

filtrate and white solid on the filter. The solvent was reduced to 20 ml *in vacuo* and the rest left in an open vial in the glove box. While the solvent evaporated over the next month, no crystals formed: only an orange-brown tar.

Experiment 27 JP-II-38 Attempted Synthesis of ViMeSiFl$_2$ZrCl$_2$

Bis(fluorenyl)vinylmethylsilane (1.97g, 4.92 mmol, II-28) was dissolved in 100 ml ether in a 300 ml schlenk flask equipped with a magnetic stir bar. Methyllithium (7.04 ml, 9.86 mmol, Aldrich 1.4 M in ether) was added slowly at room temperature, and the solution became milky yellow; no exotherm was observed. This was stirred for at room temperature 45 min. after evolution of gas ceased. Solid ZrCl$_4$ (1.15 g, 4.93 mmol, Strem 98%, freshly sublimed) was added slowly under argon counterflow; the reaction mixture became dark red, with a reddish precipitate. It was stirred at room temperature overnight, then the solvent removed *in vacuo*. Pentane was added and the yellow solvent layer removed by filter cannula. The remaining solid was dissolved in dichloromethane and filtered through celite, leaving a clear burgundy solution. Some of the solvent was removed *in vacuo*, and the remaining solution left at -30 °C under argon. After four days some solid appeared; this was removed, and the solution concentrated under vacuum and returned to the -30 °C freezer. No further solids appeared, despite repeated incremental solvent removal over the next month. The solid collected (0.08 g, 3%) had an ^{1}H NMR spectrum (CD$_2$Cl$_2$, ppm) with peaks as would be expected, but the areas of the peaks
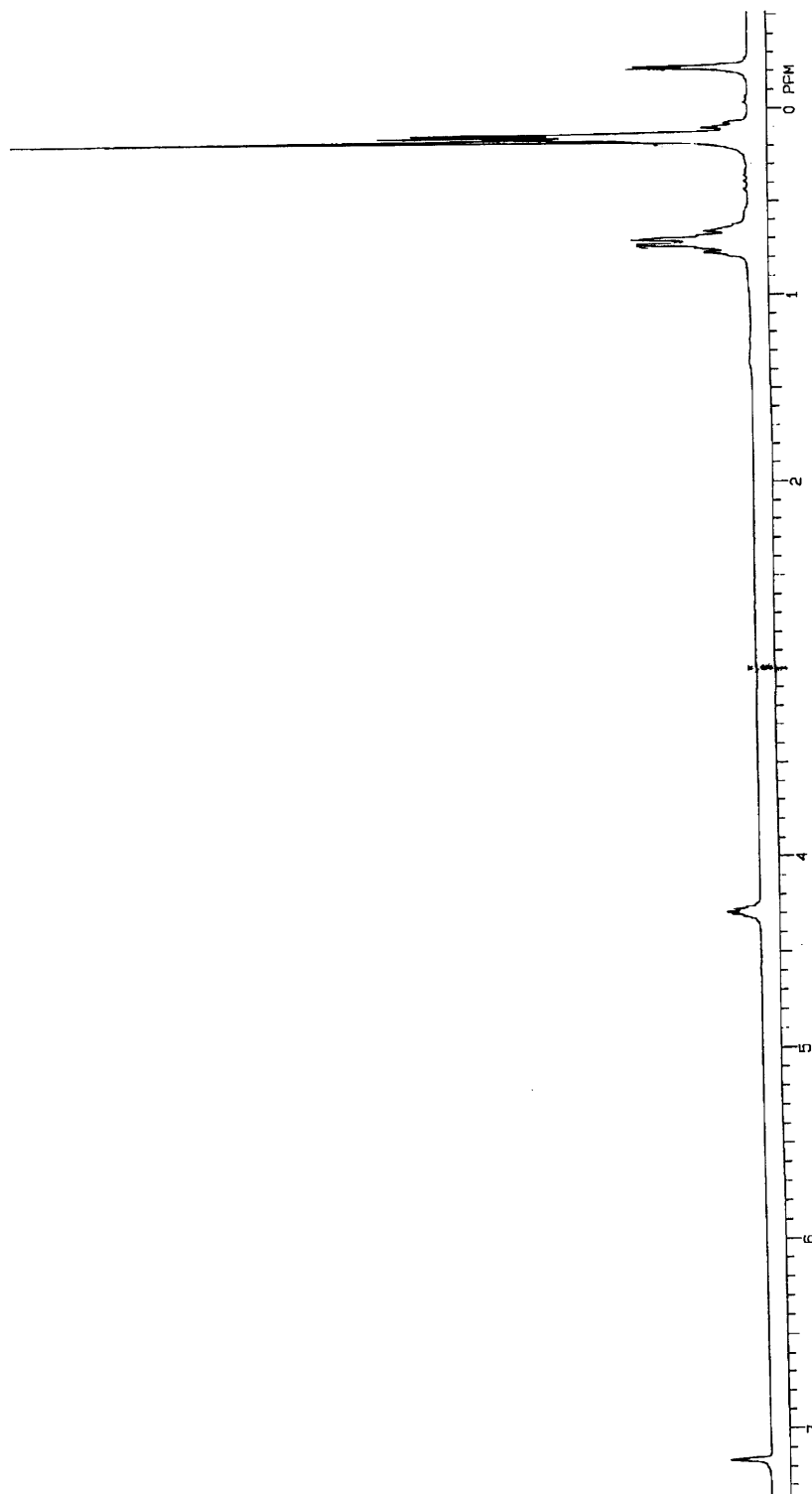
were far off from the appropriate values. Unreacted fluorenyl ligand was present.

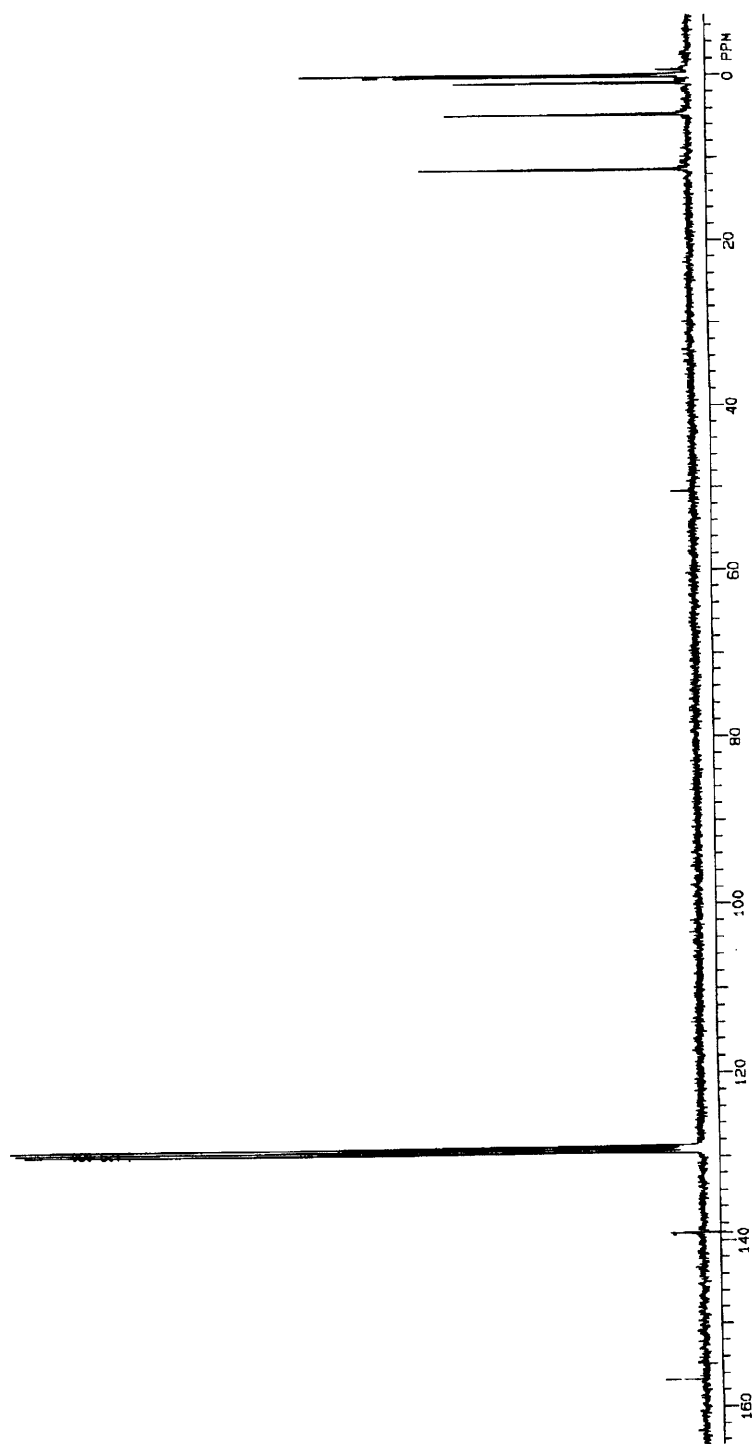Elemental: Expected 62.12% C, 3.96 % H; found 55.52% C, 4.71 % H. (Figure 10.22)

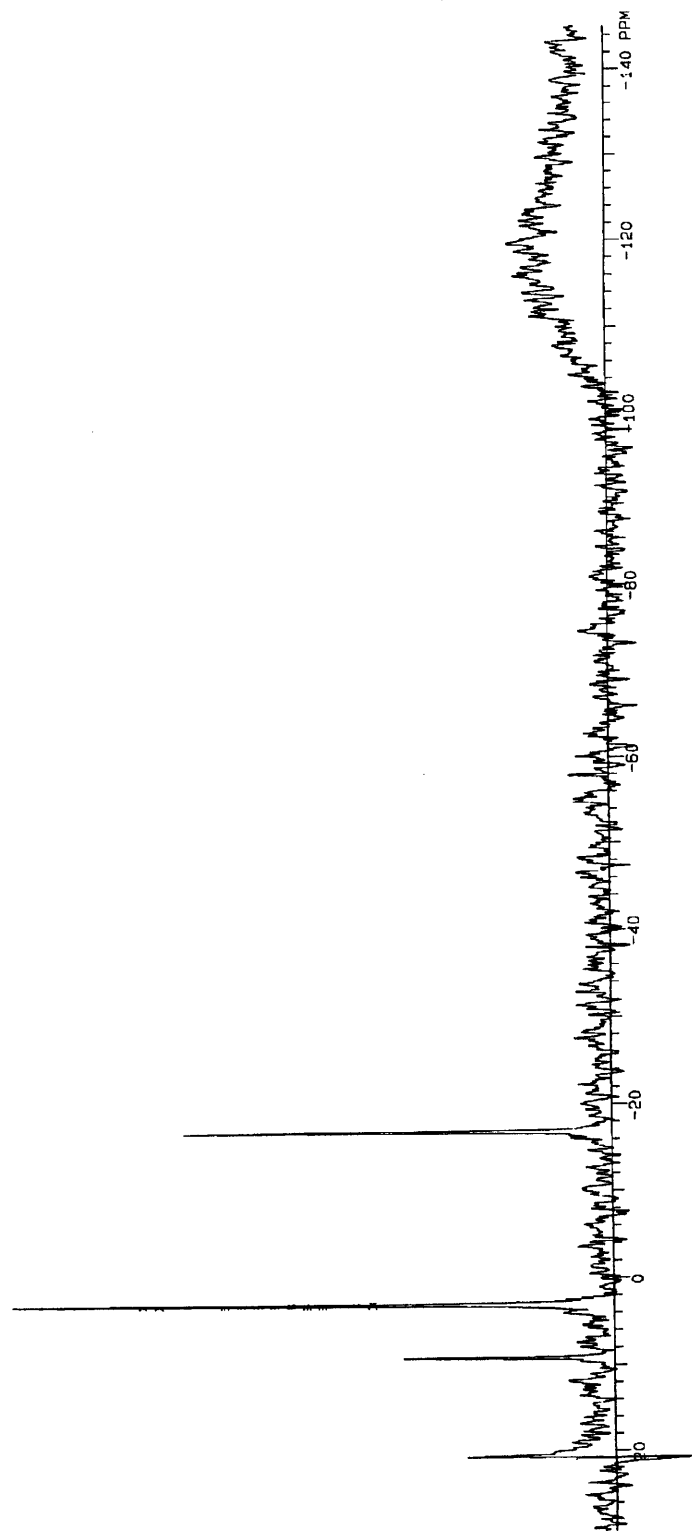(This was repeated on II-48 with much the same result.)

Figure 10.6 (a): ^{1}H NMR spectrum of I-83,
$Si(CH_2Si(Me)_2CH_2Si(Me)_2H)_4$.

Figure 10.6 (b): ^{13}C NMR spectrum of I-83,
$Si(CH_2Si(Me)_2CH_2Si(Me)_2H)_4$.

Figure 10.6 (c): ^{29}Si NMR spectrum of I-83,

Si(CH₂Si(Me)₂CH₂Si(Me)₂H)₄.

Figure 10.7 (a): ^{1}H NMR spectrum of I-107,

$Si(CH_2CH_2Si(Me)_2CH_2SnBu_3)_4$, immediately after isolation.
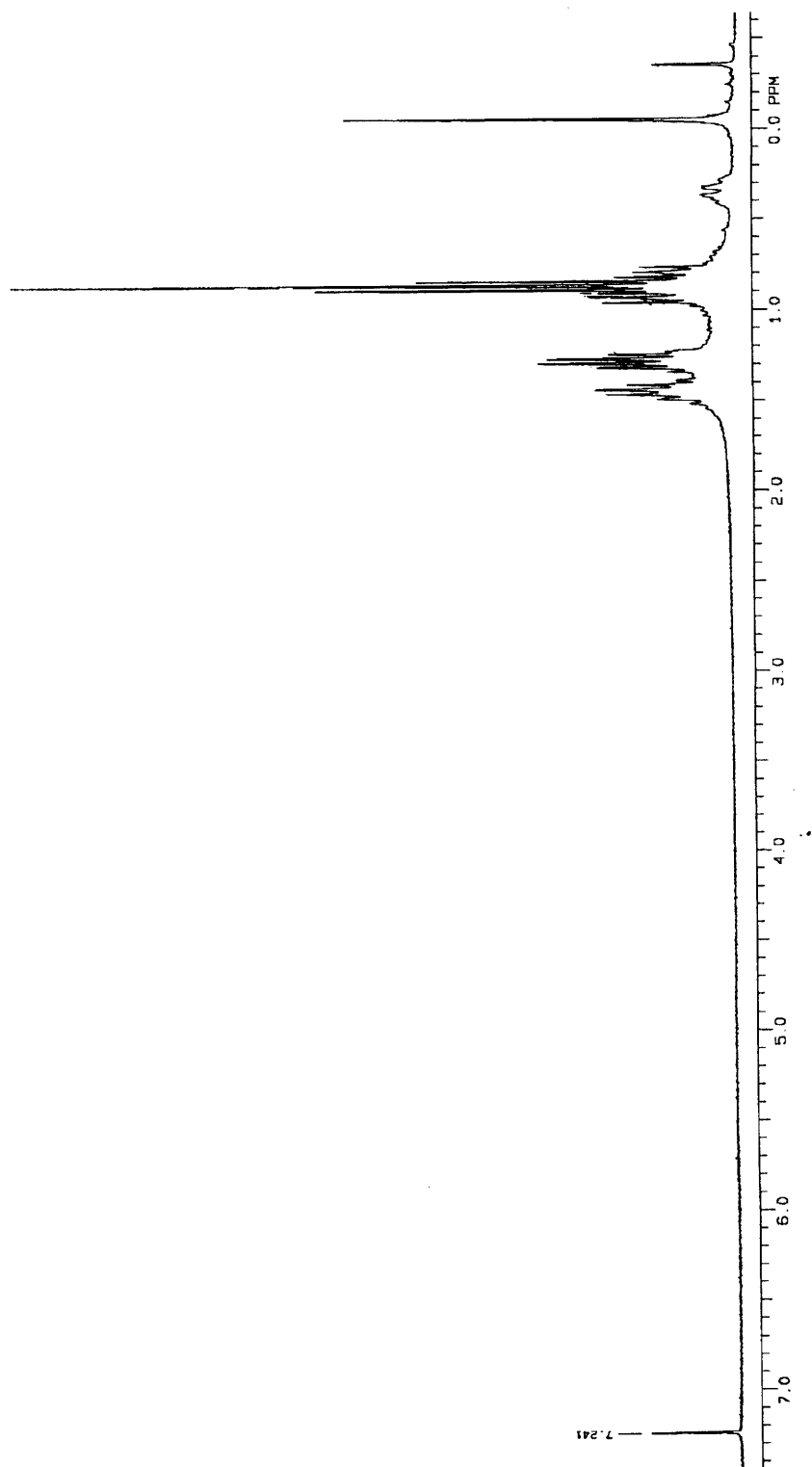
Figure 10.7 (b): ^1H NMR spectrum of I-107, Si(CH$_2$CH$_2$Si(Me)$_2$CH$_2$SnBu$_3$)$_4$, immediately after isolation.
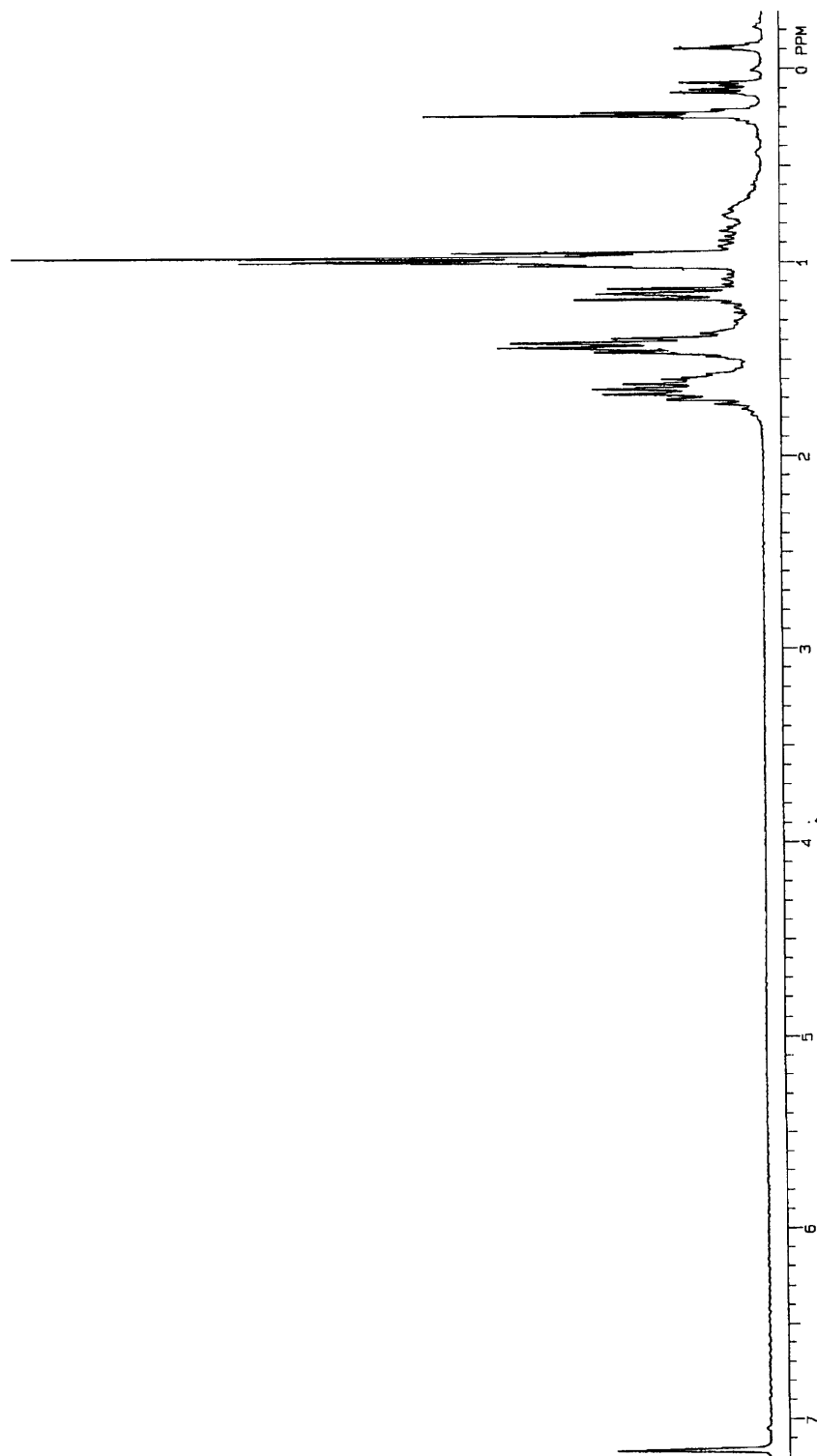
10.4 References

1)Tomalia, D. A.; Baker, H.; Dewald, J.; Hall, M.; Kallos, G.; Martin, S.; Roeck, J.; Ryder, J.; Smith, P. *Polymer J.* **1985**, *17*, 117.

2)Tomalia, D. A.; Naylor, A. M.; Goddard, W. A. *Angew. Chem. Int. Ed. Engl.* **1990**, *29*, 138.

3)Ardoin, N.; Astruc, D. *Bull. Soc. Chim. Fr.* **1995**, *132*, 875.

4)Barth, R. F.; Adams, D. M.; Soloway, A. H.; Alam, F.; Darby, M. V. *Bioconj. Chem.* **1994**, *5*, 58.

5)Tomalia, D. A.; Wilson, L. R., U.S. Patent Appl. 897,455, 1986.

6)Watson, A. D., U.S. Patent Appl. 772,349, 1991.

7)Watanabe, S.; Regen, S. L. *J. Am. Chem. Soc.* **1994**, *116*, 8855.

8)Coen, M. C.; Lorenz, K.; Kressler, J.; Frey, H.; Mulhaupt, R. *Macromol.* **1996**, *29*, 8069.

9)Alonso, B.; Cuadrado, I.; Moran, M.; Losada, J. *J. Chem. Soc. Chem. Commun.* **1994**, 2575.

10)Wyra, R., Final Report on Reserach in the Seyferth Group, unpublished.

11)Lungwitz, B., Final Report on Research in the Seyferth Group, unpublished.

12)Jansen, J. F. G. A.; de Brabander-van den Berg, E. M. M.; Meijer, E. W. *Science* **1994**, *266*, 1226.

13)Shahlai, K.; Hart, H. *J. Am. Chem. Soc.* **1990**, *112*, 3687.

14)Hawker, C. J.; Frechet, J. M. J. *J. Am. Chem. Soc.* **1990**, *112*, 7638.

15)Roovers, J.; Zhou, L.-L.; Toporowski, P. M.; van der Zwan, M.; Iatrou, H.; Hadjichristidis, N. *Macromol.,* **1993**, *26,* 4324.

16)van der Made, A. W.; van Leeuwen, P. W. N. M. *J. Chem. Soc. Chem. Commun.* **1992**, 1400.

17)Roovers, J.; Toporowski, P. M.; Zhou, L.-L. *Polym. Prepr. (Am. Chem. Soc. Div. Polym. Chem.)* **1992**, *33*, 182.

18)Zhou, L.-L.; Roovers, J. *Macromol.* **1993**, *26*, 963.

19)Seyferth, D.; Son, D. Y.; Rheingold, A. L.; Ostrander, R. L. *Organometallics* **1994**, *13*, 2682.

20)Krska, S. W., Ph.D. Thesis; Massachusetts Institute of Technology: Cambridge, MA, 1997.

21)Onopchenko, A.; Sabourin, E. T. *J. Org. Chem.* **1987**, *52*, 4118.

22)Eaborn, C. *Organosilicon Compounds*; Academic Press: New York, 1960.

23)Capka, M.; Svoboda, P.; Hetflejs, J. *Coll. Czechoslov. Chem. Commun.* **1973**, *38*, 3830.

24)Whitmore, F. C.; Sommer, L. H. *J. Am. Chem. Soc.* **1946**, *68*, 481.

25)Sommer, L. H.; Whiltmore, F. C. *J. Am. Chem. Soc.* **1946**, *68*, 485.

26)Jensen, F. R.; Bedard, R. L. *J. Org. Chem.* **1959**, *24*, 874.

27)Lai, Y.-H. *Synthesis* **1981**, 585.

28)Rieke, R. D.; Bales, S. E. *J. Chem. Soc. Chem. Commun.* **1973**, 879.

29)Rieke, R. D.; Bales, S. E. *J. Am. Chem. Soc.* **1974**, *96*, 1775.

30)Finkelstein, H. *Ber.* **1910**, *43*, 1528.

31)Willy, W. E.; McKean, D. R.; Garcia, B. A. *Bull. Chem. Soc. Jpn.* **1976**, *49*, 1989.

32)Lennon, P. J.; Mack, D. P.; Thompson, Q. E. *Organometallics* **1989**, *8*, 1121.

33)Wakefield, B. J. *Chemistry of Organolithium Compounds*; Pergamon Press: New York, 1974.

34) Wakefield, B. J. *Organomagnesium Methods in Organic Synthesis*; Academic Press: New York, 1994.

35) March, J. *Advanced Organic Chemistry: Reactions, Mechanisms, and Structure*; 4th ed.; Wiley-Interscience: New York, 1992.

36) Eaborn, C.; Harrison, M. R.; Walton, D. R. M. *J. Organomet. Chem.* **1971**, *31*, 43.

37) El-Durini, N. M. K.; Jackson, R. A. *J. Organomet. Chem.* **1982**, *232*, 117.

38) Collman, J. P.; Hegedus, L. S.; Norton, J. R.; Finken, R. G. *Principles and Applications of Organotransition Metal Chemistry*; University Science Books: Mill Valley, California, 1987.

39) Chen, Y.-X.; Rausch, M. D.; Chien, J. C. W. *Macromol.* **1995**, *28*, 5399.

40) Chen, Y.-X.; Rausch, M. D.; Chien, J. C. W. *J. Organomet. Chem.* **1995**, *497*, 1.

41) Ewen, J. A.; Jones, R. L.; Razavi, A.; Ferrara, J. D. *J. Am. Chem. Soc.* **1988**, *110*, 6255.

42) Alt, H. G.; Samuel, D. *Chem. Soc. Rev.* **1998**, *27*, 323.

43) Schneider, N.; Huttenloch, M. E.; Stehling, U.; Kirsten, R.; Schaper, F.; Brintzinger, H. H. *Organometallics* **1997**, *16*, 3413.

44) Morawietz, M. J. A., Ph.D. Thesis; Technical University of Munich: Munich, Germany, 1995.

45) Patsidis, K.; Alt, H. G.; Palackal, S. J.; Elawley, G. R. *Russ. Chem. J.* **1996**, *45*, 2216.

46) Ewen, J. A.; Elder, M. J.; Jones, R. L.; Haspeslagh, L.; Atwood, J. L.; Bott, S. G.; Robinson, K. *Makromol. Chem., Macromol. Symp.* **1991**, *48/49*, 253.

47)Diamond, G. M.; Rodewald, S.; Jordan, R. F. *Organometallics* **1995**, *14*, 5.

48)Herrmann, W. A.; Morawietz, M. J. A. *J. Organomet. Chem.* **1994**, *482*, 169.

49)Hopper, S.P.; Tramelling; M.J. Ginsberg, R.J.; Mendelowitz, P.C *J. Organomet. Chem.* **1977**, *134*, 173.

50)Rosenberg, S.D.; Walburn, J.J.; Stankovich, T.D.; Balint, A.E.; Ramsden, H.E. *J. Org. Chem.* **1957**, *22*, 1200.